

Surender Reddy Salkuti
Papia Ray *Editors*

Next Generation Smart Grids: Modeling, Control and Optimization

Lecture Notes in Electrical Engineering

Volume 824

Series Editors

Leopoldo Angrisani, Department of Electrical and Information Technologies Engineering, University of Napoli Federico II, Naples, Italy

Marco Arteaga, Departament de Control y Robótica, Universidad Nacional Autónoma de México, Coyoacán, Mexico

Bijaya Ketan Panigrahi, Electrical Engineering, Indian Institute of Technology Delhi, New Delhi, Delhi, India
Samarjit Chakraborty, Fakultät für Elektrotechnik und Informationstechnik, TU München, Munich, Germany

Jiming Chen, Zhejiang University, Hangzhou, Zhejiang, China

Shanben Chen, Materials Science and Engineering, Shanghai Jiao Tong University, Shanghai, China

Tan Kay Chen, Department of Electrical and Computer Engineering, National University of Singapore, Singapore, Singapore

Rüdiger Dillmann, Humanoids and Intelligent Systems Laboratory, Karlsruhe Institute for Technology, Karlsruhe, Germany

Haibin Duan, Beijing University of Aeronautics and Astronautics, Beijing, China

Gianluigi Ferrari, Università di Parma, Parma, Italy

Manuel Ferre, Centre for Automation and Robotics CAR (UPM-CSIC), Universidad Politécnica de Madrid, Madrid, Spain

Sandra Hirche, Department of Electrical Engineering and Information Science, Technische Universität München, Munich, Germany

Faryar Jabbari, Department of Mechanical and Aerospace Engineering, University of California, Irvine, CA, USA

Limin Jia, State Key Laboratory of Rail Traffic Control and Safety, Beijing Jiaotong University, Beijing, China

Janusz Kacprzyk, Systems Research Institute, Polish Academy of Sciences, Warsaw, Poland

Alaa Khamis, German University in Egypt El Tagamoa El Khames, New Cairo City, Egypt

Torsten Kroeger, Stanford University, Stanford, CA, USA

Yong Li, Hunan University, Changsha, Hunan, China

Qilian Liang, Department of Electrical Engineering, University of Texas at Arlington, Arlington, TX, USA

Ferran Martín, Departament d'Enginyeria Electrònica, Universitat Autònoma de Barcelona, Bellaterra, Barcelona, Spain

Tan Cher Ming, College of Engineering, Nanyang Technological University, Singapore, Singapore

Wolfgang Minker, Institute of Information Technology, University of Ulm, Ulm, Germany

Pradeep Misra, Department of Electrical Engineering, Wright State University, Dayton, OH, USA

Sebastian Möller, Quality and Usability Laboratory, TU Berlin, Berlin, Germany

Subhas Mukhopadhyay, School of Engineering & Advanced Technology, Massey University, Palmerston North, Manawatu-Wanganui, New Zealand

Cun-Zheng Ning, Electrical Engineering, Arizona State University, Tempe, AZ, USA

Toyoaki Nishida, Graduate School of Informatics, Kyoto University, Kyoto, Japan

Federica Pascucci, Dipartimento di Ingegneria, Università degli Studi "Roma Tre", Rome, Italy

Yong Qin, State Key Laboratory of Rail Traffic Control and Safety, Beijing Jiaotong University, Beijing, China

Gan Woon Seng, School of Electrical & Electronic Engineering, Nanyang Technological University, Singapore, Singapore

Joachim Speidel, Institut of Telecommunications, Universität Stuttgart, Stuttgart, Germany

Germano Veiga, Campus da FEUP, INESC Porto, Porto, Portugal

Haitao Wu, Academy of Opto-electronics, Chinese Academy of Sciences, Beijing, China

Walter Zamboni, DIEM - Università degli studi di Salerno, Fisciano, Salerno, Italy

Junjie James Zhang, Charlotte, NC, USA

The book series *Lecture Notes in Electrical Engineering* (LNEE) publishes the latest developments in Electrical Engineering - quickly, informally and in high quality. While original research reported in proceedings and monographs has traditionally formed the core of LNEE, we also encourage authors to submit books devoted to supporting student education and professional training in the various fields and applications areas of electrical engineering. The series cover classical and emerging topics concerning:

- Communication Engineering, Information Theory and Networks
- Electronics Engineering and Microelectronics
- Signal, Image and Speech Processing
- Wireless and Mobile Communication
- Circuits and Systems
- Energy Systems, Power Electronics and Electrical Machines
- Electro-optical Engineering
- Instrumentation Engineering
- Avionics Engineering
- Control Systems
- Internet-of-Things and Cybersecurity
- Biomedical Devices, MEMS and NEMS

For general information about this book series, comments or suggestions, please contact leontina.dicecco@springer.com.

To submit a proposal or request further information, please contact the Publishing Editor in your country:

China

Jasmine Dou, Editor (jasmine.dou@springer.com)

India, Japan, Rest of Asia

Swati Meherishi, Editorial Director (Swati.Meherishi@springer.com)

Southeast Asia, Australia, New Zealand

Ramesh Nath Premnath, Editor (ramesh.premnath@springernature.com)

USA, Canada:

Michael Luby, Senior Editor (michael.luby@springer.com)

All other Countries:

Leontina Di Cecco, Senior Editor (leontina.dicecco@springer.com)

**** This series is indexed by EI Compendex and Scopus databases. ****

More information about this series at <https://link.springer.com/bookseries/7818>

Surender Reddy Salkuti · Papia Ray
Editors

Next Generation Smart Grids: Modeling, Control and Optimization

 Springer

Editors

Surender Reddy Salkuti
Department of Railroad and Electrical
Engineering
Woosong University
Daejeon, Korea (Republic of)

Papia Ray
Department of Electrical Engineering
Veer Surendra Sai University of Technology
Burla, Odisha, India

ISSN 1876-1100

ISSN 1876-1119 (electronic)

Lecture Notes in Electrical Engineering

ISBN 978-981-16-7793-9

ISBN 978-981-16-7794-6 (eBook)

<https://doi.org/10.1007/978-981-16-7794-6>

© The Editor(s) (if applicable) and The Author(s), under exclusive license to Springer Nature Singapore Pte Ltd. 2022

This work is subject to copyright. All rights are solely and exclusively licensed by the Publisher, whether the whole or part of the material is concerned, specifically the rights of translation, reprinting, reuse of illustrations, recitation, broadcasting, reproduction on microfilms or in any other physical way, and transmission or information storage and retrieval, electronic adaptation, computer software, or by similar or dissimilar methodology now known or hereafter developed.

The use of general descriptive names, registered names, trademarks, service marks, etc. in this publication does not imply, even in the absence of a specific statement, that such names are exempt from the relevant protective laws and regulations and therefore free for general use.

The publisher, the authors and the editors are safe to assume that the advice and information in this book are believed to be true and accurate at the date of publication. Neither the publisher nor the authors or the editors give a warranty, expressed or implied, with respect to the material contained herein or for any errors or omissions that may have been made. The publisher remains neutral with regard to jurisdictional claims in published maps and institutional affiliations.

This Springer imprint is published by the registered company Springer Nature Singapore Pte Ltd.

The registered company address is: 152 Beach Road, #21-01/04 Gateway East, Singapore 189721, Singapore

Preface

Economically functioned power systems that can house a high penetration of renewable energy are of global interest. Recently, there has been a significant deployment of smart grids and a consequent rise in renewable power generation, resulting in the decarbonization of electrical power systems. However, due to the variability and intermittency of the renewable sources, significant uncertainty in power systems occurs, implying a more complex operation and control. Research activities are needed to provide adequate modeling and optimization techniques that account for variability and randomness in the proposed grid. The output of a renewable energy system is affected by the intermittency of resources. The storage system plays a vital role in overcoming the intermittency and provides a reliable and smooth supply to the demand. In smart grid networks, sustainability requires using renewable energy resources (RERs), communication technologies, and controls to improve environmental security and minimizing the cost of the system's capacity and planning. For the next generation of smart grids, several computational technologies are required to design and study the long- and short-term energy independence based on RERs.

Adequate modeling of RERs is needed to handle the variability of resources and uncertainties of the loads to meet the generation and load demand. Optimal allocation of different types of renewable energy for distributed generation (DG) penetration into the distribution network minimizes losses and costs, improving system security and reliability. Distribution grids are being transformed from passive to active networks due to new smart grids with RERs. In this context, smart grids are an emerging trend in electrical power systems to achieve both economic and environmental objectives while contributing to the reliability of energy supply to the consumers. Existing smart grids require technical expertise to be run, monitored, and maintained and cannot be deployed as standalone modules. However, to address this issue, an intelligent smart grid can be built using technologies like the Internet of Things (IoT) and machine learning. The scope of this book is to bridge the gap between traditional power consumption methods and modern consumption methods using smart computation methods. The goal is to develop an evidence-based, economically sound, and validated approach to enhancing the resilience of smart power grids, accounting for their interdependence with other infrastructure systems.

This book aims to develop the next generation of smart grid-connected RERs and load with variability and randomness. Renewable energy's behavior becomes unpredictable in a changing environment, and it becomes pretty challenging to optimize the smart grid's non-stationary distributed energy resources with static optimization methods. Under this situation, reliable operation of the power system becomes critical. Optimization and control strategies are needed to be developed to manage the stochastic nature of the resources while ensuring the stability of the RER-connected system. The contents of this book include the introduction of various energy optimization techniques, modeling and control in renewable and power domain, smart grid architectures and cyber and physical security, the impact of smart grid in distributed energy generation, integration of energy sources for smart grid efficiency improvement, intelligent learning models for the monitoring of energy management systems, electricity markets for power systems with high penetration of RERs, storage and electric vehicles, implementation of demand response programs in smart grids, and the intelligent computing applications for electrical power energy systems. This book also presents the application of artificial intelligence, machine learning, and IoT in the operation of smart grids, application of various optimization techniques in design and operation of smart grids, optimization and protection of power systems with RERs and energy storage, reliability, and resiliency analysis of smart grid, smart electric vehicles: optimization, security and privacy issues, and optimal generation scheduling using smart power computations techniques.

The book's primary emphasis is to develop a computational platform for modeling, control, performance analysis, and optimization of next generation hybrid energy systems. Further, this book leads toward cost-effective and environmentally benign utilization of a future energy system portfolio by providing a cyber-enabled sustainable pathway toward deep integration of intelligent decision-makers in the smart distribution grid. The results of this book will significantly advance state of the art in power systems operations under uncertainty and will also considerably extend the methods in solving general multi-stage robust optimization problems. This book is an effort to educate the next generation of academicians and researchers proficient in advanced analytics and improve national energy sustainability. The book is organized into 17 chapters. This book covers various fields to satisfy control and power engineers and researchers. The major topics covered in the book are modeling, control, and optimization of the smart grid and its various applications.

Chapter "[Overview of Next Generation Smart Grids](#)" provides a basic concept of the smart grid and the different challenging issues that the power sector faces in modeling and control and their solutions. It also focuses on the concept of cyber-enabled intelligence network communication, big data, machine learning, and blockchain technology in smart grids (SGs). In Chapter "[Modeling of Various Renewable Energy Resources for Smart Electrical Power Systems](#)", the modeling of power output from different renewable energy resources and the uncertainty in handling solar photovoltaic and wind energy systems is discussed. Chapter "[Smart Grid Communication: Recent Trends and Challenges](#)" focuses on the evolution of communication technology from wired networks to wireless networks and the smart grid architecture; various standards and protocols related to smart grid communi-

cation are also presented. In Chapter “[Comparison of Selected MPPT Techniques Using Different Performance Features](#)”, the investigation is carried out to extract the highest power from the photovoltaic generator, even in general situations, with the help of maximum power point tracking methods, namely perturb and observe, incremental conductance, and temperature control methods. Chapter “[Short Term Active Power Load Forecasting Using Machine Learning with Feature Selection](#)” proposes an artificial neural network (ANN) architecture designed, implemented, and tested in a Microsoft Azure Notebook environment to predict a 33/11 kV electric power distribution substation load. In Chapter “[Evaluation of Algorithms for Fundamental and Harmonic Impacts of Integration of Renewable Energy Sources in Smart Power Distribution Networks](#)”, a new power flow algorithm for fundamental and harmonic analysis of smart power distribution network with the integration of renewable energy-based DG and the nonlinear loads is proposed. Different case studies are also carried out in this chapter on IEEE-13 bus and IEEE-34 bus test feeders for analyzing the impacts of multiple integrations of synchronous based-renewable DG and power electronic based-renewable DG. Chapter “[A Comprehensive Review of Active Islanding Detection Methods and Islanding Assessment in a Grid Connected Solar Based Microgrid](#)” gives an overview of different islanding detection methods (IDMs) of the power system network consisting of distribution systems along with Distributed Generator (DG). This chapter also gives a techno-economical comparison of various IDMs based on recent trends related to monitoring islanding events. Additionally, a simulation study for a grid-connected solar-based microgrid is also presented in this chapter to analyze five different islanding detection methods under unintentional islanding. Chapter “[A Comparative Analysis of PI and Predictive Control Strategy for HESS Based Bi-directional DC-DC Converter for DC Microgrid Applications](#)” presents a comparative analysis of proportional–integral (PI) and model predictive control (MPC) of multiple input bidirectional DC-DC converter (MIPC) for hybrid energy storage systems (HESS) in DC microgrid applications. In this chapter, the simulation results are developed for the comparative performance of MPC over the PI control schemes, and it is concluded from the simulation results that the proposed MPC is better DC grid voltage restoration to step-change in PV generation and load demand over traditional PI control scheme. In Chapter “[Parameters Estimation of Solar PV Using Jaya Optimization Technique](#)”, a novel algorithm-specific parameter-free optimization named Jaya Algorithm is used to predict the solar PV module parameters accurately for three different technologies, i.e., poly-crystalline (Shell S75), mono-crystalline (Shell SM55), and thin-film (Shell ST36). The MATLAB simulation is carried out in this chapter for evaluating the PV module parameters for various environmental conditions. Chapter “[Integration of Photovoltaic Distributed Generation into Grid](#)” focuses on extracting maximum power from the photovoltaic solar plant at various working conditions using a maximum power point tracking algorithm. An active shunt filter is designed in this chapter to minimize the harmonics injected due to inverter operation. In Chapter “[Transient Stability Enhancement of Power System with Grid Connected DFIG Based Wind Turbine](#)”, the impact of a doubly-fed induction generator (DFIG)

on the transient stability (TS) of the power system connected to the grid is investigated, and the implementation of the rotor resistance control method to enhance the TS of the system is presented. Chapter “[Design and Analysis of BLDC Motor Driver for Hybrid Electric Vehicles](#)” presents the design and analysis of brushless DC (BLDC) motor drivers for hybrid electric vehicles (EVs). This chapter presents the relative evaluation of the EV powered by a brushless DC (BLDC) motor and the corresponding impact on the state of ripples and charge in the DC voltage at the battery power. Chapter “[A Novel Approach for Power Quality Improvement in Microgrid](#)” proposes an approach to improve the power quality (PQ) of the three-phase system by manipulating the grid-connected smart Photovoltaic Distribution Static Compensator (PV D-STATCOM) system with the help of a proposed dynamic voltage restorer (DVR) and a reweighted zero attracting (RZA) control technique containing adaptive features with P and O (perturb and observe) approach-based maximum power point tracking (MPPT) method. In Chapter “[Characterization of Bifacial Passivated Emitter and Rear Contact Solar Cell](#)”, the characterization of bifacial p-type Passivated Emitter and Rear Contact Cell (PERC) solar cell with various proportions of tallness and width, back silicon nitrate layer with various thickness are streamlined for better efficiency than the standard cell which are reaching their physical limits. Chapter “[Network Reconfiguration of Distribution System with Distributed Generation, Shunt Capacitors and Electric Vehicle Charging Stations](#)” presents a heuristic-based technique for solving the optimal network reconfiguration (ONR) in a radial distribution system (RDS) using the fuzzy-based multi-objective methodology. Minimization of real power losses and deviation of node voltage is considered as the multiple objectives in this work, and they are modeled with fuzzy sets. The developed algorithm determines the optimal reconfiguration of feeders with the minimum number of tie-line switch operations. Chapter “[Role of Advanced Control Technologies in the Evolution of Smart](#)” presents a discussion on the various challenges in the execution of smart grid and some of the recently proposed control techniques designed and applied to handle those issues. Also, various control applications in the smart grid are supplemented in this chapter with appropriate test bench problems and experimental or simulation results. Chapter “[Application of Solar Energy as Distributed Generation for Real Power Loss Reduction in Radial Distribution Network](#)” discusses the integration of solar energy as distribution generation in radial distribution systems and improves the system reliability and integrity by minimizing the power losses caused in the distribution lines.

Unlike many other books, in this book, individual chapters are unlike most technical publications as they are journal-type chapters and are not textbooks in nature that focus on the in-depth coverage of the topic. This book is written for researchers, utility engineers, and advanced teaching in power and control engineering.

Enjoy Reading!

Daejeon, South Korea
Sambalpur, India

Surender Reddy Salkuti
Papia Ray

Contents

Overview of Next Generation Smart Grids	1
Surender Reddy Salkuti, Papia Ray, and Sravanthi Pagidipala	
Modeling of Various Renewable Energy Resources for Smart Electrical Power Systems	29
Surender Reddy Salkuti	
Smart Grid Communication: Recent Trends and Challenges	49
Ishan Srivastava, Sunil Bhat, and Arvind R. Singh	
Comparison of Selected MPPT Techniques Using Different Performance Features	77
Salauddin Ansari and Om Hari Gupta	
Short Term Active Power Load Forecasting Using Machine Learning with Feature Selection	103
Venkataramana Veeramsetty, D. Rakesh Chandra, and Surender Reddy Salkuti	
Evaluation of Algorithms for Fundamental and Harmonic Impacts of Integration of Renewable Energy Sources in Smart Power Distribution Networks	125
R. Satish, K. Vaisakh, and Almoataz Y. Abdelaziz	
A Comprehensive Review of Active Islanding Detection Methods and Islanding Assessment in a Grid Connected Solar Based Microgrid	153
Kumari Namrata, Akshit Samadhiya, and Papia Ray	
A Comparative Analysis of PI and Predictive Control Strategy for HESS Based Bi-directional DC-DC Converter for DC Microgrid Applications	181
Srinivas Punna, Udaya Bhasker Manthathi, and C. R. Arunkumar	

Parameters Estimation of Solar PV Using Jaya Optimization Technique	221
C. Srinivasarathnam, Gurappa Battapothula, Anil Annamraju, and Chandrasekhar Yammani	
Integration of Photovoltaic Distributed Generation into Grid	257
Neelakanteshwar Rao Battu, Perka Krishna, and Venu Yarlagadda	
Transient Stability Enhancement of Power System with Grid Connected DFIG Based Wind Turbine	279
D. Rakesh Chandra, Surender Reddy Salkuti, and Venkataramana Veeramsetty	
Design and Analysis of BLDC Motor Driver for Hybrid Electric Vehicles	297
Seong-Cheol Kim, Narasimha Sangam, Sravanthi Pagidipala, and Surender Reddy Salkuti	
A Novel Approach for Power Quality Improvement in Microgrid	313
Arvind R. Singh, Papia Ray, and Surender Reddy Salkuti	
Characterization of Bifacial Passivated Emitter and Rear Contact Solar Cell	333
Suresh Kumar Tummala, Phaneendra Babu Bobba, and Satyanarayana Kosaraju	
Network Reconfiguration of Distribution System with Distributed Generation, Shunt Capacitors and Electric Vehicle Charging Stations	355
Surender Reddy Salkuti	
Role of Advanced Control Technologies in the Evolution of Smart	377
Raseswari Pradhan	
Application of Solar Energy as Distributed Generation for Real Power Loss Reduction in Radial Distribution Network	403
Aliva Routray, Khyati D. Mistry, and Sabha Raj Arya	
Author Index	433
Subject Index	435

Editors and Contributors

About the Editors

Dr. Surender Reddy Salkuti received the Ph.D. degree in electrical engineering from Indian Institute of Technology, New Delhi, India, in 2013. He was a Post-doctoral Researcher at Howard University, Washington, DC, USA, from 2013 to 2014. He is currently working as an Associate Professor in the Department of Railroad and Electrical Engineering, Woosong University, Daejeon, Republic of Korea. His current research interests include power system restructuring issues, ancillary service pricing, real and reactive power pricing, congestion management, and market clearing, including renewable energy sources, demand response, smart grid development with integration of wind and solar photovoltaic energy sources, battery storage and electric vehicles, artificial intelligence applications in power systems, and power system analysis and optimization. He received Distinguished Researcher Award from Woosong University Educational Foundation, Republic of Korea in 2016, and POSOCO Power System Award (PPSA), India in 2013. He is a Member of IEEE and IEEE Power and Energy Society.

Dr. Papia Ray received the Ph.D. degree in Electrical Engineering from the Indian Institute of Technology, New Delhi, India, in 2013. She is currently working as an Associate Professor in the Department of Electrical Engineering, Veer Surendra Sai University of Technology, Burla, Odisha, India and is having more than 17 years of teaching experience. Her current research interests include power system protection, power quality, wide-area measurement systems, artificial intelligence applications in power system protection and microgrid protection. She is the recipient of the Young Scientist Award from DST in 2015. She has published several research papers in various journals and conferences and is also an active reviewer for several reputed journals. She is a Senior Member of IEEE, Life Member of Indian Society for Technical Education, and Member of Institution of Engineer's India Ltd. She has edited a book on *Microgrid: Operation, Control, Monitoring and Protection* published by Springer.

Contributors

Almoataz Y. Abdelaziz Faculty of Engineering and Technology, Future University in Egypt, Cairo, Egypt

Anil Annamraju Department of Electrical and Electronics Engineering, School of Engineering, Malla Reddy University, Telangana, India

Salauddin Ansari Department of Electrical Engineering, National Institute of Technology Jamshedpur, Jamshedpur, Jharkhand, India

C. R. Arunkumar Electrical Engineering Department, NIT Warangal, Warangal, Telangana, India

Sabha Raj Arya Department of Electrical Engineering, Sardar Vallabhbhai National Institute of Technology Surat, Gujarat, India

Gurappa Battapothula Department of Electrical and Electronics Engineering, B.V. Raju Institute of Technology, Narsapur, Telangana, India

Neelakanteshwar Rao Battu Department of Electrical and Electronics Engineering, VNR VJIET, Hyderabad, Telangana, India

Sunil Bhat Electrical Engineering Department, Visvesvaraya National Institute of Technology, Nagpur, India

Phaneendra Babu Bobba Electrical and Electronics Engineering Department, Gokaraju Rangaraju Institute of Engineering and Technology, Hyderabad, India

Om Hari Gupta Department of Electrical Engineering, National Institute of Technology Jamshedpur, Jamshedpur, Jharkhand, India

Seong-Cheol Kim Department of Railroad Electrical Systems, Woosong University, Daejeon, Republic of Korea

Satyanarayana Kosaraju Mechanical Engineering Department, Gokaraju Rangaraju Institute of Engineering and Technology, Hyderabad, India

Perka Krishna Department of Electrical and Electronics Engineering, VNR VJIET, Hyderabad, Telangana, India

Udaya Bhasker Manthathi Electrical Engineering Department, NIT Warangal, Warangal, Telangana, India

Khyati D. Mistry Department of Electrical Engineering, Sardar Vallabhbhai National Institute of Technology Surat, Gujarat, India

Kumari Namrata Department of Electrical Engineering, National Institute of Technology Jamshedpur, Jamshedpur, India

Sravanthi Pagidipala Department of Electrical Engineering, National Institute of Technology Andhra Pradesh (NIT-AP), Andhra Pradesh, India

Raseswari Pradhan Department of Electrical Engineering, VSSUT, Burla, Odisha, India

Srinivas Punna Electrical and Electronics Engineering Department, BVRIT Hyderabad College of Engineering for Women, Hyderabad, Telangana, India

D. Rakesh Chandra Department of Electrical and Electronics Engineering, Kakatiya Institute of Technology and Science, Warangal, India

Papia Ray Department of Electrical Engineering, Veer Surendra Sai University of Technology (VSSUT), Burla, Odisha, India

Aliva Routray Department of Electrical Engineering, Sardar Vallabhbhai National Institute of Technology Surat, Gujarat, India

Surender Reddy Salkuti Department of Railroad Electrical Systems, Woosong University, Daejeon, Republic of Korea

Akshit Samadhiya Department of Electrical Engineering, National Institute of Technology Jamshedpur, Jamshedpur, India

Narasimha Sangam Department of Electrical and Electronics Engineering, TKR College of Engineering and Technology, Hyderabad, India

R. Satish Department of Electrical and Electronics Engineering, ANITS (A), Visakhapatnam, Andhra Pradesh, India

Arvind R. Singh School of Electrical Engineering, Shandong University, Jinan, China

C. Srinivasarathnam Department of Electrical and Electronics Engineering, Vasavi College of Engineering, Ibrahimbagh, Hyderabad, Telangana, India

Ishan Srivastava Electrical Engineering Department, Visvesvaraya National Institute of Technology, Nagpur, India

Suresh Kumar Tummala Electrical and Electronics Engineering Department, Gokaraju Rangaraju Institute of Engineering and Technology, Hyderabad, India

K. Vaisakh Department of Electrical Engineering, Andhra University, AUCE (A), Visakhapatnam, Andhra Pradesh, India

Venkataramana Veeramsetty Center for Artificial Intelligence and Deep Learning, SR Engineering College, Warangal, India

Chandrasekhar Yammani Department of Electrical Engineering, National Institute of Technology, Warangal, Telangana, India

Venu Yarlagadda Department of Electrical and Electronics Engineering, VNR VJIET, Hyderabad, Telangana, India

Overview of Next Generation Smart Grids



Surender Reddy Salkuti, Papia Ray, and Sravanthi Pagidipala

Abstract Due to the integration of renewable energy resources (RERs), the electric power system is undergoing a significant change in operation, maintenance, and planning. The advancement into a smart grid (SG) using advanced automation and control approaches produces new challenges and opportunities. In this work, an overview of next generation smart grids has been presented by highlighting the latest and recent innovations in the SG fields. Advantages, barriers, and opportunities of smart grids are provided in this work. Challenges of integrating the RERs into the grid and various energy storage technologies are reviewed. The output of RERs is affected by the uncertain nature of resources. The energy storage system plays a vital role to handle this uncertain nature of RERs and provides a smooth and reliable supply to the load demand. Smart energy systems present various challenges and opportunities in designing, integrating, and implementing electrical grids with network and communication technologies and essential privacy and security issues of various components within the electrical grid. Therefore, this work presents the concepts of cyber-enabled intelligence network communication, big data, machine learning, and blockchain technology in smart grids (SGs). This work also demonstrates the impact of SGs in distributed energy generation and the comparative study on electric vehicles (EVs) along with the classification, i.e., battery, hybrid electric, and plug-in electric vehicles, current issues and challenges on the EV technology. Further, a discussion is also provided on SG protection issues and their remedy.

S. R. Salkuti (✉)

Department of Railroad and Electrical Engineering, Woosong University, Daejeon 34606, Republic of Korea
e-mail: surender@wsu.ac.kr

P. Ray

Department of Electrical Engineering, Veer Surendra Sai University of Technology (VSSUT), Burla, Odisha, India
e-mail: papiaray_ee@vssut.ac.in

S. Pagidipala

Department of Electrical Engineering, National Institute of Technology Andhra Pradesh (NIT-AP), Andhra Pradesh, India

Keywords Renewable energy · Machine learning · Demand response · Big data · Smart grid · Energy storage · Electrical vehicles · Optimal control

Nomenclature

BEV	Battery electric vehicle
CHP	Combined heat and power
DG	Distributed generation
DR	Demand response
DER	Distributed energy resources
DMS	Distribution management system
PV	Photovoltaic
VVO	Voltage/VAR optimization
AMI	Advanced metering infrastructure
GIS	Geographic information system
OMS	Outage management system
WAMS	Wide area measurement system
ML	Machine learning
PMU	Phasor measurement unit
EMS	Energy management system
IED	Intelligent electronic device
SG	Smart grid
RERs	Renewable energy resources
WT	Wind turbine
ICE	Internal combustion engine
PHEV	Plug-in hybrid electric vehicle
IoE	Internet of energy
IED	Integrated electronic device

1 Introduction

A smart grid (SG) is an advanced distribution and transmission grid that uses information, control, and communication technologies to enhance the electrical grid's security, efficiency, economy, and reliability. The conventional grid can be changed into the SG by smart metering, advanced network operation and control, faster fault identification, and self-healing capabilities using grid automation. SG can be defined as an interconnected system of information, communication technologies, and control systems used to interact with automation and business processes across the entire power sector, encompassing electricity generation, transmission, distribution, and consumers [1]. Smart renewable energy control centres which can forecast

and monitor renewable energy availability and potentially use energy storage to manage the dispatch of power to match grid conditions or manage demand through demand response (DR) programs to match capacity availability are expected to become critical to the future integration of renewable energy.

In recent days, the power generation from renewable energy resources (RERs) is increasing significantly, and the power generated from renewable energy will play a significant role soon. To enhance the integration of renewable power in the conventional power network, it has to deliver the liabilities acted to the network due to the irregular nature of these resources. Because of their effect on system adjusting, reserves procurement, scheduling and commitment of generating units, changeability, and ramp or slope events in power output are the fundamental difficulties to the system administrators [2]. With the integration of RERs such as solar PV and wind, significant uncertainty into the power system is developed. It is a tremendous challenge for system operators to maintain reliable operation and efficient electricity markets with simultaneous maximum utilization of renewable energy. As the electric market structures change to improve the management of renewable sources, advances in the design and pricing aspects of energy and ancillary services markets are needed [3].

Distributed generation (DG) is from many small energy sources connected directly on the customer side of the meter or to the distribution network. DGs are also termed as embedded generation or dispersed generation or decentralized generation, or on-site generation. Optimal size and location of DGs can reduce the power losses in the system, improve system voltage, maximise DG capacity, enhance system reliability, and minimise investment. Power companies generally generate electricity with a relatively fixed amount of energy over short periods, regardless of the daily fluctuation of the energy demand. The energy demand fluctuation leads to energy storage techniques to supply enough electricity to consumers during peak demand. Electricity storage techniques allow power companies to provide electricity when needed [4]. The electricity is first generated and then stored in storage devices to be used during the peak load.

Oil, natural gas, uranium are all power sources that the world has been using for a long time and they all have the potential to run out at any time. RERs are the sources that can last longer than the human race. Most renewable energies are environmentally friendly, fight against global warming by reducing carbon emission. Renewable energies are sustainable, reliable, and cost less compared to fossil fuels and other nonrenewable energies. Solar energy initial installation remains expensive, but it is increasingly being used around the globe, especially in the rural world where people don't have access to electricity or simply can't afford to pay for their monthly electric bills. Biomass is one of the most renewable energies used today due to its advantages [5]. In addition to the fact that biomass energy does not pollute the air allows countries to protect their environments by burning the wastes. Renewable energy is a resource used all over the world. Renewable energy produces from natural resources such as wind, solar photovoltaic (PV), biomass, geothermal, etc., and is known to be beneficial to the earth. Table 1 presents the various characteristics of the traditional power grid and the SG [6].

Table 1 Characteristics of the traditional power grid and smart grid

Characteristics	Traditional power grid	Smart grid (SG)
Technological aspect	The traditional power grid is electromechanical. As a result, it has no means of communication and there is minimal internal regulation	SG uses advanced digital technology. It allows for communication between devices and promotes self-regulation
Distribution system	It involves the one-way distribution of power. Power is only distributed from the main power plant with the help of traditional infrastructure	It allows for the two-way distribution of power, i.e., power can also go back to the distribution lines from a secondary power provider
Generation	The generation infrastructure is highly centralized. All the power is generated from a central system that minimises incorporating alternative energy sources into the grid	The generation infrastructure is scattered and distributed. It allows the power to be distributed from multiple power sources, which help in balancing the load and limit power outages
Incorporation of sensors	It involves limited sensors as the infrastructure is unable to handle sensors making detection of problems difficult	SG infrastructure system allows multiple sensors throughout the line, which helps to pinpoint problems
Monitoring of power plants	Traditional infrastructure is minimal. As a result, energy distribution has to be manually monitored	The SG involves advanced technology and can monitor itself, which prevents troubleshoot outages
Restoration and repairing	For restoration purposes, technicians must physically go to the failure location and make corresponding repairs to prevent excessive power outages	In the case of SG technology, the sensors can detect, analyze and rectify the required problems without the need for physical intervention
Equipment	Due to the ageing and limited capacity of the traditional power grid, it is prone to failures and blackouts	In the case of an SG system, alternative energy sources limit the area that is impacted by the power outage
Control of energy	In the case of traditional power infrastructure, energy companies have no control over the distribution of energy	With the availability of sensors and innovative infrastructure, energy providers have pervasive control over the power distribution
Choices of consumers	The traditional power grid system does not provide consumers with any flexibility in receiving their electricity	SG allows consumers to have more choices in the way they receive energy

A smart grid (SG) network should possess

- **Better communication:** This deals with interaction with the network and within the network itself. An illustration of this will be the automatic shutting off of power supplied to the home when people living in a house. In light of that, it is easy to see that a lot of work goes into sensing and feedback circuitry built into the grid as it receives information about the power grid itself.
- **Self-healing capability:** SG employs technologies that assist in self-healing in response to natural faults or breakdown without human intervention.
- **Adaptiveness and flexibility:** SG should be able to adapt to variations in conditions within the grid, especially regarding ever-changing load and the direction of flow of power.
- **Resilience:** This refers to the ability of the SG to withstand attack, i.e., both human and natural.
- **Real-time measurements and control:** In monitoring the central generation, distribution generation, and other plants in the system, the grid must be capable of making real-time measurements and controlling the grid due to the sensitivity of generated power even within just microseconds.
- **Reliable technology:** SG uses state estimation technologies, which improves fault detection and allows self-healing of the corresponding system without the need of the technicians to intervene [7]. This ensures a proper reliable supply of electricity and reduces related vulnerabilities.
- **Flexibility in networking:** SG technology enables better handling of the bidirectional flow of energy, allowing for distributed generation. This includes solar panels, fuel cells, electric batteries, wind turbines, and other such sources.
- **Increased efficiency:** SG technology has resulted in numerous contributions towards the overall improvement in the efficiency of the power grid system and energy infrastructure. The demand-side management has highly benefitted from the smart infrastructure. This includes the voltage/VAR optimization (VVO) technique which reduces the power usage through the distribution lines during idle time and advanced metering infrastructure (AMI) systems which improve the outage management of usage data [8]. All these have resulted in better efficiency and greater utilization of energy resources.
- **Peak curtailment-usage and pricing:** Communication systems and metering technologies have reduced demand during high cost and peak usage hours. Smart devices allow users to track the energy demand and usage of electricity. Moreover, it also allows utility companies to reduce consumptions and avoid system overloads. This is done by increasing the electricity cost during peak hours which is termed peak curtailment.
- **Sustainability:** The SG system is supposed to be highly flexible as it allows the correlation of various RERs such as solar and wind energy without any additional storage.
- **Demand response:** Demand response allows loads and generators to interact amongst themselves in an automated real-time manner [9]. This, in turn, eliminates

the additional costs of reserve generators and increases the life expectancy of power systems [10].

- **Advanced services in the near future:** The use of robust two-way communications combined with technologically advanced sensors and distributed technology will drastically improve the efficiency, productivity, reliability, and safety of power generation, transmission, and distribution.

SG combines various technologies and applications to provide efficient, clean, reliable, easily accessible, and low-cost energy. The need of the hour is to perform complex testing and improve applied techniques and improve threshold and optimized operation of the SG, keeping in mind the sustainable development of the environment [11]. Various applications of SGs include:

- Improve response and adaptivity of transmission and distribution systems.
- Enables quicker detection and recovery from faults, disturbances, and outages in the distribution lines and feeders.
- Reduces the cost and peak demand for energy.
- Allows for integration and scalability of various alternative sources of energy such as wind and solar power.
- Utilizes sharing of load, which in turn reduces the load on a large scale.
- Many other technologies have also helped to optimize the SG on a large scale, such as advanced metering infrastructure (AMI), distribution management system (DMS), geographic information system (GIS), outage management system (OMS), wide area measurement system (WAMS), phasor measurement unit (PMU) and energy management systems (EMS).

The international energy roadmap study ranks windmills, biomass, solar PV, and tidal power as future renewable power sources to sustain the world's economy. Progress in the field of sustainable energy scenario over the previous period has been exceptional. The two primary sustainable energy resources are the sun and the wind. The growth in electricity generation from renewables was substantially increased [12, 13]. The IEA ventures by 2050, around (15–18)% of worldwide power will be created from the wind, with sun-powered PV contributing as high as 16% [14, 15] regardless of its different favourable circumstances.

2 Smart Grids: Advantages, Barriers, and Opportunities

A smart grid (SG) is a system that utilizes digital processing and communications technology to manage resources connected to a power grid. The heavy dependence on technology and hence power supply that aid the operation of these technologies across all facets of life from the auto industry to medical equipment, households, and so on has increased the need for efficient management of the assets to maximize

productivity [16]. The ageing power grid, workforce also compound this, and infrastructure within the US SG will help ensure better communication between human beings and the power grid.

2.1 Advantages and Barriers of Smart Grids

Advantages of SG include:

- **Growth of economic sector:** The manufacture, installation, maintenance, and corresponding operation of the SG and its respective components will create opportunities for skilled and unskilled job sectors [17]. Moreover, it will help in growth in business along with providing advanced technological solutions.
- **Cost efficiency:** SG technologies tend to be cheaper than traditional energy sources. Moreover, with advancements in technologies, energy expenses reduce over time.
- **Greater customer satisfaction:** The improved reliability and lower costs have resulted in greater customer satisfaction [18]. Additionally, SG provides better customer control over energy distribution and usage.
- **Better reliability:** SG reduces power outages and, at the same time, improves power efficiency.
- **Environment:** SG results in a positive impact on the environment as it helps reduce greenhouse gas emissions by enabling alternate RERs and electric vehicles (EVs) [19]. Moreover, it also reduces oil consumption because of efficient power generation.
- **Intelligence:** SGs enhance the capacity and capability of the existing power grid. Also, they have predictive maintenance and self-healing capabilities.

Barriers of SG include:

- **Security and privacy concerns:** As the SG is void of human interference, it is highly prone to hacking and cyber-attacks. It may lead hackers to gain access to numerous smart meters and manipulate the data [20]. Also, since the system is fully automatic, privacy concerns are raised over data collection and the use of smart meters.
- **Lack of government norms and policies:** As SG technology is still in its budding stage, there is a lack of proper stringent government policies to avoid thrift, loss, and misuse of the power system. Also, there are no standard regulations regarding the safety and threshold limitations of SG systems.
- **Higher installation costs:** The present energy infrastructure scenario is inadequate and insufficient to develop SG technologies [21]. As a result, SG systems require a higher installation cost as it involves the procurement of smart meters and various other sensors for monitoring and data distribution.
- **Congestion in network topology:** Smooth operation of a SG requires a continuous network channel. This may result in network traffic, especially during peak

hours. Moreover, there is no guaranteed service during abnormal conditions such as heavy rainfall, storm, and lightning conditions.

2.2 Challenges

There are bound to be vital challenges with the rapid growth in digital technologies and their widespread applications. These include insecurity and privacy issues along with a lack of government policies [22]. The most common challenges regarding SG include:

- **Privacy issues:** With the involvement of technology, there are bound to be privacy concerns. There is a possibility of some people hijacking the system to gain sensitive data regarding the consumers.
- **Security issues:** SG technology is prone to attack by hackers who may gain access to the power system and disrupt the underlying technology to gain an advantage by hampering the net-metering system [23].
- **Grid volatility:** SG is considered to be a volatile network, being highly intelligent at both the transmission end and distribution end but a bit vulnerable along the way due to a lack of complete network intelligence.

Various processes and systems to overcome the above challenges include:

- **Increasing the grid strength:** The power grid should have enough tensile strength to withstand the power requirement. The power grid is one of the most complex inter-connected physical systems in the world. Hence, absolute care should be taken to sustain the grid network.
- **Communication systems:** SG should be optimized to integrate all kinds of sensors and digital devices to enhance and upgrade the level and performance of the grid. Additionally, there should be proper coordination and communication among all the components to ensure reliable operation. Fiber optics has enabled faster travel of data signals, thus reducing propagation time.
- **Advanced metering infrastructure (AMI):** It involves a net-metering system that includes a smart meter and the infrastructure to allow for two-way communication of energy. With the help of broadband and radio technology, it has become possible for grids to communicate with other grids. Moreover, it is also a viable option for energy sustenance and reduces consumer costs.
- **Economic dispatch and integration of various sources:** It involves cost optimization of electrical power analysis and minimises production and distribution costs. Also, the integration of various energy sources like solar and wind is achieved with the intermittent coordination of multiple generators.
- **Advanced power system monitoring:** Use of synchronised PWMs and SCADA has enabled better monitoring of SGs and proper control over the utility. AMI has helped real-time measurements of voltage and current phasors. GPS has allowed us to pinpoint the fault location and reduce the outage time precisely.

3 Technologies Required for the Smart Grid Development

SG has a set of diverse necessities. To accomplish all the requirements, various technologies have been enabled and utilized [24].

3.1 Sensing and Measurement Technologies

These technologies include:

- **Phasor measurement units (PMU) and Wide area monitoring, protection and control (WAMPAC):** These help in maintaining the security and reliability of the power grid [1].
- **Intelligent electronic devices (IED):** These devices are used for protection relays and determining faults. These involve integrated sensors and automated systems for rapid analysis and diagnosis and results in timely resolutions. They also function to minimize network congestion and reduce the risk of outages. As a result, these devices enhance the efficiency and operation of the resultant SG.
- **Smart appliances:** These devices form the control and communication part of the power grid system [25]. They monitor the operation of consumer appliances and try to maximize their efficiency, reliability, and safety.
- **Smart meter and its associated software:** These form the building blocks of the entire SG system. It provides better electricity control and allows consumers greater control over their electricity consumption. They also make the consumers responsible by providing real-time info and proper bills.

3.2 Communication Technologies

The various technologies include:

- **Two-way communication:** It enables a back and forth bridge to allow a two-way flow of electrical energy across various loads in a power system.
- **Advanced architecture:** It allows for technologies regarding EVs, micro-generation, and plug-play home appliances.
- **Communication technology:** Along with the corresponding software, communication technology aims to provide the energy consumers with better opportunities and more meaningful information [26].
- **Hardware and software:** These formed the building blocks of the system and were responsible for maintaining the security and reliability of the utility.

3.3 Smart Meters and Advanced Metering Infrastructure (AMI)

AMI is defined as the integration and interconnection of numerous smart meters and communication equipment that work in cohesion to enable a two-way flow of power in the power grid between utilities and consumers. It involves data management systems and advanced sensors that make the SG capable of monitoring its power requirements. Smart meters are equipped with power monitoring software technologies that enable faster detection and diagnosis of faults along with ways to resolve power problems [27]. Moreover, AMI prepares the grid with self-healing capability by monitoring power outages, enabling faster detections of faults. Various other features of AMI include:

- Power generation systems and storage components can be analyzed and controlled at the consumer level. It provides data to improve the operation and management of the utility network.
- Before AMI enables auto-detection of faults and outages, it also informs the repair crew of the location of the fault.
- An AMI system provides accurate records and notifications regarding outages and their corresponding restoration through the smart meter sensors. This helps in quicker resolution of outages and also enables faster providing of power supply.
- AMI implementation reduces the daily reading of meters as the readings are taken automatically at regular intervals [28].
- It implements built-in analysis tools and software which detect and prevent possible energy theft and tampering.
- By combining with SCADA, the AMI systems automatically generate investigation reports for field managers making their work easier.

4 Renewable Energy and Energy Storage

Renewable energy is a resource needed to transform the electric power system by enhancing the SG's performance, sustainability, and reliability. Distributed energy resources (DER) in a microgrid would include photovoltaic (PV), small wind turbines (WT), heat or electricity storage, combined heat and power (CHP), and controllable loads. Renewable energy sources are practically inexhaustible in that most of their energy is from nature and sources that will continue to exist like the sun. Renewable energy is an area that will continue to grow in research and development; more money has gone into the exploration of both new and existing renewable sources. Solar, the most commonly used, has improved its application in our world drastically with the advents of solar-powered cars, light, and houses [29]. More work needs to be done to eradicate non-renewable energy in our society to create a world where green power is the dominant energy source used. Finally, for renewable energy to facilitate energy shortage, extensive research on utilising the available RER to its maximum efficiency

is needed. Also, areas throughout the world should implement primary RER based on their most vital natural resource. For example, areas with the strong wind will implement more hydropower, and regions with constant sunlight will use solar.

4.1 Renewable Energy

Renewable energy resources (RERs) could be harnessed from technological sources like solar, wind, biomass, biogas, geothermal, and hydroelectric. There has been an improvement in technologies and advancement in the equipment and use of renewable energy. More companies, through research and government incentives, have increased the operational experience of renewable energy technologies. The issue of renewable energy and its application presents questions on the efficiency, reliability, tracking, and accountability of these resources. However, most renewable energy technologies struggle to compete economically with conventional fuel technologies making the budget and funds for renewable energy smaller than its counterpart [30]. The regulatory commission has categorized the utility industry into three; generation companies cover utility and non-utility companies, transmission companies, and distribution companies.

The intermittent nature of wind generation makes its operation and planning a complex problem, and there is a need for the current analytical models to consider this uncertainty appropriately. Current electricity market clearing schemes cannot fully integrate the essential features of non-dispatchable generation such as wind power. This limitation is becoming an issue for grid operators as there is more and more public and political pressure to increase the penetration of renewable generation. This is due to the uncertainty associated with wind forecasts. As wind cannot be forecast to a high degree of accuracy, additional reserve capacity needs to be carried by the system in addition to the reserves already allocated to cater for unit outages and demand forecast errors. Renewable energy could be discussed regarding connectivity, sustainability, cost, environmental impact, security, etc.

- **Connectivity:** Renewable energies usually require different levels before they could be used as power for its consumers' stages from generation to transmission to distribution and the utilization levels in its connectivity. Based on a particular renewable technology, this varies [31]. Some RERs could be stand-alone, grid-connected, or hybrid, which combines both stand-alone and grid-connected. In comparison to non-renewable energies, the connectivity for renewable energy technologies is quite challenging.
- **Sustainability:** This is one of the strong positives of renewable energy. In comparison to non-renewable energies, it's readily available to be harnessed. Since most RER are gotten from nature like the wind, sun, water, it's always bound to exist, and others RER like bio-mass will exist due to human waste.
- **Cost:** The amount necessary to have RE technologies is said to cost less than the amount used in electricity production. Most massive amounts go into research on

renewable technologies and how to utilize these sources rather than how they are set up effectively.

- **Environmental impact:** Renewable energy is considered green power due to its friendliness to the environment. Most RERs have a significantly low carbon emission rate and insignificant waste. In regards to areas of scenery, wildlife, and land utilization, it has a negative impact. Most facilities/instruments for RERs are huge, land-consuming, and disquieting to the area.
- **Security and regulations:** An essential concern to RERs is how safe the facilities, devices, and instruments used in the operations are? From the production to transmission to distribution and then utilization, companies try to fight off vandalisms, wastage and enforce rigid standards on how the procedure should be.

A summary of some of the advantages of renewable energy [32] could be the following:

- The abundance of these sources used in renewable energy technologies.
- RE sources are considered environmentally friendly and green due to low carbon emissions.
- The research and development in this field provide thousands of jobs and employment opportunities to the society, thereby helping the economy of its subsequent country.
- Like in non-renewable sources where some resources are gotten from other countries and either imported or exported, all renewable sources are present everywhere in all countries as it is abundant in nature.
- Renewable sources cost less than the current price of electricity. Crude oil is projected to increase its price in the coming years.
- Various tax incentives in the form of credit deductions, tax waivers are available for businesses and individuals who use renewable resources.

4.2 Energy Storage

RERs such as solar and wind are not available throughout the year, i.e., seasonal. So, it is of utmost importance to store the maximum amount of energy possible with minimum losses. The SG requires energy storage directly or indirectly. In the present scenario, the pumped hydroelectric storage technology is considered bulk energy storage technology. Proper storage units connected with OFF-grid systems are further connected to the utility to form a hybrid system, improve robustness, and prevent intermittent outages. Older storage units include batteries, flywheels, and compressed air systems. Nowadays, a hydrogen network is connected in parallel to the grid utility as a storage unit. Storage devices, including batteries, supercapacitors, and flywheels, could be used to match generation with demand in SGs [33]. The storage systems can supply generation deficiencies, reduce load surges by providing a ride-through capability for short periods, reduce network losses, and improve the

protection system by contributing to fault currents. V2G and EV mobility can reduce the SG reliance on the grid supply.

5 Big Data, Machine Learning, and Blockchain Technology in Smart Grids

5.1 Big Data

Data identification and collection, data storage and data filtering, data classification and extraction, data cleaning and data summarization, data analysis and processing, and data visualization are the various life cycle of big data analysis. Apache Spark, Apache Hadoop, Apache Storm, Apache Flink, Apache Kafka, and Apache Samza are the big data processing tools that are being developed. But the main challenge faced during the data collecting is a time delay in receiving data [34]. This problem is resolved by using 5G technologies, which can reduce the time delay problem. Big data applications in power and energy systems include transient power prediction, distribution and utility systems, SG applications, fault detection and prevention, weather data and wind speed prediction, etc. Table 2 presents the applications of big

Table 2 Applications of big data in various industries

Industries	Applications of big data
Power and energy	Distribution systems, generation systems, utility systems, SG applications
Health care and life sciences	Clinical trials data analysis, disease pattern analysis, chain management, drug discovery and development analysis, patient care quality, and program analysis
Telecommunications	Customer churn prevention, call detail record analysis, mobile user location analysis, network performance and optimization, revenue assurance, and price optimization
Web and digital media	Large scale clickstream analytics, abuse, click-fraud prevention, social graph analysis and profile segmentation, campaign management, and loyalty programs
Retail/consumers	Supply chain management and analytics, market and consumer segmentation, event and behaviour-based targeting, merchandising, and market-based analysis
Finance and fraud services	Compliance and regulatory reporting, risk analysis and management, fraud detection and security analytics, credit risk, scoring, and analysis
E-commerce and customer service	Cross-channel analytics, event analytics, right offer at the right time, next best option, or following best action

Table 3 Challenges, state of the art, current status, and recent developments in big data

Challenges	State of the art, current status, and recent developments
<ul style="list-style-type: none"> • Privacy • Data miming • Integration of data • Cybersecurity • Demand prediction through analytics processing in SG applications • Data quality and cost balance • Industrial fault diagnosis using big data • Quantum cryptography for data security in smart grids 	<ul style="list-style-type: none"> • Big data technique to handle a large amount of information in a short time using meter data management • Big data requirements and enhancements throughout the entire power network dispatching and planning • Fault diagnosis on bogies of the high-speed train with big databases on deep neural networks • Schedulable capacity forecasting technique for thermostatically controlled load by big data analysis • Concept of device electrocardiogram in fault diagnosis using big data • Tensor-based big data management scheme in SG systems • The artificial neural network approach is used for efficient electricity generation forecasting

data in various industries [35, 36]. Multiple challenges, state of the art, current status, and recent developments in big data are presented in Table 3.

5.2 Machine Learning (ML)

A myth is that artificial intelligence (AI) is only one application that is robotics. Still, AI has much application such as medical sector, education sector, agriculture sector, pharmacy sector, research sector, energy sector, transport sector, etc. AI makes it possible for the machine to work as a human, learn like a human, and resemble the behaviour of humans. AI can be divided into artificial general intelligence (AGI) and artificial narrow intelligence (ANI). ANI is a type of AI in which a machine would perform only some specific task. AGI is a type of AI in which machines perform any given task that humans can perform or many more. In the future, all the sectors are upgraded with AI. Various AI applications in the SG are power load forecasting, power generation forecast of renewable energy, fault diagnosis, and protection of flexible equipment, electricity consumption behaviour, network security protection, and energy supply. Machine learning can be classified into two groups one is based on the learning model, and another one is based on learning methods. The learning model can be classified into supervised learning, unsupervised learning, and reinforcement learning [37, 38]. The learning model can be classified into Deep learning

and traditional machine learning. The various application of ML is electrical power and energy, transportation, education, healthcare, financial services, and marketing and sales.

5.3 Blockchain Technology

Blockchain technology can overcome all the difficulties faced by power utility sectors, and it will effectively help in the futuristic vision of economic herald in the energy distribution sector. The distributed ledger can start experimenting on blockchain to adopt new business strategies and goals. There are many applications of blockchain. One of those is electrical energy distribution. By using blockchain, one can effectively convert electrical energy into electronic money for transaction purposes, and it can be converted to any form. Blockchain provides a crystal clear, secure, and transparent form of transaction. Some of the technical challenges for applying blockchain technology in electricity trading, checking, and certifications. It gives a comprehensive view of the implementation of smart contracts under varied blockchain technologies in power systems. At the same time, implementing this technology [39]. The most important two items that must be handled with utmost care in blockchain application are the time frame and data privacy in power systems applications.

In recent time there is a massive demand for energy, primarily electrical energy. We are surrounded by innumerable electrical equipment. So, it becomes an integral part of the generating stations to fulfil this electricity demand and supply of electricity stably. Prosumers are the producers of electricity, and consumers, on the other hand, consume electricity. With the help of SG, one can fulfil the objective of consumers and keep an eye on the transmission losses, which can be minimized to a large extent. The transaction can be done in a peer-to-peer fashion among the prosumer and the consumer. To have this type of transaction, blockchain comes into the role to initiate a centralized transaction system which would be very costly in other means [40]. By using blockchain, one can solve complex problems that may arise in a SG.

With the help of blockchain technology, the trade of electricity became easier without any intervention from a third party. A trust is created between the prosumer and consumer. It has few advantages as we have real-time market records, less transaction cost because of simple structure, more privacy within the grid. In a centralized structure of energy systems where there is a large-scale implementation of industrial and commercial loads and environmental hazards, the power generation center has been located from the load centres at a far distance. High voltage (HV) transmission with distribution is used to transfer the power generated from the source to the load centres [41]. Currently, three technological trends provide a new dimension of the transformation in energy fields:

Table 4 Advantages and disadvantages of centralized and distributed systems

System	Advantages	Disadvantages
Centralized system	This system is rapid, and it can make effective decisions. No duplicity in any transactions. This system has an efficient bureaucratic chronology	In this system, the central government controls and handles all power and authority. Applications run on a single process. The component constitutes a single failure point
Distributed system	There are multiple processes for cooperating and executing the application processes Workloads can be distributed to different machines in this system The limit to tolerate faults is relatively high All data can be shared in different networks, but all the decision-making processes will only be held at one particular node	There may be privacy issues Complexity is more with very little predictability They require a lot of effort to managing all the systems operating Synchronization problems may arise

- The energy sector is more and more interested in shifting away from the direct energy consumption of non-renewable energy sources commercially toward the integration of different sources or hybrid grids.
- The increasing use of RERs and grids facilitates the decentralization of the energy field and increases the versatility in real-time operation in the power-system applications.
- Large parts of the energy value chain are digitalized due to the increased digital elements in a grid.

Blockchain technology works on a decentralized system having a peer-to-peer network, which signifies a collective model of trust among the peers who are unknown to each other and an immutable ledger of records of transactions (distributed). Decentralization means a user-to-user basis network. A Distributed immutable ledger means data that is stored in it cannot be further modified or deleted. Transactions in blockchain are just the transfer of values in Bitcoin. UTXO, an unspent transaction output, defines input and output in the transaction of bitcoin.

Once a block is verified algorithmically, and when a data miner agrees to it, it is added to the blockchain chain. An unspent transaction output (UTXO) can be spent as a currency unit in further transactions. The main operation in a blockchain is validation and block creation of transactions with the consensus of the users participating in the transaction. There are also many underlying operations. A smart contract gives the capability for code execution in business logic on a Blockchain. Miner nodes in the network receive, verify, gather and execute the transaction. Significant innovations like smart contracts have broadened the applications of blockchain technologies. Private and permitted blockchains to allow for access to the blockchain in

a controlled manner, enabling much more diverse business models. Table 4 presents the advantages and disadvantages of centralized and distributed systems.

Blockchain technology has a significant impact on utility industries. It has three levels of technologies benefitting both permissioned and private ledgers [42]. These levels are classified based on different technology attributes for the adaptability of the leading utility.

5.3.1 Level 1: Foundational Technology

Foundational technology consists of bill pay, electric vehicle charging transactions etc. It enhances the reliability and security of transactions inside the grid framework. The transaction is unified from disrupting generating stations in the energy ecosystem. Some common application include

- **Bill pays:** there are a lot of startup companies that are facilitating effective methodology for transactions. Such as prepaid energy meter, transaction through cryptocurrency, bitcoins, etc.
- **Solar renewable energy certificates:** Blockchain technology is used in trading and earning credit certificates related to renewable energy. One example is the solar coin that can be made for the generation of solar energy individually.
- **EV charging:** In the US, most people use an EV and blockchain-based transaction is there to charge EVs in certain charging stations. Some of the companies which are using blockchain are bloch charge, innogy. This technology enables the user for digital payments
- **Customer switching:** There is a UK-based company known as electron. It is a blockchain-based company. It enables the user for faster switching of suppliers.

Because of blockchain security and tracking of transactions, this application is quite fruitful without intermediaries.

5.3.2 Level 2: Medium for Sustaining Business

Utility technology should adopt blockchain as well as internal business units to sustain the investment made in technology. There should be some regulatory board to keep an eye on all the transactions [43]. Appropriate support model to ensure guard of interest of utility business. Some examples of experimental permissioned blockchain applications with relevance for the utility sector are:

- **Microgrids:** specific distributed energy systems such as microgrids function independently. Distributed energy systems like microgrids mainly operate independently from a centralized system due to the small size of the operation. Blockchain is much more relevant for managing all transactions.

Table 5 Current market shortcomings and the possible role for blockchain

Current market shortcoming	Possible role for blockchain
The cost of production is much more than electric markets	The combination of the Internet of things, records and information about generation time/demand, location, type of generation/demand, and other aspects of predicting the price for electric market customers
Integration renewable energy sources integration into the electric grid	Blockchain can be used for de-centralized and automatic grid management and control systems. As there are many producers and consumers in the distribution grid, blockchain technology balances the supply of electricity and demand for auto verification of grid components
Adequate power resource	Cryptocurrencies can be used as a token for creating new markets and business models. There will co-ownership for such models
Increase in coordination in-between operators of system	Blockchain can give promising results in developing an automated decentralized and completely efficient asset control and management of such assets, including a better balance between demand and supply at different networks
Integrating demand response for ancillary services	Smart contracts are designed to engage and reward willing customers for helping in DR activity for maintaining the grid more economically
Much adequate cross-border data exchange in power system	Cross-border data exchange incurs costs and data flows through multiple intermediates, which add time delays in decision making and thus a potential loss of data. Blockchains can streamline this process by removing intermediaries, removing delays, and maintaining data integrity as data is not transferred but immutably shared

- Grid settlements and wholesale market trading: independent power producers integrate a small number of people in a microgrid grid settlement, and wholesale markets involve many users within industry regulations, so blockchain does provide scalability and regulatory compliance to all those units. Table 5 presents the current market shortcomings and the possible role of blockchain.

6 Electric Vehicles (EVs)

This section focuses on EVs, which are trending in the latest era for meeting the energy needs replacing the internal combustion engine (ICE) vehicles. In recent years, EV's have much attention as compared to conventional internal combustion engine vehicles. This contemplation is due to the economic and environmental trouble

concerns linked with the utilization of natural gas and petroleum fuels. These are used as fuel in ICE vehicles. More advancement and researches on vehicles like fuel cell and hybrid cars, pure battery-powered electric vehicles, etc., are pursued actively [44]. Because these vehicles are reasoned to serve as an efficient means to deal with global warming caused by the tail pipe-auto emissions. In eco vehicles, the compatibility between safety and running performance has to be ensured, especially in EVs where electric devices like batteries, converters, and inverters are part of their propulsion force-producing system. If such an electric device fails during the motion of the EV, the EVs shall fail to run safely and comfortably. This kind of failure in motion may constitute series of traffic accidents like rear-end collisions. As an advancement for developing the next generation of EVs, fail-safe functions must be interlinked within the propulsion force-generating system. The EV can persist in running safely even if malfunctions occur during EV motion. The hybrid electric vehicles (HEV), which mainly contains at a minimum of two sources of power, first one is a primary power source, and the other one is named as a secondary power source, which has the favours of both the EV and conventional ICE vehicles also could vanquish their disadvantages. Considering the HEVs and PHEVs, more electrical components are utilized in the making. Electric machines, power electronic converters, batteries, ultra-capacitors, sensors, and microcontrollers are examples of various such features. Besides these electrification components and their subsystems, the traditional internal combustion engine or other mechanical and hydraulic systems have also been present. Those difficulties generated due to the modern propulsion systems demand the advanced design of powertrain components, namely power electronic converters, energy storage, and other electric machines. This power management system includes modelling, simulation of the powertrain, hybrid control theory and optimization control of vehicle [45].

Characteristics of EVs:

- The EV's are designed to steer with high voltage electrical energy stored batteries. In this way, the exhaust emissions can be excluded, which further reduces air pollution since gasoline or other fossil fuels are not required for the propulsion.
- The engine's noises and vibrations are negligibly small during the entire driving range compared to traditional ICEs. The electric motor employed in EVs is generally higher performance motors.
- During the downhill or decelerating motion of the said vehicle, the restoring of brake energy by regeneration can be employed and stored in the high voltage batteries. Thereby the driving range from single charging will be extended and also reduce the loss during braking.
- If the battery's existing charge is not adequate to drive the vehicle, various charging methods like AC or DC charge are applicable. The trickle charge can also be applied.

6.1 Battery Electric Vehicles (BEVs)

A battery electric vehicle (BEV) runs entirely on a battery and electric drive train without an internal combustion engine. To recharge their batteries, these vehicles must be plugged into an external electricity source. A hybrid electric vehicle (HEV) with an internal combustion engine and an electric motor together with an engine or generator depends on one or more energy sources [46]. A plug-in hybrid electric vehicle (PHEV) uses rechargeable batteries or other power storage systems that can be recharged by connecting them to external electricity sources.

Instead of an ICE vehicles, EVs have an electrical motor. The electric battery vehicle uses a large traction battery pack to power the electric motor and, since it operates on electricity, it must be plugged into the charging station. The vehicle emits no exhaust from the tailpipe and does not contain the fuel components such as fuel pump, fuel line, and fuel tank. The battery pack used to store the electrical energy that drives the motor is used in the car. By plugging the vehicle into an electric power source, batteries are charged. BEVs are more costly than conventional hybrid vehicles.

The battery stores the energy necessary for the vehicle to operate. The battery supplies the motor with an electric current. And the engine, thus, drives the greater the battery size, the greater the range of the vehicle. Lithium-ion type batteries are the most widely used batteries. The higher energy density of these batteries is capable of storing more energy [47]. Using an inverter, the battery energy in the DC is converted to AC. The AC is transmitted to the induction motor from the inverter, which generates a spinning magnetic field that allows the motor to turn.

The single-speed transmission transfers power to the wheels from the induction motor. This electric motor converts electrical energy into mechanical energy that turns the wheels to move forward. The car uses more energy during the acceleration, but the energy transforms through the induction motor into electricity during the stop. This power is stored in the battery pack and can be used when more energy is required. An electric vehicle battery can be charged by plugging it into an outlet or charging station. Advantages of BEV are less air pollution, less noise pollution, higher efficiency, low fuel and operating cost, and low maintenance cost. The disadvantages of BEVs include are high prices and low range.

6.2 Hybrid Electric Vehicles (HEVs)

The phrase *hybrid vehicle* makes reference to a vehicle with the least of two power sources. Among the two sources of power for HEV, an electric motor acts as one energy source. In contrast, the other source of motive power can be extracted within several divergent technologies. But the most used secondary source of power will be an ICE destined to run either on gasoline or petroleum fuel [48]. As put forward by the technical committee of the international electrotechnical commission (electric

road vehicles), an HEV is a vehicle in which propulsion energy is available from two or more types of energy sources, and at least one of them can deliver electrical energy. Predicted on the definition by the commission, various kind of energy combinations of HEVs are:

- The battery and gasoline IC engine combo
- Battery and ICE with diesel
- Fuel cell and battery combo
- Battery with ultra-capacitor
- Battery along with flywheel combo
- Hybrid battery and other batteries

Incorporating an ICE with an electric motor is the most widely used combo for the generation of propulsion force in hybrid EVs. With this integration, energy efficiency will be improved and vehicle emissions will be fall off due to the electric motor. The driving range will be extended because of the ICE in contemplation of advancements in the HEV. The stereotypical ICE vehicles bestow good performances and an extensive operating range because of the high energy density yielded by the petroleum products. But these standard ICE vehicles have the disbenefit of indigent fuel economy and more significant risks of environmental contamination [49]. By far, the reasons behind their indigent fuel economy are:

- The contrast between real operation requirements and the vehicles fuel expertise
- Operating in urban areas, the wastage of kinetic energy during braking
- Due to the stop-and-go driving pattern, the productivity of hydraulic transmission in current day automobiles.

The EVs powered by battery packs have dominance over typical ICE vehicles by high energy productivity and almost zero environmental contamination. The comparison of these vehicles based on the performance of their driving range per battery charge ICEs holds the upper hand. However, HEVs can outsmart both traditional ICEs and EVs due to the use of two power sources.

An ICE and an electric motor that utilizes energy stored in the battery are powered by HEVs. Instead of charging the batteries by regenerative braking and an ICE, a hybrid car cannot be plugged in to charge the battery. A smaller engine could theoretically allow for the extra power provided by the electric motor. When stopped, the battery can also control auxiliary loads such as sound systems and headlights and decrease engine idling. Together, these characteristics result in increased fuel economy. During coasting or braking, the regenerative braking mechanism restores energy normally lost. It uses the wheels' forward motion to spin the engine. This provides energy which makes the vehicle slow down.

6.3 *Plug-In Hybrid Electric Vehicles (PHEVs)*

A battery and an electric motor are available for PHEVs. They also have an ICE and a fuel tank. The PHEV works with electricity until the battery is almost empty. In the engine, the fuel is then burned to create extra electricity for the electric motor or power the wheels. With plug-in supplies and a regenerative braking system, the PHEV batteries can be recharged.

As proposed in the name itself, it's also a shade of hybrid electric vehicle (HEVs). Also named as electric vehicles with an extended running range that utilizes battery packs to deliver energy to an electric motors and an alternate source of energy like fuel or gasoline to satisfy the energy demands of ICE employed. i.e., similar to HEVs, PHEVs also make use of both the electrical and mechanical power path with the help of conventional ICE and general electric machines. The batteries could be charged alongside plugging through an electric power source or regenerative braking with the ICE. The PHEV may have larger battery packs than common HEVs [50]. The PHEVs gain almost all their power while running through urban areas with the already stored electricity in the battery packs. Before even beginning, one must ensure the battery is sufficiently charged. In case of distress or complete depletion of batteries, ICEs may power the vehicle during situations where sudden acceleration, at high speeds, or when rigorous heating or air conditioning is needed. The dissimilarities of PHEVs and HEVs depend on the capacity of the battery and their recharging techniques. PHEV's are furnished with larger capacities of batteries that can operate only with battery power within a reasonable driving range, also called an all-electric driving range.

The utilization of fuel/gasoline in PHEVs depends upon the total distance travelled within the complete discharging period. The tailpipe emissions of a PHEV are zero if it's driven only with battery power. Even if it's operating with an ICE alone, gasoline consumption will be practically lesser and produce lower emissions than similar conventional vehicles do. Comparing with the traditional ICEs that blindly rely on fossil fuels, PHEVs offer consumers to choose between alternate cheap and clean energy, thereby diminishing the dependence on a single source of energy.

Two fuel sources, an electric motor and a combustion engine, drive PHEVs. PHEVs use less fuel and emit fewer emissions than traditional ICE vehicles powered only by combustion engines. In contrast to HEVs, PHEV uses a high-capacity battery for energy storage. The greater battery capacity allows the vehicle to cover longer electric-mode driving distances than hybrid vehicles. The electric motor alone or the combustion engine powers the car, depending on the driving conditions [51]. The high voltage battery either absorbs energy or emits it. The high voltage battery releases energy while the electric motor is running, via regenerative braking, the battery is partially charged by kinetic energy while driving. You should plug the vehicle in to recharge your high-voltage battery. Charging can be done at any location with domestic electricity installed. From the public charging stations, they can also charge. The car must be parked with the ignition switched off before being

charged. The charging indicator illuminates until the vehicle is fully charged when the charging cable is attached.

The vehicle functions in two modes to encapsulate it. The first mode is called the charge depleting mode, in which only the electric motor powers the vehicle before the high voltage battery reaches a low energy level [52]. When the battery level is low, the mode of the vehicle switches to the hybrid mode's charge sustaining mode. It's the second mode of driving. The vehicle uses power from the electric motor to drive in hybrid mode during mild acceleration, providing enough pickup to help increase speed. The gasoline engine and the electric motor are used to get the desired speed when the acceleration is higher or uphill motion. The machine goes to power assist mode while cruising at a relatively steady rpm, where the gasoline engine is the primary source of drive power [53]. The device captures energy through a regenerative braking system as the vehicle's speed decreases and stores it in the battery for future use. As mentioned above, external charging is often used to optimize high voltage levels. Table 6 presents different types of EVs and their characteristics.

7 Protection of Smart Grid

A grid would be more efficient when more resiliency is added into the existing electric network and made ready for diffident unavoidable tragedies and natural calamities. Therefore, if some extra powerful features are supplemented to the existing grid, it becomes a SG. The extra powerful features can be advanced protection schemes in grid operation. This will make the existing grid network more efficient, faster in power transmission and self-repair after power disturbances, inexpensive, improved security etc.

Protection in SG refers to the protection of devices connected to the SG against unintentional failures like fault, overload etc. One of the power system protection applications in the SG is quick to fault diagnosis to prevent fluctuations in voltage and power outages. When some schemes protect the physical infrastructures of SG, it is referred to as physical protection of SG. This type of protection refers to inadvertent situations because of equipment failure, errors created by human's, natural disasters etc. In this type of protection, two essential things have to be looked into. One is the reliability of the system and the other one is protection scheme failure. Reliability refers to SG's component's reliability and the way they are placed and they are achieved in four various ways:

- Reliability of distributed generation
- Reliability of measurement infrastructure
- Reliability of network before action
- Decision-making performance by sub-station

RERs are used as DG in a SG whose penetration into the system makes coordination between them with other protection devices quite challenging. As a result reliability and stability of the system becomes a concern for the protection engineer.

Table 6 Different types of electric vehicles (EVs) and their characteristics

Type of electric vehicle	Battery electric vehicle	Hybrid electric vehicle	Plug-in hybrid electric vehicle	Fuel cell hybrid electric vehicle
Propulsion	Electric motor	International combustion engine (ICE) and electric motor	International combustion engine (ICE) and electric motor	Electric motor
Energy system	Battery	ICE unit and battery	ICE unit and battery	Fuel cell along with battery and ultra-capacitor to enhance power density
Energy source	Electric grid charging	Gasoline station	Electric grid charging and gasoline station	Hydrogen, Hydrogen production, transportation, and infrastructure
Characteristics	Zero-emission, high energy efficiency, and high initial cost, readily available	Low emission, high fuel economy, long-range of driving, high cost, commercially available	Low emission, large battery capacity, long driving range in road trips, and high cost	Zero-emission or ultra-low emission, high energy efficiency, high cost, less dependent on fossil fuels
Challenges and issues	Battery management, high cost of charging facilities	Control of multiple energy sources, battery management	Control of multiple sources, maintenance cost	High fuel cell cost, fuel cell durability, and reliability, Hydrogen infrastructure

One SG operation requirement is the smart measurement infrastructure, which helps monitor network reliability, stability, and healthiness, which can be met with a phasor measurement unit (PMU). Suppose the decision making performance by sub-station can be achieved. In that case, the time span can be reduced as it does not have to wait for the control network’s decision and the system achieves better stability and reliability. Failure prevention and prediction are two important aspects of SG physical protection. Prediction means identifying the failure event in the SG, and prevention means to inhibit the failure from an occurrence. Recovery is another important aspect of the SG that can be achieved by developing efficient techniques. For example, a smart meter is used to recover missing data from the system. Because of the inverter-based DGs into the SG, the operating characteristics differ from standard distribution systems, making the protection engineer challenging. Another challenge

before power system engineer's is to attain reliability and efficiency in a wired and wireless communication network for control and data transfer purpose. For proper unit protection and to optimize the relay coordination in SG, internet of energy (IoE) based communication technology is recently used, which mainly exchanges information that is further collected by integrated electronic devices (IED). This type of protection scheme is called i-protection, which precisely identifies the fault with the help of IEDs and IoE through a wide-area wireless network.

8 Conclusion

Smart grid (SG) has been the most impactful technology in recent times and is still rising because of its significant benefits. But like any other more substantial change, transition to the SG system from a conventional power grid system is highly tedious and time-consuming. At the same time, it is a great decision to meet the growing electricity demand of modern civilization. The successful transition requires meticulous preparation, thorough understanding, and proper knowledge, along with their corresponding impacts on every part of the ecosystem. The distributed energy resource (DER) applications would increase the efficiency of the energy supply and reduce the electricity delivery cost and carbon footprint in the SG. The SG needs to be well-designed, robust structure to withstand the tension, efficient and reliable, sustainable with the environment, intelligent enough to discover outages and fault locations, secured and safe from cyber-attacks, able to monitor real-time data and act upon it, scalable and integrable with other sources of energy. Various features of the SG need to be implemented cost-effectively to form a symbiotic relationship and benefit grid operators, energy providers, consumers, and the environment. There are many challenging issues of protection in SGs like maintaining reliability, stability, coordination etc. All these can be solved by developing optimized algorithms, which is also ongoing research.

Acknowledgements This research work was funded by “Woosong University’s Academic Research Funding—(2021–2022)”.

References

1. Fan D, Ren Y, Feng Q, Liu Y, Wang Z, Lin J (2021) Restoration of smart grids: current status, challenges, and opportunities. *Renew Sustain Energy Rev* 143. <https://doi.org/10.1016/j.rser.2021.110909>
2. Patil H, Sharma S, Raja L (2020) Study of blockchain based smart grid for energy optimization. *Mater Today Proc* 2020. <https://doi.org/10.1016/j.matpr.2020.11.013>
3. Feng C, Wang Y, Chen Q, Ding Y, Strbac G, Kang C (2021) Smart grid encounters edge computing: opportunities and applications. *Adv Appl Energy* 1. <https://doi.org/10.1016/j.adaen.2020.100006>

4. Neffati OS, Sengan S, Thangavelu KD, Kumar SD, Setiawan R, Elangovan M, Mani D, Velayutham P (2021) Migrating from traditional grid to smart grid in smart cities promoted in developing country. *Sustain Energy Technol Assess* 45. <https://doi.org/10.1016/j.seta.2021.101125>
5. Alotaibi I, Abido MA, Khalid M, Savkin AV (2020) A comprehensive review of recent advances in smart grids: a sustainable future with renewable energy resources. *Energies* 13. <https://doi.org/10.3390/en13236269>
6. Zhou J, He L, Li C, Cao Y, Liu X, Geng Y (2013) What's the difference between traditional power grid and smart grid?—from dispatching perspective. In: *IEEE PES Asia-Pacific power and energy engineering conference (APPEEC)*, Hong Kong, China, pp 1–6. <https://doi.org/10.1109/APPEEC.2013.6837107>
7. Butt OM, Zulqarnain M, Butt TM (2021) Recent advancement in smart grid technology: future prospects in the electrical power network. *Ain Shams Eng J* 12(1):687–695. <https://doi.org/10.1016/j.asej.2020.05.004>
8. Moulema P, Mallapuram S, Yu W, Griffith D, Golmie N (2017) Chapter 24—Integrating renewable energy resources in smart grid toward energy-based cyber-physical systems. In: *Cyber-physical systems - foundations, principles and applications, intelligent data-centric systems* 377–398. <https://doi.org/10.3390/en14092657>
9. Du P, Lu N, Zhong H (2019) *Demand response in smart grids*. Energy Renew Green Energy. Springer. ISBN: 978-3-030-19769-8
10. Gelazanskas L, Gamage KAA (2014) Demand side management in smart grid: a review and proposals for future direction. *Sustain Cities Soc* 11:22–30. <https://doi.org/10.1016/j.scs.2013.11.001>
11. Ekanayake JB, Jenkins N, Liyanage K, Wu J, Yokoyama A (2012) *Smart grid: technology and applications*. Wiley. ISBN: 978-1-119-96909-9
12. GWEC: Global wind report 2016, annual market update, Technical Report, Global Wind Energy Council (GWEC)
13. PVPS Annual report 2016, Technical Report, Photovoltaic Power Systems Technology Collaboration Programme
14. IEA: Technology roadmap, wind energy, Technical Report, Energy Technology Perspectives, 2013 edition, International Energy Agency
15. IEA-PVPS: Technology roadmap, solar photovoltaic energy, Technical Report, Energy Technology Perspectives, 2014 edition, International Energy Agency
16. Moura PS, Lopez GL, Moreno JI, Almeida ATD (2013) The role of smart grids to foster energy efficiency. *Energy Efficiency* 6:621–639. <https://doi.org/10.1007/s12053-013-9205-y>
17. Acakpovi A, Abubakar R, Asabere NY, Majeed IB (2019) Barriers and prospects of smart grid adoption in Ghana. *Proc Manuf* 35:1240–1249. <https://doi.org/10.1016/j.promfg.2019.06.082>
18. Matisoff DC, Beppler R, Chan G, Carley S (2020) A review of barriers in implementing dynamic electricity pricing to achieve cost-causality. *Environ Res Lett* 15(9). <https://doi.org/10.1088/1748-9326/ab9a69>
19. Mikalauskas I (2015) Economic, social and environmental benefits of smart grids. *Eur J Interdisc Stud* 7(2):30–39
20. Smart Grid Economic and Environmental Benefits (2013) A review and synthesis of research on smart grid benefits and costs. Technical Report, Smart Grid Consumer Collaborative
21. El-hawary ME (2014) The smart grid—state-of-the-art and future trends. *Electr Power Compon Syst* 42(3–4):239–250
22. Kezunovic M, McCalley JD, Overbye TJ (2012) Smart grids and beyond: achieving the full potential of electricity systems. *Proc IEEE* 100:1329–1341. <https://doi.org/10.1109/JPROC.2012.2187131>
23. Kappagantu R, Daniel SA (2018) Challenges and issues of smart grid implementation: a case of Indian scenario. *J Electr Syst Inf Technol* 5(3):453–467. <https://doi.org/10.1016/j.jesit.2018.01.002>
24. Dileep G (2020) A survey on smart grid technologies and applications. *Renew Energy* 146:2589–2625. <https://doi.org/10.1016/j.renene.2019.08.092>

25. Rohde F, Hielscher S (2021) Smart grids and institutional change: emerging contestations between organisations over smart energy transitions. *Energy Res Soc Sci* 74. <https://doi.org/10.1016/j.erss.2021.101974>
26. Lalle Y, Fourati M, Fourati LC, Barraca JP (2021) Communication technologies for smart water grid applications: overview, opportunities, and research directions. *Comput Netw* 190. <https://doi.org/10.1016/j.comnet.2021.107940>
27. Yu K, Arifuzzaman M, Wen Z, Zhang D, Sato T (2015) A key management scheme for secure communications of information centric advanced metering infrastructure in smart grid. *IEEE Trans Instrum Measure* 64(8):2072–2085. <https://doi.org/10.1109/TIM.2015.2444238>
28. Ghosal A, Conti M (2019) Key management systems for smart grid advanced metering infrastructure: a survey. *IEEE Commun Surv Tutor* 21(3):2831–2848. <https://doi.org/10.1109/COMST.2019.2907650>
29. Iris Ç, Lam JSL (2021) Optimal energy management and operations planning in seaports with smart grid while harnessing renewable energy under uncertainty. *Omega*. <https://doi.org/10.1016/j.omega.2021.102445>
30. Shi Y, Tuan HD, Savkin AV, Lin CT, Zhu JG, Poor HV (2021) Distributed model predictive control for joint coordination of demand response and optimal power flow with renewables in smart grid. *Appl Energy* 290. <https://doi.org/10.1016/j.apenergy.2021.116701>
31. Alarifi A, AlZubi AA, Alfarraj O, Alwadain A (2021) Automated control scheduling to improve the operative performance of smart renewable energy systems. *Sustain Energy Technol Assess* 45. <https://doi.org/10.1016/j.seta.2021.101036>
32. Carpejani P, de Jesus ET, Catapan BLSB, Gouvea da Costa SE, Pinheiro de Lima E, Tortato U, Machado CG, Richter BK (2020) Affordable and clean energy: a study on the advantages and disadvantages of the main modalities. In: Leal Filho W, Borges de Brito P, Frankeberger F (eds) *International business, trade and institutional sustainability*. World sustainability series. Springer, Cham. https://doi.org/10.1007/978-3-030-26759-9_35
33. Salkuti SR (2020) Energy storage technologies for smart grid: a comprehensive review. *Majlesi J Electr Eng* 14(1):39–48
34. Tu C, He X, Shuai Z, Jiang F (2017) Big data issues in smart grid—a review. *Renew Sustain Energy Rev* 79:1099–1107. <https://doi.org/10.1016/j.rser.2017.05.134>
35. Munshi AA, Mohamed YARI (2017) Big data framework for analytics in smart grids. *Electr Power Syst Res* 151:369–380. <https://doi.org/10.1016/j.epr.2017.06.006>
36. Lai CS, Lai LL (2015) Application of big data in smart grid. In: *IEEE international conference on systems, man, and cybernetics*, Hong Kong, China, pp 665–670. <https://doi.org/10.1109/SMC.2015.126>
37. Hossain E, Khan I, Un-Noor F, Sikander SS, Sunny MSH (2019) Application of big data and machine learning in smart grid, and associated security concerns: a review. *IEEE Access* 7:13960–13988. <https://doi.org/10.1109/ACCESS.2019.2894819>
38. Günel K, Ekti AR (2019) Exploiting machine learning applications for smart grids. In: *16th international multi-conference on systems, signals and devices (SSD)*, Istanbul, Turkey, pp 679–685. <https://doi.org/10.1109/SSD.2019.8893252>
39. Musleh AS, Yao G, Muyeen SM (2019) Blockchain applications in smart grid-review and frameworks. *IEEE Access* 7:86746–86757. <https://doi.org/10.1109/ACCESS.2019.2920682>
40. Agung AAG, Handayani R (2020) Blockchain for smart grid. *J King Saud Univ Comput Inf Sci*. <https://doi.org/10.1016/j.jksuci.2020.01.002>
41. Dutta SD, Prasad R (2020) Digitalization of global cities and the smart grid. *Wireless Pers Commun* 113:1385–1395. <https://doi.org/10.1007/s11277-020-07478-w>
42. Hasankhani A, Hakimi SM, Niasar MB, Shafie-khah M, Asadolahi H (2021) Blockchain technology in the future smart grids: a comprehensive review and frameworks. *Int J Electr Power Energy Syst* 129. <https://doi.org/10.1016/j.ijepes.2021.106811>
43. Patil H, Sharma S, Raja L (2020) Study of blockchain based smart grid for energy optimization. *Mater Today Proc*. <https://doi.org/10.1016/j.matpr.2020.11.013>
44. El Bassam N (2021) Chapter Thirteen—Energy storage, smart grids, and electric vehicles. In: El Bassam N (ed) *Distributed renewable energies for off-grid communities*, 2nd edition. Elsevier, pp 263–295. <https://doi.org/10.1016/B978-0-12-821605-7.00008-8>

45. Pournaras E, Jung S, Yadhunathan S, Zhang H, Fang X (2019) Socio-technical smart grid optimization via decentralized charge control of electric vehicles. *Appl Soft Comput* 82. <https://doi.org/10.1016/j.asoc.2019.105573>
46. Brenna M, Foadelli F, Zaninelli D, Graditi G, Somma MD (2021) Chapter 10—The integration of electric vehicles in smart distribution grids with other distributed resources. In: Graditi G, Somma MD (eds) *Distributed energy resources in local integrated energy systems*, Elsevier, pp 315–345. <https://doi.org/10.1016/B978-0-12-823899-8.00006-6>
47. Ahmadian A, Sedghi M, Elkamel A, Fowler M, Golkar MA (2018) Plug-in electric vehicle batteries degradation modeling for smart grid studies: review, assessment and conceptual framework. *Renew Sustain Energy Rev* 81(2):2609–2624. <https://doi.org/10.1016/j.rser.2017.06.067>
48. Salehpour MJ, Tafreshi SMM (2020) Contract-based utilization of plug-in electric vehicle batteries for day-ahead optimal operation of a smart micro-grid. *J Energy Storage* 27. <https://doi.org/10.1016/j.est.2019.101157>
49. Hariiri AM, Hejazi MA, Dezaki HH (2021) Investigation of impacts of plug-in hybrid electric vehicles' stochastic characteristics modeling on smart grid reliability under different charging scenarios. *J Clean Prod* 287. <https://doi.org/10.1016/j.jclepro.2020.125500>
50. Kong P, Karagiannidis GK (2016) Charging schemes for plug-in hybrid electric vehicles in smart grid: a survey. *IEEE Access* 4:6846–6875. <https://doi.org/10.1109/ACCESS.2016.2614689>
51. Karthikeyan A, Vijayarajan S (2020) A comprehensive review on electric vehicles. *Int J Sci Technol Res* 9(2):2071–2079
52. Zheng Y, Niu S, Shang Y, Shao Z, Jian L (2019) Integrating plug-in electric vehicles into power grids: a comprehensive review on power interaction mode, scheduling methodology and mathematical foundation. *Renew Sustain Energy Rev* 112:424–439. <https://doi.org/10.1016/j.rser.2019.05.059>
53. Mwasilu F, Justo JJ, Kim EK, Do TD, Jung JW (2014) Electric vehicles and smart grid interaction: a review on vehicle to grid and renewable energy sources integration. *Renew Sustain Energy Rev* 34:501–516. <https://doi.org/10.1016/j.rser.2014.03.031>

Modeling of Various Renewable Energy Resources for Smart Electrical Power Systems



Surender Reddy Salkuti

Abstract This chapter presents the modeling of various renewable energy resources (RERs) such as solar photovoltaic (PV), wind, small hydro, pumped hydro, geothermal, biomass, and battery energy storage. RERs are an infinitely sustainable and environmentally friendlier form of energy that will help reduce the dependency on traditional fossil fuels-based electrical power generation. The abundance of wind and solar irradiation in nature makes wind and solar PV energy the resources with great potential if accuracy in planning and technology compiled together. Modeling of power output from different RERs and the uncertainty handling of solar PV and wind energy systems are described in this chapter. Battery storage systems provide energy to the system when the supply from RERs cannot meet the required load demand. Battery storage units are used to store the extra amount of power produced by the RERs. Small hydropower generators work at variable speeds as the water flows at various speeds. Geothermal thermal energy involves accessing underground hot water or steam from wells several miles into the earth. Sustainable biomass energy can be generated by burning several types of biomass fuels which are converted into several forms of energy after combustion. The modeling of all these resources along with their advantages and disadvantages are discussed in this chapter.

Keywords Battery storage · Biomass · Geothermal · Pumped hydro · Wind energy · Solar PV · Smart grid · Small hydro

1 Introduction

The fluctuating/intermittent nature of the renewable energy resources (RERs) is an important factor that limits their large-scale integration into the utility grid. The penetration of RERs has been increased as they can reduce the environmental impact and meet the increased power demand. All nations throughout the world are promoting

S. R. Salkuti (✉)

Department of Railroad and Electrical Engineering, Woosong University, Daejeon 34606, Republic of Korea

e-mail: surender@wsu.ac.kr

the construction of renewable power plants. The European Union (EU) and the USA have set targets of 100% and 80% of power generation by RERs by 2050. Recently several countries have set targets for the reduction of emissions of greenhouse gases by increasing the share of RERs. New installations of RERs have been dominated by wind and solar photovoltaic (PV) power plants. However, one needs to develop suitable models to characterize their intermittent and variable behavior to incorporate in the planning and operation of electrical power systems [1]. The amount of renewable power generation from the solar PV and wind energy systems purely depends on meteorological conditions such as solar irradiance, ambient temperature, and wind speed which are directly associated with the site/location. Therefore, the analysis of solar insolation and wind speed characteristics at a particular installed site plays a vital role in utilizing solar and wind energy systems efficiently. Presently, the share of hydro-power generation is almost 58% of the electricity generated by renewable sources throughout the world. To meet the ever-increasing load demand and for efficient power-sharing with the change in climate conditions and subsequent change in load an intelligent and robust control techniques are needed [2].

In recent days the power generation from RERs is increasing in a significant way and the power generated from renewable power sources is going to play a significant role shortly. To increase the integration of RERs in the conventional power network, it has to deliver the liabilities acted to the entire system as a consequence of the irregular nature of these RERs. Because of their effect on system adjusting, scheduling, reserves management, and commitment of generating units, changeability, and a ramp or slope events in the power output are the major difficulties to the system administrators [3, 4].

The European power system with ambitious de-carbonization with the efficient coupling of RERs to conventional energy systems has been presented reference [5]. Reference [6] proposes a combined energy system, i.e., an energy hub consisting of electrical, heating, and cooling equipment, demand response, and the optimization of RERs. The changes of optimization techniques brought by large-scale integration of RERs are presented in [7]. Reference [8] presents the importance of long-term uncertainty modeling approaches to evaluate various support policies of renewable and de-carbonization. A simulation model based on a systems dynamics methodology for representing the complex behavior of the national electricity market under different scenarios analysis has been presented in [9]. An approach of utilizing multi-type demand-side reserve offers to smooth fluctuations in RERs forecast on various time scales has been presented in [10]. An optimal energy management problem of microgrids with RERs and energy storage systems has been presented in reference [11].

The aim of this chapter is to presents the modeling of various renewable energy resources (RERs) such as solar, wind, small hydro, pumped hydro, geothermal, and biomass. The rest of this work is organized as follows: Sect. 2 describes the modeling of the wind energy system and its uncertainty handling approach. Modeling of output power from solar PV energy system and its uncertainty handling approach is described in Sect. 3. Section 4 presents the modeling of a battery energy storage system. Modeling of small hydro and pumped hydro energy systems is described in

Sect. 5. Sections 6 and 7 describe the modeling of geothermal energy and biomass energy. Section 8 summarizes the major contributions with concluding remarks.

2 Wind Energy System

Wind energy is the kinetic energy (KE) of the air in motion which is more economical, reliable, and the operation of a wind turbine (WT) is quite simple. As the wind blows through the blades of WT with the pressure exerted on the surface area of the blade. Aerodynamic forces cause the blade to turn the rotor. The generator and gearbox are kept together in a single unit behind the blades. The output of the generator is passed through for conversion from DC to AC. The WT converts the KE from the wind into mechanical energy. This energy could then be used to generate electricity. It is one of the renewable energies that were discovered to transform electric power by enhancing the sustainability, performance, and reliability of the smart grid [12]. After converting the wind into mechanical energy, that energy can be used to produce electricity is by using a wind generator. WTs are manufactures in the range of vertical and horizontal axis types and each type of wind turbine is used for a specific purpose. For example, large wind turbines are used in the production of commercial electric power whereas the smallest turbines are used to provide additional power on boat sailing or battery charging.

Wind energy is environmentally friendly and produced naturally as there is no need for burning fuels to generate wind power. Wind turbines don't require a lot of space because windmills cover only a few square meters and the rest of the land can be used for farming or agriculture purposes. However, the wind turbine can make a disturbing noise, for those who live a hundred meters from the wind power station [13]. Wind turbines can be used for standalone or hybrid power supply. A power regulator is usually used to regulate the power output between the turbines' output and the load. Transformers are used to step the voltages down or up depending on the use of voltages.

A WT has an expected average life of 20–25 years, which makes it a great source of alternate power. It is being recognized as a vital component of sustainable environmental and economic well-being, long-term, and security of energy supply and price. Although wind energy is reliable and inexpensive, it requires windmills to be built in areas where the wind is not only strong but also steady, which may be a disadvantage for some countries. Offshore may be the best place for wind power because winds are usually strong and steady over there. The height of the turbine is a huge factor in its power generation as the impact of a taller is considered to give higher winds in the WT also, and the surface winds can be affected easily by the roughness or irregularities of the earth surface [14]. Wind turbine also produces no emission, and their efficiency in its application area as green power is top-notch. The common issue with the turbine is its most suited application, i.e., for peak shaving applications and the power it produces is dependent on strong winds. The wind turbine is fairly inexpensive compare to the PV system.

The working of wind turbines depends on several factors such as the shape and size of the rotors, height of the blades, and location of the turbine. Advantages of the wind turbine technology include: environmentally friendly, low cost in its generation of energy, a big source of energy and large industrial base already exists, it could be scaled down to small turbines used in companies to power small institutions, offshore advantage allows the mounting of the huge turbine to produce a large amount of energy [15]. However, there are some disadvantages such as the intermittent nature of wind power, noise generated from the rotating blade and motor, loss of scenery, requirement of large amounts of land.

2.1 Modeling of Wind Turbines (WTs)

The WT is connected to an inductive/asynchronous machine that consumes the reactive power (Q) and generates the active power (P_m) [16]. This active power output is given by,

$$P_m = \frac{1}{2} \rho \pi r^2 v^3 C_p \quad (1)$$

where r is the radius of WT (in m), v is wind speed (in m/s), ρ is air density (kg/m^3), C_p is turbine power coefficient. Then the electrical power (P_e) is given by,

$$P_e = n_0 P_m \quad (2)$$

where $n_0 = n_m n_g$. n_g and n_m are efficiencies of generator and turbine, respectively.

2.2 Modeling of Wind Speed

The stochastic behavior of wind speed can be analyzed statistically by using the Weibull Probability Distribution Function (PDF). Weibull PDF of a certain wind speed at a particular time (t) can be expressed as,

$$f^t(v) = \left(\frac{k_t}{c_t}\right) \left(\frac{v}{c_t}\right)^{(k_t-1)} \exp\left[-\left(\frac{v}{c_t}\right)^{(k_t-1)}\right] \quad (3)$$

The scale factor (c_t) and shape factor (k_t) at a particular time (t) can be evaluated by using [17],

$$c_t = \frac{\mu_v^t}{\Gamma\left(1 + \frac{1}{k_r}\right)} \quad (4)$$

$$k_t = \left(\frac{\sigma_v^t}{\mu_v^t}\right)^{-1.086} \quad (5)$$

where $\Gamma()$ is the gamma function. σ_v^t and μ_v^t are the standard deviation and mean of wind speed (v_t) at a particular time t .

2.3 Modeling of Wind Power Output

The amount of power output from wind energy generators (WEG) falls in three different regions. When the wind speed (v_t) is less than the v_{cin} or higher than the v_{cout} , then the WEG/WT will produce zero power output (i.e., $P_w^t = 0$). When v_t is between v_{cin} and v_r , then the wind power will increase linearly (as represented in Eq. (6) and it is called the continuous range. When v_t is between v_r and v_{cout} , then it is going to generate rated wind power (i.e., P_w^r), and it is a discrete PDF. In the similar lines, below the v_{cin} or above the v_{cout} , the WT will not produce any real power and it is also considered as a discrete range. Then the power output can be expressed as [18],

$$P_w^t = \begin{cases} 0 & v_t < v_{cin} \text{ and } v_t > v_{cout} \\ \left(\frac{P_w^r}{v_r - v_{cin}}\right)v_t - \left(\frac{v_{cin}P_w^r}{v_r - v_{cin}}\right) & v_{cin} \leq v_t \leq v_r \\ P_w^r & v_r \leq v_t \leq v_{cout} \end{cases} \quad (6)$$

Generally, the wind power output is dependent on wind speed. The (P_w^t) with wind speed can also be expressed as a cubical [19]. The amount of wind power generated from a WT at a particular time 't' can be expressed as,

$$P_w^t = \begin{cases} 0 & v_t < v_{cin} \text{ and } v_t > v_{cout} \\ \left(\frac{P_w^r}{v_r^3 - v_{cin}^3}\right)v_t^3 + \left(\frac{v_{cin}^3 P_w^r}{v_r^3 - v_{cin}^3}\right) & v_{cin} \leq v_t \leq v_r \\ P_w^r & v_r \leq v_t \leq v_{cout} \end{cases} \quad (7)$$

where v_t is the average wind speed at a particular time t . v_r , v_{cout} and v_{cin} are the rated, cut-out, and cut-in wind speeds. P_w^r is rated/maximum wind power. The amount of wind power generated can also be expressed as,

$$P_w^t = \frac{1}{2} \rho K_{max} A_f v_t^3 \quad (8)$$

where K_{max} is power coefficient, ρ is the air density, and A_f is swept area by the rotor of WT. The wind technology option uses modeling techniques like Gaussian, Weibull, Rayleigh, and Beta PDFs due to its intermittent and variable behavior.

2.3.1 Wind Power Output in Continuous Range

In continuous range (i.e., the (P_w^t) in the region between cut-in to rated wind speeds), the random variable transformation is used to transform the wind speed random variable (v_t) to the wind power output (P_w^t) random variable. In this continuous range, the Weibull PDF can be expressed as [19],

$$f_p(p) = \frac{k(v_r - v_i)}{c^k * p_r} \left[v_i + \frac{p}{p_r} (v_r - v_i)^{k-1} \right] \exp \left[- \left[\frac{v_i + \frac{p}{p_r} (v_r - v_i)}{c} \right]^k \right] \quad (9)$$

where $f_p(p)$ is the WEG/wind power PDF. The above PDF (i.e., Eq. (9)) is valid only for the continuous range.

2.3.2 Wind Power Output in Discrete Range

From Eqs. (6) and (7), it can be seen that two different discrete probabilities occur when there is no power output from the wind plant ($P_w^t = 0W$) and the rated power output ($P_w^t = P_w^r$) [20]. The probability of an event at ($P_w^t = 0$) is given by,

$$P_r(P = 0) = P_r(V < v_i) + P_r(V \geq v_o) = 1 - e \left(- \left(\frac{v_i}{c} \right)^k \right) + e \left(- \left(\frac{v_o}{c} \right)^k \right) \quad (10)$$

The probability of an event at ($P_w^t = P_w^r$) is given by,

$$P_r(P = P_r) = P_r(v_r < V < v_o) = e \left(- \left(\frac{v_r}{c} \right)^k \right) + e \left(- \left(\frac{v_o}{c} \right)^k \right) \quad (11)$$

From the above Eqs. (9), (10), and (11), it is clear that it is a mixed probability function with continuous and discrete power outputs.

3 Solar PV Energy System

Solar energy is an inexhaustible energy source. It is one of the renewable energies which transform the electric power system. Scientists have found ways to harness

the power of the sun. The process consists of converting the sunlight into electricity, using photovoltaic (PV) cells. PV converts light into electric current using the PV effect. Solar energy works very well in areas where the sun shines almost every day. A Photoelectric system converts light energy to electricity. It consists of multiple components. There are three main models of solar PV systems, i.e., grid-connected, independent/stands alone and integrated models. The grid-connected solar PV system operates a DC power to a power conduction unit converter that converts the DC to AC, whereas the standalone model is equipped with a battery energy storage and generator for backup power. For instance, the power produced by panels can be used to supply homes or buildings or a power grid. Since the energy production by solar PV panels is DC, an inverter is used to convert it to AC and a regulator is used to regulate the power. Transformers are used to step the voltages down or up depending on the use of those voltages. Whereas in the integrated system, the solar PV system is coupled directly to their loads without major power conducting device or the storage battery. This PV system is friendlier to the environment due to its no emission, pollution, and minimal health hazards [21].

Two main factors considered for the solar PV systems include insolation/irradiance and emission. Insolation is the availability of solar PV energy conversion to electricity. Various factors affecting solar irradiance include the operating temperature of the solar cells, position of the solar panel, and intensity of light. Different materials applied for solar PV cells are amorphous silicon and cadmium telluride, these are environmentally friendly. The cost of power from solar technology is expected to reduce in the nearest future. Due to its stationary parts and constant availability of the sun increases the lifetime of the solar PV system.

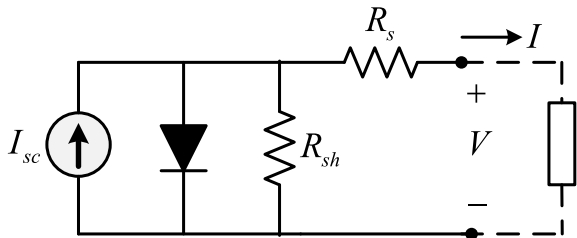
Applications of solar PV energy systems include solar power, solar vehicles, agriculture, solar lighting, water heating, water cookers, water treatments, etc. Some of the advantages of solar PV systems include abundant availability, quick installation, low cost in the application and processing, low maintenance, and easy customization [22]. However, the disadvantages include higher cost than fossil energy, dependent on the sun, high capital investment, and finding suitable locations for building solar PV plants. Solar technology is going to play a larger role in the future, as there are new developments that could result in lower costs and improved efficiency.

3.1 Modeling of Power Output from Solar PV Plant

In setting up of solar PV plants and systems, data typically gotten over a year takes to account hourly global direct insolation, temperature and wind speed data, array geometry, and balance of the system. Generally, the solar PV panels are tilted to get maximum solar irradiance on them. Beam and diffuse radiation incident on solar PV panels surface govern the amount of electricity generation. Total hourly solar irradiation on a titled surface (G_t in W/m^2) can be expressed as [22],

$$G_t = G_b R_b + G_d R_d + (G_b + G_d) R_r \quad (12)$$

Fig. 1 Equivalent circuit of the solar PV cell



where G_b and G_d are the beam part and diffused part of solar irradiancies. R_b , R_d and R_r are the tilt factors for beam, diffused, and reflected part of solar radiations. The active power output from solar PV power (P_{pv}) can be represented by [23],

$$P_{pv} = \eta AG_t \quad (13)$$

where η is the photoelectric conversion efficiency and A is the surface area of solar PV systems (in m^2). The most commonly used model for PV technology and the equivalent of solar PV cell circuit model has been depicted in Fig. 1.

The amount of current flowing through a load of the solar PV cell (I) is given by,

$$I = I_{sc} - I_{os} \left[e^{\left(\frac{q(V + IR_s)}{nKT} \right)} - 1 \right] - \left(\frac{V + IR_s}{R_{sh}} \right) \quad (14)$$

where K is Boltzmann's constant, I_{sc} is short circuit current, q is electron charge (1.6×10^{-19} C), R_s and R_{sh} are series and shunt resistances for cells. T is the absolute temperature of the p-n junction; V is the voltage across solar cell, n is the ideality factor, which is a number between 1 and 2. Saturation current (I_{os}) is given by,

$$I_{os} = AT^\gamma e^{\left(\frac{-E_g}{nKT} \right)} \quad (15)$$

where A is temperature constant, γ is temperature dependency exponent, E_g is energy gap. The current of an ideal solar cell (I_d) is given by,

$$I_d = I_{sc} - I_{os} \left[e^{\left(\frac{q}{nKT} E_d \right)} - 1 \right] \quad (16)$$

However, for an array of ($N_s \times N_{sh}$) solar PV cells,

$$I_d = \frac{I_d^{mod}}{N_{sh}} \quad (17)$$

$$E_d^{mod} = E_d \times N_s \quad (18)$$

$$R_s^{mod} = R_s \left(\frac{N_s}{N_{sh}} \right) \quad (19)$$

$$R_{sh}^{mod} = R_{sh} \left(\frac{N_s}{N_{sh}} \right) \quad (20)$$

where N_s , N_{sh} are the number of series and parallel cell junctions of a PV module. R_s^{mod} is series resistance, R_{sh}^{mod} is shunt resistance, E_d^{mod} is voltage and I_d^{mod} is current of the entire module. The power output of solar PV panel is given by [24],

$$P_{pv}(G) = F_{PV} \frac{G_t}{G_{std}} P_{pv}^r [1 + \gamma(T_t - T_{std})] \quad (21)$$

G_t is solar irradiance (in W/m^2) at time t, G_{std} is standard solar irradiance ($1000 W/m^2$), F_{PV} is the factor reflecting the shading and wiring losses, P_{pv}^r is the rated power output, T_t is the temperature at time t, T_{std} is standard test conditions temperature ($25^\circ C$), γ is the maximum correction for temperature. Some of the factors that determine the output given by solar technologies include the type of material, the area and intensity of the sun in the region, the cross-sectional area of the solar PV panel, and the type of connectivity it operates.

By neglecting the solar PV cell temperature, the amount of power output from solar PV cell ($P_{pv}(G)$) can be represented by [25],

$$P_{pv}(G) = \begin{cases} P_{pv}^r \left(\frac{G_t}{G_{std} R_c} \right) & \text{for } 0 < G_t < R_c \\ P_{pv}^r \left(\frac{G_t}{G_{std}} \right) & \text{for } G_t > R_c \end{cases} \quad (22)$$

where R_c is a certain solar PV irradiation point (say $150 W/m^2$).

3.2 Uncertainty Modeling of Solar PV Unit

Solar power is free after the recovery of the initial investment, and it is also environmentally friendly. Solar energy does not require expensive maintenance and finally, it does not pollute our air and it operates silently. Solar energy can be harness asong as the sunshine and the energy can be stored in batteries for the evening and overnight use. Solar panels don't require a lot of maintenance and 90% of the solar panels last 30 years or more. At a selected location, the solar irradiation follows a bi-modal PDF, which can be modeled as two unimodal PDFs. The unimodal PDF can be modeled by using the Beta PDF, Weibull PDF, and Log-normal PDF. The modeling of hourly solar irradiation by using Weibull PDF can be represented by [25],

$$f_G(G) = \omega \left(\frac{k_1}{c_1}\right) \left(\frac{G_t}{c_1}\right)^{k_1-1} \exp\left[-\left(\frac{G_t}{c_1}\right)^{k_1}\right] + (1-\omega) \left(\frac{k_2}{c_2}\right) \left(\frac{G_t}{c_2}\right)^{k_2-1} \exp\left[-\left(\frac{G_t}{c_2}\right)^{k_2}\right] \quad (23)$$

where ω is the weight parameter ($0 < \omega < 1$). c_1 , c_2 , k_1 and k_2 are scale and shape factors, respectively. As mentioned earlier, the solar irradiance follows a Beta PDF. This Beta distribution of solar irradiance (G_t) at a particular time t can be expressed as [26],

$$f_G^T(G) = \frac{\Gamma(\alpha^t + \beta^t)}{\Gamma(\alpha^t)\Gamma(\beta^t)} G_t^{(\alpha^t-1)} (1 - G_t)^{(\beta^t-1)} \quad (24)$$

where α^t and β^t are the shape parameter at a particular time t , and they are calculated by using,

$$\beta^t = (1 - \mu_G^t) \left[\frac{\mu_G^t (1 + \mu_G^t)}{(\sigma_G^t)^2} - 1 \right] \quad (25)$$

$$\alpha^t = \frac{\mu_G^t \beta^t}{(1 - \mu_G^t)} \quad (26)$$

where μ_G^t and σ_G^t are the mean and standard deviation of solar irradiance (G_t) at a particular time t . The expectation (E) and variance (Var) of the random variables (X) of the Beta distribution are expressed using,

$$E(X) = \frac{\alpha^t}{\alpha^t + \beta^t} \quad (27)$$

$$Var(X) = \frac{\alpha^t \beta^t}{(\alpha^t + \beta^t)^2 (1 + \alpha^t + \beta^t)} \quad (28)$$

4 Battery Storage Modeling

The battery storage system is employed as a backup to store the excess of power when the supply from RERs exceeds the load demand. This battery will also provide energy to the system when the supply from RERs cannot meet the required load demand. Battery storage units are used to store the extra amount of power produced by the RERs. Generally, Lithium-ion (Li-ion) batteries are used for storage. Li-ion battery has a low-self discharge rate, higher better energy capacity, and the ability to be recharged hundreds of thousands of times than other battery types. The Li-ion

batteries have high power density, high efficiency, high energy density, and longer life cycle [27]. For the longer life of the battery, the minimum SOC is considered as 20% and the round trip efficiency is considered as 80%. The amount of energy stored in a battery is expressed as,

$$Q_B = Q_B^0 + \int_0^t V_B I_B dt \quad (29)$$

The state of charge (SoC) of a battery is expressed as,

$$SoC_t^B = \left(\frac{Q_B}{Q_B^{\max}} \right) \times 100 \quad (30)$$

where Q_B is the total energy of battery at time t , Q_B^0 is energy available at the beginning of the scheduling interval. Storage systems play a vital role in changing the generation to suit the requirement which leads to enhancing the consistency and performance of the system against the uncertainties [28]. The SoC of the storage system (in Wh) is expressed as,

$$SoC_t = SoC_{t-1} + \eta_c^B \left(\frac{P_c^t}{\Delta t} \right) - \left(\frac{P_d^t}{\Delta t} \right) \quad (31)$$

where η_c^B is the charging efficiency of the battery, Δt is the scheduling interval (say 1 h). P_d^t and P_c^t are the discharging and charging powers of the battery storage system. The SoC for the battery is considered an important parameter to be controlled [29]. The variation of battery SoC is expressed by using,

$$SoC_t = SoC_0 + \frac{1}{Q} \int_0^t i dt \quad (32)$$

where Q is maximum capacity and $i dt$ is the instantaneous capacity of the battery bank. Maintaining the SoC within the limits is essential to prevent it from any overcharging or under discharging, and for a longer lifetime of the battery, and this constraint can be expressed as [30],

$$SoC_{\min} \leq SoC_t \leq SoC_{\max} \quad (33)$$

Batteries are degraded by the depth of discharge (DOD), temperature, and SoC, which minimizes the charging and discharge sequence of the storage system. The degradation cost of battery (C_d^t) is given by [31],

$$C_B = \frac{IC_B P_B^t \Delta t}{N_c^t S_B \eta_c^B \eta_d^B} \quad (34)$$

Degradation cost during charging ($C_{d,ch}^t$) can be expressed as,

$$C_{d,ch}^t = \frac{\alpha P_{b,ch}^t \eta_c C_p}{T_c N \eta_d \tau} \quad (35)$$

Degradation cost during discharging ($C_{d,disch}^t$) can be expressed as,

$$C_{d,disch}^t = \frac{(1 - \alpha) P_{b,disch}^t \eta_c C_p}{T_d N \eta_d \tau} \quad (36)$$

where T_c and T_d are the average number of charging and discharging hours per day. τ is the time period after which the decay is measured. N is charging and discharging cycles of the storage system, α is the ratio of average charging time to total operating time per day, C_p is the capital cost of the storage system. The cost function of the battery storage system in terms of DOD during the charging and discharging operation can be represented by [32],

$$C_B = \frac{I C_B P_B^t \Delta t}{N_c^t S_B \eta_c^B \eta_d^B} \quad (37)$$

$I C_B$ is the investment cost of battery storage, Δt is the time step (say 1 h), P_B^t is power output from storage battery at time t, N_c^t is the number of cycles of energy storage at a particular DOD at time t, S_B is the total capacity of the battery storage system in Wh. η_d^B and η_c^B are discharging and charging efficiencies of the battery.

5 Small Hydro and Pumped Hydro Energy Systems

Water is another form of renewable energy that creates hydroelectric power is usually located on dams where there is an abundance of moving water. To produce water energy the industrials that produce water energy push water through pipes to turn a turbine which is hooked to a generator. Once the turbine is in motion it then turns the generator which produces electricity. This process consists of releasing kinetic energy, which is transformed into mechanical energy, and then the production of electricity. The working principle of a pumped-hydro storage plant is similar to the traditional hydropower plant. Small hydropower generators work at variable speeds as the water flows at various speeds.

The main advantage of hydro energy is the fact that water is natural and it can be retained in one location and to be used later for energy production. As hydropower is fueled by water, it is a clean source of power as it does not pollute the air as fossil fuels do. This power can be made readily available on-demand (very high ramp up and ramp down limits) as the flow of water through the turbines can be controlled. Hydropower facilities create reservoirs that provide some kind of recreational activities [33].

The hydro-electric power dams are very expensive to build and require adequate preparation to execute. These dams are believed to last 100 years and since we will continue to have water as a resource, then this technology is quite sustainable. These plants do not produce any emissions or create waste but the dams disturb the scenery, aquatic ecosystem, and surrounding lands.

5.1 Modeling of Small Hydro Power

The power plants that create hydroelectric power are usually located on dams where there is an abundance of moving water. To produce water energy the industrials that produce water energy push water through pipes to turn a turbine which is hooked to a generator and the generator generates electricity. Large-scale hydro energy dams are used to power grids. Transformers are used to step the voltages down or up depending on the use of those voltages. The small hydro generator allows the cases of the high head with a low volumetric rate of flow or a high volumetric rate of flow with a low head for operation. The amount of electrical power obtained from small hydro generator (P_H) can be represented by using [34],

$$P_H = \frac{g\eta_h h_{eff} \rho_w Q_w}{1000W/kW} \quad (38)$$

where ρ_w is the water density (kg/m^3), g is acceleration due to gravity (9.81 m/s^2), h_{eff} is the effective height (m), Q_w is the flow rate of water (m^3/s), η_h is the efficiency of the small hydro generator (%). This potential energy (E) of hydropower can be represented by,

$$E = mgh \quad (39)$$

Relating power to mass flow rate can be expressed as,

$$\frac{E}{t} = \frac{m}{t} gh \quad (40)$$

Hence, for the hydro-electric power (P) can be expressed as,

$$P = \rho\varphi gh = hr gk \quad (41)$$

where m is mass, k is efficiency coefficient, and φ is the rate of fluid flow.

5.2 Modeling of Pumped Hydro Storage Plant

The working principle of a pumped-hydro storage plant is similar to the traditional hydropower plant. The amount of power generated from the pumped hydro plant during the generating mode (P_{gen}) can be expressed as [35],

$$P_{gen} = \eta_g Q_w h_{eff} g \quad (42)$$

The amount of power used by the pumped hydropower plant to pump the water (P_{pump}) is given by,

$$P_{pump} = \frac{Q_w h_{eff} g}{\eta_p} \quad (43)$$

where η_p is the pumping efficiency.

6 Geothermal Energy

It is clean and sustainable energy. It saves about 80% cost of fossil fuels. Also, it decreases our dependence on fossil fuels since geothermal energy does not use fuel to generate power. Another important benefit of geothermal energy is the fact that geothermal energy does not pollute the air and people use this resource to heat/cool their homes, prepare their foods, which is a creation of jobs for the local people. The installation of a power plant to get steam from deep within the earth requires high investments. The process requires recruiting highly skilled people for the job, and those workers are usually relocated since this type of energy power is not widely used. Another disadvantage is the geothermal site can run out of steam after injecting heavy investments on that site which will make companies lose a lot of money. This energy is available only in the regions where the temperatures are low and can produce steam for a long period of time [36]. However, geothermal energy is not environmentally friendly and may contain poisonous gases that can escape from the holes dug by the workers.

Due to the large electrical energy output, geothermal plants can only be connected to a grid to supply power to a city, town, etc. Transformers are used to step the voltages down or up depending on the use of those voltages. The cost of geothermal energy varies based on different criteria, such as temperature, depth of area drilled, etc. They are connected to a grid in regards to the power supply. Generally, there are three main types of geothermal power units:

- **Dry-steam power units:** These plants/units use the steam from underground to drive the turbines to produce electricity.

- **Flash-power units:** These plants pull water at high pressure from underground. As the water rises, the pressure drops, and hence, the water vaporizes into steam which drives the turbine. Any leftover water or condensed steam is condensed and renewed.
- **Binary cycle power units:** These use heat from hot water from underground to boil a working fluid that vaporizes in a heat exchanger and then it turns to the turbine.

6.1 Modeling of Geothermal Energy

As mentioned earlier, geothermal energy involves accessing the hot water and underground steam from the wells to several miles into the earth. The main feature of this technology is the steam turbine. Essentially, the steam that comes out of the earth's crust is used to drive a turbine which activates a generator and ultimately produces the power required. Some power plants use steam obtained directly to power a turbine, while some others use hot water obtained to vaporize a liquid which in turn turns a turbine. The heat energy (H) equation is given by [37],

$$H = m \times C_p \times \Delta T \quad (44)$$

where ΔT is change in temperature, m is mass, C_p is specific heat. The maximum heat power generated from a geothermal source is given by [38],

$$P_{\max} = kv(T - T_g) = kv\Delta T \quad (45)$$

where k is thermal conductivity, v is water outflow capacity. T and T_g are water and border temperatures, respectively.

Geothermal technologies are clean, sustainable, cost-effective, and reliable. It requires no fuel and it is relatively environmental-friendly as it does not produce as much pollution as fossil fuels. However, although the technological advancements have led to the broadening of the range and scale of power obtained here, it has broadly been limited to areas close to tectonic plate boundaries. Drilling and exploration of wells/pipes for deep underground resources are very expensive. Geothermal wells release greenhouse gases trapped underground. But, these gases are far less pollutant than the gases emitted by fossil fuels.

A lot of gases including carbon dioxide, hydrogen sulfide, and ammonia are get carried by water from underground. This eventually leads to the release of pollutants into the atmosphere which could cause acid rain, global warming, or other conditions. It is important to note that these pollutants do not have as much negative impact as fossil fuels. Also, the drilling and construction of wells to provide access to geothermal energy sometimes affects land adversely and could trigger earthquakes as part of hydraulic faulting.

7 Biomass Energy

Biomass energy is sustainable. This energy is produced from biomass organic matter like wheat, corn, soybeans, and raisins that can generate materials and chemicals which we generally get from petroleum. Biomass energy is generated by burning many types of biomass fuels such as wood, municipal solid waste, refused derived fuel, etc. The biomass fuels are converted into many forms of energy after combustion: hot water, hot air, electricity, etc. Bio-power can also be derived from the gasification process. This is the conversion of gas to a gas turbine to produce electricity. The Biomass energy conversion process utilizes the concept of pyrolysis of oil. Biomass can be converted directly into fluid fuels, most common fuels are bio-diesel or ethanol. Organic material will be always available to be used as energy resources. This means that biomass plants can last longer than the human race. Biomass power can only be produced when sufficient bio-products are available and converted. Its efficiency is still very low and is also not an ideal green/sustainable power due to pollutants emission.

Biomass causes no increase in carbon dioxide emissions to the atmosphere. Carbon is removed from the atmosphere as the trees and plants grow, and the use of biomass energy does not contribute to global climate change, which is a huge advantage to the world. Also, using biomass to produce energy is a way of disposing of the waste material and preventing our environment from being deteriorated by those wastes. For example, burning the waste from particular cities would prevent those cities from having wasted all over the places or in the countryside. Another advantage of this source is that biomass energy is available throughout the world. Biomass plants generate AC power to supply a grid. This is due to the fact biomass plants produce large output power. However, the burning of biomass causes pollution and global warming [39].

The main advantages of bio-energy include the use of waste products, carbon-neutral, continuous source unlike solar or wind; cost of resources is low, reduced level of methane, and easy availability. However, burning the biomass causes pollution and global warming. Other disadvantages include limited potentials, require top-notch management, may create air pollution if not handled carefully and fear of health hazards if close to residential homes.

7.1 Modeling of Biomass Energy

Biogas production is made from biomass feedstock, i.e., agriculture residue, household waste, and forest residue in this case study biomass is used to produce biogas. The biomass feedstock potential estimation is made considering the efficiency of 75% as collection rate and the average collected feedstock of 160 kg/ha/yr. 80% of the total biomass feedstock potential is suggested to use as electricity conversion using a gasified biomass-based system. The hourly power output from biomass generator

(P_{Bio} in kW) can be calculated by using [40],

$$P_{Bio} = \frac{\eta_{Bio} F_A C V_{Bio} \times 1000}{365 \times 860 \times Oh_{day}} \quad (46)$$

η_{Bio} is the efficiency of biomass generator (%), F_A is total fuel availability (in tons/year), CV_{Bio} is the caloric value of biomass, Oh_{day} represents the number of operating hours per day.

8 Conclusions

Renewable power generation from the solar PV and wind energy systems for a particular region is almost complimentary as the wind speed is high during the night and solar irradiance is high during the day. Therefore, obtaining an optimum mixture will give maximum potential benefits to the system. This chapter has presented the modeling of various renewable energy resources (RERs) such as solar PV, wind, small hydro, pumped hydro, geothermal, and biomass. Biogas has stated benefits (cleaner combustion, high efficiency, ameliorates control) over solid biomass though having a low heating value in comparison to fossil fuels. The main advantage of geothermal energy is that geothermal energy is relatively cheap compared to fossil fuel.

Acknowledgements This research work was funded by “Woosong University’s Academic Research Funding—2021”.

References

1. Akintande OJ, Olubusoye OE, Adenikinju AF, Olanrewaju BT (2020) Modeling the determinants of renewable energy consumption: evidence from the five most populous nations in Africa. *Energy* 206. <https://doi.org/10.1016/j.energy.2020.117992>
2. Assi AF, Isiksal AZ, Tursoy T (2021) Renewable energy consumption, financial development, environmental pollution, and innovations in the ASEAN + 3 group: evidence from (P-ARDL) model. *Renew Energy* 165(1):689–700. <https://doi.org/10.1016/j.renene.2020.11.052>
3. Mohammed NA, Al-Bazi A (2021) Management of renewable energy production and distribution planning using agent-based modelling. *Renew Energy* 164:509–520. <https://doi.org/10.1016/j.renene.2020.08.159>
4. Bramstoft R, Pizarro-Alonso A, Jensen IG, Ravn H, Münster M (2020) Modelling of renewable gas and renewable liquid fuels in future integrated energy systems. *Appl Energy* 268. <https://doi.org/10.1016/j.apenergy.2020.114869>
5. Bernath C, Deac G, Sensfuß F (2021) Impact of sector coupling on the market value of renewable energies—a model-based scenario analysis. *Appl Energy* 281. <https://doi.org/10.1016/j.apenergy.2020.115985>
6. Li L, Ling L, Yang Y, Poursoleiman R (2021) Modeling and optimal energy operation considering probabilistic and sustainable renewable energy models and demand side management. *Energy Build* 231. <https://doi.org/10.1016/j.enbuild.2020.110557>

7. Deng X, Lv T (2020) Power system planning with increasing variable renewable energy: a review of optimization models. *J Clean Prod* 246. <https://doi.org/10.1016/j.jclepro.2019.118962>
8. Scott IJ, Botterud A, Carvalho PMS, Silva CAS (2020) Renewable energy support policy evaluation: the role of long-term uncertainty in market modelling. *Appl Energy* 278. <https://doi.org/10.1016/j.apenergy.2020.115643>
9. Valencia-Calvo J, Olivar-Tost G, García-Ortega M (2020) Model and simulation of a renewable energy market: integration of renewable energy sources with the conventional generation system. In: 15th Iberian conference on information systems and technologies, Sevilla, Spain, pp 1–7. <https://doi.org/10.23919/CISTI49556.2020.9140987>
10. Yi W, Zhang Y, Zhao Z, Huang Y (2018) Multi objective robust scheduling for smart distribution grids: considering renewable energy and demand response uncertainty. *IEEE Access* 6:45715–45724. <https://doi.org/10.1109/ACCESS.2018.2865598>
11. Rahbar K, Chai CC, Zhang R (2018) Energy cooperation optimization in micro-grids with renewable energy integration. *IEEE Trans Smart Grid* 9(2):1482–1493. <https://doi.org/10.1109/TSG.2016.2600863>
12. Rekioua D (2014) Wind power electric systems—modeling, simulation and control. In: *Green energy and technology*, Springer-Verlag London. ISBN: 978-1-4471-6425-8
13. Soriano LA, Yu W, Rubio JJ (2013) Modeling and control of wind turbine. *Math Probl Eng*. <https://doi.org/10.1155/2013/982597>
14. Yaakoubi AE, Amhaimar L, Asselman A (2020) Wind energy conversion system modeling toward different approaches. In: Maalawi KY (ed) *Design optimization of wind energy conversion systems with applications*, IntechOpen. <https://doi.org/10.5772/intechopen.89066>
15. Afanasyeva S, Saari J, Kalkofen M, Partanen J, Pyrhönen O (2016) Technical, economic and uncertainty modelling of a wind farm project. *Energy Convers Manage* 107:22–33. <https://doi.org/10.1016/j.enconman.2015.09.048>
16. Evangelopoulos VA, Georgilakis PA (2014) Optimal distributed generation placement under uncertainties based on point estimate method embedded genetic algorithm. *IET Gener Transm Distrib* 8(3):389–400. <https://doi.org/10.1049/iet-gtd.2013.0442>
17. Hetzer J, Yu DC, Bhattarai K (2008) An economic dispatch model incorporating wind power. *IEEE Trans Energy Convers* 23(2):603–611. <https://doi.org/10.1109/TEC.2007.914171>
18. Liu X, Xu W (2010) Minimum emission dispatch constrained by stochastic wind power availability and cost. *IEEE Trans Power Syst* 25(3):1705–1713. <https://doi.org/10.1109/TPWRS.2010.2042085>
19. Reddy SS, Bijwe PR, Abhyankar AR (2015) Joint energy and spinning reserve market clearing incorporating wind power and load forecast uncertainties. *IEEE Syst J* 9(1):152–164. <https://doi.org/10.1109/JSYST.2013.2272236>
20. Reddy SS, Bijwe PR, Abhyankar AR (2015) Optimal posturing in day-ahead market clearing for uncertainties considering anticipated real-time adjustment costs. *IEEE Syst J* 9(1):177–190. <https://doi.org/10.1109/JSYST.2013.2265664>
21. Vinod KR, Singh SK (2018) Solar photovoltaic modeling and simulation: as a renewable energy solution. *Energy Rep* 4:701–712. <https://doi.org/10.1016/j.egy.2018.09.008>
22. Mazidi M, Zakariazadeh A, Jadid S, Siano P (2014) Integrated scheduling of renewable generation and demand response programs in a micro-grid. *Energy Convers Manage* 86:1118–1127. <https://doi.org/10.1016/j.enconman.2014.06.078>
23. Chauhan A, Saini RP (2014) A review on integrated renewable energy system based power generation for stand-alone applications: configurations, storage options, sizing methodologies and control. *Renew Sustain Energy Rev* 38:99–120. <https://doi.org/10.1016/j.rser.2014.05.079>
24. Rajanna S, Saini RP (2016) Modeling of integrated renewable energy system for electrification of a remote area in India. *Renew Energy* 90:175–187. <https://doi.org/10.1016/j.renene.2015.12.067>
25. Reddy SS, Momoh JA (2015) Realistic and transparent optimum scheduling strategy for hybrid power system. *IEEE Trans Smart Grid* 6(6):3114–3125. <https://doi.org/10.1109/TSG.2015.2406879>

26. Atwa YM, El-Saadany EF, Salama MMA, Seethapathy R (2010) Optimal renewable resources mix for distribution system energy loss minimization. *IEEE Trans Power Syst* 25(1):360–370. <https://doi.org/10.1109/TPWRS.2009.2030276>
27. Ganesan S, Subramaniam U, Ghodke AA, Elavarasan RM, Raju K, Bhaskar MS (2020) Investigation on sizing of voltage source for a battery energy storage system in micro-grid with renewable energy sources. *IEEE Access* 8:188861–188874. <https://doi.org/10.1109/ACCESS.2020.3030729>
28. Rancilio G, Lucas A, Kotsakis E, Fulli G, Merlo M, Delfanti M, Masera M (2019) Modeling a large-scale battery energy storage system for power grid application analysis. *Energies* 12. <https://doi.org/10.3390/en12173312>
29. Bera A, Tian Y, Almasabi S, Mitra J, Borges C (2019) Modeling of battery energy storage systems for system reliability studies. In: *IEEE power and energy society general meeting, Atlanta, GA, USA*, pp 1–5. <https://doi.org/10.1109/PESGM40551.2019.8973773>
30. Sarasua AE, Molina MG, Mercado PE (2013) Dynamic modelling of advanced battery energy storage system for grid-tied AC micro-grid applications. In: *Zobaa AF (ed) Energy storage—technologies and applications*, IntechOpen. <https://doi.org/10.5772/52219>
31. Salkuti SR (2020) Optimal day-ahead renewable power generation scheduling of hybrid electrical power system. In: *Ray P, Biswal M (eds) Micro-grid: operation, control, monitoring and protection, Lecture notes in electrical engineering*, vol 625. Springer, Singapore. https://doi.org/10.1007/978-981-15-1781-5_2
32. Dubarry M, Baure G, Fernández CP, Yu TF, Widanage WD, Marco J (2019) Battery energy storage system modeling: a combined comprehensive approach. *J Energy Storage* 21:172–185. <https://doi.org/10.1016/j.est.2018.11.012>
33. Gil-González W, Montoya OD, Garces A (2020) Modeling and control of a small hydro-power plant for a DC micro-grid. *Electr Power Syst Res* 180. <https://doi.org/10.1016/j.epsr.2019.106104>
34. Kusakana K (2016) Optimal scheduling for distributed hybrid system with pumped hydro storage. *Energy Convers Manage* 111:253–260. <https://doi.org/10.1016/j.enconman.2015.12.081>
35. Gupta A, Saini RP, Sharma MP (2010) Steady-state modelling of hybrid energy system for off grid electrification of cluster of villages. *Renew Energy* 35(2):520–535. <https://doi.org/10.1016/j.renene.2009.06.014>
36. Blank L, Rioseco EM, Caiazzo A, Wilbrandt U (2020) Modeling, simulation, and optimization of geothermal energy production from hot sedimentary aquifers. *Comput Geosci*. <https://doi.org/10.1007/s10596-020-09989-8>
37. Deo M, Roehner R, Allis R, Moore J (2014) Modeling of geothermal energy production from stratigraphic reservoirs in the great basin. *Geothermics* 51:38–45. <https://doi.org/10.1016/j.geothermics.2013.10.011>
38. Sanchez E, Torres CF, Guillen P, Larrazabal G (2013) Modeling and simulation of the production process of electrical energy in a geothermal power plant. *Math Comput Model* 57(9–10):2140–2148. <https://doi.org/10.1016/j.mcm.2011.03.021>
39. Baruah D, Baruah DC (2014) Modeling of biomass gasification: a review. *Renew Sustain Energy Rev* 39:806–815. <https://doi.org/10.1016/j.rser.2014.07.129>
40. Upadhyay S, Sharma MP (2014) A review on configurations, control and sizing methodologies of hybrid energy systems. *Renew Sustain Energy Rev* 38:47–63. <https://doi.org/10.1016/j.rser.2014.05.057>

Smart Grid Communication: Recent Trends and Challenges



Ishan Srivastava, Sunil Bhat, and Arvind R. Singh

Abstract The complexity of power distribution network is increasing day by day with rapid increase in power demand. For monitoring and control of this complex power network, application of smart grid technologies is essential. These technologies can also improve the overall system reliability and system security. A two-way communication network is the main requirement for optimal operation of a smart grid. In modern grid, different sensors and Intelligent Electronic Devices (IED) are installed at various locations. All these devices share different information related to the state of the network like voltage, current, power flow etc., through a two-way communication channel. Maximum utilization of the network communication system resources like sensors, IEDs and smart meters can ensure most economical operation of the grid. However, this communication channel can be subjected to various challenges like cyber attacks, interference and data loss which can be a major hurdle in deployment grid automation strategies. In this chapter, the evolution of communication technology from wired network to wireless network along with architecture of the smart grid is discussed; various standards and protocols related to smart grid communication are presented. The authors also explained different challenges and their possible solutions for two-way communication infrastructure of smart grid.

Keywords Smart grid · Wireless communication · Smart grid standards · Cyber-security · Compressive sensing

I. Srivastava · S. Bhat
Electrical Engineering Department, Visvesvaraya National Institute of Technology,
Nagpur 440010, India
e-mail: ishansrivastava@students.vnit.ac.in

S. Bhat
e-mail: ssbhat@eee.vnit.ac.in

A. R. Singh (✉)
School of Electrical Engineering, Shandong University, Jinan, P.R. China

© The Author(s), under exclusive license to Springer Nature Singapore Pte Ltd. 2022
S. R. Salkuti and P. Ray (eds.), *Next Generation Smart Grids: Modeling, Control and Optimization*, Lecture Notes in Electrical Engineering 824,
https://doi.org/10.1007/978-981-16-7794-6_3

Nomenclature

SG	Smart Grid
RES	Renewable Energy Sources
IED	Intelligent Electronic Device
AMI	Advanced Metering Infrastructure
AMR	Automatic Meter Reading
NIST	National Institute of Standards and Technology
DG	Distributed Generation
ISO	Independent System Operator
RTO	Regional Transmission Operators
SCR	Silicon Controlled Rectifier
IoT	Internet-of-Things
LAN	Local Area Network
NAN	Neighborhood Area Network
QoS	Quality of Service
HTC	Human Type Communication
DMS	Distribution Management System
PLC	Power Line Communication
WMN	Wireless Mesh Network
TVE	Total Vector Error
FE	Frequency Error
X	Synchrophasor value
\hat{X}	Reconstructed value
f	Frequency of original signal
\hat{f}	Frequency of reconstructed signal
FDIR	Fault Detection, Identification, Isolation and Power Restoration

1 Introduction

The energy demand is increasing across the globe with the advancement of new technologies. In the modern era, most of this energy is supplied in the form of electricity. Due to the rise in number of customers and the loads, the modern grid's complexity is also increasing. The concept of Smart Grid (SG) is introduced to manage this highly complex power network efficiently. Advancement in the field of material science, communication engineering and power electronics is the basis of the emergence of SG. The modern grid must be designed, expanded and operated to meet the following demands:

1. The energy transmission and distribution must be economical.
2. The energy cost for the consumers must be less.
3. System security must be maintained.
4. Service restoration must be fast in the case of a fault event.

5. The environmental impacts must be appropriately monitored, and more number of Renewable Energy Sources (RES) must be connected in the grid.
6. Better management and integration of RES.

The key feature of a modern grid is the presence of RES. The presence of RES can help in providing clean energy and also it can be effective in supplying different loads during peak demand. Conventionally, the energy flows from generating station to consumers in a vertical power structure. But, due to the presence of RES in the modern grid, the power can flow in the reverse direction as well, i.e. the power can be generated at customer end and can be fed to the grid. This reverse power flow can further increase the complexity in the operation of modern grid. Therefore, a two-way communication channel is used in the SG for proper monitoring and control.

SG is equipped with a large number of different sensors at various grid nodes compared to a limited number of sensors in the conventional grid. The overall infrastructure of an SG consists of smart power generation, transmission and distribution elements. Additionally, smart information system, including smart meter, sensors, and phasor measurement units, is also present. Data exchange among various components of the grid is of high importance for the grid's smooth operation. This data helps in monitoring, analysis, optimization and control of various parameters of the power grid. This data exchange is possible through inter-operability of measuring, monitoring and controlling devices present in the grid. For example, the smart meter component present in the customer domain must be able to communicate with any component present in the generation domain, market domain or service domain. This kind of information exchange needs proper protocols and standards. Furthermore, this kind of information transfer must be done on a secured server as it is prone to cyber-attacks. To make the grid smarter, more number of sensors, intelligent electronic devices (IEDs) or PMUs are getting connected to the grid on a regular basis. But with more number of such devices, the size of real-time data generated is also increasing. Therefore, SG must be equipped with resources for data management and storage. To manage this large data, different data pre-processing, data cleaning, data analysis and data prediction agents must be incorporated in the smart information system domain of the SG. This chapter's subsequent sections present SG architecture's concept, standards related to SG, wired and wireless mode of communication in SG and cyber-security aspects associated with SG.

The main differences in the conventional grid and the SG is reported in [1–3]. The existing or conventional grid is having a limited number of sensors compared to an SG infrastructure. These sensors are responsible for providing sufficient data for real-time monitoring and control of the grid. Since there is the provision of reverse power flow in the modern grid, the communication network for the SG must be designed for two way communication. This two-way communication is also essential for implementing Advanced Metering Infrastructure (AMI) in SG. The metering system is electro-mechanical in the conventional power grid; this arrangement can't be used for real-time data transfer. Consequently, for the deployment of automation strategies like Automatic Meter Reading (AMR) for AMI, the digital metering system is an essential SG requirement. These automation strategies are responsible for

collection of data from smart meters, and secure data transmission through the communication network. This data can be utilized for billing, troubleshooting issues in the grid and analyzing various patterns. Another important duty of SG components is to restore the power to customers in case of power interruption. The service must be restored to the customers in a timely manner. The amount of time taken by the utility for restoring the power supply is directly affecting the reliability of the system. In the conventional grid, the process of fault detection, identification, isolation and power restoration (FDIR) is done manually by the utility. As a result, the time requirement for FDIR is more. In SG, with the concept of distribution automation and self-healing network, the FDIR time can be drastically reduced, thus improving the system's overall reliability.

2 Architecture of SG

According to the National Institute of Standards and Technology (NIST) [4], an SG architecture is the model that describes different domains or entities present in the system and various interactions within the system. This architecture covers different design aspects of the system along with the protocols and standards, defined for the proper operation of the grid. According to NIST, the SG consists of seven major domains:

1. Bulk generation
2. Transmission
3. Distribution
4. Customers
5. Markets
6. Service provider
7. Operations.

2.1 Bulk Generation

The significant part of energy demand is fulfilled by non-renewable sources of energy like coal and nuclear. This approach is mainly adopted in the power sector because the related technology is matured, the system's reliability is high, and the management of power flow is smooth. On the other hand, the emission of greenhouse gases that can be very harmful to the environment is the major drawback of this approach. Additionally, the availability of non-renewable resources is limited, and the global increase in energy demand will create an imbalance in supply and demand, in the near future. Therefore, the use of RES becomes essential in the current scenario. The fundamental difference in terms of generation in SG environment compared to conventional grid is the use of these RES. As the grid is becoming more complex with

more customers, there is a need to generate electricity on a small scale at different locations in the grid. This concept is known as Distributed Generation (DG). These DGs and energy storage elements like battery are collectively known as DERs. It is desired that most of these DGs present in the SG must be of renewable nature. The power generation capacity of these DGs can range from 3 to 10,000 kW [3]. In SG having DG penetration, with proper monitoring and control, the reliability of the system can also be achieved equivalent to the reliability of the conventional grid [5]. The burden from the main grid can be reduced by using DGs in the power network. The load demands or peak demands can be fulfilled with the help of DGs in the system, and this approach is more economical compared to traditional grid. This kind of cost-effective operation is the main reason for reduced transmission losses in the SG, equipped with DG.

There are a lot of challenges associated with the use of DER in SG. The main challenge is to design a proper control system for the microgrid, as there are fluctuations at the DG's input side. Also, with increased DG penetration, the inertia of the main grid can be reduced, which creates stability issues for the grid. Therefore, SG must be equipped with components for monitoring and controlling. Power electronics plays a crucial role in the integration and controlling of DGs.

The major components of bulk generation domain in SG architecture are:

- **Control:** It is responsible for overall control over the generation which is based on the data available through WAMS or SCADA system. Load generation balance is the crucial aspect for the stability of the grid. Bulk generation domain is responsible for maintaining this balance, and therefore, power generation control becomes very important.
- **Measurement:** All the data, which can be relevant for power generation is collected through the SCADA system.
- **Protection:** This component ensures protection of all the equipment incorporated for a bulk generation.
- **Record:** The various records related to system status are stored for analysis and forecasting purposes.
- **Asset management:** It deals with the management of equipment. It involves regular maintenance, repair and replacement of faulty equipment.

2.2 Transmission Domain

The transfer of power from generating station to distribution level is done through a transmission network. In the SG, through various substations, the power can be transferred from the bulk generating station to the distribution network via the power transmission system. The system operator's main responsibility is to maintain the grid's stability by managing the load generation balance. Additionally, these Independent System Operators (ISOs) or Regional Transmission Operators (RTOs) perform various tasks to ensure the smooth operation of the network [6]. Various tasks

like planning, data acquisition and data analysis also come under top priorities for smooth operation. With the increase in load demand, the transmission network can become congested if proper planning and expansion strategy is not implemented. The data acquired from smart devices like phasor measurements units, smart protection relays, and power quality monitors becomes essential for monitoring and controlling the modern electric grid. The authors in [6] described the following relevant features related to the present smart transmission grid:

- **Digitalization:** Two-way communications throughout the grid requires digital signals for transfer of data. Therefore, the transmission substations must be equipped with the devices which are compatible with digital communication. Additionally, the devices present in the transmission domain must communicate with the devices present in other domains. Therefore, a standard digital communication channel is required for interoperability.
- **Flexibility:** The transmission domain must have the feature for up-gradation and expansion, in order to meet the demands of dynamic load patterns, dynamic market structure, and increased DER penetration in the grid. Also, decentralized control schemes must be incorporated for better grid control.
- **Intelligence:** The system must be equipped with smart technologies capable of doing predictions and making decisions which is necessary in an automated environment. For example, in case of service restoration, IEDs can play a crucial role in automatically restoring the power to the customers of the healthy section of the network. This self-healing capability of the system is essential to maintain reliability.

Smart transmission network must have smart substations which must possess some basic characteristics. For example, each substation must be connected to all the other substations and the control centres present in the grid. Additionally, these substations must have enough resources to monitor and control the grid's different zone independently. These substations must process the historical and real-time data quickly to predict the probable events, which helps prepare contingency plans for problems like blackouts, instability etc. The data obtained from PMUs contains a time-stamping; this allows the system operator to deploy necessary strategies to control the grid on time.

2.3 Distribution Domain

In the conventional grid with the limited number of sensors, complete grid data is not available. This will delay service restoration in the case of a fault condition or in case of disturbances created by extreme events. The reliability of the system is inferior for such scenario. Also, the increase of DG penetration in the distribution side is making the monitoring and control procedure more complicated. Therefore, to meet the demands of modern grid, the smart distribution system is necessary.

Smart meters, various sensors and IEDs are used to collect the data in the smart distribution system. This data can help plan and deploy various strategies like outage management, fault detection, isolation and service restoration procedure, demand-side management etc. The combination of these schemes is known as the Distribution Management System (DMS). Smart meters are installed at customer premises and are responsible for collecting different types of data like the voltage, real power flow, and reactive power flow at the customer node. This data can be transferred to the electric utility in every 15 min. But, generally, this time interval depends upon the various factors and applications. The data transfer is done using a Local Area Network (LAN) from the customer node to some customer utility interface like Meter Data Management System (MDMS) which uses Zigbee technology [7]. The data collected from smart meters are used for billing, load modelling, load forecasting, state estimation, reactive power compensation management.

The other major distribution automation strategy is service restoration. Distribution network is generally designed to operate in a radial manner. Therefore, whenever a fault occurs in the system, some healthy part of the system gets disconnected. In that situation, the utility is to take some step to re-route the power to the healthy section of the network. The strategy mentioned above can be deployed by changing the topology of the network, which can be done by operating the switches present in the network. The use of remotely controlled switches instead of manually controlled switches can reduce the overall restoration process time and thus improve system's reliability. Modern distribution network must be equipped with these power electronic-based remotely controlled switches. The modern distribution network is becoming complicated day-by-day, so decentralized control strategy is more suitable for better monitoring and control, which may further reduce the overall time of operation for various distribution automation strategies.

2.4 Customer Domain

The customer in the power sector can be broadly classified into three categories, home customers (energy range ≤ 20 kW), commercial customers (energy range 20–200 kW) and industrial customer (energy range ≥ 200 kW). The link which connects these customers to the utility is called as Energy Service Interface (ESI). This interface plays a critical role in customers, utility interaction process. Every type of customer is provided with the metering facility and a gateway for the proper transfer of data.

AMI is needed for two-way communication through ESI. LAN or Home Area Network (HAN) can be used for communication between the customer domain and ESI. Distribution network also contains micro-generation units which can be of the renewable type or non-renewable type. Connection and disconnection of these units is very import aspect in overall control of the grid. The customers who feed the

power back to the grid must be adequately compensated. Therefore, smart meters at customer premises must be required when there are micro-generation units like rooftop PV present in the system.

2.5 Market Domain

The market domain provides a platform for buying and selling of energy or grid assets. This domain's main responsibility is to decide various electricity market prices with proper judgment and planning. Furthermore, these prices must be known to the customers, independent system operators and other concerned authorities, so this information transfer is managed by market domain. The market-related details, like pricing and other relevant information must also be communicated to all the other domains for planning and management purposes. This exchange of information is possible with interoperability among different domains. Interoperability is the ability of communication among various devices present in all the domains and sub-domains of the SG.

The other significant role of the market domain is to promote aggregators by expanding their capabilities. The contribution of small utilities in the power sector is of high relevance. Therefore, these small players must be provided with a transparent platform for participation in the big electricity market. The market domain is also responsible for making regulations for retailing and wholesaling of electrical energy. In the future grid, it can be expected that the complete information will be readily available to the customers like the price of electricity at different times of the day, the tariff information corresponding to different players present in distribution domain for power supply. It will help demand-side management and peak reduction, by providing a more economical energy choice to the customers.

2.6 Service Provider Domain

Service provider domain has a wide range of responsibilities, ranging from traditional utility services like billing and customer account management to managing the SG's overall ecosystem. Service provider personnel are mainly responsible for the installation and maintenance of various components at the customer end. Furthermore, home management, building management, automation, account management, billing and customer management also comes under the umbrella of utility services.

2.7 Operation Domain

This domain is responsible for maintaining, monitoring and controlling all the other domains of the grid so that all the operations run smoothly in the system. The main duties of the operation domain include:

1. Maintenance and construction
2. Manage finances
3. Manage supply chain logistics
4. Records and assets management
5. Ensure security
6. Communication infrastructure management
7. Expansion planning
8. Smooth network operations which include smooth power flow in the network and high reliability of the network.

3 Wired and Wireless Technology for Smart Grid Communication

A common understanding is that a two-way communication channel is required for information transfer in the SG. But, there is a difference in opinion on the kind of technology which should be used for communication [8]. The main reason for this debate is the variety of network types. SG infrastructure has enterprise bus, wide area networks, field area networks and premises networks [3].

The communication network either wired or wireless, must possess certain qualities like reliability, the network must have provision for fast data transfer with privacy and security.

3.1 Wired Communication Technology

There are mainly two technologies used in wired communication system namely fibre-optic communication and Power Line Communication (PLC).

3.1.1 Fiber-Optic Communication

The main features related to this kind of communication channel are high bandwidth, immunity towards electromagnetic/radio interference, suitable dielectric characteristic for high voltage application. The main disadvantage of deploying fibre-optic communication is the cost of installation, which is very high relative to other forms of communication methods [9]. Therefore, despite having the advantages mentioned

above, this type of communication channel is used when high bandwidth is required in the network. As the data size increases day by day with more sensors in the system, this communication method is becoming relevant.

3.1.2 Power Line Communication

PLC technology uses the infrastructure which was mainly deployed for electrical power transfer between two nodes. These lines deliver AC power (50 Hz or 60 Hz) or DC power. Additionally, the communication signal is transmitted, which is having a frequency range from a few hundred Hz to a few thousand MHz [10]. There are various terminology used for PLC technology [10] which are listed in Table 1. The main advantage of using PLC over other communication medium is that the infrastructure required for PLC is already present. For SG applications, the utilities can control the information transfer directly [11]. PLC has “through the-grid” property [12], which enables it to send information about lines, switches, loads etc. present in the grid. Additionally, real-time diagnostics and monitoring can be performed by utilities using the information collected through PLC. With the use of power electronics, it is possible to inject data signals or any other type signal into a power distribution line which carries electrical power [13].

Table 1 Various terminology used for PLC technology

Terminology	Description
Carrier-current systems	Transmit carrier-modulated data signals Can be used to transmit narrowband frequency signal (500 kHz)
Power line carrier	Transmit carrier modulated signal Used for the systems with operating frequency of less than 500 kHz
Distribution line carrier	Technology used in distribution network Relatively complicated to deploy compared to transmission network Used for system with frequency less than 500 kHz
Broadband over power line communication (BPL)	Used in distribution domain Signal of frequency range from 2 to 30 MHz can be transmitted Data transfer rate up to hundreds of Mbps
Power line tele-communication (PLT)	Similar advantages that of broadband over power line communication More popular in European countries

Some of the methods for PLC schemes in medium-voltage lines are as follows:

- a. Zero-crossing shift method: In this technique, with the help of the power electronic circuit, a slight shift is created at the point of zero-crossing of the power signal. This zero-crossing point is selected based on the time at which the additional signal needs to be injected. Consequently, after injection of communication signal, there is a shift in the power signal. The injected signal can be detected at the receiver end by comparing the duration of sending end and receiving end waveform, as shown in Fig. 1. An example of the power electronics circuit is shown in Fig. 2, which can create the required shift in the waveform of phase A [13].

As shown in the circuit (Fig. 2), when there is no communication signal injection, the series arm remains inactive, and thus no shift is observed in phase A waveform. When a signal is injected in the power waveform, the shunt arm gets de-energized, and series arm injects signal in waveform corresponding to phase A.

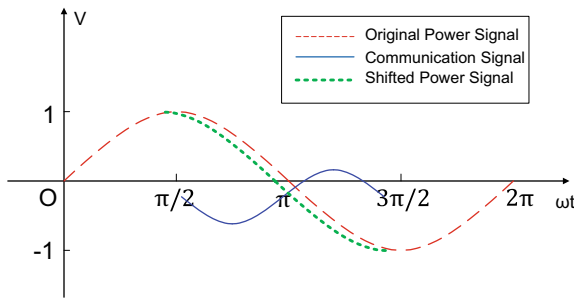


Fig. 1 Waveform showing zero-crossing shift in power signal

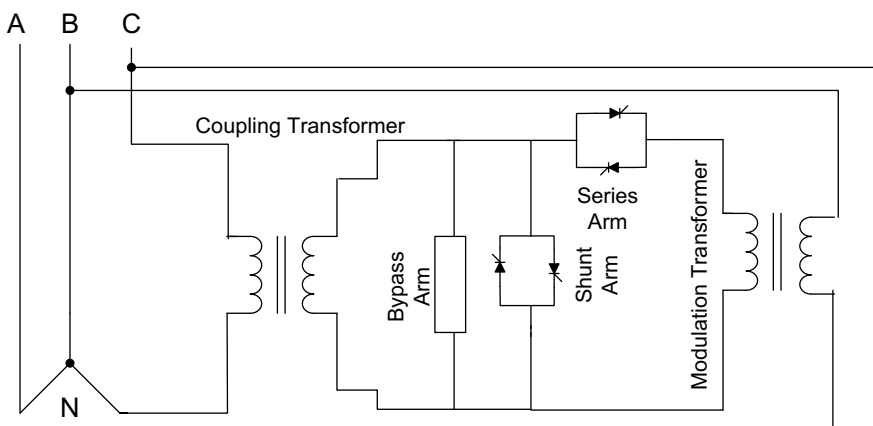
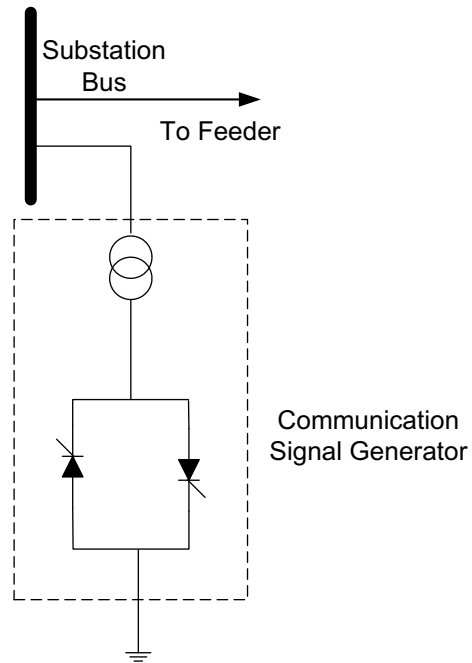


Fig. 2 Circuit for creating zero-crossing shift in power signal

Fig. 3 Scheme to create voltage sag at zero-crossing point for outbound signal generation



- b. Zero-crossing distortion technique: This technology is useful and simple for inbound [14] and outbound [15] communication through PLC. The outbound signal is created with the circuit shown in Fig. 3 [13]. In this method, the substation bus is connected to a power electronics switch like SCR and whenever an information signal needs to be injected, or perturbation needs to be done in the voltage waveform, this power electronic switch is turned on in a controlled manner near the zero-crossing point of the voltage waveform. Consequently, voltage sag is created near the zero-crossing point of the voltage waveform. This injection is done in only one of the two cycles of the voltage waveform. The signal insertion is done in this manner because the original signal can be easily retrieved by subtracting two consecutive voltage waveform cycles. Additionally, this procedure ensures the absence of voltage harmonics or noise in the obtained information signal.

Whenever a piece of information needs to be transferred from a point where this power electronics circuit is present to the load points located in the downstream region, this technique can be incorporated. Alternatively, for the applications such as automatic meter reading where the information is transferred from load end to the utility, a power electronic circuit shown in Fig. 4a can be used to generate a current pulse near the zero-crossing point of the voltage waveform as shown in Fig. 4b. This current pulse is created by switching the SCR in a controlled manner; thus, a temporary short circuit is obtained near load end.

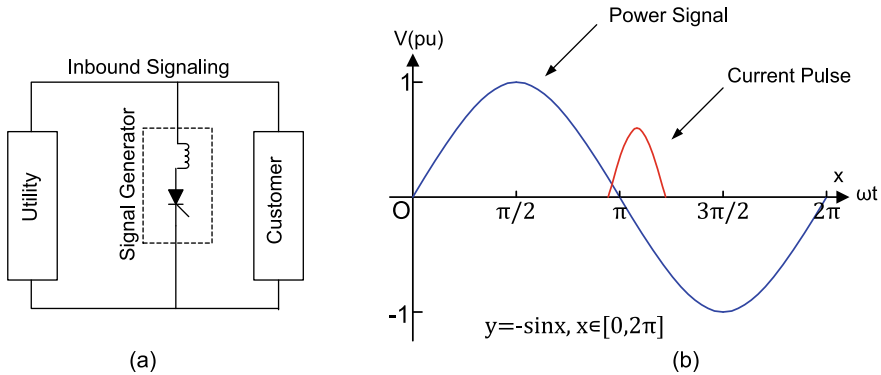


Fig. 4 **a** Power electronic circuit to create current pulse near zero crossing point of voltage waveform. **b** Resultant waveform

Due to this short-circuit, a current pulse is drawn from the power supply, which the utilities can detect as an information signal.

- c. Ripple signalling technique: A ripple signal is a high-frequency signal superimposed in the carrier signal of frequency 50 Hz or 60 Hz. This signalling technique based on ripple control is commonly used in PLC. The ripple control can be carried out using electronic or power electronics-based circuit [13]. The ripple signal produces a distortion in the voltage waveform. By analyzing this distortion, the original communication signal can be retrieved. Some of the ripple based technique is proposed in [16–18].
- d. Summary: For smart metering infrastructure or AMI, narrowband PLC can be used [19]. For data transfer from SG controllers to a home network, broadband PLC can be used [3]. For SG ecosystems, technologies like Internet-of-Things (IoT) can be used along with PLC technology to improve the grid’s overall performance. This kind of integration helps to deploy automation strategies more smoothly [2]. Powerline channel modelling is challenging since the communication channel can be affected by external factors such as noise, emissions, impedance alterations etc. [3]. Therefore, a lot more focus is required in channel modelling for PLC. Some of the proposed research work in this area is reported in [20–22].

3.2 Wireless Communication in Smart Grid

There are many advantages of using wireless technology over wired communication, such as less installation cost, mobility, and fast deployment. One of the benefits of using wireless technology is the remote end application [3]. In the earlier stages of SG development, wireless technology is not considered for two way communication

because of low data rates and limited bandwidth. But, for the recent scenario, with more mature wireless communication technology, it can be used effectively for SG application. Following wireless methods of communication can be used for two way communication in SG:

- a. **Wireless Mesh Network (WMN):** The critical components of WMN are mesh routers and mesh clients. These routers and clients are the nodes for the communication network, and are connected through a wireless network. This network can dynamically configure and organize the required ad-hoc networks responsible for connectivity with all other nodes [23]. Some of the reported benefits [3] of using WMN technology are mentioned below:
 - I. **Improved communication channel reliability:** The WMN network has some redundant paths for communication. These paths become useful when some problems like path failure or node failure arise in the system. Consequently, the reliability of the communication network will improve.
 - II. **Aids automation in SG:** As already mentioned, WMN mesh routers can self-configure and self-organize the required ad-hoc network which connects all the nodes. Therefore, the automation process needed for the SG ecosystem becomes smooth with WMN.
 - III. **High data transfer rate:** Wireless broadband communication like WiMAX based on IEEE:802.16 standards, can be used for transferring data at a high rate and over long distances. The basic architecture of WMN is shown in Fig. 5.
- b. **Cellular communication system:** This technology is widely used in the telecom sector. The main reason for using a cellular network is its mature technology which is improving further with time. For SG paradigm, cellular technology can be useful. A survey is presented in [24], which discusses the role of cellular network in Neighborhood Area Network (NAN). In the case of the power distribution network, an LTE-based communication standard can be beneficial. The advantages of using LTE-based communication network are Quality of Service (QoS), broad coverage, and low latency [24]. The LTE network is originally designed for Human Type Communication (HTC) which is different from the type of communication carried out in the SG paradigm. Also, there are limited numbers of users connected to the base station in the case of HTC. On the other hand, the number of nodes that generates and sends the data to the base station is relatively large for SG application. Consequently, the LTE technology needs modification for future SG [24]. Since the deployment of 3G (3rd generation) cellular technology in 2001, the data transfer rate has significantly improved in a cellular network. The data used in 3G technology is digital broadband packet data which operates on the spectrum range of 824–894 MHz [25]. The data transmission rate can go up to 2 Mbps. The 3G technology is based on WCDMA, UMTS, CDMA 2000, while the subsequent 4G (4th generation) cellular technology uses MiMAX or LTE. The frequency range is from 850 to 2600 MHz, and the maximum speed up to 100 Mbps is attainable. In recent advancement,

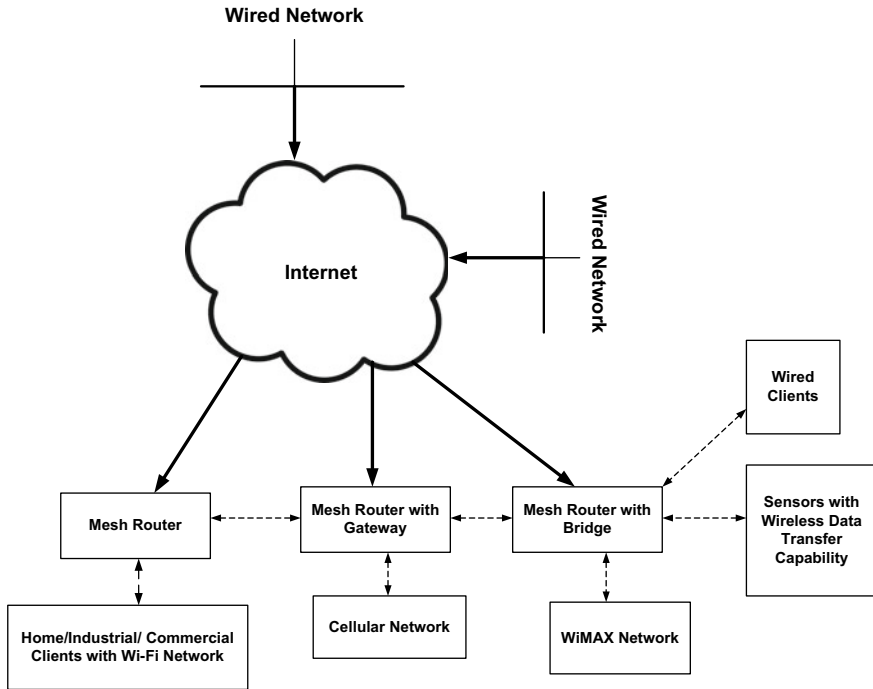


Fig. 5 Architecture of WMN network

5G (5th generation) cellular technology is ready for SG application deployment. This 5G network has added advantage of low latency, less call dropout rates, and speed up to 10 Gbps with a frequency range of 3–90 GHz [26]. The main drawbacks of using the cellular network for SG application are the call drop out the problem, which can affect the data transferred. Also, the monthly charges for cellular service may be costly for data transfer on a regular basis [25]. WMN and cellular networks are used for NAN or Field Area Network (FAN).

For Home Area Network (HAN) or Building Area Network (BAN) or Industrial Area Network (IAN), the following wireless technologies can be used.

1. ZigBee: ZigBee Alliance designed this technology for radio-frequency applications. The main features of this technology are reliability, security and cost-effectiveness. It is compatible with the IEEE 802.15.4 standard and is mostly used in the customer domain for communication. Additionally, this technology can be used for information transfer through smart meters [3]. ZigBee uses DSSS modulation technique to operate in the frequency range of 868 MHz, 915 MHz and 2.4 GHz [25]. The data rate through ZigBee technology is of range from 20–50 kbps.
2. Wireless Local Area Network (WLAN): This network follows the IEEE 802.11 standard. The main features of this technology are high data rate, which can be

up to 150 Mbps, low latency, and a coverage range of 250 m [27]. Different data rates are obtained according to the applications based on standards IEEE 802.11a, IEEE 802.11g and IEEE 802.11i. WLAN technology can be used for substation automation applications that use IEC 61850 protocol for two-way communication with respect to SG paradigm. WLAN technology in the distribution network in the presence of DER can play a crucial role in monitoring and controlling the grid, which is equipped with smart sensors and IEDs. The main challenge in deploying WLAN technology for smart grid is the interference problem with other communication networks and electromagnetic interference in high voltage applications.

Other modes of communications:

- a. Satellite communication: Satellite communication can be cost-effective in scenarios where the monitoring and control need to be done through remote substation [3]. In [28], the authors showed a cost-effective communication method for remote generation deployment application. This cost-effective solution can be obtained by minimizing data transmission through satellite and maximizing telemetry data [28].

Although satellite communication may provide economical solutions for some scenarios, it can't act as a primary data transmission network for the smart grid. The primary reason for the same is the delay in data transmission when compared to terrestrial communication. So, the more feasible prospect is to keep the satellite communication channel as a backup network. In case of faults in the terrestrial network, this backup network takes over, ensuring good reliability of the communication system.

- b. Microwave communication: This kind of communication technology is used in SG as a backhaul network between power generation and power distribution control centres. For the SG application, a medium-haul to long haul communication microwave band can be used, which has a frequency range of 3–15 GHz. For point-to-point communication, microwave technology has the advantage of high bandwidth, and the antenna size requirement is also feasible. This technology is useful for communication in remote areas [3]. Microwave communication is a line of sight communication technology which means obstacles in the path can distort the communication signal.

4 Smart Grid Standards

Standards are written agreements which are prepared by experts of respective fields. Standards contain technical specifications or other criteria that can be used to operate a system or perform specific tasks. There are rules, guidelines and definitions associated with each standard which are essential for better understanding and smooth operation of the system. Standards ensure the delivery of any product or service in a consistent and harmonized way.

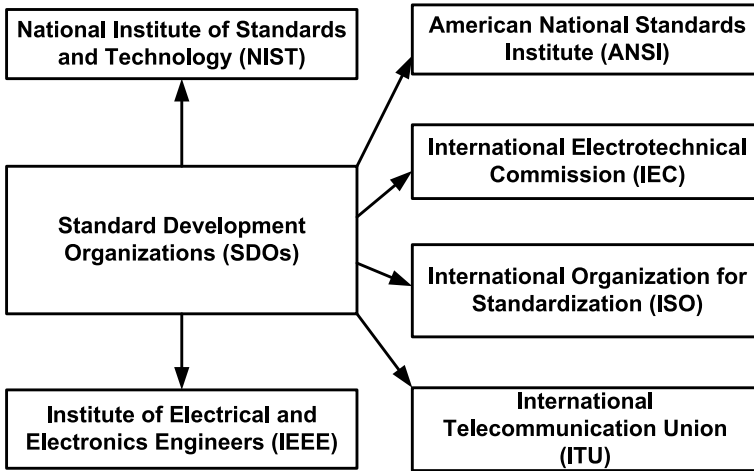


Fig. 6 Major standards development organizations

In the SG paradigm, the communication elements, monitoring elements, protection elements and control elements must have some rules, guidelines and specifications for their smooth operation. The presence of DER in the smart grid also need some standard aspects such as rules for its connection and disconnection, rules for maintaining its characteristics, guidelines for power supply through DER, guidelines for maintaining electrical constraints at the point of common coupling. Similarly, the communication system, which is the backbone of the SG's ecosystem must have proper rules, guidelines and definitions for data transfer among various components of the power system.

There are various Standards Development Organizations (SDOs) present, which are responsible for drafting, maintaining, and updating the standards with experts' help. Some major organizations are shown in Fig. 6.

In the SG paradigm, based on the field of interest, various standards have been approved by SDOs which are shown in Fig. 7.

Various standards for a different type of communication network are listed in Table 2.

Some of the standards related to smart grid are discussed below:

1. IEEE 1547: The criteria and requirements for interconnection of DER with the electricity grid are documented in this standard. This standard also provides the guidelines for interoperability and smooth operation, testing, safety, and maintenance requirements. IEEE 1547 has amended over the years since it was first published in 2003. The IEEE 1547 series of standards provides information about the test procedure (IEEE 1547.1), application guide (IEEE 1547.2), monitoring, exchange of information and control (IEEE 1547.3), a guide for design, operation and integration of DER (IEEE 1547.4), recommended practice for interconnecting DER with secondary distribution network (IEEE 1547.6).

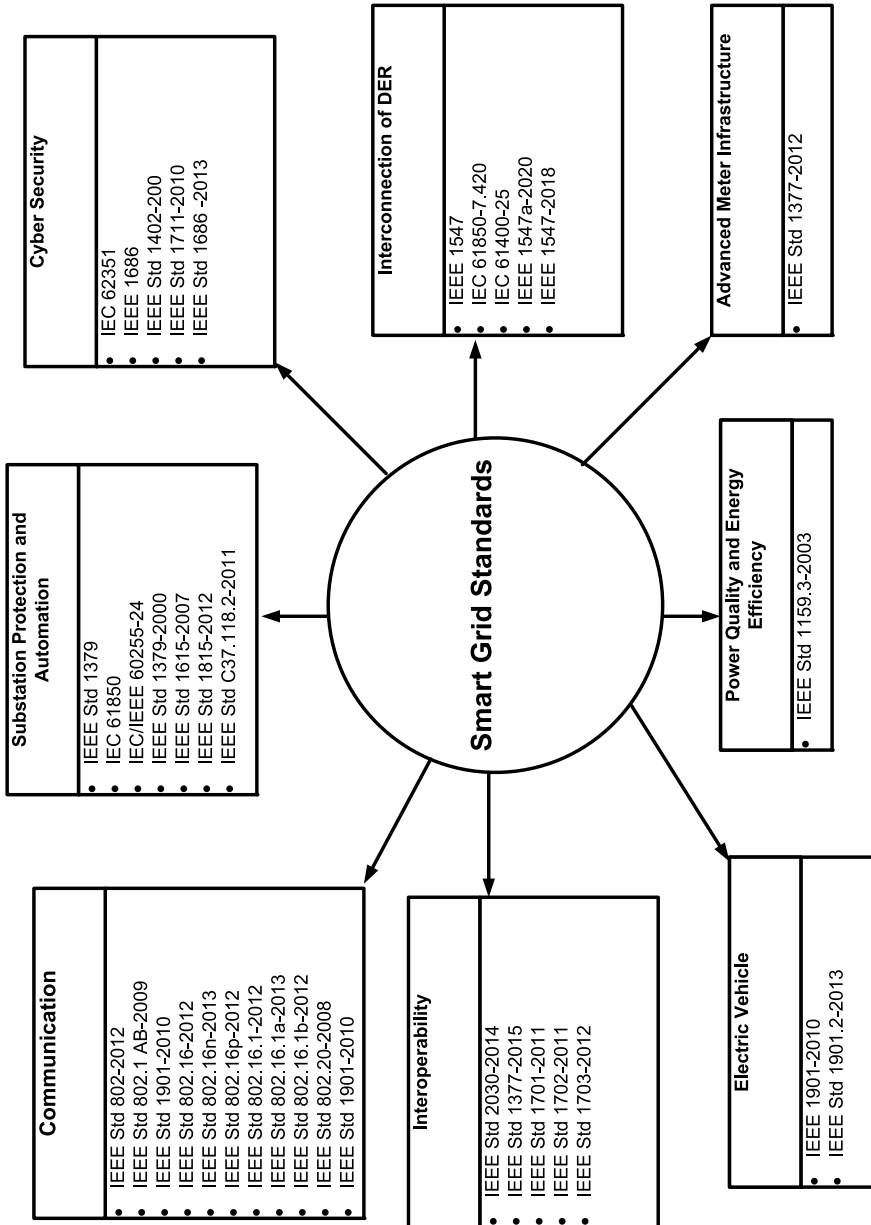


Fig. 7 Various approved standards for smart grid applications

Table 2 Standards related to different type of communications in smart grid

Network type	Range	Data rate	Standards	
			Wireless communication	Wired communication
HAN/BAN/IAN	1–100 m	1–100 kbps	IEEE 802.11 IEEE 802.15.4	IEEE 802.1 IEEE 802.3 IEEE 1901 IEEE 1901.2 IEEE 1905.1
Smart meters	–	–	IEEE SC31 (1377,1701,1703,P1704)	
NAN/FAN	100 m–10 km	100 kbps–10 Mbps	IEEE 802.11 IEEE 802.15.4 IEEE 802.16	IEEE 802.1 IEEE 802.3 IEEE 1901
WAN	10–100 km	10 Mbps–1 Gbps	IEEE 802.16d/e IEEE 802.20 IEEE 802.22	IEEE 802.1 IEEE 802.3
Substation	–	–	LAN IEEE 1815 IEC 61850	

2. IEEE C37.118-2005: This standard defines the method for evaluation of PMU data. The error in the synchrophasor data is calculated in terms of Total Vector Error (TVE), and this standard provides the guidelines for maximum permissible TVE in steady-state scenarios. IEEE C37.118 is spitted into two parts; IEEE C37.118.1 defines synchrophasor measurements under steady-state as well as under dynamic conditions. The frequency measurement and rate of change of frequency measurement techniques and guidelines are also defined in this standard. IEEE C37.118.2 defines the method for exchanging real-time synchronized PMU data among various types of power system equipment.
3. IEEE 802 series of standards: IEEE 802 consists of a series of standards that cover the system’s networking aspects. In SG, where wireless communication is important for data exchange, these set of standards play a crucial role. IEEE 802 series covers specifications related to LAN and Metropolitan Area Network (MAN). The protocols for the data-link layer and physical layer are defined in IEEE 802 series of standards. Protocols for LAN (IEEE 802.1), Ethernet (IEEE 802.3), wireless PAN (IEEE 802.15), vehicular mobility (IEEE 802.20-2008), wireless MAN (IEEE 802.16.1-2012), along with some other essential protocols are defined in IEEE 802 series.

5 Challenges in Smart Grid Communication

The major challenges for SG communication are as follows:

5.1 Active Control Challenges

Modern grid is getting more complex with time as more loads with different characteristics are added to the network. DERs are deployed in large numbers across the distribution grid to manage these loads and maintain the system's reliability. The DERs or the micro-grids need proper controlling as the two way power flow can be dangerous if not handled properly. Intelligent controllers are required for managing the power flow through micro-grids. These controllers need to perform tasks in full coordination with other controllers and de-centralized control stations present in the network. It is a more practical approach to control the electricity network in a decentralized manner compared to a centralized one. To demonstrate the suitability of decentralized control, consider an example of fault event between bus A and bus B in the system shown in Fig. 8. In case of the centralized control scheme, for the fault event, to re-energize the load at bus B, any of the tie-switches T1 or T2 must be operated. The centralized control station will decide to operate the switch, and the overall procedure from decision making to deployment can be very time-consuming. On the other hand, with a decentralized control scheme, the intelligent controller associated with the DER will make a quick decision to close the switch S1 and feed the load with DER if sufficient power is available. The main drawback using a DG unit is the variable output characteristics and complicated grid integration procedure.

From the communication perspective, the connectivity among these intelligent controllers is essential for proper coordination [29]. Most of the controlling is required for real-time decision making. Therefore, the data transfer rate and the bandwidth must be optimum. The connectivity is also needed between intelligent controllers and the sensors which are deployed in the network. The health of the sys-

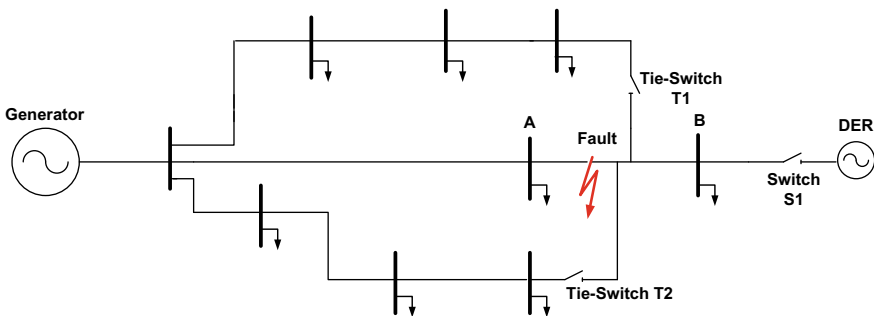


Fig. 8 Test system to demonstrate effectiveness of de-centralized control scheme

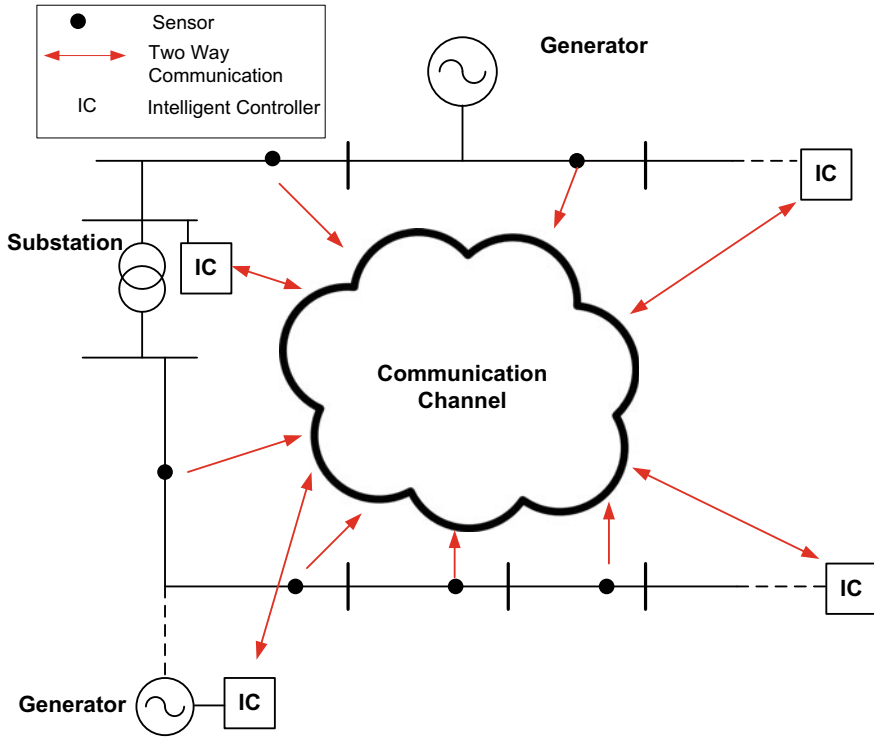


Fig. 9 Communication network for active controlling in distribution grid

tem, as well as the corrective action required in case of fault event, can be predicted from the data collected through sensors. Therefore, more number of sensors with reliable data transfer network is also needed for the SG. Figure 9 shows a typical communication network for active controlling in the distribution grid.

5.2 Cyber-Security

Data exchange in SG paradigm is very frequent. The data generated by sensors, smart meters and PMUs may contain critical information about the customer and the grid. This data can be easily misused by hackers, resulting in the breach of customer privacy and compromise grid security. There are four basic criteria for information security in the SG [30].

1. Confidentiality: The customer data or the propriety information must remain confidential. This means only authorized personnel can access this data. All the information collected by the sensors or other measuring devices must be used by only the utility in the grid. It must not be disclosed to any other unauthorized

person or organization. The data exchange or the information transfer must be done through the proper channel in a lawful manner. The critical data related to the customer or the grid can be used for malicious purpose.

2. **Availability:** The data in the grid must be available in a timely manner since this information exchange is necessary for most of the control operations in the grid. If due to some reason if any critical information is missing, then smooth operation of the grid can be obstructed. Therefore, the operator needs to ensure a consistent flow of data in the grid's communication network.
3. **Integrity:** The data obtained from the measurement devices must be transferred entirely without any modifications. The data must be genuine and it must not be altered at any stage by any unauthorized individual or entity. For instance, in the conventional grid, electromechanical meters are used for registering the amount of electricity consumed by a household or an industry. In this setup, it is a common practice in developing countries to alter the reading of the energy meters to pay a reduced amount of bill to the utility. This is a typical example when the integrity of information is compromised. In SG paradigm, with smart meters, the hackers are regularly trying to take control over the network server so that they can manipulate data for their own personal gains. Also, this activity is not limited to the customer domain but also other domains with vulnerabilities which are prone to attacks and can lead to serious issues in the grid's operation.
4. **Accountability:** The activities of authorized person responsible for collecting or monitoring data exchange is recorded, so that any unauthorized exchange of information can be easily tracked. This kind of practice in the SG is necessary so that the person-in-charge dealing with critical data can be held accountable for his/her unauthorized actions.

There are four steps in which any hacker tries to attack and control the SG [31]. The first step is called reconnaissance, in which the attacker attempts to gather all the information related to the target. In this step, the attackers will do traffic analysis and try different authorized and unauthorized sources for collection of information about the system [30]. The next step is the scanning; in this move, the attacker attempts to find and analyze the system's vulnerabilities. The attacker tries to collect information related to IPs, ports and services of the system. The third step is the exploitation stage. The attackers try to take control of the system using the vulnerabilities and weaknesses of the system. The type of activities the attacker tries to do is to violate integrity and privacy in the system, try to various channels, and try to inject viruses and Trojan in the system [30]. The final step is to maintain the access of the system; the attacker tries to gain permanent control of the system once the security is breached.

5.2.1 Countermeasures to Cyberattacks

In [30], the authors have proposed a three-step cyber security process.

1. **Pre-attack:** In this phase, the authorized persons and organizations take the appropriate step to upgrade the existing system's security. It can be achieved by iden-

tifying the vulnerabilities of the system. Different components and resources of the system prone to attacks are identified and recommended security measures are implemented to further enhance safety. The pre-attack countermeasures are divided into three parts:

- I. Network security: For network security, firewalls can provide a primary layer of protection, but this layer is relatively weak and can be easily bypassed by many attackers. Therefore, the firewall that allows or denies the connection in a network must be associated with other security features. Intrusion Detection System (IDS), Network Data Loss Prevention (DLP), Security Information and Event Management Systems (SIEM) are some technologies which can be used with firewall [29].
 - II. Cryptography technique: These techniques can ensure the exchanged information's confidentiality and integrity by encryption methods. The encryption can be of a single-key type, where a single key is used to encrypt and de-encrypt the information or it can be two-key encryption where separate private and public keys are used for encryption and de-encryption. For power system applications, various key management frameworks are proposed. For SCADA system, single-key, key establishment scheme, key management architecture, and advanced key management architecture are proposed.
 - III. Device security: The SG components are interconnected; therefore, any weak link in the system may compromise the security of the whole system. So, performing regular configuration checks and other security checks becomes utmost important. An additional system can be created to regularly check the devices and equipments for weakness regarding cyber-security to perform such a task.
2. Under-attack: This step comprises two parts, (1) detect the attack: in this phase, the concerned authority will try to detect the identity of the attacker, determine the severity of the attack and identify part of the system or network where actually the attack has been done. Part (2): deployment of countermeasure strategies against the attack, which include pushback and reconfiguration methods. In the pushback method, the network administrator will block all the incoming traffic so that attacker loses all the unauthorized control. In the reconfiguration method, the network topology is changed which is required to isolate the attacker. Also, some anti-jamming methods can be employed as countermeasures.
 3. Post-attack: In this step, the attacks are analyzed to protect the grid from any malicious activity in future. An investigation is carried out to find the system's weakness, the virus and Trojan details used in the attack, cyber-security loopholes, the leaked information and the attacker details. Furthermore, based on the collected information, the current security database is updated to prevent future attacks.

5.3 Data-Loss Problem and Mitigation Techniques

In the SG, the data can be lost or distorted during transmission due to various reasons, such as radio interference, hardware or software malfunctioning, less bandwidth availability for data transmission. This data loss problem can compromise the integrity and availability aspects of information in the grid. Therefore, the data loss problem must be resolved promptly. Some of the data loss mitigation techniques involve improving the communication network's reliability by performing regular inspection of hardware and software involved in information exchange by increasing the bandwidth of the wireless communication channel so that data congestion can be avoided and some mathematical techniques can also be used for reconstruction of lost signal in SG.

In [32], the authors proposed a compressive sensing based technique to reconstruct the synchrophasor data obtained through the PMUs. The compressive sensing based technique can also be used to compress the data without compromising its integrity. Consequently, the bandwidth requirement also gets reduced if the data is appropriately compressed without the loss of any information [33]. In the compressive sensing based method, the signal from PMU or the synchrophasor data is made sparse by applying discrete wavelet transform and thresholding techniques. The obtained samples are encoded at the sending end before their transfer over the communication channel in the next step. When the samples are received at the receiving end, then l_1 optimization method followed by inverse wavelet transform is applied to get the reconstructed signal.

To find the error in the reconstruction process, TVE and Frequency Error (FE) are calculated. TVE is given as:

$$TVE(n) = \sqrt{\frac{(X_{real}(n) - \tilde{X}_{real}(n))^2 + (X_{img}(n) - \tilde{X}_{img}(n))^2}{(X_{real}(n))^2 + (X_{img}(n))^2}} \quad (1)$$

$$FE = |f - \hat{f}| \quad (2)$$

where $n = 1, 2, 3 \dots N$, X and \hat{X} represents synchrophasor value and reconstructed value respectively. f is the original frequency signal and \hat{f} is reconstructed frequency signal.

The TVE and FE obtained by the compressive sensing method is less than 1% [33], which is within limits prescribed in the IEEE C37.118-2005 standard.

6 Conclusion

The electricity grid is becoming more complex with time; the primary reasons for the same are increased DG penetration, variable load characteristics and dynamic electricity market structure. The need for proper coordination among various components of the grid is of utmost importance. Interoperability is the key for the SG's smooth operation, which requires reliable and secures two-way communication channel for smooth information flow among the grid components. For better management, the SG is divided into different domains: generation, transmission, distribution, market, operations, service and customer domain. Each domain is guided by specific rules and is assigned with different responsibilities. Various standards and protocols are managing this SG system. These standards are essential for the proper operation of the grid. For example, there are standards defined for running various grid activities like connecting DERs in the grid, operating the grid's communication system, maintaining security aspects of the grid, etc. These standards ensure the proper delivery of the service along with the economical operation of various components of the grid. The communication channel is prone to multiple cyber-attacks. Therefore, various provisions are being made and updated in a timely manner to tackle security problems.

References

1. Nafi NS, Ahmed K, Gregory MA, Datta M (2016) A survey of smart grid architectures, applications, benefits and standardization. *J Netw Comput Appl* 76:23–36. <https://doi.org/10.1016/j.jnca.2016.10.003>
2. Kabalci E, Kabalci Y (eds) (2019) Smart grids and their communication systems. Springer, pp 18–19. <https://doi.org/10.1007/978-981-13-1768-2>
3. Fang X, Misra S, Xue G, Yang D (2011) Smart grid—the new and improved power grid: a survey. *IEEE Commun Surv Tutor* 14(4):944–980. <https://doi.org/10.1109/SURV.2011.101911.00087>
4. Greer C, Wollman DA, Prochaska DE, Boynton PA, Mazer JA, Nguyen CT et al (2014) NIST framework and roadmap for smart grid interoperability standards, release 3.0. <https://doi.org/10.6028/NIST.SP.1108r3>
5. Agency IE (2002) Distributed generation in liberalised electricity markets. <https://doi.org/10.1787/9789264175976-en>
6. Li F, Qiao W, Sun H, Wan H, Wang J, Xia Y, Zhang P (2010) Smart transmission grid: vision and framework. *IEEE Trans Smart Grid* 1(2):168–177. <https://doi.org/10.1109/TSG.2010.2053726>
7. Jiang Y, Liu CC, Xu Y (2016) Smart distribution systems. *Energies* 9(4):297. <https://doi.org/10.3390/en9040297>
8. Souryal M, Gentile C, Griffith D, Cypher D, Golmie N (2010) A methodology to evaluate wireless technologies for the smart grid. In: 2010 first IEEE international conference on smart grid communications, Oct 2010. IEEE, pp 356–361. <https://doi.org/10.1109/SMARTGRID.2010.5622067>
9. Gore RN, Valsan SP (2018) Wireless communication technologies for smart grid (WAMS) deployment. In: 2018 IEEE international conference on industrial technology (ICIT), Feb 2018. IEEE, pp 1326–1331. <https://doi.org/10.1109/ICIT.2018.8352370>

10. Lampe L, Tonello AM, Swart TG (eds) (2016) Power line communications: principles, standards and applications from multimedia to smart grid. Wiley. <https://doi.org/10.1002/9781118676684>
11. Ahmed MO, Lampe L (2013) Power line communications for low-voltage power grid tomography. *IEEE Trans Commun* 61(12):5163–5175. <https://doi.org/10.1109/TCOMM.2013.111613.130238>
12. Galli S, Scaglione A, Wang Z (2011) For the grid and through the grid: the role of power line communications in the smart grid. *Proc IEEE* 99(6):998–1027. <https://doi.org/10.1109/JPROC.2011.2109670>
13. Xu W, Wang W (2010) Power electronic signaling technology—a new class of power electronics applications. *IEEE Trans Smart Grid* 1(3):332–339. <https://doi.org/10.1109/TSG.2010.2066293>
14. Mak ST, Moore TG (1984) TWACSTM, a new viable two-way automatic communication system for distribution networks. Part II: inbound communication. *IEEE Trans Power Appar Syst* 8:2141–2147. <https://doi.org/10.1109/TPAS.1984.318524>
15. Mak ST (1984) A new method of generating TWACS[®] type outbound signals for communication on power distribution networks. *IEEE Trans Power Appar Syst* 8:2134–2140. <https://doi.org/10.1109/TPAS.1984.318523>
16. Foord PM (1989) U.S. Patent No. 4,868,539. U.S. Patent and Trademark Office, Washington, DC. <https://patents.google.com/patent/US4868539/en>
17. Galloway JH, Berman AM (1980) U.S. Patent No. 4,215,394. U.S. Patent and Trademark Office, Washington, DC. <https://patents.google.com/patent/US4215394>
18. Hunt PC (2000) Low frequency bilateral communication over distributed power lines. United States Patent No. US6154488A. <https://patents.google.com/patent/US6154488A/en>
19. Rieken DW, Walker MR II (2011) Ultra low frequency power-line communications using a resonator circuit. *IEEE Trans Smart Grid* 2(1):41–50. <https://doi.org/10.1109/TSG.2010.2099674>
20. Konate C, Kosonen A, Ahola J, Machmoum M, Diouris JF (2008) Power line channel modelling for industrial application. In: 2008 IEEE international symposium on power line communications and its applications, Apr 2008. IEEE, pp 76–81. <https://doi.org/10.1109/ISPLC.2008.4510402>
21. Meng H, Chen S, Guan YL, Law CL, So PL, Gunawan E, Lie TT (2004) Modeling of transfer characteristics for the broadband power line communication channel. *IEEE Trans Power Deliv* 19(3):1057–1064. <https://doi.org/10.1109/TPWRD.2004.824430>
22. Zimmermann M, Dostert K (2002) Analysis and modeling of impulsive noise in broad-band powerline communications. *IEEE Trans Electromagn Compat* 44(1):249–258. <https://doi.org/10.1109/15.990732>
23. Akyildiz IF, Wang X (2005) A survey on wireless mesh networks. *IEEE Commun Mag* 43(9):S23–S30. <https://doi.org/10.1109/MCOM.2005.1509968>
24. Kalalas C, Thrybom L, Alonso-Zarate J (2016) Cellular communications for smart grid neighborhood area networks: a survey. *IEEE Access* 4:1469–1493. <https://doi.org/10.1109/ACCESS.2016.2551978>
25. Parikh PP, Kanabar MG, Sidhu TS (2010) Opportunities and challenges of wireless communication technologies for smart grid applications. In: IEEE PES general meeting, July 2010. IEEE, pp 1–7. <https://doi.org/10.1109/PES.2010.5589988>
26. Sofana RS, Dragičević T, Siano P, Prabaharan S (2019) Future generation 5G wireless networks for smart grid: a comprehensive review. *Energies* 12(11):2140. <https://doi.org/10.3390/en12112140>
27. Mahmood A, Javaid N, Razaq S (2015) A review of wireless communications for smart grid. *Renew Sustain Energy Rev* 41:248–260. <https://doi.org/10.1016/j.rser.2014.08.036>
28. Deep UD, Petersen BR, Meng J (2009) A smart microcontroller-based iridium satellite-communication architecture for a remote renewable energy source. *IEEE Trans Power Deliv* 24(4):1869–1875. <https://doi.org/10.1109/TPWRD.2009.2028803>

29. Bouhafis F, Mackay M, Merabti M (2014) Communication challenges and solutions in the smart grid. Springer. <https://doi.org/10.1007/978-1-4939-2184-3>
30. El Mrabet Z, Kaabouch N, El Ghazi H, El Ghazi H (2018) Cyber-security in smart grid: survey and challenges. *Comput Electr Eng* 67:469–482. <https://doi.org/10.1016/j.compeleceng.2018.01.015>
31. Knapp ED, Samani R (2013) Applied cyber security and the smart grid: implementing security controls into the modern power infrastructure. Newnes. <https://doi.org/10.1016/C2012-0-01113-1>
32. Srivastava I, Bhat S, Singh AR (2020) Fault diagnosis, service restoration, and data loss mitigation through multi-agent system in a smart power distribution grid. *Energy Sources Part A Recov Util Environ Eff* 1–26. <https://doi.org/10.1080/15567036.2020.1817190>
33. Thadikemalla VSG, Srivastava I, Bhat SS, Gandhi AS (2020) Data loss mitigation mechanism using compressive sensing for smart grids. In: 2020 IEEE international conference on power electronics, smart grid and renewable energy (PESGRE2020), Jan 2020. IEEE, pp 1–6. <https://doi.org/10.1109/PESGRE45664.2020.9070414>

Comparison of Selected MPPT Techniques Using Different Performance Features



Salauddin Ansari and Om Hari Gupta

Abstract In the last few decades, the tendency and necessity to drift towards renewable sources of energy for power generation have captivated scientists moving to photovoltaic (PV) systems. Since the characteristics of the PV generator is non-linear and its output power changes with solar irradiance and atmospheric temperature, the need for advanced maximum power point tracking (MPPT) technique has always been fascinated. To withdraw the highest power from the PV generators, MPPT is essential. So, to extract the highest power from the photovoltaic generator, even in general situations, maximum power point tracking methods namely perturb and observe, incremental conductance, and temperature control methods are simulated in MATLAB/Simulink. Different parameters of solar energy conversion system—obtained using different algorithms—are compared for different temperatures and irradiances.

Keywords Maximum power point tracking · Perturb and observe · Incremental conductance · Temperature control · Duty ratio

Nomenclature

PV	Photovoltaic
MPPT	Maximum Power Point Tracking
SECS	Solar Energy Conversion System
PO	Perturb and Observe
IC	Incremental Conductance
TC	Temperature Control
MSE	Mean Square Error
FF	Fill Factor
IR	Solar Irradiance

S. Ansari · O. H. Gupta (✉)

Department of Electrical Engineering, National Institute of Technology Jamshedpur, Jamshedpur, Jharkhand, India

T	Temperature
d	Duty ratio
MPP	Maximum Power-Point
Δd	Incremental duty ratio
ΔV	Ripple in PV Voltage
ΔP	Ripple in PV Output Power
t_{dpo}	Delay time for PO algorithm
t_{dic}	Delay time for IC algorithm
t_{dtc}	Delay time for TC algorithm
t_{rpo}	Rise time for PO algorithm
t_{ric}	Rise time for IC algorithm
t_{rtc}	Rise time for TC algorithm
t_{ppo}	Peak time for PO algorithm
t_{pic}	Peak time for IC algorithm
t_{ptc}	Peak time for TC algorithm
E_{ppo}	MSE of PV output power for PO algorithm
E_{pic}	MSE of PV output power for IC algorithm
E_{ptc}	MSE of PV output power for TC algorithm
E_{vpo}	MSE of PV voltage for PO algorithm
E_{vic}	MSE of PV voltage for IC algorithm
E_{vtc}	MSE of PV voltage for TC algorithm
E_{ipo}	MSE of PV current for PO algorithm
E_{iic}	MSE of PV current for IC algorithm
E_{itc}	MSE of PV current for TC algorithm
FF_{po}	Fill factor for PO algorithm
FF_{ic}	Fill factor for IC algorithm
FF_{tc}	Fill factor for TC algorithm
η_{ipo}, η_{opo}	Input and Overall efficiency for PO algorithm
η_{iic}, η_{oic}	Input and Overall efficiency for IC algorithm
η_{itc}, η_{otc}	Input and Overall efficiency for TC algorithm

1 Introduction

One of the vast threats of the 21st era is the increasing risk of pollution and drop of energy surety for the upcoming generation. However, since the need for energy continues to increase day by day, we have to take measures and promote new technologies based on yielding energy from sources that are ample and do not endanger the environment. Due to the fullness and sustainability of the sun, solar energy is taking into consideration as one of the sustainable renewable sources at present and future [1–3]. With the advancement in material science, photovoltaic (PV) energy system efficiency continues increasing and the price constantly continues decreasing [4–7].

In addition to many benefits, such as easy installation, no pollution, and easy maintenance, the life of these systems is also very long [8, 9]. The technical improvements in the photovoltaic system have decreased the price and increased the solar energy conversion system (SECS) efficiency. There is still a long way to reach the desired level of energy generation. Some of the important studies to harvest a maximum of available power out of the PV system i.e., MPPT algorithms are included in this chapter.

The MPPT plays a very important role in solar power generation since it extracts maximum power output from its PV system for different atmospheric situations and thereby, maximizing the system's efficiency. In this way, MPPT can reduce the total cost of the entire system. The MPPT technique continuously searching the operating point corresponding to maximum power output and keep it at that point. Several MPPT techniques are introduced in the literature [10–12]. However, the perturb and observe (PO) and incremental conductance (IC) are the two specific methods and remain the most extensively used methods in commercial photovoltaic MPPT systems. Apart from these two, a temperature control (TC)-based MPPT method is also discussed in this chapter. The main emphasis of this study is the comparison of the aforementioned MPPT techniques for SECS by considering various features/parameters. These features/parameters are as follows:

- PV voltage and its ripple
- PV current and its ripple
- PV power and its ripple
- delay time, rise time, and peak time
- PV internal and overall efficiency
- mean square error (MSE)
- fill factor (FF).

The remaining chapter is formulated according to the following. Section 2 introduced the different parameters/terms related to SECS. Section 3 presents the working principle of SECS. Section 4 describes different MPPT techniques, Sect. 5 describes heuristic approaches of the MPPT Technique and then, in Sect. 6, results and discussions are included. Finally, the Conclusion is added to Sect. 7.

2 Different Parameters Related to SECS

- **Fill factor:** The fill factor (FF) is a figure of merit of PV cell. It tells how good or how bad a PV cell is. Figure 1 depicts the concept of fill factor. The FF is nothing but a ratio of maximum accessible power ($V_{mpp} \times I_{mpp}$) to the maximum theoretical power ($V_{oc} \times I_{sc}$). Mathematically, it can be written as given in (1).

$$FF = \frac{(V_{mpp} \cdot I_{mpp})}{(V_{oc} \cdot I_{oc})} \quad (1)$$

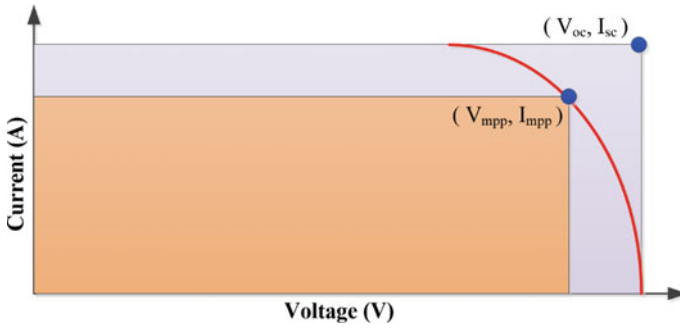


Fig. 1 Fill factor representation

- **MSE:** It is the mean of the squares of the errors—that is, the mean squared changes between the predicted value and the true value. Mathematically, MSE can be written as

$$MSE = \frac{1}{n} \sum_{i=1}^n (X_i - \hat{X}) \tag{2}$$

where n is the no. of samples of data points

X is the vector of true value

\hat{X} is the vector of the predicted value.

- **Delay time:** The delay time is termed as the amount of time needed for the response of a system to reach 50% of its final value within the first cycle of oscillation.
- **Rise time:** The rise time is termed as the amount of time needed for the response of a system to reach from 10% of its final value to 90% of its final value within the first cycle of oscillation.
- **Peak time:** The peak time is termed as the amount of time needed for the response of a system to reach its first peak.

Different times i.e., delay time (t_d), rise (t_r) and peak time (t_p) are depicted in Fig. 2.

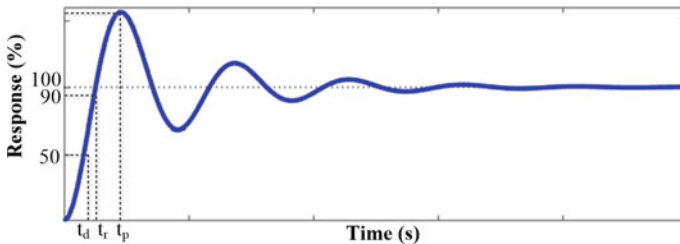


Fig. 2 Delay time (t_d), rise time (t_r), and peak time (t_p)

3 Working Principle of Solar Energy Conversion System

The Photovoltaic panels are made up of semiconductor material designed to transform solar irradiation into usable electrical energy. Since the solar irradiance (IR) and temperature (T) randomly changes throughout the day, the power output also changes. Figure 3 explains the concept of a solar energy conversion system that represents the block diagram of SECS which comprises of PV panel, MPPT controller, DC–DC boost converter connected through DC load R_L . When sun light falls on the PV panel, it generates PV voltage V_{pv} and current I_{pv} which has nonlinear relation as illustrated in Fig. 4. To withdraw the maximum available electrical power from the PV panel, an MPPT controller is employed. MPPT controller senses the PV voltage “ V_{sense} ” and current “ I_{sense} ” and next computes the optimum duty ratio (d) corresponding to the MPP which modifies the input impedance of boost converter.

Finally, the boost converter is cascaded with DC load, R_L to transfer power to the load R_L . The variations in PV current, power, and impedance with PV voltage are illustrated in Fig. 4, where slopes S_1 and S_2 represent the load lines—one corresponding to the fixed load impedance (S_1) and another corresponding to load impedance modulated by the boost converter (S_2). The slope S_1 will be equal to $1/R_L$ while slope S_2 will be $1/R_L(1 - d)^2$. If load “ R_L ” is directly coupled to the PV panel it may extract the power P_1 which is not the maximum available power. To the withdraw maximum power from the PV panel, the DC–DC boost converter is introduced between the PV panel and the load R_L which modulates the load impedance to $R_L(1 - d)^2$. Alternatively stated, the converter is shifting the operating point along the locus of maximum power point (MPP) and fixing the operating point at MPP. Hence, the maximum power “ P_{mpp} ” is extracted from the PV panel. From Fig. 4, it is clear that if we have to shift the operating point at MPP, the slope of the line should be decreased and the input impedance of converter $R_{in} = R_L(1 - d)^2$ should be increased. To increase R_{in} , d must be decreased, until the MPP is reached. After the measurement of voltage and current, the MPPT technique computes d so as to transfer maximum power to the load. The converter chosen can also be a boost, buck, or buck-boost converter, but in this chapter, a boost converter is employed, due to its greater efficiency and higher range control [13].

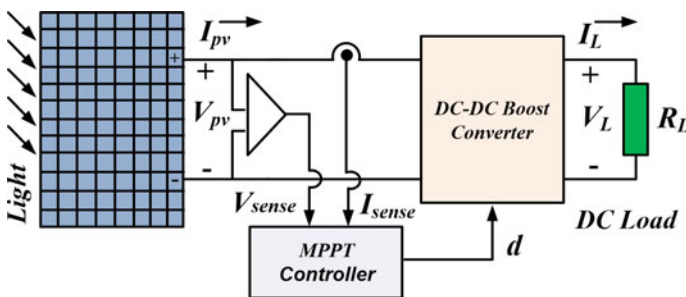
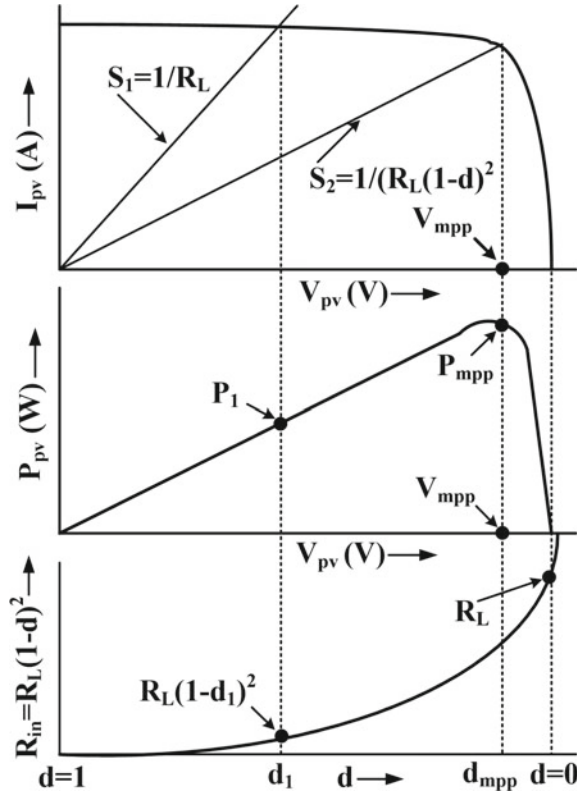


Fig. 3 Equivalent diagram of a SECS with MPPT

Fig. 4 Intersection between load line, current–voltage, and power–voltage curve



4 MPPT Techniques

Three MPPT techniques are included for comparative analysis and discussed next.

4.1 Perturb and Observe

The perturb and observe (PO) [14–19] technique is the most frequently used and discussed MPPT technique. In this method, initially, the PV output voltage $V(k)$ and current $I(k)$ are captured, and then PV output power $P(k) = V(k) \times I(k)$ is calculated. From calculated power and voltage, the change in PV output power “ ΔP ” and voltage “ ΔV ” are obtained as follows:

$$\Delta P = P(K) - P(K - 1) \tag{3}$$

$$\Delta V = V(K) - V(K - 1) \tag{4}$$

Now, if the changes in PV output power and voltage are zero i.e., $\Delta P = 0$ and $\Delta V = 0$, the algorithm returns to the start position. If the change in PV output power is negative i.e., $\Delta P < 0$, the change in voltage will be checked. Now, if $\Delta V < 0$, the operating voltage is increased else it will be decreased. While if the change in PV output power is not negative i.e., $\Delta P \geq 0$, the change in the voltage (ΔV) is checked, and if $\Delta V < 0$, the operating voltage is decreased else it will be increased. After shifting the operating voltage, the algorithm returns to the start position. The corresponding flow diagram is given in Fig. 5. The PO technique has two primary drawbacks. Initially, the value of perturbation given to the system is crucial and determines the amount of oscillations under steady-state at MPP. Besides, the speed of convergence of output power towards MPP is slower. The greater the perturbations, quickly the algorithm finds the MPP. However, greater perturbation results in a high value of oscillation at MPP.

At the same time, if the value of perturbation is too small, the oscillation about MPP will decrease, though the speed of convergence towards MPP will also decrease. This means that there will be a compromise among the speed of convergence and steady-state oscillations.

To resolve this drawback, the amount of perturbation may be decreased as it approaches towards the MPP—the same is proposed in [20, 21]. When the output power is far-off from the MPP, larger perturbations are used while smaller perturbations are used when the output power is closed to MPP. Overall, the amount of perturbations is selected based on the power–current curve slope. However, it results in complexity and a costly technique. Further, whenever the operating point of the system changes rapidly, the method can settle to an erroneous operating point. To resolve such drawbacks, different methods have been proposed [22, 23]. The key facts related to PO algorithm are:

- (a) Two sensors are required, one, for voltage and the other for current.
- (b) Slow rate of convergence to MPP.
- (c) It fails to follow MPP if the environmental conditions vary quickly.
- (d) Under steady-state, response will be oscillatory about the MPP.

4.2 Incremental Conductance

The IC [24–28] technique uses the slope of the power–voltage curve of the PV generator to track MPP. The slope of the power–voltage curve (Fig. 4) of the PV panel is zero at MPP. The slope will be positive if the PV output power is less than MPP and negative if the PV output power is more than MPP. Mathematically, can write the aforementioned discussion as given below in Eq. (5).

$$\left. \begin{aligned} \frac{dP}{dV} &= 0; \text{ at MPP} \\ \frac{dP}{dV} &> 0; \text{ left of MPP} \\ \frac{dP}{dV} &< 0; \text{ right of MPP} \end{aligned} \right\} \quad (5)$$

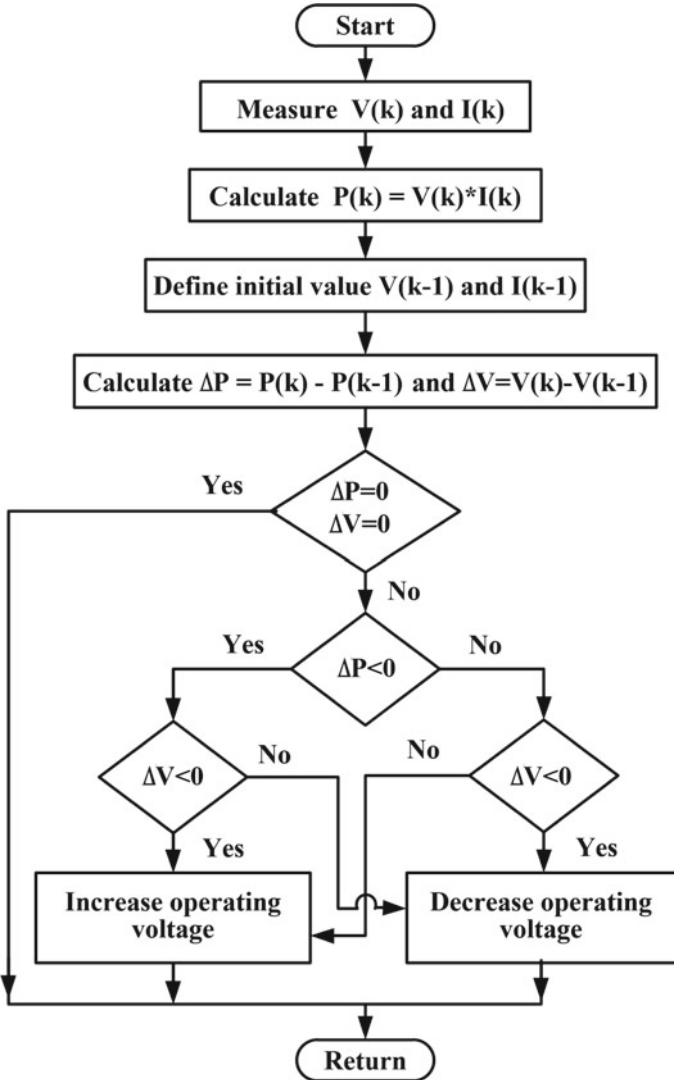


Fig. 5 Flow diagram of PO algorithm

For maximum output power, the PV output power differentiation with respect to voltage should be zero, i.e.:

$$\frac{dP}{dV} = \frac{d(VI)}{dV} = I + V \frac{dI}{dV} \cong I + V \frac{\Delta I}{\Delta V} = 0 \tag{6}$$

Equation (6) can be modified as given in (7) below.

$$\frac{\Delta I}{\Delta V} \cong \frac{-I}{V} \quad (7)$$

Now, Eq. (5) can be expressed as:

$$\left. \begin{aligned} \frac{\Delta I}{\Delta V} &= \frac{-I}{V}; \text{ at } MPP \\ \frac{\Delta I}{\Delta V} &> \frac{-I}{V}; \text{ left of } MPP \\ \frac{\Delta I}{\Delta V} &< \frac{-I}{V}; \text{ right of } MPP \end{aligned} \right\} \quad (8)$$

Thus, it is possible to detect whether the PV generator is working at MPP, left of MPP, or right of MPP. So, as per Eq. (8), the MPP can be tracked by comparing instantaneous conductance (I/V) with the incremental conductance ($\Delta I/\Delta V$). The flow diagram of the IC method is given in Fig. 6. Initially, PV output voltage $V(k)$ and current $I(k)$ are captured. Then the initial and old values of voltage and current are updated. From the captured voltage and current, ΔV is determined as given in (4) and ΔI is determined as given in Eq. (9) below.

$$\Delta I = I(K) - I(K - 1) \quad (9)$$

Now, if the change in PV output voltage is zero i.e., $\Delta V = 0$, the change in the current ΔI is to be checked, and if $\Delta I = 0$, the algorithm returns to the start position. If $\Delta I > 0$, the operating voltage is to be decreased else it is to be increased. While if PV output voltage is not zero i.e., $\Delta V \neq 0$, the change in ($\Delta I/\Delta V$) and instantaneous conductance ($I(k)/V(k)$) are checked and if $\Delta I/\Delta V = -I(k)/V(k)$, the algorithm returns to the start position. If $\Delta I/\Delta V > -I(k)/V(k)$, the operating voltage is increased else it will be decreased. The speed of tracking the MPP depends upon the amount of change in the magnitude of operating voltage. If increment or decrement in operating voltage is large, the algorithm tracks the MPP faster but the system cannot remain at MPP but oscillates around it. If the size of increment or decrement in operating voltage is too small, the response becomes slower but the oscillations close to MPP are lesser. So, again, there is a compromise between the speed of convergence and oscillations. There are mainly two advantages of this algorithm, first, it gives effective results even during the rapid change in atmospheric conditions. Second, it has low oscillations about MPP as compared to the PO algorithm. The main drawback of this technique is that it requires complex control circuitry. The key facts related to this algorithm are:

- (a) Two sensors are required—one for voltage another for current.
- (b) More complicated than the PO algorithm.
- (c) Fast dynamic tracking regardless the atmospheric conditions.
- (d) Under steady-state, lesser oscillations about the MPP.

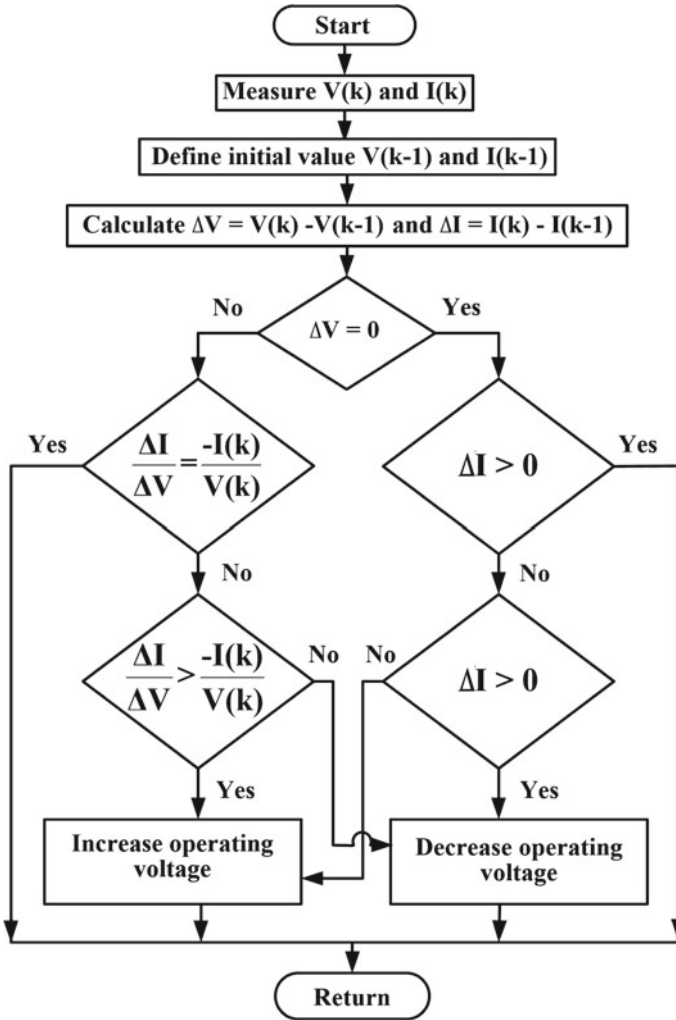


Fig. 6 Flow diagram of the IC algorithm

4.3 Temperature Control

The TC [29–31] technique is originated on the concept that the output voltage of the PV module depends on the surface temperature of the PV panel. The relation is described by Eq. (10) below [32].

$$V_{mpp}(T) = V_{mpp}(T_o) + \alpha_{V_{mpp}}(T - T_o) \tag{10}$$

$$\Delta d = [V - V_{mpp}(T)] S_{\Delta d} \tag{11}$$

$$d(k) = \Delta d + d(k - 1) \quad (12)$$

where

$V_{mpp}(T)$	MPP voltage at the measured temperature
$V_{mpp}(T_o)$	MPP voltage at a measured temperature from the datasheet
α_{Vmpp}	Temperature coefficient from the datasheet
T	Measured temperature
T_o	Reference temperature from the datasheet.

From Eq. (10), it is obvious that MPP voltage V_{mpp} relies on the measured temperature T because $V_{mpp}(T_o)$, α_{Vmpp} , and T_o are the datasheet information. The flowchart used to implement the TC technique is described in Fig. 7. First, the system starts to sense the PV output voltage V and PV module surface temperature T . With the help of measured temperature T , the optimized value of MPP voltage $V_{mpp}(T)$ is calculated from Eq. (10). Also, the incremental duty ratio (Δd) is proportional to the change in the actual PV module output voltage V and the desired MPP voltage $V_{mpp}(T)$ according to Eq. (11). Where constant $S_{\Delta d}$ is the step size of Δd and the value of $S_{\Delta d}$ decides the convergence rate of the technique. For a higher value of $S_{\Delta d}$, the algorithm tracks the MPP faster and for a smaller value of $S_{\Delta d}$, it tracks the MPP at a slower rate. Finally, to ensure the PV output voltage to be as near as possible to MPP voltage V_{mpp} , $d(k)$ is upgraded according to Eq. (12) which is the sum of the Δd and the previous value of duty ratio $d(k - 1)$. Now, $d(k)$ and minimum duty ratio (d_{min}) are compared and if the duty ratio is less than the minimum duty ratio i.e., $d(k) < d_{min}$, it is updated as $d(k) = d_{min}$ and then the algorithm returns to the start position. While if the duty ratio is greater than the maximum limit i.e., $d(k) > d_{max}$, it is again limited to d_{max} and then the algorithm returns to the start position. Else if the duty ratio is within the upper and lower limits, the algorithm returns to the start position.

Since the temperature on the PV panel changes gradually because of the thermal inertia, the voltage of the PV terminal will also change smoothly. At the same time, the PV output current is directly in proportion to the surface IR; therefore, its dynamic is faster than the dynamics of temperature. Thus, it is obvious that the PV output power includes two separate dynamics due to the slow change in temperature and the fast fluctuations of the IR. However, when the TC technique is used, only temperature measurements are taken into account. Therefore, fast dynamics is eliminated from the technique and makes tracking more smooth, stable, and faster.

The key facts related to this algorithm are:

- Two sensors are required one for voltage other for temperature.
- It is constructed on the concept that the PV output voltage is directly related to the temperature.
- Here, only the slow dynamic is taken into consideration and the fast dynamic is eliminated and therefore, the tracking trend is more smooth, stable, and faster.

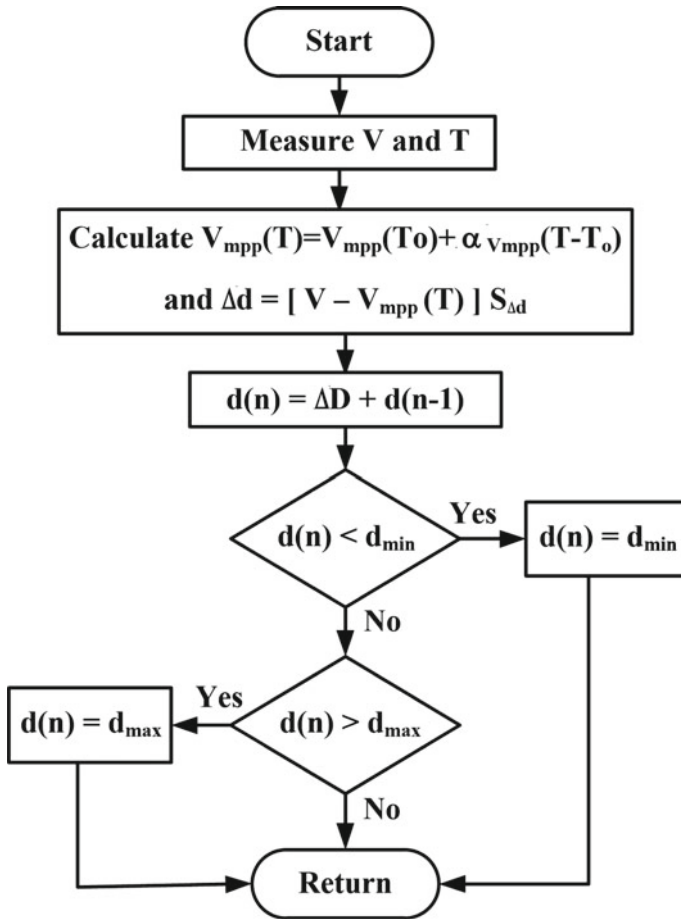


Fig. 7 Flow chart of TC algorithm

5 Implementation of Heuristic Approaches of the MPPT Technique

Figure 8 shows the implementation of heuristic approaches of the MPPT Technique which is composed of a PV panel, MPPT controller, Boost converter, load, and filter connected to the utility grid. Initially, solar energy is converted to electrical energy with the help of a solar panel. Then, output voltage and current of the solar panel are measured—which are utilized by the MPPT controller to produce a duty cycle for the Boost converter corresponding to its maximum power. Since the output of the Boost converter is DC in nature so to convert it into AC, an inverter is used. An inverter control block generates switching pulses for the inverter by utilizing the output voltage and current of the inverter. Therefore, the SECS generate AC active

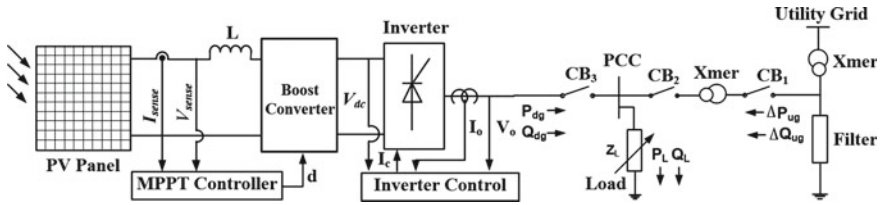


Fig. 8 Implementation of heuristics approaches of the technique

power (P_{dg}) and reactive power (Q_{dg}). A local load is connected to the system then finally, SECS is attached to the utility grid through a step-up transformer. A filter is used to eliminate any lower order harmonics from the supply. If the load is less than the generated power of SECS then surplus power ΔP_{ug} and ΔP_{ug} are supplied by the utility grid.

6 Results and Discussion

For the verification of all three algorithms i.e., PO, IC, and TC, MATLAB/Simulink simulations were executed considering a readily available PV module ‘Sun Earth Solar Power TPB156*156-60-P225W’. The DC–DC boost converter is employed for MPPT. The electrical specifications of the PV panel are presented in Table 1 and the PV Power, voltage, and current, obtained from the power–voltage curve, are given in Table 2. To obtain a comparative analysis, two aspects are taken into consideration i.e., changes in IR and temperature. The influence of change in IR and temperature on different parameters such as voltage, current, power, ripples in voltage, current, and power are recorded in the present analysis. Moreover, Mean Squared Error (MSE), Fill factor (FF), delay time, rise time, peak time, internal (or PV) efficiency, and overall efficiency are also obtained. Different results of the mentioned cases are included next.

6.1 Voltage and Voltage Ripples in Varying Atmospheric Conditions

Figure 9 represents the PV output voltages obtained for PO, IC, and TC algorithms (i.e., V_{po} , V_{ic} , and V_{tc} respectively) at a fixed temperature (25 °C) and varying IR. It can be observed from Fig. 9 that as the IR rises from 400 to 1200 W/m² in the steps of 200, PV output voltages by PO and IC algorithms (i.e., V_{po} and V_{ic} , respectively) are decreased slightly while that of TC algorithm (V_{tc}) has increased. It is also found that the TC algorithm gives slightly lesser PV output voltages for IR of 400–600 W/m² while for 800–1200 W/m², all the three algorithms gave approximately the same

Table 1 Specifications of ‘Sun Earth Solar Power TPB156*156-60-P225W’ PV module

<i>Array data</i>	
Parallel string	2
Series connected module per string	2
<i>Module data</i>	
Maximum power P_{max}	225.04 W
Voltage at MPP V_{mpp}	29 V
Current at MPP I_{mpp}	7.76 A
Voltage in open circuit condition V_{oc}	36.5 V
Temperature coefficient of V_{oc}	-0.34/°C
Short circuit current I_{sc}	8.26 A
Temperature coefficient of I_{sc}	0.07/°C
Cells per module	60
<i>Module parameters</i>	
Current due to light I_{lt}	8.2671 A
Saturation current through diode I_o	$1.3914 * 10^{-10}$ A
Diode ideality factor	0.95481
Resistance in shunt R_{sh}	476.1198 Ω
Resistance in series R_{se}	0.41169 Ω

Table 2 PV power, voltage and current at different temperature T and irradiance IR obtained from PV curve

T (°C)	IR (W/m ²)	P_{pv} (W)	V_{pv} (V)	PV current (A)
25	400	367.3	58.9	6.236
25	600	550	58.78	9.357
25	800	727.9	58.54	12.43
25	1000	900.2	58	15.52
25	1200	1066	57.4	18.58
30	1000	881.6	56.67	15.56
40	1000	864.1	54.18	15.58
50	1000	806.3	51.69	15.6

PV output voltages. Figure 10 shows the PV output voltages for the variations in temperature (30, 40, and 50 °C) with IR kept constant at 1000 W/m². It is found that as the temperature increases, PV output voltages obtained from PO, IC and TC algorithms decrease. It is also observed that the TC algorithm gives slightly less PV output voltage as well as slightly fewer ripples in PV output voltage as compared to PO and IC algorithms.

For better comparative analysis, Fig. 11 includes the comparison bars of PV voltages obtained from different MPPT techniques and the PV voltage, corresponding

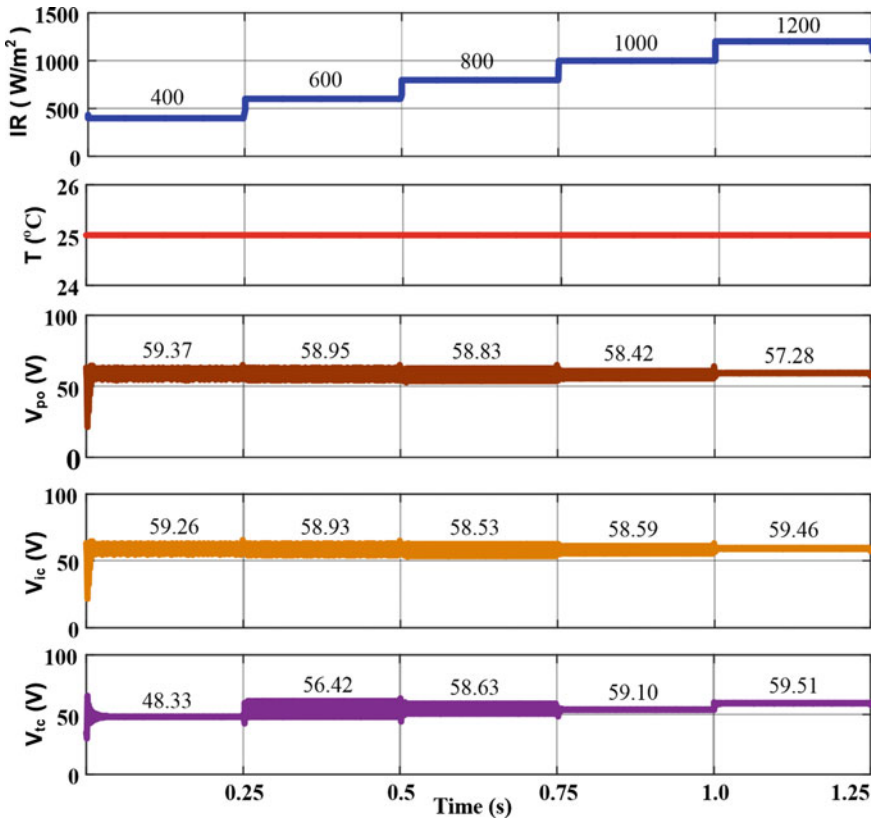


Fig. 9 PV output voltage with PO, IC, and TC algorithm when irradiance varied

to MPP i.e., V_{pv} —obtained from the PV characteristics for a given temperature and IR. It can be concluded that all the methods give quite accurate results. In some of the cases, particularly at 25 °C and 1200 W/m², the voltages obtained from PO, IC, and TC methods are equal and slightly more than V_{pv} . Similarly, Fig. 12 represents the ripple in PV voltage ΔV at different temperatures and IR for different methods. It is observed that minimum ripples are there in the case of the TC method, followed by IC and PO methods. It is also observed that as the temperature and IR are increased, the value of ripples in PV voltage decreases. For example, at 25 °C and 400 W/m², the ripples in PV voltage (ΔV) is about 7 V but at 40 °C and 1000 W/m², its value is about 2 V.

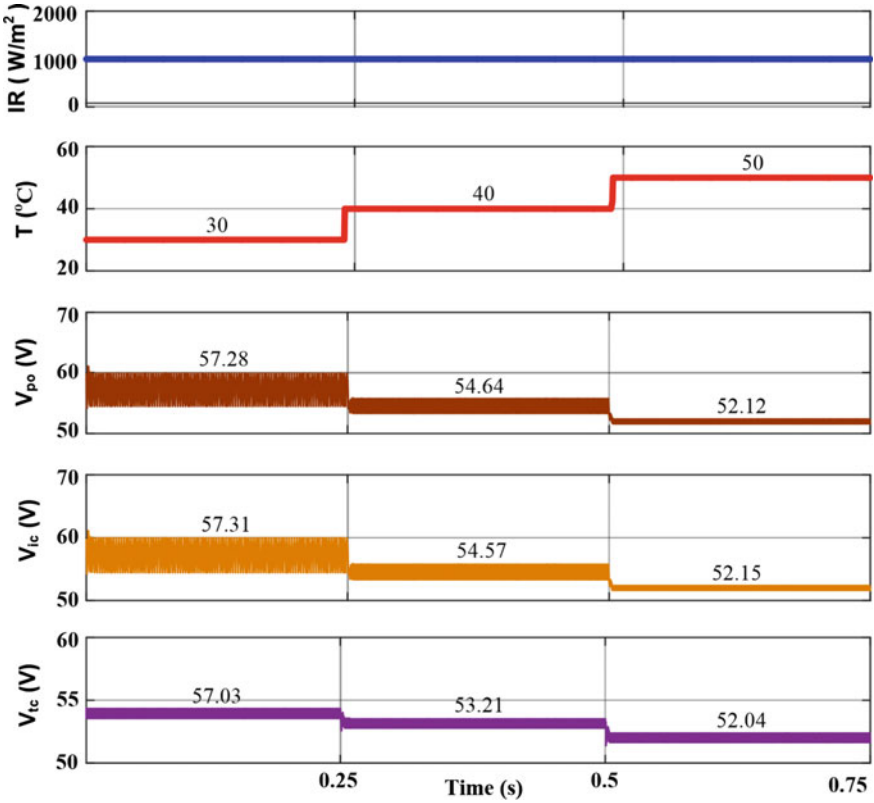


Fig. 10 PV output voltage with PO, IC, and TC algorithm when temperature varied

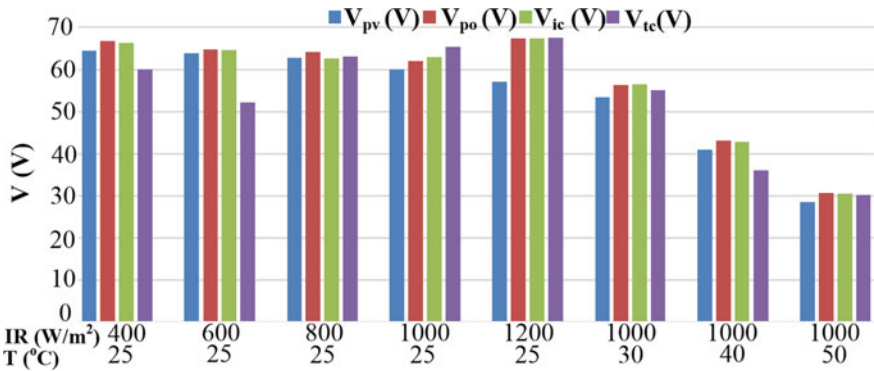


Fig. 11 Comparison of PV output voltage with PO, IC, and TC algorithm when both temperature and irradiance are varied

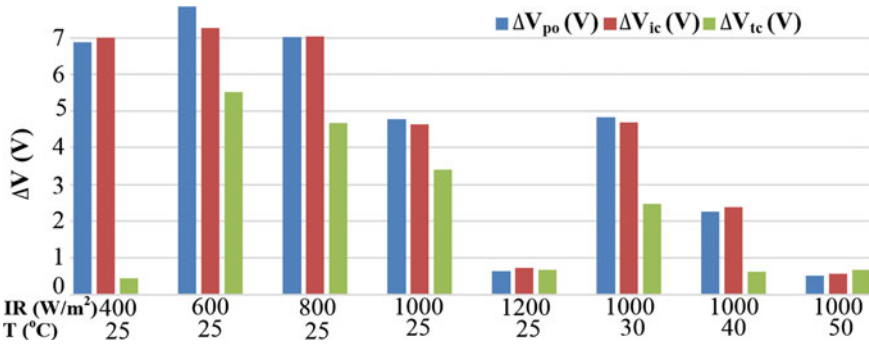


Fig. 12 Ripple in PV output voltage with PO, IC, and TC algorithm when both temperature and irradiance are varied

6.2 Power and Power Ripples in Varying Atmospheric Conditions

Figure 13 represents the PV output powers P_{po} , P_{ic} and P_{tc} obtained for PO, IC, and TC algorithms, respectively at 25 °C and different IR (400–1200 W/m²). It can be noticed from this figure that all three techniques successfully track the MPP and as the IR increases, PV output power also increases. For example, for time 0.75 s to 1 s, the PV output power obtained from PV characteristics (P_{pv}) is 900.2 W—given in Table 2—while PO, IC, and TC algorithms (i.e., P_{po} , P_{ic} , P_{tc} , respectively) provide 891.25 W, 890.95 W and 892 W of power, respectively. The obtained powers are very close to P_{pv} . Initially, due to the presence of transients from 0 to 0.25 s, the TC algorithm provides lesser PV output power as compared to that of IC and PO algorithms. Figure 14 presents PV output powers for different temperatures (30, 40, and 50 °C) with a fixed IR of 1000 W/m². It can be noted from the figure that, even in transient-period i.e., from 0 to 0.25 s, power by TC algorithm is almost equal to P_{pv} —providing the most accurate result in comparison to other methods. Moreover, for better understanding, PV output powers obtained from different algorithms at different temperatures and IR are compared magnitude wise in Fig. 15. Finally, Fig. 16 represents the ripples in PV output powers for different algorithms under the same environmental conditions. It can be noticed that ripples in output power ΔP are maximum at 25 °C and 800 W/m² which is about 27 W while it is minimum at 50 °C and 1000 W/m² which is about 2 W. That means upon increasing the IR and temperature, ripples in PV output power (ΔP) decreases.

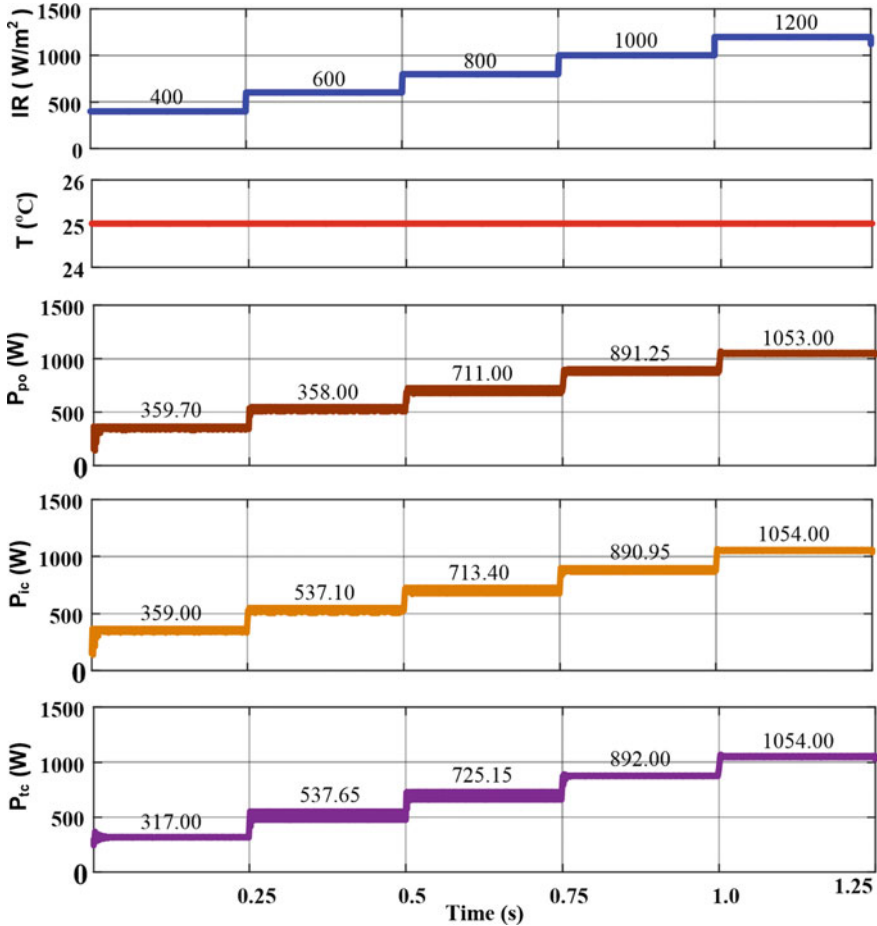


Fig. 13 PV output power with PO, IC and TC algorithm when irradiance is varied

6.3 Current and Current Ripples in Varying Atmospheric Conditions

Figure 17 shows the comparison of PV currents obtained from PO, IC, and TC methods (I_{po} , I_{ic} , I_{ic} , respectively) with ideal PV current obtained from characteristic I_{pv} for different temperatures and IR. It is found that all the three algorithms work similarly and the currents are almost the same as obtained from PV characteristic (I_{pv}). It is also noticed that as the IR increases, the PV output current goes on increasing while it is almost constant if IR is kept constant and only the temperature is varied. Further, Fig. 18 represents the ripples in the PV output currents for changed IR and temperature. It can be noticed in this figure that ripples in PV output current

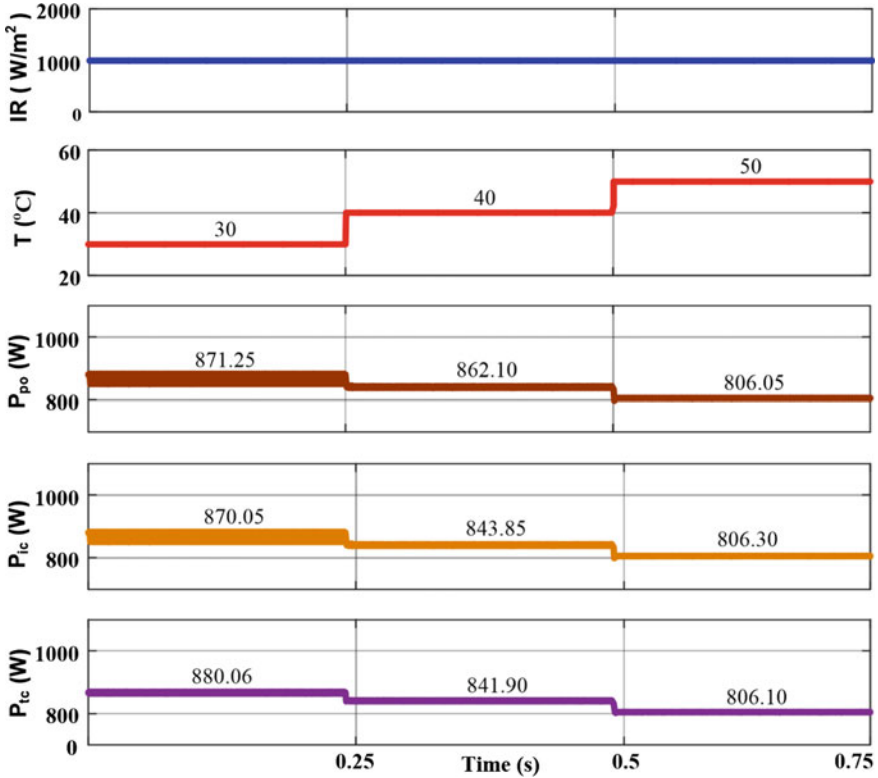


Fig. 14 PV output power with PO, IC and TC algorithm when the temperature is varied

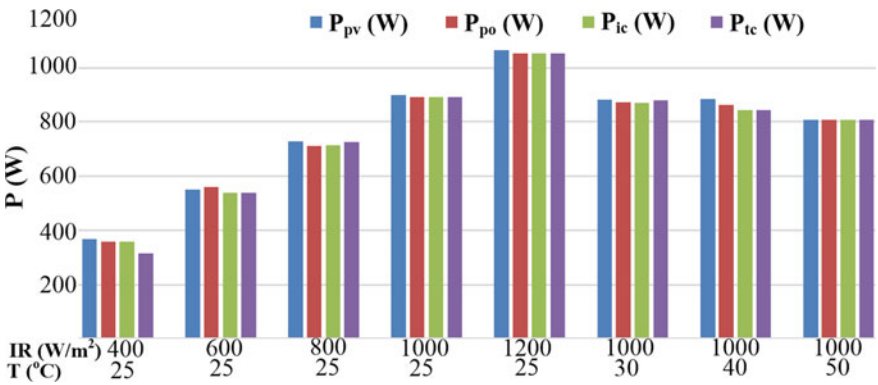


Fig. 15 Comparison of PV output power with PO, IC and TC algorithm when both temperature and irradiance are varied

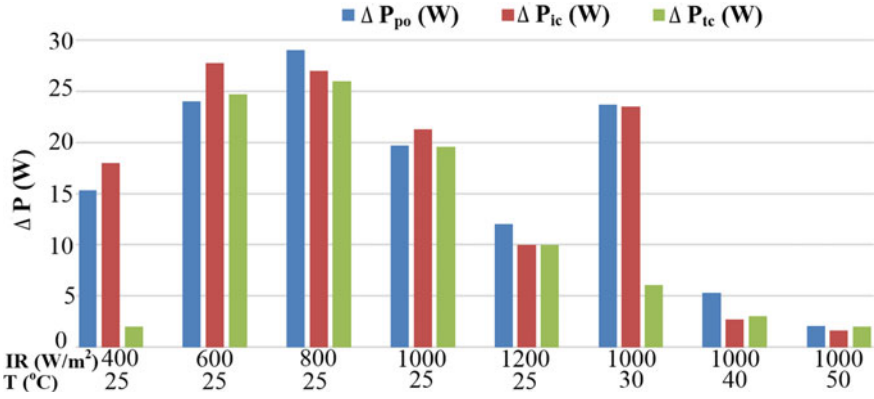


Fig. 16 Ripple in PV output power with PO, IC and TC algorithm when both temperature and irradiance are varied

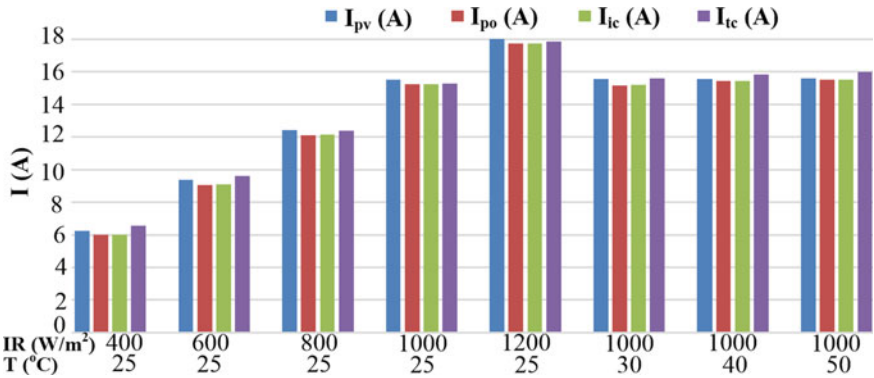


Fig. 17 Comparison of PV output current with PO, IC, and TC algorithm when both temperature and irradiance are varied

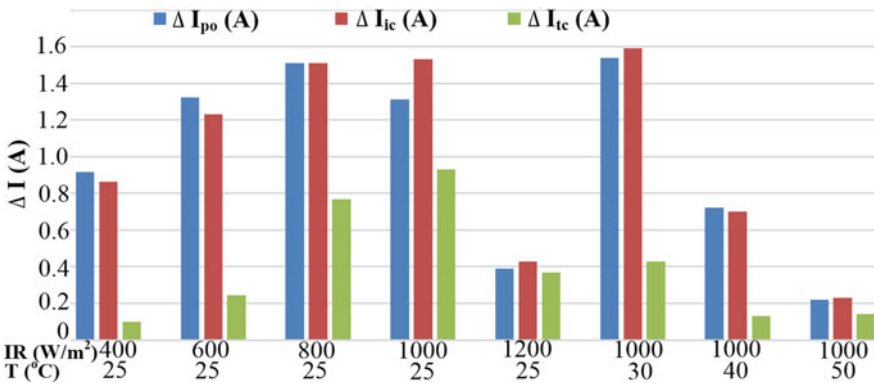


Fig. 18 Ripple in PV output current with PO, IC, and TC algorithm when both temperature and irradiance are varied

by the TC algorithm are minimum as compared to that of PO and IC algorithms. The ripples in PV output currents obtained from PO and IC algorithms are almost equal.

6.4 Tracking Performance and Efficiency

Figure 19 presents the delay times, rise times, and peak times for PO, IC, and TC algorithms which give an idea about the tracking performances of the MPPT methods. It can be observed from this figure that the delay time is minimum for the TC algorithm (i.e., t_{dtc})—equal to 0.415 ms. The rise time is minimum for the IC algorithm (i.e., t_{ric})—equal to 2.465 ms whereas the peak time is minimum for PO method (i.e., t_{ppo})—equal to 2.94 ms. Figure 20 shows the mean squared errors (MSEs) for PV output power, voltage, and current for PO, IC, and TC algorithms (considering 1000 samples for each case). The MSE of PV output powers for all methods (i.e., E_{ppo} ,

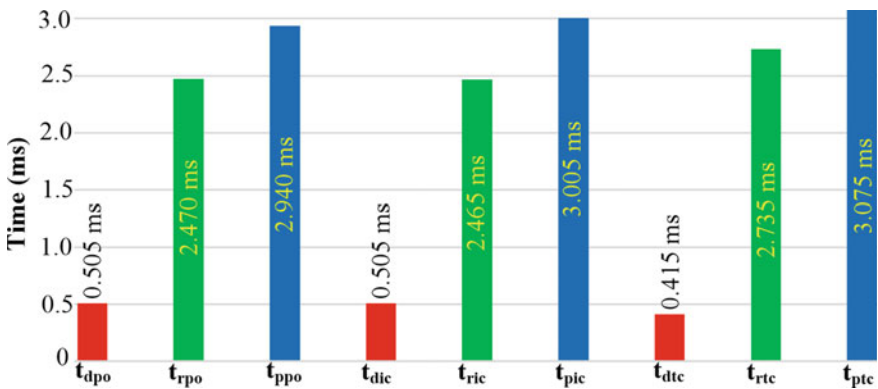


Fig. 19 Delay time, rise time, and peak time with PO, IC, and TC algorithm

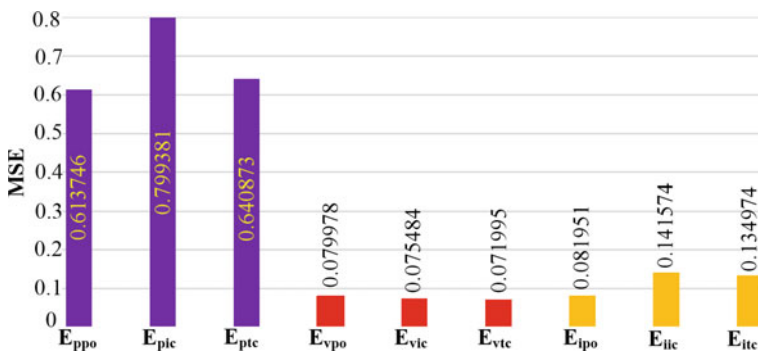


Fig. 20 MSE of PV output power, voltage, and current with PO, IC, and TC algorithm

E_{pic} , and E_{ptc} for PO, IC, and TC algorithms, respectively) are calculated and it is found that, out of them, MSE is minimum for the PO algorithm.

Similarly, MSEs for the PV output voltages (i.e., E_{vpo} , E_{vic} , and E_{vtc} for PO, IC, and TC algorithms, respectively) are calculated and it is found that all the methods have almost the same voltage MSE. Finally, MSEs for the PV output currents (i.e., E_{ipo} , E_{iic} , and E_{itc} for PO, IC, and TC algorithms, respectively) are calculated and it is observed that the value of MSE is minimum for the PO algorithm. Figure 21 represents the fill factors, FF_{po} , FF_{ic} , and FF_{tc} —obtained for PO, IC, and TC algorithms, respectively—at different temperatures and IR. It is observed from this figure that as the IR and temperature are increased, fill factors obtained by all the three algorithms decrease slightly. It is also clear from the figure that, out of the three algorithms, the TC algorithm gives the highest fill factor. Figure 22 presents the internal and overall efficiencies η_{ipo} , η_{lopo} , η_{lic} , η_{loic} , η_{litc} and η_{lotc} for PO, IC and TC algorithms, respectively. It is observed from this figure that both internal and overall efficiencies for the IC algorithm have the highest values out of all algorithms. For the internal

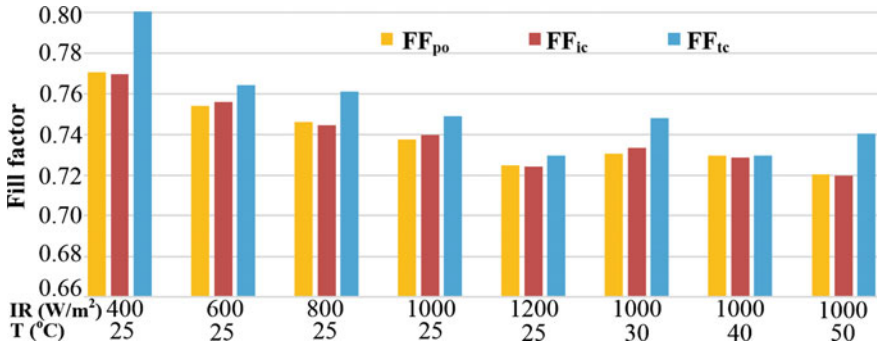


Fig. 21 Fill Factor with PO, IC and TC algorithm when both temperature and irradiance are varied

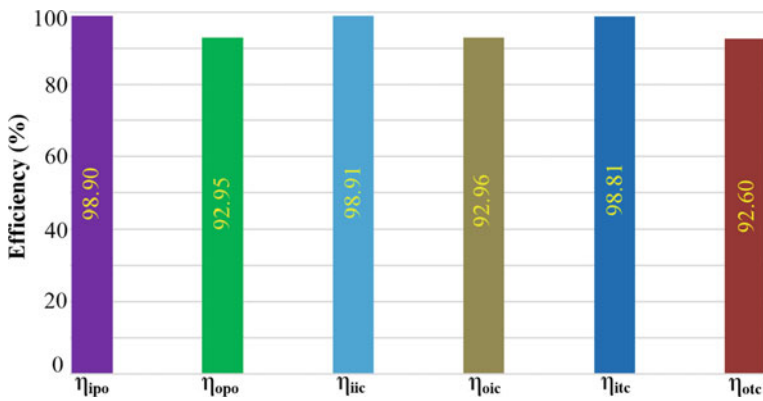


Fig. 22 Internal and overall efficiency with PO, IC and TC algorithm

efficiency calculation, PV output power is considered while for the calculation of overall efficiency, the load output power is considered. That means, for internal efficiency calculation, output power equal to the product of V_{pv} and I_{pv} while for overall efficiency calculation, the output power is equal to the product of V_L and I_L as given in Fig. 3.

7 Conclusion

Three different MPPT techniques (i.e., PO, IC and TC) are tested on PV systems by using MATLAB/Simulink offline simulations. The techniques have been compared in terms of delay time, rise time, peak time, MSE, ripple content in voltage, current, and power, internal efficiency, overall efficiency and fill factor for different IRs and temperatures. It is found that all three MPPT techniques are successfully tracking the MPP and obtained results are comparable. However, for a particular parameter, one technique is found to be superior to another viz., TC method provides a better fill factor, the PO method gives better MSE and the IC method provides better internal and overall efficiencies.

References

1. Qazi A, Hussain F, Rahim NABD, Hardaker G, Alghazzawi D, Shaban K, Haruna K (2019) Towards sustainable energy: a systematic review of renewable energy sources, technologies, and public opinions. *IEEE Access* 7:63837–63851. <https://doi.org/10.1109/ACCESS.2019.2906402>
2. Akhtar I, Kirmani S, Jamil M (2019) Analysis and design of a sustainable microgrid primarily powered by renewable energy sources with dynamic performance improvement. *IET Renew Power Gener* 13:1024–1036. <https://doi.org/10.1049/iet-rpg.2018.5117>
3. Koraki D, Strunz K (2018) Wind and solar power integration in electricity markets and distribution networks through service-centric virtual power plants. *IEEE Trans Power Syst* 33:473–485. <https://doi.org/10.1109/TPWRS.2017.2710481>
4. Hegedus S, Luque A (2011) Achievements and challenges of solar electricity from photovoltaics. In: *Handbook of photovoltaic science and engineering*. Wiley, pp 1–38. <https://doi.org/10.1002/9780470974704.ch1>
5. Branker K, Pathak MJM, Pearce JM (2011) A review of solar photovoltaic leveled cost of electricity. <https://doi.org/10.1016/j.rser.2011.07.104>
6. Singh PP, Singh S (2010) Realistic generation cost of solar photovoltaic electricity. *Renew Energy* 35:563–569. <https://doi.org/10.1016/j.renene.2009.07.020>
7. Yang CJ (2010) Reconsidering solar grid parity. *Energy Policy* 38:3270–3273. <https://doi.org/10.1016/j.enpol.2010.03.013>
8. Ansari S, Gupta OH, Tripathy M (2021) An islanding detection methodology for SOFC-based static DG using DWT. In: *Lecture notes in electrical engineering*. Springer Science and Business Media Deutschland GmbH, pp 95–107. https://doi.org/10.1007/978-981-15-7994-3_9
9. Ansari S, Gupta OH (2021) Voltage ripple-based islanding technique on modified IEEE-13 bus test feeder for photovoltaic inverter. In: *Lecture notes in electrical engineering*. Springer Science and Business Media Deutschland GmbH, pp 139–155. https://doi.org/10.1007/978-981-15-7994-3_13

10. Logeswaran T, SenthilKumar A (2014) A review of maximum power point tracking algorithms for photovoltaic systems under uniform and non-uniform irradiances. *Energy Procedia* 228–235. <https://doi.org/10.1016/j.egypro.2014.07.266>
11. Soualmia A, Chenni R (2017) A survey of maximum peak power tracking techniques used in photovoltaic power systems. In: *FTC 2016—proceedings of future technologies conference*. Institute of Electrical and Electronics Engineers Inc., pp 430–443. <https://doi.org/10.1109/FTC.2016.7821645>
12. Husain MA, Tariq A, Hameed S, Arif MSB, Jain A (2017) Comparative assessment of maximum power point tracking procedures for photovoltaic systems. <https://doi.org/10.1016/j.gee.2016.11.001>
13. Balasubrahmanyam CHS, Gupta OH (2020) Detailed study of solar energy conversion system using boost converter—a new MPPT technique. *J Inst Eng India Ser B* 101:631–639. <https://doi.org/10.1007/s40031-020-00478-1>
14. Wasynczuk O (1983) Dynamic behavior of a class of photovoltaic power systems. *IEEE Power Eng Rev* PER-3:36–37. <https://doi.org/10.1109/MPER.1983.5519293>
15. Hua C, Lin JR (1996) DSP-based controller application in battery storage of photovoltaic system. In: *IECON proceedings (industrial electronics conference)*. IEEE, pp.1705–1710. <https://doi.org/10.1109/iecon.1996.570673>
16. Hua C, Lin J, Shen C (1998) Implementation of a DSP-controlled photovoltaic system with peak power tracking. *IEEE Trans Ind Electron* 45:99–107. <https://doi.org/10.1109/41.661310>
17. Abdelsalam AK, Massoud AM, Ahmed S, Enjeti PN (2011) High-performance adaptive perturb and observe MPPT technique for photovoltaic-based microgrids. *IEEE Trans Power Electron* 26:1010–1021. <https://doi.org/10.1109/TPEL.2011.2106221>
18. Bianconi E, Calvente J, Giral R, Mamarelis E, Petrone G, Ramos-Paja CA, Spagnuolo G, Vitelli M (2013) Perturb and observe MPPT algorithm with a current controller based on the sliding mode. *Int J Electr Power Energy Syst* 44:346–356. <https://doi.org/10.1016/j.ijepes.2012.07.046>
19. Kumar N, Hussain I, Singh B, Panigrahi BK (2018) Framework of maximum power extraction from solar PV panel using self predictive perturb and observe algorithm. *IEEE Trans Sustain Energy* 9:895–903. <https://doi.org/10.1109/TSST.2017.2764266>
20. Huynh P, Cho BH (1996) Design and analysis of a microprocessor-controlled peak-power-tracking system. *IEEE Trans Aerosp Electron Syst* 32:182–190. <https://doi.org/10.1109/7.481260>
21. John R, Mohammed SS, Zachariah R (2018) Variable step size perturb and observe MPPT algorithm for standalone solar photovoltaic system. In: *Proceedings of the 2017 IEEE international conference on intelligent techniques in control, optimization and signal processing, INCOS 2017*. Institute of Electrical and Electronics Engineers Inc., pp 1–6. <https://doi.org/10.1109/ITCOSP.2017.8303163>
22. Yu GJ, Jung YS, Choi JY, Choy I, Song JH, Kim GS (2002) A novel two-mode MPPT control algorithm based on comparative study of existing algorithms. In: *Conference record of the IEEE photovoltaic specialists conference*, pp 1531–1534. <https://doi.org/10.1109/pvsc.2002.1190903>
23. Hua C, Lin J (2003) An on-line MPPT algorithm for rapidly changing illuminations of solar arrays. *Renew Energy* 28:1129–1142. [https://doi.org/10.1016/S0960-1481\(02\)00214-8](https://doi.org/10.1016/S0960-1481(02)00214-8)
24. Hussein KH, Muta I, Hoshino T, Osakada M (1995) Maximum photovoltaic power tracking: an algorithm for rapidly changing atmospheric conditions. *IEE Proc Gener Transm Distrib* 142:59–64. <https://doi.org/10.1049/ip-gtd:19951577>
25. Liu F, Duan S, Liu F, Liu B, Kang Y (2008) A variable step size INC MPPT method for PV systems. *IEEE Trans Ind Electron* 55:2622–2628. <https://doi.org/10.1109/TIE.2008.920550>
26. Mei Q, Shan M, Liu L, Guerrero JM (2011) A novel improved variable step-size incremental-resistance MPPT method for PV systems. *IEEE Trans Ind Electron* 58:2427–2434. <https://doi.org/10.1109/TIE.2010.2064275>
27. Zakzouk NE, Elsharty MA, Abdelsalam AK, Helal AA, Williams BW (2016) Improved performance low-cost incremental conductance PV MPPT technique. *IET Renew Power Gener* 10:561–574. <https://doi.org/10.1049/iet-rpg.2015.0203>

28. Alsumiri M (2019) Residual incremental conductance based nonparametric MPPT control for solar photovoltaic energy conversion system. *IEEE Access* 7:87901–87906. <https://doi.org/10.1109/ACCESS.2019.2925687>
29. Mutoh N, Matuo T, Okada K, Sakai M (2002) Prediction-data-based maximum-power-point-tracking method for photovoltaic power generation systems. In: *PESC record—IEEE annual power electronics specialists conference*, pp 1489–1494. <https://doi.org/10.1109/psec.2002.1022386>
30. Park M, Yu IK (2004) A study on the optimal voltage for MPPT obtained by surface temperature of solar cell. In: *IECON proceedings (industrial electronics conference)*, pp 2040–2045. <https://doi.org/10.1109/iecon.2004.1432110>
31. Swaraj K, Mohapatra A, Sahoo SS (2017) Combining PV MPPT algorithm based on temperature measurement with a PV cooling system. In: *International conference on signal processing, communication, power and embedded system, SCOPES 2016—proceedings*. Institute of Electrical and Electronics Engineers Inc., pp 482–489. <https://doi.org/10.1109/SCOPES.2016.7955876>
32. Coelho RF, Concer FM, Martins DC (2010) A MPPT approach based on temperature measurements applied in PV systems. In: *2010 IEEE international conference on sustainable energy technologies, ICSET 2010*. <https://doi.org/10.1109/ICSET.2010.5684440>

Short Term Active Power Load Forecasting Using Machine Learning with Feature Selection



Venkataramana Veeramsetty, D. Rakesh Chandra,
and Surender Reddy Salkuti

Abstract Active power load forecasting is an essential task for electric utilities in order to operate network more reliable and also to participate successfully in energy trading. In this chapter a new artificial neural network (ANN) topology is designed to predict the load. The most efficient input features to predict the load have been selected using correlation factors. The active power load data has been taken from 33/11 kV electric power distribution substation. The proposed ANN architecture is designed, implemented and tested in Microsoft Azure Notebook environment. Based on the simulation results, it has been observed that the proposed ANN model predicts the load with good accuracy.

Keywords Active power · Artificial neural network · Feature selection · Load forecasting · Machine learning

1 Introduction

In order to preserve the equilibrium of the load requirement And supply, electrical power companies forecasts the load. Electrical load estimation is becoming one of the core processes for periodic planning and expansion of power company facilities

V. Veeramsetty

Center for Artificial Intelligence and Deep Learning, SR Engineering College,
Warangal, Telangana, India

D. Rakesh Chandra

Department of Electrical and Electronics Engineering, KITS, Warangal, Telangana, India
e-mail: drc.eee@kitsw.ac.in

S. R. Salkuti (✉)

Department of Railroad and Electrical Engineering, Woosong University, Daejeon,
Republic of Korea
e-mail: surender@wsu.ac.kr

[1]. Electric power load estimation is categorized into three categories based on time horizons such as short-term, medium-term and long-term load forecasting [2, 3]. Short term power prediction is used to schedule the generation and transmission. Time horizon for short term prediction is from few hours to days. Medium term electric power prediction is used to purchase the fuel. Time horizon for medium term prediction is from few weeks to months. Long term prediction is used to develop the generation, transmission and distribution systems. Time horizon for long term prediction is from one to ten years.

The estimate of short-term energy demand is a really an important problem for proper management and delivery of electricity to avoid repeated power failures. It's just an essential prerequisite for the economic delivery of generation units in power plants [4]. Strong control in the short term Load forecasting methodology must be more precise in order to be more reliable It lets consumers pick a more efficient method of energy use, minimizes production costs and optimizes output costs [5].

Machine learning (ML) has become an integral part in many fields like automobiles, international business, educational institution [6], civil engineering applications [7, 8], image processing [9] and also, electrical power system applications [10]. ML analyses the system and makes forecasts based on previous existing data.

Many scholars have focused on active power Load prediction with various estimation methods. Multiple linear regression model was used in [11] to predict the active power load using hourly load demand and temperatures of South Sulawesi electrical system. Active power load was estimated in [12] using Artificial neural networks and multiple linear regression model. Active power load was predicted in [13] based on load data of last four hours. Active power load was estimated in [10, 14, 15] based load data for last four hours and load data at same hour for the last two days. Active power load was predicted using support vector regression model in [16]. In this methodology, the authors did not consider the load on weekends. A hybrid approach based on decision tree and expert system was developed in [17] to predict the active power load southeast of Brazil. Fourier-series forecast model with least-squares was proposed in [18] to predict the hourly load data. A novel approach was developed in [19] to forecast the active power load based on auto encoder and gated recurrent unit (GRU). Auto encoder is used to compress the input features and GRU used to forecast the load. An ANN model was developed in [20] to forecast the half-hourly electric load demand in Tunisia. Authors have used Levenberg–Marquardt learning algorithm to train the ANN model. Prediction of electricity demand and price one day ahead using functional models was discussed in [21]. Estimation of electric power consumption in Shanghai using grey forecasting model was discussed in [22]. All of these approaches make useful contributions to load estimation, but lack certain essential functionality, such as dimensional reduction, to boost the efficiency of the model.

In this chapter active power load on a 33/11 kV substation was predicted using artificial neural network (ANN). A new approach is used to predict the load at particular hour of the day based on load at previous two hours and at same hour but in previous three days. Stochastic gradient descent optimizer [23] was used to update the weight and bias parameters in the ANN. Dimensionality reduction using correlation concept has been used to find more suitable input features among $L(T-1)$, $L(T-2)$,

$L(T-24)$, $L(T-48)$ and $L(T-72)$. Lightweight ANN model is designed with more suitable input features to predict the load. The proposed ANN topology with learning algorithm is validated by comparing it with models developed in [13, 14].

The main contributions of this chapter are as follows:

- Complex and compact ANN models were developed to predict the active power load.
- A new approach i.e. predict the active power load based on load at last two hours and load at same time but in last three days was used.
- Dimensionality reduction with correlation concept was used to reduce the complexity of the model so that over fitting problem was removed.
- Data analytic tools were used to process the data before feed it to the model.

The remaining of the chapter was organized as follows. Section 2 deliberates on the ANN models to forecast the load on substation. Section 3 presents result analysis, and conclusions of this chapter are described in Sect. 4.

2 Methodology

2.1 ANN Topology Design

The architecture of ANN that has been used in this chapter to predict the load $L(T)$ at particular hour (T) of the day based on load at last previous two hours [$L(T-1)$ and

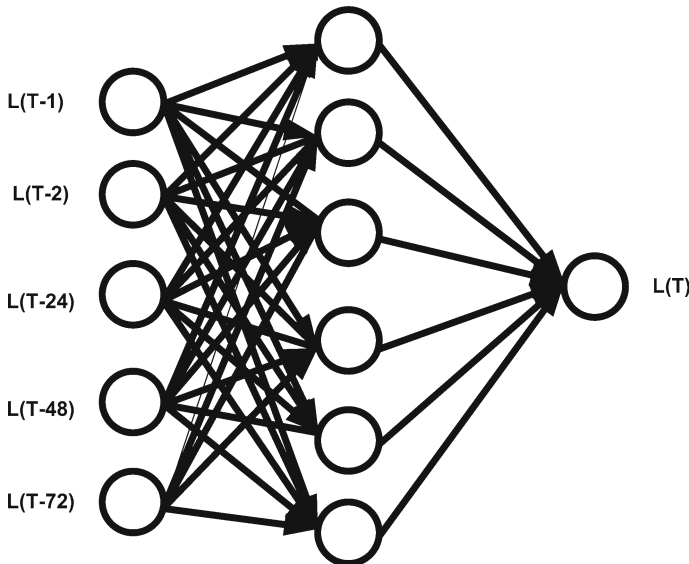


Fig. 1 Complex ANN architecture to predict load on 33/11 kV substation

Table 1 ANN model parameters

Variable	Parameters
W_{ih}	30
W_{ho}	6
b_h	6
b_o	1
Total parameters: 43	
Hidden layer activation: softmax	
Output layer activation: softmax	

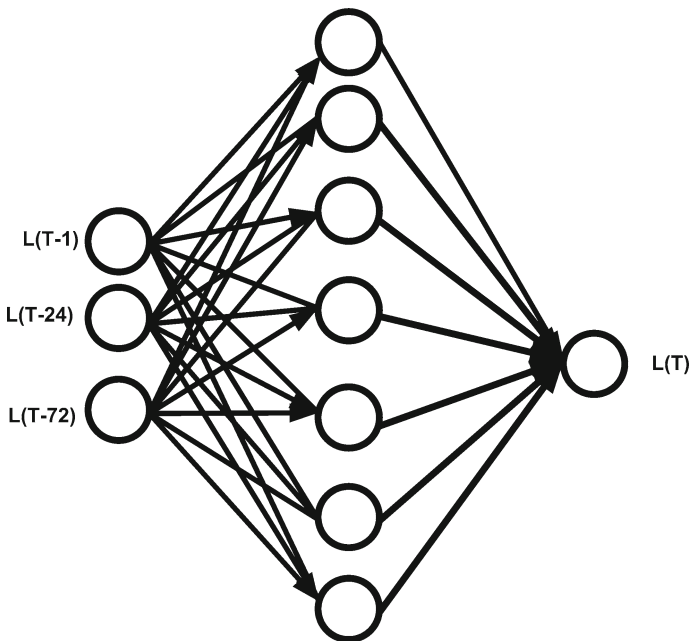


Fig. 2 Lightweight ANN architecture to predict load on 33/11 kV substation

$L(T-2)$] and load at same time but last three days [$L(T-24)$, $L(T-48)$, $L(T-72)$] is shown in Fig. 1. Complete information of trainable parameters of the ANN model are presented in Table 1.

The architecture of lightweight ANN that has been developed based on most important features that have been selected using correlation concept is shown in Fig. 2. Complete information of trainable parameters of the light weight ANN model are presented in Table 2. Based on correlation concept $L(T-1)$, $L(T-24)$ and $L(T-48)$ have been considered as most important features.

Table 2 Lightweight ANN model parameters

Variable	Parameters
W_{ih}	21
W_{ho}	7
b_h	7
b_o	1
Total parameters: 36	
Hidden layer activation: softmax	
Output layer activation: softmax	

2.2 Dimensionality Reduction—Correlation

Correlation between the any two input features has been computed using Eq. 1. If correlation between any of two input features is greater than 0.7 then one of them will be removed from dataset. In this chapter 0.7 is considered as a threshold correlation value to identify most important features.

$$correlation(L(T - 1), L(T - 2)) = \frac{1}{n - 1} \frac{\sum_{L(T-1)} \sum_{L(T-2)} (L(T - 1) * mean(L(T - 1)))(L(T - 2) * mean(L(T - 2)))}{Std(L(T - 1))Std(L(T - 2))} \quad (1)$$

2.3 Stochastic Gradient Descent Optimizer

In this chapter back propagation based on stochastic gradient descent optimizer has been used to train the ANN models. Back propagation Algorithm that has been used to train the ANN based on stochastic gradient descent optimizer is presented in Algorithm 1.

3 Result Analysis

Historical load data at each hour of the day for the period from September-2018 to November-2018 was taken from 33/11 kV substation near Kakathiya University in Warangal [24]. Date processing techniques for observing the data distribution and outliers, and for data normalization have been used before using this data to train and test the ANN models. The proposed ANN models have been implemented and tested in cloud computing environment using Microsoft Azure Notebook [25].

Algorithm 1 Back Propagation Algorithm Using Stochastic Gradient Descent Optimizer

Inputs

- 1: Read Dataset and initialize weight matrices W_{ih} and W_{ho} , and bias parameters b_h and b_o
- 2: set $\eta=0.01$, epochs=100, batch size=1

Steps

- 1: Set iteration $t=1$
- 2: Set Sample $i=1$
- 3: **while** $t \leq itermax$ **do**
- 4: **while** $i \leq n_s$ **do**
- 5: Compute net input (net_h) to hidden layer for input 'X[i]' using Eq. 2.

$$net_h = [W_{ih}]^T * X[i] + b_h \quad (2)$$

- 6: Compute output (o_h) of hidden layer using Eq. 3.

$$o_h = \frac{1}{1 + e^{-net_h}} \quad (3)$$

- 7: Compute net input (net_o) to output layer using Eq. 4.

$$net_o = [W_{ho}]^T * o_h + b_o \quad (4)$$

- 8: Compute output (o_o) of output layer using Eq. 5.

$$o_o = \frac{1}{1 + e^{-net_o}} \quad (5)$$

- 9: Update weights between hidden and output layer using Eq. 6 and bias using 7.

$$W_{ho} = W_{ho} + \eta * (d - O) * O * (1 - O) * O_h \quad (6)$$

$$b_o = b_o + \eta * (d - O) * O * (1 - O) \quad (7)$$

- 10: Update weights between input and hidden layer using Eq. 8 and bias at hidden layer using 9.

$$W_{ih} = W_{ih} + \eta * (d - O) * O * (1 - O) * W_{ho} * O_h * (1 - O_h) * X[i] \quad (8)$$

$$b_h = b_h + \eta * (d - O) * O * (1 - O) * W_{ho} * O_h * (1 - O_h) \quad (9)$$

- 11: $i=i+1$
- 12: **end while**
- 13: $t=t+1$
- 14: **end while**

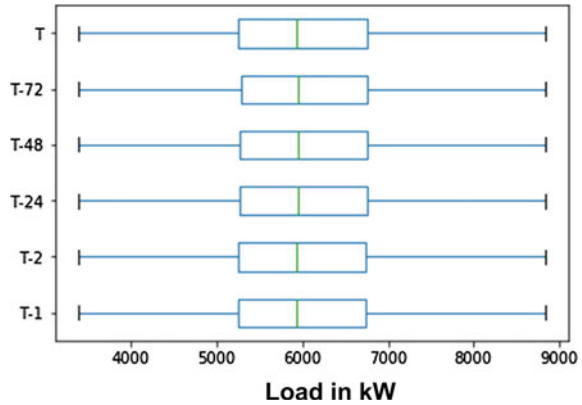
- 15: Print final weights W_{ih} and W_{ho}

- 16: Compute error MSE and MAE for both training and testing dataset using Eqs. 10 and 11 respectively

$$MSE = \frac{1}{n_s} \sum_{i=1}^{n_s} (d_i - O_i)^2 \quad (10)$$

$$MAE = \frac{1}{n_s} \sum_{i=1}^{n_s} |d_i - O_i| \quad (11)$$

Fig. 3 Box plot for active power load dataset



3.1 Data Analysis

Active power load data is analyzed for normal distribution and also for outliers using box plot as shown in Fig. 3. In the box plot seen in Fig. 3, Median shows that there is no left or right skew in the data at the centre of the inter-quartile spectrum and also indicates that the data meets the ideal normal distribution. Box plot was also used to identify the outliers in the data set. Outlier is identified as data points with a value less than the minimum represented by the left most vertical line and more than the maximum represented by the right most vertical line in the box plot. The box plot shown in Fig. 3 confirms that there is no outliers in the active power load dataset.

Complex ANN model performance The ANN model with five input neurons corresponding to five input features $L(T-1)$, $L(T-2)$, $L(T-24)$, $L(T-48)$ and $L(T-72)$ and one output neuron corresponding to output variable $L(T)$ is simulated with different number of hidden layers and neurons. The performance of various architectures are presented in Table 3 in terms of MSE and MAE. From Table 3, it has been observed that ANN model with one hidden layer with 6 hidden neurons is performing well in terms of training MSE and MAE i.e. 0.0108 and 0.0736 and testing MSE i.e. 0.0121. Finally the complex model with 5 input neurons, 1 output neuron and 6 hidden neurons with one hidden layer is considered for active power load prediction.

Comparison between actual load and load that predicted using complex ANN having testing MSE 0.0121, training MSE 0.0108 and training MAE 0.0736 is presented in Fig. 4. From Fig. 4, it has been observed that load predicted with complex ANN is almost follows the actual load.

Table 3 Complex ANN model training and testing performance

Layers	Stage	Error	Hidden neurons		
			6	7	8
1	Training	MSE	0.0108	0.0113	0.0116
		MAE	0.0736	0.0766	0.0784
	Testing	MSE	0.0121	0.0128	0.0257
		MAE	0.0768	0.0767	0.0775
2	Training	MSE	0.0113	0.0113	0.0115
		MAE	0.0768	0.0767	0.0775
	Testing	MSE	0.0129	0.0129	0.0134
		MAE	0.1185	0.0761	0.0812
3	Training	MSE	0.0219	0.0112	0.0122
		MAE	0.1185	0.0761	0.0812
	Testing	MSE	0.0230	0.0127	0.0128
		MAE	0.1185	0.0761	0.0812

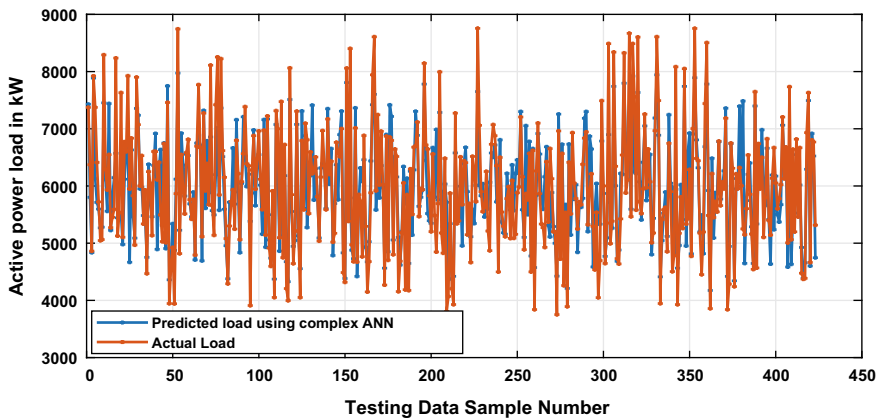


Fig. 4 Comparison between actual and predicted load using complex ANN

3.2 *Lightweight ANN Model Performance*

The light ANN model with three input neurons corresponding to three most important input features $L(T-1)$, $L(T-24)$ and $L(T-72)$ and one output neuron corresponding to output variable $L(T)$ is simulated with different number of hidden layers and neurons. The performance of various architectures are presented in Table 4 in terms of MSE and MAE. From Table 4, it has been observed that ANN model with one hidden layer with 7 hidden neurons is performing well in terms of training MSE and MAE i.e. 0.0112 and 0.0758 and testing MSE i.e. 0.0128. Finally the lightweight model with 3 input neurons, 1 output neuron and 7 hidden neurons with one hidden layer is considered for active power load prediction.

Comparison between actual load and load that predicted using lightweight ANN having testing MSE 0.0128, training MSE 0.0112 and training MAE 0.0758 is pre-

Table 4 Lightweight ANN model training and testing performance

Layers	Stage	Error	Hidden neurons			
			5	6	7	8
1	Training	MSE	0.0114	0.0113	0.0112	0.0113
		MAE	0.0763	0.0762	0.0758	0.0758
	Testing	MSE	0.0130	0.0128	0.0128	0.0128
2	Training	MSE	0.0114	0.0115	0.0115	0.0115
		MAE	0.0767	0.0775	0.0769	0.0771
	Testing	MSE	0.0132	0.0132	0.0131	0.0131
3	Training	MSE	0.0349	0.0367	0.0116	0.0262
		MAE	0.1523	0.1562	0.0777	0.1311
	Testing	MSE	0.0394	0.0134	0.0132	0.02713

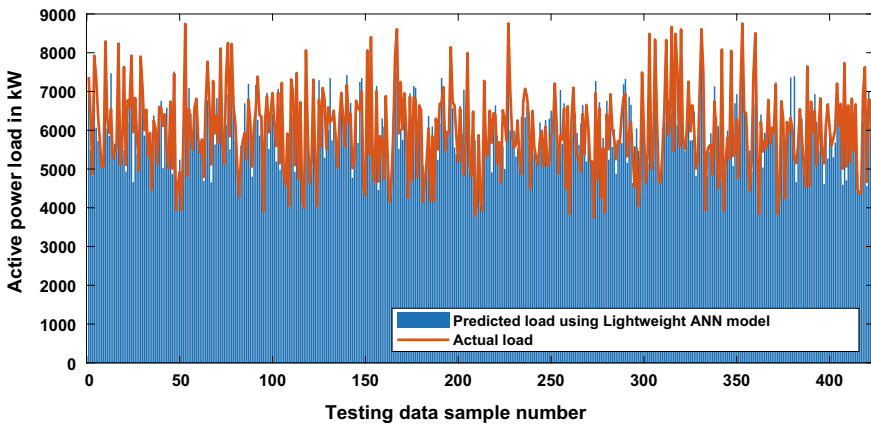


Fig. 5 Comparison between actual and predicted load using complex ANN

sented in Fig. 5. From Fig. 5, it has been observed that lightweight ANN model predicts the load almost equal the actual load.

Converging characteristics representing the variation in both training and testing MSE during the training of complex ANN model is shown in Fig. 6a and lightweight ANN model is shown in Fig. 6b. From Fig. 6 it has been observed that as training is progress, the weights are updated in such a way that the difference between actual and predicted load is decreasing. Validation loss is high comparing to training loss but not have much difference that shows model is well trained and does not have under fitting problem.

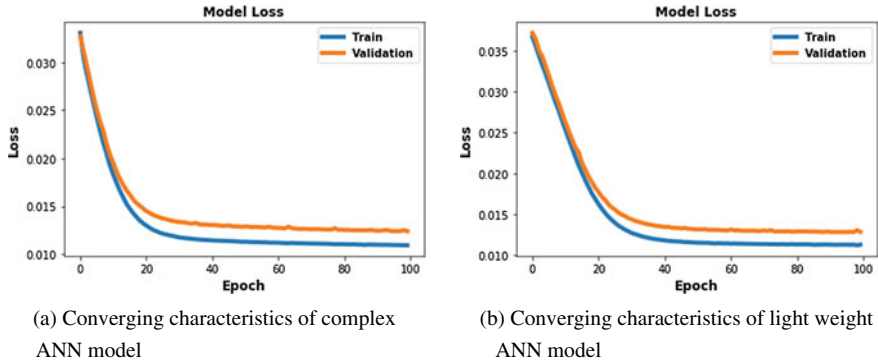


Fig. 6 Converging characteristics

Table 5 Comparison between ANN models

Model	Trainable parameters	Training			Testing
		MSE	MAE	MSE	MSE
Complex ANN	43	0.0108	0.0736	0.0121	
Lightweight ANN	36	0.0112	0.0758	0.0128	
% of absolute change	16.28	3.7	3.0	5.8	

3.3 Comparative Analysis

Comparison of the complex ANN model and the lightweight ANN model is shown in Table 5. The size of the lightweight ANN model is small with 36 parameters compared to the complex ANN model with 43 parameters. Owing to the distortion of the model with reduced dimensionality, the lightweight ANN model had good training and testing losses compared to the complex ANN model. Even though “Lightweight ANN model” was compressed by 16.28% in terms of training parameters, losses i.e. MSE, MAE and testing MSE are just increased by 3.7%, 3.0% and 5.8% respectively.

The proposed ANN models were validated by comparison with the load forecasting models available in literature such as [10, 13, 14] based on training and testing of MSE as described in Table 6. For Table 6, it has been observed that the proposed ANN models predict loads with good accuracy compared to the existing models.

Table 6 Comparisons in terms of testing MSE

Model	MSE	
	Training	Testing
[13]	0.29	1.59
[14]	0.23	0.44
[10]	0.2	0.32
Complex ANN	0.0108	0.0121
Lightweight	0.0112	0.0128

4 Conclusions

In this chapter short term load forecasting was implemented using ANN based on load at last two hours and load at same time but previous three days. Feature selection based on correlation concepts was utilized to reduce the complexity of the model by reducing number of input features. Light weight ANN model was also predicted load like a complex model with less number of trainable parameters with loss of small amount of accuracy. Practical historical load to train and test the ANN models was collected from 33/11 kV substation near Kakathiya University in Warangal city.

The proposed model can be helpful to utilities to trade energy in hourly ahead markets successfully by estimation the load with good accuracy. The discussed short term load forecasting problem can be further extended using sequence models like RNN, LSTM and GRU, also by using various dimensionality reduction techniques like PCA and FA.

Acknowledgements This research work was supported by “Woosong University’s Academic Research Funding - (2021–2022)”.

Appendix

This section demonstrates the mathematical derivation for the expressions presented in Eqs. 6, 7, 8 and 9. Also, explains how weights and bias parameters of ANN model update using stochastic gradient descent optimizer with help of numerical calculations.

Mathematical Derivation

Forward pass

During forward pass stage of back propagation algorithm ANN model will estimate the output as shown in Eqs. 2, 3, 4 and 5.

Backward pass

Backward stage of back propagation algorithm will help to update weights and bias parameters using specified optimizer. In this chapter stochastic gradient descent optimizer has been used to updated the model parameters.

Change in weights between hidden and output layer

$$\Delta W_{ho} = -\eta * \frac{\partial 0.5 * MSE}{\partial W_{ho}} = -\eta * \frac{\partial 0.5 * (d - o_o)^2}{\partial W_{ho}} \quad (12)$$

where $MSE = (d - o_o)^2$ and $o_o = \frac{1}{1+e^{-net_o}}$ and $net_o = W_{ho}^T + O_h + b_o$

$$\Delta W_{ho} = -\eta * \frac{\partial 0.5 * MSE}{\partial W_{ih}} = -\eta * 0.5 * \frac{\partial MSE}{\partial o_o} \frac{\partial o_o}{\partial net_o} \frac{\partial net_o}{\partial W_{ho}} \quad (13)$$

where $\frac{\partial MSE}{\partial o_o} = -2 * (d - o_o)$ and $\frac{\partial o_o}{\partial net_o} = o_o * (1 - o_o)$ and $\frac{\partial net_o}{\partial W_{ho}} = o_h$. Replace all these mathematical derivatives in Eq. 13 then will get the mathematical expression for ΔW_{ho} as shown in Eq. 14.

$$\Delta W_{ho} = \eta * (d - o_o) * o_o * (1 - o_o) * o_h \quad (14)$$

Change in bias parameters at output layer

$$\Delta b_o = -\eta * \frac{\partial 0.5 * MSE}{\partial b_o} = -\eta * \frac{\partial 0.5 * (d - o_o)^2}{\partial b_o} \quad (15)$$

$$\Delta b_o = -\eta * \frac{\partial 0.5 * MSE}{\partial b_o} = -\eta * 0.5 * \frac{\partial MSE}{\partial o_o} \frac{\partial o_o}{\partial net_o} \frac{\partial net_o}{\partial b_o} \quad (16)$$

where $\frac{\partial net_o}{\partial b_o} = 1$. Replace it in Eq. 16 then will get the mathematical expression for Δb_o as shown in Eq. 17.

$$\Delta b_o = \eta * (d - o_o) * o_o * (1 - o_o) \quad (17)$$

Change in weights between input and hidden layer

$$\Delta W_{ih} = -\eta * \frac{\partial 0.5 * MSE}{\partial W_{ih}} = -\eta * \frac{\partial 0.5 * (d - o_o)^2}{\partial W_{ih}} \quad (18)$$

$$\Delta W_{ih} = -\eta * \frac{\partial 0.5 * MSE}{\partial W_{ih}} = -\eta * 0.5 * \frac{\partial MSE}{\partial net_h} \frac{\partial net_h}{\partial W_{ih}} \quad (19)$$

where $\frac{\partial net_h}{\partial W_{ih}} = X$ and $\frac{\partial MSE}{\partial net_h} = \frac{\partial MSE}{\partial o_h} * \frac{\partial o_h}{\partial net_h}$. Replace all these mathematical derivatives in Eq. 19 then will get the mathematical expression as shown in Eq. 20.

$$\Delta W_{ih} = \eta * 0.5 * X * \frac{\partial MSE}{\partial o_h} * \frac{\partial o_h}{\partial net_h} \quad (20)$$

where $\frac{\partial o_h}{\partial net_h} = o_h * (1 - o_h)$ and $\frac{\partial MSE}{\partial o_h} = \frac{\partial MSE}{\partial net_o} * \frac{\partial net_o}{\partial o_h}$. Replace all these mathematical derivatives in Eq. 20 then will get the mathematical expression as shown in Eq. 21.

$$\Delta W_{ih} = \eta * 0.5 * X * o_h * (1 - o_h) * \frac{\partial MSE}{\partial net_o} * \frac{\partial net_o}{\partial o_h} \quad (21)$$

where $\frac{\partial net_o}{\partial o_h} = W_{ho}$ and $\frac{\partial MSE}{\partial net_o} = \frac{\partial MSE}{\partial o_o} * \frac{\partial o_o}{\partial net_o}$. Replace all these mathematical derivatives in Eq. 21 then will get the mathematical expression as shown in Eq. 22.

$$\Delta W_{ih} = \eta * 0.5 * X * o_h * (1 - o_h) * W_{ho} * \frac{\partial MSE}{\partial o_o} * \frac{\partial o_o}{\partial net_o} \quad (22)$$

where $\frac{\partial MSE}{\partial o_o} = (-2 * (d - o_o))$ and $\frac{\partial o_o}{\partial net_o} = o_o * (1 - o_o)$. Replace all these mathematical derivatives in Eq. 22 then will get the mathematical expression for ΔW_{ih} as shown in Eq. 23.

$$\Delta W_{ih} = \eta * X * o_h * (1 - o_h) * W_{ho} * (d - o_o) * o_o * (1 - o_o) \quad (23)$$

Change in bias parameters at hidden layer

$$\Delta b_h = -\eta * \frac{\partial 0.5 * MSE}{\partial b_h} = -\eta * \frac{\partial 0.5 * (d - o_o)^2}{\partial b_h} \quad (24)$$

$$\Delta b_h = -\eta * \frac{\partial 0.5 * MSE}{\partial b_{ih}} = -\eta * 0.5 * \frac{\partial MSE}{\partial net_h} \frac{\partial net_h}{\partial b_h} \quad (25)$$

where $\frac{\partial net_h}{\partial b_{ih}} = 1$ and $\frac{\partial MSE}{\partial net_h} = \frac{\partial MSE}{\partial o_h} * \frac{\partial o_h}{\partial net_h}$. Replace all these mathematical derivatives in Eq. 25 then will get the mathematical expression as shown in Eq. 26.

$$\Delta b_h = \eta * 0.5 * \frac{\partial MSE}{\partial o_h} * \frac{\partial o_h}{\partial net_h} \quad (26)$$

where $\frac{\partial o_h}{\partial net_h} = o_h * (1 - o_h)$ and $\frac{\partial MSE}{\partial o_h} = \frac{\partial MSE}{\partial net_o} * \frac{\partial net_o}{\partial o_h}$. Replace all these mathematical derivatives in Eq. 26 then will get the mathematical expression as shown in Eq. 27.

$$\Delta b_h = \eta * 0.5 * o_h * (1 - o_h) * \frac{\partial MSE}{\partial net_o} * \frac{\partial net_o}{\partial o_h} \quad (27)$$

where $\frac{\partial net_o}{\partial o_h} = W_{ho}$ and $\frac{\partial MSE}{\partial net_o} = \frac{\partial MSE}{\partial o_o} * \frac{\partial o_o}{\partial net_o}$. Replace all these mathematical derivatives in Eq. 27 then will get the mathematical expression as shown in Eq. 28.

Table 7 Sample dataset in MW

Dataset	L(T-1)	L(T-24)	L(T-72)	L(T)
Training	0.5	0.4	0.7	0.6
Testing	0.4	0.3	0.6	0.5

Table 8 Weights between input and hidden layer (W_{ih})

Input neuron	Hidden neuron						
	1	2	3	4	5	6	7
1	-0.1	0.1	0.2	-0.2	0.3	-0.3	0.4
2	0.1	0.2	-0.2	0.3	-0.3	0.4	-0.1
3	0.2	-0.2	0.3	-0.3	0.4	0.1	-0.1

$$\Delta b_h = \eta * 0.5 * o_h * (1 - o_h) * W_{ho} * \frac{\partial MSE}{\partial o_o} * \frac{\partial o_o}{\partial net_o} \quad (28)$$

where $\frac{\partial MSE}{\partial o_o} = -2 * (d - o_o)$ and $\frac{\partial o_o}{\partial net_o} = o_o * (1 - o_o)$. Replace all these mathematical derivatives in Eq. 22 then will get the mathematical expression for Δb_h as shown in Eq. 29.

$$\Delta b_h = \eta * o_h * (1 - o_h) * W_{ho} * (d - o_o) * o_o * (1 - o_o) \quad (29)$$

Numerical Calculations

Problem Update weights and bias parameters of an ANN model to estimate the load at particular hour of the day L(T) based on load available at one hour, one day and two days before i.e. L(T-1), L(T-24) and L(T-72). Architecture of ANN model is presented in Fig. 2. Assume dataset as shown in Table 7.

Initialize weights and bias parameters

Initial random weights W_{ih} and W_{ho} are shown in Tables 8 and 9 respectively. Similarly Initial random bias parameters b_h and b_o are shown in Table 10.

Forward pass calculations

Calculate net input (net_h) to hidden layer using Eq. 2 as presented below

Table 9 Weights between hidden layer and output layer (W_{ho})

Hidden neuron	Output neuron 1
1	-0.1
2	0.1
3	0.2
4	-0.2
5	0.3
6	-0.3
7	0.4

Table 10 Bias parameters (b_h) and (b_o)

Hidden neurons							Output neuron
b_h							b_o
1	2	3	4	5	6	7	1
-0.1	0.1	0.2	-0.2	0.3	-0.3	0.4	-0.4

$$\begin{aligned}
 net_h = W_{ih}^T * X + b_h = & \begin{bmatrix} -0.1 & 0.1 & 0.2 \\ 0.1 & 0.2 & -0.2 \\ 0.2 & -0.2 & 0.3 \\ 0.2 & 0.3 & -0.3 \\ 0.3 & -0.3 & 0.4 \\ -0.3 & 0.4 & 0.1 \\ 0.4 & -0.1 & -0.1 \end{bmatrix} \\
 * \begin{bmatrix} 0.5 \\ 0.4 \\ 0.7 \end{bmatrix} + & \begin{bmatrix} -0.1 \\ 0.1 \\ 0.2 \\ -0.2 \\ 0.3 \\ -0.3 \\ 0.4 \end{bmatrix} = & \begin{bmatrix} 0.03 \\ 0.09 \\ 0.43 \\ -0.39 \\ 0.61 \\ -0.22 \\ 0.49 \end{bmatrix}
 \end{aligned}$$

Calculate output (o_h) for hidden layer using Eq. 3 as presented below

$$o_h = \frac{1}{1 + e^{-net_h}} = \begin{bmatrix} 1.9704 \\ 1.9139 \\ 1.6505 \\ 2.4770 \\ 1.5434 \\ 2.2461 \\ 1.6126 \end{bmatrix}$$

Calculate net input (net_o) to output layer using Eq. 4 as presented below

$$net_o = W_{ho}^T * o_h + b_o = [-0.1 \ 0.1 \ 0.2 \ -0.2 \ 0.3 \ -0.3 \ 0.4] \\ * \begin{bmatrix} 1.9704 \\ 1.9139 \\ 1.6505 \\ 2.4770 \\ 1.5434 \\ 2.2461 \\ 1.6126 \end{bmatrix} - 0.1 = 0.1633$$

Calculate output (o_o) for output layer using Eq. 5 as presented below

$$o_o = \frac{1}{1 + e^{-net_o}} = \frac{1}{1 + e^{-0.1633}} = 0.5407$$

Backward pass calculations

Calculate change in weights (ΔW_{ho}) using Eq. 14. Assume learning rate $\eta = 0.1$.

$$\Delta W_{ho} = \eta * (d - o_o) * o_o * (1 - o_o) * o_h = 0.1 * (0.6 - 0.5407) * 0.5407 \\ * (1 - 0.5407) * \begin{bmatrix} 1.9704 \\ 1.9139 \\ 1.6505 \\ 2.4770 \\ 1.5434 \\ 2.2461 \\ 1.6126 \end{bmatrix} = \begin{bmatrix} 0.0029 \\ 0.0028 \\ 0.0024 \\ 0.0036 \\ 0.0023 \\ 0.0033 \\ 0.0024 \end{bmatrix}$$

Update weights between hidden and output layers using Eq. 6 as shown below

$$W_{ho} = W_{ho} + \Delta W_{ho} = \begin{bmatrix} -0.1 \\ 0.1 \\ 0.2 \\ -0.2 \\ 0.3 \\ -0.3 \\ 0.4 \end{bmatrix} + \begin{bmatrix} 0.0029 \\ 0.0028 \\ 0.0024 \\ 0.0036 \\ 0.0023 \\ 0.0033 \\ 0.0024 \end{bmatrix} = \begin{bmatrix} -0.0971 \\ 0.1028 \\ 0.2024 \\ -0.1964 \\ 0.3023 \\ -0.2967 \\ 0.4024 \end{bmatrix}$$

Calculate change in bias parameter (Δb_o) at output layer using Eq. 17 as shown below.

$$\begin{aligned}\Delta b_o &= \eta * (d - o_o) * o_o * (1 - o_o) = 0.1 * (0.6 - 0.5407) \\ &* 0.5407 * (1 - 0.5407) = 0.0015\end{aligned}$$

Update bias parameter at output layer as shown below

$$b_o = b_o + \Delta b_o = -0.1 + 0.0015 = -0.0985$$

Calculate change in weights (ΔW_{ih}) between input and hidden layer using Eq. 23 as shown below.

Change in weights connected to first hidden neuron (h = 1) i.e. ΔW_{i1}

$$\begin{aligned}\Delta W_{i1} &= 0.1 * 1.9704 * (1 - 1.9704) * (-0.0971) * (0.6 - 0.5407) \\ &* 0.5407 * (1 - 0.5407) * \begin{bmatrix} 0.5 \\ 0.4 \\ 0.7 \end{bmatrix} \\ \Delta W_{i1} &= \begin{bmatrix} 0.00013 \\ 0.00011 \\ 0.00019 \end{bmatrix}\end{aligned}$$

Change in weights connected to second hidden neuron (h = 2) i.e. ΔW_{i2}

$$\begin{aligned}\Delta W_{i2} &= 0.1 * 1.9139 * (1 - 1.9139) * (0.1028) * (0.6 - 0.5407) \\ &* 0.5407 * (1 - 0.5407) * \begin{bmatrix} 0.5 \\ 0.4 \\ 0.7 \end{bmatrix} \\ \Delta W_{i2} &= \begin{bmatrix} -0.00013 \\ -0.00011 \\ -0.00019 \end{bmatrix}\end{aligned}$$

Change in weights connected to third hidden neuron (h = 3) i.e. ΔW_{i3}

$$\begin{aligned}\Delta W_{i3} &= 0.1 * 1.6505 * (1 - 1.6505) * (0.2024) * (0.6 - 0.5407) \\ &* 0.5407 * (1 - 0.5407) * \begin{bmatrix} 0.5 \\ 0.4 \\ 0.7 \end{bmatrix}\end{aligned}$$

$$\Delta W_{i3} = \begin{bmatrix} -0.00016 \\ -0.00013 \\ -0.00022 \end{bmatrix}$$

Change in weights connected to fourth hidden neuron (h = 4) i.e. ΔW_{i4}

$$\begin{aligned} \Delta W_{i4} &= 0.1 * 2.477 * (1 - 2.477) * (-0.1964) * (0.6 - 0.5407) \\ &\quad * 0.5407 * (1 - 0.5407) * \begin{bmatrix} 0.5 \\ 0.4 \\ 0.7 \end{bmatrix} \end{aligned}$$

$$\Delta W_{i4} = \begin{bmatrix} 0.00053 \\ 0.00042 \\ 0.00074 \end{bmatrix}$$

Change in weights connected to fifth hidden neuron (h = 5) i.e. ΔW_{i5}

$$\begin{aligned} \Delta W_{i5} &= 0.1 * 1.5434 * (1 - 1.5434) * (0.3023) * (0.6 - 0.5407) \\ &\quad * 0.5407 * (1 - 0.5407) * \begin{bmatrix} 0.5 \\ 0.4 \\ 0.7 \end{bmatrix} \end{aligned}$$

$$\Delta W_{i5} = \begin{bmatrix} -0.00019 \\ -0.00015 \\ -0.00026 \end{bmatrix}$$

Change in weights connected to sixth hidden neuron (h = 6) i.e. ΔW_{i6}

$$\begin{aligned} \Delta W_{i6} &= 0.1 * 2.2461 * (1 - 2.2461) * (-0.2967) * (0.6 - 0.5407) \\ &\quad * 0.5407 * (1 - 0.5407) * \begin{bmatrix} 0.5 \\ 0.4 \\ 0.7 \end{bmatrix} \end{aligned}$$

$$\Delta W_{i6} = \begin{bmatrix} 0.00061 \\ 0.00049 \\ 0.00086 \end{bmatrix}$$

Change in weights connected to seventh hidden neuron (h = 7) i.e. ΔW_{i7}

$$\begin{aligned} \Delta W_{i7} &= 0.1 * 1.6126 * (1 - 1.6126) * (0.4024) * (0.6 - 0.5407) \\ &\quad * 0.5407 * (1 - 0.5407) * \begin{bmatrix} 0.5 \\ 0.4 \\ 0.7 \end{bmatrix} \end{aligned}$$

$$\Delta W_{i7} = \begin{bmatrix} -0.00029 \\ -0.00023 \\ -0.00041 \end{bmatrix}$$

Update the weights between input and hidden layers as shown below

$$W_{ih} = W_{ih} + \Delta W_{ih} = W_{ih} + [\Delta W_{i1} \Delta W_{i2} \Delta W_{i3} \Delta W_{i4} \Delta W_{i5} \Delta W_{i6} \Delta W_{i7}]$$

$$\begin{aligned} W_{ih} &= \begin{bmatrix} -0.1 & 0.1 & 0.2 & -0.2 & 0.3 & -0.3 & 0.4 \\ 0.1 & 0.2 & -0.2 & 0.3 & -0.3 & 0.4 & -0.1 \\ 0.2 & -0.2 & 0.3 & -0.3 & 0.4 & 0.1 & -0.1 \end{bmatrix} \\ &+ \begin{bmatrix} 0.000137 & -0.000132 & -0.000160 & 0.000529 & -0.000187 & 0.000611 & -0.000293 \\ 0.000109 & -0.000106 & -0.000128 & 0.000423 & -0.000149 & 0.000489 & -0.000234 \\ 0.000191 & -0.000185 & -0.000224 & 0.000741 & -0.000261 & 0.000856 & -0.000410 \end{bmatrix} \\ &= \begin{bmatrix} -0.0999 & 0.0999 & 0.1998 & -0.1995 & 0.2998 & -0.2994 & 0.3997 \\ 0.1001 & 0.1999 & -0.2001 & 0.3004 & -0.3001 & 0.4005 & -0.1002 \\ 0.2002 & -0.2002 & 0.2998 & -0.2993 & 0.3997 & 0.1009 & -0.1004 \end{bmatrix} \end{aligned}$$

Calculate change in bias parameters (Δb_h) at hidden layer using Eq. 29 as shown below.

Change in bias parameters connected to first hidden neuron ($h = 1$) i.e. Δb_1

$$\begin{aligned} \Delta b_1 &= 0.1 * 1.9704 * (1 - 1.9704) * (-0.0971) * (0.6 - 0.5407) * 0.5407 \\ &* (1 - 0.5407) = 0.00027 \end{aligned}$$

Change in bias parameter connected to second hidden neuron ($h = 2$) i.e. Δb_2

$$\begin{aligned} \Delta b_2 &= 0.1 * 1.9139 * (1 - 1.9139) * (0.1028) * (0.6 - 0.5407) \\ &* 0.5407 * (1 - 0.5407) = -0.00026 \end{aligned}$$

Change in bias parameter connected to third hidden neuron ($h = 3$) i.e. Δb_3

$$\begin{aligned} \Delta b_3 &= 0.1 * 1.6505 * (1 - 1.6505) * (0.2024) * (0.6 - 0.5407) \\ &* 0.5407 * (1 - 0.5407) = -0.00032 \end{aligned}$$

Change in bias parameter connected to fourth hidden neuron ($h = 4$) i.e. Δb_4

$$\begin{aligned} \Delta b_4 &= 0.1 * 2.477 * (1 - 2.477) * (-0.1964) * (0.6 - 0.5407) \\ &* 0.5407 * (1 - 0.5407) = 0.0011 \end{aligned}$$

Change in bias parameter connected to fifth hidden neuron ($h = 5$) i.e. Δb_5

$$\Delta b_5 = 0.1 * 1.5434 * (1 - 1.5434) * (0.3023) * (0.6 - 0.5407) \\ * 0.5407 * (1 - 0.5407) = -0.00037$$

Change in bias parameter connected to sixth hidden neuron ($h = 6$) i.e. Δb_6

$$\Delta b_6 = 0.1 * 2.2461 * (1 - 2.2461) * (-0.2967) * (0.6 - 0.5407) \\ * 0.5407 * (1 - 0.5407) = 0.0012$$

Change in weights connected to seventh hidden neuron ($h = 7$) i.e. Δb_7

$$\Delta b_7 = 0.1 * 1.6126 * (1 - 1.6126) * (0.4024) * (0.6 - 0.5407) \\ * 0.5407 * (1 - 0.5407) = -0.00059$$

Update the bias parameters at hidden layer as shown below

$$b_h = b_h + \Delta b_h = b_h + [\Delta b_1; \Delta b_2; \Delta b_3; \Delta b_4; \Delta b_5; \Delta b_6; \Delta b_7]$$

$$b_h = \begin{bmatrix} -0.1 \\ 0.1 \\ 0.2 \\ -0.2 \\ 0.3 \\ -0.3 \\ 0.4 \end{bmatrix} + \begin{bmatrix} 0.0003 \\ -0.0003 \\ -0.0003 \\ 0.0011 \\ -0.0004 \\ 0.0012 \\ -0.0006 \end{bmatrix} = \begin{bmatrix} -0.0997 \\ 0.0997 \\ 0.1997 \\ -0.1989 \\ 0.2996 \\ -0.2988 \\ 0.3994 \end{bmatrix}$$

Forward pass on testing data

Calculate net input (net_h) to hidden layer using Eq. 2 as presented below

$$net_h = W_{ih}^T * X + b_h = \begin{bmatrix} -0.0999 & 0.1001 & 0.2002 \\ 0.0999 & 0.1999 & -0.2002 \\ 0.1998 & -0.2001 & 0.2998 \\ -0.1995 & 0.3004 & -0.2993 \\ 0.2998 & -0.3001 & 0.3997 \\ -0.2994 & 0.4005 & 0.1009 \\ 0.3997 & -0.1002 & -0.1004 \end{bmatrix} * \begin{bmatrix} 0.4 \\ 0.3 \\ 0.6 \end{bmatrix} \\ + \begin{bmatrix} -0.0997 \\ 0.0997 \\ 0.1997 \\ -0.1989 \\ 0.2996 \\ -0.2988 \\ 0.3994 \end{bmatrix} = \begin{bmatrix} 0.0105 \\ 0.0795 \\ 0.3994 \\ -0.3682 \\ 0.5694 \\ -0.2379 \\ 0.4690 \end{bmatrix}$$

Calculate output (o_h) for hidden layer using Eq. 3 as presented below

$$o_h = \frac{1}{1 + e^{-net_h}} = \begin{bmatrix} 0.5026 \\ 0.5199 \\ 0.5986 \\ 0.4090 \\ 0.6386 \\ 0.4408 \\ 0.6151 \end{bmatrix}$$

Calculate net input (net_o) to output layer using Eq. 4 as presented below

$$net_o = W_{ho}^T * o_h + b_o = [-0.0971 \ 0.1028 \ 0.2024 \ -0.1964 \ 0.3023 \ -0.2967 \ 0.4024] * \begin{bmatrix} 0.5026 \\ 0.5199 \\ 0.5986 \\ 0.4090 \\ 0.6386 \\ 0.4408 \\ 0.6151 \end{bmatrix} - 0.0985 = 0.2567$$

Calculate output (o_o) for output layer using Eq. 5 as presented below

$$o_o = \frac{1}{1 + e^{-net_o}} = \frac{1}{1 + e^{-0.2567}} = 0.5638$$

Error computation

In this example considered only one sample in testing dataset with target load $L(T) = 0.5$. So MSE and MAE values are computed using Eqs. 10 and 11 respectively with $n_s = 1$ and presented below.

$$MSE = (0.5 - 0.5638)^2 = 0.0041$$

$$MAE = |0.5 - 0.5638| = 0.0638$$

References

1. Almeshaiei E, Soltan H (2011) Alex Eng J 50(2):137. <https://doi.org/10.1016/j.aej.2011.01.015>
2. Alfares HK, Nazeeruddin M (2002) Int J Syst Sci 33(1):23. <https://doi.org/10.1080/00207720110067421>
3. Su P, Tian X, Wang Y, Deng S, Zhao J, An Q, Wang Y (2017) Energies 10(9):1303. <https://doi.org/10.3390/en10091303>

4. Mi J, Fan L, Duan X, Qiu Y (2018) *Math Probl Eng* 2018. <https://doi.org/10.1155/2018/3894723>
5. Hu R, Wen S, Zeng Z, Huang T (2017) *Neurocomputing* 221:24. <https://doi.org/10.1016/j.neucom.2016.09.027>
6. Lau E, Sun L, Yang Q (2019) *SN Appl Sci* 1(9):982. <https://doi.org/10.1007/s42452-019-0884-7>
7. Kumar BA, Sangeetha G, Srinivas A, Awoyera P, Gobinath R, Ramana VV (2020) *Soft computing for problem solving*. Springer, pp 677–690. https://doi.org/10.1007/978-981-15-0184-5_58
8. Awoyera P, Akinmusuru J, Krishna AS, Gobinath R, Arunkumar B, Sangeetha G (2020) *Soft computing for problem solving*. Springer, pp 197–207. https://doi.org/10.1007/978-981-15-0035-0_15
9. Veeramsetty V, Singal G, Badal T (2020) *Multimed Tools Appl* 79:22569. <https://doi.org/10.1007/s11042-020-09031-0>
10. Veeramsetty V, Deshmukh R (2020) *SN Appl Sci* 2(5):1. <https://doi.org/10.1007/s42452-020-2601-y>
11. Amral N, Ozveren C, King D (2007) In: 2007 42nd international universities power engineering conference. IEEE, pp 1192–1198. <https://doi.org/10.1109/UPEC.2007.4469121>
12. Kumar S, Mishra S, Gupta S (2016) In: 2016 second international conference on computational intelligence & communication technology (CICT). IEEE, pp 184–186. <https://doi.org/10.1109/CICT.2016.44>
13. Shaloudegi K, Madinehi N, Hosseinian S, Abyaneh HA (2012) *IEEE Trans Power Syst* 27(2):811. <https://doi.org/10.1109/TPWRS.2011.2175254>
14. Veeramsetty V, Chintham V, Vinod Kumar D (2018) *Int Trans Electr Energy Syst* 28(8):e2573. <https://doi.org/10.1002/etep.2573>
15. Veeramsetty V, Chintham V, Vinod Kumar DM (2018) *Int J Energy Sect Manag* 12(3). <https://doi.org/10.1108/IJESM-03-2017-0002>
16. Chen Y, Xu P, Chu Y, Li W, Wu Y, Ni L, Bao Y, Wang K (2017) *Appl Energy* 195:659. <https://doi.org/10.1016/j.apenergy.2017.03.034>
17. Salgado RM, Lemes RR (2013) *J Control Autom Electr Syst* 24(6):854. <https://doi.org/10.1007/s40313-013-0067-5>
18. Yang ZC (2015) *J Control Autom Electr Syst* 26(4):430. <https://doi.org/10.1007/s40313-015-0186-2>
19. Ke K, Hongbin S, Chengkang Z, Brown C (2019) *Evol Intell* 12(3):385. <https://doi.org/10.1007/s12065-018-00196-0>
20. Houimli R, Zmami M, Ben-Salha O (2019) *Energy Syst* 1–19. <https://doi.org/10.1007/s12667-019-00324-4>
21. Lisi F, Shah I (2019) *Energy Syst* 1–33. <https://doi.org/10.1007/s12667-019-00356-w>
22. Li K, Zhang T (2019) *Energy Syst* 1–16. <https://doi.org/10.1007/s12667-019-00344-0>
23. Shamir O, Zhang T (2013) In: *International conference on machine learning*, pp 71–79. <http://arxiv.org/abs/1212.1824>
24. Veeramsetty V (2020) *Mendeley data*. <https://doi.org/10.17632/ycfwywyx7d.2>
25. Barga R, Fontana V, Tok WH, Cabrera-Cordon L (2015) *Predictive analytics with Microsoft Azure machine learning*. Springer. <https://doi.org/10.1007/978-1-4842-0445-0>

Evaluation of Algorithms for Fundamental and Harmonic Impacts of Integration of Renewable Energy Sources in Smart Power Distribution Networks



R. Satish, K. Vaisakh, and Almoataz Y. Abdelaziz

Abstract With the development of renewable energy sources (RES), distributed generation (DG), microgrid, electric vehicles etc., in traditional distribution network which was earlier supply-side driven, single power supply, one-way service and basic reliance on manual management of business model turns into the direction of user interaction, the trend of two-way flow and highly automated and these changes gradually formed the smart power distribution network (SPDN). The rapid advancement in power electronic devices increases the fast growth of RES into SPDN and also increases the non-linear portion of loads on the network. Due to this, harmonic currents may inject into distribution networks. This chapter proposes new power flow algorithms (PFAs) for fundamental and harmonic analysis of SPDN with the integration of renewable energy based DG and presence of non-linear loads. The proposed methodology completely exploits the radial feature in distribution networks and developed BUS_NUM and BRANCH_NUM matrices. These matrices make the implementation of PFAs simple. The accuracy of fundamental and harmonic PFAs is tested on IEEE-13 bus test feeder and they are found to be accurate with the literature. Different case studies are carried on IEEE-13 bus and IEEE-34 bus test feeders for analyzing the impacts of multiple integration of synchronous based-renewable DG and power electronic based-renewable DG.

Keywords Power flow · Unbalanced networks · Linear loads · Non-linear loads · Distributed generation · Renewable energy sources · Harmonic distortion · Smart distribution networks

R. Satish (✉)

Department of Electrical and Electronics Engineering, ANITS (A), Visakhapatnam, Andhra Pradesh, India

K. Vaisakh

Department of Electrical Engineering, Andhra University, AUCE (A), Visakhapatnam, Andhra Pradesh, India

A. Y. Abdelaziz

Faculty of Engineering and Technology, Future University in Egypt, Cairo, Egypt

Nomenclature

RES	Renewable Energy Sources
DG	Distributed Generation
RDN	Radial Distribution Network
SPDN	Smart Power Distribution Network
PFA	Power Flow Algorithm
PEC	Power Electronic Converter
FPFA	Fundamental Power Flow Algorithm
HPFA	Harmonic Power Flow Algorithm
THD	Total Harmonic Distortion
FSIG	Fixed Speed Induction Generator
DFIG	Doubly Fed Induction Generator
SVCM	Static Voltage Characteristic Model

1 Introduction

RES such as photovoltaic, wind, fuel cells, etc., uses synchronous/induction generators or induction generators combined with PECs or only PECs to transfer AC power to the grids. Therefore RES can be a synchronous-based or a power electronic-based. Renewable energy can make a contribution to improve power quality, minimize peak loads and reduce the greenhouse gas emission. The connection of DG with the utility grid is specified in [1]. In [2], proposed a three-phase PFA for real-time distribution networks. It gives some primary discussions on PV node concept. DG modeling and their integration to the distribution networks is presented in [3, 4]. Harmonics may cause localized overheating, winding insulation stresses and torque pulsations with torsional vibrations on electric machines, additional power losses on devices, light flicker, communication interference and equipment loss of life or even damage if resonance conditions occur. Therefore HPFAs are essential for finding the harmonic distortion level in the presence of non-linear loads and renewable DG. The authors of [5, 6] propose a HPFA based on backward/forward sweep method. The improvement of power quality using fuel cell and fuzzy based controller is discussed in [7]. By using this controller, the quality of power in the grid system especially in micro grid connected with non-linear and unbalanced load is enhanced. For the fair allocation of active power losses [8, 9], develops a new active power loss allocation technique which eradicates the influence of cross-term analytically from loss formulation without any assumptions and approximations. A new active power loss allocation scheme is developed by eliminating the influence of cross-term mathematically from loss equation for allocating losses to the network participants with/without DGs [10]. This method assigns losses to the consumers/DG units with due consideration to their power consumptions/injections and physical locations in the radial distribution network.

This chapter proposes a new FPFA and HPFA for three-phase SPDN using BUS_NUM and BRANCH_NUM matrices. These algorithms use basic principles of circuit theory and hence they can be easily understood. In this chapter, a new scheme is developed to divide the distribution network into new sections. The bus numbers and branch numbers of these newly created sections are stored in row entries of BUS_NUM and BRANCH_NUM matrices respectively. These matrices make the PFA simple. The impacts of multiple installations of synchronous based-DG, power electronic based-DG and presence of non-linear loads on fundamental and harmonic voltage profile, fundamental and harmonic power loss and THD % are analyzed through the proposed algorithms. The compensation-based method [2] is used to handle the DGs in the proposed PFAs. This chapter is organized in the following order. The modeling of network components is discussed in Sect. 2. Methodology for developing BUS_NUM and BRANCH_NUM matrices is discussed in Sect. 3. FPFA for SPDN is presented in Sect. 4. Integration of renewable DGs into FPFA is presented in Sect. 5. HPFA for SPDN with integration of renewable DGs and presence of non-linear loads is presented in Sect. 6. Case studies and discussions with case studies on IEEE-13 node test feeder are presented in Sect. 7. Case studies and discussions with case studies on IEEE-34 node test feeder are presented in Sect. 8. The conclusions are presented in Sect. 9.

2 Modeling of Network Components

The modeling of lines, loads, capacitor banks, voltage regulators and distribution transformers for three-phase analysis is presented in [11]. The linear loads can be modeled in several ways [12] for harmonic analysis. Each model will show different impact on the network. In this chapter, the linear loads are modeled as impedances with series combination of resistance and reactance. The non-linear loads are modeled as constant current sources [13] with magnitude obtained from the typical harmonic spectrum and rated load current obtained from the fundamental power flow. The phase angle of the current source is obtained from the phase angle of rated current at fundamental frequency and phase angle of the harmonic source current spectrum. The modeling of other network components for harmonic analysis is presented in [14].

2.1 Renewable DG

The type of device used to interface the renewable DG to grid depends on its application and the type of energy source utilized. For example a wind turbine may employ a squirrel cage induction generator, called a FSIG, a DFIG or a PEC connected generator. DC sources or those generating at higher frequency, such as photovoltaic systems, fuel cells require a PEC to interface them into SPDN. Figure 1 gives the

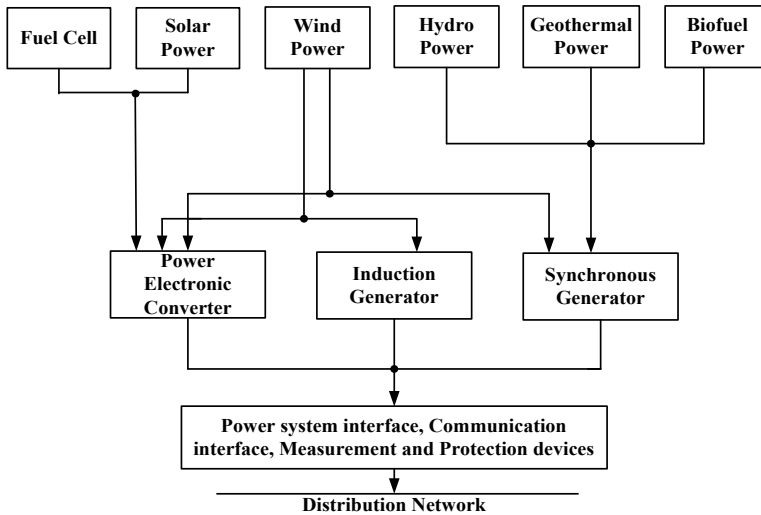


Fig. 1 Possible combination of renewable DG

possible interfacing of renewable DG with SPDN. The modeling of renewable DG for PFA requires the knowledge of operation and control on the characteristics of the interfacing devices. A brief modeling of interfacing devices is extracted as follows.

2.1.1 Synchronous Generator

Based on the excitation system the synchronous generators are of two types [3]. The first one is fixed excitation voltage type and the second one is regulating excitation voltage type. In regulating excitation voltage type the excitation can be controlled in two ways. One is maintaining the constant terminal voltage (voltage control mode) and the other is maintaining the constant power factor (power factor control mode). In PFAs the synchronous generator which maintains constant terminal voltage is considered as PV bus and which maintains constant power factor is treated as PQ bus. The synchronous generator with fixed excitation voltage [15] is treated as a SVCN.

2.1.2 Induction Generator

The active and reactive powers developed by the induction generator are functions of both slip and bus voltage [16]. Assuming the active power developed as constant and neglecting the very low dependency of reactive power with the slip, the induction generator can be modeled as SVCN and further since the bus voltage is nearer to

1 p.u in steady state cases, the reactive power is also constant. Hence the induction generator is modeled as PQ bus in PFA.

2.1.3 Power Electronic Converter

The modeling of PECs in PFA depends on the control method employed in converter control circuit. The PEC is modeled as PV bus if the control circuit in converter is designed to control both P and V independently [14]. If it is designed to control P and Q independently then it is modeled as PQ bus [17].

For HPFA, the power electronic based-renewable DG is considered as the sources for harmonics. The current spectrum of the power electronic based-renewable DG is taken from [18]. For synchronous based-renewable DG the harmonic current injection is taken as zero.

3 Methodology for Developing BUS_NUM and BRANC_NUM Matrices

The PFA of SPDN requires systematic numbering of buses and branches since it saves the memory and it is also strengthen the numerical performance of the solution methods. The numbering scheme adopted here is taken from [19]. In Fig. 2 starting with the bus 1 ('1' is enclosed in circle) in the lateral-1 ('1' is in square brackets) and then sequentially considering buses until it finds one that has more than one branch leaving from it and is labeled as section-I. So that section-I is formed with buses

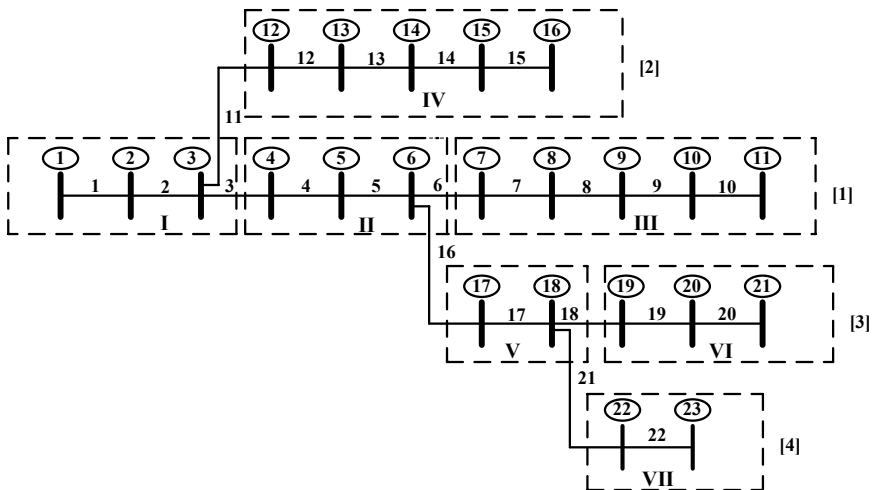


Fig. 2 Divided sections for the sample RDN

Table 1 Sections information from Fig. 2

Section No.	Bus numbers	Head bus	Tail bus	Branch numbers which are ahead of buses	Head branch	Tail branch
I	1, 2, 3	1	3	1, 2	1	2
II	4, 5, 6	4	6	3, 4, 5	3	5
III	7, 8, 9, 10, 11	7	11	6, 7, 8, 9, 10	6	10
IV	12, 13, 14, 15, 16	12	16	11, 12, 13, 14, 15	11	15
V	17, 18	17	18	16, 17	16	17
VI	19, 20, 21	19	21	18, 19, 20	18	20
VII	22, 23	22	23	21, 22	21	22

from 1 to 3. Then start proceeding from bus 4 until it find the one that has more than one branch leaving from it and it is labeled as section-II. Therefore section-II has buses from 4 to 6. Likewise the section-III created with buses from 7 to 11 in it. Once all buses in lateral-1 are over then repeat the same procedure for all other laterals After the entire distribution network is divided into sections we can have the following information as in Table 1.

A MATLAB code is developed to divide the network in to sections and to store the information of bus numbers and branch numbers of these sections in the following matrix entries.

BUS_NUM =	1	2	3	0	0	→ Section-I
	4	5	6	0	0	→ Section-II
	7	8	9	10	11	→ Section-III
	12	13	14	15	16	→ Section-IV
	17	18	0	0	0	→ Section-V
	19	20	21	0	0	→ Section-VI
	22	23	0	0	0	→ Section-VII

BRANCH_NUM =	1	2	0	0	0	→ Section-I
	3	4	5	0	0	→ Section-II
	6	7	8	9	10	→ Section-III
	11	12	13	14	15	→ Section-IV
	16	17	0	0	0	→ Section-V
	18	19	20	0	0	→ Section-VI
	21	22	0	0	0	→ Section-VII

4 Fundamental Power Flow Algorithm for SPDN

After the BUS_NUM and BRANCH_NUM matrices are developed for the SPDN, the following steps illustrate the iterative procedure for PFA.

1. The voltages at all busses are assigned as substation bus voltage.

$$\begin{bmatrix} V_a \\ V_b \\ V_c \end{bmatrix} = \begin{bmatrix} 1\angle 0^\circ \\ 1\angle -120^\circ \\ 1\angle 120^\circ \end{bmatrix} \text{ p.u} \tag{1}$$

2. Find the load current at all buses with the specified load power, type of load and voltage at the bus.
3. The power flow program should start with collecting current at bus 23 (the tail bus in section-VII as in BUS_NUM) thereby find the current in branch 22 (the tail branch in section-VII as in BRANCH_NUM). Then proceed towards head bus (i.e., bus 22) and head branch (i.e., branch 21) in finding the bus currents and branch currents respectively. This is illustrated with a sample section consists of three buses as shown in Fig. 3.

$$[I_{abc}]_k = [IL_{abc}]_k + [Ish_{abc}]_k + [IC_{abc}]_k \tag{2}$$

$$[I_{abc}]_{jk} = [I_{abc}]_k \tag{3}$$

$$[I_{abc}]_j = [I_{abc}]_{jk} + [IL_{abc}]_j + [Ish_{abc}]_j + [IC_{abc}]_j \tag{4}$$

$$[I_{abc}]_{ij} = [I_{abc}]_j \tag{5}$$

$$[I_{abc}]_i = [I_{abc}]_{ij} \tag{6}$$

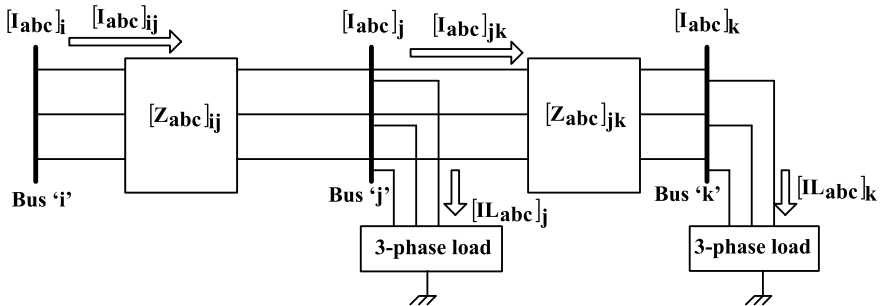


Fig. 3 A sample section consists of three busses

where,

$[I_{abc}]_k$: Three-phase current at bus 'k'.

$[I_{abc}]_{jk}$: Three-phase current in branch 'jk'.

$[I_{L_{abc}}]_k$: Three-phase load current at bus 'k'.

$[I_{sh_{abc}}]_k$: Three-phase current drawn by shunt admittance at bus 'k'.

$[I_{C_{abc}}]_k$: Three-phase current drawn by capacitor bank at bus 'k' if any.

4. Then go to section-VI and repeat the above step in finding head bus current and head branch current. Likewise, move up to section-I and find current at head bus in section-I (bus 1) and head branch in section-I (branch-1).
5. Now start with bus 1 (head bus in section-I), and proceed towards the tail bus in finding the bus voltages with Eq. 7.

$$\begin{bmatrix} V_a \\ V_b \\ V_c \end{bmatrix}_j = \begin{bmatrix} V_a \\ V_b \\ V_c \end{bmatrix}_i - \begin{bmatrix} Z_{aa} & Z_{ab} & Z_{ac} \\ Z_{ba} & Z_{bb} & Z_{bc} \\ Z_{ca} & Z_{cb} & Z_{cc} \end{bmatrix}_{ij} \bullet \begin{bmatrix} I_a \\ I_b \\ I_c \end{bmatrix}_{ij} \quad (7)$$

6. Then go to section-II and proceed towards the tail bus in finding the bus voltages. Likewise move up to bus 23 (tail bus in section-VII).
7. Repeat the steps 3 to 6 until the voltage magnitude mismatches at all buses in successive iterations is below the tolerance limit.

$$|[V_{abc}]_i^r - [V_{abc}]_i^{r-1}| \leq [\varepsilon_{abc}] \quad (8)$$

where, 'r' is the iteration number.

8. Find the power losses in all the branches are obtained with Eq. 9.

$$\begin{bmatrix} S_{Loss_a} \\ S_{Loss_b} \\ S_{Loss_c} \end{bmatrix}_{ij} = \begin{bmatrix} (V_a)_i \cdot (I_a)_{ij}^* \\ (V_b)_i \cdot (I_b)_{ij}^* \\ (V_c)_i \cdot (I_c)_{ij}^* \end{bmatrix} - \begin{bmatrix} (V_a)_j \cdot (I_a)_{ji}^* \\ (V_b)_j \cdot (I_b)_{ji}^* \\ (V_c)_j \cdot (I_c)_{ji}^* \end{bmatrix} \quad (9)$$

The flowchart of this algorithm is shown in Fig. 4.

5 Integration of Renewable DGs into FPPA of SPDN

The detailed iterative procedure for integration of renewable DG is illustrated with the following steps:

1. Run the power flow as presented in section-4. After the power flow is converged, select the locations of renewable DG.

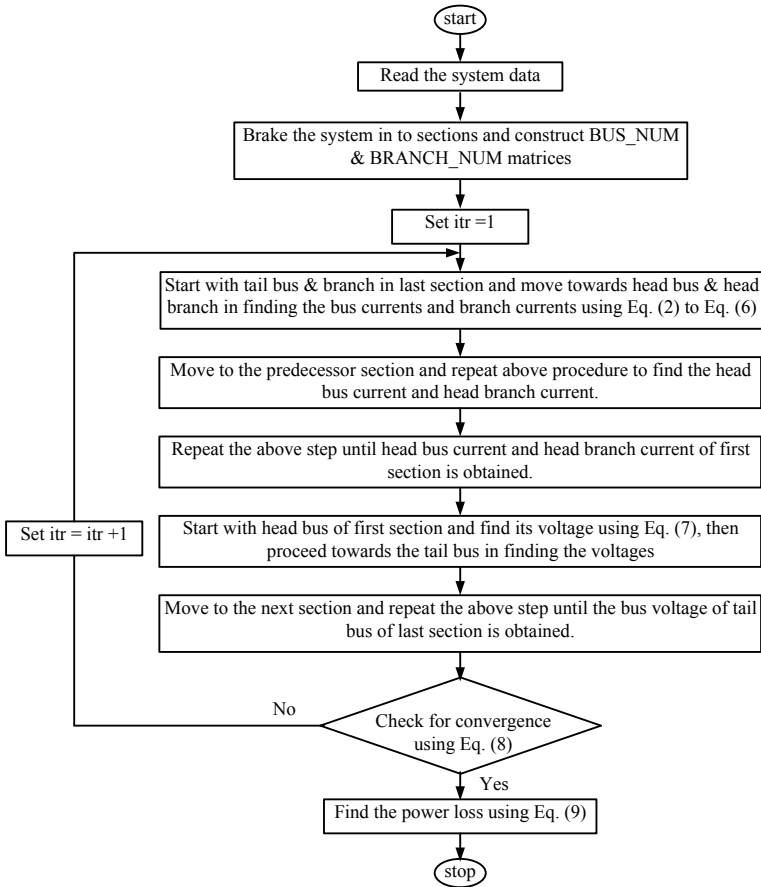


Fig. 4 Flowchart of FPFA

2. Then for the outside γ th iteration, check the type of renewable DG available.
3. If the renewable DG is modeled as PQ at bus say ' j ', then the current injected by the renewable DG is obtained with the specified power rating $[S_{G,abc}]_j$ and the bus voltage $[V_{abc}]_j$ as,

$$[I_{G,abc}]_j^\gamma = \left[\begin{matrix} (S_{G,a}/V_a)^* \\ (S_{G,b}/V_b)^* \\ (S_{G,c}/V_c)^* \end{matrix} \right]_j^\gamma \tag{10}$$

4. If the renewable DGs are modeled as PV buses. Then calculate the voltage mismatches at all the PV buses as,

$$\begin{bmatrix} \Delta V_a \\ \Delta V_b \\ \Delta V_c \end{bmatrix}^\gamma = \begin{bmatrix} V_a^{sp} \\ V_b^{sp} \\ V_c^{sp} \end{bmatrix} - \begin{bmatrix} V_a^{cal} \\ V_b^{cal} \\ V_c^{cal} \end{bmatrix}^\gamma \quad \text{PV buses } \forall \quad (11)$$

where,

$[\Delta V_{abc}]^\gamma$: Voltage mismatch matrix for outside γ th iteration. Its size is $3 \cdot n \times 1$ for 'n' PV buses in the network.

$|V_{abc}^{sp}|$: Magnitude of specified voltage at i th PV buses.

$|V_{abc}^{cal}|^\gamma$: Magnitude of voltage calculated at i th PV buses for outside k th iteration.

5. If the voltage mismatches are not less than the specified tolerance value, then incremental current injections at PV buses in order to maintain the specified voltages is calculated with Eq. 12.

$$[\Delta I]^\gamma = [Z_{pv}]^{-1} \cdot [\Delta V]^\gamma \quad (12)$$

$[Z_{pv}]$ is the PV bus sensitivity matrix. The $[Z_{pv}]$ can be formed by observing the following numerical properties of its entries [2]. The diagonal entry Z_{pp} is equal to the modulus of the sum positive sequence impedance of all line sections between PV buses 'p' and the substation bus. Since all the lines are three phase line sections, the size of Z_{pp} is 3×3 . If any two PV nodes, 'p' and 'q', have different paths from root node, then the off diagonal entry Z_{pq} (size 3×3) is zero. If 'p' and 'q' share a piece of common path to the root node, then Z_{pq} is equal to the modulus of the sum positive sequence impedance of all line sections on this common path. The dimension of $[Z_{pv}]$ is equal to $3 \cdot n \times 3 \cdot n$.

6. If the reactive power generations of renewable DGs are unlimited for the specified real power generation, then incremental reactive current to be injected at the j th PV bus is obtained with Eq. 13.

$$\begin{bmatrix} \Delta I_{G,a} \\ \Delta I_{G,b} \\ \Delta I_{G,c} \end{bmatrix}_j^\gamma = \begin{bmatrix} |\Delta I_a| \cdot (\cos(90^\circ + \delta_{v,a}) + j \sin(90^\circ + \delta_{v,a})) \\ |\Delta I_b| \cdot (\cos(90^\circ + \delta_{v,b}) + j \sin(90^\circ + \delta_{v,b})) \\ |\Delta I_c| \cdot (\cos(90^\circ + \delta_{v,c}) + j \sin(90^\circ + \delta_{v,c})) \end{bmatrix}_j^\gamma \quad (13)$$

$\delta_{v,a}$, $\delta_{v,b}$ and $\delta_{v,c}$ are the voltage angles at the j th PV bus.

7. Now, find the current in branch 'ij' from Fig. 5.

$$\begin{bmatrix} I_a \\ I_b \\ I_c \end{bmatrix}_{ij}^\gamma = \begin{bmatrix} I_{L,a} \\ I_{L,b} \\ I_{L,c} \end{bmatrix}_j^\gamma - \begin{bmatrix} \Delta I_{G,a} \\ \Delta I_{G,b} \\ \Delta I_{G,c} \end{bmatrix}_j^\gamma \quad (14)$$

With $[V_{abc}]_j^\gamma$ and $[I_{abc}]_{ij}^\gamma$ the reactive power flow in the line $[Q_{abc}]_{ij}^\gamma$ is evaluated. Then incremental reactive power injection is evaluated with Eq. 15.

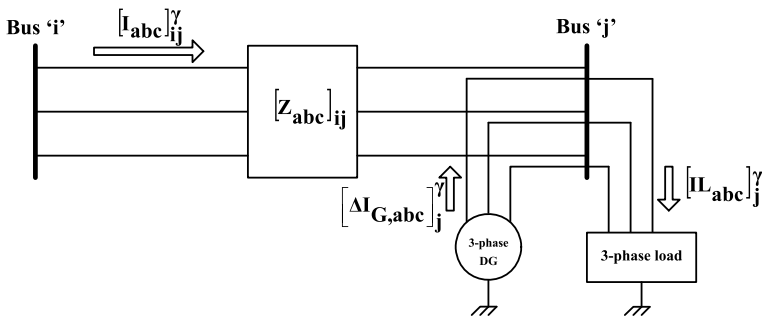


Fig. 5 A sample two nodes in the system with renewable DG placed at bus 'j'

$$\begin{bmatrix} \Delta Q_{G,a} \\ \Delta Q_{G,b} \\ \Delta Q_{G,c} \end{bmatrix}_j^\gamma = \begin{bmatrix} Q_{L,a} \\ Q_{L,b} \\ Q_{L,c} \end{bmatrix}_j^\gamma - \begin{bmatrix} Q_a \\ Q_b \\ Q_c \end{bmatrix}_{ij}^\gamma \tag{15}$$

Find the reactive power generation needed at j th PV bus using Eq. 16.

$$\begin{bmatrix} Q_{G,a} \\ Q_{G,b} \\ Q_{G,c} \end{bmatrix}_j^\gamma = \begin{bmatrix} Q_{G,a} \\ Q_{G,b} \\ Q_{G,c} \end{bmatrix}_j^{\gamma-1} + \begin{bmatrix} \Delta Q_{G,a} \\ \Delta Q_{G,b} \\ \Delta Q_{G,c} \end{bmatrix}_j^\gamma \tag{16}$$

Find the complex power generation at PV bus using Eq. 17.

$$\begin{bmatrix} S_{G,a} \\ S_{G,b} \\ S_{G,c} \end{bmatrix}_j^\gamma = \begin{bmatrix} P_{G,a} \\ P_{G,b} \\ P_{G,c} \end{bmatrix}_j + j * \begin{bmatrix} Q_{G,a} \\ Q_{G,b} \\ Q_{G,c} \end{bmatrix}_j^\gamma \tag{17}$$

where,

$[P_{G,abc}]_j$: Specified three-phase real power generation of the renewable DG at j th bus.

8. With the complex power obtained in Eq. 18, the current injected by the renewable DG is calculated with Eq. 10.
9. If the reactive power generations by the renewable DG were limited, then reactive power generation limits must be checked first. The total three phase reactive power needed at j th PV node is the sum of reactive power of three phases.

$$(Q_G)_j^\gamma = (Q_{G,a})_j^\gamma + (Q_{G,b})_j^\gamma + (Q_{G,c})_j^\gamma \tag{18}$$

If $Q_{j,\min} \leq (Q_G)_j^\gamma \leq Q_{j,\max}$, then complex power generation is as Eq. 17.

If $(Q_G)_j^y \leq Q_{j,\min}$ then set $(Q_G)_j^y = Q_{j,\min}$ and $(Q_{G,a})_j^y = (Q_{G,b})_j^y = (Q_{G,c})_j^y = Q_{j,\min}/3$.

If $(Q_G)_j^y \geq Q_{j,\max}$ then set $(Q_G)_j^y = Q_{j,\max}$ and $(Q_{G,a})_j^y = (Q_{G,b})_j^y = (Q_{G,c})_j^y = Q_{j,\max}/3$.

Where, $Q_{j,\min}$ and $Q_{j,\max}$ are the minimum and maximum reactive power generation limits of renewable DG at j^{th} PV bus.

These reactive power generations are combined with active power generations at PV buses and find the current injections by renewable DG as in Eq. 10.

10. Now set $\gamma = \gamma + 1$ and run the power flow with the current injections at renewable DG.
11. Power flow will be stopped when it attains convergence criterion.

The flowchart for this algorithm is shown in Fig. 6.

6 HPFA for SPDN with Integration of Renewable DGs and Presence of Non-linear Loads

The detailed iterative procedure for HPFA with integration of renewable DGs is illustrated with the following steps,

1. Run the FPFA with integrations of renewable DGs as presented in section-5.
2. With the converged bus voltages and specified loads, the impedance of linear loads is calculated for the harmonic order-h of interest.
3. Find the harmonic current injections of non-linear loads and power electronic based-renewable DGs for the selected harmonic order-h from the current spectra of the non-linear loads and DGs respectively.
4. The harmonic voltage at the substation bus is taken as zero since the supply voltage is assumed as a pure sinusoidal voltage waveform.
5. Find the net harmonic currents at all the buses with the harmonic current drawn by linear loads and harmonic current injections of non-linear loads and renewable DGs. The current drawn by the linear loads at all the buses is zero for the first iteration. The calculation of harmonic currents is illustrated with the sample section as shown in Fig. 7. The net harmonic current at node 'j' is given by Eq. 19 and the harmonic current in branch 'ij' is given by Eq. 20.

$$[I_{abc}]_j^h = -[IS_{abc}]_j^h - [IG_{abc}]_j^h + [IL_{abc}]_j^h \quad (19)$$

$$[I_{abc}]_{ij}^h = [I_{abc}]_j^h \quad (20)$$

Using the BUS_NUM and BRANCH_NUM matrices, the harmonic currents in all branches are to be obtained by moving up to the substation.

Where,

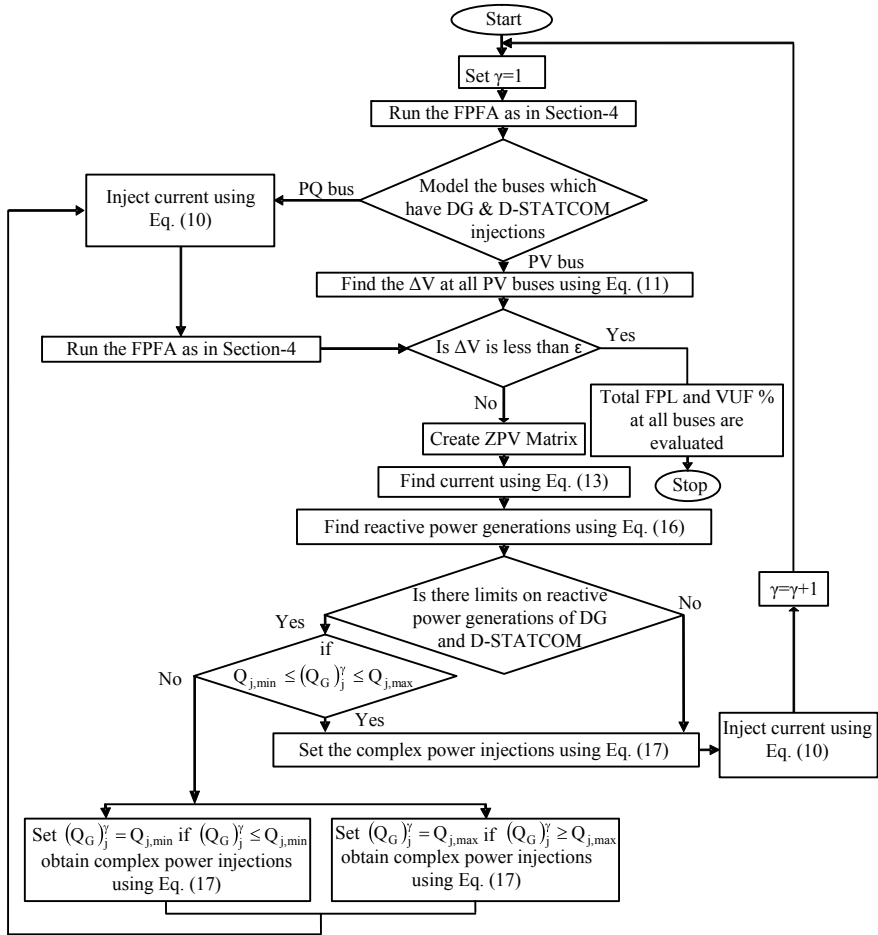


Fig. 6 Flowchart of FPFA with multiple renewable DG integrations

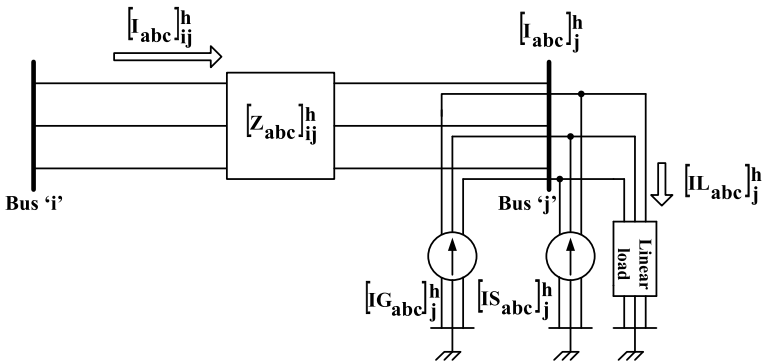


Fig. 7 A sample section of two buses for HPFA

$[I_{abc}]_j^h$: Three-phase harmonic current at bus 'j' for harmonic order-h.

$[I_{abc}]_{ij}^h$: Three-phase harmonic current in branch 'ij' for harmonic order-h.

$[IL_{abc}]_j^h$: Three-phase harmonic current drawn by linear load at bus 'j' for harmonic order-h.

$[IS_{abc}]_j^h$: Three-phase harmonic current injection by non-linear load at bus 'j' for harmonic order-h.

$[IG_{abc}]_j^h$: Three-phase current injection by renewable DG at bus 'j' for harmonic order-h.

6. Now, start with section-I and find the harmonic bus voltages by moving towards the tail bus using Eq. 21.

$$\begin{bmatrix} V_a \\ V_b \\ V_c \end{bmatrix}_j^h = \begin{bmatrix} V_a \\ V_b \\ V_c \end{bmatrix}_i^h - \begin{bmatrix} Z_{aa} & Z_{ab} & Z_{ac} \\ Z_{ba} & Z_{bb} & Z_{bc} \\ Z_{ca} & Z_{cb} & Z_{cc} \end{bmatrix}_{ij}^h \bullet \begin{bmatrix} I_a \\ I_b \\ I_c \end{bmatrix}_{ij}^h \quad (21)$$

Move to the next section and repeat this procedure until harmonic voltage at tail bus in last section is obtained.

7. Repeat the steps 5 and 6 until the magnitude mismatch of harmonic voltages of h-order at all the busses is within the tolerance limit.
8. The complex power loss for h-order harmonic is obtained with Eq. 22.

$$\begin{bmatrix} S_{Loss_a} \\ S_{Loss_b} \\ S_{Loss_c} \end{bmatrix}_{ij}^h = \begin{bmatrix} (V_a)_i \cdot (I_a)_{ij}^* \\ (V_b)_i \cdot (I_b)_{ij}^* \\ (V_c)_i \cdot (I_c)_{ij}^* \end{bmatrix}^h - \begin{bmatrix} (V_a)_j \cdot (I_a)_{ji}^* \\ (V_b)_j \cdot (I_b)_{ji}^* \\ (V_c)_j \cdot (I_c)_{ji}^* \end{bmatrix}^h \quad (22)$$

9. Find the total real power loss due to harmonics frequency of order-h using Eq. 23.

$$[P_loss]^h = \sum_{br=1}^{Nbr} [\text{real}([S_{Loss}]_{br}^h)] \quad (23)$$

10. Repeat the steps from 2 to 9 for all harmonics (order: 3, 5, 7, 9, 11, 13 and 15) of the selected range of frequency.
11. The total power loss due to all harmonics is,

$$[\text{Total_loss}] = \sum_{h=h_0}^{h_m} \sum_{br=1}^{Nbr} [\text{real}([S_{Loss}]_{br}^h)] \quad (24)$$

12. The r.m.s value of voltage at bus 'i', say phase 'a' is calculated as,

$$(V_a)_i = \sqrt{|(V_a)_i^1|^2 + \sum_{h=h_0}^{h_m} |(V_a)_i^h|^2} \quad (25)$$

13. The total harmonic distortion at every bus is defined as,

$$(THD)_i^a = \frac{\sqrt{\sum_{h=h_0}^{h_m} |(V_a)_i^h|^2}}{|(V_a)_i^1|} \quad (26)$$

where

h_0 : Minimum harmonic order

h_m : Maximum harmonic order

br: Branch number

Nbr: Total number of branches.

The flowchart for HPFA with multiple injections of renewable DGs is shown in Fig. 8.

7 Case Studies and Discussions on IEEE-13 Bus Feeder

7.1 Case Study 1: Fundamental Power Flow Solution

The data for IEEE-13 bus feeder shown in Fig. 9 is taken from [20]. The FPFA is developed on MATLAB software with convergence tolerance of 10^{-4} . The base values selected for the system are 5000 kVA and 4.16 kV. This FPFA is converged after 5 iterations. For testing the accuracy of FPFA, the voltage solution of IEEE-13 bus test feeder is presented Table 2 in comparison with the IEEE results. The maximum mismatches for voltage magnitudes and angle are found to be 0.0005 p.u and 0.010° respectively and are of insignificant. Therefore the test results are almost matches the IEEE results [20] in terms of accuracy. The power loss of the network in comparison with IEEE results is presented in Table 3.

7.2 Case Study 2: Harmonic Power Flow Solution

The regulator between buses 650 and 632 is removed and the capacitor banks at bus 675 and 611 are removed from the network. The data for harmonic load composition and current spectra of harmonic loads is taken from [21]. The convergence tolerance

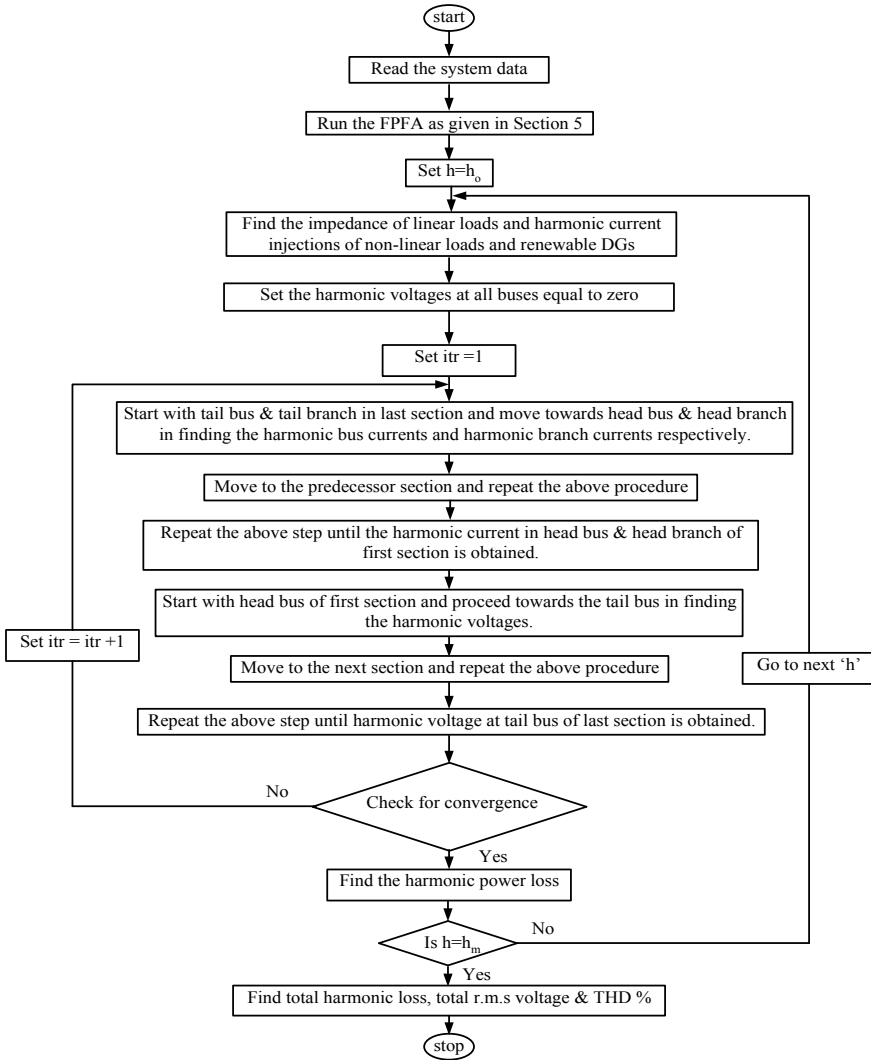
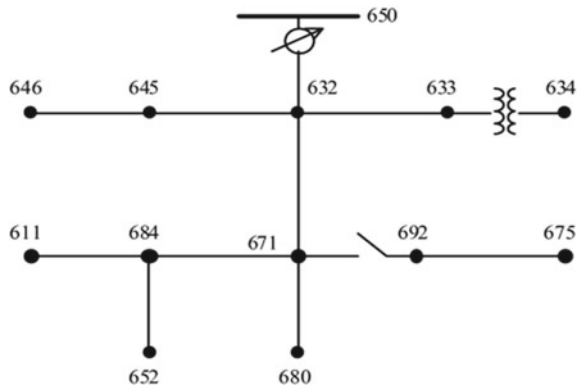


Fig. 8 Flowchart of HPFA with multiple integrations of renewable DGs

is taken as 10^{-4} . Table 4 presents the harmonic losses for harmonic frequencies of order 3, 5, 7, 9, 11, 13 and 15, total harmonic loss of the network and total power loss of the network including fundamental and harmonic loss. Total harmonic voltage profile and THD % for the selected range of harmonics of order 3, 5, 7, 9, 11, 13 and 15 are presented in Table 5. From the Table 5 it is observed that, the maximum THD % on the network is 5.2263 at bus 611 for c-phase and in [22] it was reported that maximum THD % at bus 611 for c-phase is 5.23. Therefore the results of the proposed HPFA are almost matches the literature in terms of accuracy. The THD%

Fig. 9 IEEE 13 bus test feeder



more than 5 is not desirable according to [23]. It is found that, the number of phases in the network with THD% more than 5 is 2.

7.3 Case Study 3: Harmonic Power Flow Solution with Multiple Integrations of Renewable DGs

One renewable DG is placed at bus 634 and other renewable DG placed at bus 675. The renewable DG at bus 634 is taken as PQ model with per phase real and reactive power generations are 300 kW and 197 kVAR respectively. Another renewable DG placed at bus 675 is taken as PV model with its per phase real power generation is 260 kW and the range of three-phase reactive power generation is 100 kVAR to 650 kVAR. The phase voltages specified at this bus are 1 p.u. In this case, the harmonic impacts are analyzed by treating both the renewable DGs as power electronic based in case-A and synchronous based in case-B. The convergence tolerance is taken as 10^{-4} . Table 6 presents the harmonic power loss for harmonic frequencies of order 3, 5, 7, 9, 11, 13 and 15, total harmonic loss of the network and total power loss of the network including fundamental and harmonic loss for case studies A and B. Table 7 presents the total r.m.s voltages and THD % for case studies A and B in case study 3.

7.4 Discussions

The results of case-2 such as voltage profile, power loss and THD % are used as benchmarks to see the fundamental and harmonic impacts of renewable DGs. In case-A of case-3, in which both DGs are power electronic based, the maximum THD% is observed to be 5.7280 at bus 611 for c-phase which is more than THD% in reported in case-2. The number of phases in buses with THD % more than 5 is

Table 2 Fundamental voltage solution for case study 1

Bus	Phase	Calculated results	IEEE Results [20]	Error in voltage Mag	Error in voltage Ang
650	a	$1 \angle 0^\circ$	$1 \angle 0^\circ$	0.0000	0.00
	b	$1 \angle -120^\circ$	$1 \angle -120^\circ$	0.0000	0.00
	c	$1 \angle 120^\circ$	$1 \angle 120^\circ$	0.0000	0.00
RG	a	$1.0625 \angle 0^\circ$	$1.0625 \angle 0^\circ$	0.0000	0.00
	b	$1.0500 \angle -120^\circ$	$1.0500 \angle -120^\circ$	0.0000	0.00
	c	$1.0687 \angle 120^\circ$	$1.0687 \angle 120^\circ$	0.0000	0.00
632	a	$1.0210 \angle -2.49^\circ$	$1.0210 \angle -2.49^\circ$	0.0000	0.00
	b	$1.0420 \angle -121.72^\circ$	$1.0420 \angle -121.72^\circ$	0.0000	0.00
	c	$1.0175 \angle 117.83^\circ$	$1.0170 \angle 117.83^\circ$	-0.0005	0.00
671	a	$0.9900 \angle -5.30^\circ$	$0.9900 \angle -5.30^\circ$	0.0000	0.00
	b	$1.0529 \angle -122.34^\circ$	$1.0529 \angle -122.34^\circ$	0.0000	0.00
	c	$0.9778 \angle 116.03^\circ$	$0.977 \angle 116.02^\circ$	0.0001	-0.01
680	a	$0.9900 \angle -5.30^\circ$	$0.9900 \angle -5.30^\circ$	0.0000	0.00
	b	$1.0529 \angle -122.34^\circ$	$1.0529 \angle -122.34^\circ$	0.0000	0.00
	c	$0.9778 \angle 116.03^\circ$	$0.977 \angle 116.02^\circ$	0.0001	-0.01
633	a	$1.0180 \angle -2.55^\circ$	$1.0180 \angle -2.56^\circ$	0.0000	0.01
	b	$1.0401 \angle -121.77^\circ$	$1.0401 \angle -121.77^\circ$	0.0000	0.00
	c	$1.0148 \angle 117.82^\circ$	$1.0148 \angle 117.82^\circ$	0.0000	0.00
634	a	$0.9940 \angle -3.23^\circ$	$0.9940 \angle -3.23^\circ$	0.0000	0.00
	b	$1.0218 \angle -122.22^\circ$	$1.0218 \angle -122.22^\circ$	0.0000	0.00
	c	$0.9960 \angle 117.35^\circ$	$0.9960 \angle 117.34^\circ$	0.0000	-0.01
645	b	$1.0328 \angle -121.90^\circ$	$1.0329 \angle -121.90^\circ$	0.0001	0.00

(continued)

Table 2 (continued)

Bus	Phase	Calculated results	IEEE Results [20]	Error in voltage Mag	Error in voltage Ang
	c	1.0155 ∠ 117.86°	1.0155 ∠ 117.86°	0.0001	0.00
646	b	1.0311 ∠ -121.98°	1.0311 ∠ -121.98°	0.0000	0.00
	c	1.0134 ∠ 117.90°	1.0134 ∠ 117.90°	0.0000	0.01
692	a	0.9900 ∠ -5.30°	0.9900 ∠ -5.31°	0.0000	0.01
	b	1.0529 ∠ -122.34°	1.0529 ∠ -122.34°	0.0000	0.00
	c	0.9778 ∠ 116.03°	0.9777 ∠ 116.02°	-0.0001	-0.01
675	a	0.9835 ∠ -5.55°	0.9835 ∠ -5.56°	0.0000	0.01
	b	1.0553 ∠ -122.52°	1.0553 ∠ -122.52°	0.0000	0.00
	c	0.9759 ∠ 116.04°	0.9758 ∠ 116.03°	-0.0001	-0.01
684	a	0.9881 ∠ -5.32°	0.9881 ∠ -5.32°	0.0000	0.00
	c	0.9758 ∠ 115.92°	0.9758 ∠ 115.92°	0.0000	0.00
611	c	0.9738 ∠ 115.78°	0.9738 ∠ 115.78°	0.0000	0.00
652	a	0.9825 ∠ -5.24°	0.9825 ∠ -5.25°	0.0000	0.01

Table 3 Fundamental power loss for case study 1

Phase	Calculated power loss		IEEE results [20]	
	Active	Reactive	Active	Reactive
	(kW)	(kVAR)	(kW)	(kVAR)
a	39.13	152.62	39.107	152.585
b	-4.74	42.27	-4.697	42.217
c	76.59	129.69	76.653	129.850
Total	110.98	324.57	111.063	324.653

Table 4 Harmonic power loss in case study 2

Harmonic order	Harmonic power loss	
	Active (kW)	Reactive (kVAR)
3	0.7958	6.5165
5	0.0856	1.1483
7	0.0072	0.1183
9	0.0043	0.0902
11	0.0008	0.0164
13	0.0008	0.0226
15	0.0010	0.0340
Total harmonic loss	0.8983	7.9464
Total power loss	148.23	441.49

found to be 6. In case-B of case-3, in which both DGs are synchronous based, the maximum THD% is observed to be 5.2442 at bus 611 for c-phase which is more than THD % reported in case-2. The number of phases in buses with THD % more than 5 is found to be 6. Figure 10 compares the fundamental voltage profile between case 2 and case 3. From Fig. 10, the improvement in voltage profiles is observed with the integrations of renewable DGs as in case 2. Figure 11 compares the THD% of case-A in case-3, case-B in case-3 with the THD % of case 2 and it is observed from Fig. 11 that, the THD% is more for case-A, in which the renewable DGs are power electronic based.

8 Case Studies and Discussions on IEEE-34 Bus Feeder

The data for IEEE-34 bus feeder is taken from [20]. The convergence tolerance is 10^{-4} . The base values selected for the system are 2500 kVA and 24.9 kV. The load composition at spot loads for harmonic analysis is presented in Table 8. The current spectra of the non-linear loads are taken from [21]. The description of different case studies on IEEE-34 bus feeder is presented in Table 9. The test results of the case-1 are used as benchmark to see the fundamental and harmonic impacts of renewable DGs on the network.

Figure 12 compares the fundamental voltage profile between case-1 and case-2. From Fig. 12, improvement in voltage profile is absorbed with the integrations of renewable DGs. Figure 13 compares the THD % between the case studies 1 and 2. From Fig. 14, the maximum THD % is observed in case-A of case-2, which has integrations of two power electronic based-DGs. From Fig. 15, it is observed that the number of phases effected with THD% more than 5 is 19 for case-A of case-2 and zero for case-B of case-2. From Figs. 13, 14 and 15 it is seen that, the integrations of renewable synchronous based-renewable DGs reduces the THD%, reduces the

Table 5 Harmonic power flow solution for case study 2

Bus	Phase	S. No.	Fundamental r.m.s voltage	Total r.m.s voltage	THD %
650	a	1	$1 \angle 0^\circ$	0	0
	b	2	$1 \angle -120^\circ$	0	0
	c	3	$1 \angle 120^\circ$	0	0
632	a	4	$0.9498 \angle -2.7462^\circ$	0.9500	1.9173
	b	5	$0.9839 \angle -121.6817^\circ$	0.9839	0.4974
	c	6	$0.9300 \angle 117.8000^\circ$	0.9302	2.2737
671	a	7	$0.9109 \angle -5.8987^\circ$	0.9117	4.0623
	b	8	$0.9875 \angle -122.2091^\circ$	0.9875	1.0363
	c	9	$0.8717 \angle 115.9500^\circ$	0.8728	4.9409
680	a	10	$0.9109 \angle -5.8987^\circ$	0.9117	4.0623
	b	11	$0.9875 \angle -122.2091^\circ$	0.9875	1.0363
	c	12	$0.8717 \angle 115.9500^\circ$	0.8728	4.9409
633	a	13	$0.9466 \angle -2.8223^\circ$	0.9468	1.9098
	b	14	$0.9819 \angle -121.7315^\circ$	0.9819	0.4919
	c	15	$0.9271 \angle 117.7946^\circ$	0.9273	2.2648
634	a	16	$0.9207 \angle -3.6073^\circ$	0.9209	1.8801
	b	17	$0.9624 \angle -122.2445^\circ$	0.9624	0.4873
	c	18	$0.9064 \angle 117.2178^\circ$	0.9066	2.2406
645	b	19	$0.9745 \angle -121.8646^\circ$	0.9745	0.4991
	c	20	$0.9283 \angle 117.8225^\circ$	0.9286	2.2769
646	b	21	$0.9729 \angle -121.9382^\circ$	0.9729	0.5000
	c	22	$0.9264 \angle 117.8696^\circ$	0.9267	2.2815
692	a	23	$0.9109 \angle -5.8987^\circ$	0.9117	4.0623
	b	24	$0.9875 \angle -122.2091^\circ$	0.9875	1.0363
	c	25	$0.8717 \angle 115.9500^\circ$	0.8728	4.9409
675	a	26	$0.9025 \angle -6.0795^\circ$	0.9034	4.3128
	b	27	$0.9887 \angle -122.3037^\circ$	0.9887	1.0491
	c	28	$0.8678 \angle 116.0660^\circ$	0.8689	5.0687
684	a	29	$0.9093 \angle -5.9502^\circ$	0.9100	4.0765
	c	30	$0.8684 \angle 115.9163^\circ$	0.8695	5.0741
611	c	31	$0.8651 \angle 115.8365^\circ$	0.8663	5.2263
652	a	32	$0.9041 \angle -5.8755^\circ$	0.9049	4.0900

Table 6 Harmonic power loss for case-A and case-B in case study 3

Harmonic order	Harmonic power loss			
	Case-A in Case-3		Case-B in Case-3	
	Active (kW)	Reactive (kVAR)	Active (kW)	Reactive (kVAR)
3	0.7529	6.1520	0.8228	6.7138
5	0.2015	2.5941	0.0913	1.2239
7	0.0835	1.3267	0.0081	0.1341
9	0.0041	0.0857	0.0048	0.1018
11	0.0169	0.3981	0.0009	0.0186
13	0.0193	0.5764	0.0009	0.0259
15	0.0009	0.0322	0.0011	0.0404
Total harmonic loss	1.0791	11.1652	0.9299	8.2585
Total power loss	69.93	197.41	69.78	194.50

number of phases in buses with THD% less than 5 and reduces the maximum THD % on the network and the integrations of power electronic based-renewable DGs increases the THD %, increases the number of phases in buses with THD% less than 5 and increases the maximum THD % on the network with respect to case-1. Figure 16 compares the total power loss in different case studies.

9 Conclusion

The impacts of renewable DG on fundamental voltage, fundamental power loss and combined harmonic impacts of renewable DG and non-linear loads on harmonic voltage profile, harmonic power loss and THD % are analyzed with the proposed FPFA and HPFA. The proposed algorithm is accurate and easy to understand and effectively handling all types of renewable DG models. The use of BUS_NUM and BRANCH_NUM matrices makes the PFAs simple. The integration of synchronous based-renewable DG the network can reduce the harmonic pollution on the network in terms of THD% at different buses of the network, number of phases in buses with THD% more than 5 and maximum THD% on the network.. However the improvement in fundamental voltage profile and reduction in power loss can be achieved with any type of renewable DG. The location, type and size of renewable DGs are the three main factors that can affect the power quality and this can limit the amount of renewable DG penetration. In the case of a utility owned DG installation the utility has to optimally plan the location and size of the DG in order to improve network benefits and reliability. In practice, one is not always able to site DG at the locations determined by an optimization algorithm. In the case of customer owned DG

Table 7 Harmonic power flow solution for case study 3

Bus	Ph	S. No.	Fundamental r.m.s voltage	Total r.m.s voltage for case-A in case-3	THD %	Total r.m.s voltage for case-B in case-3	THD%
650	a	1	1 $\angle 0^\circ$	0	0	0	0
	b	2	1.0000 $\angle -120^\circ$	0	0	0	0
	c	3	1.0000 $\angle 120^\circ$	0	0	0	0
632	a	4	0.9730 $\angle -1.68^\circ$	0.9732	2.1494	0.9732	1.9959
	b	5	0.9973 $\angle -120.48^\circ$	0.9973	1.0734	0.9973	0.6219
	c	6	0.9540 $\angle 118.98^\circ$	0.9544	2.7960	0.9543	2.3845
671	a	7	0.9429 $\angle -4.10^\circ$	0.9437	4.1935	0.9437	4.0844
	b	8	1.0045 $\angle -120.42^\circ$	1.0046	1.5876	1.0046	1.2144
	c	9	0.9056 $\angle 117.88^\circ$	0.9070	5.4857	0.9067	4.9782
680	a	10	0.9429 $\angle -4.10^\circ$	0.9437	4.1935	0.9437	4.0844
	b	11	1.0045 $\angle -120.42^\circ$	1.0046	1.5876	1.0046	1.2144
	c	12	0.9056 $\angle 117.87^\circ$	0.9070	5.4857	0.9067	4.9782
633	a	13	0.9749 $\angle -1.64^\circ$	0.9752	2.2474	0.9751	2.0059
	b	14	1.0006 $\angle -120.40^\circ$	1.0006	1.2622	1.0006	0.6309
	c	15	0.9574 $\angle 119.06^\circ$	0.9578	2.9268	0.9577	2.3982
634	a	16	0.9950 $\angle -1.00^\circ$	0.9957	3.7010	0.9952	2.0365
	b	17	1.0249 $\angle -119.60^\circ$	1.0254	3.0848	1.0249	0.6456
	c	18	0.9828 $\angle 119.94^\circ$	0.9838	4.5109	0.9831	2.4403
645	b	19	0.9880 $\angle -120.66^\circ$	0.9880	1.0792	0.9880	0.6240
	c	20	0.9523 $\angle 119.00^\circ$	0.9527	2.8009	0.9526	2.3878
646	b	21	0.9863 $\angle -120.73^\circ$	0.9864	1.0810	0.9863	0.6250
	c	22	0.9503 $\angle 119.05^\circ$	0.9507	2.8067	0.9506	2.3927
692	a	23	0.9429 $\angle -4.10^\circ$	0.9437	4.1935	0.9437	4.0844
	b	24	1.0045 $\angle -120.42^\circ$	1.0046	1.5876	1.0046	1.2144
	c	25	0.9056 $\angle 117.87^\circ$	0.9070	5.4857	0.9067	4.9782
675	a	26	0.9379 $\angle -4.19^\circ$	0.9388	4.4480	0.9388	4.3096
	b	27	1.0080 $\angle -120.44^\circ$	1.0082	1.6510	1.0081	1.2267
	c	28	0.9047 $\angle 118.08^\circ$	0.9061	5.6530	0.9058	5.0896

(continued)

Table 7 (continued)

Bus	Ph	S. No.	Fundamental r.m.s voltage	Total r.m.s voltage for case-A in case-3	THD %	Total r.m.s voltage for case-B in case-3	THD%
684	a	29	0.9411 $\angle -4.15^\circ$	0.9420	4.2097	0.9419	4.0965
	c	30	0.9023 $\angle 117.84^\circ$	0.9037	5.5985	0.9035	5.1023
611	c	31	0.8990 $\angle 117.77^\circ$	0.9005	5.7280	0.9003	5.2442
652	a	32	0.9358 $\angle -4.07^\circ$	0.9366	4.2311	0.9366	4.1047

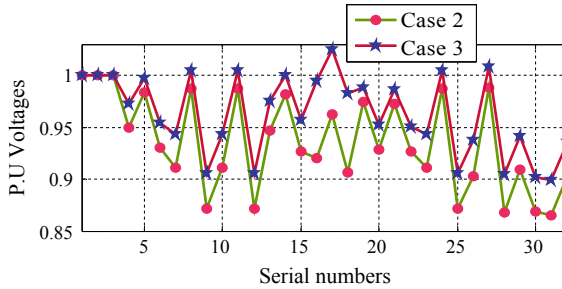


Fig. 10 Comparison of fundamental voltage profile between case 2 and case 3 for IEEE-13 bus feeder

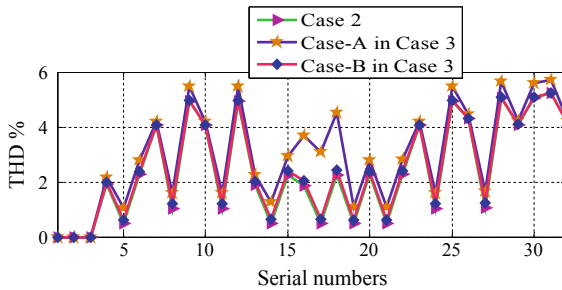


Fig. 11 Comparison of THD % between case 2 and case 3 for IEEE-13 bus feeder

installation, the utility planner should conduct feasibility and assessment study to evaluate any technical issues resulting from the new installation of customer owned DG installation.

Table 8 Load composition of spot loads on IEEE-34 bus feeder

Bus No.	Load composition			
	Non-linear loads			Linear loads
	Fluorescent light banks	Adjustable speed drives	Composite residential loads	
830	None	None	80	20
844	30	30	30	10
848	30	30	30	10
890	30	None	60	10
860	30	30	30	10
840	30	30	30	10

Table 9 Case studies on IEEE-34 bus feeder

Case study	Description	
Case-1	<ul style="list-style-type: none"> Removed voltage regulators between buses 614 and 650 and 852 and 832 Removed capacitor banks at buses 844 and 848 Load composition of spot loads as in Table 9 	
Case-2	<ul style="list-style-type: none"> 3-phase DG is placed at bus 848 is modeled as PQ bus with capacity, P = 150 kW and Q = 99 kVAR for each phase 3-phase DG is placed at bus 890 is modeled as PV bus with P = 130 kW per phase and three phase reactive power limits: $50 \leq Q \leq 325$ kVAR 	Case-A: Both DGs are Power electronic based Case-B: Both DGs are Synchronous based

Fig. 12 Comparison of fundamental voltage profile between case 1 and case 2 for IEEE-34 bus feeder

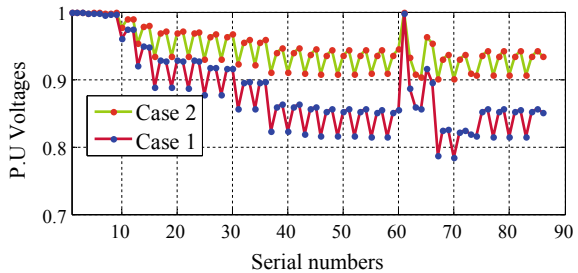


Fig. 13 Comparison of THD % between case 1 and case 2 for IEEE34 bus feeder

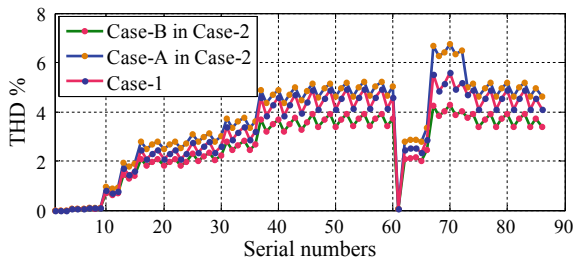


Fig. 14 Comparison of maximum THD % in different case studies for IEEE-34 bus feeder

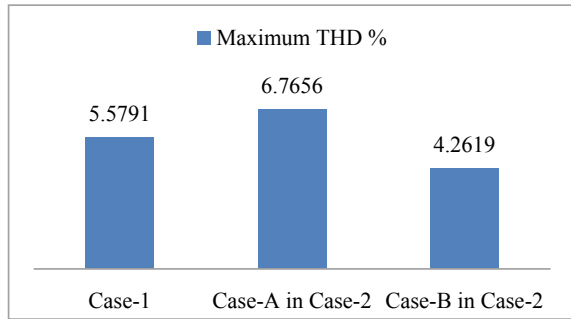


Fig. 15 Comparison of number of phases in buses with THD % more than 5 in different case studies for IEEE-34 bus feeder

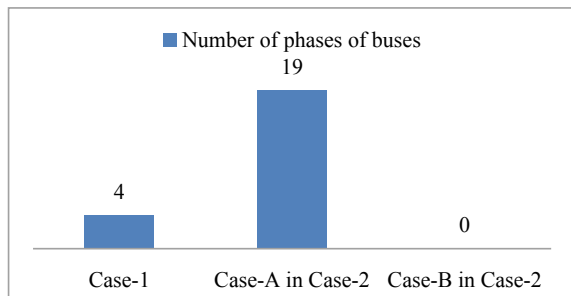
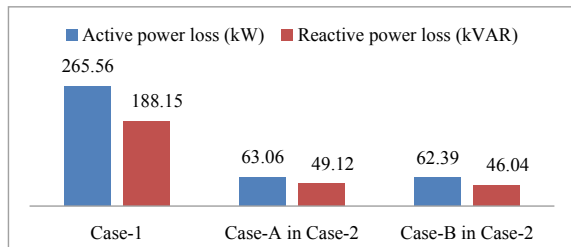


Fig. 16 Comparison of total power loss in different case studies for IEEE-34 bus feeder



References

1. IEEE Standard 1547-2003, IEEE Standard for Interconnecting Distributed Resources with Electric Power Systems, pp 1–16. <https://doi.org/10.1109/IEEESTD.2003.94285>.
2. Cheng CS, Shirmohammadi D (1995) A three-phase power flow method for real-time distribution system analysis. IEEE Trans Power Syst 10:671–679. <https://doi.org/10.1109/59.387902>
3. Losi A, Russo M (2005) Dispersed generation modeling for object-oriented distribution load flow. IEEE Trans Power Deliv 20:1532–1540. <https://doi.org/10.1109/TPWRD.2004.838634>
4. Moghaddas-Tafreshi SM, Mashhour E (2009) Distributed generation modeling for power flow studies and a three-phase unbalanced power flow solution for radial distribution systems considering distributed generation. Electr Power Syst Res 79:680–686. <https://doi.org/10.1016/j.epsr.2008.10.003>

5. Teng J-H, Chang C-Y (2007) Backward/forward sweep-based harmonic analysis method for distribution systems. *IEEE Trans Power Deliv* 22:1665–1672. <https://doi.org/10.1109/TPWRD.2007.899523>
6. Amini MA, Jalilian A, Behbahani MRP (2019) Fast network reconfiguration in harmonic polluted distribution network based on developed backward/forward sweep harmonic load flow. *Electr Power Syst Res* 168:295–304. <https://doi.org/10.1016/j.epsr.2018.12.006>
7. Das SR, Mishra DP, Ray PK, Salkuti, A. K. Sahoo (2020) Power quality improvement using fuzzy logic based compensation in a hybrid power system. *Int J Power Electron Drive Syst* 11. <https://doi.org/10.11591/ijpeds.v12.i1.pp576-584>
8. Hota P, Mishra S, Mishra DP, Salkuti SR (2020) Allocating active power loss with network reconfiguration in electrical power distribution systems, *Int J Power Electron Drive Syst* 11. <https://doi.org/10.11591/ijpeds.v12.i1.pp130-138>
9. Hota P, Mishra SK, Mishra DP (2020) Loss allocation strategies in active power distribution networks: a review. *Adv Electr Control Signal Syst Sel Proc AECSS* 665:889–902. https://doi.org/10.1007/978-981-15-5262-5_68
10. Hota P, Mishra SK, Mishra DP (2020) A new active power loss allocation method for radial distribution networks with DGs. *Adv Electr Control Signal Syst Sel Proc AECSS* 665:501–514. https://doi.org/10.1007/978-981-15-5262-5_37
11. Kersting WH (2017) *Distribution system modeling and analysis*, 4th edn. CRC Press
12. Burch R, Cheng G, Hatziaioniu C et al (2003) Impact of aggregate linear load modeling on harmonic analysis: a common practice and analytical models. *IEEE Trans Power Delivery* 18:625–630. <https://doi.org/10.1109/TPWRD.2003.810492>
13. Task Force on Harmonic Modeling and Simulation (1996) Modeling and simulation of the propagation of harmonics in electric power networks Part I: concepts, models and simulation techniques. *IEEE Trans Power Deliv* 11:452–465. <https://doi.org/10.1109/61.484130>
14. Arrillaga J, Watson NR (2003) *Power system harmonics*, 2nd edn. Wiley, New York
15. Chen H, Chen J, Shi D, Duan X (2006) Power flow study and voltage stability analysis for distribution systems with distributed generation. In: *IEEE power engineering society general meeting*, pp 1–8. <https://doi.org/10.1109/PES.2006.1709198>
16. Naka S, Genji T, Fukuyama Y (2001) Practical equipment models for fast distribution power flow considering interconnection of distributed generators. In: *Power engineering society summer meeting*, pp 1007–1012. <https://doi.org/10.1109/PSS.2001.970196>
17. Nehrir H, Wang C, Shaw SR (2006) Fuel cells: promising devices for distributed generation. *IEEE Power Energy Mag* 4:47–53. <https://doi.org/10.1109/MPAE.2006.1578531>
18. RavikumarPandi V, Zeineldin HH, Xiao W (2013) Determining optimal location and size of distributed generation resources considering harmonic and protection coordination limits. *IEEE Trans Power Syst* 28:1245–1254. <https://doi.org/10.1109/TPWRS.2012.2209687>
19. Das D, Nagi HS, Kothari DP (1994) Novel method for solving radial distribution networks. *IEE Proc Gen Transm Distrib* 141:291–298. <https://doi.org/10.1049/ip-gtd:19949966>
20. Radial Distribution Test Feeders. <http://sites.ieee.org/pes-testfeeders/resources>
21. Abu-Hashim R, Burch R, Chang G et al (1999) Test systems for harmonic modeling and simulation. *IEEE Trans Power Deliv* 14:579–587. <https://doi.org/10.1109/61.754106>
22. Yang NC, Le MD (2016) Three-phase harmonic power flow by direct Z_{BUS} method for unbalanced radial distribution systems with passive power filters. *IET Gen Transm Distrib* 10:3211–3219. <https://doi.org/10.1049/iet-gtd.2015.1368>
23. IEEE Standard 519-2014, IEEE recommended practice and requirements for harmonic control in electric power systems, pp 1–17. <https://doi.org/10.1109/IEEESTD.2014.6826459>

A Comprehensive Review of Active Islanding Detection Methods and Islanding Assessment in a Grid Connected Solar Based Microgrid



Kumari Namrata, Akshit Samadhiya, and Papia Ray

Abstract In this literature, different islanding and their detection techniques are overviewed for the power system network consisting of distribution system along with Distributed Generator (DG). As penetration of renewable energy utilization and DG are increasing continuously, it is important for a power system engineer to detect and mitigate any possible occurrence of islanding event. Islanding Detection Methods (IDMs) are divided as remote and local methods. Remote methods requires communication system for efficient operation while local methods are again categorised into three types active, passive and hybrid methods. Active methods are based on direct interaction with the power system operation via perturbation and passive methods are based on utilization of local parameters while hybrid methods are the amalgamation of active and passive. These IDMs for DG are described and analysed as per detection time, advantage, disadvantage, Non Detection Zone (NDZ) and power quality issues. This work will give a broad idea for selecting the better one of IDMs. Selection of IDMs are based on four relevant performance indices. A better IDM has a minimum NDZ with lower detection time without degrading the power quality. Integration of Renewable energy sources can pose technical challenges. Unintentional Islanding may result in issues such as system instability, degradation in power quality and malfunctioning of protection system. Fast and efficient methods needs to be developed to prevent unintentional islanding. To achieve better reliability and high accuracy, different islanding detection methods (IDMs) have been discussed in this research work. An extensive analysis of IDMs based on different technical aspects is presented. A techno-economical comparison of IDMs is presented based on recent trends related to monitoring islanding events. Additionally, a simulation study for a grid connected Solar based Microgrid is presented to analyze five different islanding

K. Namrata (✉) · A. Samadhiya

Department of Electrical Engineering, National Institute of Technology Jamshedpur, Jamshedpur, India

e-mail: namrata.ee@nitjsr.ac.in

P. Ray

Department of Electrical Engineering, Veer Surendra Sai University of Technology, Burla, Odisha, India

e-mail: papiaray_ee@vssut.ac.in

detection methods under unintentional islanding. Comparison of IDMs is based on trip signal generation under two different loading scenarios during an islanding event.

Keywords Islanding · Distributed generator · Local parameters · Non detection zone · Power quality · Photovoltaic · Utility grid

Nomenclature

IDMs	Islanding Detection Methods
MG	Micro-grid
DG	Distributed Generator
NDZ	Non Detection Zone
PQ	Power quality
P	Active Power
Q	Reactive Power
CB	Circuit Breaker
AI	Anti-Islanding
ID	Islanding Detection
PCC	Point of common coupling
ΔP	Active Power mismatch
ΔQ	Reactive Power mismatch
Δt	Detection time
Ed	Error detection ratio
RID	Remote islanding detection
LID	Local islanding detection
PID	Passive islanding detection
AID	Active islanding detection
HID	Hybrid islanding detection
TT	Transfer trip
SCADA	Supervisory control and data acquisition
OUV	Over/Under voltage
OUF	Over/Under frequency
PJD	Phase jump detection
PLL	Phase Locked Loop
VU	Voltage unbalance
PSV	Positive Sequence Voltage
THD	Total harmonic distortion
CBSS	Circuit breaker switching strategy
AFD	Active frequency drift
C_f	Chopping fraction
T_z	Zero or dead time
SFS	Sandia frequency shift
SVS	Sandia voltage shift

APS	Automatic phase drift
IM	Impedance measurement
NCCI	Negative component of current injection

1 Introduction

Global consumption pattern has seen continual annual growth over the last two decades and is expected that the demand may even double in coming 10 years [1]. A shift towards renewable based low carbon technologies in power generation has been observed. Key factors such as technological advancement in semiconductors, Solar cells and wind turbines, decarbonisation of power sector, efficient power electronics converters and advanced control strategies allows accelerated deployment of renewable energy sources. Renewable based Microgrids ensures less transmission losses and can even improve the power quality and voltage profile of the Grid [2]. However, increasing penetration of renewable based energy system can pose certain challenges to the power quality, stability and safety of the Grid [3].

Renewable based generation systems or Distributed generations (DGs) as shown in Fig. 1 can either operate in grid connected mode or isolate itself to provide power to local loads. However, events related to unintentional islanding of DGs may occur which needs prompt attention. These events leads to instability, transient

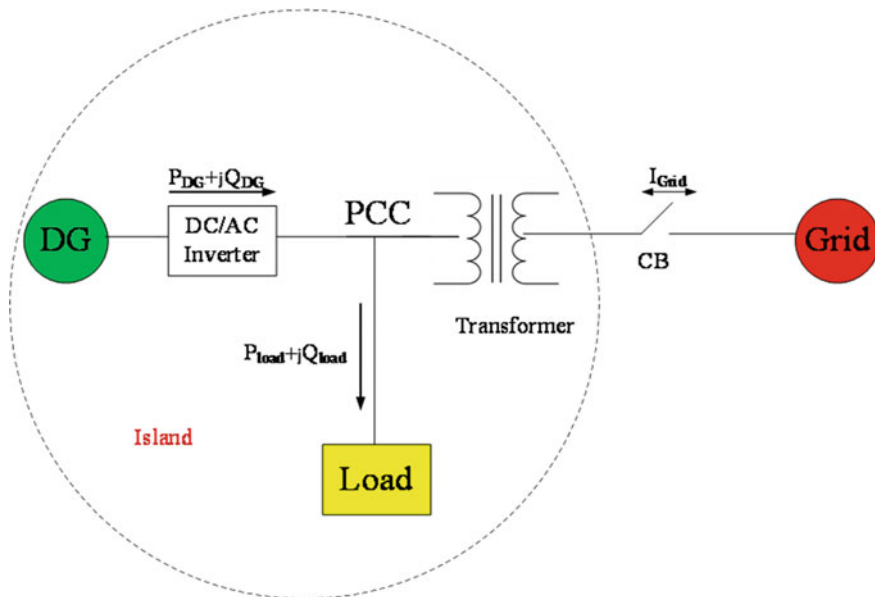
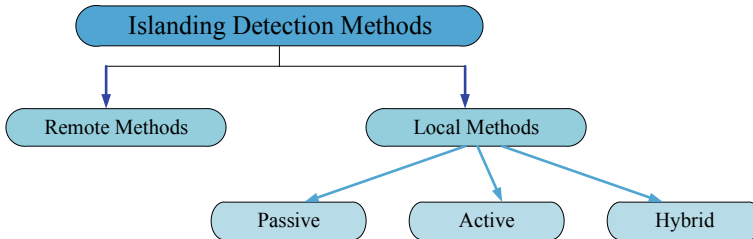


Fig. 1 Power islanding condition

Table 1 Technical requirements and guidelines defined by various for monitoring islanding events in grid connected DGs [4, 5]

Standards	Quality factor	$t_{\text{detection}}$ (ms)	Allowable frequency range (Hz)	Allowable voltage range (%)
IEEE:1547	1	<2000	49.3–50.5	88–110
IEC:62116	1	<2000	$f_0 - 1.5 \leq f \leq f_0 + 1.5$	88–110
IEEE:929-2000	2.5	<2000	49.3–50.5	88–110

**Fig. 2** Taxonomy of islanding detection methods

overvoltage, frequency deviation, malfunction of protection system that degrades the power quality of the system. Certain standards are adopted widely to address unintentional islanding issues for grid connection of DG units. Some standards are listed in Table 1 that provides technical requirement for Anti islanding capability of DG units before integration in the power system network.

For detection of the islanding phenomena different methods are shown in Fig. 2 remote islanding and local islanding methods. Again local islanding methods are categorised as passive, active and hybrid methods [6]. A detailed assessment and comparison of various Islanding Detection (ID) methods along with benefits and limitations are presented for monitoring islanding based activities.

- Considering the future outlook of the electric power industry, wide scale penetration of renewable technologies such as solar, wind, fuel cell etc. in the form of distributed generation requires efficient converters, adoption of advance control strategies and latest technological advancements.
- Detection of islanding condition is also an important issue to deal with.
- Due to challenges related to the power quality of the system, progress in the field of islanding detection have gained momentum in recent years.
- However, very few publications have discussed about the fundamental problem, comparison between contemporary and advance detection techniques, classification of IDMs, performance indices for assessing IDMs, advantages and disadvantages of each IDMs in terms of Non detection zones (NDZ), detection time and power quality. Hence, a comprehensive analysis on various aspects of islanding detection is worth to review and compile.

The work is segregated into following sections. Section 2 deals with challenges related to unintentional islanding and its effect on the power system. Section 3 discusses about various performance indices for selecting a better IDM. Section 4 broadly discusses about different types of local, remote, active and Hybrid islanding detection methods. Section 5 compares different types of IDM based on NDZ, detection time and power quality.

2 Certain Challenges with Islanding

Unintentional islanding into the system leads a big concern since integrated power distribution networks was implemented. Such integrated system together with inverter or non-inverter-based DG systems, different load conditions, and compounded control strategy give rise to many challenge to power system network reliability [7]. There are numerous IDMs presented in research paper, which uses different tolls for effective capacity building, tools name as complex computing and signal analysis [8]. Though, still some problems remain that need to be examined in the field of islanding detection, example as performance of IDMs for concurrent operations, interaction between different DG systems which are fitted with AI devices, when islanding occurs. Tackling mentioned challenges and highlighting the responsiveness of the AI devices, IDMs are analytically analysed in this review. If an island of the power system is created unintentionally, it causes trouble and serious harms. Some of the important harms are discussed as.

- The voltage and frequency may get affected and not remain in their appropriate standard level.
- Line staff safety may be vulnerable by DGs feeding into a system after opening and tagging of primary sources.
- Instant reclosing may cause phase difference. This causes huge torques mechanically and huge difference in current (I) /voltage (V), might shatter the physical systems [9]. Sharp rise leads to devastation of the appliances also.

3 Indices / Parameters of Islanding Detection Methods

The objective of the islanding detection techniques is to monitor certain system parameters such as rate of change of frequency, Voltage, current, ΔP , ΔQ and accordingly determine any possible occurrence of grid disconnection based on the threshold value of the parameters. The salient characteristics of an effective and reliable IDM are listed below:

- Minimum NDZ
- Minimum detection time

- High Power quality (lower value of THD)
- Error detection ratio close to 1 i.e. minimum events of false detection.

Hence, IDMs can be assessed on the basis of four relevant performance indices namely Non detection Zone (NDZ). Detection time (Δt), power quality and error detection ratio (E_d).

3.1 Non Detection Zone (NDZ)

NDZ became the primary cause for failing of IDMs. NDZ methods is build up by observing of V, I and f deviation that lead to power mismatch. Power mismatch between output of DG and load utilization when distributed generator operates in islanding condition are due to fluctuation of V and f at a point of common coupling (PCC). When ΔP and ΔQ are almost to zero, at that time V and f fluctuation are not enough to detect the islanding. The range of power mismatch (ΔP , ΔQ), which can't cause V and f crossing the threshold set value to detect islanding is known non detection zone (NDZ) [6, 10]. NDZ in power mismatch space is shown by [11].

$$\left(\frac{V}{V_{\max}}\right)^2 - 1 \leq \frac{\Delta P}{P} \leq \left(\frac{V}{V_{\min}}\right)^2 - 1 \quad (1)$$

$$Q_f \left(1 - \left(\frac{f}{f_{\min}}\right)^2\right) \leq \frac{\Delta Q}{P} \leq Q_f \left(1 - \left(\frac{f}{f_{\max}}\right)^2\right) \quad (2)$$

where $[V_{\min}, V_{\max}]$ is the allowable voltage range, f_{\min} is minimum frequency and f_{\max} is maximum frequency, V and P are rated voltage and active power, and Q_f is the quality factor. NDZ region is shown in Fig. 3. NDZ stands “non-detection zone” the range of conditions where a real grid failure will be filtered out.

NDZ is a very useful feature used for evaluating and examining the effectiveness of the islanding detection technique. Figure 3, shows ΔP versus ΔQ plane and this power imbalance happen due to V and f variations. Out of the shaded region AI device sense the islanding condition and thus disconnect the DG but this would not be possible in case of power difference came within power mismatch space and thus it became threat for the safety unit.

3.2 Detection Time

Time interval between the disconnecting of the main grid and detecting islanding b IDMs that is expressed as

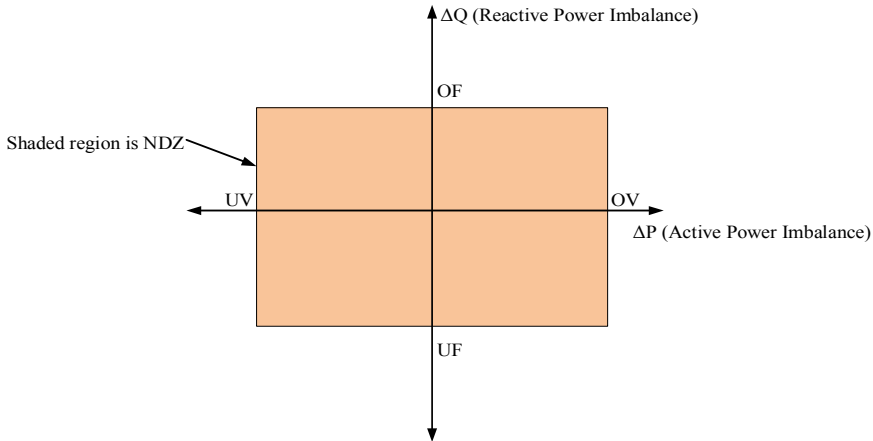


Fig. 3 Power mismatch space or NDZ region

$$\Delta t = t_{IDM} - t_{trip} \tag{3}$$

where Δt is the detection time, t_{IDM} is the instant at which islanding detected and t_{trip} is the instant at which circuit breaker of the main grid get trip and isolate the DGs.

3.3 Power Quality

For the power quality, several aspects have to be taken in consideration like voltage, current and frequency stability as well as continuous supply of power and there waveform. Due to all these concerns it doesn't have the particular definition and thus it is also known as service quality, voltage and current quality but judging the all parameters it can defined as the calculation, analysis, and betterment of the line parameters to maintain a reference waveform.

3.4 Error Detection Ratio

It is related to the false detection of islanding by IDMs whenever utility grid and micro grid (MG) are interconnected. Error measurement caused primarily by disturbance, which results in measured units exceeding the set points [12]. It is described as

$$E_d = \frac{N_{error\ detected}}{N_{error\ detected} + N_{correct\ detected}} \tag{4}$$

where E_d is error detection ratio, $N_{error\ detected}$ is count of time false detection and $N_{correct\ detected}$ is count of time correct detection.

4 Islanding Detection Methods

Various detection methods are being identified the researchers across the world. Typically, these can be classified into remote islanding detection (RID) and local islanding detection (LID) methods. RID methods are based on measurement and calculation of technical parameters at the central side [13–18], while LID methods are based realization at DG side. LID methods can be further divided into passive islanding detection (PID) [19–53], active islanding detection (AID) and hybrid islanding detection (HID) methods as shown in Fig. 2. In this work, Active Islanding [54–64] and Hybrid Islanding techniques [57, 65, 66] are extensively reviewed. Passive detection techniques are discussed in our recent review article [67].

4.1 Active Islanding Detection Methods

In these AID methods, intentionally injecting small perturbation at the output end of the DGs, that injecting signal do some significant changes in the system parameters and if that changes exceed the predefined value then trip signal get activated of the islanding condition and thus DG get disconnected. Remarkably AID methods have advantage as their low or zero NDZ, but major demerit is that these methods deteriorate the power quality. The basic flow chart of AID methods is shown in Fig. 4, and then different AID methods discussed briefly.

4.1.1 Active Frequency Drift (AFD)

Electrical parameters voltage and current are associated with the magnitude, frequency and phase. AFD uses the frequency/phase related parameters. In this method a small disruption current is injected into the main system, and whenever the islanding phenomena occurs, frequency drift take place by adding a zero time in inverter current and make the inverter current waveform distorted with respect to the original waveform i.e., shown in Fig. 5, however it is not affected during the grid connected system. Distortion meaning is phase difference between inverter output waveform (current) and original waveform of utility voltage at PCC. Due to distortion, inverter detect phase error, and participate in drifting the DG/inverter current to make the phase error zero. To make the drift occurs, DG connected inverter should work at unity power factor, and frequency drift is compared with OUF relay for islanding to be detected. For this a parameter is defined name as chopping fraction (cf) shown in Eq. (5).

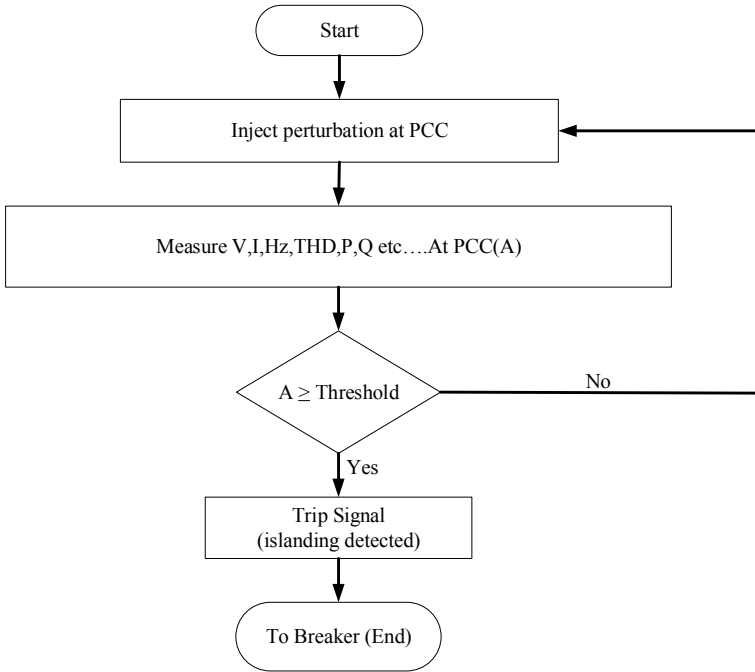


Fig. 4 Flow chart of AID methods

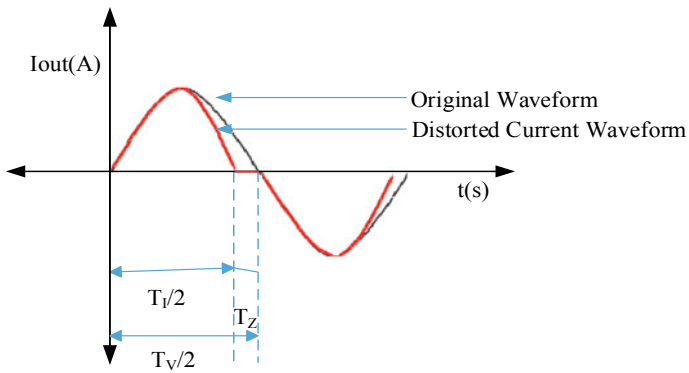


Fig. 5 Operational waveform of AFD method [54]

$$cf = \frac{T_z}{T_v/2} \tag{5}$$

where, T_z = zero or dead time and T_v = time period of utility voltage. It is easy in implementation and having small NDZ compare to novel PID methods. Drawbacks

are, effective for purely resistive load, as NDZ became large during large values of capacitance (C) and inductance (L), also wouldn't suitable for parallel inverter systems, and have issue with the power quality [54].

4.1.2 Active Frequency Drift with Positive Feedback (AFDPF)

For suppressing drawbacks of AFD (multi-inverter and NDZ issue), a positive feedback is used along with AFD. This feedback amplify the chopping fraction (cf) or dead time and assist the frequency drift at higher rate. Due to increase in the rate of frequency detection, it leads to detect the islanding condition fastly compared to AFD.

$$cf_k = cf_{k-1} + G(\Delta\omega_k) \quad (6)$$

where cf_k and cf_{k-1} are k th chopping fraction and $(k - 1)$ th chopping fraction, $\Delta\omega_k = \text{frequency difference} = \omega_{k-1} - \omega_0$, G is positive gain constant. No matter cf is positive or negative, AFDFP reinforced the frequency drift for any load, but the power quality degradation is still continued due to injected disturbance [55].

4.1.3 Sandia Frequency Shift (SFS)

This method is also an add-on of AFD, using a positive feedback for the frequency of the output voltage at the inverter end, whose chopping fraction is expressed as

$$cf = cf_0 + K(f_{PCC} - f_{line}) \quad (7)$$

where, cf_0 is chopping fraction without frequency variation, K is accelerating gain, f_{PCC} is frequency of voltage at PCC and f_{line} is the frequency of the original line.

During normal operation DG sets try to change the frequency but system stability maintain the same frequency, but during utility grid disconnected mode, there is rise in the frequency attempted at PCC and thus increase the chopping fraction. Whenever the frequency at the inverter end crosses the set value then islanding is detected. SFS method has very small NDZ, as well as detecting efficiency and power quality is improved [56].

4.1.4 Sandia Voltage Shift (SVS)

This method uses the same principle as SFS, just change is that it uses a positive feedback of magnitude of voltage at PCC and changes the current and power. When grid is linked there is no effect shown of this positive feedback, but during open linked voltage is reduced at PCC and thus current and power reduced. For that reduction

of voltage a UV relay is used for the protection. Possibility is also of rising of voltage, and hence OUV relay is used, if the PCC voltage reaches OUV standards then islanding is detected [57]. Among all AID methods this method is quite easy in implementation, having small NDZ but facing the problem of power quality issue.

4.1.5 Slip Mode Frequency Shift (SMFS)

Practice is carried out by applying positive feedback to the phase of the PCC voltage. A small perturbation in the phase will cause frequency deviation during the grid disconnected, but a small disturbance in phase during grid connected mode will not lead to frequency deviation, hence phase difference in normal operation is almost zero as unity power factor maintain by the inverter. A SMFS curve Fig. 9, using Eq. (8).

$$\theta_{SMFS}(k) = \theta_m \sin\left(\frac{\pi}{2} \frac{(f^{(k-1)} - f_0)}{(f_m - f_0)}\right) \tag{8}$$

where θ_m is maximum phase deviation which occur at maximum frequency f_m and $f^{(k-1)}$ is previous cycle frequency and f_0 is rated frequency. Equation (8) is showing the relation between frequency and phase angle. Working principle also validate that slope of the SMFS line is greater than the load line during unstable region. When grid get disconnected, operation will move towards the new stable point (shown by dotted as $f1$ and $f2$), during going through unstable to stable a set threshold value of inverter frequency crossed in either direction and thus islanding get detected by OUF relay. Problem with this method is having large NDZ and quality of power issue [58].

4.1.6 Automatic Phase Drift (APS)

This method is extension of SMFS, used to rectify the problem of NDZ of AFD and SMFS methods by utilizing positive feedback to the phase angle of output current of inverter. Hence only starting angle of inverter current alter consistently by using previous frequency of voltage, expression is shown as

$$\theta_{APS}^{(k)} = \frac{1}{\alpha} \left(\frac{f^{(k-1)} - f_0}{f_0} \right) 360^\circ + \theta_0^{(k)} \tag{9}$$

where $\theta_{APS}^{(k)}$ is beginning angle of inverter I, α is constant and $\theta_0^{(k)}$ is additional phase shift induced each time in the terminal voltage.

$$\theta_0^{(k)} - \theta_0^{(k-1)} = \Delta\theta * sgn(\Delta f_s) \tag{10}$$

where $\Delta\theta = \text{constant}$, $\Delta f_s = \text{change in steady state frequency}$, $\text{sgn} = \text{sign or signum function i.e., defined as}$:

$$\text{sgn}(\Delta f_s) = \begin{cases} 1 & \text{if } f_s > 0 \\ 0 & \text{if } f_s = 0 \\ -1 & \text{if } f_s < 0 \end{cases} \quad (11)$$

Due to additional phase shift, frequency deviate of the voltage to stabilizing to new operating point, and during islanding this deviation of the frequency leads the OUF standards, thus islanding get detected. Disadvantages of this method are speed is slow and not suited for nonlinear load [59].

4.1.7 Variation in Active and Reactive Power

Method is based on the capacity of inverter to produce both active power and reactive power independently. During the utility disconnected mode, DG has to supply active power, and depending upon the load condition, voltage will rise or fall as voltage is related directly to the active power. When the change in the voltage exceeds the set threshold value, then islanding condition is detected by the help of OUV relay.

Similarly reactive power cause frequency variation, and it's detected by the OUF relay. The detection time is around 0.3–0.75 s, easy in implementation and has small NDZ. Weaknesses are it can't support multi-inverter as false detection sometime raised, power quality issue continued [60].

4.1.8 Negative Component of Current Injection (NCCI)

This method is involving the use of small injection of negative component of current (less than 3%) to the voltage source inverter (VSI) at the PCC terminal, leads to disturbing the PCC voltage as unbalancing of the voltage occurs during the grid disconnected. In normal mode NCC flow into grid without affecting the PCC voltage. Thus islanding get detected if negative sequence voltage exceeds the threshold value within 60–70 ms. Method is beneficial for any load, zero NDZ and detecting fast compare to positive sequence voltage [61, 62]. This method can also use to detect islanding by negative sequence impedance as it's the ratio of negative component of voltage and current.

4.1.9 Impedance Measurement (IM)

Ratio of rate of change of voltage (ROCOV) to the rate of change of current (ROCO) of the inverter gives the impedance. This (dv/di) technique is used for the detection as during normal operation variation in the voltage is very less and hence impedance is

low, but during grid disconnected mode voltage varies significantly by perturbation in the current and thus impedance crosses the threshold value and islanding get detected. Detection time is around 700–900 ms [63]. It's advantage is that NDZ is low and work effectively in case of single inverter and synchronously connected multi inverter, but all time synchronously would not be possible and thus multi inverter is became demerit for it.

4.1.10 Impedance Detection at Specific Frequency

This technique is exceptional case of harmonic detection method. A perturbation of the special frequency harmonics of the current are injected in the inverter. Due to this abruptly change occurs in the voltage of inverter placed at PCC terminal when the utility is disconnected, but not significant change during utility connected to the DGs. Due to production of harmonic voltage in the system, impedance can be measure and if it crosses more than the set point, then islanding detected. It is not appropriate for the multi inverter system [64].

4.2 Hybrid Islanding Detection Methods

As passive and active methods are suffering from large NDZ and power quality issue respectively. To eradicate both the problems, a HID methods are used, that combine both PID and AID methods. In this case AID methods apply after the use of the PID methods as shown in the flow chart of Fig. 6. Some of the HID methods are discussed in brief as the following.

4.2.1 Voltage Unbalance (VU) and Frequency Set Point

As VU (passive) is more sensitive to the load fluctuation, so instead of VU/THD (passive), this method uses VU as a passive parameter. Other active parameter should be needed that is completed by positive feedback to the voltage or current that leads to deviation in the frequency by using SFS/SVS. Whenever some changes in the system occur the voltage spike rises suddenly, and from precaution of the false detection due to load switching or transient, a maximum VU is set for their threshold i.e., around 35 times of the VU average as per the Menon and Nehrir proposal [65]. Voltage spike also leads to frequency deviation, if the frequency change in a specified time is greater than the threshold value then islanding condition get detected. Technique have advantages as very small NDZ, very low power quality issue and clearly discriminate islanding and non-islanding conditions.

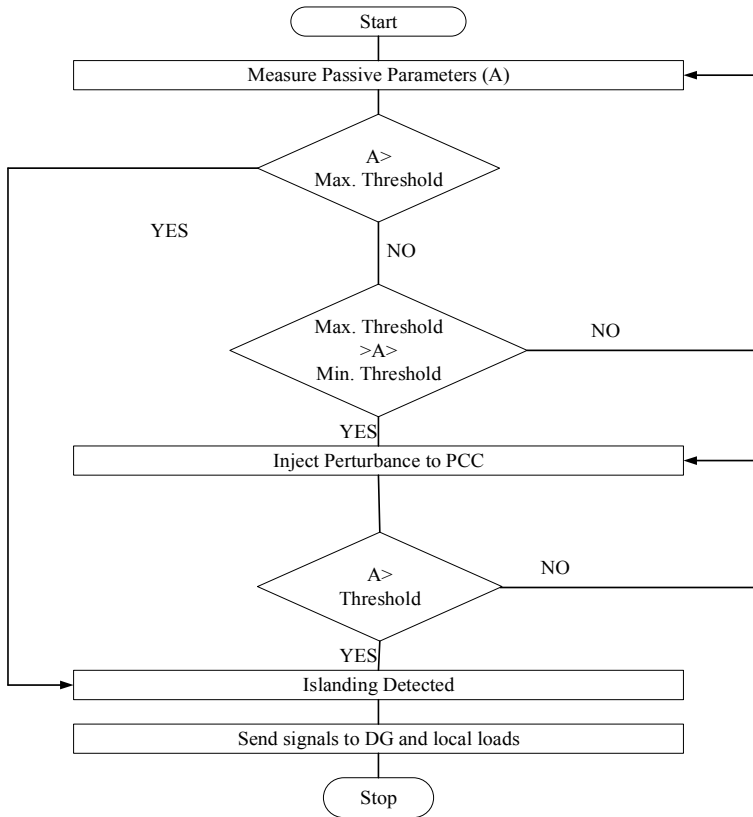


Fig. 6 Flow chart of HID methods

4.2.2 Voltage Fluctuation Injection

This method consist of ROCOF/ROCOV (passive) and chopping fraction, CF (active) method. As shown in the HID flow chart, if the rate of change of F/V is greater than the large (maximum) setting value of threshold then islanding is confirmed directly, and when the ROCOF/V is greater than the small (minimum) setting value of threshold then immediately AID method get activated [57]. In AID chopping frequency (CF) is checked, and if CF value is also more to their corresponding threshold value then islanding detected, otherwise it would be considered as non-islanding case.

4.2.3 SFS and Q-f (ROCOF) Technique

This method is based on the integration of the Sandia frequency shift, SFS (active) and ROCOF (passive) technique [66]. For large power variation, islanding confirmed directly by ROCOF method only, but if the variation is in between the large and small

then active method (SFS) will come into the action and by perturbation the islanding can be detected. Similarly many HID methods (like ROCOV and P, ROCOF and IM, ROCOF and frequency injection) can be formed by implementing the integrated passive and active IDMs.

5 Comparison of IDMs

Key technical factors such as (NDZ), detection time and power quality were considered for comparing RID, PID, AID and HID methods. A fair comparison of widely adopted IDMs has been presented in in Table 2. Each method has its own pros and cons which are listed in Table 3. Selection of IDMs are dependent on number of factors such as system power rating, network loading conditions, cost effectiveness, protection devices and integration guidelines and allowable limits. In terms of cost, PID has advantages over the others. RID requires high initial and maintenance costs.

6 System Architecture of a Grid Connected Solar Based DG

Figure 7 shows a Solar photovoltaic based DG connected to the 110 kV Utility grid. A DC-DC boost converter stabilizes the output of the PV arrays at a constant DC voltage of 500 V. A 3 level DC/AC power converter is used to process the power to the local loads and the main grid. CB1 and CB2 are the breakers for 20 and 110 kV bus respectively. Two local loads are connected to 20 kV feeder. Five different islanding detections methods are modelled to provide a trip signal during islanding events. They are Over/Under Voltage IDM, Over/Under Current IDM, Over/Under Frequency IDM, modified ROCOF IDM and Vector Shift IDM.

7 Results and Discussion

Five different IDMs are modelled and tested on a grid connected Solar photovoltaic based Distributed Generation system in MATLAB/SIMULINK environment. The PV inverter is connected to a 20 kV Bus through a 3- Φ 100 kVA Δ/Y transformer. Circuit breaker CB1 connects the two local loads to the 20 kV Bus. The DG units and local loads are connected to 110 kV, 2500 MVA, 50 Hz Utility Grid through a circuit breaker CB2. Islanding event is achieved by opening CB2 at $t = 0.1$ s. Unintentional islanding usually pose power quality issues when the local generation capacity is adequately not enough to supply the local consumer demands. Hence, two loading scenarios have been considered for the simulation study. Trip Signal is generated on successful detection of islanding event in two cases described below:

Table 2 Technical comparison of different IDMs based on three key performance metrics

Method's name (RID)	NDZ	Δt (ms)	PQ
PLC	Nil	200	No effect
TT	Nil	–	No effect
SCADA	Nil	Slow speed in busy grid	No effect
Method's name (PID)	NDZ	Δt (ms)	PQ
OUV/OUF	Large	4 to 2000	No effect
ROCOF	Large	24	No effect
ROCOP	<than OUV/OUF	>One cycle	No effect
ROCOFOP	<ROCOF	100	No effect
ROCOFORP	Very small	–	No effect
PJD	Large	10–20	No effect
VU	Large	53	No effect
THD (V/I)	Large, (Q high)	45	No effect
VU AND THD	Small	25 to 2000	No effect
ROCOV and CPF	Small	35	No effect
ROCONSV (ac)	Nil	80	No effect
ROCOPSV (ac)	Nil	10	No effect
ROCO (PSV and PSC)	Nil	10	No effect
ROCOEVORP	Nil	–	No effect
ROCOEV with CBSS	Nil	100 to 300	No effect
PANSVNSC	Nil	Within 4.16	No effect
FHO	Very small	Upto 440	No effect
Method's name (AID)	NDZ	Δt (ms)	PQ
AFD	Very small	Within 2000	Degrade
AFDPF	Very small	<AFD	Slight degrade
SFS	Very small	500	Degrade
SVS	Small	–	Slight degrade
SMFS	<AFD	400	Spike in system
APS	Small	Small	Degrade
NCCI	Zero	60	–
IM	Small	700–900	Slight degrade
Method's name (HID)	NDZ	Δt (ms)	PQ
VU and SFS/SVS	Very small	–	Slight degrade
ROCOV and P	Small	Within 2000	Slight degrade
ROCOF and IM	Small	216	

Table 3 Merits and Demerits of Different Islanding Detection Methods

Islanding detection methods	Merits	Demerits
Remote islanding methods (RID)	<ul style="list-style-type: none"> Highly reliable 	<ul style="list-style-type: none"> Quiet expensive especially for low-medium power Microgrid
Passive islanding methods (PID)	<ul style="list-style-type: none"> Lower detection time Does not disturb the system Reliable in extreme loading conditions 	<ul style="list-style-type: none"> Less effective in low loading conditions Requires attention while deciding the threshold levels
Active islanding methods (AID)	<ul style="list-style-type: none"> Reliable even when generation matches the demand Small NDZ 	<ul style="list-style-type: none"> Perturbs the system Slow response System stability may disturb under perturbations
Hybrid islanding methods (HID)	<ul style="list-style-type: none"> Injects disturbances only when islanding is suspected Smaller NDZ Power quality better than active islanding case 	<ul style="list-style-type: none"> Detection time is more

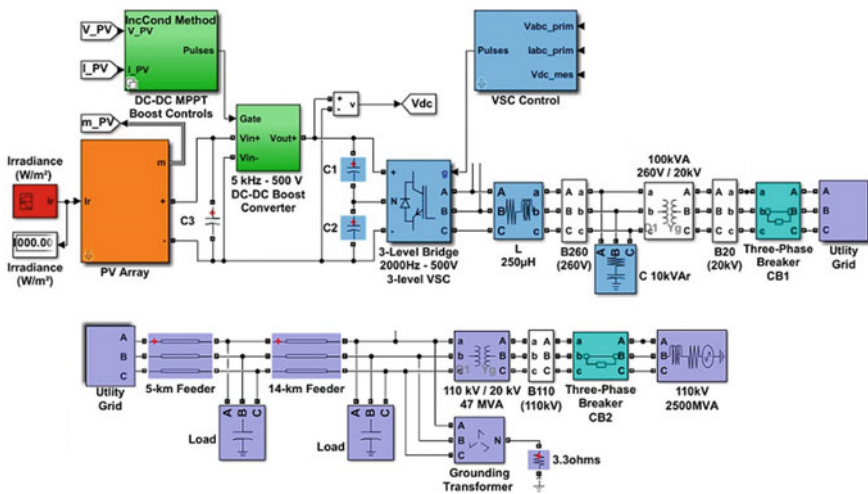


Fig. 7 Grid connected solar photovoltaic based DG under study

- Local generating capacity is either equal to the local load requirement
- Local generating capacity is less than the local load requirement

In this study, Over/Under voltage, Over/Under current, Over/Under Frequency, modified ROCOF and vector shift methods are examined.

7.1 Case 1: Local Load is Equal to Local Generation

This test is performed at the 20 kV feeder where local loads are connected. Load 1 and Load 2 demands 50 kW each.

For the performing the islanding test, circuit breaker (CB2) of the main grid is opened at the instant of 0.1 s and reclose at instant of 0.25 s. Within the time interval of CB2 open condition (islanding condition) many parameters are changed, and if any parameters are crossed the corresponding threshold value then trip signal is generated for the removal of DG.

As seen in Fig. 8, when the islanding events occurred, suddenly voltage and current parameters are affected. In Fig. 9 change of frequency and modified ROCOF are observed. RMS Value of Phase voltages can be observed in Fig. 10. Trip signal is generated when the selected parameters crosses the set threshold values. Islanding is detected by OUV, OUC, OUF, m-ROCOF and VS within 10 m, 15 ms, 65 ms, 25 ms and 25 ms respectively as shown in Fig. 11. During reclosing of the load at 0.25 s, a transient is seen which is suppressed within few cycles.

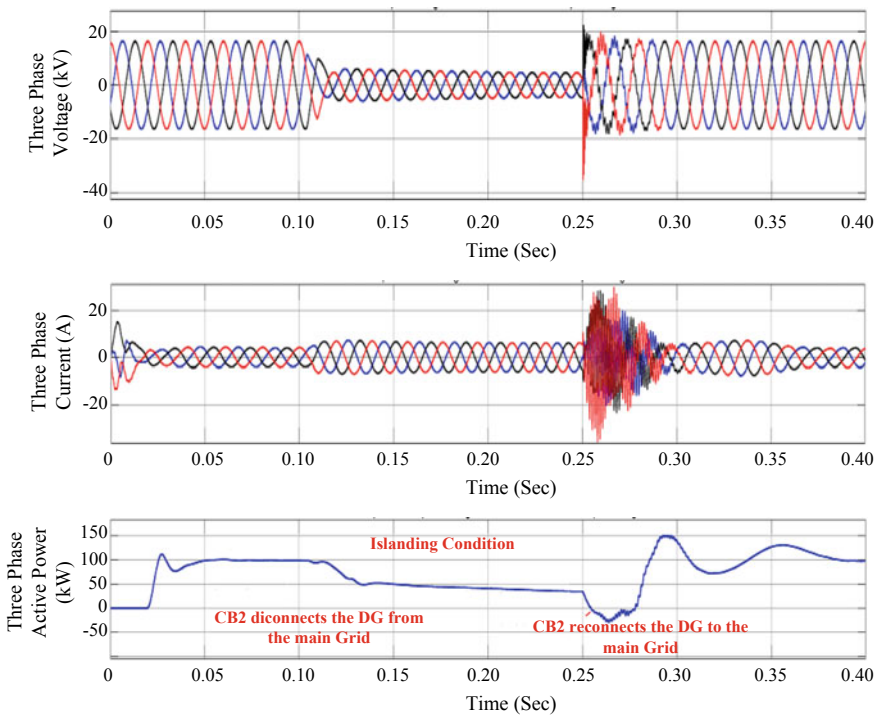


Fig. 8 Variation of three phase voltage, current and active power in case local load equals PV generation

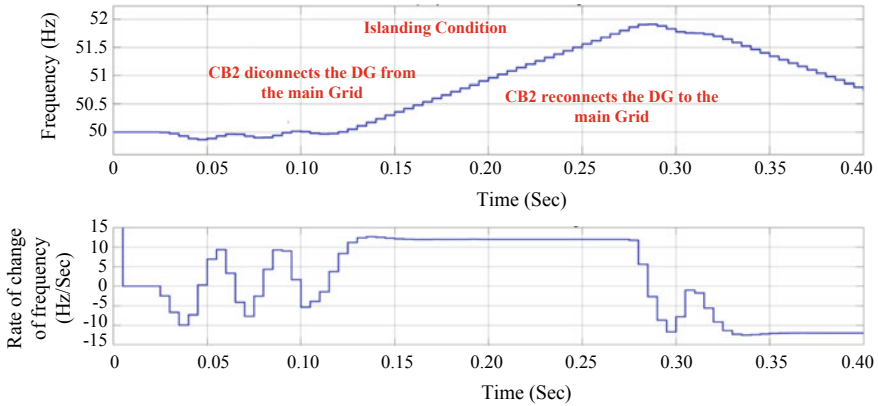


Fig. 9 Variation of frequency (50 Hz), and ROCOF in case local load equals PV generation

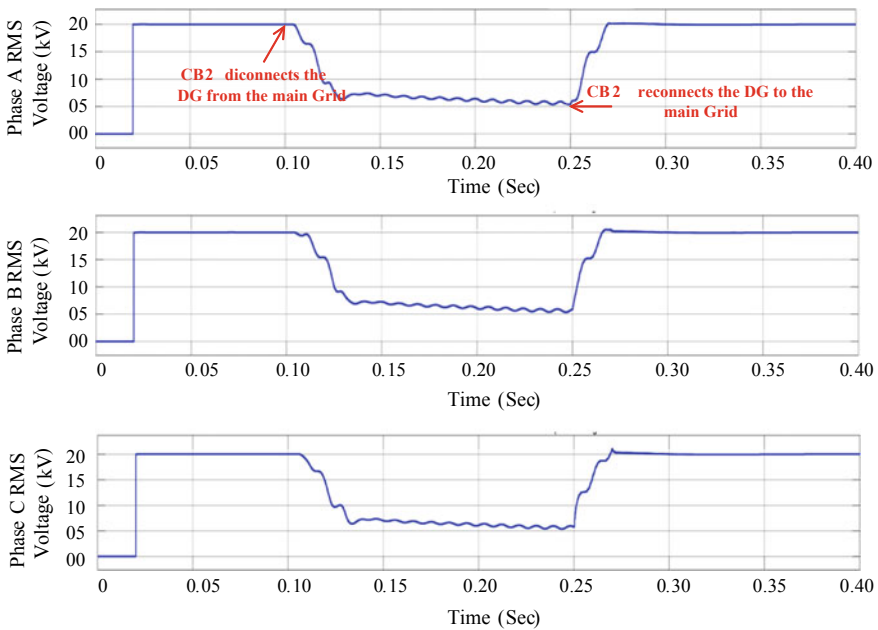


Fig. 10 Variation of Variation in RMS value of voltage Va, Vb and Vc in case local load equals PV generation

7.2 Case 2: Local Load Exceeds Local Generation

This test is also performed at the 20 kV feeder where local load are connected as per the specification: load 1 requires 2 MW and load 2 requires 30 MW and 2 MVAR (lagging) respectively. For performing the islanding test CB2of the main

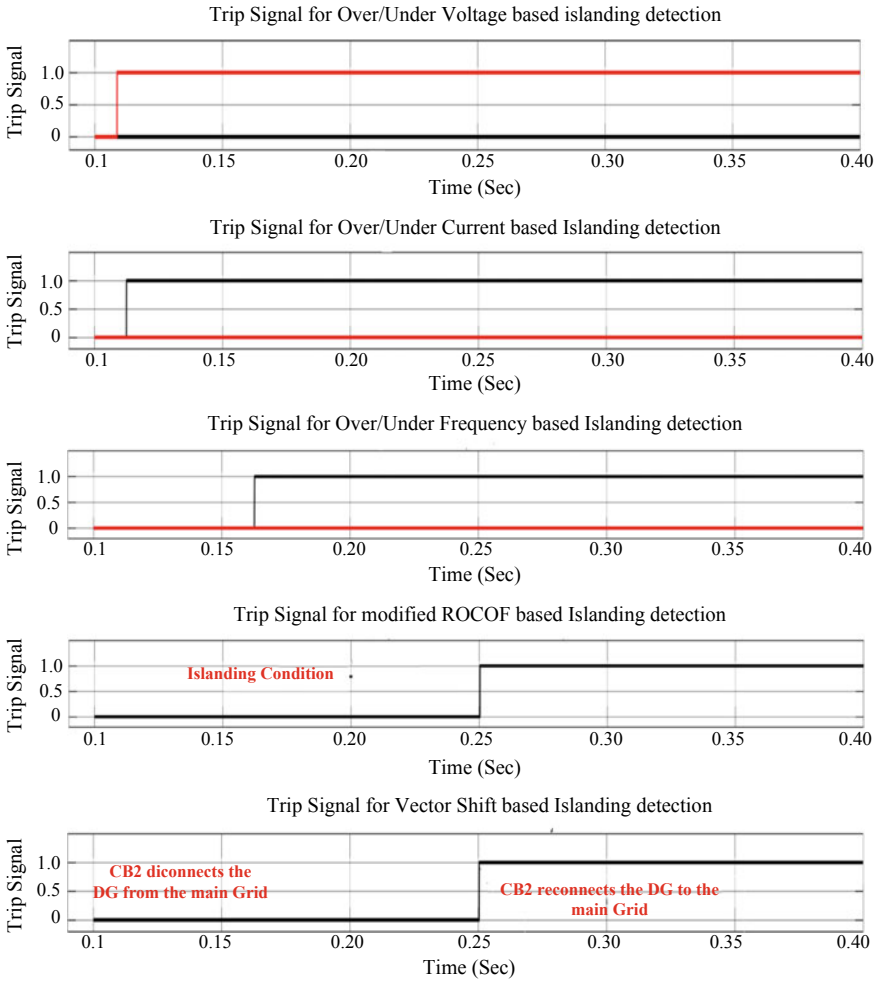


Fig. 11 Islanding detection (trip signal) in case local load equals PV generation

grid is opened for some time i.e., from 0.1 to 0.25 s. Within this period, electrical parameters crosses the set threshold value then islanding get realized. In Fig. 12, during islanding events, sudden change of voltage and current magnitude is seen, and the change crosses the threshold value, hence islanding get detected. The detection time of the OUV is around 7 ms, while detection time of over/under current is around 12 ms, i.e., the fast detection corresponding to the previous case discussed. Variation in active power is also shown in Fig. 12, i.e., sudden dip of power during islanding event. PV based DG is unable to supply the load resulting in load shedding.

In Fig. 13 change of frequency and modified ROCOF are seen and islanding is detected with the corresponding detection time as 54 ms and 65 ms respectively. RMS value of Phase voltages can be observed in Fig. 14. A vector shift is also detected

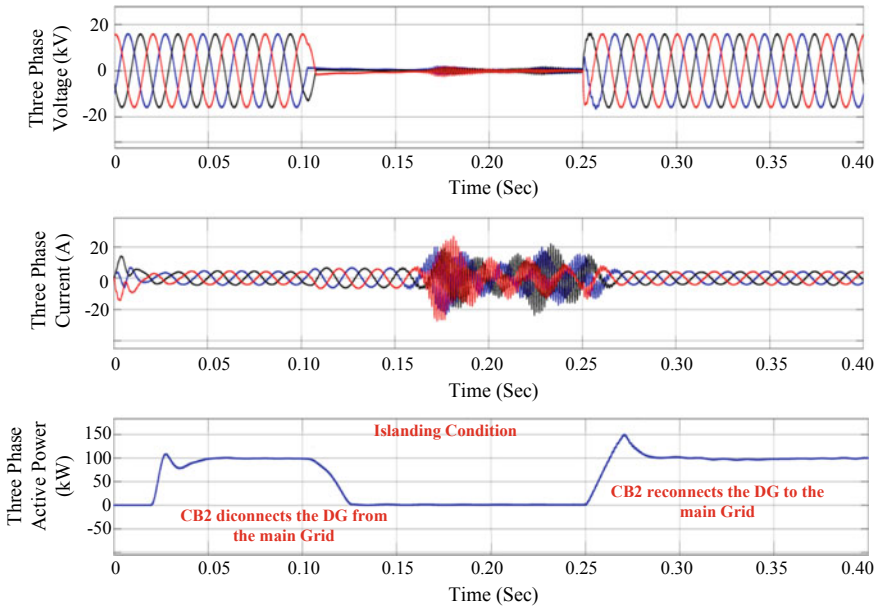


Fig. 12 Variation of three phase voltage, current and active power in case local load exceeds PV generation

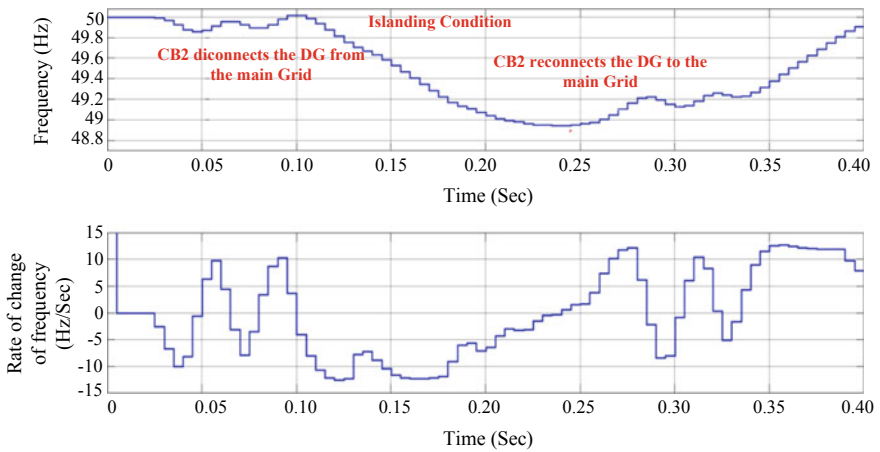


Fig. 13 Variation of frequency (50 Hz), and modified ROCOF in case local load exceeds PV generation

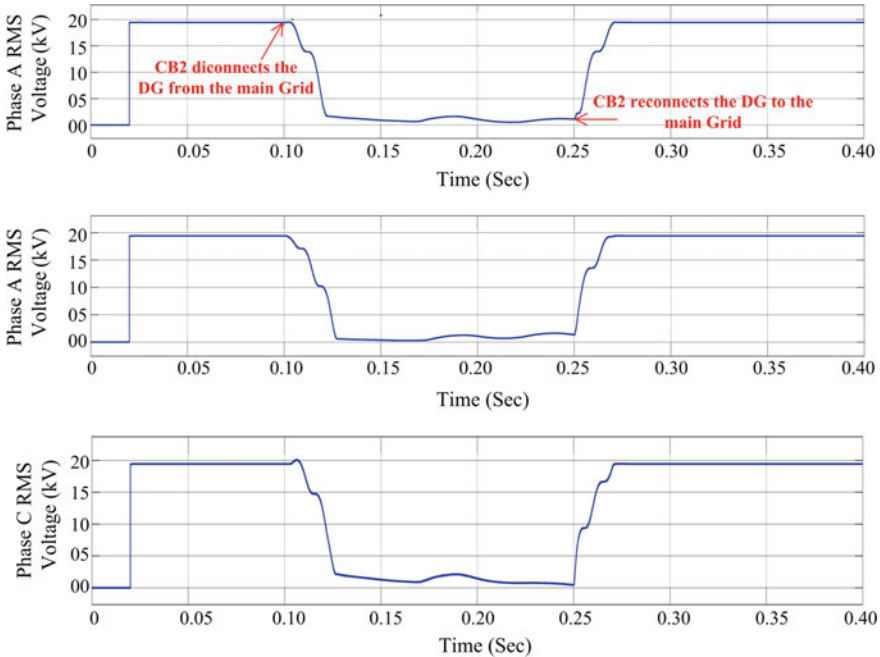


Fig. 14 Variation in RMS value of voltage V_a , V_b and V_c in case local load exceeds PV generation

having the detection time is equal to 64 ms. Trip signals are generated on successful islanding detection using OUV, OUC, OUF, m-ROCOF and VS as shown in Fig. 15.

Out of these five, three methods OUV, over/under current and OUF are based on the magnitude comparison of voltage, current and frequency. It is observed that the fast detection is done by OUV and followed by over/under current but problem with these are having large false detection. So, further methods modified ROCOF and voltage vector shift are observed and found that, it eliminate the false detection condition to somehow. Hence, accuracy is improved in both methods as two passive parameters are checked there and hence detection time increased. Detection time and non-islanding conditions are discussed in Table 4.

8 Conclusion

In this paper, active islanding detection techniques have been described for the utility connected micro grid system. The IDMs comparison is based on standards listed in Table 1, mainly IEEE 1547. Remote methods requires noise free, efficient and faster communication infrastructure, and hence the cost is high but is most reliable, as NDZs are minimized and prevents degradation of power quality. An active method has very small NDZ but degrade the power quality and that is why hybrid methods come into

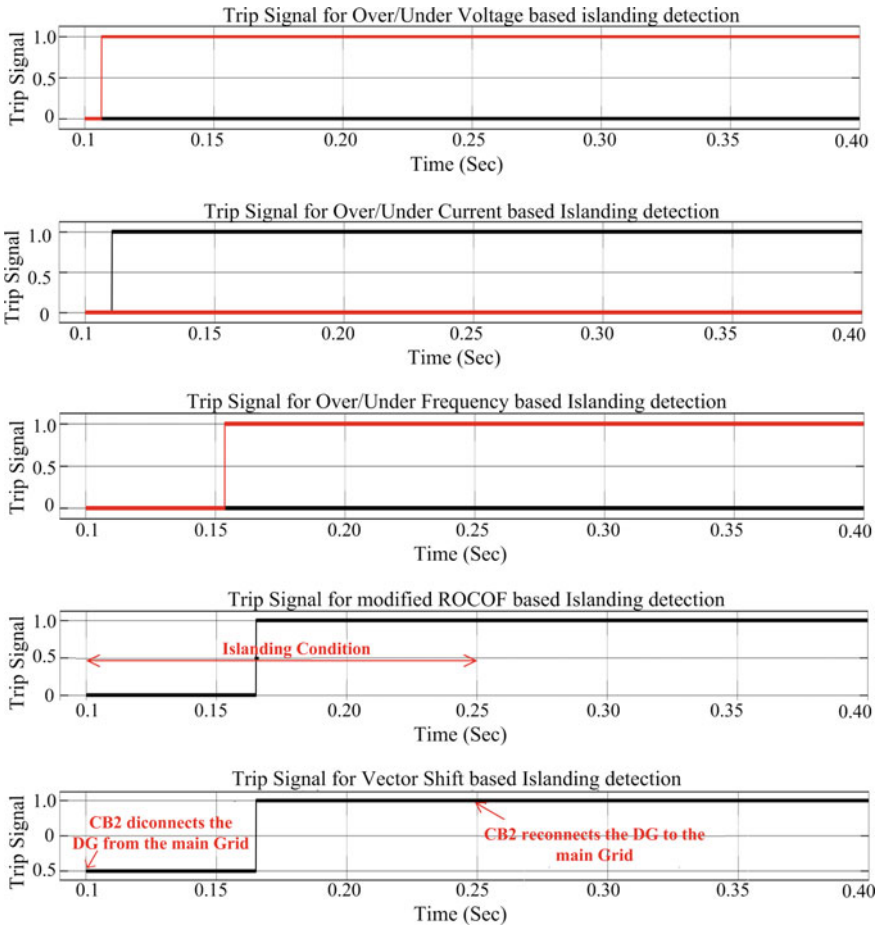


Fig. 15 Islanding detection (trip signal) in case local load exceeds PV generation

Table 4 Islanding detection time for each IDM

Technique's name	$t_{\text{detection}}$ (ms) Case 1	$t_{\text{detection}}$ (ms) Case 2
OUV	10	1
Over/under current	15	12
OUF	62	54
Modified ROCOF	150	65
Voltage vector shift	150	54

the picture to eradicate the high NDZ of passive and power quality issue of active, by combining the both methods (passive and active), detection time became prolonged. Generally passive detection time is low compared to both active (for seeing the response after perturbation, needed somehow more time) and hybrid. After being easy installation and lesser cost of PID methods, still it is not chosen because of their limitation with multi inverter systems and NDZ during balance islanding. In most of the cases AID are being used, but future trend will be hybrid and RID as both giving the good result over islanding and non-islanding, and capable of use of multi inverter systems with good reliability. Hence, this literature is providing a good concept over islanding detection, and it will be helpful for the future research. A grid connected architecture of a Solar based Distributed generation system is examined under islanding events using five IDMs. Modified ROCOF and voltage vector shift are observed to be more effective than conventional under/over voltage, current and frequency detections as they eliminates false detection conditions.

References

1. Dutta S, Sadhu PK, Reddy MJB, Mohanta DK (2018) Shifting of research trends in islanding detection method—a comprehensive survey. *Protect Control Modern Power Syst* 3(1). <https://doi.org/10.1186/s41601-017-0075-8>
2. Acharya N, Mahat P, Mithulananthan N (2006) An analytical approach for DG allocation in primary distribution network. *Int J Electr Power Energy Syst* 28:669–678. <https://doi.org/10.1016/j.ijepes.2006.02.013>
3. Chiang WJ, Jou HL, Wu JC (2012) Active islanding detection method for inverter-based distribution generation power system. *Int J Electr Power Energy Syst* 42(1):158–166. <https://doi.org/10.1016/j.ijepes.2012.03.038>
4. Basso TS (2014) IEEE 1547 and 2030 standards for distributed energy resources interconnection and interoperability with the electricity grid. National Renewable Energy Laboratory, Golden, CO, USA, vol 15013. <https://doi.org/10.2172/1166677>
5. Reddy CR, Reddy KH (2019) Islanding detection techniques for grid integrated DG—a review. *Int J Renew Energy Res* 9(2):960–977
6. Li C, Cao C, Cao Y, Kuang Y, Fang B (2014) A review of islanding detection methods for microgrid. *Renew Sustain Energy Rev* 35:211–220. <https://doi.org/10.1016/j.rser.2014.04.026>
7. Vahedi H, Noroozian R, Jalilvand A, Gharehpetian GB (2011) A new method for islanding detection of inverter-based distributed generation using DC-link voltage control. *IEEE Trans Power Deliv* 26:1176–1186. <https://doi.org/10.1109/TPWRD.2010.2093543>
8. Khamis A, Xu Y, Dong ZY, Zhang R (2018) Faster detection of microgrid islanding events using an adaptive ensemble classifier. *IEEE Trans Smart Grid* 9:1889–1899. <https://doi.org/10.1109/TSG.2016.2601656>
9. Walling RA, Miller NW (2002) Distributed generation islanding implications on power system dynamic performance. *IEEE Power Eng Soc Summer Meeting* 1:92–96. <https://doi.org/10.1109/PESS.2002.1043183>
10. Bahrani B, Karimi H, Irvani R (2011) Non-detection zone assessment of an active islanding detection method and its experimental evaluation. *IEEE Trans Power Deliv* 26(2):517–525. <https://doi.org/10.1109/TPWRD.2009.2036016>
11. Ye Z, Kolwalkar A, Zhang Y, Du P, Walling R (2004) Evaluation of anti-islanding schemes based on nondetection zone concept. *IEEE Trans Power Electron* 19(5):1171–1176. <https://doi.org/10.1109/TPEL.2004.833436>

12. Vieira JCM, Salles D, Freitas W (2011) Power imbalance application region method for distributed synchronous generator anti-islanding protection design and evaluation. *Electr Power Syst Res* 81(10):1925–1960. <https://doi.org/10.1016/j.epsr.2011.06.009>
13. Mahat P, Chen Z, Bak-Jensen B (2008) Review of islanding detection methods for distributed generation. In: *Third international conference on electric utility deregulation and restructuring and power technologies*, pp 2743–2748. <https://doi.org/10.1109/DRPT.2008.4523877>
14. Rumbayan M (2017) Development of power system infrastructure model for the island communities: a case study in a remote island of Indonesia. In: *International conference on advanced mechatronic systems*, pp 515–518. <https://doi.org/10.1109/ICAMechS.2017.8316470>
15. Wang W, Kliber J, Zhang G, Xu W, Howell B, Palladino T (2007) A power line signaling based scheme for anti-islanding protection of distributed generators: Part II: field test results. *IEEE Trans Power Deliv* 22:1767–1772. <https://doi.org/10.1109/TPWRD.2007.899620>
16. Raza S, Mokhlis H, Arof H, Laghari JA, Wang L (2015) Application of signal processing techniques for islanding detection of distributed generation in distribution network: a review. *Energy Convers Manage* 96:613–624. <https://doi.org/10.1016/j.enconman.2015.03.029>
17. Kim MS, Haider R, Cho GJ, Kim CH, Won CY, Chai JS (2019) Comprehensive review of islanding detection methods for distributed generation systems. *Energies* 12(5):837. <https://doi.org/10.3390/en12050837>
18. Xiao H, Fang Z, Li C, Xu D, Venkatesh B, Singh BN (2017) Anti islanding protection relay for medium voltage feeder with distributed generator. *IEEE Trans Ind Electron* 64(10):7874–7885. <https://doi.org/10.1109/TIE.2017.2694394>
19. Guha B, Haddad RJ, Kalaani Y (2015) A novel passive islanding detection technique for converter based distributed generation systems. In: *IEEE power & energy society innovative smart grid technologies conference*, pp 1–5. <https://doi.org/10.1109/ISGT.2015.7131907>
20. Zhao J, Zhang D, He J (2017) A passive islanding detection method based on interharmonic impedance. In: *IEEE conference on energy internet and energy system integration*, pp 1–6. <https://doi.org/10.1109/EI2.2017.8245574>
21. IEEE 929 (2000) IEEE recommended practice for grid interface of photovoltaic (PV) systems. Institute of Electrical and Electronics Engineers, New York. <https://doi.org/10.1109/IEEESTD.2000.91304>
22. Timbus A, Oudalov A, Ho CN (2010). Islanding detection in smart grids. In: *2010 IEEE energy conversion congress and exposition*, pp 3631–3637. <https://doi.org/10.1109/ECCE.2010.5618306>
23. Jones RA, Sims TR, Imece AF (1990) Investigation of potential islanding of a self-commutated static power converter in photovoltaic systems. *IEEE Trans Energy Convers* 5(4):624–631. <https://doi.org/10.1109/60.63131>
24. Gupta P, Bhatia RS, Jain DK (2016) Active ROCOF relay for islanding detection. *IEEE Trans Power Delivery* 32(1):420–429. <https://doi.org/10.1109/TPWRD.2016.2540723>
25. Warin J, Allen WH (1990) Loss of mains protection. In: *ERA conference on circuit protection for industrial and commercial installations*, pp 4–3
26. Guha B, Haddad RJ, Kalaani Y (2015) A passive islanding detection approach for inverter-based distributed generation using rate of change of frequency analysis. In: *IEEE South east conference*, pp 1–6. <https://doi.org/10.1109/SECON.2015.7133024>
27. Ahmad KNEK, Selvaraj J, Rahim NA (2013) A review of the islanding detection methods in grid-connected PV inverters. *Renew Sustain Energy Rev* 21:756–766. <https://doi.org/10.1016/j.rser.2013.01.018>
28. Aghdam HN, Ghadimi N, Farhadi P, Hashemi F, Ghadimi R (2011) Detecting the anti-islanding protection based on combined changes of active and reactive output powers of distributed generations. In: *3rd international conference on computer research and development*, Shanghai, pp 285–289. <https://doi.org/10.1109/ICCRD.2011.5764196>
29. Reddy CR, Reddy KH (2017) Islanding detection method for inverter based distributed generation based on combined changes of ROCOAP and ROCORP. *Int J Pure Appl Math* 117(19):433–440

30. Menon D, Antony A (2016) Islanding detection technique of distribution generation system. In: International conference on circuit, power and computing technologies, pp 1–5. <https://doi.org/10.1109/ICCPCT.2016.7530126>
31. Nikolovski S, Baghaee HR, Mlakic D (2019) Islanding detection of synchronous generator-based DGs using rate of change of reactive power. *IEEE Syst J* 13(4):4344–4354. <https://doi.org/10.1109/JSYST.2018.2889981>
32. Raza S, Mokhlis H, Arof H, Mohamad H, Laghari JA (2016) Prioritization of different passive parameters for islanding detection on the basis of response analysis. In: IEEE international conference on power and energy, pp 615–619. <https://doi.org/10.1109/PECON.2016.7951634>
33. Raza S, Mokhlis H, Arof H, Laghari JA, Mohamad H (2016) A sensitivity analysis of different power system parameters on islanding detection. *IEEE Trans Sustain Energy* 7(2):461–470. <https://doi.org/10.1109/TSTE.2015.2499781>
34. Hu W, Sun Y (2009) A compound scheme of islanding detection according to inverter. In: Asia-Pacific power and energy engineering conference, pp 1–4. <https://doi.org/10.1109/APP/EEC.2009.4918040>
35. Khichar S, Lalwani M (2018) An analytical survey of the islanding detection techniques of distributed generation systems. *Technol Econ Smart Grids Sustain Energy* 3(10). <https://doi.org/10.1007/s40866-018-0041-1>
36. Singam B, Hui LY (2006) Assessing SMS and PJD schemes of anti-islanding with varying quality factor. In: IEEE international power and energy conference, pp 196–201. <https://doi.org/10.1109/PECON.2006.346645>
37. Mahat P, Chen Z, Bak-Jensen B (2011) Review on islanding operation of distribution system with distributed generation. In: IEEE power and energy society general meeting, pp 1–8. <https://doi.org/10.1109/PES.2011.6039299>
38. Jang S, Kim KH (2004) An islanding detection method for distributed generations using voltage unbalance and total harmonic distortion of current. *IEEE Trans Power Deliv* 19(2):745–752. <https://doi.org/10.1109/TPWRD.2003.822964>
39. Tzelepis D, Dyśko A, Booth C (2016) Performance of loss-of-mains detection in multi-generator power islands. In: 13th International conference on development in power system protection, pp 1–6. <https://doi.org/10.1049/cp.2016.0066>
40. Jose BK, Vincent G (2017) Harmonic current based islanding detection for grid connected PV systems. In: 2017 IEEE international conference on circuits and systems, pp 191–195. <https://doi.org/10.1109/ICCS1.2017.8325988>
41. Zeineldin HH, Kirtley JH (2009) A simple technique for islanding detection with negligible nondetection zone. *IEEE Trans Power Deliv* 24(2):779–786. <https://doi.org/10.1109/TPWRD.2009.2013382>
42. Laaksonen H (2012) New multi-criteria-based algorithm for islanding detection in smart grids. In: 3rd IEEE PES innovative smart grid technologies, pp 1–8. <https://doi.org/10.1109/ISGTEurope.2012.6465661>
43. Danandeh A, Seyedi H, Babaei E (2012) Islanding detection using combined algorithm based on rate of change of reactive power and current THD techniques. In: Asia-Pacific power and energy engineering conference, pp 1–4. <https://doi.org/10.1109/APPEEC.2012.630746>
44. Jun L, Liang HX, Xiao-Hu C, Miao X, Wen X (2010) Two islanding detection circuits based on the impedance variation for the micro-grid. In: The 2nd international symposium on power electronics for distributed generation systems, pp 859–863. <https://doi.org/10.1109/PEDG.2010.5545813>
45. Salman SK, King DJ, Weller G (2001) New loss of mains detection algorithm for embedded generation using rate of change of voltage and changes in power factors. In: International conference on developments in power system protection, pp 82–85. <https://doi.org/10.1049/cp:20010105>
46. Kumar KM, Naresh M, Singh NK, Singh AK (2016) A passive islanding detection approach for distributed generation using rate of change of negative sequence voltage and current. In: IEEE international conference on electrical, computer and electronics engineering, pp 356–360. <https://doi.org/10.1109/UPCON.2016.7894679>

47. Rostami A, Jalilian A, Naderi SB, Negnevitsky M, Davari P, Blaabjerg F (2017) A novel passive islanding detection scheme for distributed generations based on rate of change of positive sequence component of voltage and current. In: Australasian universities power engineering conference, pp 1–5. <https://doi.org/10.1109/AUPEC.2017.8282394>
48. Reddy CR, Reddy KH (2018) An efficient passive islanding detection method for integrated DG system with zero NDZ. *Int J Renew Energy Res* 8:1994–2002
49. Rostami A, Bagheri M, Naderi SB, Negnevitsky M, Jalilian A, Blaabjerg F (2017) A novel islanding detection scheme for synchronous distributed generation using rate of change of exciter voltage over reactive power at DG-Side. In: Australasian universities power engineering conference, pp 1–5. <https://doi.org/10.1109/AUPEC.2017.8282417>
50. Naveen G, Reddy KH, Reddy CR, Ramakrishna B, Bramaramba P, Reddy LB (2018) Passive islanding detection method for integrated DG system with balanced islanding. *Int J Pure Appl Math* 120(06):4041–4058
51. Rostami A, Jalilian A, Hagh MT, Muttaqi KM, Olamaei J (2018) Islanding detection of distributed generation based on rate of change of exciter voltage with circuit breaker switching strategy. *IEEE Trans Ind Appl* 55(1):954–963. <https://doi.org/10.1109/IAS.2017.8101799>
52. Bashir J, Jena P, Pradhan AK (2014) Islanding detection of a distributed generation system using angle between negative sequence voltage and current. In: 18th National power systems conference, pp 1–5. <https://doi.org/10.1109/NPSC.2014.7103855>
53. Bakhshi M, Noroozian R, Gharehpetian GB (2017) Novel islanding detection method for multiple DGs based on forced helmholtz oscillator. *IEEE Trans Smart Grid* 9(6):6448–6460. <https://doi.org/10.1109/TSG.2017.2712768>
54. Sundar DJ, Kumaran MS (2015) A comparative review of islanding detection schemes in distributed generation systems. *Int J Renew Energy Res* 5(4):1016–1023
55. Reis MV, Villalva MG, Barros TA, Moreira AB, Ruppert E (2015) Active frequency drift with positive feedback anti-islanding method for a single phase two-stage grid-tied photovoltaic system. In: 13th Brazilian power electronics conference and 1st southern power electronics conference, pp 1–6. <https://doi.org/10.1109/COBEP.2015.7420121>
56. Zeineldin HH, Kennedy S (2009) Sandia frequency-shift parameter selection to eliminate nondetection zones. *IEEE Trans Power Deliv* 24(1):486–487. <https://doi.org/10.1109/TPWRD.2008.2005362>
57. Khamis A, Shareef H, Bizkevelci E, Khatib T (2013) A review of islanding detection techniques for renewable distributed generation systems. *Renew Sustain Energy Rev* 28:483–493. <https://doi.org/10.1016/j.rser.2013.08.025>
58. Akhlaghi S, Akhlaghi A, Ghadimi AA (2016) Performance analysis of the Slip mode frequency shift islanding detection method under different inverter interface control strategies. In: IEEE power and energy conference, pp 1–7. <https://doi.org/10.1109/PEEL.2016.7459250>
59. Hung GK, Chang CC, Chen CL (2003) Automatic phase-shift method for islanding detection of grid-connected photovoltaic inverters. *IEEE Trans Energy Convers* 18(1):169–173. <https://doi.org/10.1109/TEC.2002.808412>
60. De Mango F, Liserre M, Dell' Aquila A (2006) Overview of anti-islanding algorithms for pv systems. Part II: active methods. In: 12th international power electronics and motion control conference, pp 1884–1889. <https://doi.org/10.1109/EPEPEMC.2006.4778680>
61. Alsharidah M, Ahmed NA, Alothman AK (2014) Negative sequence injection for islanding detection of grid interconnected distributed generators. In: IEEE electrical power and energy conference, pp 267–274. <https://doi.org/10.1109/EPEC.2014.38>
62. Karimi H, Yazdani A, Iravani R (2008) Negative-sequence current injection for fast islanding detection of a distributed resource unit. *IEEE Trans Power Electron* 23(1):298–307. <https://doi.org/10.1109/TPEL.2007.911774>
63. Nale R, Biswal M (2017) Comparative assessment of passive islanding detection techniques for microgrid. In: Innovations in information, embedded and communication systems, pp 1–5. <https://doi.org/10.1109/ICIIECS.2017.8275935>
64. PVPS I (2002) Evaluation of islanding detection methods for photovoltaic utility-interactive power systems. Report IEA PVPS T5-09

65. Menon V, Nehrir MH (2007) A hybrid islanding detection technique using voltage unbalance and frequency set point. *IEEE Trans Power Syst* 22(1):442–448. <https://doi.org/10.1109/TPWRS.2006.887892>
66. Khodaparastan M, Vahedi H, Khazaeli F, Oraee H (2017) A novel hybrid islanding detection method for inverter-based DGs using SFS and ROCOF. *IEEE Trans Power Deliv* 32(5):2162–2170. <https://doi.org/10.1109/TPWRD.2015.2406577>
67. Shastri R, Samadhiya A, Namrata K (2021) A comprehensive review of remote and passive IDMs of utility grid integrated MG system—Part I. In: *Lecture Notes in Electrical Engineering*, vol 699, pp 485–496. https://doi.org/10.1007/978-981-15-7994-3_45

A Comparative Analysis of PI and Predictive Control Strategy for HESS Based Bi-directional DC-DC Converter for DC Microgrid Applications



Srinivas Punna, Udaya Bhasker Manthati, and C. R. Arunkumar

Abstract In modern electric grid system easy integration with renewable energy sources (RES), energy storage systems (ESSs) and electric load is an attractive technology of DC microgrid. This chapter presents with a comparative analysis of proportional integral (PI) and model predictive control (MPC) of multiple input bi-directional DC-DC converter (MIPC) for hybrid energy storage systems (HESS) in DC microgrid applications. The contrasting characteristics of battery and supercapacitor (SC) is the perfect combination of HESS. This MIPC, provides decoupled control of battery and SC power along with energy exchange between storage devices. A controller is designed for DC microgrid applications, modified operation of controller made it possible for both HESS charging and discharging operation thus make it a unified controller. When batteries are used as energy storage, their rate of charge and discharge is very low. So there are current stresses on the battery and reduced life cycle, SC have high power density and can react immediately to sudden load variations. SC alone can't be used as energy storage device, because it can't supply power to the load for longer duration. The simulation results are developed for comparative performance of MPC over the PI control schemes. The proposed MPC was better DC grid voltage restoration to step change in PV generation and load demand over traditional PI control scheme.

Keywords Battery · Supercapacitor · HESS · Bi-directional converter · PI controller · MPC · Power quality

S. Punna (✉)

Electrical and Electronics Engineering Department, BVRIT Hyderabad College of Engineering for Women, Hyderabad, Telangana 500090, India
e-mail: srinu240@student.nitw.ac.in

U. B. Manthati · C. R. Arunkumar

Electrical Engineering Department, NIT Warangal, Warangal, Telangana 506004, India
e-mail: ub@nitw.ac.in

C. R. Arunkumar

e-mail: acr_research@student.nitw.ac.in

Nomenclature

HESS	Hybrid Energy Storage Systems
MIPC	Multiple input Bidirectional DC-DC Converter
SC	Supercapacitor
ESSs	Energy Storage Systems
PV	Photovoltaic
MPPT	Maximum Peak Power Point
P&O	Perturb and Observe
ZVS	Zero Voltage Switching
SOC	State of Charge
PI	Proportional Integral
MPC	Model Predictive Control
ESR	Equivalent Series Resistance
RPS	Regulated Power Supply
V_{DC}	DC grid Voltage
d_S	Supercapacitor duty cycle
d_B	Battery duty cycle
V_S	Supercapacitor Voltage
V_B	Battery Voltage
i_{SC}	Supercapacitor current
i_B	Battery current
$G_{i_{SC}d_{SC}}$	Control to supercapacitor current transfer function
$G_{v_{DC}i_{SC}}$	Current to voltage transfer function
$G_{i_Bd_B}$	Control to battery current transfer function
G_{PI}	PI Control transfer function
Q_{SC}	Supercapacitor charge
i_{CH}	Supercapacitor charge current
LPF	Low Pass Filter
i_{ref}	Total Reference current
$i_{B,ref}$	Battery Reference current
$i_{SC,ref}$	Supercapacitor Reference current
PWM	Pulse Width Modulation
$i_b(k + 1)$	Predicted battery current
$i_{sc}(k + 1)$	Predicted supercapacitor current

1 Introduction

Due to easy integration with renewable energy sources as well as proliferation of dc-compatible loads, DC microgrids are gaining popularity [1, 2]. High penetration of these intermittent renewable energy sources into DC microgrids cause power mismatch between generation and load sides culminating in dc bus voltage variations.

Energy Storage Systems (ESS) of diverse variety and characteristics are used to tackle this problem. The most commonly used ESS is battery. The battery is preferred for high energy density and supercapacitor is preferred for high power density in ESS applications [3, 4]. Intermittent renewable energy sources demand ESS with high energy density whereas loads with high-pulse requirement demand ESS with high power density. Hence a Hybrid Energy Storage System (HESS) was formed by integrating battery and supercapacitor which fulfill the aforementioned requirements of a DC grid [5–9]. In addition to this, HESS improves the stability of power converter based microgrids which otherwise would be low due to low rotational inertia [10].

The advantages of both battery and supercapacitor are exploited by different HESS topologies as shown in [11]. The most widely employed HESS configuration, that has the advantage of individual battery and supercapacitor control is as shown in Fig. 1a. It is possible to exchange energy between the components ESSs in this active parallel configuration of HESS that is the battery ESS can charge the supercapacitor ESS or vice versa. However, the energy exchange process is through DC microgrid and this may push the grid operating limits beyond desired range.

Multiple input bidirectional (MIBD) converters, as in Fig. 1b, have better energy exchange performance between input sources compared to multiple single-input bidirectional dc-dc (MSIBD) converters in active parallel configuration. This makes the former for a better choice for applications like hybrid electric vehicle (HEV) and microgrids. The main advantage of MIBD converter over the MSIBD converter are (i) Better energy exchange between input sources (ii) reduces the system size (iii) reduces the cost of the converter [12]. The salient features of the two HESS configurations are summarized in Table 1. In this study, Fig. 1b is selected, since it offers lesser components and smaller size.

The DC microgrid setup by PV source supported by battery-supercapacitor HESS is shown in Fig. 2.

Several multiple input topologies have been proposed which can interface multiple sources with contrasting characteristics to a common load. In [13], multiple ESSs

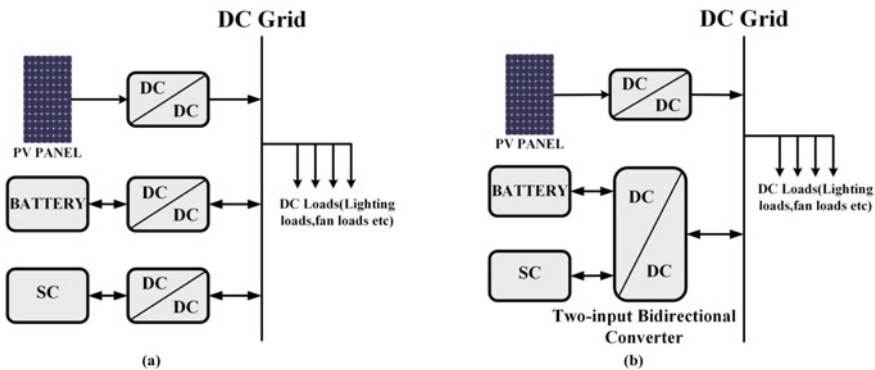


Fig. 1 Different configurations of HESS, comprising of battery and SC, interfaced to DC microgrid. **a** Two separate bidirectional converter modules used. **b** Single double-input bidirectional converter

Table 1 Comparisons of HESS configurations

Configuration	Figure 1a	Figure 1b
Number of converters	2	1
Controlled DC link voltage	Yes	Yes
Controlled battery current	Yes	Yes
Controlled SC current	Yes	Yes
DC link voltage swing	High	High

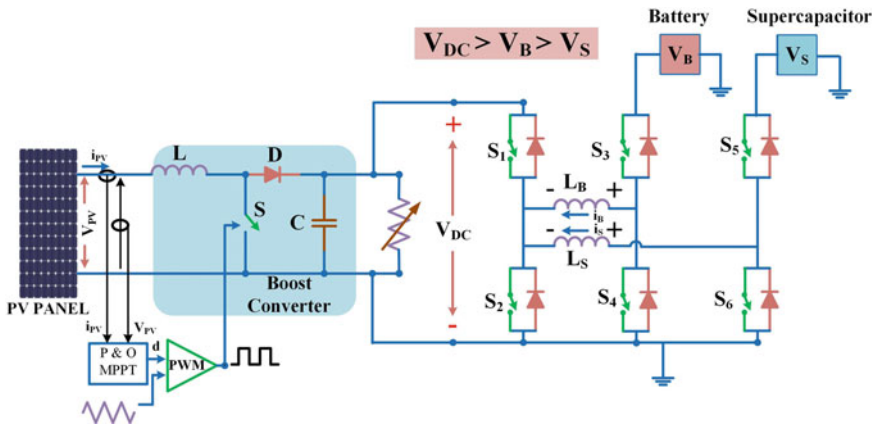


Fig. 2 DC microgrid architecture setup powered by PV-HESS

are interfaced to a three-winding high frequency transformer wherein each source is connected through a full-bridge circuit. For battery-supercapacitor HESS connected number of switches required is eight which may affect the overall efficiency as far as DC microgrid application is concerned. An Isolated multiport dc-dc converter was presented in [14, 15] which can manage power from multiple energy sources to a common load. But power flow between the sources, if they were replaced by ESSs, was not explored. Even though isolated converters support wide range of voltage levels as well as safety in the form of isolation, energy management of multiple sources is difficult compared to that of non-isolated converters.

A number of multiple input non-isolated dc-dc bidirectional converters for interfacing multiple sources can be found in literature which offers far more flexibility in implementation and power management than isolated ones [16–28]. In [16] a procedure for developing all possible double-input single-output dc-dc converters was described and was experimentally verified for a system with battery as one input. But bidirectional power flow between the two input ports was not considered which is necessary for HESS in microgrid applications. A multi-input dc-dc converter for various energy sources of diverse characteristics was proposed in [17] but with no power sharing option between the input sources.

Wang et al. [18] has presented single inductor based multi-port converter for HESS. The computation and controller effort are much more since the paper uses model predictive control. More over SOC based analysis is required for the validity of control strategy. Faraji et al. [19] proposes a multiport hybrid energy system with PV and battery. The independent use of battery alone will increase the stress on the battery. Also the proposed converter is not suitable for SC applications. Sato et al. [20] also proposing multi-port converter for PV and battery. The proposed circuit able to integrate battery with PV, however during various disturbances, the stress on the battery will be high. A unified control of the PV-Battery-based grid energy management system for both grid-connected and island operation was introduced by Yi et al. [21]. In the proposed control method, battery balances the power flow inside the AC micro grid and DC micro grid in all different operating conditions. This increases the battery stress, system cost and life cycle of battery. A high efficiency dual input interleaved converter was proposed in [26] which is especially suitable for energy storage sources. However, Dual input interleaved converter circuit requires eight switches makes the control strategy to be complicated. Few multi-input converters for grid-tied and/or solar applications are reported in [27–29]. Similarly, multi-input converters are also widely used in hybrid electric vehicle (HEV) applications as in [30–33]. However, in all above multiple input converter topologies does not maintain SOC_{SC} in the predefined limits and protecting SC from over charge and discharge is difficult.

Even though a large number of works about multi-input bidirectional converters are available in literature, less or little importance has been given to their controller development methods. A multi-input bidirectional dc-dc converter, proposed in [34], is used to interface the HESS to microgrid. The converter in [34] has been modified in operation to suit for HESS operation in DC microgrid applications. One attractive attribute of this converter is that all the switches are turned on with zero voltage switching (ZVS) which can improve its efficiency. Apart from controlling the charging/discharging of HESS, the unified controller can also share current between battery and supercapacitor in such a way that the former is subjected to less current stress which helps in extending its lifetime. Total HESS current (charging/discharging) bifurcates such that high frequency component of the current is being supplied by power density element supercapacitor and average or low frequency current is being fed by energy density unit battery. The main contributions of the chapter are as follows.

- A multi input converter based DC microgrid voltage stabilization is proposed in this chapter.
- Detailed controller design and analysis is presented for HESS based Multiple-Input Bidirectional converter. The presented small signal model based controller for multi input converter can ensure stability in all operating regions.
- Implementation of energy management system for Multiple-Input Bidirectional converter with HESS is presented for different PV and load conditions. The EMS can easily track the SC SOC and enable different mode to ensure safe operation.

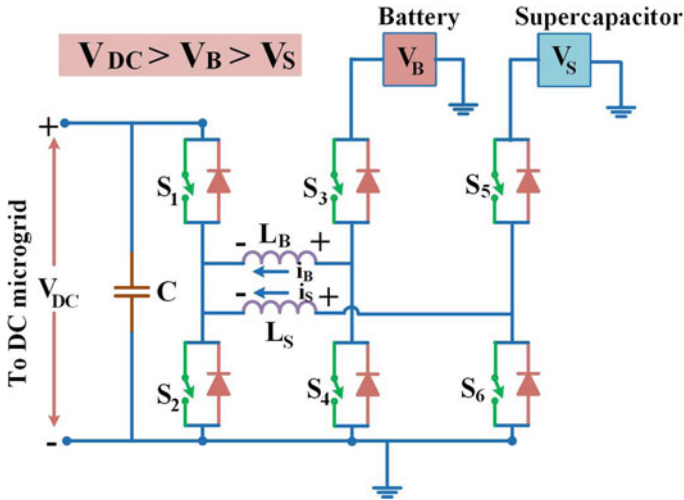


Fig. 3 Two-input bidirectional converter topology for HESS [34]

- The main advantage of designed double-input Bidirectional converter is its energy exchange mode where we can charge the SC independently from battery. Other than that, there are several advantages to the double-input bidirectional converter, such as efficient power distribution between the various ESSs, rapid regulation of DC link voltage to PV power fluctuations and load variations.
- The performance evaluation of MPC over PI control scheme with step change in PV generation and load demand for peak overshoot and settling time to restore DC grid voltage are presented.

Two-input bidirectional DC-DC converter for HESS is shown in Fig. 3.

The chapter is organized as follows: The modeling of PV panel and P and O MPPT algorithm is discussed in Sect. 2. Section 3 reviews the multiple input bidirectional converter proposed in [34] and detailed modified operation as two-input bidirectional dc-dc converter for HESS operation is elaborated. Small signal linear averaged model of the two-input converter is developed in Sect. 4, which is crucial for the development of unified controller for HESS charging/discharging with current sharing between ESSs. Study of MPC for HESS is discussed in Sect. 5. Section 6 deals with the development for state of charge (SOC) controller for supercapacitor. Simulation and experimental validation is presented in Sects. 7 and 8. Results and inferences are concluded in Sect. 9.

2 Modelling of PV Panel

The PV panel consist of photodiodes that converts light energy in to electrical energy. The basic unit of PV panel is known as PV cell. The PV cells are connected in series and parallel to form a PV panel to meet the necessary power ratings. The series and parallel combination of PV panels are utilized to make PV array. Further, the PV array is designed based on the power, voltage and current rating required by the DC microgrid. The electrical equivalent of PV array is shown in Fig. 4a [35].

The characteristic equation defined here is based on the PV array single diode model. In general, the characteristics of the current and voltage (I-V) of the PV cell shows non-linear, as shown in Fig. 4b. The characteristics equation of the PV array can be given in Eq. (1),

$$i_{pv} = N_p I_{ph} - N_p I_{rs} \left(e^{\frac{q \left(\frac{V_{pv}}{N_s} + \frac{i_{pv}}{N_{pv}} \right)}{\Delta K T}} - 1 \right) - \frac{\frac{N_p V_{pv}}{N_s} + i_{pv} R_s}{R_{sh}} \tag{1}$$

where N_p : Total number of Parallel connected PV cells, N_s : Total number of series connected PV cells. I_{ph} : total photo-current generated from PV array. I_{rs} represents reverse saturation current of PV cell. R_s and R_{sh} represent the series and parallel resistances. A : diode ideal factor, T : PV cell’s working temperature, K : Boltzmann’s constant (1.38×10^{23} J/k). V_{pv} and I_{pv} represent PV array voltage and current. The current equation of PV panel is non-linear and dependent on weather conditions like insolation and temperature. To find the maximum power point on non-linear PV curve maximum power point tracking algorithm is engaged.

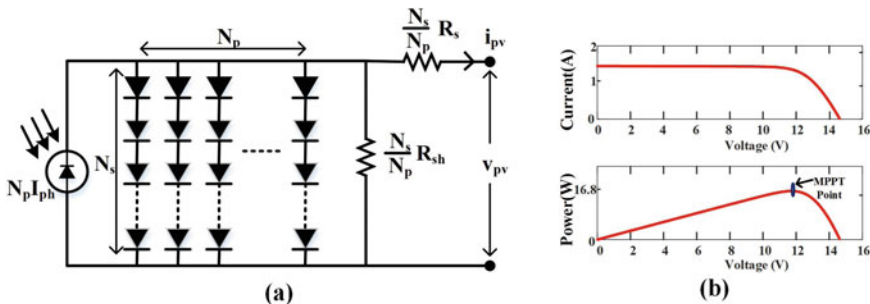


Fig. 4 a Equivalent circuit representation of PV array, b I-V and P-V Characteristics of PV

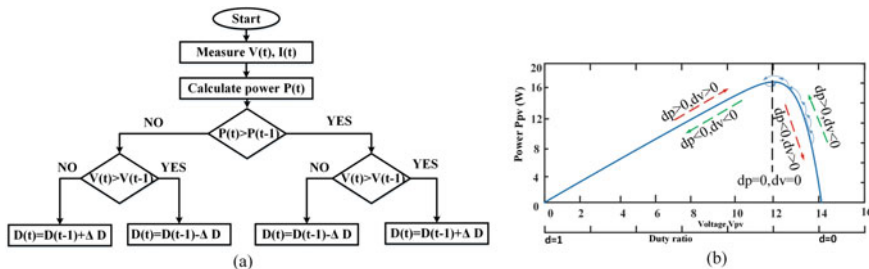


Fig. 5 a P&O MPPT flowchart, b P-V characteristics

2.1 P&O MPPT Algorithm

The maximum power from a PV panel is extracted by using MPPT algorithms. Perturb and observe (P&O) is the conventional MPPT algorithm for maximum power extraction. In this method extracted power is observed by varying the duty based on comparing the power output. The change in power (ΔP_{PV}) and voltage (ΔV_{PV}) between two samples are recoded and compared to generate the duty for the next sample. As, it can also be observed from the flowchart of P&O algorithm shown in Fig. 5a, when both ΔP_{PV} and ΔV_{PV} are positive or ΔP_{PV} and ΔV_{PV} are negative duty factor increases while, alternation of positive and negative sign in ΔP_{PV} and ΔV_{PV} leads to reduces of duty factor.

3 Two-Input Bidirectional DC-DC Converter (TIBC) Operation

The two input bidirectional converter, various modes of operation are elaborated in detail in [34]. Modified operation of the converter is explained here. It consists of three switch-legs. Battery (V_B) and supercapacitor (V_S) modules are connected to legs 2 and 3 respectively. DC microgrid (V_{DC}) is connected to leg 1. In this topology, the operating voltages are selected such a way that the DC grid voltage is greater than ESSs voltages and SC voltage is selected as less than the battery voltage. The inductor L_B and L_S are connected across legs 1, 2 and 1, 3 respectively. The operating modes of presented TIBC is explained as follows:

3.1 HESS Discharging Mode

Whenever there exists a mismatch between PV output and load power, DC microgrid voltage varies from steady state value. When the load exceeds PV generation capacity

Table 2 Switching state in different time intervals

Time scale	T_1	T_2	T_3
Operating switches	S_2, S_3, S_5	S_2, S_4, S_5	S_1, S_4, S_6

or when the power produced by PV falls due to decreased solar irradiation, the DC microgrid voltage decreases. The deficient power must be supplied by HESS during this period. So power flows in this mode from HESS to DC microgrid, by regulating the bidirectional converter properly. The proposed converter switching sequence for discharging mode is given in Table 2.

The converter operation using equivalent circuits and switching model can be divided into three intervals as shown in Figs. 6 and 7 respectively. Switch pairs S_1/S_2 , S_3/S_4 and S_5/S_6 always work in complimentary fashion. Switch pair S_2/S_5 and S_1/S_6 always switch together in this mode and their gating pulses are complimentary to each other. At time instant t_0 , switches S_2, S_3 and S_5 are turned on which will increase inductor currents i_B and i_S linearly with slopes V_B/L_B and V_S/L_S respectively. At t_1 ,

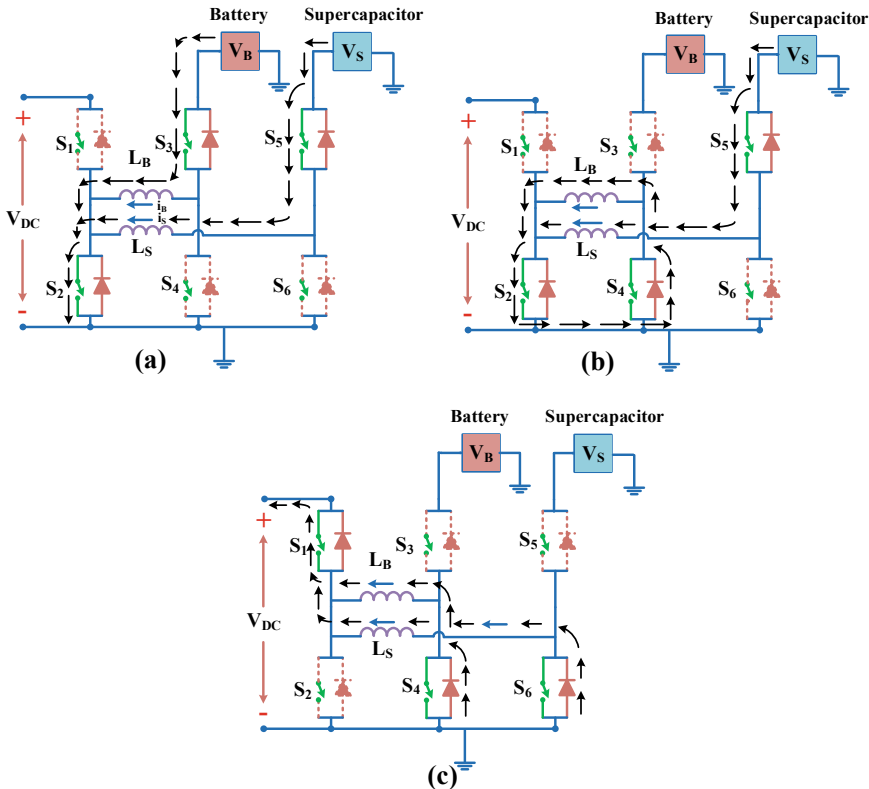
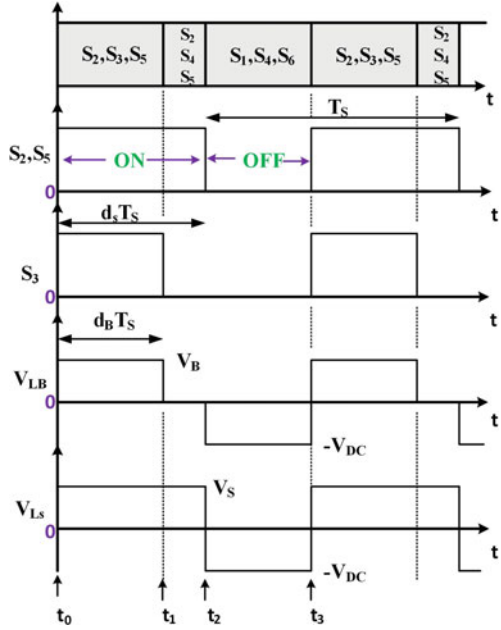


Fig. 6 Switching equivalent circuit of two-input bi-directional converter, **a** S_2, S_3, S_5 operates, **b** S_2, S_4, S_5 operates, **c** S_1, S_4, S_6 operates

Fig. 7 Operational waveforms for HESS discharging mode



switch S_3 is turned off to provide a free-wheeling path for current i_B through body diode of S_4 . After dead time interval for switch pair S_3/S_4 , switch S_4 is turned on. Since body diode of S_4 is already conducting when gating signal was given, S_4 turns on with ZVS. At t_2 , switches S_2 and S_5 are turned off causing inductor current i_{L2} to flow through body diodes of switches S_1 and S_6 with a negative slope of V_{DC}/L_S . Inductor current i_B also flows body diode of S_1 with a negative slope of V_{DC}/L_B . Switches S_1 and S_6 are gated on after dead time interval of switch pairs S_2/S_1 and S_5/S_6 . Similar to the turn on of S_4 , switches S_1 and S_6 are also turned on with ZVS since body diodes of respective switches are already in conduction. At t_3 , switches S_1 , S_4 and S_6 are turned off. Consequently, body diodes of switches S_2 , S_3 and S_5 will conduct in order to maintain the flow of inductor currents. Currents, i_B and i_S , flow with positive slopes of V_B/L_B , and V_S/L_S respectively. After dead time interval, gating pulses are given to switches S_2 , S_3 and S_5 which turn on with ZVS. If d_B is duty cycle of gating pulse given to switch S_3 and d_S is duty cycle of gating pulse given to switches S_2 , S_3 and S_5 , applying volt-second balance to inductors L_S and L_B gives

$$V_{DC} = \frac{d_S}{1 - d_S} \cdot V_S \tag{2}$$

$$V_{DC} = \frac{d_B}{1 - d_S} \cdot V_B \tag{3}$$

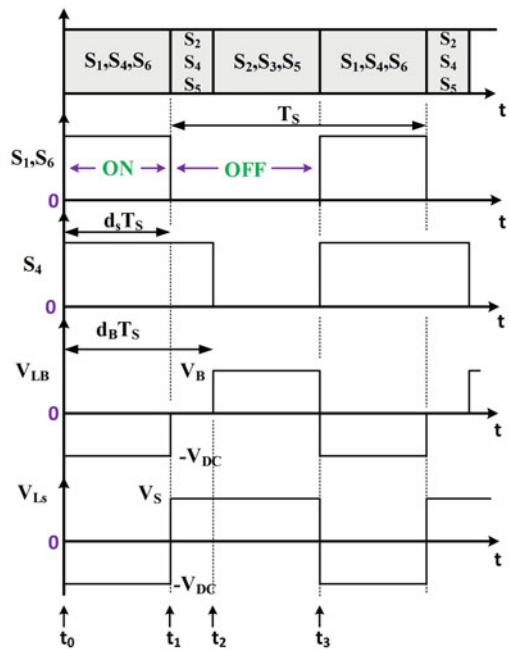
Since V_B is greater than V_S , d_B will always be lesser than d_S . Therefore, by controlling d_B and d_S , power flow from battery and supercapacitor to dc grid can be controlled independently.

3.2 HESS Charging Mode

Whenever PV generation exceeds the load power demand or reduction in load power, there exist an excess power in the DC microgrid that leads to increase in DC microgrid voltage. This excess power utilized to charge the HESS and hence the direction of power flow is from DC microgrid to HESS. The converter operation using equivalent circuits and switching model can be divided into three intervals as shown in Figs. 8 and 9. Switch pair S_1 and S_6 are switched simultaneously. Switch pair S_2 and S_5 are also gated simultaneously but with complimentary pulses to that of S_1 and S_6 . Similarly switches S_4 and S_3 are also gated in complimentary fashion. At t_0 , switches S_1 , S_4 and S_6 are gated on to increase the inductor currents, i_B and i_S , in negative direction linearly with slopes V_{DC}/L_B and V_{DC}/L_S respectively. Operating switches in each time interval is tabulated in Table 3.

Inductors, L_B and L_S , store energy in this time interval until instant t_1 . At t_1 , switch pair S_1/S_6 are turned off. In order to maintain inductor current i_S , body diodes of switches S_2 and S_5 turn on. Energy stored in inductor L_S is now used up to charge

Fig. 8 Operational waveforms for HESS charging mode



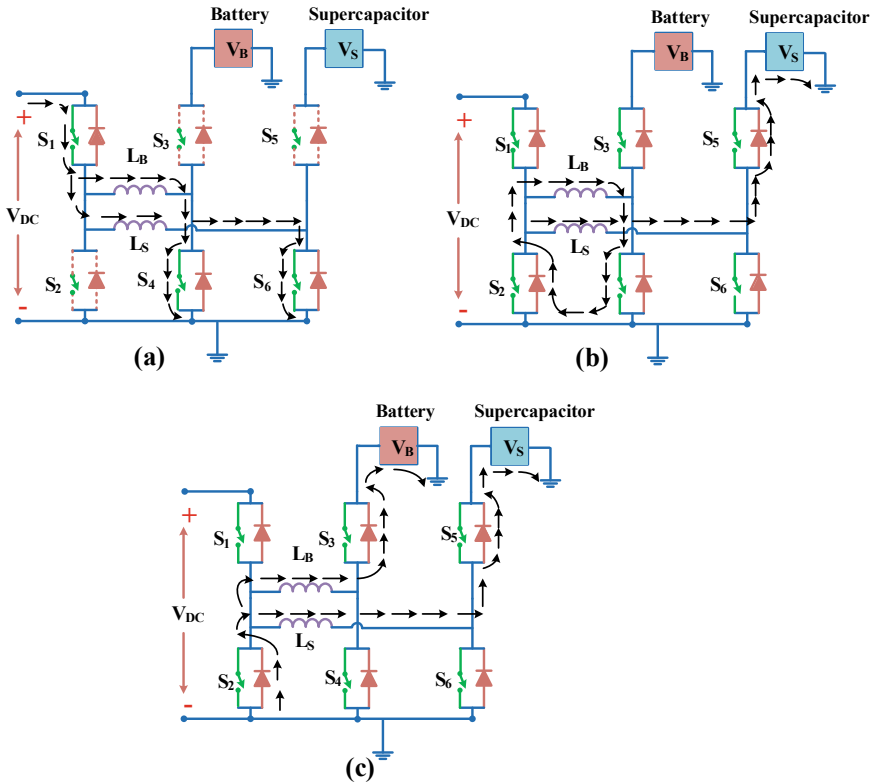


Fig. 9 Switching equivalent circuit of two-input bi-directional converters, **a** S_1, S_4, S_6 operates, **b** S_2, S_4, S_5 operates, **c** S_2, S_3, S_5 operates

Table 3 Switching states in different time intervals

Time scale	T_1	T_2	T_3
Operating switches	S_1, S_4, S_6	S_2, S_4, S_5	S_2, S_3, S_5

supercapacitor. Inductor current i_B free-wheels through body diode of switch S_2 . After dead time interval for switch pair S_1/S_6 and S_2/S_5 , gating pulses are given to S_2 and S_5 which turns them on with ZVS since body diodes of respective switches are already in conduction. At time instant t_2 , switch S_4 is turned off. Inductor current i_S increase linearly with slope V_S/L_S through body diode of switch S_3 . After dead time interval of switch pair S_4/S_3 , gating pulse to S_3 is applied to turn it on with ZVS. Energy stored in inductor L_B is now used to charge battery. At instant t_3 , switches S_2, S_3 and S_5 are turned off, consequently body diodes of switches S_1, S_4 and S_6 turns on to maintain flow of inductor currents. Gating pulses are given to S_1, S_4 and S_6 after dead time interval to turn them on with ZVS. If d_S is duty cycle of gating pulse to S_1/S_6 switch pair and d_B is duty cycle of gating pulse to switch S_4 , applying

volt-second balance to inductors L_S and L_B gives

$$V_S = \frac{d_S}{1 - d_S} \cdot V_{DC} \tag{4}$$

$$V_B = \frac{d_S}{1 - d_B} \cdot V_{DC} \tag{5}$$

Since V_B is greater than V_S which in turn is smaller than V_{DC} , d_B is always greater than d_S . By controlling d_B and d_S , power flow from DC microgrid to HESS can be controlled.

3.3 HESS Energy Exchange Mode

Supercapacitor in HESS is a power density unit. It cannot supply energy for long duration continuously like battery due to its high self-discharging effect. For proper functioning of HESS in DC microgrid applications it is necessary that component ESSs of HESS should have enough energy stored in it. To maintain supercapacitor charge within desired limits, it has to be charged whenever needed from the energy density unit battery for proper functioning of HESS. This mode constitutes power flow from battery to supercapacitor. Circuit topology in this mode is given in Fig. 10a. Steady state waveforms are as shown in Fig. 10b.

In this mode, first switch leg is inactive (switches S_1 and S_2 are off) thus effectively isolating the DC microgrid from HESS during supercapacitor charging process. Switch pairs S_5/S_6 and S_3/S_4 work in complimentary manner. Switch S_5 is always on in this mode which cause switch S_6 to be always off. Switch S_3 is operated upon with duty cycle d . Power flow from battery to supercapacitor involves buck operation of switch S_3 . Inductors, L_B and L_S , are in series and this considerably reduce the

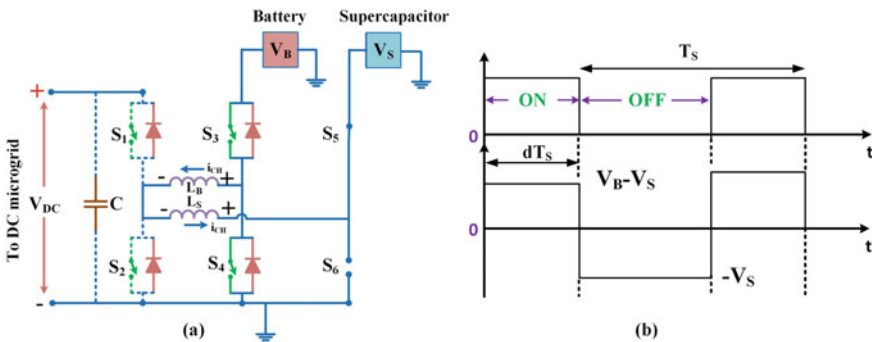


Fig. 10 HESS energy exchange mode of operation. **a** Active circuit through which current flows, **b** steady-state waveforms

current ripple. By controlling d , power flow from battery to supercapacitor can be controlled. Applying volt-second balance to equivalent series inductor L ($L = L_B + L_S$) gives

$$V_S = d \cdot V_B \tag{6}$$

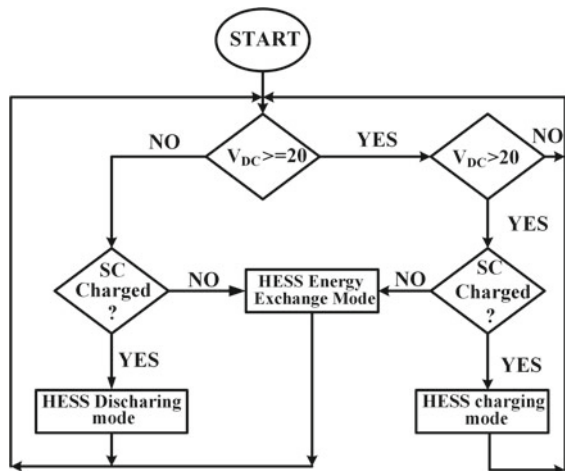
Similarly, power flow from supercapacitor to battery is possible by complimentary operation of switch S_3 . This indicates boost operation of switch S_4 . Operation is similar to that explained above.

3.4 Mode Transitions

The mode of operation is determined from present condition of DC microgrid and continuous monitoring of supercapacitor SOC. Battery SOC is not considered in this work since it is assumed that battery energy is not depleted fast compared to supercapacitor. Flow chart for simple mode transition logic is shown in Fig. 11. When DC microgrid voltage exceeds the set reference, HESS is put into charging mode, provided supercapacitor SOC is within prescribed limits. When DC microgrid voltage is less than set reference value, HESS is put into discharging mode, provided supercapacitor SOC is in safe limits. If supercapacitor SOC violates the prescribed limits, HESS is put into energy exchange mode, thus isolating the DC microgrid electrically from HESS. Supercapacitor SOC working range and its mathematical expression using coulomb’s counting method are

$$SOC_{MIN} \leq SOC \leq SOC_{MAX} \tag{7}$$

Fig. 11 Transitions to different modes represented using a flow chart



$$\% SOC = \left[SOC_i + \left(\frac{1}{Q_{SC}} \int i_{CH} dt \right) \right] \times 100 \tag{8}$$

where SOC_i is initial SOC of supercapacitor, Q_{SC} is rated supercapacitor charge and i_{CH} is supercapacitor charging current.

3.5 Mathematical Design Calculations of Filter Parameters

The design of filter inductor assumes that the bidirectional DC-DC converter always operates in continuous conduction mode (CCM). Mathematical modeling of filter inductor and capacitor for various converters is given in [36–38]. Equivalent circuit of ON time period and OFF time period of boost converter are shown in Fig. 12.

Calculation of peak-to-peak inductor (Δi_L) current during switch ON duration is calculated as

$$\Delta i_L = i_L(DT) - i_L(0) \tag{9}$$

$$\Delta i_L(ON) = \frac{V_{PV} \cdot DT}{L} = \frac{V_{PV} \cdot D}{f_s L} = \frac{V_{DC} \cdot D \cdot (1 - D)}{f_s L} \tag{10}$$

Similarly Δi_L during switch OFF duration of time

$$\Delta i_L = i_L(DT) - i_L(T) \tag{11}$$

$$\Delta i_L(OFF) = \frac{(V_{DC} - V_{PV})(1 - D)T}{L} = \frac{V_{DC} \cdot D \cdot (1 - D)}{f_s L} \tag{12}$$

In this work, the rating of the PV panel are: MPP voltage (V_{PV}): 32 V, MPP current (i_{PV}): 3 A and maximum power (P_{max}): 96 W. For designing DC microgrid voltage (V_{DC}) to 48 V, load resistance can be selected as follows,

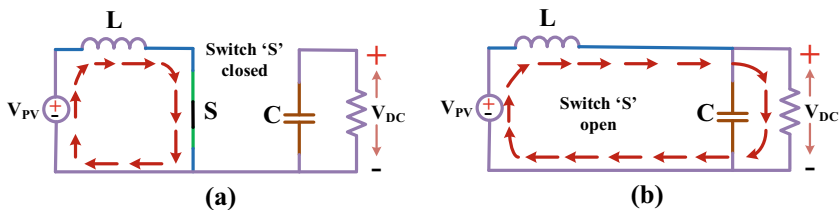


Fig. 12 Equivalent circuit of boost converter, a turn ON, b turn OFF

$$R_{load} = \frac{V_{DC}^2}{P_{max}} = \frac{48^2}{96} = 24 \Omega \quad (13)$$

For designing filter inductor, the peak-to-peak inductor current (Δi_L) is limited to 5% of total current in this work, inductor (L) is defined as follows,

$$L = \frac{V_{PV} \cdot D}{f_s \cdot \Delta i_L} \quad (14)$$

Similarly, the output filter capacitor (C) reduces the voltage ripple, thus can be calculated as

$$C = \frac{D \cdot V_{DC}}{f_s \cdot R_{load} \cdot \Delta V_{DC}} \quad (15)$$

4 Small Signal Linear Averaged Model of 2-Input Bidirectional Converter for PI Controller Design

Small signal averaged model is the basis for development of unified controller for charging/discharging of HESS. An effective model will contribute a controller which will not only provide good closed loop performance but also provide stable operation amidst converter dynamics and external disturbances.

As per circuit operation as explained in previous sections, independent control of power flow is possible from battery and supercapacitor to DC microgrid. Hence, decoupled small signal model can be developed for battery stage as well as for supercapacitor stage which is similar to developing dynamic model of two single-input bidirectional converter. This decoupled averaged small signal model of battery and supercapacitor power flow stage aids in designing simpler controllers which otherwise would be complicated due to presence of multi-input multi-output control systems [22]. Small signal model of battery to DC microgrid as well as supercapacitor to DC microgrid are developed as follows.

A unified controller for battery/supercapacitor charging and discharging will suffice since both the circuit operations share same small signal transfer function due to complimentary action of switches. For developing linear models, HESS discharging mode of operation is considered. Control system description for bifurcation of battery and supercapacitor power is shown in Fig. 13. The outer voltage loop is designed based on supercapacitor stage because of its inherent fast dynamic response.

Thus control system description of supercapacitor stage consists of an inner current loop and an outer voltage loop as depicted in Fig. 14a. Similarly, battery current reference is regulated by a current controller as in Fig. 14b. Inner current loop of supercapacitor is designed for a higher bandwidth than that of battery for

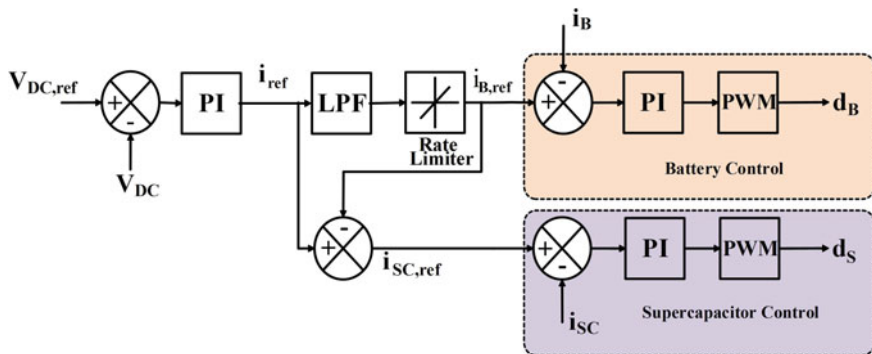


Fig. 13 Overall control system description for current bifurcation between SC and battery units

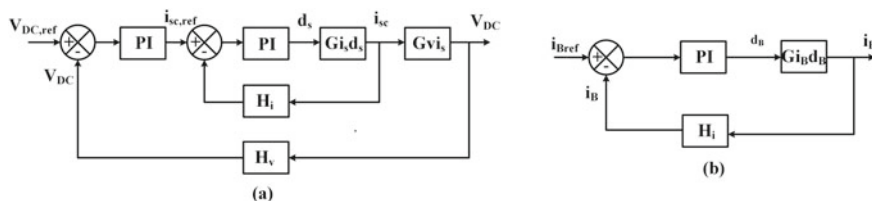


Fig. 14 Supercapacitor and battery control logic. **a** Control system description for supercapacitor control. **b** Control system description for battery control

fast response. Inner current loop operate at a faster rate compared to that of outer voltage loop. Hence voltage loop bandwidth is maintained lesser than inner current loop. Switching frequency considered is 10 kHz.

4.1 Small Signal Linear Averaged Model of Supercapacitor-DC Microgrid Stage

From Fig. 7 and as per operation explained in Sect. 3, during time interval ($t_0 \sim t_2$) the state equations are as follows.

$$L_s \frac{di_{L_s}}{dt} = v_{sc} \tag{16}$$

$$C \frac{dv_{DC}}{dt} = -\frac{v_{DC}}{R} \tag{17}$$

During time interval ($t_2 \sim t_3$), the state equations are as follows.

$$L_s \frac{di_{Ls}}{dt} = -v_{DC} \tag{18}$$

$$C \frac{dv_{DC}}{dt} = i_{Ls} - \frac{v_{DC}}{R} \tag{19}$$

After perturbation and linearization of above state equations, control-to-inductor current and inductor current-to-voltage small signal transfer functions are obtained as follows.

$$G_{i_{sc}d_{sc}} = \frac{i_{SC}(s)}{d_{SC}(s)} = \frac{V_{DC}(1 + D_{SC})}{R(1 - D_{SC})^3} \left[\frac{1 + s \frac{RC}{1+D_{SC}}}{s^2 \frac{L_{SC}C}{(1-D_{SC})^2} + s \frac{L_{SC}}{R(1-D_{SC})^2} + 1} \right] \tag{20}$$

$$G_{v_{DC}i_{sc}} = \frac{v_{DC}(s)}{i_{SC}(s)} = \frac{R(1 - D_{SC})}{(1 + D_{SC})} \left[\frac{1 - s \frac{D_{SC}L_{SC}}{R(1-D_{SC})^2}}{1 + s \frac{RC}{1+D_{SC}}} \right] \tag{21}$$

The inner current loop PI controller is built based on the above model with a bandwidth of 1.6 kHz and a phase margin of 60°. The Bode plot is shown in Fig. 15 for compensated and uncompensated current loop transfer functions. The PI transfer function is given by

$$G_{pi_{is}} = 0.4124 + \frac{2291}{s} \tag{22}$$

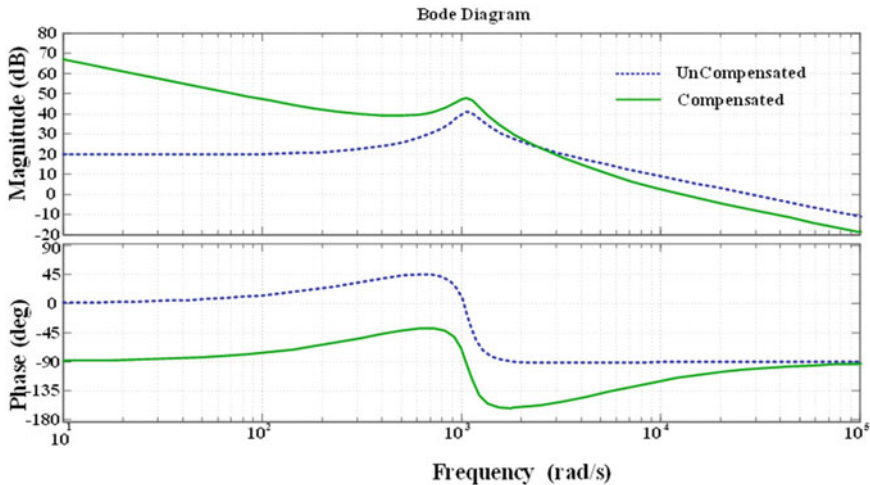


Fig. 15 Bode plot of inner current controller of SC Control logic, with and without compensation

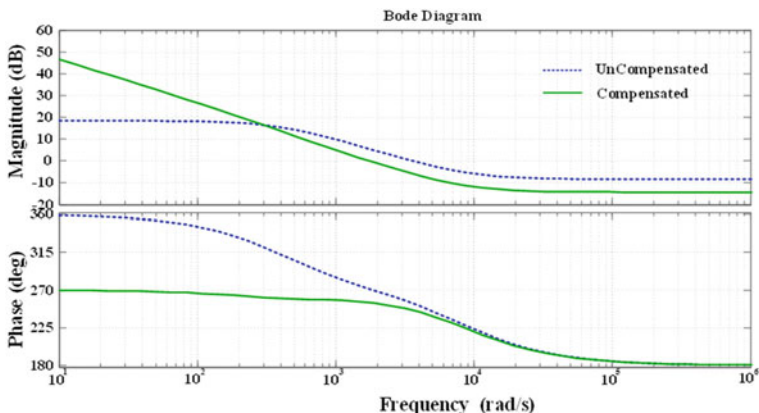


Fig. 16 Bode plot of outer voltage control loop for with and without compensation

The outer voltage loop’s PI controller is also constructed based on the average model. The bandwidth must be smaller than the right half plane zero. The designed voltage controller has a bandwidth of 200 Hz and phase margin of 60°. Bode plot for the same is as shown in Fig. 16. The transfer function is given by

$$G_{pi_v} = 0.5054 + \frac{266}{s} \tag{23}$$

4.2 Small Signal Linear Averaged Model of Battery-DC Micro Grid Stage

Discharge operation of battery is completed in three time intervals as shown in Fig. 7. As explained in Sect. 3, during time interval ($t_0 \sim t_1$), the state equations are as follows.

$$L_B \frac{di_B}{dt} = v_B \tag{24}$$

$$C \frac{dv_{DC}}{dt} = -\frac{v_{DC}}{R} \tag{25}$$

The above system of state equations can be represented in matrix form after converting to frequency domain which takes the following form

$$\frac{dX}{dt} = AX + BU \tag{26}$$

$$Y = CX + EU \quad (27)$$

where X is a matrix containing all state variables (i_B , v_{DC}), U is a matrix containing inputs and Y is a matrix containing all the system outputs. Equations (24) and (25) can be rewritten in matrix form as

$$\begin{bmatrix} \frac{di_B}{dt} \\ \frac{dv_{DC}}{dt} \end{bmatrix} = [A_1] \begin{bmatrix} i_B \\ v_{DC} \end{bmatrix} + [B_1][v_{DC}] \quad (28)$$

$$[i_B] = [C_1] \begin{bmatrix} i_B \\ v_{DC} \end{bmatrix} + [E_1][v_{DC}] \quad (29)$$

where $A_1 = \begin{bmatrix} 0 & 0 \\ 0 & -\frac{1}{RC} \end{bmatrix}$, $B_1 = \begin{bmatrix} \frac{1}{L_B} \\ 0 \end{bmatrix}$, $C_1 = [1 \ 0]$ and $E_1 = [0]$.

Similarly, for second time interval ($t_1 \sim t_2$), the state equations and its matrix form can be represented as follows.

$$L_B \frac{di_B}{dt} = 0 \quad (30)$$

$$C \frac{dv_{DC}}{dt} = -\frac{v_{DC}}{R} \quad (31)$$

$$\begin{bmatrix} \frac{di_B}{dt} \\ \frac{dv_{DC}}{dt} \end{bmatrix} = [A_2] \begin{bmatrix} i_B \\ v_{DC} \end{bmatrix} + [B_2][v_{DC}] \quad (32)$$

$$[i_B] = [C_2] \begin{bmatrix} i_B \\ v_{DC} \end{bmatrix} + [E_2][v_{DC}] \quad (33)$$

where $A_2 = \begin{bmatrix} 0 & 0 \\ 0 & -\frac{1}{RC} \end{bmatrix}$, $B_2 = \begin{bmatrix} 0 \\ 0 \end{bmatrix}$, $C_2 = [1 \ 0]$ and $E_2 = [0]$.

In third time interval ($t_2 \sim t_3$), the state equations and state model in matrix form are expressed as follows.

$$L_B \frac{di_B}{dt} = -v_{DC} \quad (34)$$

$$C \frac{dv_{DC}}{dt} = i_B - \frac{v_{DC}}{R} \quad (35)$$

$$\begin{bmatrix} \frac{di_B}{dt} \\ \frac{dv_{DC}}{dt} \end{bmatrix} = [A_3] \begin{bmatrix} i_B \\ v_{DC} \end{bmatrix} + [B_3][v_{DC}] \quad (36)$$

$$[i_B] = [C_3] \begin{bmatrix} i_B \\ v_{DC} \end{bmatrix} + [E_3][v_{DC}] \quad (37)$$

where $A_3 = \begin{bmatrix} 0 & -\frac{1}{L_B} \\ \frac{1}{C} & -\frac{1}{RC} \end{bmatrix}$, $B_3 = \begin{bmatrix} 0 \\ 0 \end{bmatrix}$, $C_3 = [1 \ 0]$ and $E_3 = [0]$.

From Fig. 7 it is evident that the bidirectional converter will be subjected to state model represented by Eqs. (28) and (29) for a time duration of $(d_B \cdot T_S)$ after which it will undergo transition to the model represented by Eqs. (32) and (33) where it stays for a duration of $[(d_S - d_B) \cdot T_S]$. The duration of third time interval is $[(1 - d_S) \cdot T_S]$ for which the model is Eqs. (36) and (37). Thus, averaged state model of the converter is obtained as follows.

$$A = A_1 \cdot d_B + A_2 \cdot (d_S - d_B) + A_3 \cdot (1 - d_S) \quad (38)$$

$$B = B_1 \cdot d_B + B_2 \cdot (d_S - d_B) + B_3 \cdot (1 - d_S) \quad (39)$$

$$C = C_1 \cdot d_B + C_2 \cdot (d_S - d_B) + C_3 \cdot (1 - d_S) \quad (40)$$

$$E = E_1 \cdot d_B + E_2 \cdot (d_S - d_B) + E_3 \cdot (1 - d_S) \quad (41)$$

$$\frac{dx}{dt} = Ax + Bu \quad (42)$$

$$y = Cx + Eu \quad (43)$$

Assuming perturbations in state variables \hat{x} around the steady state DC value of X , then

$$x = X + \hat{x} \quad (44)$$

Similarly, assuming perturbations in duty cycles (d_B and d_S) and input (u),

$$d_S = D_S + \hat{d}_S \quad (45)$$

$$d_B = D_B + \hat{d}_B \quad (46)$$

$$u = U + \hat{u} \quad (47)$$

For obtaining small signal model, the perturbations are assumed to be very small compared to steady state DC values, i.e., $\hat{d}_S \ll D_S$, $\hat{d}_B \ll D_B$ and $\hat{u} \ll U$. Also, these perturbations are assumed to be constant during one switching period.

Substituting Eqs. (44)–(47) into Eqs. (42) and (43) and linearizing by neglecting second-order terms, the state space model of the converter is obtained as below.

$$\dot{\hat{x}} = \frac{d\hat{x}}{dt} = A\hat{x} + B\hat{u} + F\hat{d}_B + G\hat{d}_S \quad (48)$$

$$\hat{y} = C\hat{x} + (C_1 - C_2)X\hat{d}_B + (C_2 - C_3)X\hat{d}_S \quad (49)$$

where $F = (A_1 - A_2)X + (B_1 - B_2)U$, $G = (A_2 - A_3)X + (B_2 - B_3)U$ and $X = -A^{-1}BU$. Applying Laplace transform to Eqs. (48) and (49) and rearranging, control-to-output transfer function of battery stage is obtained as

$$\frac{\hat{y}(s)}{\hat{d}_B(s)} = C(sI - A)^{-1}F + (C_1 - C_2)X \quad (50)$$

where I is identity matrix. Substituting the values for C , A , F , C_1 , C_2 and X from Eqs. (42), (43), (48), (49), (28), (29), (32) and (33), the control-to-inductor current transfer function of battery loop is given as:

$$G_{i_B d_B} = \frac{\hat{i}_B(s)}{\hat{d}_B(s)} = \frac{V_{DC}}{D_B R(1 - D_S)} \cdot \left[\frac{1 + sRC}{s^2 \frac{L_B C}{(1 - D_S)^2} + s \frac{L_B}{R(1 - D_S)^2} + 1} \right] \quad (51)$$

The PI controller is designed to regulate battery current based on the above transfer function in Eq. (51). The bandwidth of the designed controller is selected such a way that it is less than that of supercapacitor stage. The controller is designed with a bandwidth of 1 kHz and phase margin of 60°. Bode plot for battery current loop with compensated and uncompensated plant is shown in Fig. 18. Transfer function of PI controller is given by

$$G_{pi_{i_B}} = 1.971 + \frac{7300}{s} \quad (52)$$

5 Control Scheme Using Model Predictive Controller

The block diagram of MPC based HESS control scheme is represented in Fig. 19. The outer voltage control loop generates the total current reference (i_{ref}) to be handled by the HESS. The battery reference current (i_{bref}) and SC reference current (i_{scref}) used as current reference to the battery and SC systems. The MPC generates optimal switching states to maintain battery and SC current according to their reference currents.

5.1 Outer Voltage Control Loop

The output of the outer voltage control loop is to calculate the total current demand handled by the HESS to ensure the constant DC grid voltage. Expression for the prediction of total reference current is as follows.

The output capacitor current is given by the equation:

$$i_c = C \frac{dV_{dc}}{dt} \quad (53)$$

$$i_c = C \times \frac{V(k+1) - V(k)}{T_s} \quad (54)$$

where, $v(k+1)$ is the control target and the $v(k)$ is the DC bus voltage to be regulated. In other words, '(K+1)th' state represents the reference input and kth value indicates the measured value.

Total reference current can be written as sum of output capacitor current (i_c) and output DC bus current (i_{dc})

$$i_{ref} = i_c + i_{dc} \quad (55)$$

$$i_c(k+1) = C \times \frac{[V_{ref} - V(dc)]}{N \times T_s} \quad (56)$$

Total reference current can be written as:

$$i_{ref}(k+1) = i_c(k+1) + i_{dc}(k) \quad (57)$$

5.2 Inner Current Control

In HESS, battery supplies the average power required by the load and SC supports the transient power requirement. Hence total current reference can be written as:

$$i_{ref}^* = i_{b,ref}^* + i_{sc,ref}^* \quad (58)$$

To allocate the predicted HESS current properly between battery and SC, a LPF with cutoff frequency of ω_r is used. The corresponding battery reference current (i_{bref}) and SC current reference (i_{scref}) are as follows:

$$i_{b,ref}^* = \frac{w_r}{(S + w_r)} \cdot i_{ref}^* \quad (59)$$

$$i_{SC,ref}^* = \left(1 - \frac{w_r}{(S + w_r)}\right) \cdot i_{ref}^* \quad (60)$$

It is important to calculate the battery current and SC current for the regulation of DC bus voltage. The battery and SC currents are predicted from inductors current equations. Thus, d_b and d_{sc} can be calculate to regulate the DC bus voltage by the following prediction equations.

$$L_b \frac{di_b}{dt} = V_b d_b - V_{dc}(1 - d_b) \quad (61)$$

$$L_{sc} \frac{di_{sc}}{dt} = V_{sc} d_{sc} - V_{dc}(1 - d_b) \quad (62)$$

$$L_b \frac{i_b(k+1) - i_b(k)}{T_s} = V_b(k) d_b(i) - V_{dc}(k)(1 - d_b(i)) \quad (63)$$

$$i_b(k+1) = \frac{T_s}{L_b} \times [V_b(k) d_b(i) - V_{dc}(k)(1 - d_b(i))] + i_b(k) \quad (64)$$

$$i_{sc}(k+1) = \frac{T_s}{L_{sc}} \times [V_{sc}(k) d_{sc}(i) - V_{dc}(k)(1 - d_b(i))] + i_{sc}(k) \quad (65)$$

6 Supercapacitor State-of-Charge Controller

Unlike batteries, supercapacitors have low ESR. So it cannot retain energy for long duration. In order to prevent supercapacitor energy from getting depleted beyond a minimum permissible point, a control logic is devised to maintain the SOC within required limits of Eq. (7). Whenever this desired range of SOC is violated, the converter enters into HESS Energy exchange mode explained in Sect. 3. When SOC of supercapacitor falls below prescribed minimum limit, it is charged with a constant current, I_{CH} , with battery power. When SOC exceeds the maximum safe limit, supercapacitor is allowed to discharge its excess energy to battery with a constant current- I_{CH} . Thus SOC of supercapacitor is maintained within the limits by either buck (SC charging) or boost (SC discharging) operation as explained in Sect. 3. The control logic for SOC controller is shown in Fig. 17. A PI controller is used to regulate the supercapacitor current. The controller is designed based on buck mode control-to-output transfer function. Since its design is not within the scope, it is not shown here. Same controller is sufficient for buck and boost operation in HESS Energy exchange mode explained above since transfer function is same for both the operations. It is to be noted that whenever HESS Energy exchange mode is active, either due to low SOC or high SOC, DC microgrid is isolated from HESS electrically.

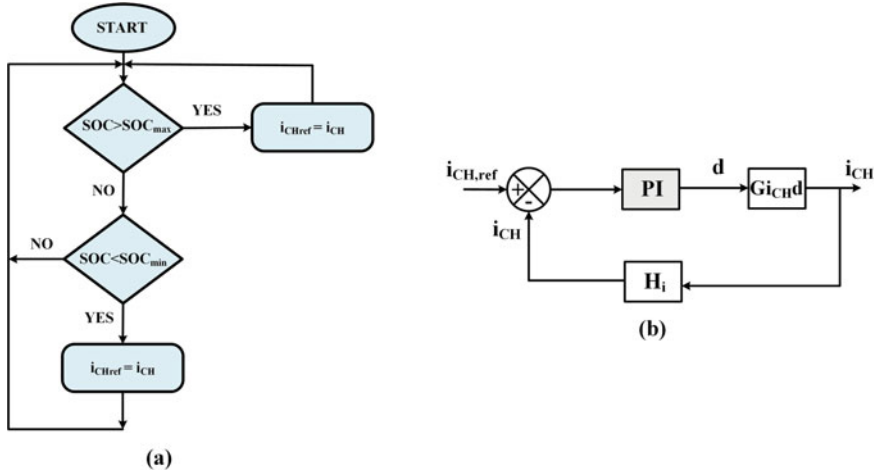


Fig. 17 SOC charge controller for supercapacitor. **a** Logic to select between charging and discharging. **b** Control logic diagram

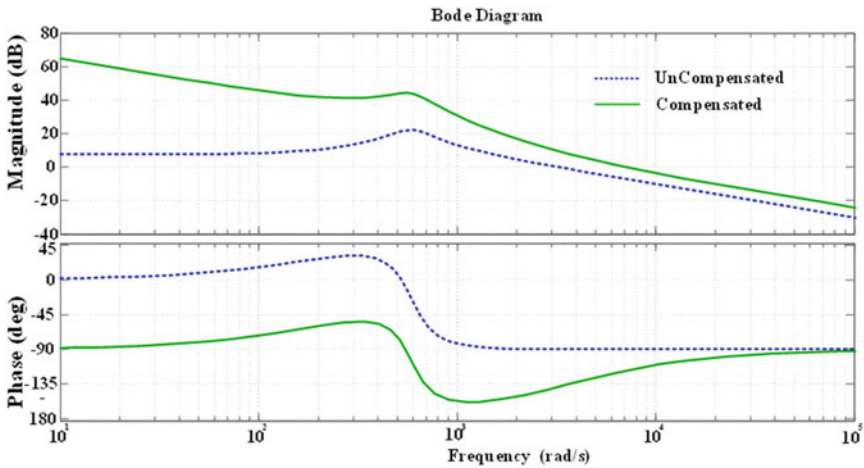


Fig. 18 Bode plot for battery inner current control logic

7 Simulation Study and Discussion

In this segment, the results of the PI and MPC control schemes are displayed for four test cases. The nominal parameters for simulation study are presented in Table 4. The entire model is implemented using MATLAB. The model consists of two bidirectional converters—one for battery and other for SC. The PV array is a unidirectional, which is connected to the boost converter. The different operating cases are presented in the following sections for step change in PV generation and load demand.

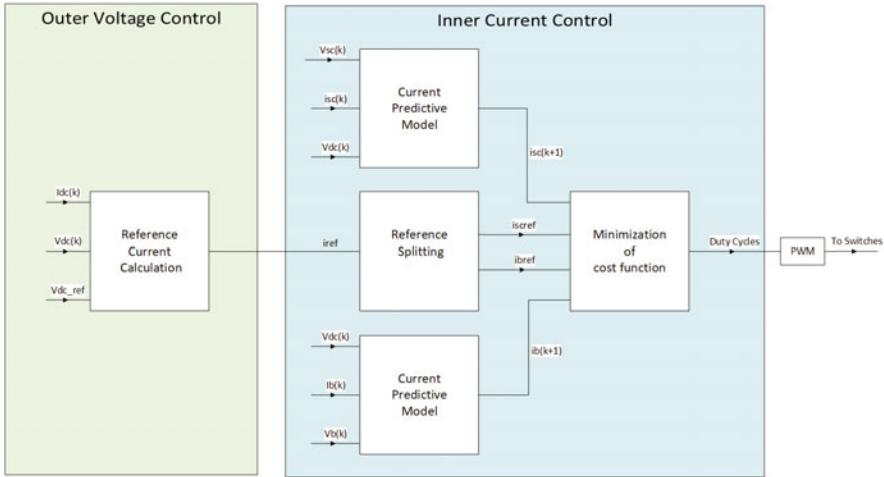


Fig. 19 Block diagram representation of MPC based control scheme

Table 4 System parameters for simulation study

S. No.	Parameters	Value
1	MPPT Voltage (V_{mppt})	32 V
2	MPPT Current (I_{mppt})	3 A
3	MPPT Power (P_{mppt})	96 W
3	SC Voltage (V_{SC})	32 V
4	SC inductance (L_S)	0.355 mH
5	Battery voltage (V_B)	24 V
6	Battery inductance (L_B)	0.3 mH
7	Boost inductance (L)	4.1 mH
8	Resistance (R)	24 Ω
9	DC grid voltage (V_{DC})	48 V
10	Capacitance (C)	300

7.1 Step Change in PV Generation Using PI Control Scheme

The simulation results for step change in PV generation using PI control scheme as shown in Fig. 20. Due to atmospheric variation power produced by the PV panel changed from 96 to 192 W at $t = 0.2$ s and bring back to 96 W at $t = 0.4$ s. For that PV current increases from 3 to 6 A at 0.2 s and bring back to 3 A at 0.4 s. In this case load power requirement constant at 96 W. At $t = 0.2$ s PV power is more than load power requirement by 96 W, DC grid voltage increases more than 48 V. Immediately SC absorbs excess power of 96 W in short duration until battery can regulate the DC grid voltage to 48 V. The battery and SC charge according to energy

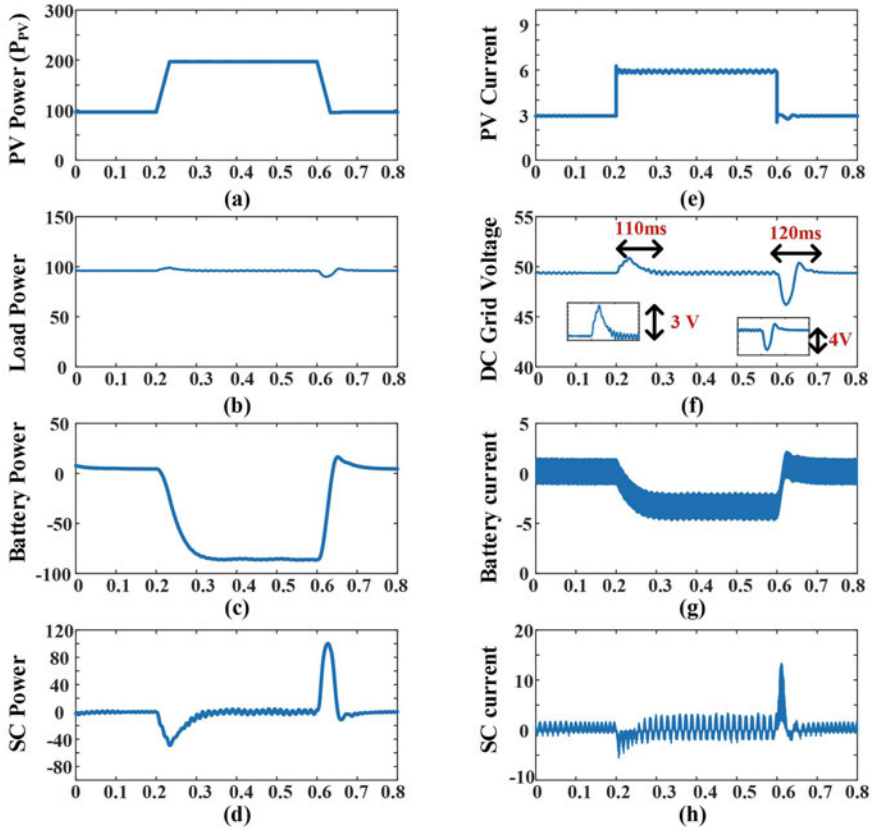


Fig. 20 Simulation results for step change in PV generation using PI control scheme, **a** PV power, **b** load power, **c** battery power, **d** SC power, **e** PV current, **f** DC grid voltage **g** battery current, **h** SC current

management scheme to maintain DC grid voltage constant at 48 V. From obtained results shows that settling time, step increase in PV generation at $t = 0.2$ s is 110 ms and step decrease in PV generation at $t = 0.4$ s is 120 ms.

7.2 Step Change in Load Demand Using PI Control Scheme

The simulation results for step change in load demand as shown in Fig. 21. At a time instant $t = 0.2$ s load power demand increases from 96 to 192 W. This increases the load current from 2 to 4 A. During this state PV current is constant at 3 A. At $t = 0.2$ s, when load power increases to 192 W which is the beyond range of PV power generation. Due to this, power imbalance between source and load power. Due to sudden load fluctuations will affect the DC grid voltage. HESS respond immediately

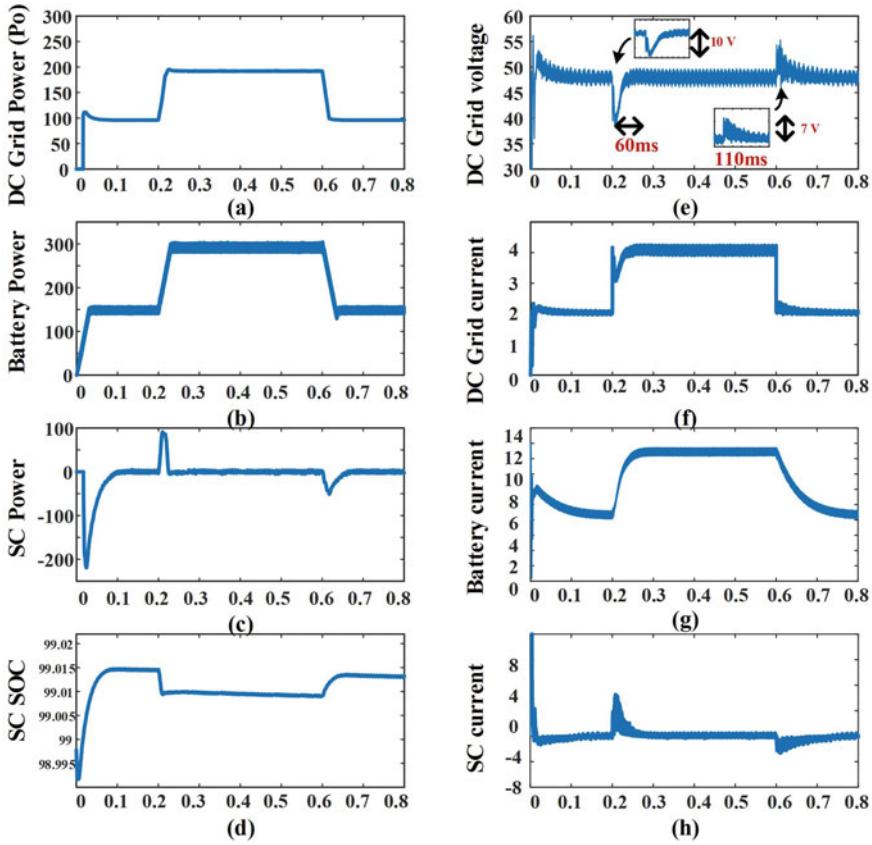


Fig. 21 Simulation results for step change in load demand using PI Control scheme, **a** DC grid power, **b** battery power, **c** SC power, **d** SC SOC, **e** DC grid voltage, **f** DC grid current, **g** battery current, **h** SC current

to these sudden load fluctuations to handle the excess power in DC microgrid. The SC handles the high frequency power transients and study state component of power handled by the battery. The time taken to restore the voltage, at $t = 0.2$ s is 60 ms and $t = 0.4$ s is 110 ms.

7.3 Step Change in PV Generation Using MPC

The simulation results for step change in PV generation using MPC scheme are presented in Fig. 22. Due to the atmospheric variations power produced by the PV panel changes from 96 to 192 W, bring back to 96 W at 0.2 s and 0.4 s respectively. The step change in PV generation causes, step change in PV current at 0.2 s and 0.4 s.

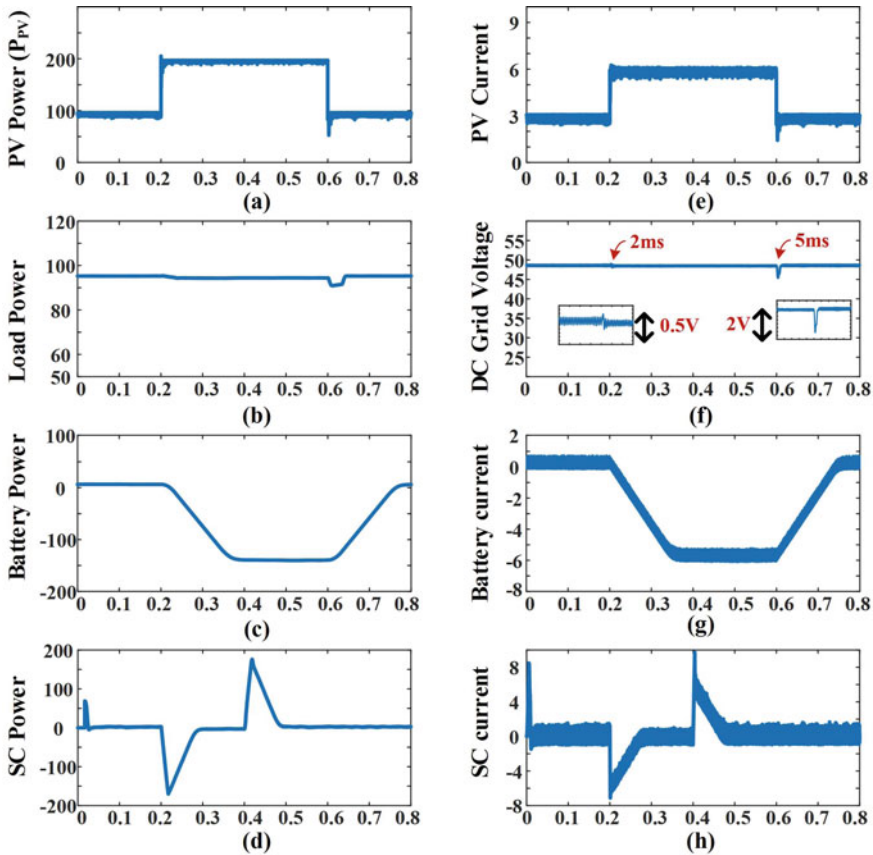


Fig. 22 Simulation results for Step change in PV generation using MPC control, **a** PV power, **b** load power, **c** battery power, **d** SC power, **e** PV current, **f** DC grid voltage, **g** battery current, **h** SC current

At time instant 0.2 s and 0.4 s the DC grid voltage is almost constant at 48 V with negligible settling time of 2 ms and 5 ms. From the results MPC control scheme is faster with less peak overshoot of DC grid voltage compared to PI control scheme.

7.4 Step Change in Load Demand Using MPC

The simulation results for step change in load demand for MPC control scheme are shown in Fig. 23. The maximum power produced by the PV panel is limited to 96 W. The load power requirement increased to 192 W at $t = 0.2$ s. Which is more than the PV power generation. Due to this power imbalance between PV generation and load power demand, DC grid voltage falls below 48 V. The proposed control scheme

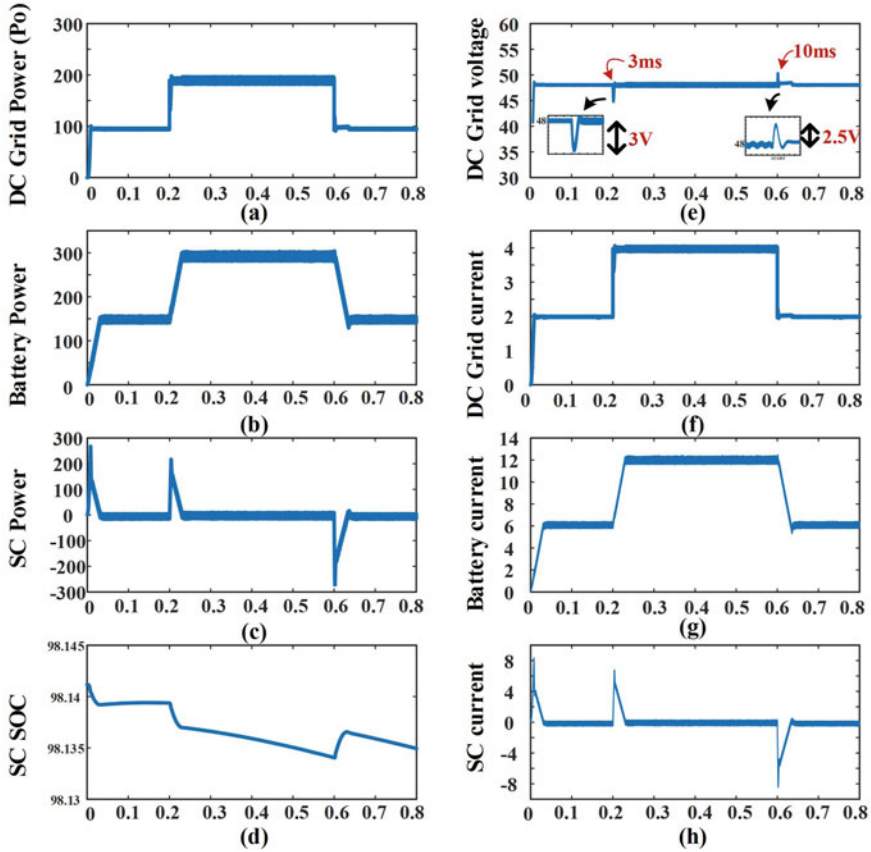


Fig. 23 Simulation results for step change in load demand using MPC control, **a** DC grid power, **b** battery power, **c** SC power, **d** SC SOC, **e** DC grid voltage, **f** DC grid current, **g** battery current, **h** SC current

controls the bidirectional converter, so that HESS supply excess power of 96 W to maintain the DC grid voltage constant at 48 V. The voltage restored to set reference value by using MPC scheme is about 3 ms and 10 ms which 10 times lesser than PI control scheme.

7.5 Comparative Performance Evaluation

The performance evaluation of MPC scheme over the PI control scheme with step change in PV generation and load demand for the peak overshoot and settling time to restore DC grid voltage. The maximum peak overshoot can be calculated during step change in PV generation and load demand as follows.

$$\%MP = \frac{|V_{DC,ref} - V_{max}|}{V_{DC,ref}} \times 100 \tag{66}$$

The comparative performance of PI and MPC schemes are shown in Fig. 24. By graphical results represents, MPC control scheme is faster and reduced peak overshoot compared to PI control scheme. The MPC control scheme is designed such that, SC supports the HESS up to battery steady state operation. The MPC control scheme is faster DC grid regulation and robust control.

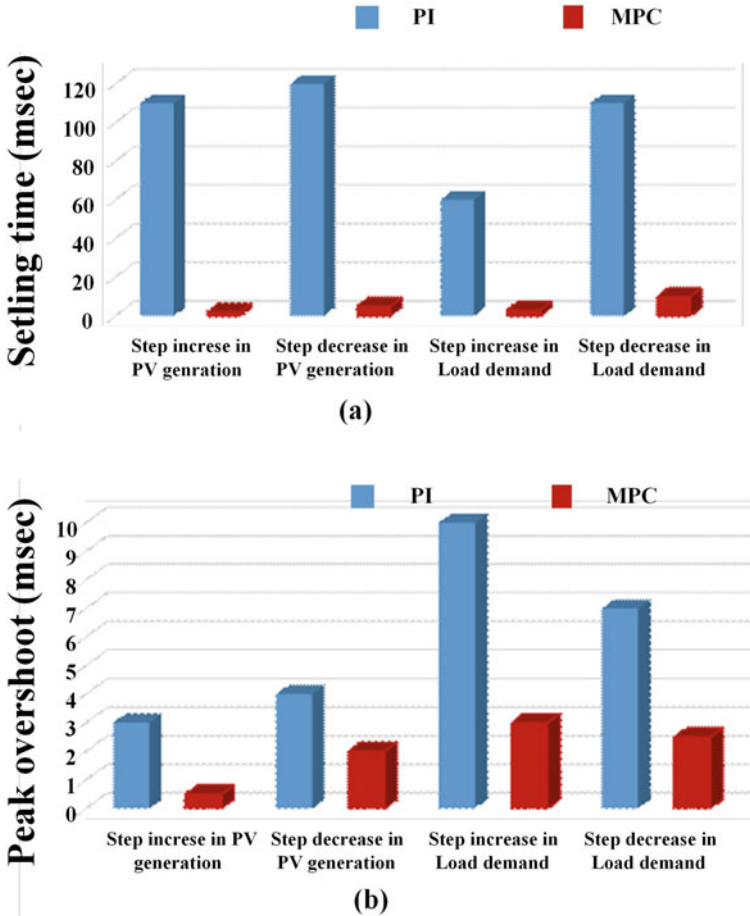


Fig. 24 Graphical comparative performance of PI controller over MPC, **a** settling time **b** peak overshoot

8 Experimental Results

The experimental setup developed for validation of proposed MPC controller for two-input bidirectional converter as shown in Fig. 25. The dSPACE-DS1104 digital controller used in this work. The current sensor LA 55-P and voltage sensor LV 25-P are used for current and voltage measurements in the experimental validation. The regulated power supply (RPS) acts like PV emulator whose current controlled by boost converter. HESS is wired up using one unit of Exide Chloride 12 V, 7 Ah lead-acid battery and Maxwell BMOD0058 16 V, 58F supercapacitor. The bidirectional converter is connected using six MOSFET switches IRFP460.

The performance of DC microgrid supported by HESS is verified for different cases. (1) Step variation of DC grid reference voltage (2) Step variation of PV generation (3) Step variation of load demand (4) Energy exchange mode. System parameters for DC grid are given Table 5. DC microgrid is designed at a nominal voltage of 20 V.

8.1 Step Variation of DC Grid Reference Voltage

The experimental results for step change in DC grid voltage reference as shown in Fig. 26. At time instant t_1 , $V_{DC,ref}$ is step changed from 18 to 20 V as shown in Fig. 26a. In this case load resistance and PV generation kept constant at 25 Ω and 1.3 A respectively. The smooth transition of DC grid voltage is observed. The HESS

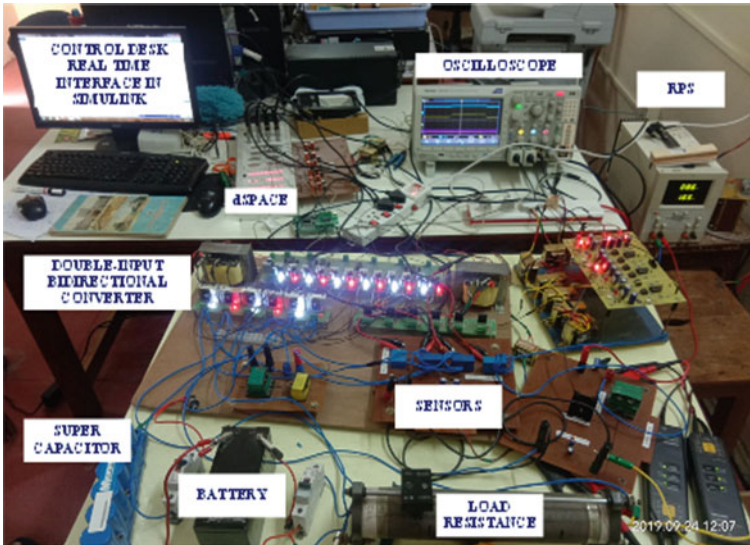


Fig. 25 Hardware prototype developed for HESS

Table 5 Nominal parameters of DC microgrid

S. No.	Parameter	Value
1	SC Voltage (V_{SC})	10 V
2	SC inductance (L_S)	1.43 mH
3	Battery voltage (V_B)	12 V
4	Battery inductance (L_B)	4.8 mH
5	Boost inductance (L)	4.1 mH
6	Resistance (R)	25 Ω
7	DC grid voltage (V_{DC})	20 V
8	Capacitance (C)	150

supplies required power to maintain the DC grid stability. SC supports transient current demand and battery supports steady state demand to maintain the DC grid stability. Similarly, $V_{DC,ref}$ step changed from 20 to 18 V at time t_2 as shown in Fig. 26b. Figure 26c shows the experimental results of step increase and decrease of DC grid reference ($V_{DC,ref}$). At time t_3 , $V_{DC,ref}$ changed from 18 to 21 V immediately HESS supplies required power to maintain the DC grid stability. At time t_4 , $V_{DC,ref}$ changed from 21 to 18 V immediately HESS responds transient component of current charging SC and steady state component of current charging battery to maintain DC grid voltage stability.

8.2 Step Variation of PV Generation

The experimental results for step change in PV generation waveforms are given in Fig. 27. At time t_1 , PV generation suddenly increases to 40 W from 30 W this can be emulated by increasing PV current to 2 A from 1.5 A as shown in Fig. 27a. Then immediately HESS responds to store excess power of 10 W in short duration of time, transient component of current charge SC until battery can regulate the DC grid voltage to 20 V. At time t_2 , PV generation brought back to original condition of 30 W from 40 W power as shown in Fig. 27b. Then immediately HESS responds such way that supplies deficient 10 W power in short duration of time. At time instants t_1 and t_2 , DC grid voltage is almost stable at 20 V as shown in Fig. 27a, b. Figure 27c shows the experimental results for sudden increase and decrease for PV generation at time t_3 and t_4 respectively. With the implementation of proposed control strategy better DC grid voltage regulation is achieved.

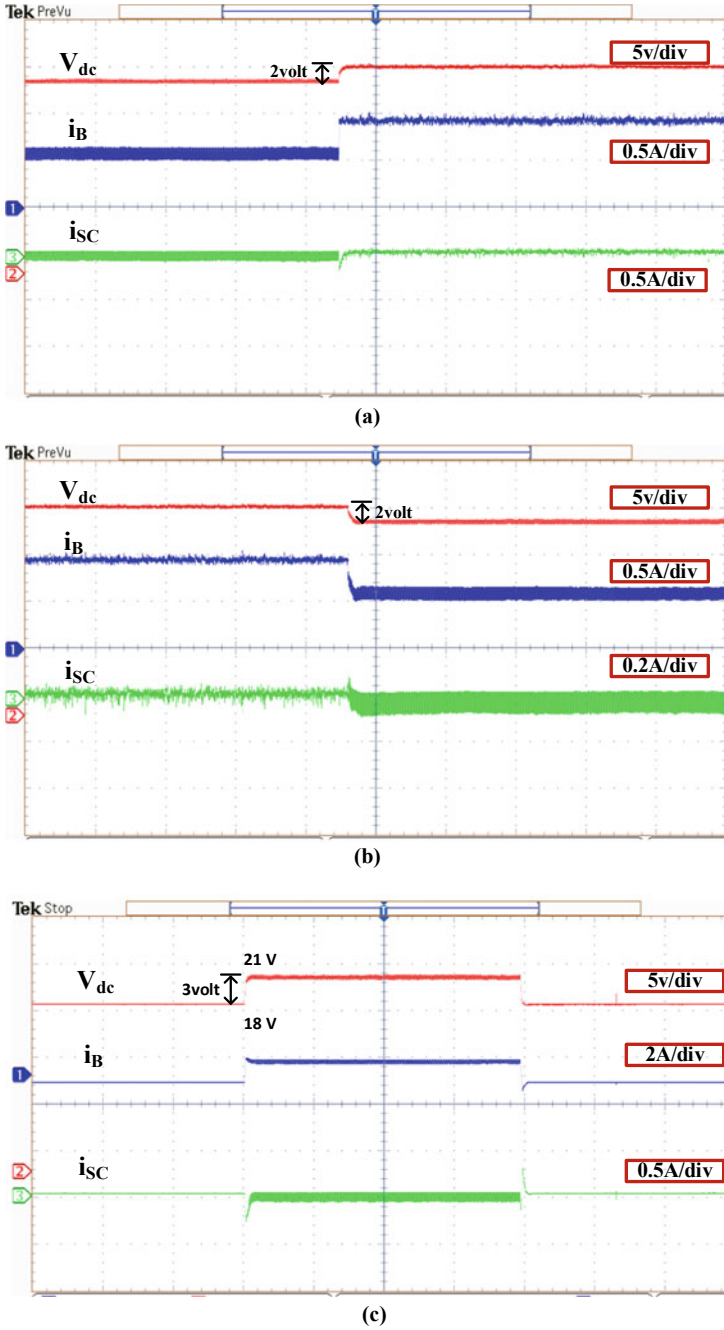


Fig. 26 Experimental results for step change in DC grid voltage reference, a step increase in reference, b step decrease in reference, c step increase and decrease reference voltage

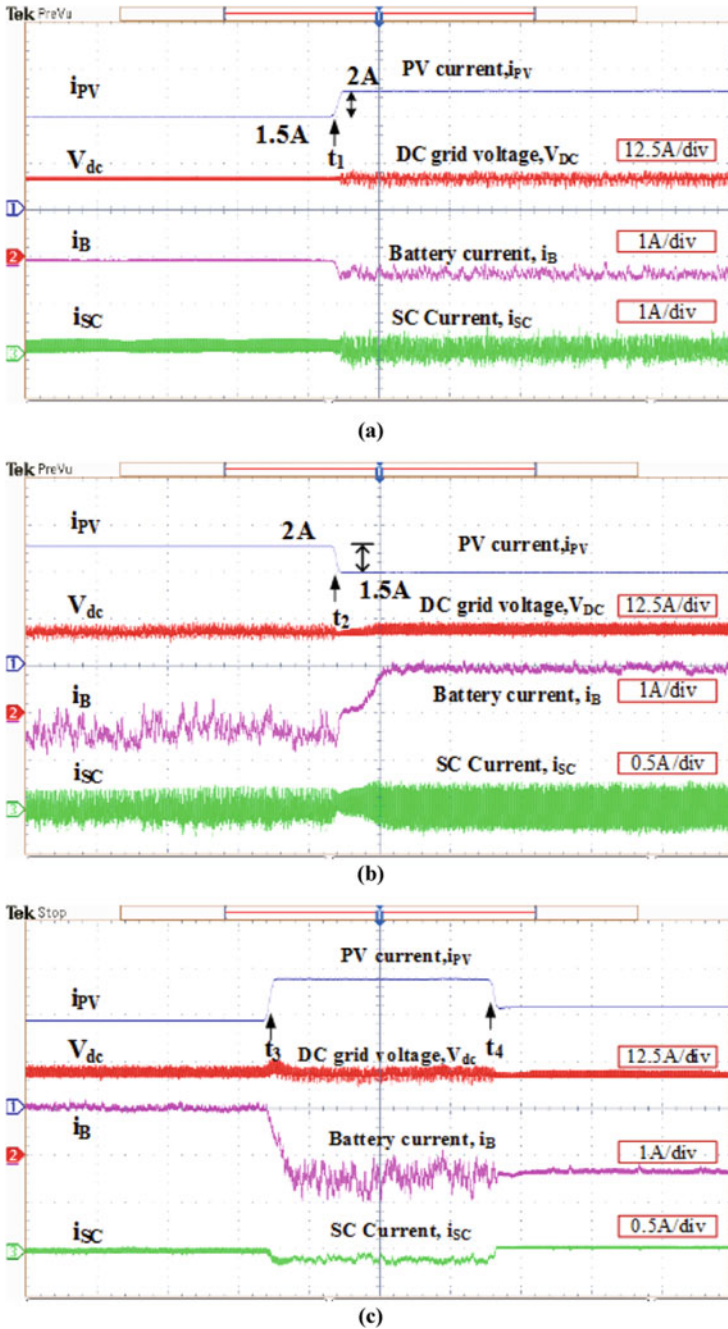
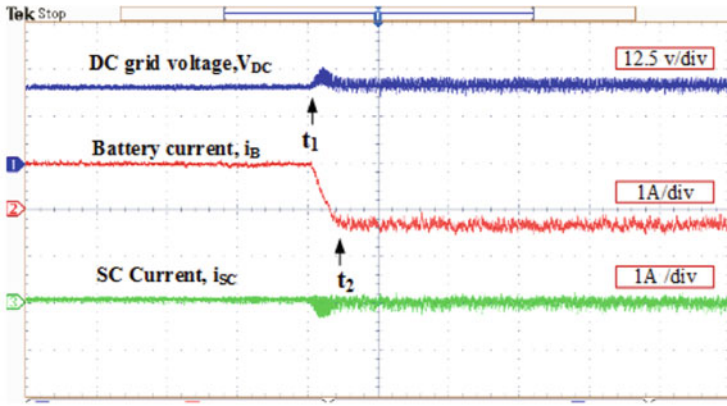
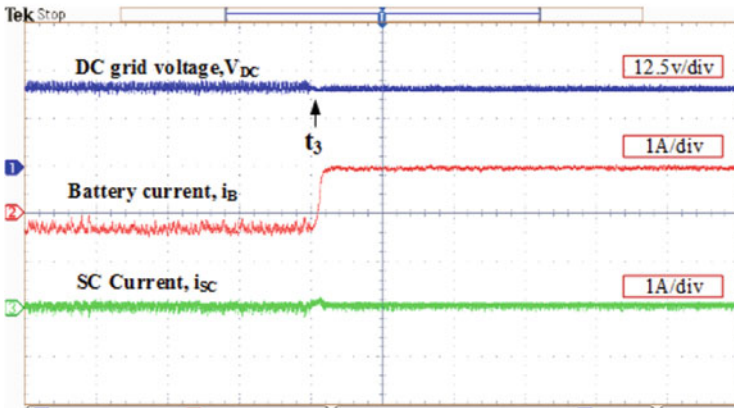


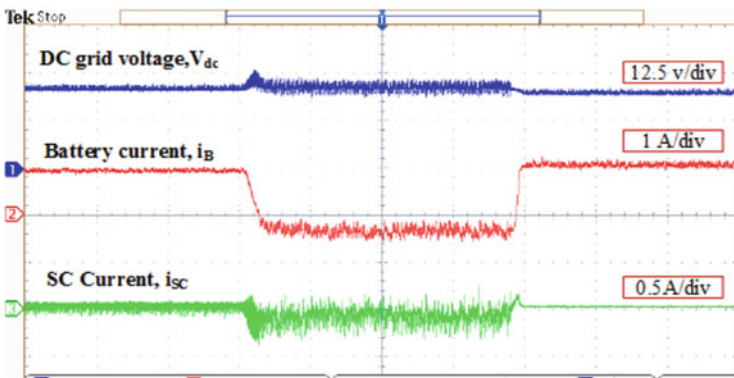
Fig. 27 Experimental results for HESS, **a** step increase in PV generation, **b** step decrease in PV generation, **c** step increase and decrease PV generation



(a)



(b)



(c)

Fig. 28 Experimental results for HESS, **a** step decrease in load demand, **b** step increase in load demand, **c** step increase and decrease load demand

8.3 Step Variation of Load

Experimental results for step change in load demand as shown in Fig. 28. In this case i_{PV} is kept constant at 1.3 A and RPS connected to the boost converter maintaining input voltage to 12 V. Initially load resistance is 25 Ω up to instant t_1 . At time t_1 , load resistance increased to 35 Ω as result decrease in load demand as shown in Fig. 28a. The surge in grid voltage due to excess energy at DC microgrid. At that instant HESS stores excess energy at DC microgrid to maintain grid voltage constant at 20 V. Transient component of current is charging SC and battery charging current is slowly increasing to steady state at up to the instant t_2 .

The load resistance is brought back to original condition $R = 25 \Omega$ at instant t_3 as shown in Fig. 28b. As a result increase in load demand is analyzed. At instant t_3 , small dip in DC grid voltage due to power mismatch between PV generation and load demand. The HESS supplies deficient power to maintain grid voltage constant by discharging battery and SC. Transient component of current met by SC and steady state component of current supplies battery can be shown by using current waveforms. The experimental study for both decrease in load and increase in load as shown in Fig. 28c. DC grid voltage is almost constant at 20 V, small spikes due to fast dynamics of power semiconductor devices.

8.4 Energy Exchange Mode

The power flow from battery to SC is illustrated in this mode. Experimental results for energy exchange mode as shown in Fig. 29. Before time instant t_1 HESS disconnected from DC microgrid, in this period grid voltage 18 V due to reduced PV generation.

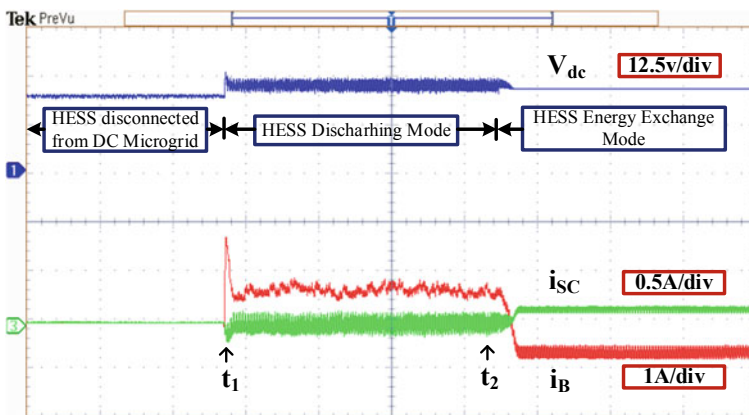


Fig. 29 Experimental results for HESS energy exchange mode. DC microgrid voltage (V_{DC}), battery current (i_B), SC current (i_S). Transition from discharging mode to energy exchange mode

At time instant t_1 , HESS is connected for discharging of battery and SC to regulate DC grid voltage to 20 V. At time instant t_2 , supercapacitor SOC reduced to below 50%, which is taken as prescribed lower limit of SOC range than HESS shifts from discharging mode to energy exchange mode. Now SC will charge from battery with a constant current of $i_{CH} = 0.8$ A. During energy exchange mode, HESS disconnected from DC microgrid which is now evident from voltage waveform not being at nominal voltage of 20 V.

9 Conclusion

In this chapter, two different control schemes for the two-input bidirectional converter for HESS control. The performance of designed controllers are analyzed in various test cases for the application of voltage regulation in DC microgrid. Both the controllers are effectively stabilize DC microgrid against disturbances from step change in PV generation as well as load variations. It could utilize inherent fast dynamics of supercapacitor for absorbing incoming transients to the microgrid. This unified controller proved to be enough for both charging and discharging operation of HESS. Moreover, decoupled, separate and independent control of supercapacitor and battery power was achieved as well as power flow between them. It can also be used in the case of hybrid electric vehicle applications where two or more sources supply power. The performance evaluation of MPC over PI control scheme with step change in PV generation and load demand for peak overshoot and settling time to restore DC grid voltage are tested.

References

1. Xiao J, Wang P, Setyawan L (2016) Implementation of multiple-slack-terminal DC microgrids for smooth transitions between grid-tied and Islanded States. *IEEE Trans Smart Grid* 7(1):273–281. <https://doi.org/10.1109/TSG.2015.2445834>
2. Karbalaye Zadeh M, Gavagsaz-Ghoachani R, Pierfederici S, Nahid-Mobarakeh B, Molinas M (2016) Stability analysis and dynamic performance evaluation of a power electronics-based DC distribution system with active stabilizer. *IEEE J Emerg Sel Top Power Electron* 4(1):93–102. <https://doi.org/10.1109/JESTPE.2015.2484218>
3. Graditi G, Ippolito MG, Telaretti E, Zizzo G (2015) An innovative conversion device to the grid interface of combined RES-based generators and electric storage systems. *IEEE Trans Ind Electron* 62(4):2540–2550. <https://doi.org/10.1109/TIE.2014.2336620>
4. Choi ME, Kim SW, Seo SW (2012) Energy management optimization in a battery/supercapacitor hybrid energy storage system. *IEEE Trans Smart Grid* 3(1):463–472. <https://doi.org/10.1109/TSG.2011.2164816>
5. Feng X, Gooi HB, Chen SX (2014) Hybrid energy storage with multimode fuzzy power allocator for PV systems. *IEEE Trans Sustain Energy* 5(2):389–397. <https://doi.org/10.1109/TSST.2013.2290543>

6. Gao L, Dougal RA, Liu S (2005) Power enhancement of an actively controlled battery/ultracapacitor hybrid. *IEEE Trans Power Electron* 20(1):236–243. <https://doi.org/10.1109/TPEL.2004.839784>
7. Gee AM, Robinson FVP, Dunn RW (2013) Analysis of battery lifetime extension in a small-scale wind-energy system using supercapacitors. *IEEE Trans Energy Convers* 28(1):24–33. <https://doi.org/10.1109/TEC.2012.2228195>
8. Zheng JP, Jow TR, Ding MS (2001) Hybrid power sources for pulsed current applications. *IEEE Trans Aerosp Electron Syst* 37(1):288–292. <https://doi.org/10.1109/7.913688>
9. Punna S, Manthathi UB (2020) Optimum design and analysis of a dynamic energy management scheme for HESS in renewable power generation applications. *SN Appl Sci* 2:495. <https://doi.org/10.1007/s42452-020-2313-3>
10. Inthamoussou FA, Pegueroles-Queralt J, Bianchi FD (2013) Control of a supercapacitor energy storage system for microgrid applications. *IEEE Trans Energy Convers* 28(3):690–697. <https://doi.org/10.1109/TEC.2013.2260752>
11. Laldin O, Moshirvaziri M, Trescases O (2013) Predictive algorithm for optimizing power flow in hybrid ultracapacitor/battery storage systems for light electric vehicles. *IEEE Trans Power Electron* 28(8):3882–3895. <https://doi.org/10.1109/TPEL.2012.2226474>
12. Wang B, Xian L, Manandhar U, Ye J, Ukil A, Beng Gooi H (2017) A stand-alone hybrid pv/fuel cell power systems using single-inductor dual-input single-output boost converter with model predictive control. In: 2017 Asian conference on energy, power and transportation electrification (ACEPT), Oct 2017, pp 1–5. <https://doi.org/10.1109/ACEPT.2017.8168569>
13. Zhao C, Round SD, Kolar JW (2008) An isolated three-port bidirectional DC-DC converter with decoupled power flow management. *IEEE Trans Power Electron* 23(5):2443–2453. <https://doi.org/10.1109/TPEL.2008.2002056>
14. Zeng J, Qiao W, Qu L, Jiao Y (2014) An isolated multiport DC-DC converter for simultaneous power management of multiple different renewable energy sources. *IEEE J Emerg Sel Top Power Electron* 2(1):70–78. <https://doi.org/10.1109/JESTPE.2013.2293331>
15. Wang Y, Han F, Yang L, Xu R, Liu R (2018) A three-port bidirectional multi-element resonant converter with decoupled power flow management for hybrid energy storage systems. *IEEE Access* 6. <https://doi.org/10.1109/ACCESS.2018.2872683>
16. Yang P, Tse CK, Xu J, Zhou G (2015) Synthesis and analysis of double-input single-output DC/DC converter. *IEEE Trans Ind Electron* 62(10):6284–6295. <https://doi.org/10.1109/TIE.2015.2424396>
17. Khaligh A, Cao J, Lee YJ (2009) A multiple-input DC-DC converter topology. *IEEE Trans Power Electron* 24(3):862–868. <https://doi.org/10.1109/TPEL.2008.2009308>
18. Wang B, Xian L, Manandhar U, Ye J, Zhang X, Gooi HB, Ukil A (2019) Hybrid energy storage system using bidirectional single-inductor multipleport converter with model predictive control in DC microgrids. *Electr Power Syst Res* 173(April-2019):38–47. <https://doi.org/10.1016/j.epsr.2019.03.015>
19. Faraji R, Farzanehfard H (2018) Soft-switching nonisolated high step-up three-port DC-DC converter for hybrid energy systems. *IEEE Trans Power Electron* 33. <https://doi.org/10.1109/TPEL.2018.2791840>
20. Sato Y, Uno M, Nagata H (2020) Nonisolated multiport converters based on integration of PWM converter and phase-shift-switched capacitor converter. *IEEE Trans Power Electron* 35(1). <https://doi.org/10.1109/TPEL.2019.2912550>
21. Yi Z, Dong W, Etemadi AH (2018) A unified control and power management scheme for PV-battery-based hybrid microgrids for both grid-connected and islanded modes. *IEEE Trans Smart Grid* 9(6). <https://doi.org/10.1109/TSG.2017.2700332>
22. Behjati H, Davoudi A (2013) Power budgeting between diversified energy sources and loads using a multiple-input multiple-output DC-DC converter. *IEEE Trans Ind Appl* 49(6):2761–2772. <https://doi.org/10.1109/TIA.2013.2265251>
23. Filsoof K, Lehn PW (2016) A bidirectional multiple-input multiple-output modular multilevel DC-DC converter and its control design. *IEEE Trans Power Electron* 31(4):2767–2779. <https://doi.org/10.1109/TPEL.2015.2448112>

24. Wai RJ, Lin CY, Chen BH (2012) High-efficiency DC-DC converter with two input power sources. *IEEE Trans Power Electron* 27(4):1862–1875. <https://doi.org/10.1109/TPEL.2011.2170222>
25. Nejabatkhah F, Danyali S, Hosseini SH, Sabahi M, Niapour SM (2012) Modeling and control of a new three-input DC–DC boost converter for hybrid PV/FC/battery power system. *IEEE Trans Power Electron* 27(5):2309–2324. <https://doi.org/10.1109/TPEL.2011.2172465>
26. Wai RJ, Chen BH (2014) High-efficiency dual-input interleaved DC-DC converter for reversible power sources. *IEEE Trans Power Electron* 29(6):2903–2921. <https://doi.org/10.1109/TPEL.2013.2275663>
27. Chen CW, Liao CY, Chen KH, Chen YM (2015) Modeling and controller design of a semi-isolated multiinput converter for a hybrid PV/wind power charger system. *IEEE Trans Power Electron* 30(9):4843–4853. <https://doi.org/10.1109/TPEL.2014.2367594>
28. Danyali S, Hosseini SH, Gharehpetian GB (2014) New extendable single-stage multi-input DC–DC/AC boost converter. *IEEE Trans Power Electron* 29(2):775–788. <https://doi.org/10.1109/TPEL.2013.2256468>
29. Guo F, Fu L, Zhang X, Yao C, Li H, Wang J (2016) A family of quasi-switched-capacitor circuit-based dual-input DC/DC converters for photovoltaic systems integrated with battery energy storage. *IEEE Trans Power Electron* 31(12):8237–8246. <https://doi.org/10.1109/TPEL.2016.2519394>
30. Gummi K, Ferdowsi M (2010) Double-input DC–DC power electronic converters for electric-drive vehicles—topology exploration and synthesis using a single-pole triple-throw switch. *IEEE Trans Ind Electron* 57(2):617–623. <https://doi.org/10.1109/TIE.2009.2032762>
31. Ahrabi RR, Ardi H, Elmi M, Ajami A (2017) A novel step-up multiinput DC–DC converter for hybrid electric vehicles application. *IEEE Trans Power Electron* 32(5):3549–3561. <https://doi.org/10.1109/TPEL.2016.2585044>
32. Akar F, Tavlasoglu Y, Ugur E, Vural B, Aksoy I (2016) A bidirectional nonisolated multi-input DC–DC converter for hybrid energy storage systems in electric vehicles. *IEEE Trans Veh Technol* 65(10):7944–7955. <https://doi.org/10.1109/TVT.2015.2500683>
33. Nahavandi A, Hagh MT, Sharifian MBB, Danyali S (2015) A nonisolated multiinput multi-output DC–DC boost converter for electric vehicle applications. *IEEE Trans Power Electron* 30(4):1818–1835. <https://doi.org/10.1109/TPEL.2014.2325830>
34. Hintz A, Prasanna UR, Rajashekara K (2015) Novel modular multiple-input bidirectional DC–DC power converter (MIPC) for HEV/FCV application. *IEEE Trans Industr Electron* 62(5):3163–3172. <https://doi.org/10.1109/TIE.2014.2371778>
35. Kollimalla SK, Mishra MK (2014) A novel adaptive p&o mppt algorithm considering sudden changes in the irradiance. *IEEE Trans Energy Convers* 29(3):602–610. <https://doi.org/10.1109/TEC.2014.2320930>
36. Erickson RW, Maksimovic D (2007) *Fundamentals of power electronics*. Springer Science and Business Media. <https://doi.org/10.1007/978-3-030-43881-4>
37. Prasanth S, Manthathi UBVP, Punna S (2019) Efficient interleaved buck converter driver for LED applications. In: 2019 IEEE international conference on sustainable energy technologies and systems (ICSETS), Bhubaneswar, India, 2019, pp 206–212. <https://doi.org/10.1109/ICSETS.2019.8744943>
38. Arunkumar CR, Manthathi UB (2019) Design and small signal modelling of battery-supercapacitor HESS for DC microgrid. In: TENCON 2019—2019 IEEE region 10 conference (TENCON), Kochi, India, pp 2216–2221. <https://doi.org/10.1109/TENCON.2019.8929544>

Parameters Estimation of Solar PV Using Jaya Optimization Technique



C. Srinivasarathnam, Gurappa Battapothula, Anil Annamraju,
and Chandrasekhar Yammani

Abstract Integration of Renewable Energy Sources into the Power Systems is increasing day-by-day because of greater importance to environmental protection, in addition to gradual depletion of fossil fuels. Among all the Renewable Energy Sources, Photo-Voltaic (PV) System has become most popular due to its abundant availability, clean and environmentally pollution-free, noise-free and low maintenance cost. For efficient scheduling of PV system, to meet the load demand and also to reduce the uncertainty, accurate estimation of PV power generation is essential. Thus, estimating PV system parameters accurately has become a research topic of great interest. The mathematical model of the PV system is non-linear in nature. The data provided by the PV manufacturer is inadequate for accurate system analysis. In view of the above, in this chapter, a novel algorithm-specific parameter-free optimization, named Jaya Algorithm is used to predict the Solar PV modules parameters accurately for three different technologies i.e., Poly-crystalline (Shell S75), Mono-crystalline (Shell SM55) and Thin film (Shell ST36). The MATLAB simulation is

C. Srinivasarathnam (✉)

Department of Electrical and Electronics Engineering, Vasavi College of Engineering,
Ibrahimbagh, Hyderabad, Telangana, India
e-mail: crsrinu@staff.vce.ac.in

G. Battapothula

Department of Electrical and Electronics Engineering, B.V. Raju Institute of Technology,
Narsapur, Telangana, India
e-mail: gurappa.b@bvrit.ac.in

A. Annamraju

Department of Electrical and Electronics Engineering, School of Engineering, Malla Reddy
University, Telangana, India
e-mail: anilkumar.a@mallareddyuniversity.ac.in

C. Yammani

Department of Electrical Engineering, National Institute of Technology, Warangal, Telangana,
India
e-mail: chandrayammani@nitw.ac.in

carried out for evaluating the PV module parameters for various environmental conditions. The effectiveness of the proposed method has been validated upon comparison with other optimization techniques available in the literature and with experimental data.

Keywords Renewable energy · Solar PV power · Parameters estimation · Single-diode model · Optimization

Nomenclature

RES	Renewable Energy Sources
GDP	Gross Domestic Product
GW	Giga Watts
kWh	Kilo Watt Hour
PV	Photo-Voltaic
RMSE	Root Mean Square Error
AE	Absolute Error
a	Diode ideality factor
R_s	Series resistance
R_p	Shunt Resistance
I_0	Diode reverse saturation current
I_{ph}	Photo current generated by the module
ω	Inertia weight
V_{ij}^t	Particle 'i' velocity towards dimension 'j' at iteration 't'
X_{ij}^t	Position vector of particle 'i' in dimension 'j' at iteration t
$P_{best,i}^t$	Personal best position of particle 'i' in the iteration t
G_{best}	Global best position of all particle through all iterations
C_1 and C_2	Positive acceleration constants which are used to level the contribution of the cognitive and social components respectively
r_{1j}^t and r_{2j}^t	Random numbers from uniform distribution at iteration t

1 Introduction

Human life is very much dependent on energy. Industries, commercial, and day-to-day activities cannot be progressed without energy. However, energy is available in different forms such as Chemical energy, Thermal energy, Radiant energy, Nuclear energy, Electrical energy, Motion energy, etc., as shown in Fig. 1 [1]. According to the "Law of Conservation of energy," energy can be transformed from one form to another, but neither can it be created nor destroyed. Out of various forms of energy, electrical energy is the most important as it can efficiently be generated (converted

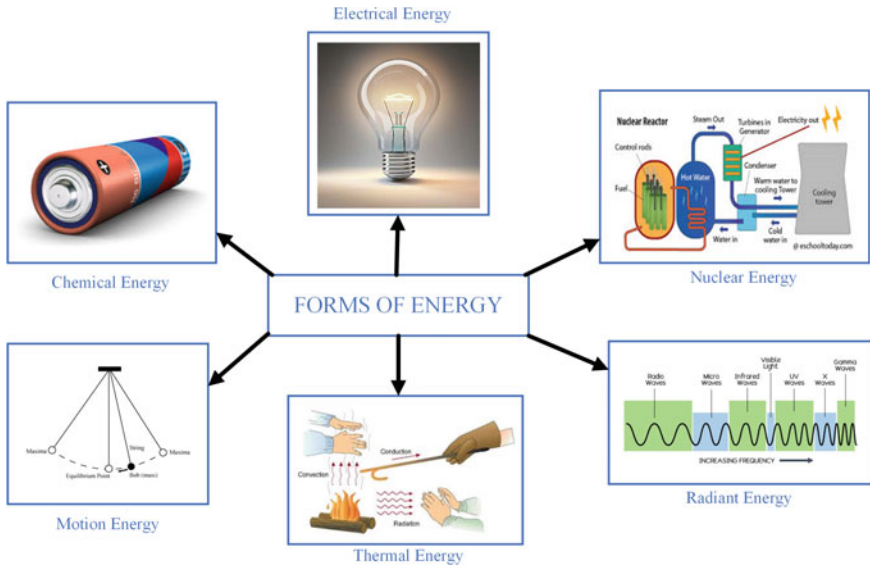


Fig. 1 Various forms of energy

from other forms of energy), easily transmitted, and for a reasonable cost, it can be utilized. The ease of transmission of electrical energy gives rise to a possibility of generating electrical energy in bulk at centralized places and transmit it over a long distance, to be used ultimately by a large number of users [2]. Because of ease in generation, transmission, and utilization, throughout the World, the demand for electrical energy is increasing day-by-day.

As stated in [3], electrical power systems is a technical wonder, and according to the National Academy of Engineering, electricity and its accessibility are the greatest engineering achievements of the twentieth century, ahead of computers and airplanes. The authors in [4, 5] stated that adult literacy rate, life expectancy at birth, GDP per capita (the level of economic development), consumption expenditure per capita, urbanization rate are the five indices that reflect the human development. The per capita electricity consumption should be strengthened to enhance the level of welfare of society and human development. Therefore, special attention is being paid to the generation of electricity. India has installed a capacity of 1.36 GW during Independence whereas it has raised to 365 GW as on October 31, 2019 [6]. As a reflection, the per capita energy consumption of electricity in India has grown from 16 kWh during 1946–47 to 1181 kWh in the year 2018–19, as shown in Fig. 2. The per capita energy consumption of electricity by various countries is shown in Fig. 3. It is clear from Fig. 3 that the per capita energy consumption of electricity in India is much lower than the developed countries and is lesser than the world’s average consumption. Further, the world’s average electricity consumption is much lower than the developed countries’ electricity consumption. Thus, there is a need to think of supplying reliable power to the consumer at an affordable price.

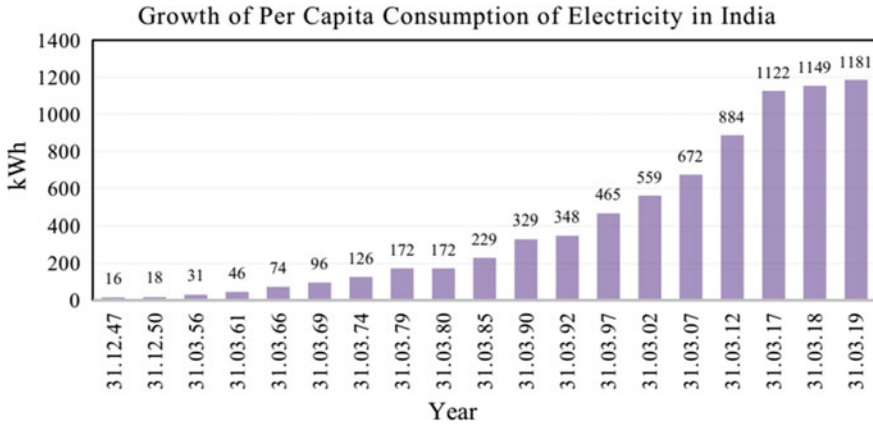


Fig. 2 Growth in per capita consumption of electrical energy in India

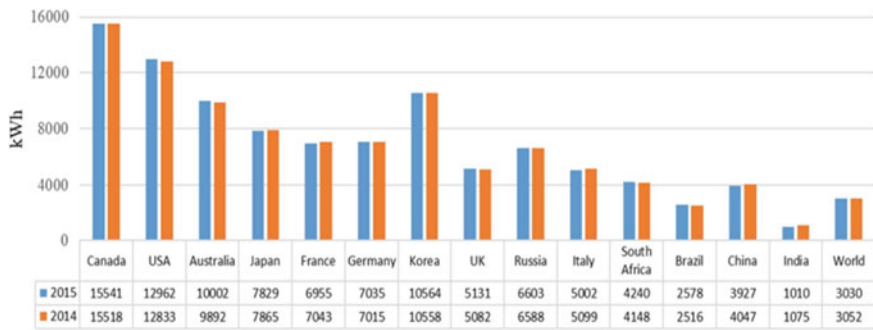


Fig. 3 Per capita energy consumption of electrical energy in various countries

In addition to the above problem, for developing countries with spurring social and economic progress, it is pivotal to have affordable and reliable electricity in rural areas. It is proclaimed by Ministry of Power, Government of India [7] that still 13.90 lakhs households in India are yet to be electrified as on 31.10.2019, and as per the World Bank report, the percentage of the World’s population having access of electricity up to 2018 is 89.59% [8] as depicted in Fig. 4. The Indian Government, by grid expansion, has made remarkable progress on rural electrification. However, copious householders have no electricity access. Thus, it is a challenge to the power systems engineers to supply electrical power to the remote locations where geographically grid expansion is not feasible.

The power generation from the conventional energy sources encounters challenges such as run out of fossil fuels such as coal and oil, change in climate conditions, continuous increase in energy demand [9]. Further, combustion of fossil fuels releases harmful gases which include Carbon dioxide, Sulphur dioxide, Nitrogen oxide, which causes global warming and acid rains. To address these challenges faced by the power

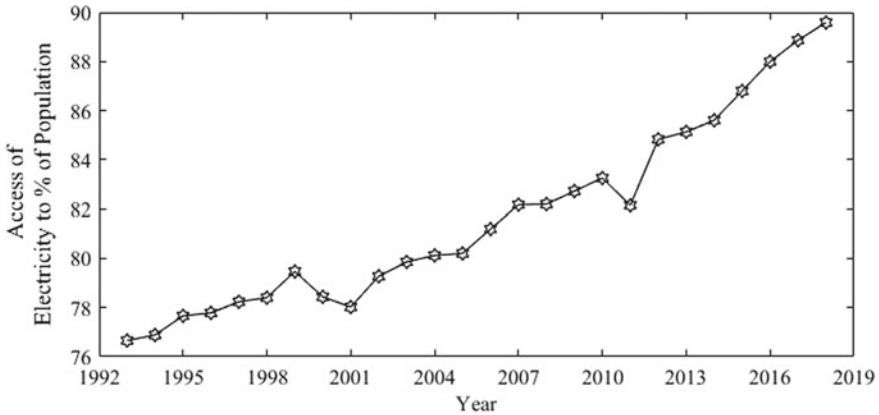


Fig. 4 Access of electricity to percentage of population in the world

systems engineers, researchers are focusing on alternate energy sources. Considering the capital investment and environment condition, Renewable Energy Sources (RES) are found to be the best alternate [10]. Among the RES (Solar power and Wind power), Solar Photo-Voltaic (PV) power generation is deemed to be popular around the world being ubiquitous in urban and rural areas, its abundant availability in nature, long lifecycle time, clean and environmentally pollution-free, noise-free, negligible maintenance as it does not rely on moving parts and reliable [11]. Further, modularity is the salient feature of PV technology, wherein the existing PV system can be easily upgradable within a short period of time, without replacing the entire existing system. The PV system is found to be ideal for earth applications as well as space applications due to its flexibility and benefits [12, 13].

Optimal utilization of solar energy is essential due to its high initial investment cost. Thus, the proper design of the PV system is crucial for increasing system efficiency. The accuracy of predicting the solar panel characteristics is decided by the determination of PV model parameters exactly. An accurate estimation of the PV system is necessary for (a) Demand side management in power systems, (b) Design of Maximum Power tracking of Solar system (c) Efficiency estimation, at different weather conditions [14]. In view of this, parameter estimation of the PV cell accurately has become an interesting topic for the researchers today.

To determine the performance and non-linear behavior of the PV system, several mathematical models are available in the literature. Among the available methods, single diode modeling and two diode modeling are popular [15]. Due to simplicity in modeling and a reduced number of model components, the single diode model is mostly preferred. Furthermore, the parameters extraction methods of any model have been categorized into (a) Deterministic algorithms and (b) Stochastic algorithms.

Deterministic methods normally use algebraic manipulation which involves numerical iterations. The traditional optimization algorithms, such as Dynamic Programming, Nonlinear Programming, Geometric Programming, Sequential

Programming, etc., have certain limitations in their search mechanism. The search mechanism of these algorithms depends on the type of objective and constraint functions, modeling of variables type. The efficiency of these algorithms relies on the solution space size, the structure of solution space, the number of variables. The above problems associated with traditional techniques have been surmounted with population-based optimization techniques over the past two decades.

The authors in reference [16] addressed the PV parameters estimation for three different PV modules, which are multi-crystalline (Kyocera KC200GT), monocrystalline (Shell SQ80), and thin-film (Shell ST40). An Iterative method based on the Gauss-Siedel iterative resolution algorithm has been attempted on a Single diode model and an analytical method tested on two diode model to evaluate the PV parameters accurately. The author has considered both Absolute Error (AE) and Root Mean Square Error (RMSE) to validate the reliability of the methods. In reference [17], an iterative and the Lambert W function has been attempted by the authors for PV parameters estimation of single diode model. The authors have tested the performance of the proposed model on multi-crystalline, mono-crystalline and thin-film models. RMSE has been considered to address the accuracy of the proposed model results with experimental results. A non-linear least-squares optimization method which depends on the modification of Newton method with Levenberg parameters has been attempted by the author in reference [18].

Though computationally deterministic methods are fast, certain approximations are required, in order to ensure the model is analytically manageable, which leads to compromise in the accuracy of the solution. Moreover, the analytical methods are tedious, computationally complex and time consuming [11]. Thus, now-a-days, most of the researchers are opting stochastic algorithms.

Stochastic algorithms such as Genetic Algorithm(GA) [19], Particle Swarm Optimization(PSO) [20], Enhanced Learner Particle Swarm Optimization [21] Teaching Learning Based Optimization(TLBO) [22], Simulation Annealing (SA), Jaya algorithm [23] etc., generate population randomly in the search space and these population get update their position randomly to identify the best solution in the search space.

The author in [24] attempted Shuffled Frog Leaping Algorithm (SFLA) technique to evaluate the PV parameters considering Single diode model. The models examined by the author are Kyocera KC200GT and SolarexMSX-60. Power error function has been treated as an objective function such that the power output at MPP by the proposed method and the experimental method are to be closure. It was proved that simulation results by SFLA coincide with the experimental details. The author has proclaimed that SFLA results are superior that Genetic Algorithm and Iterative modeling algorithm.

In reference [11], the authors have attempted the Bacterial Foraging Algorithm to estimate the PV parameters of single diode model. The results obtained are compared with the Genetic Algorithm and Artificial Immune System. The authors have claimed that the proposed algorithm is superior in terms of accuracy, consistency, speed of convergence and absolute error.

Differential evolutionary (DE) algorithm has been addressed by the authors in [25] to evaluate the PV parameters. The parameters Diode ideality factor (a) and series

resistance (R_s) are evaluated using DE and other parameters Shunt Resistance (R_p), Diode reverse saturation current (I_0) and Photocurrent generated by the module (I_{ph}) are evaluated analytically. The authors proclaimed that by using DE and analytical method, the computation burden had reduced drastically and substantial improvement had been found in the results.

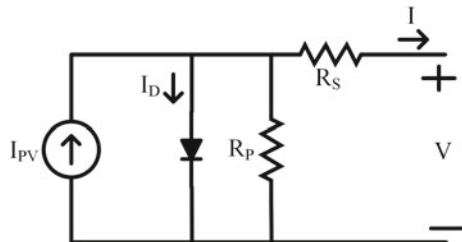
Based on the above literature, considering the advantages of the meta-heuristic techniques and to reduce the computational burden in evaluating the PV parameters, in this chapter, both meta-heuristic methods and analytical methods are considered together to evaluate the PV parameters of a single diode model. To validate the results, different technologies of PV panels are considered, which are (1) Poly-crystalline (Shell S75), (2) Mono-crystalline (Shell SM55) and (3) Thin-film (Shell ST36).

The remainder of this chapter is organized as follows: Sect. 2 describes Mathematical modeling of PV model. The problem formulation of parameters estimation of single diode model is presented in Sect. 3. Meta-heuristic techniques applied to solve the parameter estimation problem are PSO and Jaya algorithm, which are described in Sects. 4 and 5 respectively. Section 6 presents the algorithm and flow chart respectively using PSO and Jaya algorithms for the proposed problem. Simulation results and analysis are presented in Sect. 7. Section 8 summarizes the major contributions with concluding remarks.

2 Mathematical Modeling of PV Model

Due to average complexity and accuracy in results, the single diode model is mostly used electrical model to represent the characteristics of a solar PV module. The ideal model of a Solar PV module is a Current source (I_{PV}) in parallel with a diode. However, due to leakage current in the semiconductor device, a shunt resistance (R_p) is added in parallel to the device. Further, due to resistance offered for the current flow by the semiconductor material, metal grid in the module and leads contact resistance, a resistance in series (R_s) is added to the model. Thus, the practical Solar PV model is represented in Fig. 5. From the Fig. 5, by applying KCL, we get the current (I) as per Eq. (1).

Fig. 5 Single-diode PV equivalent circuit



$$I = I_{PV} - I_D - \frac{V}{R_P} \quad (1)$$

where V is the terminal voltage/voltage across the diode, I_D is the diode current, I_{PV} is the Photo current generated by the module.

The general form of a diode current equation is given by Eq. (2).

$$I_D = I_o \left(e^{\frac{V}{aV_t}} - 1 \right) \quad (2)$$

where I_o is the diode reverse saturation current, a is diode ideality factor and V_t is the thermal voltage across the diode, which is given by Eq. (3).

$$V_t = \frac{KT}{q} \quad (3)$$

where q is charge of electron which is given by $-1.602 \times 10^{-19} \text{C}$, T is cell temperature measured in Kelvin, K is Boltzmann constant given by $1.380649 \times 10^{-23} \text{J.K}^{-1}$. By applying KVL in Fig. 5, we get

$$V_D = V + IR_S \quad (4)$$

where V_D is the voltage across the diode. Thus, the parameters to be estimated in this single diode model are Diode ideality factor (a), Series resistance (R_s), Shunt Resistance (R_p), Diode reverse saturation current (I_o) and Photo current generated by the module (I_{pv}).

3 Problem Formulation

As illustrated above, in the single diode model, five parameters a , R_s , R_p , I_o and I_{ph} need to be evaluated for modelling the solar PV characteristics. In this chapter, both analytical method and optimization techniques are used to evaluate these parameters. Shunt resistance (R_p), diode reverse saturation current (I_o) and Photocurrent generated by the module (I_{ph}) are determined analytically to reduce the computational complexity and diode ideality factor (a), Series resistance (R_s) are evaluated using an optimization technique. These parameters are assessed such that the error between the calculated value and experimental values is maintained as minimum as possible. Also, due to the change in environmental conditions particularly temperature and irradiance, these parameter values get varied. The parameters of the Solar PV model need to be evaluated such that the error is minimum under different operating conditions.

From the manufacturer's data sheet, the known parameters of the model are short circuit current (I_{SC}), open circuit voltage (V_{OC}), Maximum power point operating current (I_M) and operating voltage (V_M) and current temperature coefficient (K_I). The photocurrent of a PV panel is determined using the Eq. (5) which is defined as follows.

$$I_{PV} = \frac{G}{G_{STC}} (I_{SC,STC} + K_I(T - T_{STC})) \quad (5)$$

where $I_{SC,STC}$ is short circuit current at STC, G is irradiance at which surface of the panel is exposed to environment, G_{STC} is irradiance at STC i.e., 1000 W/m^2 , T_{STC} is temperature at STC i.e., $25 \text{ }^\circ\text{C}$. During open circuit condition, the output voltage and current values are

$$V = V_{OC} \quad (6)$$

$$I = 0 \quad (7)$$

Substituting Eqs. (6) and (7) in Eq. (1), which gives

$$0 = I_{PV} - I_D - \frac{V_{OC}}{R_P} \quad (8)$$

On substituting Eqs. (2) in (8), we get Eq. (9) as below

$$0 = I_{PV} - I_o \left(e^{\frac{V_{oc}}{aV_t}} - 1 \right) - \frac{V_{oc}}{R_P} \quad (9)$$

From the above Eq. (9), I_o can be evaluated as follows,

$$I_o = \frac{I_{PV} - \frac{V_{oc}}{R_P}}{\left(e^{\frac{V_{oc}}{aV_t}} - 1 \right)} \quad (10)$$

The I_o in Eq. (10) depends on R_P , which is an unknown parameter. Thus, to make I_o independent of R_P , the following procedure is followed. We know, during MPP condition,

$$V = V_M \quad (11)$$

$$I = I_M \quad (12)$$

On substituting the following conditions in Eq. (1), we get

$$I_M = I_{PV} - I_o \left(e^{\frac{V_M + I_M R_S}{aV_t}} - 1 \right) - \frac{V_M + I_M R_S}{R_p} \tag{13}$$

From the Eq. (13), R_p is evaluated as

$$R_p = \frac{V_M + I_M R_S}{I_{PV} - I_o \left(e^{\frac{V_M + I_M R_S}{aV_t}} - 1 \right) - I_M} \tag{14}$$

On substituting Eqs. (14) in (10), we get an equation for I_o which only depends on known parameters and independent of unknown parameters. Thus, I_o is defined as per Eq. (15).

$$I_o = \frac{I_{PV} + \frac{V_{oc}}{V_M + I_M R_S} (I_M - I_{PV})}{\left(e^{\frac{V_{oc}}{aV_t}} - 1 \right) - \left(e^{\frac{V_M + I_M R_S}{aV_t}} - 1 \right) \left(\frac{V_{oc}}{V_M + I_M R_S} \right)} \tag{15}$$

3.1 Evaluation of Fitness Function

From the P-V characteristics of a solar panel, at Maximum Power Point (MPP), the slope is equals to zero, irrespective of irradiance and temperature condition. Therefore, the slope at MPP can be written as

$$\left(\frac{dP}{dV} \right)_{MPP} = 0 \tag{16}$$

We know from the characteristics that power (P) is given as product of voltage (V) and current (I). Thus,

$$P = VI \tag{17}$$

Upon derivating the Eq. (17) with respect to V, we get

$$\left(\frac{dP}{dV} \right)_{MPP} = \frac{dI}{dV} V + I = 0 \tag{18}$$

Considering the Eq. (18) as a fitness function (J), the objective is to minimize J , which is defined as per Eq. (19).

$$J = \left(\frac{dP}{dI} \right)_{MPP} = \left| \frac{dI_M}{dV_M} V + \frac{I_M}{V_M} \right| = 0 \tag{19}$$

The term $\frac{dI_M}{dV_M}$ in Eq. (19) can be evaluated as follows. From the Eq. (13),

$$I_M = I_{PV} - I_o \left(e^{\frac{V_M + I_M R_S}{aV_t}} - 1 \right) - \frac{V_M + I_M R_S}{R_p} \quad (20)$$

Upon derivating the Eq. (20) w.r.t V_M , we get

$$\frac{dI_M}{dV_M} = \frac{-\frac{I_o}{aV_t} e^{\frac{V_M + I_M R_S}{aV_t}} - \frac{1}{R_p}}{\frac{I_o}{aV_t} R_s e^{\frac{V_M + I_M R_S}{aV_t}} - \frac{R_s}{R_p}} \quad (21)$$

From the Eq. (21), fitness function can be evaluated such that, objective function value must be minimum. This can be achieved by applying stochastic algorithms as discusses above. To analyze the performance of the proposed algorithm, Root Mean Square Error (RMSE), an index, which is defined in Eq. (22) has been utilized, which depends on experimental current (I_{exp}) and the current obtained using optimization technique, denoted as (I_{meas}) at a given voltage. Minimum the value of RMSE, the closure is the measured value of the current to the experimental value.

$$RMSE = \sqrt{\frac{\sum_{i=1}^N (I_{exp,i} - I_{meas,i})^2}{N}} \quad (22)$$

4 Particle Swarm Optimization

The Particle Swarm Optimization (PSO) algorithm [26, 27] is a multi-agent parallel search technique. In this optimization technique, a swarm of particles are generated in the search space randomly and each particle represents a potential solution in the swarm. These particles move in a multi-dimensional search space, such that the particles adjust their position to find the global best solution, based on their own experience and that of their neighbors.

In this optimization technique, each individual solution $i = (1, 2, 3, \dots, n)$, $n > 1$ is called as particle. Each particle will have a current position in search space X_i . These particles will move to evaluate the global best solution with a current velocity V_i . Each particle throughout its journey will have a best solution, identified as personal best, $P_{best,i}$. This personal best $P_{best,i}$ can be treated as a minimum objective function value or maximum objective function value in the search space by this particle 'i' alone, for minimization function or for maximization function respectively. A swarm of such particles $i = (1, 2, 3, \dots, n)$, $n > 1$, will have each individual best positions and the particle having lowest objective function value or

highest objective function value can be treated as Global best solution for minimization function or for maximization function respectively, which is denoted as G_{best} .

During the iterative process of the optimization technique, the personal best $P_{best,i}$ and the Global best G_{best} values are updated. The mathematical representation of evaluating the personal best position of a particle ‘i’ for the next iteration (t + 1) is defined as per Eq. (23) for objective function of minimization type.

$$\begin{cases} P_{best,i}^{t+1} = P_{best,i}^t & \text{if } f(x_i^{t+1}) > P_{best,i}^t \\ x_i^{t+1} & \text{if } f(x_i^{t+1}) \leq P_{best,i}^t \end{cases} \quad (23)$$

where f is the objective function.

Similarly, the Global best position of the solution set for the next iteration is evaluated as per Eq. (24), which is defined as follows.

$$G_{best} = \min(P_{best,i}^{t+1}) \quad (24)$$

where $i \in [1,2,\dots,n]$ and $n > 1$.

From the above, it is important to understand that the personal best $P_{best,i}$ is the best position so far achieved by the particle i’, during its journey, on the other hand, global best position G_{best} is the best position of any particle is the entire swarm during their journey. The velocity and position of particle are updated as per Eqs. (25) and (26) respectively, which are defined as follows.

$$V_{ij}^{t+1} = \omega V_{ij}^t + c_1 r_{1j}^t [P_{best,i}^t - X_{ij}^t] + c_2 r_{2j}^t [G_{best} - X_{ij}^t] \quad (25)$$

$$X_{ij}^{t+1} = X_{ij}^t + V_{ij}^{t+1} \quad (26)$$

4.1 PSO Algorithm Parameters

It is a well-known fact that for any optimization technique, there will be a few algorithm-specific parameters that affect the performance of the algorithm in terms of finding the global best solution, convergence speed etc. Among all the algorithm-specific parameters, some of the parameters have a significant impact and the other parameters have a very small impact on its performance. The algorithm-specific parameters for PSO algorithm that are noticeable are population size/swarm size, maximum number of iterations, velocity and acceleration coefficients, inertia weight etc.

4.1.1 Swarm Size

The number of particles in the swarm is called as population size or swarm size. However, each particle represents a solution to the objective function. With the consideration of larger swarm size, the particles cover the larger part of the search space for identifying the global solution. Thus, the number of iterations required for identifying global solution shall be reduced with the higher number of swarm size. However, computational complexity per iteration and time to complete an iteration will be more by the consideration of huge swarm size. In view of this, in the literature based on a number of empirical studies, it is recommended to consider a swarm size of $n \in [20, 80]$.

4.1.2 Iteration Numbers

Based on the nature of the objective function/problem, the number of iterations may vary to identify the global solution. Lower the number of iterations, the optimization technique may be struck at a local minima/premature convergence. On contrary, a too large number of iterations makes lead to unnecessary computational complexity to the system and it requires more time.

4.1.3 Velocity Components

Updation of the velocity of the particle is an important step in the PSO Algorithm. It is evident from the Eq. (24), the updation equation has three different contributions to the particle movement.

- (a) The term ω is called inertia weight. The contribution of ωV_{ij}^t term in the velocity updating Eq. (25) is that it decides the current flight direction of a particle, based on the memory of the previous flight direction. If $\omega = 1$, then the current particle velocity is fully influenced by the previous velocity. On the other hand, if $0 < \omega < 1$, then the particle velocity is less influenced by the velocity of the previous flight, thus provide change for exploring more search area.
- (b) The second term in the Eq. (25) is $c_1 r_{1j}^t [P_{best,i}^t - X_{ij}^t]$, which is called the cognitive component. The basic idea behind this term is that as the particle X_{ij}^t move away from its P_{best} position, the difference term indicated in braces increases and thus the particle is attracted towards its own best position.
- (c) The third and the final term in the Eq. (25) is $c_2 r_{2j}^t [G_{best} - X_{ij}^t]$, which is called social component or social learning rate. The idea behind this term is to share the information of best solution achieved by the swarm so far in their flight, regardless of which particle has reached the best. This component pulls the particles towards the best solution achieved so far by the swarm.

4.1.4 Acceleration Coefficients

The variables C_1 and C_2 are called acceleration coefficients and are positive values. The terms C_1r_1 and C_2r_2 represents the stochastic influence of cognitive and social components of the particle's velocity respectively. The random number r_1 and r_2 varying in the region $[0,1]$ randomly. C_1r_1 weighs the importance of particle's own previous experiences whereas C_2r_2 weighs the importance of the global learning of the swarm. In general, the values of C_1 and C_2 are static in nature throughout the iterative process. The values of these coefficients are found empirically. Initializing these values wrongly may lead to divergence of the problem. Based on the literature, the empirical values for these coefficients are found to be $C_1 = C_2 = 2$.

5 Jaya Algorithm

There are different types of population-based algorithms such as Evolutionary Algorithms (EA) and Swarm Intelligence (SI) algorithms. These probabilistic algorithms require tuning of control parameters, some of which are common parameters of all algorithms such as population size, number of iterations etc. and the rest are algorithm-specific parameters such as crossover probability, mutation probability, elitism probability in the Genetic Algorithm (GA), inertia weight, maximum velocity, and cognitive parameters in Particle Swarm Optimization (PSO) algorithm, harmony memory in Harmon Search (HS) algorithm. These parameters play a vital role in finding the global optimum in the search space and improper tuning of these parameters leads to premature convergence.

Considering the stated facts, a novel meta-heuristic algorithm which is *independent of algorithm-specific parameters* rather needs only common control parameters such as population size and the maximum number of iterations i.e., Jaya Algorithm has been considered in this chapter. Jaya Algorithm was proposed by Prof. R. Venkata Rao in 2016 and it is a simple and powerful global optimization algorithm. The Jaya Algorithm procedure is described as follows.

Let 'f' be the objective function to be minimized. Assuming that there are k number of design variables of the objective function f . In this algorithm, in the beginning, generate P_{size} (Population size) number of initial solutions (X) randomly. The random solutions must be within the search space, bounded by the lower and upper limits of the design variables. Now, evaluate the objective function value for all the P_{size} initial solutions. Upon evaluation of objective function value, the three common phases of Jaya Algorithm are to be followed to produce the next generation population.

5.1 Evaluation of the Best Solution Candidate and the Worst Solution Candidate Phase

In each iteration, the candidate solution which provides minimum objective function value and maximum objective function value are treated as the Best solution candidate ($X_{i,best,k}$) and the Worst solution candidate ($X_{i,worst,k}$) among the total population ($X_{i,j,k}$) respectively. Here ‘ i ’ stands for iteration number, varies from zero to the maximum number of iterations/generations, ‘ j ’ indicates the candidate number in the population, which varies from one to population size (P_{size}) and ‘ k ’ points out the design variable, varies from one to the maximum number of design variables of the objective function. On identification of Best solution candidate and Worst solution candidate, the candidates have to be modified as specified in the ‘*Updation Phase*’ which is as follows.

5.2 Updation Phase

On obtaining the Best solution candidate and the Worst candidate solution of the population, each candidate solution will be updated using the Eq. (27).

$$X_{i,j,k}^1 = X_{i,j,k} + r_{i,j,1}(X_{i,best,k} - |X_{i,j,k}|) - r_{i,j,2}(X_{i,worst,k} - |X_{i,j,k}|) \quad (27)$$

where $X_{i,j,k}$ indicate the value of the k th variable for the j th candidate during the i th iteration, $X_{i,best,k}$ and $X_{i,worst,k}$ represents the Best candidate solution and the Worst candidate solution in i th iteration respectively, $r_{i,j,1}$ and $r_{i,j,2}$ represents the two random numbers of the k th variable during i th iteration in the range $[0,1]$ and $X_{i,j,k}^1$ represents corresponding updated candidate.

The term “ $r_{i,j,1}(X_{i,best,k} - |X_{i,j,k}|)$ ” implies that the candidate tendency to move towards the Best candidate solution and the term “ $-r_{i,j,2}(X_{i,worst,k} - |X_{i,j,k}|)$ ” indicates the tendency of the candidate to avoid the worst solution. The updated candidates ($X_{i,j,k}^1$) and the previous candidate ($X_{i,j,k}$) are given as inputs to the ‘*Comparison Phase*’.

5.3 Comparison Phase

Upon completion of Updation phase, compute the fitness values of $X_{i,j,k}$ and the updated candidate $X_{i,j,k}^1$. The fitness value of the candidate solution is evaluated as per Eq. (28),

$$fitness(X) = \frac{1}{1 + objective\ function\ value} \quad (28)$$

If the fitness of the updated candidate $X_{i,j,k}^1$ is better than the fitness of $X_{i,j,k}$, then replace the candidate $X_{i,j,k}$ with $X_{i,j,k}^1$ for the next generation, otherwise retain $X_{i,j,k}$ for the next generation and discard the updated candidate. This comparison has to be performed for all the candidates of the population.

With the above, one iteration of the Jaya algorithm gets completed. All the fittest candidates in the ‘*Comparison phase*’ at the end of the iteration are saved in the memory and these values become the input to the next iteration. Repeat the above process until the convergence criterion is satisfied. Thus, the algorithm tries to get closer to the global optimal.

6 Algorithm for Estimation of Solar PV Parameters

The algorithm for the Solar PV parameters estimation using Jaya Algorithm and Particle Swarm Optimization Algorithms are described in the following sections.

6.1 Algorithm for Estimation of Solar PV Parameters Using Jaya Algorithm

1. Read PV module specifications, i.e., short circuit current (I_{SC}), open circuit voltage (V_{OC}), maximum power point operating current (I_M) and operating voltage (V_M) and current temperature coefficient (K_T).
2. Read irradiance values and temperature values at which parameters to be estimated.
3. Read Jaya algorithm parameters: population size (P_{size}) and maximum number of iterations ($iter_{max}$).
4. Initialize the population randomly for Diode ideality factor (a), Series resistance (R_s) in the search space.
5. Set iteration count ($iter$) = 1.
6. Evaluate the Shunt Resistance (R_p), Diode reverse saturation current (I_0) and Photo current generated by the module (I_{ph}) analytically.
7. Calculate the fitness using Eq. (28).
8. Evaluate the Best fitness candidate and the Worst fitness candidate in the population.
9. Update the candidate using updation phase as indicated in Eq. (27).
10. Go to Comparison phase and based on updated candidate fitness value either replace the candidate or retain the candidate.
11. Increment iteration count ($iter = iter + 1$) and repeat above steps (Step 6–Step 10) until a convergence criterion is met.
12. Evaluate RMSE value using Eq. (22) at different points.
13. Stop the program and print the results.

6.2 Algorithm for Estimation of Solar PV Parameters Using Particle Swarm Optimization

1. Read PV module specifications, i.e., short circuit current (I_{SC}), open circuit voltage (V_{OC}), maximum power point operating current (I_M) and operating voltage (V_M) and current temperature coefficient (K_I).
2. Read irradiance values and temperature values at which parameters to be estimated.
3. Read PSO algorithm parameters: population size (P_{size}), maximum number of iterations ($iter_max$), Boundaries of velocities (V), Inertia weight (w), Cognitive and Social parameters.
4. Initialize the population randomly for Diode ideality factor (a), Series resistance (R_s) in the search space.
5. Set iteration count ($iter$) = 1.
6. Evaluate the Shunt Resistance (R_P), Diode reverse saturation current (I_0) and Photo current generated by the module (I_{ph}) analytically for all the particles.
7. Calculate the fitness using Eq. (28) for all the particles.
8. Identify Personal best ($P_{best,i}^{t+1}$) and the Global best (G_{best}) for the population using Eqs. (23) and (24).
9. Update the particle velocity using Eq. (25).
10. Check for velocity limits.
11. Update the particle using Eq. (26).
12. Check whether the updated particle is violating their limits. If violated, keep within their limits
13. Increment iteration count ($iter = iter + 1$) and repeat above steps (Step 6–Step 12) until a convergence criterion is met.
14. Evaluate RMSE value using Eq. (22) at different points.
15. Stop the program and print the results.

6.3 Flowchart for PV Parameters Estimation

The flowchart for parameters estimation of solar PV module is presented in the Figs. 6 and 7 using Jaya algorithm and PSO algorithm respectively.

7 Results and Analysis

In this section, the results attained for PV parameters using the proposed Jaya Algorithm are demonstrated and are validated by comparison with the well-proven algorithm in the literature named Particle Swarm Optimization (PSO) and the experimental results. The simulation work has been carried out on MATLAB Simulink

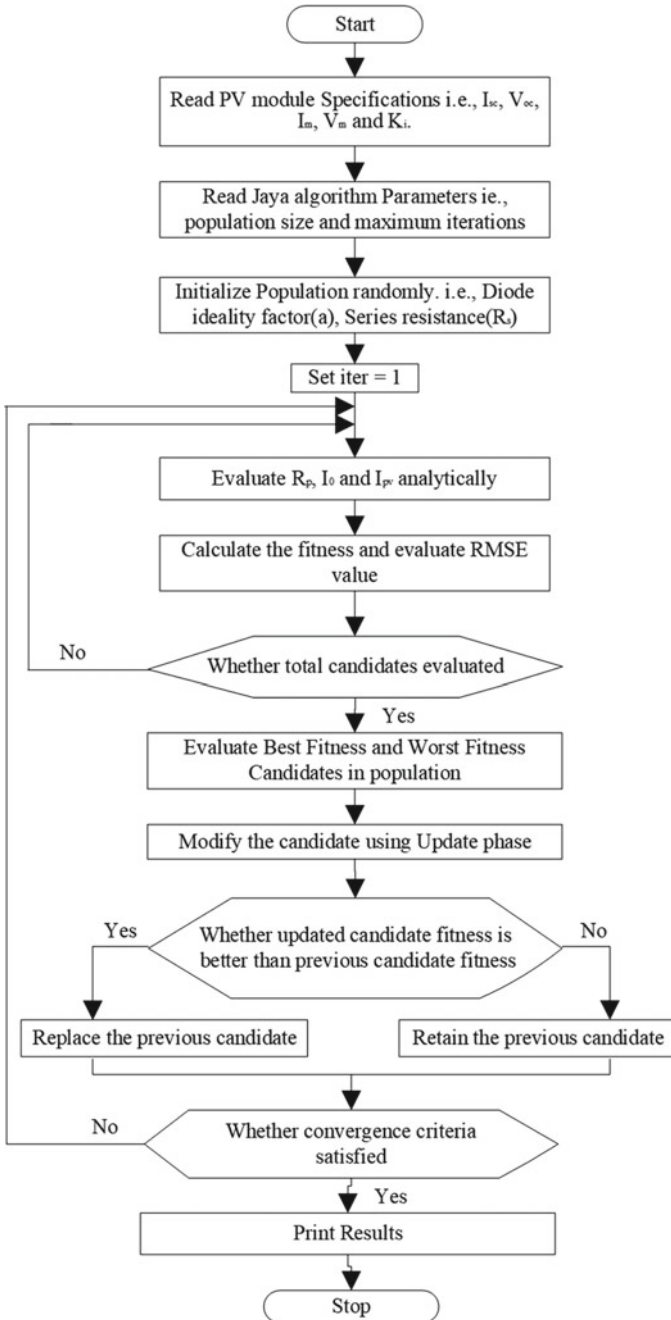


Fig. 6 Flowchart of parameter estimation of solar PV model using Jaya algorithm

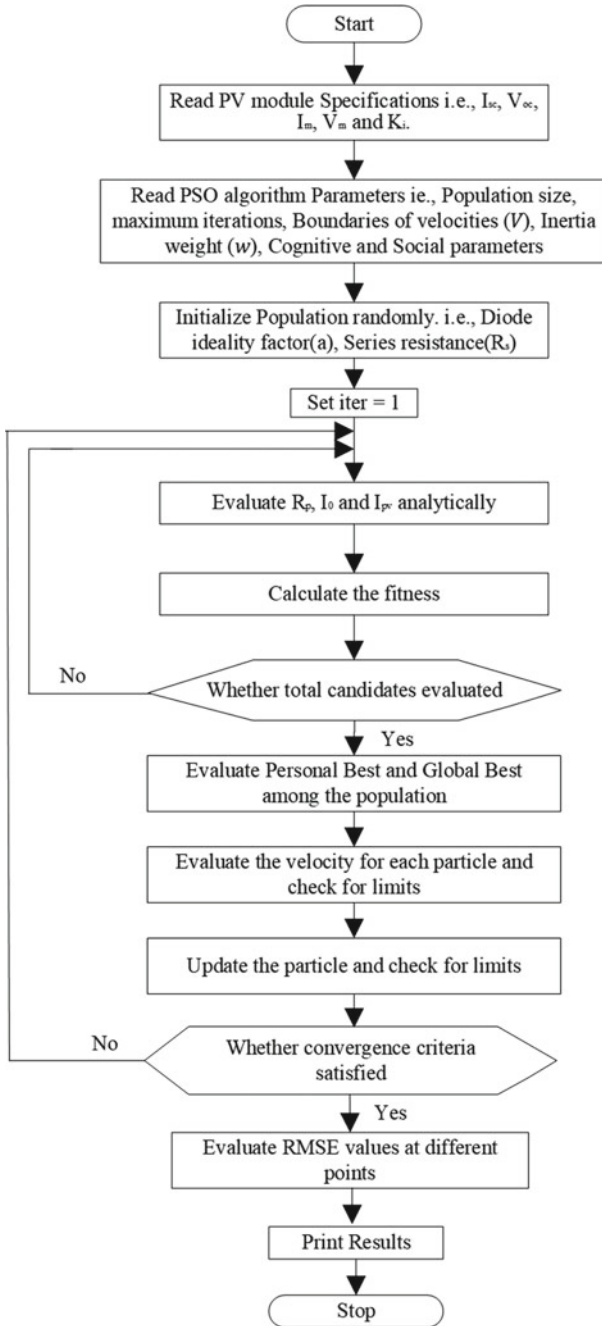


Fig. 7 Flowchart of parameter estimation of solar PV model using PSO algorithm

environment 2017a. The simulation work has been carried out on three different technologies of PV modules namely (1) Poly-crystalline (Shell S75), (2) Mono-crystalline (Shell SM55) and (3) Thin-film (Shell ST36) and the results are demonstrated. The optimization parameters considered in this work are (a) Jaya algorithm: Population size = 80, maximum iterations = 200. (b) PSO algorithm: Population size = 80, maximum iterations = 200, $C_1 = 2$, $C_2 = 2$, inertia weight $w =$ linearly decreases from 0.9 to 0.4.

As deliberated, the parameters provided by the manufacturer's datasheet for a PV module are short circuit current (I_{SC}), open-circuit voltage (V_{OC}), Maximum power point operating current (I_M) and operating voltage (V_M) and current temperature coefficient (K_I). However, for accurate modeling of PV model characteristics at various irradiance (G) and operating temperatures (T), these parameters are inadequate and need to estimate the other parameters of the system, which are Shunt Resistance (R_P), Series resistance (R_S), Diode reverse saturation current (I_0), Photo current generated by the module (I_{ph}) and diode ideality factor (a). These parameters can be obtained using meta-heuristic techniques. However, to reduce the computational complexity of the system, in this chapter, both meta-heuristic technique and analytical method have been attempted to address the problem of parameter estimation.

The PV parameters Diode ideality factor (a), Series resistance (R_S) are generated randomly in the search space within the limits using optimization techniques. From the literature, it is noticed that the series resistance value is very small in comparison to shunt resistance. Thus, the range of initial guess of R_S is taken as $[0, 2]$. The range for diode ideality factor is preferred as $[1, 2]$. Upon initialization of variables, the other parameters R_P , I_0 and I_{ph} are evaluated analytically using the equation described in mathematical modelling Sect. 3. Based on these values, fitness function value has arrived. Several runs of optimization technique have been performed to get the global solution in the search space.

From the simulation results of Poly-crystalline (Shell S75) model, the plots of I-V characteristics and P-V characteristics for constant irradiance of 1000 W/m^2 and varying temperature ($T = 20 \text{ }^\circ\text{C}$, $T = 40 \text{ }^\circ\text{C}$ and $T = 60 \text{ }^\circ\text{C}$) are illustrated in Figs. 8 and 9 respectively. Similarly, Figs. 10 and 11 depict the I-V characteristics and P-V characteristics for constant temperature of $25 \text{ }^\circ\text{C}$ and varying irradiance ($G = 1000$, $G = 800$, $G = 600$, $G = 400$ and $G = 200 \text{ W/m}^2$). From these plots, it is evident that the proposed Jaya Algorithm is exhibiting characteristics very near to the experimental results obtained. Table 1 presents the experimental current values (I_{exp}) and current measured (I_{meas}) by Proposed Jaya Algorithm and PSO Algorithm for different voltage values. From the Table 1, it is clear that the RMSE value obtained by the proposed Jaya Algorithm is 0.0008259, which is much lower than the RMSE value of 0.02784 attained by the PSO Algorithm.

Figures 12 and 13 illustrates the I-V characteristics and P-V characteristics respectively for constant irradiance of 1000 W/m^2 and varying temperature ($T = 20$, $T = 40$ and $T = 60 \text{ }^\circ\text{C}$) of Mono-crystalline (Shell SM55) model. Similarly, Figs. 14 and 15 depict the I-V characteristics and P-V characteristics for constant temperature of $25 \text{ }^\circ\text{C}$ and varying irradiance ($G = 1000$, $G = 800$, $G = 600$, $G = 400$ and $G = 200 \text{ W/m}^2$). Thus, from these plots, it is evident that the proposed algorithm works

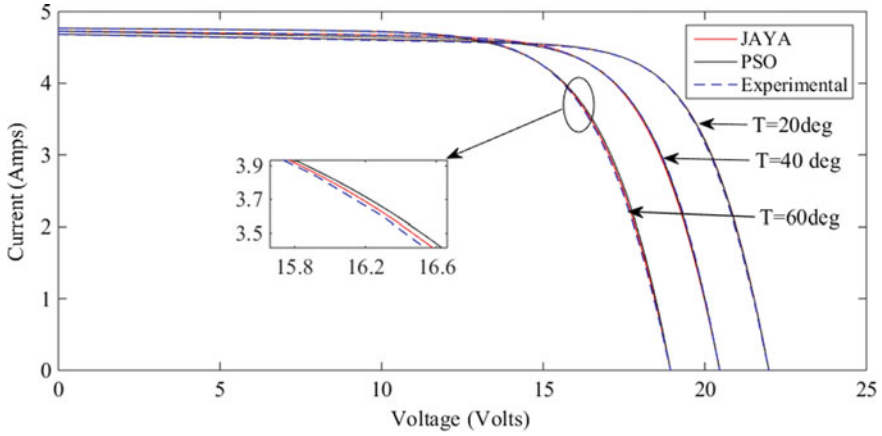


Fig. 8 V-I characteristics at varying temperature and constant irradiance for S75 model

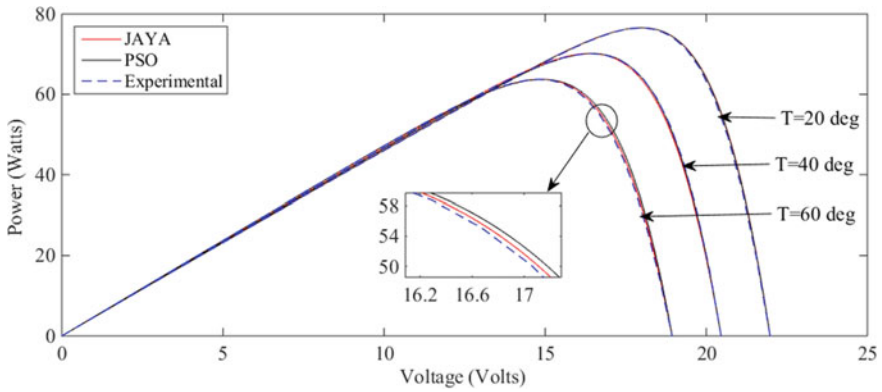


Fig. 9 P-V characteristics at varying temperature and constant irradiance for S75 model

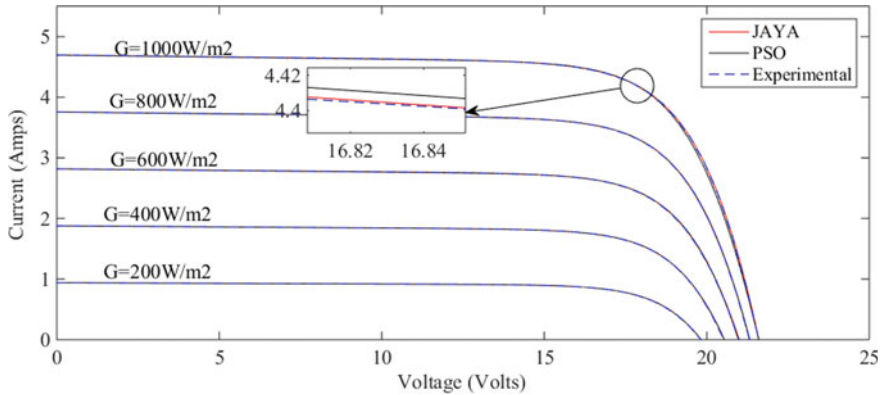


Fig. 10 V-I characteristics at varying irradiance and constant temperature for S75 model

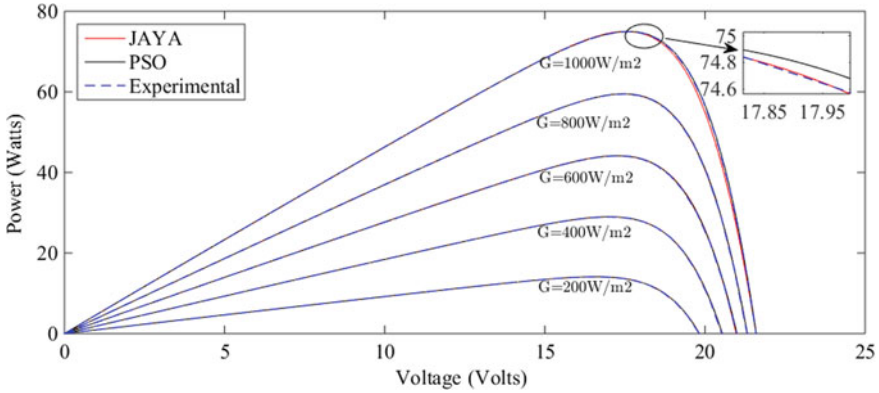


Fig. 11 P-V characteristics at varying Irradiance and constant temperature for S75 model

better for the Mono-crystalline shells. Table 2 presents the I_{exp} and I_{meas} by Proposed Jaya Algorithm and PSO Algorithm for different voltage values. From the Table 2, it is clear that the RMSE value obtained by the proposed Jaya Algorithm is 0.0062505 which is lower than the RMSE value of 0.0070137 attained by the PSO Algorithm by 10.88%.

From the simulation results of Thin-film (Shell ST36) model, the plots of I-V characteristics and P-V characteristics for constant irradiance of 1000 W/m² and varying temperature ($T = 20, T = 40$ and $T = 60$ °C) are illustrated in Figs. 16 and 17 respectively. On the other hand, Figs. 18 and 19 depicts the I-V characteristics and P-V characteristics for constant temperature of 25 °C and varying irradiance ($G = 1000, G = 800, G = 600, G = 400$ and $G = 200$ W/m²). By a close inspection of these characteristics infers that the proposed Jaya algorithm yields most accurate results. Table 3 illustrates the measured current and calculated current values at different voltage levels. It can be noticed that the proposed Jaya Algorithm is producing an RMSE index of 0.003242 lower than that of the PSO Algorithm. Table 4 illustrates the parameter values obtained for different PV technologies S75, SM55 and ST36 using PSO algorithm and the proposed Jaya algorithm at STC. The variation of model parameters under different irradiation and temperature conditions using PSO algorithm and proposed Jaya algorithm for S75, SM55 and ST36 models are presented in Tables 5, 6 and 7 respectively.

It is proclaimed in the literature that the values of R_s and R_p must increase gradually with decreasing irradiance level and the same is observed in our results for various PV modules. Thus, from the above results, it is concluded that the proposed algorithm works more accurately in tracing the experimental results in comparison to the PSO Algorithm.

Table 1 RMSE values of PSO algorithm and the proposed Jaya algorithm for S75 PV module

Measured data		PSO algorithm		Proposed Jaya algorithm	
$V_{PV}(V)$	$I_{PV}(A)$	$I_{CAL}(A)$	ΔI	$I_{CAL}(A)$	ΔI
0	4.696904	4.694773	0.002132	4.69679	0.000114
0.431	4.694183	4.69195	0.002232	4.694039	0.000144
0.864	4.691448	4.689115	0.002333	4.691275	0.000173
1.297	4.688713	4.686279	0.002434	4.688511	0.000202
1.73	4.685978	4.683443	0.002535	4.685746	0.000232
2.163	4.683243	4.680607	0.002636	4.682982	0.000261
2.596	4.680508	4.677772	0.002736	4.680217	0.000291
3.029	4.677772	4.674935	0.002836	4.677452	0.00032
3.462	4.675035	4.672099	0.002936	4.674685	0.000349
3.895	4.672297	4.669262	0.003035	4.671918	0.000379
4.328	4.669558	4.666424	0.003133	4.66915	0.000408
4.761	4.666817	4.663586	0.003231	4.66638	0.000437
5.194	4.664073	4.660746	0.003327	4.663608	0.000466
5.627	4.661327	4.657905	0.003422	4.660832	0.000495
6.06	4.658575	4.655061	0.003514	4.658051	0.000524
6.493	4.655816	4.652213	0.003603	4.655264	0.000552
6.926	4.653049	4.64936	0.003688	4.652468	0.00058
7.359	4.650268	4.6465	0.003768	4.64966	0.000608
7.792	4.64747	4.64363	0.003841	4.646835	0.000636
8.225	4.644649	4.640744	0.003904	4.643986	0.000662
8.658	4.641794	4.637838	0.003955	4.641105	0.000688
9.091	4.638893	4.634902	0.00399	4.63818	0.000713
9.524	4.635929	4.631925	0.004004	4.635192	0.000736
9.957	4.632878	4.628887	0.003991	4.63212	0.000758
10.39	4.629707	4.625764	0.003943	4.62893	0.000777
10.823	4.626371	4.622521	0.00385	4.625578	0.000793
11.256	4.622806	4.619106	0.0037	4.622002	0.000804
11.689	4.618928	4.615448	0.00348	4.618117	0.000811
12.122	4.614616	4.611445	0.003172	4.613805	0.000812
12.555	4.609708	4.606952	0.002757	4.608904	0.000805
12.988	4.603978	4.601764	0.002214	4.60319	0.000788
13.421	4.597115	4.59559	0.001525	4.596355	0.00076
13.854	4.588693	4.588019	0.000674	4.587975	0.000718
14.287	4.578125	4.578469	0.000344	4.577464	0.000661
14.72	4.564605	4.566121	0.001515	4.564019	0.000586

(continued)

Table 1 (continued)

Measured data		PSO algorithm		Proposed Jaya algorithm	
$V_{PV}(V)$	$I_{PV}(A)$	$I_{CAL}(A)$	ΔI	$I_{CAL}(A)$	ΔI
15.153	4.547031	4.549818	0.002787	4.546537	0.000494
15.586	4.523891	4.527943	0.004052	4.523506	0.000384
16.019	4.493127	4.49824	0.005112	4.492866	0.000261
16.452	4.451946	4.457586	0.00564	4.451813	0.000133
16.885	4.396574	4.401707	0.005133	4.39656	0.000014
17.318	4.321957	4.324837	0.00288	4.322029	0.000072
17.751	4.221396	4.21935	0.002046	4.22149	0.000094
18.184	4.086137	4.075442	0.010695	4.086146	0.000009
18.617	3.904952	3.880961	0.023991	3.904724	0.000228
19.05	3.663804	3.621578	0.042227	3.663153	0.000652
19.483	3.34571	3.281448	0.064262	3.344454	0.001256
19.916	2.930979	2.844461	0.086518	2.929025	0.001954
20.349	2.398001	2.295944	0.102057	2.395479	0.002522
20.782	1.724644	1.624425	0.100219	1.7221	0.002544
21.215	0.89017	0.822952	0.067218	0.888777	0.001393
21.599	0.001315	0.001781	0.000465	0.002575	0.00126
RMSE		0.02784		0.0008259	

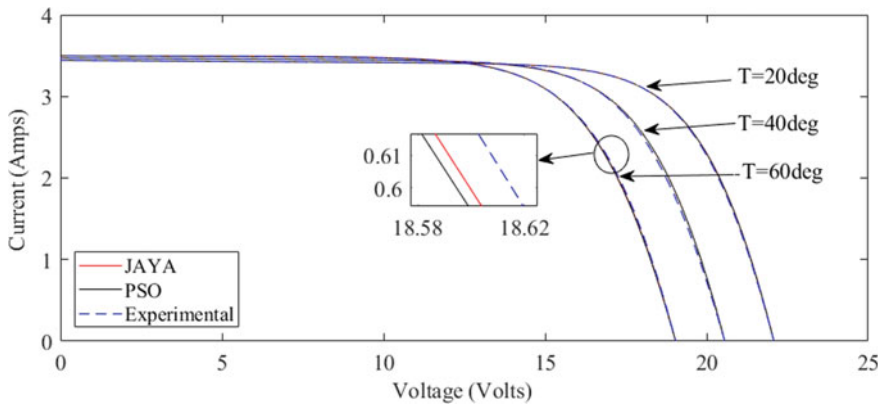


Fig. 12 V-I characteristics at varying temperature and constant irradiance for SM55 model

8 Conclusion

In this chapter, accurate modeling of the PV parameters using the single diode model has been analyzed. Out of the five parameters, Shunt Resistance (R_p), Diode reverse

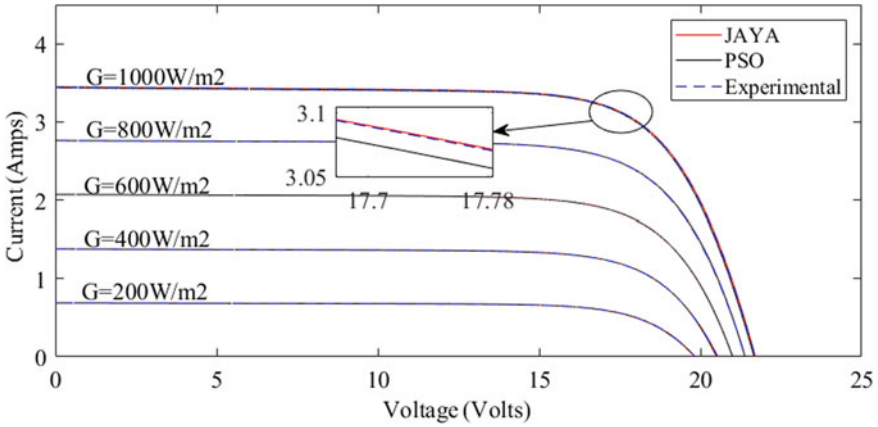


Fig. 13 P-V characteristics at varying temperature and constant irradiance for SM55 model

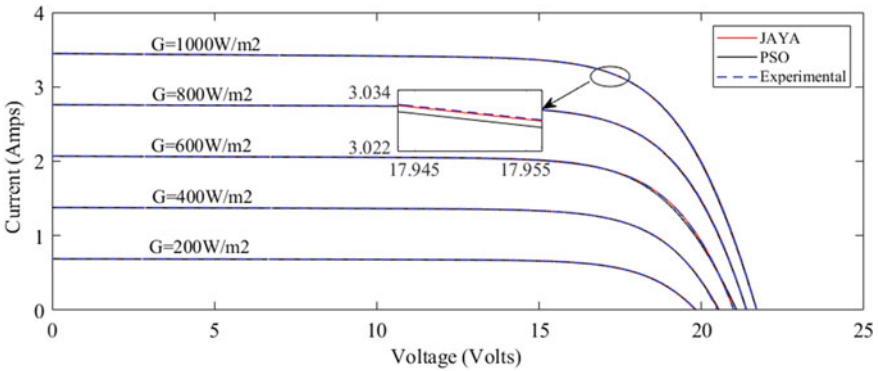


Fig. 14 V-I characteristics at varying irradiance and constant temperature for SM55 model

saturation current (I_0) and Photocurrent generated by the module (I_{ph}) are analytically computed whereas the other parameters Diode ideality factor (a), Series resistance (R_s) are optimized using different meta-heuristic techniques. To validate the results of the proposed methodology, three different types of PV modules, i.e., Poly-crystalline (Shell S75), Mono-crystalline (Shell SM55) and Thin-film (Shell ST36) are considered. From the results, it is noticed that the proposed Jaya algorithm is accurately matching the experimental data at varying irradiance condition keeping temperature constant and varying temperature condition maintaining irradiance constant. Further, an index RMSE value of the proposed algorithm is found to be lower than that of PSO method. Thus, it is envisaged that the proposed method is useful tool for accurate modeling of PV parameters.

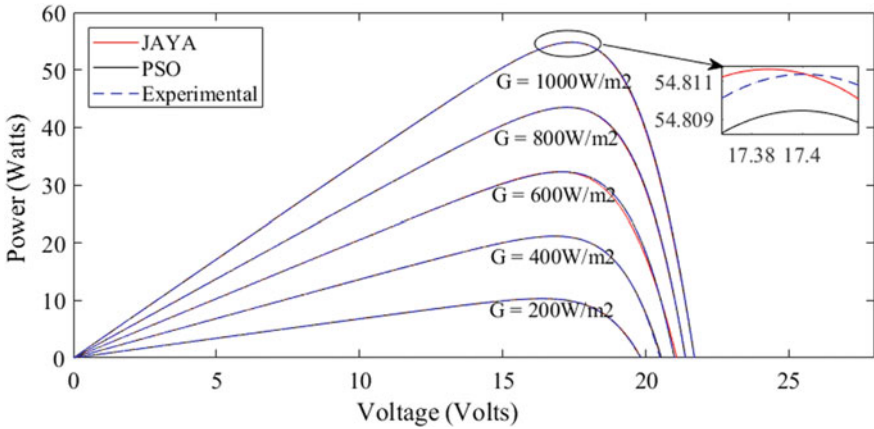


Fig. 15 P-V characteristics at varying Irradiance and constant temperature for SM55 model

Table 2 RMSE values of PSO algorithm and the proposed Jaya algorithm for SM55 PV module

Measured data		PSO algorithm		Proposed Jaya algorithm	
$V_{PV}(V)$	$I_{PV}(A)$	$I_{CAL}(A)$	ΔI	$I_{CAL}(A)$	ΔI
0.177	3.446021	3.446329	0.000308	3.446299	0.000278
0.91	3.443657	3.444013	0.000357	3.443973	0.000317
2.091	3.439847	3.440282	0.000435	3.440226	0.000379
3.391	3.435653	3.436173	0.00052	3.436099	0.000447
4.832	3.430997	3.431611	0.000614	3.431518	0.000521
5.777	3.427936	3.42861	0.000674	3.428504	0.000568
6.203	3.426552	3.427252	0.0007	3.427141	0.000589
7.266	3.423076	3.423839	0.000763	3.423714	0.000638
8.093	3.420332	3.421137	0.000806	3.421002	0.000671
9.298	3.416188	3.41704	0.000851	3.416891	0.000703
10.34	3.412292	3.413153	0.000861	3.412995	0.000703
11.73	3.405898	3.406683	0.000784	3.40652	0.000622
12.51	3.400939	3.401604	0.000665	3.401445	0.000506
13.08	3.396081	3.396607	0.000526	3.396454	0.000373
14.31	3.378468	3.378511	0.000043	3.378388	0.00008
15.11	3.356667	3.356277	0.00039	3.356185	0.000482
16.21	3.297256	3.296392	0.000864	3.296337	0.000919
16.95	3.220708	3.220067	0.000641	3.22	0.000708

(continued)

Table 2 (continued)

Measured data		PSO algorithm		Proposed Jaya algorithm	
$V_{PV}(V)$	$I_{PV}(A)$	$I_{CAL}(A)$	ΔI	$I_{CAL}(A)$	ΔI
17.56	3.119123	3.11948	0.000358	3.119344	0.000221
18.16	2.968063	2.970556	0.002493	2.970262	0.002199
18.62	2.805351	2.810413	0.005062	2.80992	0.004569
18.96	2.652341	2.659772	0.007431	2.659086	0.006745
19.29	2.472833	2.48279	0.009957	2.481888	0.009055
19.64	2.245118	2.257716	0.012598	2.256568	0.01145
19.97	1.992057	2.00673	0.014674	2.005359	0.013302
20.27	1.727708	1.743533	0.015826	1.74199	0.014282
20.55	1.450478	1.466402	0.015924	1.464749	0.014271
20.82	1.154836	1.169661	0.014825	1.167968	0.013133
21.11	0.806348	0.818377	0.012029	0.816738	0.01039
21.34	0.507462	0.515893	0.00843	0.514382	0.006919
21.54	0.231722	0.235923	0.004202	0.234593	0.002871
RMSE		0.0070137		0.0062505	

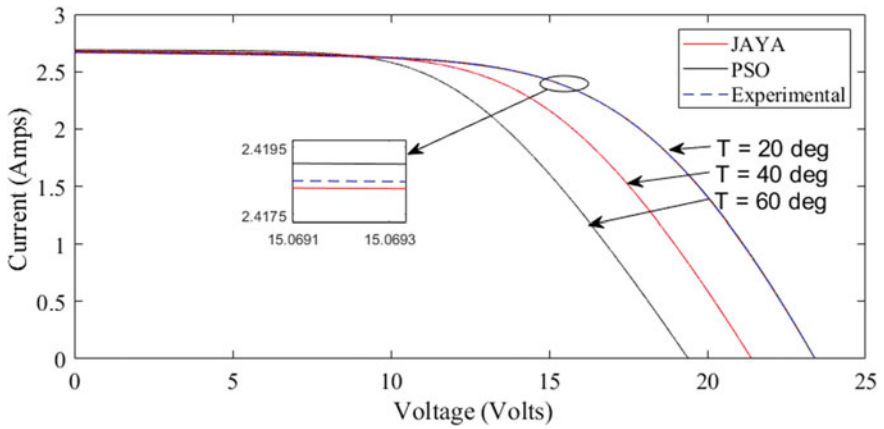


Fig. 16 V-I characteristics at varying temperature and constant irradiance for ST36 model

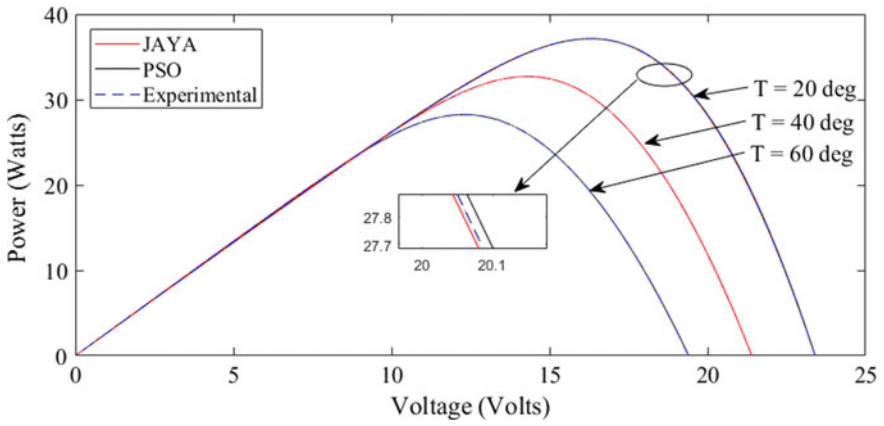


Fig. 17 P-V characteristics at varying temperature and constant irradiance for ST36 model

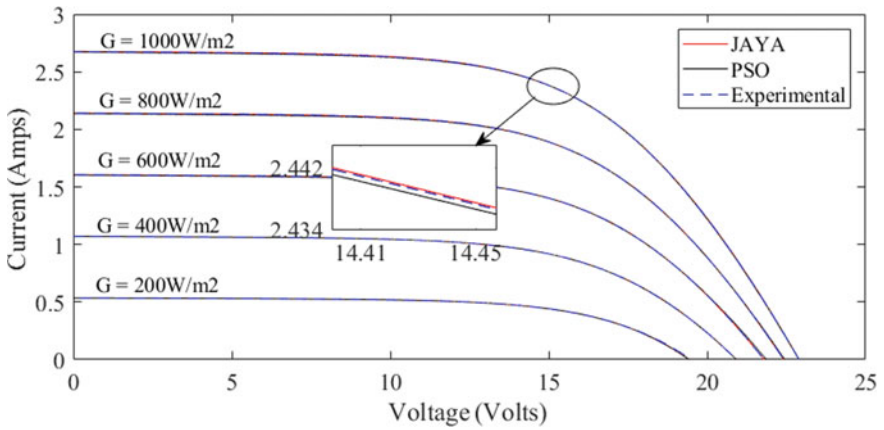


Fig. 18 V-I characteristics at varying irradiance and constant temperature for ST36 model

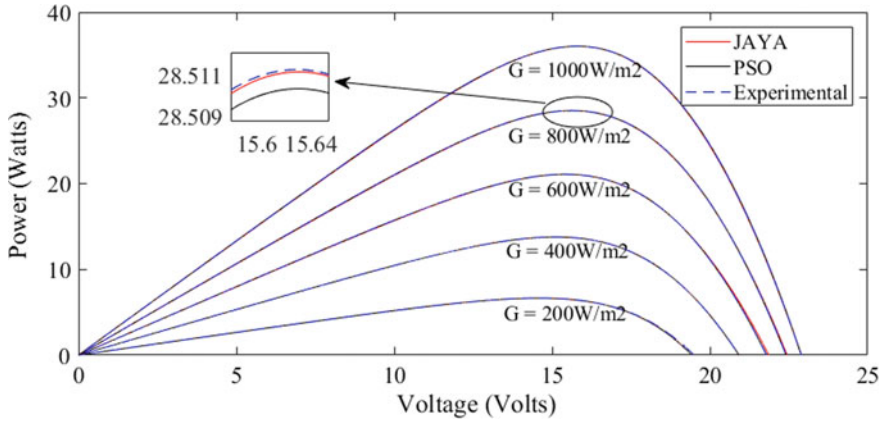


Fig. 19 P-V characteristics at varying irradiance and constant temperature for ST36 model

Table 3 RMSE values of PSO algorithm and the proposed Jaya algorithm for ST36 PV module

Measured data		PSO algorithm		Proposed Jaya algorithm	
$V_{PV}(V)$	$I_{PV}(A)$	$I_{CAL}(A)$	ΔI	$I_{CAL}(A)$	ΔI
0.106	2.671883	2.674943	0.003061	2.674039	0.002157
0.957	2.669945	2.673643	0.003699	2.672547	0.002602
2.091	2.667272	2.671794	0.004522	2.670448	0.003176
3.579	2.663484	2.669012	0.005528	2.667364	0.003388
4.714	2.660199	2.666404	0.006205	2.664553	0.004355
6.368	2.654177	2.661133	0.006956	2.659061	0.004883
7.480	2.648583	2.655801	0.007218	2.653654	0.005071
8.823	2.638642	2.645786	0.007144	2.643667	0.005025
10.45	2.617586	2.623852	0.006265	2.622005	0.004419
11.45	2.595709	2.600928	0.005219	2.5994	0.003691
12.57	2.557374	2.561014	0.00364	2.559963	0.002589
13.80	2.488798	2.490518	0.00172	2.490049	0.00125
15.03	2.378127	2.378395	0.000268	2.378376	0.00025
16.18	2.221675	2.221705	0.00003	2.22179	0.000115
17.15	2.040681	2.041566	0.000885	2.041436	0.000755
17.81	1.889276	1.89118	0.001904	1.890778	0.001501
18.47	1.714362	1.71744	0.003078	1.71672	0.002358
19.03	1.547697	1.551729	0.004031	1.55075	0.003053

(continued)

Table 3 (continued)

Measured data		PSO algorithm		Proposed Jaya algorithm	
$V_{PV}(V)$	$I_{PV}(A)$	$I_{CAL}(A)$	ΔI	$I_{CAL}(A)$	ΔI
19.59	1.364802	1.369596	0.004794	1.368415	0.003612
20.20	1.147986	1.15324	0.005254	1.151947	0.00396
20.64	0.980844	0.986111	0.005267	0.984831	0.003987
21.15	0.776545	0.781431	0.004886	0.780283	0.003738
21.54	0.613116	0.617394	0.004278	0.616442	0.003326
21.87	0.470239	0.473775	0.003536	0.473057	0.002818
22.22	0.314347	0.316861	0.002514	0.316461	0.002114
22.55	0.163465	0.164788	0.001323	0.164757	0.001293
RMSE		0.0044638		0.003242	

Table 4 Variation of model parameter values obtained using PSO and proposed Jaya Algorithm at STC conditions for various PV models

Parameters	S75		SM55		ST36	
	PSO algorithm	Proposed Jaya algorithm	PSO algorithm	Proposed Jaya algorithm	PSO algorithm	Proposed Jaya algorithm
At STC ($G = 1000 \text{ W/m}^2$, $T = 25 \text{ }^\circ\text{C}$)						
I_{PV}	4.700	4.700	3.450	3.450	2.680	2.680
I_0	4.62E-07	1.13E-07	1.67E-07	1.14E-07	4.89E-05	5.69E-05
a	1.451	1.334	1.395	1.356	1.948	1.975
R_s	0.107	0.170	0.286	0.306	1.302	1.286
R_p	156.57	152.54	316.31	314.62	624.94	736.89

Table 5 Variation of model parameter values obtained using PSO and proposed Jaya algorithm under different irradiation and temperature conditions for S75 model

		PSO algorithm					Proposed Jaya algorithm				
		I_{PV}	I_0	a	R_s	R_P	I_{PV}	I_0	a	R_s	R_P
Constant T (= 25 °C) varying G (W/m ²)	G	Varying irradiance									
	1000	4.700	4.62E-07	1.451	0.107	156.57	4.700	1.13E-07	1.334	0.170	152.54
	800	3.760	1.47E-07	1.355	0.142	165.99	3.760	1.25E-07	1.342	0.150	164.28
	600	2.820	4.93E-08	1.274	0.191	196.10	2.820	9.42E-08	1.321	0.150	207.23
	400	1.880	3.46E-08	1.250	0.200	280.00	1.880	3.46E-08	1.250	0.197	277.54
	200	0.940	1.43E-08	1.194	0.200	500.00	0.940	1.42E-08	1.194	0.200	498.63
Constant G varying T (°C)	T	Varying temperature									
	20	4.690	5.97E-08	1.333	0.157	131.75	4.690	7.42E-08	1.349	0.150	134.13
	40	4.730	6.53E-07	1.337	0.146	133.23	4.730	1.19E-06	1.388	0.150	200.32
	60	4.770	1.95E-05	1.479	0.100	300.00	4.770	8.82E-06	1.390	0.150	302.30

Table 6 Variation of model parameter values obtained using PSO and proposed Jaya algorithm under different irradiation for SM55 model

		PSO algorithm					Proposed Jaya algorithm				
		I_{PV}	I_0	a	R_s	R_p	I_{PV}	I_0	a	R_s	R_p
G		Varying irradiance									
Constant T (= 25 °C) varying G (W/m ²)	1000	3.450	1.67E-07	1.395	0.286	316.31	3.45	1.14E-07	1.356	0.306	314.62
	800	2.760	8.22E-07	1.541	0.194	628.37	2.760	7.94E-07	1.537	0.196	621.62
	600	2.070	4.60E-07	1.484	0.201	653.26	2.070	4.70E-07	1.486	0.198	657.38
	400	1.380	2.13E-07	1.416	0.203	769.90	1.380	1.18E-07	1.367	0.304	690.77
	200	0.690	2.36E-08	1.250	0.500	1000.00	0.690	2.82E-08	1.262	0.479	1089.70
T		Varying temperature									
Constant G (= 1000 W/m ²) varying T (°C)	20	3.443	3.31E-07	1.505	0.232	418.24	3.443	3.45E-07	1.509	0.230	423.35
	40	3.471	1.54E-06	1.449	0.252	486.15	3.471	1.57E-06	1.451	0.251	490.75
	60	3.499	5.10E-06	1.372	0.292	650.00	3.499	7.06E-06	1.406	0.276	986.08

Table 7 Variation of model parameter values obtained using PSO and proposed Jaya algorithm under different irradiation for ST36 model

		PSO algorithm					Proposed Jaya algorithm				
		I_{PV}	I_0	a	R_s	R_P	I_{PV}	I_0	a	R_s	R_P
G		Varying irradiance									
Constant T (= 25 °C) varying G (W/m ²)	1000	2.680	4.89E-05	1.948	1.302	624.94	2.680	5.69E-05	1.975	1.286	736.89
	800	2.144	6.42E-05	1.998	1.407	841.91	2.144	6.49E-05	2.000	1.404	841.74
	600	1.608	6.47E-05	1.998	1.552	851.71	1.608	6.47E-05	1.999	1.552	851.64
	400	1.072	6.43E-05	1.989	1.650	934.21	1.072	6.39E-05	1.999	1.653	932.68
	200	0.536	5.03E-05	1.957	1.308	1161.40	0.536	6.37E-05	1.999	0.984	1228.10
T		Varying temperature									
Constant G (= 1000 W/m ²) varying T (°C)	20	2.678	2.90E-05	1.934	1.292	337.72	2.678	4.23E-05	2.000	1.253	411.10
	40	2.685	1.04E-05	1.518	1.621	606.34	2.685	8.38E-06	1.492	1.637	512.17
	60	2.691	7.98E-07	1.071	1.999	1425.70	2.691	8.14E-07	1.073	1.999	1479.90

References

1. Solar Schools, Types of Energy (2019). <https://www.solarschools.net/knowledge-bank/energy/types>
2. Kothari DP, Nagrath IJ (2008) Power systems engineering. 2nd edn. TMC
3. Mohan N (2012) Elelectric power systems: a first course. Wiley
4. Niu S, Jia Y, Wang W, He R, Hu L, Liu Y (2013) Electricity consumption and human development level: a comparative analysis based on panel data for 50 countries. *Int J Electr Power Energy Syst* 53:338–347. <https://doi.org/10.1016/j.ijepes.2013.05.024>
5. Assadzadeh A, Nategh H (2015) The relationship between per capita electricity consumption and human development indices. In: 6th IASTEM international conference, Berlin, Germany, 2015, November, pp 51–57. https://www.worldresearchlibrary.org/up_proc/pdf/117-144870270051-57.pdf
6. Ministry of New and Renewable Energy. <https://mnre.gov.in/>
7. Press Information Bureau Government of India Ministry of Power. <https://pib.gov.in/Pressreleaseshare.aspx?PRID=1592833>
8. Access to Electricity (% of Population). World Bank Open Data. <http://data.worldbank.org/indicator/EG.ELC.ACCS.ZS>
9. Chowdhury AH, Asaduz-Zaman M (2015) Load frequency control of multi-microgrid using energy storage system. In: 8th international conference on electrical computer engineering advanced technology a better tomorrow, ICECE 2014, pp 548–551. <https://doi.org/10.1109/ICECE.2014.7026975>
10. Srinivasarathnam C, Yammani C, Maheswarapu S (2019) Frequency control of autonomous hybrid multi-microgrid system. In: National power electronics conference, NPEC 2019, pp 1–6. <https://doi.org/10.1109/NPEC47332.2019.9034751>
11. Rajasekar RV, Neeraja Krishna Kumar N (2013) Bacterial foraging algorithm based solar PV parameter estimation. *Sol Energy* 97:255–265. <https://doi.org/10.1016/j.solener.2013.08.019>
12. Jacobus H, Lin B, Jimmy DH, Ansumana R, Malanoski AP, Stenger D (2011) Evaluating the impact of adding energy storage on the performance of a hybrid power system. *Energy Convers Manage* 52(7):2604–2610. <https://doi.org/10.1016/j.enconman.2011.01.015>
13. Bernal-Agustín JL, Dufo-López R, Rivas-Ascaso DM (2006) Design of isolated hybrid systems minimizing costs and pollutant emissions. *Renew Energy* 31(14):2227–2244. <https://doi.org/10.1016/j.renene.2005.11.002>
14. Humada AM, Darweesh SY, Mohammed KG, Kamil M, Mohammed SF, Kasim NK, Tahseen TA, Mekhilef S (2020) Modeling of PV system and parameter extraction based on experimental data: review and investigation. *Sol Energy* 199:742–760. <https://doi.org/10.1016/j.solener.2020.02.068>
15. Alam MBEDF, Yousri DA (2015) Flower pollination algorithm based solar PV parameter estimation. *Energy Convers Manage* 101:410–422. <https://doi.org/10.1016/j.enconman.2015.05.074>
16. Et-torabi K, Nassar-eddine I, Obbadi A, Errami Y, Rmailly R, Sahnoun S, El fajri A, Agunaou M (2017) Parameters estimation of the single and double diode photovoltaic models using a Gauss–Seidel algorithm and analytical method: a comparative study. *Energy Convers Manage* 148:1041–1054. <https://doi.org/10.1016/j.enconman.2017.06.064>
17. Nassar-eddine MAI, Obbadi A, Errami Y, El fajri A (2016) Parameter estimation of photovoltaic modules using iterative method and the Lambert W function—a comparative study. *Energy Convers Manage* 119:37–48. <https://doi.org/10.1016/j.enconman.2016.04.030>
18. Easwarakhanthan T, Bottin J, Bouhouch I, Boutrit C (2007) Nonlinear minimization algorithm for determining the solar cell parameters with microcomputers. *Int J Sol Energy* 4(1):1–12. <https://doi.org/10.1080/01425918608909835>
19. Ismail MS, Moghavvemi M, Mahlia TMI (2013) Characterization of PV panel and global optimization of its model parameters using genetic algorithm. *Energy Convers Manage* 73:10–25. <https://doi.org/10.1016/j.enconman.2013.03.033>

20. Russell Eberhart JK (1999) A new optimizer using particle swarm theory. In: Sixth international symposium on micro machine and human science, 1999, pp 39–43. <https://doi.org/10.1109/MHS.1995.494215>
21. Rezaee Jordehi A (2018) Enhanced leader particle swarm optimisation (ELPSO): an efficient algorithm for parameter estimation of photovoltaic (PV) cells and modules. *Sol Energy* 159:78–87. <https://doi.org/10.1016/j.solener.2017.10.063>
22. Rao RV, Savsani VJ, Vakharia DP (2011) Teaching–learning–based optimization: a novel method for constrained mechanical design optimization problems. *Comput Des* 43:303–315. <https://doi.org/10.1016/j.cad.2010.12.015>
23. Venkata Rao R (2016) Jaya: a simple and new optimization algorithm for solving constrained and unconstrained optimization problems. *Int J Ind Eng Comput* 7:19–34. <https://doi.org/10.5267/j.ijiec.2015.8.004>
24. Hasanien HM (2015) Shuffled frog leaping algorithm for photovoltaic model identification 6(2):509–515. <https://doi.org/10.1109/TSTE.2015.2389858>
25. Jack V, Salam Z (2015) An improved method to estimate the parameters of the single diode model of photovoltaic module using differential evolution. In: 4th international conference on electric power and energy conversion systems (EPECS), Sharjah, pp 1–6. <https://doi.org/10.1109/EPECS.2015.7368514>
26. Reddy SS, Rathnam CS (2016) Optimal power flow using glowworm swarm optimization. *Int J Electr Power Energy Syst* 80:128–139. <https://doi.org/10.1016/j.ijepes.2016.01.036>
27. Eberhart R, Kennedy J (1995) A new optimizer using particle swarm theory. In: Sixth international symposium on micro machine and human science, pp 39–43. <https://doi.org/10.1109/MHS.1995.494215>

Integration of Photovoltaic Distributed Generation into Grid



Neelakanteshwar Rao Battu, Perka Krishna, and Venu Yarlagadda

Abstract Present trend of electricity generation is from clean and green renewable energy sources; one of the prominent sources being photovoltaics (solar energy). The objective of the work presented here includes extraction of maximum power from the photovoltaic solar plant at various working conditions using maximum power point tracking algorithm. The output produced from the solar plant is a low magnitude d.c output, which is required to be boosted. The solar output is fed to a boost converter to enhance its magnitude. The enhanced d.c output is fed to a 3- ϕ , five-level voltage source inverter to convert d.c voltage to a.c equivalent of it. Conversion process through the inverter introduces harmonics into the system. Shunt active filter is designed in this work to minimize the harmonics injected due to inverter operation. Two cases are studied for the application of proposed methodology; stand alone operation of the designed photo-voltaic solar system and photovoltaics integrated to the grid. The above cases are implemented and analyzed using MATLAB software. Fast Fourier analysis is used to determine the total harmonic distortion for both the cases. The results show considerable improvement in quality of power produced due to mitigation of harmonics.

Keywords Solar PV · Irradiance · Distributed generation · Shunt active power filter · Fast Fourier analysis · Total harmonic distortion · Boost converter · Maximum power point tracking · Perturb and observe

Nomenclature

PV Photovoltaic
MPPT Maximum Power Point Tracking

N. R. Battu (✉) · P. Krishna · V. Yarlagadda
Department of Electrical and Electronics Engineering, VNR VJIET, Hyderabad, Telangana, India
e-mail: neelakanteshwarrao_b@vnrvjiet.in

V. Yarlagadda
e-mail: venu_y@vnrvjiet.in

© The Author(s), under exclusive license to Springer Nature Singapore Pte Ltd. 2022
S. R. Salkuti and P. Ray (eds.), *Next Generation Smart Grids: Modeling, Control and Optimization*, Lecture Notes in Electrical Engineering 824,
https://doi.org/10.1007/978-981-16-7794-6_10

257

PO	Perturb and Observe
VSI	Voltage Source Inverter
FFA	Fast Fourier analysis
THD	Total Harmonic Distortion
PCC	Point of common coupling
APF	Active power filter
SAPF	Shunt active power filter
PWM	Pulse width modulation
SPWM	Sinusoidal pulse width modulation
SMPS	Switched-mode power supply
V	Supply voltage
V_{out}	Output voltage
N_s	Number of turns on primary side of the transformer
N_p	Number of turns on secondary side of the transformer
I_L	Photo generated current
I_D	Diode current
I_{sh}	Shunt current
I	Output current
V_{sh}	Voltage across the shunt resistor and diode
I_0	Reverse bias saturation current
V_D	Voltage across diode
V_T	Terminal voltage
n	Ideality or quality factor

1 Introduction

Modern Power Systems are facing with everlasting power demand. To meet this increasing power demand, various means of power generation is required. The generation of power from fossil fuels leads to hazardous gases. In contrast, renewable power generation is quite useful in reducing these effects [1]. Solar plants find to be one of the promising means of generating renewable power [2]. Solar panels used in respective plants consist of solar cells. Solar cell converts the beam radiation into d.c supply. Boost converters are used in solar power plants to increase the d.c output. The d.c output provided by converter is fed to an inverter of suitable rating to convert d.c supply to a.c supply. The output voltage waveform of the inverter is not a pure sine wave. It contains harmonics which are injected by the converters. The total harmonic distortion (THD) is usually not in the acceptable limits and it can be minimized by proper design of shunt active Power filter at point of common coupling (PCC) [3].

Li Bin et al., have proposed a digital based approach for 3- \emptyset , 4-wire active power filter (APF) to reduce the harmonics [4]. Nabae et al., have discussed about control strategy used in active power filters using voltage source converters [5]. Ko et al., have discussed the impact of shunt active filters on distortions caused by harmonic

currents [6]. Singh et al., have reviewed various types of active filters and their impact on power quality improvement. [7]. Akagi et al., have discussed the new trends used in active filters for power conditioning [8]. Villalva et al., have discussed modeling of PV arrays [9]. Salmeron et al., have discussed about series and shunt active filters to improve power quality [10]. Vodyakho et al., have proposed three level inverter based shunt active power filter [11]. Viswanth et al., have proposed fuel cell based SAPF to deal with power quality issues [12]. Chandra et al., have reviewed the active filters used in power quality improvement [13].

The power produced by the solar cell/photovoltaic (PV) cell is not constant due to variations in solar radiation [14]. However, maximum power can be extracted from the available solar radiation using Maximum power point tracking (MPPT) technique [15]. Coordinated control of solar and battery management is proposed by Hareesh et al., to achieve power injection and MPPT simultaneously [16]. Amjad et al., have summarized various MPPT techniques which are used in online and offline studies under uniform and non-uniform irradiance conditions [17]. Ali et al., have proposed an MPPT technique using the estimation of climatic parameters [18]. Nishant et al., have proposed an MPPT technique based on normal harmonic search algorithm [19]. Vardan et al., have proposed circle center-line based perturb and observe algorithm for MPPT [20]. Nishant et al., have proposed leaky least logarithmic absolute difference-based control algorithm and learning based incremental conductance MPPT algorithm for PV system integrated with grid [21]. Singh et al., have proposed power normalized kernel least mean fourth algorithm based neural network and learning based hill climbing technique for MPPT [22]. Ikhlaiq et al., have proposed a hybrid Cauchy and Gaussian sine cosine optimization technique for MPPT [23]. Neeraj et al., have proposed an adaptive neuro-fuzzy inference system based particle swarm optimization technique for MPPT [24]. Bijaya et al., have proposed leaky least mean logarithmic fourth based control technique and learning based perturb and observe algorithm for MPPT in grid connected PV system [25]. Though, various techniques are available in literature for tracking or extracting maximum power from the solar radiation, among these approaches Perturb and Observe (PO) algorithm is found to be simpler and advantageous over several others [26–28].

This paper proposes design of converter and inverter for conversion of solar energy into electrical energy. It focuses on the modeling of SAPF to minimize harmonics produced during conversion of electrical energy from solar part of it. Perturb and observe based MPPT algorithm is used to control the inverter output. Fast Fourier series is used to analyze the harmonic distortion in the system. The work presented in this paper demonstrates analysis of solar power plant operating in standalone and grid connected modes.

The remaining part of this chapter is organized as follows: Sect. 2 describes about various types of non-conventional energy sources. Section 3 describes DC-DC converters. Section 4 explains various MPPT algorithms. Section 5 describes about inverters. Section 6 discusses different types of filters. Analysis of simulation results in presented in Sect. 7. Section 8 summarizes the overall work presented in this chapter.

2 Non-conventional Energy Sources

Non conventional sources are freely available in nature and generate electricity with release of less pollution as compared to conventional sources like thermal and nuclear plants. The examples of these sources are solar, wind, tidal, geo thermal and wave power plants.

2.1 Tidal Energy Source

Tidal energy is in the form of hydro power which is used to convert energy collected from tides into electricity and tides are occurred due to gravitational force on the earth. Generating electricity from these sources was first followed by Europe and America in nineteenth century. First tidal plant was established at France in 1960 and capacity of the plant is 240 MW and it is the largest power station in world. In 2011, Sinha tidal station became world's largest station in terms of output and its output is 254 MW.

2.2 Wind Energy Source

Wind energy is freely available in nature and it converts wind energy into electrical supply with help of wind turbines and generators. It generates less pollution as compared to conventional sources. Highest usage of wind power is in Denmark and it is 43.4%.

2.3 Wave Energy Source

Wave energy is in the form of waves on the surface of the water, which is converted into useful electrical supply. First wave was established in U.K in the year 2008.

2.4 Geo Thermal Energy Source

The heat produced in the crust of the earth is used to generate electricity from it in this type of sources. This source is used for industrial and agricultural purpose and usage of this source is increasing gradually.

2.5 Hydro Power

In hydro power plants, potential energy of the water is converted into electrical energy with use of turbines and generators. It is free from environmental pollution. China generates the highest output in the world and the output power generated by it is 22,500 MW. Almost 20% of total electricity generation is from this source. Hydro power plants can be classified into four types: run of river, storage, pumped storage hydro, and hydro kinetic technology.

2.6 Photovoltaic Power

Solar energy, in the form of radiation, is converted into electricity. This type of source is classified into two types; active and passive solar. In active solar type techniques like mirrors and solar heating are used. In passive solar type techniques like surface coatings, fins, micro particles, nano particles are used. Advantages of solar energy sources compared to other type of sources are as follows:

- Solar system directly converts the solar radiation into electrical supply and it doesn't need rotating devices like turbines.
- Maintenance cost is low.
- PV systems do not release sound, air and water pollution into atmosphere.
- Day-by-day its manufacturing design is enhanced to improve the efficiency.
- PV source is clean source of energy.

Disadvantages of solar energy sources are as follows:

- Manufacturing cost is high.
- Solar radiation is not available at latitude and if clouds are present.
- Fluctuation problems occur.
- Requirement of area to collect the supply is large.
- It has less efficiency.

2.7 Types of PV Cells

Based on the type of installation solar cells are classified into the following types: monocrystalline cells, polycrystalline cells and thin film cells. Monocrystalline cells are made by using silicon wafers, connected in rows and columns, by covering a glass sheet on the top view of the cell. It is also known as single crystalline panel. It offers high performance and its cost is high. Polycrystalline cells are made by using only one silicon crystal and melt together to form a wafer. It is also called as multi-crystalline silicon. It has lower efficiency as compared to mono crystalline cell and it is available in low cost. Thin film cells are made by using amorphous silicon

and cadmium and on the surface plastic is placed. It is thinner than other cells. It has low efficiency and weighs less. Also, it is portable and flexible.

3 DC-DC Converters

DC-DC converter is a device which increases one level of d.c voltage to other level. These converters are classified into two types; isolated and no-isolated type converters. Isolated converters are used for high voltage applications and have separate input and output terminals. Non-isolated converters are used for low voltage applications. Input and output terminals of such converters have same ground [29].

3.1 Isolated Converters

Isolated converters are used for high voltage applications. These converters reduce the noise and interference. These types of converters are classified into two types. They are fly back converter and forward converter. The fly back converter is used for dc-to-dc and ac-to-ac conversion. The fly back converter can act as step up or step down converter in association with a transformer, which has split inductor. It has two schemes for controlling; voltage control mode and current control mode. Forward converter is used to increase or decrease the output voltage of the transformer and provides isolation.

3.2 Non- Isolated Converters

Non-isolated converters are used in applications where low voltage is required. Both the terminals in the circuit have same ground. These types of converters produce high noise. Protection and performance of this type of converters is poor as compared to the other type. These converters are classified into three types. They are buck, boost and buck-boost converters. Buck converter is also known as step down converter. It reduces the level of output voltage. This converter is used in SMPS, which consists of two or more semi-conductor devices. To overcome the voltage variations capacitors are employed. It also improves the voltage quality. Inductor is used to resist the sudden change in current and they are connected in both supply and load side. Boost converter is called as step up converter. It increases the input voltage level. It consists of semi-conductors. Passive elements like capacitors are used to reduce the harmonics. The output voltage is higher than the source voltage. Input current is greater than load current. Buck boost converter is combination of both buck and boost converter. Depending upon the application it may be used to increase or decrease the voltage level.

4 Solar Energy

4.1 MPPT Algorithm

Maximum power point tracking algorithm is used to extract maximum power from the available irradiance. This algorithm is used for renewable energy sources. Non-conventional energy sources generally offer less efficiency and this algorithm is used to improve the efficiency. The commonly used MPPT algorithms are as follows: constant voltage method, current sweep method, perturb and observe algorithm, incremental conductance method and temperature method.

Constant voltage method is the basic type but has some demerits. This algorithm maintains a constant voltage and does not allow tracking the voltage. Maximum power cannot be extracted using this algorithm. In current sweep algorithm, current and voltage characteristics of the solar cell and waveform of the sweep is used to control the power. Perturb and Observe approach is also called as hill climbing method and it is one of the mostly used methods and the reason for it is, it is easy to implement. First, voltage and current are measured and if power tends to vary, the voltage is adjusted to extract maximum power. The flow chart for this algorithm is given in Fig. 1. In incremental conductance method array current and voltage is measured by controller to predict the effect of a voltage change. Controller has high computation. In temperature method, maximum voltage is estimated by measuring the temperature of solar cell and comparing it with the reference value [30].

4.2 PV Cell Modeling

Equivalent circuit of PV cell is shown in Fig. 2 and explained in detail in references [31, 32]. Output current flowing through the resistor ‘ R_s ’ can be expressed as

$$I = I_L - I_D - I_{sh} \tag{1}$$

where, I_L is the photo generated current, I_D is the diode current, I_{sh} is the shunt current in ampere and I is the output current.

Voltage across the current source is given by

$$V_{sh} = V + IR_s \tag{2}$$

where, V_{sh} is the voltage across the shunt resistor and diode and V is the voltage at output terminals. By using Shockley’s equation we get,

$$I_D = I_0 \left(e^{\frac{V_D}{nV_T}} - 1 \right) \tag{3}$$

Fig. 1 Flow chart of perturb and observe method

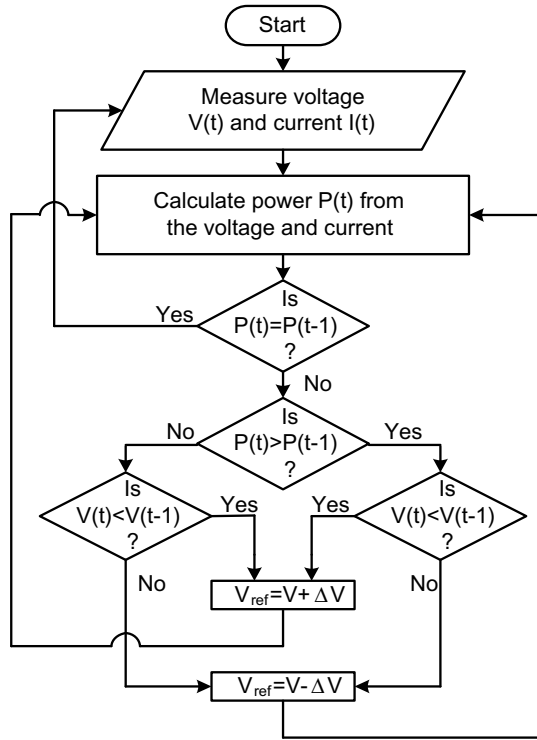
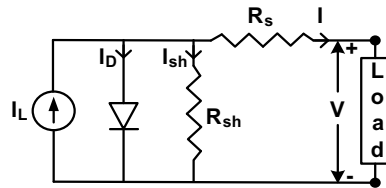


Fig. 2 Equivalent circuit of solar cell



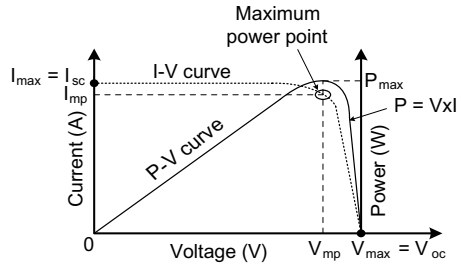
where, I_0 is the reverse bias saturation current, V_D is the voltage across diode, V_T is the terminal voltage, ‘n’ is the ideality or quality factor. By applying ohms law we get,

$$I = I_0 \left(e^{\frac{V_D}{nV_T}} - 1 \right) - \frac{V + IR_s}{R_s} \tag{4}$$

If R_{sh} is infinite we get,

$$V = nV_T \ln \left(\frac{I_L - I}{I_0} - 1 \right) - IR_s \tag{5}$$

Fig. 3 Characteristics of solar cell



Finally current equation is

$$I = I_L - I_0(e^A - 1) - B \tag{6}$$

where, $A = \frac{(V+IR_s)}{nV_T}$ and $B = \frac{V+IR_s}{R_{sh}}$.

4.3 Characteristics of PV Cell

PV cell offers electrical characteristics. The solar radiation affects the output of the cell. The output power of the PV cell is inversely proportional to temperature and directly proportional to beam radiation. Minimum current and maximum voltage is occurred at open circuit in the cell. If positive and negative terminals are short circuited voltage of the cell is minimum and current is maximum. Current versus voltage plot is shown in Fig. 3.

5 Inverters

Inverter is device which converts direct current to alternating current supply. Based on some characteristics they are classified and mentioned below.

5.1 Based on Output

Based on output the inverters are classified as sine wave inverters, square wave inverters and modified sine wave inverters. Sine wave inverter is a device which transforms the d.c voltage into an output voltage similar to supply voltage. It is one of the merits to improve the efficiency. Square wave is output of this device. But this device is rarely used. The reason is losses are very high and efficiency is very

low. Output of modified sine wave is combination of sine and square wave. Shape of output waveform nearly looks like a sine wave.

5.2 Based on Source

Based on type of source used inverters are classified as voltage source inverters and current source inverters. Input to voltage source inverters is voltage. They are used for all applications, because they have more reliability and high efficiency. Input to current source inverters is current and is used in industrial applications and is rarely used in common applications.

5.3 Based on Load

Based on type of load connected inverters are classified as single phase inverters and three phase inverters. Single phase inverters are used in household applications and commercial purpose. Again they are classified in to two categories; full and half bridge inverters. Half bridge inverter consists of two diodes and thyristors and voltage is divided into two equal parts as shown in Fig. 4.

Full bridge inverter consists of four diodes and four thyristors and we get step output and it is converted into sine wave by using filters. Diodes are used for feedback mechanism. As compared to half bridge its voltage is doubled and power is four times (Fig. 5).

Three phase inverters are used in industrial purpose and it consists of six diodes and six thyristors as shown in Fig. 6.

Operation of inverters can be divided into two modes: 180° mode and 120° mode. Thyristor conduction time is 180° in 180° mode and three thyristors act as three phases and these are in conduction mode at any time. Short circuit problems are occurred in this mode. Phase voltage looks like stepped voltage and line voltage looks like quasi-square wave. Thyristor conduction time is 120° in 120° mode and two thyristors are in conduction mode. Shapes of the both voltages are opposite to 180° mode.

Fig. 4 Half bridge inverter

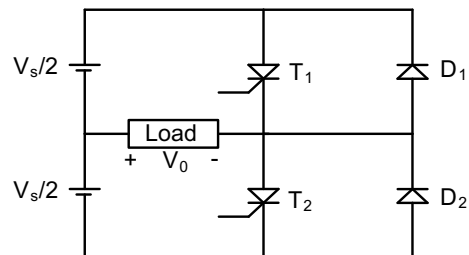


Fig. 5 Full bridge inverter

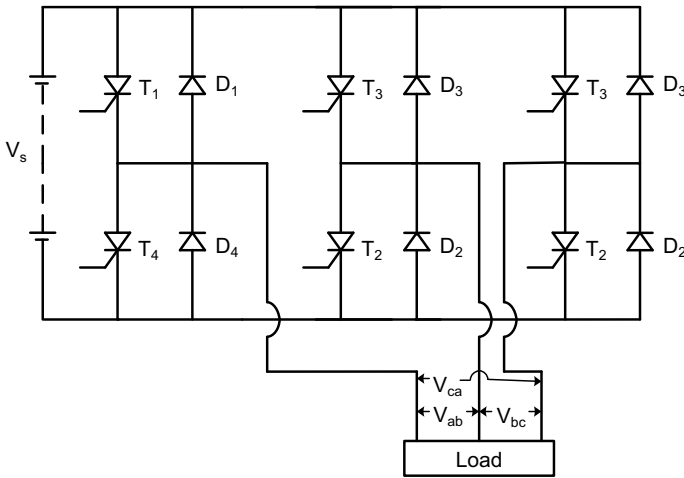
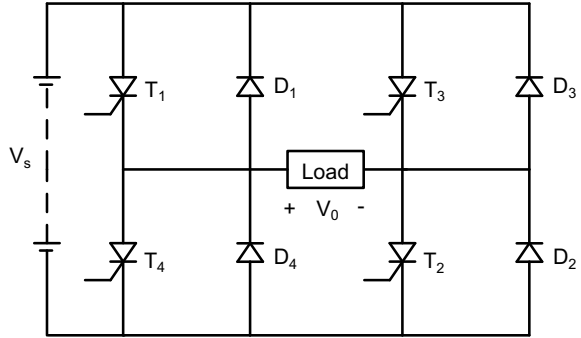


Fig. 6 Three phase inverter

5.4 Based on Technique

Based on the PWM technique used inverters are classified as single PWM inverters, multiple PWM inverters, sinusoidal PWM inverters and modified SPWM inverters. Output voltage in single PWM technique can be easily controlled using PWM technique. This technique has two signals. Square wave is reference signal and triangular wave signal act as carrier signal. By comparing both the signals gate pulse is generated. It has only one signal. Reference signal controls the output voltage. This technique is rarely used; the reason is it injects more harmonics. Multiple PWM technique has more pulses for every half cycle of voltage. Sinusoidal PWM technique is frequently used in industrial applications. Reference signal is sine wave signal. Output frequency is equal to the carrier signal frequency. Sine wave is the output. Using above techniques variation of pulse width modulation is not possible. To overcome this problem modified SPWM technique is used. At conduction period

of last and first 60° carrier signal is applied. This technique exhibits advantages like less switching losses and less switching devices.

5.5 Based on Level

Based on the output level inverters are classified as two level inverters and multiple output inverters. Two level inverter has two output levels. They are positive and negative voltages [9]. Multiple output inverters are again divided into four types. They are flying capacitor inverters, diode clamped inverters, hybrid inverters and cascaded H-type inverter.

Flying capacitor inverters have only capacitors and they allow only limited voltage. Active and reactive power is controlled by this device. It suffers with disadvantages of high switching frequency and switching losses. Diode clamped inverter consists of diodes with different voltage levels and series capacitors. The output of this inverter is less than its input voltage. By increasing the capacitors and switches the output voltage can be increased. Hybrid inverter converts beam radiation into electrical supply and it consists of battery and it stores the energy and it is very useful for back to back power consumption. Cascaded H-type inverter consists of switches like IGBT, MOSFET and capacitors. Numbers of components get reduced using this type of inverter. Based on level of inverter, the number of cells depends and each cell acts as a voltage source [5–8]. Applications of Diode clamped inverter are Static var compensation, HV lines and drives for variable speed. Applications of capacitor bank inverter are Static var, IM control and sine wave rectifiers. Applications of H-type inverter are interfacing of non-conventional source, PF compensators and active filters.

6 Filters

Power consumption is exponentially increasing and also generation of electricity is less. By using fossil fuels air pollution is occurred. To meet the increased consumption of electricity it is required to generate electricity by using green sources. Grid operates with AC supply and renewable source generates DC supply hence conversion is required. Power electronic devices are used to in DC-to-DC conversion and DC-to-AC conversion. These devices inject harmonics into the system. To eliminate these harmonics and improve power quality, filters are used. Filters are classified as follows:

6.1 *Based on Response*

Based on response the filters are classified as high pass filters, low pass filters, pass band filters and band stop filters. High pass filter allows only high frequency signals to pass through it and opposes low frequency signals. Low pass filter allows only low frequency signals to pass through it and opposes high frequency signals. Pass band filter allows a particular frequency of band and opposes other frequency signals. Band stop filter allows low and high frequency signals and opposes other frequency signals.

6.2 *Based on Their Construction*

Based on response the filters are classified as active filters and passive filters. Active filter is used to eliminate the harmonics by injections of real power with equal frequency in reverse phase to cancel those harmonics. It consists of operational amplifier or switches like transistors. Resistors and capacitors are also placed to compensate the harmonics. These filters are categorized as series and shunt filters. Series active filters are connected in series with utility grid and are used for mitigate voltage harmonics and it are operated as voltage regulators. These types of filters are frequently used for compensating voltage sag and swell problems. These filters inject fundamental voltage to compensate those problems. Shunt active filters are connected in parallel with grid and inject the fundamental current component to eliminate harmonics. These types of filters are used for mitigation of current harmonics at load side. The injected mitigation current has magnitude which is equal and phase which is opposite to that of harmonic component [13].

Passive filters consist of passive elements like resistors, capacitors and inductors. They do not require external dc source. These filters are used to eliminate the current harmonics and are mainly categorized as series, shunt and hybrid. Series filters are connected between input source and output load in series. The combination of inductor and capacitor does not allow the sudden changes in currents and voltages. Shunt filters are connected in parallel. They consist of passive elements. These filters are used to mitigate the harmonics and to balance the unbalanced voltages. Hybrid filter is a combination of both series and shunt passive filters. It mitigates both current and voltage harmonics. Advantages of active filter are: offers better performance compared to passive filter, less in weight and it has high Q factor. Advantages of passive filter are: low cost, less circuit complexity, and it does not require external supply.

7 Simulation Results

The work presented here deals with mitigation of harmonics, improvement of voltages and currents and reducing total harmonic distortion (THD) at different conditions. Shunt active power filter is used to eliminate the unwanted signal. Four case studies are performed in this work. They are (i) RL load without grid, without filter, (ii) RL load without grid with filter (iii) RL load with grid without filter and (iv) RL load with grid, with filter.

The PV system is fed to boost converter to increase the voltage level. Inverter output is fed to RL load. By conversion of dc to dc and dc to ac, current is in phase with the voltage. Harmonics are injected into system. Due to this harmonics, heat is increased. Increased harmonics results in reduced efficiency. RL load without filter is as shown in Fig. 7 and THD in this case is found to be 12.67% as shown in Fig. 8.

Due to harmonics, system performance and power quality are poor. To improve this a shunt active filter is designed and connected in parallel to load as shown in Fig. 9. It eliminates the harmonics and THD in this case is decreased to 1.70% as shown in Fig. 10.

PV system is integrated to the grid, the presence of RL load and conversion devices inject harmonics into the system. Due to these harmonics power quality problems occur. RL load with grid and without filter is as shown in Fig. 11 and THD% in this case is found to be 14.55% as shown in Fig. 12.

Shunt active filter is connected in parallel with grid. Reactive power and current harmonics are compensated by the filter. Also power factor is corrected in this case. Simulink model of grid with filter is as shown in Fig. 13. THD % in this case is decreased to 6.30 is as given in Fig. 14.

Each phase has a sub system with H-bridge cascaded model. R phase sub system is as shown in Fig. 15. The output of this model is given to the grid. Inverter output is controlled using pulse width modulation technique. Switching signal is as shown in Fig. 16.

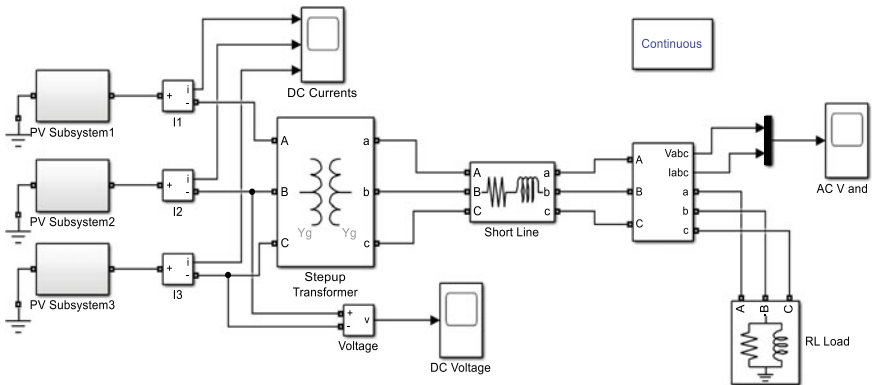


Fig. 7 RL load without grid without filter

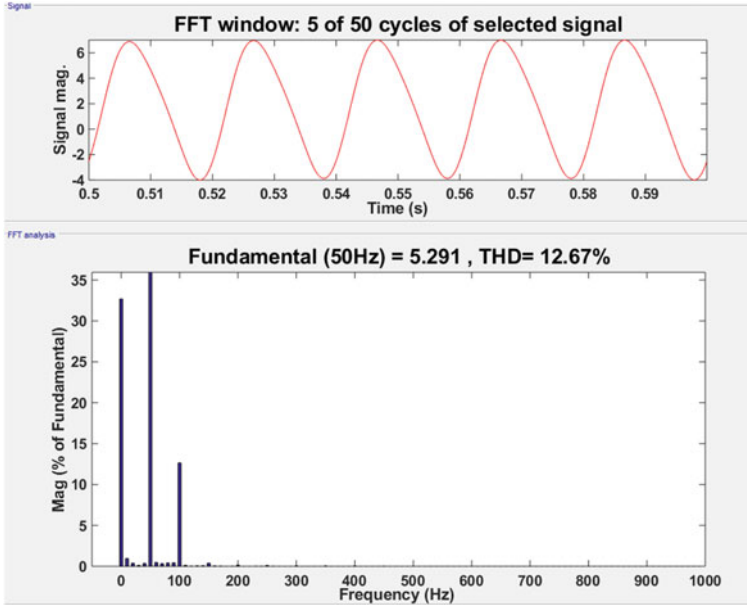


Fig. 8 THD% of RL load without filter

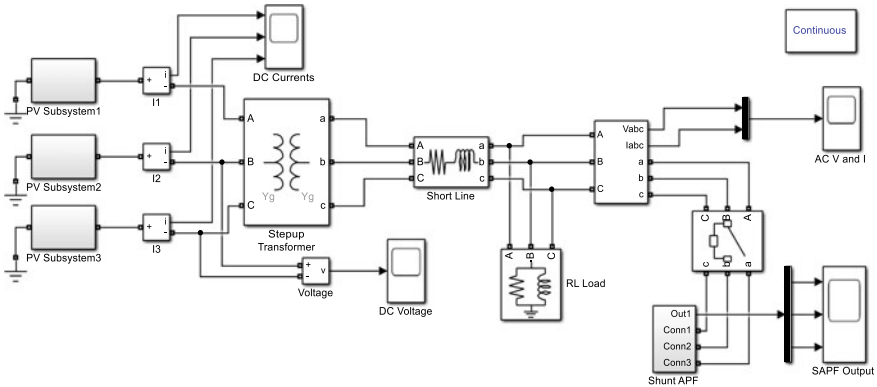


Fig. 9 RL load without grid with filter

Three phase inverter output is controlled using PWM technique. Inverter output is not sinusoidal but is nearly sinusoidal. Five level inverter offers low harmonics compared to that of three level. Output of five level inverter is as shown in Fig. 17.

Electric power distribution system is that part of utility grid which takes electrical supply from the generators and transmits it to the consumers connected to distribution system through the transmission lines. To integrate distributed generators with the grid, both must have same frequency and same voltage. The grid voltages are as

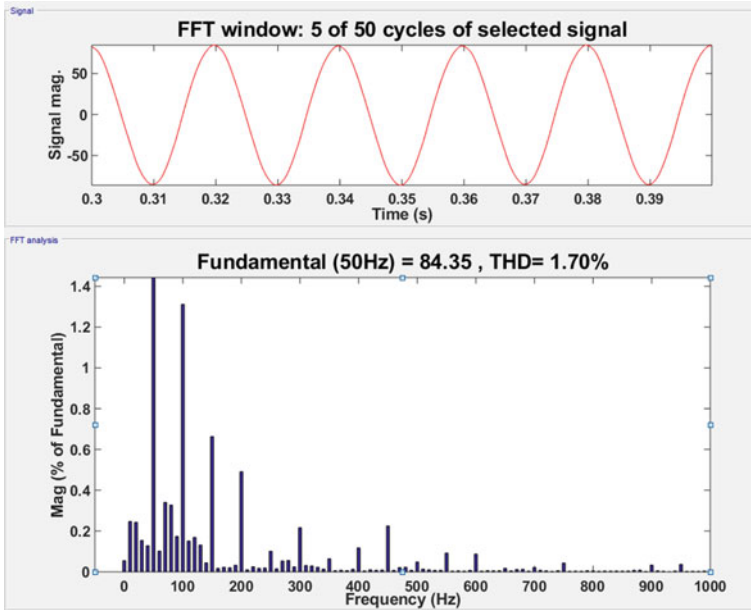


Fig. 10 THD% of RL load with filter

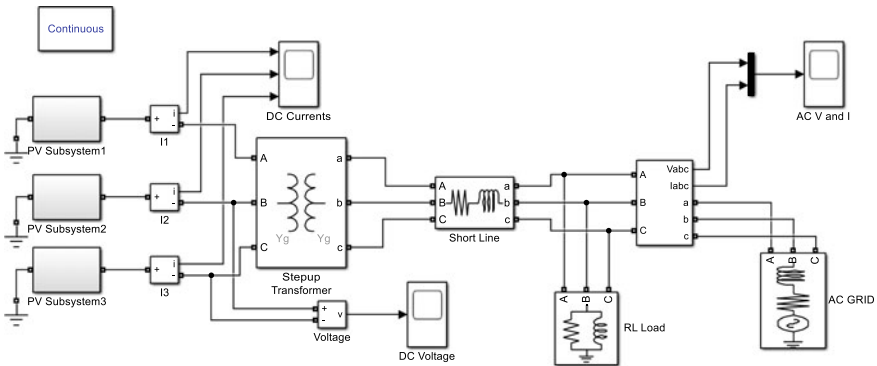


Fig. 11 RL load without filter with grid

shown in Fig. 18. If PV system is connected to the grid, total harmonic distortion is found to be quite high, that is 14.55%. Shunt active filter is connected between grid and load, to reduce the THD to 6.30%. Total harmonic distortion without and with filter is tabulated in Table 1.

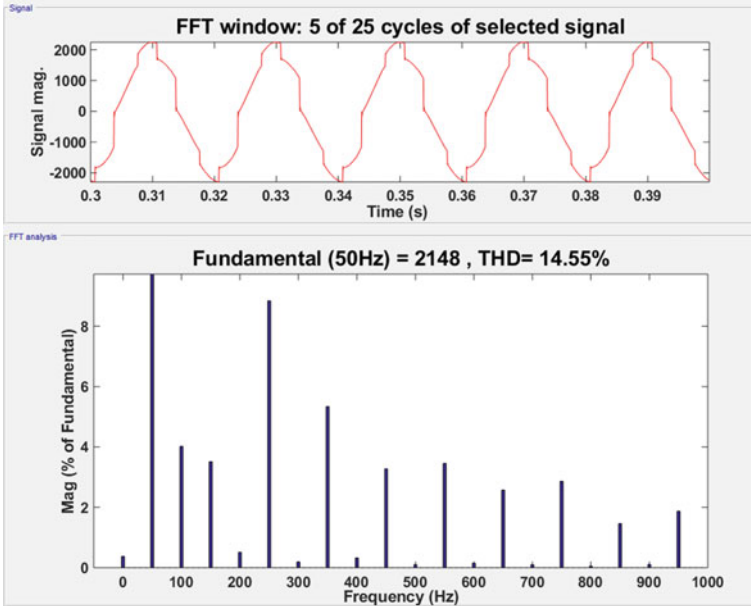


Fig. 12 THD% of grid without filter

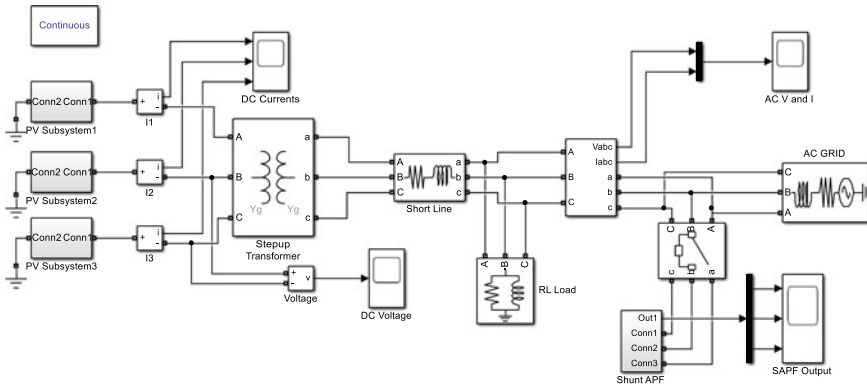


Fig. 13 RL load with grid and filter

8 Conclusion

The analysis has been made for two cases; case I focuses on harmonic analysis for the standalone photovoltaic solar system comprising of dc-dc boost converter and three phase voltage source five level H-bridge inverter and case II deals with harmonic analysis of grid connected solar system. Maximum power point tracking algorithm is implemented to extract optimal power from the solar system in both the cases.

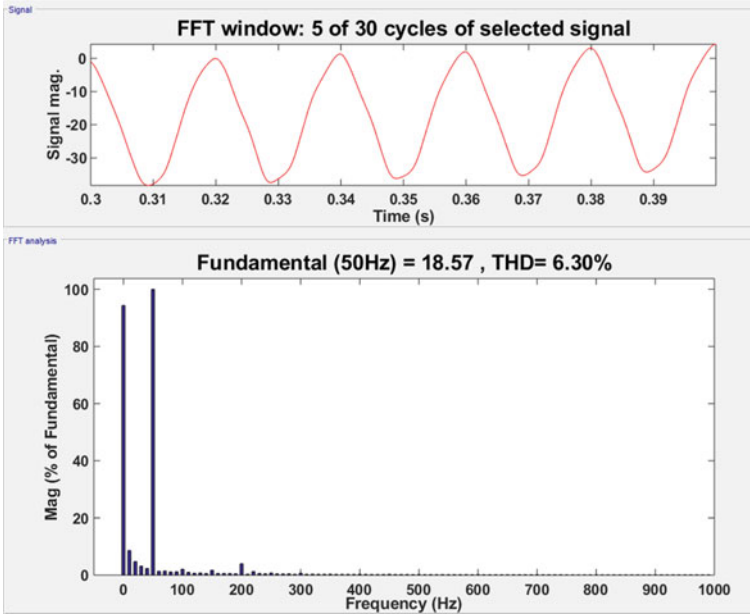


Fig. 14 THD% of grid with filter

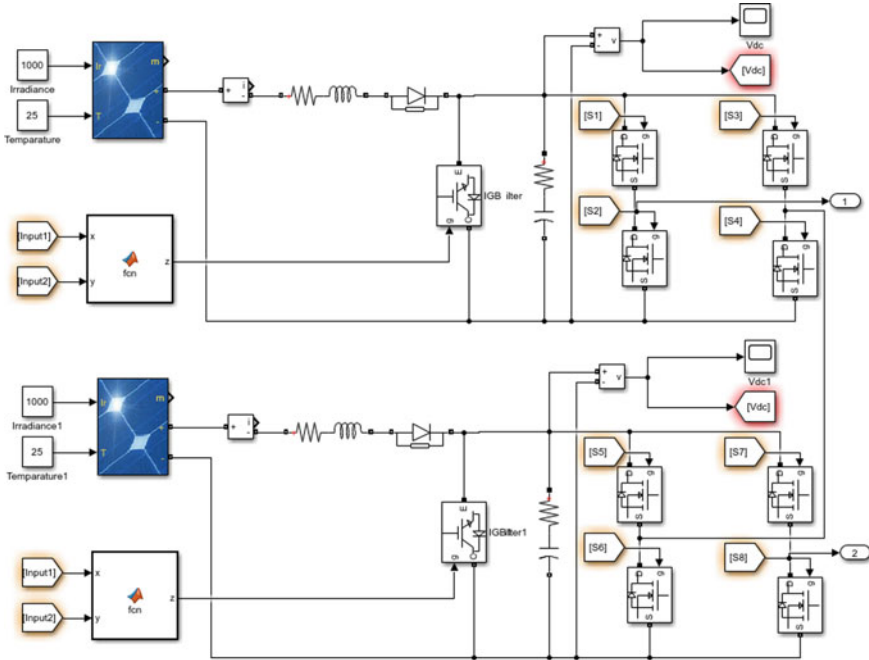


Fig. 15 R phase sub system

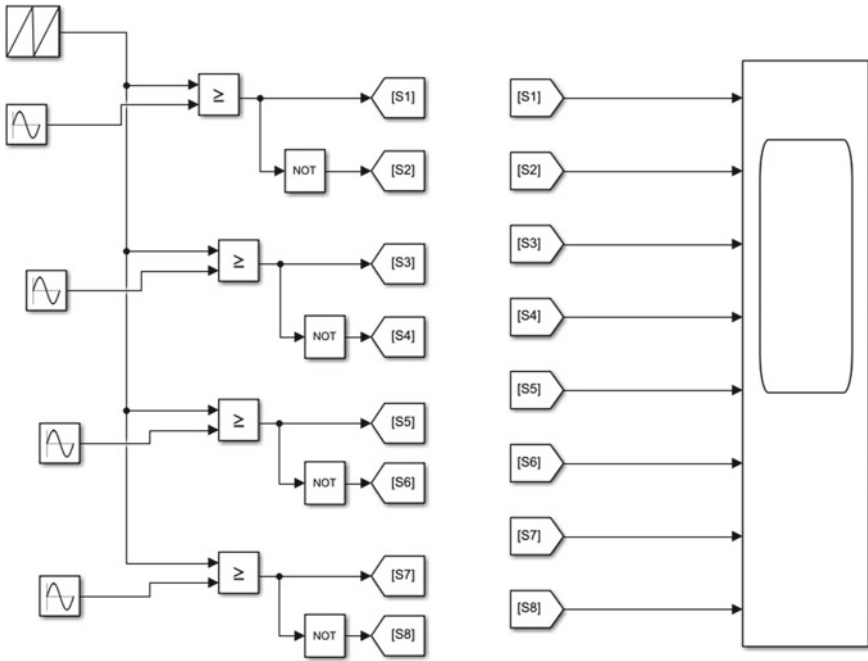


Fig. 16 PWM signals

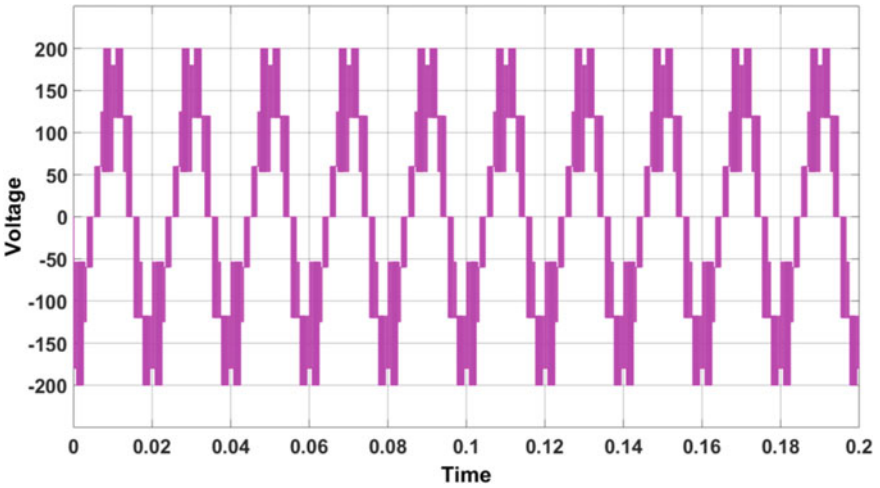


Fig. 17 Inverter output

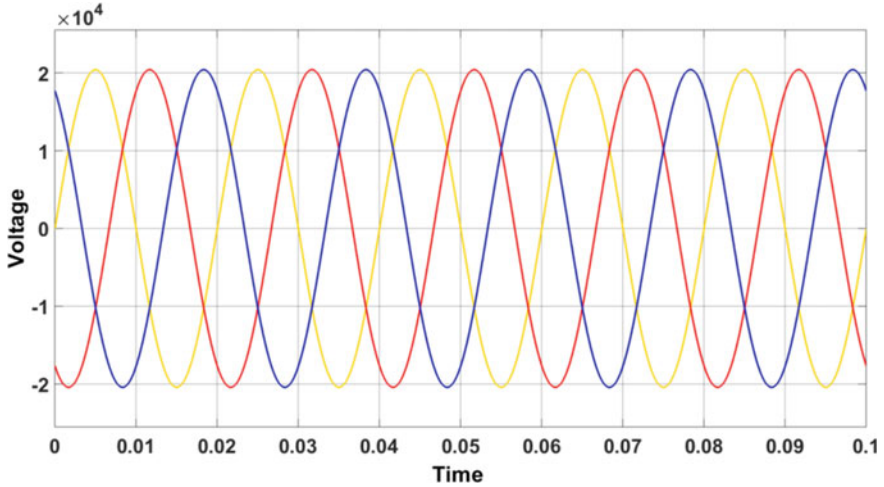


Fig. 18 Grid voltages

Table 1 THD % without and filter

Integration	Without SAPF (THD %)	With SAPF (THD %)
RL load without grid	12.67	1.70
RL load with grid	14.55	6.30

DC-to-DC converter is used to increase the dc output voltage which is fed to the cascaded H-bridge five level inverter. This inverter converts dc into ac supply which contains harmonics. Shunt active filter is designed to minimize the harmonics, which are injected by the boost converter and the inverter circuits. In case II, PV system is integrated to the grid and Fast Fourier analysis is performed to obtain its THD. Shunt active filter is designed to minimize the harmonics. Fast Fourier analysis has been done and the total harmonic distortion is obtained in both the cases. The total harmonic distortion of standalone system is observed as 12.67% without filter. SAPF is designed and implemented in the system and total harmonic distortion is reduced to 1.70%. In case 2, the solar system is integrated to grid at PCC. The total harmonic distortion is observed as 14.55% without filter. Shunt active filter is designed and connected at PCC after which the distortion was decreased to 6.30%. Thus, the shunt active power filter may be treated as the most effective filter to minimize the harmonics in both single and grid connected systems.

References

1. Salkuti SR (2019) Day-ahead thermal and renewable power generation scheduling considering uncertainty. *Renew Energy* 131: 956–65. <https://doi.org/10.1016/j.renene.2018.07.106>
2. Prasad KK, Myneni H, Kumar GS (2019) Power quality improvement and pv power injection by dstatcom with variable dc link voltage control from rsc-mlc. *IEEE Trans Sustain Energy* 10(2):876–885. <https://doi.org/10.1109/TSSTE.2018.2853192>
3. Schinke C, Vogt MR, Bothe K (2018) Optical modeling of photovoltaic modules with ray tracing simulations, Chap 3. Wiley, pp 27–91. <https://doi.org/10.1002/9781119364214.ch3>
4. Bin L, Minyong T (2012) Control method of the three-phase four-leg shunt active power filter. *Energy Proc* 14:1825–1830. <https://doi.org/10.1016/j.egypro.2011.12.1174>
5. Akagi H, Nabae A, Atoh S (1986) Control strategy of active power filters using multiple voltage-source PWM converters. *IEEE Trans Ind Appl IA-22(3)*:460–465. <https://doi.org/10.1109/TIA.1986.4504743>
6. Ko WH, Gu JC (2016) Impact of shunt active harmonic filter on harmonic current distortion of voltage source inverter-fed drives. *IEEE Trans Ind Appl* 52(4):2816–2825. <https://doi.org/10.1109/TIA.2016.2552138>
7. Singh B, Al-Haddad K, Chandra A (1999) A review of active filters for power quality improvement. *IEEE Trans Ind Electron* 46(5):960–971. <https://doi.org/10.1109/41.793345>
8. Akagi H (1996) New trends in active filters for power conditioning. *IEEE Trans Ind Appl* 32(6):1312–1322. <https://doi.org/10.1109/28.556633>
9. Villalva MG, Gazoli JR, Filho ER (2009) Comprehensive approach to modeling and simulation of photovoltaic arrays. *IEEE Trans Power Electron* 24(5):1198–1208. <https://doi.org/10.1109/TPEL.2009.2013862>
10. Salmeron P, Litran SP (2010) Improvement of the electric power quality using series active and shunt passive filters. *IEEE Trans Power Delivery* 25(2):1058–1067. <https://doi.org/10.1109/TPWRD.2009.2034902>
11. Vodyakho O, Mi CC (2009) Three-level inverter-based shunt active power filter in three-phase three-wire and four-wire systems. *IEEE Trans Power Electron* 24(5):1350–1363. <https://doi.org/10.1109/TPEL.2009.2016663>
12. Krishna VK, Dash SK, Geshma KR (2020) Development and analysis of power quality by using fuel cell based shunt active power filter. In: 2020 2nd international conference on innovative mechanisms for industry applications (ICIMIA), pp 448–452. <https://doi.org/10.1109/ICIMIA48430.2020.9074886>
13. Singh B, Al-Haddad K, Chandra A (1999) A review of active filters for power quality improvement. *IEEE Trans Industrial Electronics* 46(5):960–971. <https://doi.org/10.1109/41.793345>
14. Rao B, Krishna P, Yarlagadda V (2020) Mitigation of photovoltaic solar system harmonics using shunt active power filter. In: 2020 Fourth international conference on computing methodologies and communication (ICCMC), pp 566–571. <https://doi.org/10.1109/ICCMC48092.2020.ICCMC-000105>
15. Esram T, Chapman PL (2007) Comparison of photovoltaic array maximum power point tracking techniques. *IEEE Trans Energy Conversion* 22(2):439–449. <https://doi.org/10.1109/TEC.2006.874230>
16. Myneni H, Ganjikunta SK (2020) Energy management and control of single-stage grid-connected solar pv and bes system. *IEEE Trans Sustain Energy* 11(3):1739–1749. <https://doi.org/10.1109/TSSTE.2019.2938864>
17. Ali A, Almutairi K, Padmanaban S, Tirth V, Algarni S, Irshad K, Islam S, Zahir MH, Shafiqullah M, Malik MZ (2020) Investigation of mppt techniques under uniform and non-uniform solar irradiation condition—a retrospection. *IEEE Access* 8:127,368–127,392. <https://doi.org/10.1109/ACCESS.2020.3007710>
18. Chikh A, Chandra A (2015) An optimal maximum power point tracking algorithm for pv systems with climatic parameters estimation. *IEEE Trans Sustain Energy* 6(2):644–652. <https://doi.org/10.1109/TSSTE.2015.2403845>

19. Kumar N, Hussain I, Singh B, Panigrahi BK (2018) Normal harmonic search algorithm-based mppt for solar pv system and integrated with grid using reduced sensor approach and pnklms algorithm. *IEEE Trans Ind Appl* 54(6):6343–6352. <https://doi.org/10.1109/TIA.2018.2853744>
20. Saxena V, Kumar N, Singh B, Panigrahi BK (2021) A rapid circle centre-line concept-based mppt algorithm for solar photovoltaic energy conversion systems. *IEEE Trans Circuits Syst I Regul Pap* 68(2):940–949. <https://doi.org/10.1109/TCSI.2020.3038114>
21. Kumar N, Singh B, Panigrahi BK, Xu L (2019) Leaky-least-logarithmic-absolute-difference-based control algorithm and learning-based inc mppt technique for grid-integrated pv system. *IEEE Trans Ind Electron* 66(11):9003–9012. <https://doi.org/10.1109/TIE.2018.2890497>
22. Kumar N, Singh B, Panigrahi BK (2019) Pnklmf-based neural network control and learning-based hc mppt technique for multiobjective grid integrated solar pv based distributed generating system. *IEEE Trans Ind Inform* 15(6):3732–3742. <https://doi.org/10.1109/TII.2019.2901516>
23. Kumar N, Hussain I, Singh B, Panigrahi BK (2017) Single sensor-based mppt of partially shaded pv system for battery charging by using cauchy and gaussian sine cosine optimization. *IEEE Trans Energy Convers* 32(3):983–992. <https://doi.org/10.1109/TEC.2017.2669518>
24. Priyadarshi N, Padmanaban S, Holm-Nielsen JB, Blaabjerg F, Bhaskar MS (2020) An experimental estimation of hybrid anfis–pso-based mppt for pv grid integration under fluctuating sun irradiance. *IEEE Syst J* 14(1):1218–1229. <https://doi.org/10.1109/JSYST.2019.2949083>
25. Kumar N, Singh B, Panigrahi BK (2020) Llmlf-based control approach and lpo mppt technique for improving performance of a multifunctional three-phase two-stage grid integrated pv system. *IEEE Trans Sustain Energy* 11(1):371–380. <https://doi.org/10.1109/TSTE.2019.2891558>
26. Abdelsalam AK, Massoud AM, Ahmed S, Enjeti PN (2011) High-performance adaptive perturb and observe mppt technique for photovoltaic based microgrids. *IEEE Trans Power Electron* 26(4):1010–1021. <https://doi.org/10.1109/TPEL.2011.2106221>
27. Kollimalla SK, Mishra MK (2014) Variable perturbation size adaptive P & OMPPT algorithm for sudden changes in irradiance. *IEEE Trans Sustain Energy* 5(3):718–728. <https://doi.org/10.1109/TSTE.2014.2300162>
28. Pai FS, Chao RM (2010) A new algorithm to photovoltaic power point tracking problems with quadratic maximization. *IEEE Trans Energy Convers* 25(1):262–264. <https://doi.org/10.1109/TEC.2009.2032575>
29. Harfman Todorovic M, Palma L, Enjeti PN (2008) Design of a wide input range dc–dc converter with a robust power control scheme suitable for fuel cell power conversion. *IEEE Trans Industr Electron* 55(3):1247–1255. <https://doi.org/10.1109/TIE.2007.911200>
30. Hohm D, Ropp M (2000) Comparative study of maximum power point tracking algorithms using an experimental, programmable, maximum power point tracking test bed. In: Conference record of the twenty-eighth IEEE photovoltaic specialists conference—2000 (Cat. No.00CH37036), pp 1699–1702. <https://doi.org/10.1109/PVSC.2000.916230>
31. Sadanand DDK (2021) Modeling of photovoltaic solar cell based on cusbs absorber for the enhancement of performance. *IEEE Trans Electron Dev* 68(3):1121–1128. <https://doi.org/10.1109/TED.2020.3048326>
32. Bhuvanewari G, Annamalai R (2011) Development of a solar cell model in matlab for pv based generation system. In: 2011 annual IEEE India conference, pp 1–5. <https://doi.org/10.1109/INDCON.2011.6139509>

Transient Stability Enhancement of Power System with Grid Connected DFIG Based Wind Turbine



D. Rakesh Chandra, Surender Reddy Salkuti,
and Venkataramana Veeramsetty

Abstract Transient stability (TS) is one of the major issues of wind power grid integration. The reasons for transients are sudden severe disturbances such as faults. To save the grid from severe damage we must concentrate on transient stability management. A fixed-speed wind generator is easy to operate and reliable but it may not operate effectively under critical conditions such as transient stability. Coming to variable speed wind energy generators (WEGs) they can improve the TS of the system, and the Doubly Fed Induction Generator (DFIG) is one among the variable speed WEGs. In this work, the impact of DFIG on the TS of the power system connected to the grid has been investigated, and also rotor resistance control method is utilized to enhance the TS of the system. Here the proposed TS analysis has been implemented on a Reliability Test System (RTS)-24 bus system. All the simulation studies have been carried out in a MATLAB-compatible-based Power System Analysis Toolbox (PSAT) toolbox. From the obtained simulation studies it can be observed that in DFIG wind turbine addition of external resistance has improved system transient stability and the system could reach steady-state quickly as damping ratio is enhanced due to proportional relationship with the external resistance being added.

Keywords Renewable energy · Transient stability · Wind power · Induction generator · Power system

D. Rakesh Chandra

Department of Electrical and Electronics Engineering, Kakatiya Institute of Technology and Science, Warangal, India
e-mail: drc.eee@kitsw.ac.in

S. R. Salkuti (✉)

Department of Railroad Electrical Systems, Woosong University, Daejeon 34606, Republic of Korea
e-mail: surender@wsu.ac.kr

V. Veeramsetty

Center for Artificial Intelligence and Deep Learning, SR Engineering College, Warangal, India
e-mail: venkataramana_v@srecwarangal.ac.in

Nomenclature

TS	Transient stability
WEGs	Wind energy generators
DFIG	Doubly Fed Induction Generator
RTS	Reliability Test System
PSAT	Power System Analysis Toolbox
NN	Neural network
PLL	Phase-locked loop
MG	Microgrid
DDSG	Direct-drive synchronous generator
CSWT	Constant speed wind turbine
SCIGs	Squirrel Cage Induction Generators
GB	Gearbox
VSC	Voltage source converter

1 Introduction

Recently, power generation using renewable energy resources (RERs) is on an increase due to the considerations of green energy. At the beginning of 2020, the global installed RERs utility-scale capacity stood at 2537 GW with wind and solar PV combined contributing about 46% of the total global RERs share. In the modern world, energy has a strong relationship with the socio-economic development of a country. RERs are an adequate substitute for a conventional power system that can provide greener, consistent, quality power with low network congestion and losses. Wind energy availability is huge and it is eco-friendly. Nowadays, wind power generation has been increasing continuously throughout the world. Distributed generation in the form of RERs produces dependency on conventional energy generation and reduces the carbon footprint. Wind energy conversion system has several economic, technical, social, and environmental challenges. Economic challenges include high installation cost, technology challenges include power electronic converters (i.e., high power density converters and advanced cooling methods), controllers (pitch angle controllers, inverter-side, and grid-side converters). At present fixed and variable speeds, induction generators (IGs) are utilized for the generation of electrical power by using the wind source. Thus the integration of wind energy into the utility grid arise the issues such as rotor angle stability and transient stability (TS) problems.

In reference [1], a multilayered neural network (NN) is used to find the TS of the power system by using the PSAT software. A simple DFIG wind turbine along with its power converter model is simulated in [2] using DiGSILENT software to meet the power demand. Enhancement of both voltage stability and TS has been performed in reference [3] by using the wind energy converter with the help of P/Q control and modern voltage source converter (VSC). Comparisons among various

types of wind turbines according to their actual market share and cost-performance have been proposed in references [4, 5]. An approach to improve voltage stability by using a static compensator is proposed in references [6, 7]. The impacts of WEG on the voltage and TS of power grids are examined in reference [8] by determining the effect of variable and fixed speed grid-connected IGs on power systems voltage stability. The voltage stability of the system with grid-connected fixed and variable speed wind turbines has been investigated in reference [9]. The stability of grid-connected DFIG by taking into account the phase-locked loop (PLL) dynamics is proposed in reference [10].

The coordinated control of DFIG based WEG and the microturbine in a DC microgrid (MG) with the constant power load has been proposed in [11]. In reference [12], the performance of grid-connected DFIG based wind turbine system with gear-train backlash is analyzed. A nonlinear control method to coordinate DFIG based WEGs and static compensators in multi-machine power systems are proposed in [13]. Reference [14] presents various issues related to the stability of wind energy systems with variable speed in weak and strong grids. Reference [15] investigates the modeling and TS analysis of the integrated WEG system. Reference [16] presents a comprehensive review among three main types of wind turbines, i.e., direct-drive synchronous generator (DDSG), constant speed wind turbine (CSWT), and DFIG. The small-signal stability of a grid-connected power system with squirrel cage induction generator using a PSAT analysis with localization of Eigenvalues is proposed in reference [17]. The behavior of DFIG for grid disturbances has been simulated and validated in reference [18].

As wind energy exhibits both uncertainty and variability, wind generation cannot be dispatched on demand. It is also highly complex to forecast wind energy with precision. When it is used in combination with conventional sources, it poses a lot of challenges to grid operators in maintaining grid stability. Wind energy integration also poses challenges like power quality, effective load management in the power system. A few more issues such as power balance, wind power reserve management, and voltage control of the power system will also pose challenges to the system operator. Power quality is the deviation from original sinusoidal voltage and current waveforms such as flickers, harmonics, voltage sag, and swell. The objective of this work is to enhance transient stability (TS) of the DFIG connected system with the optimum rotor resistance control method. This work mainly concentrates on TS analysis and enhancement where it is a real challenging issue for grid-connected wind turbine systems. Time-domain simulation analysis will give the overall impact of transient stability on the system. The rotor resistance control method is used for the first time in this chapter to improve the TS of DFIG connected to the RTS-24 bus system. This chapter investigates the transient stability of the RTS 24 bus system when DFIG (at bus number 14) is connected to it. The detailed mathematical modeling of DFIG is also presented in this chapter. All these simulation studies are implemented in PSAT software of version 2.1.8.

The chapter is organized as follows: Sect. 2 describes detailed mathematical modeling of DFIG wind turbine and the implementation details of wind turbine

integrated models for TS analysis using PSAT software. The description of the Reliability Test System (RTS) 24 bus system is presented in Sect. 3. Section 4 presents the results and discussion. Lastly, the chapter is summarized in Sect. 5.

2 Modeling of Doubly Fed Induction Generator (DFIG)

Integration of wind power into utility grid via grid-connected wind turbines creates stability problems. These wind turbine generators are usually either Squirrel Cage Induction Generators (SCIGs) or Doubly Fed Induction Generators (DFIG) that use constant speed and variable speed wind turbines, respectively. The requirement of reactive power by the wind turbines causes voltage stability issues. This stability problem is also based on the amount of power integrated into the grid. The stability problem is mainly divided into small signal stability and TS. Small signal stability is due to the power system being subjected to a small disturbance that leads to small incremental change in system variables. TS is due to the power system being subjected to severe disturbances such as breaker and faults interruptions etc. In recent times the majority of wind energy generation is done by DFIG based wind turbines. The basic configuration and schematic view of DFIG are depicted in Fig. 1. The DFIG is mainly combined with a gearbox (GB), induction generator, and converter. In this work, a partial scale converter with the rating of 20% to 30% of DFIG is used so that the speed can be varied within $\pm 30\%$ of the synchronous speed. A partial scale converter makes DFIG more attractive in terms of economical point of view [19]. Generally wound rotor (slip ring) induction generators are used as DFIG.

In Fig. 1, GB is the gearbox, GSC is the grid side converter and RSC is the rotor side converter. GB is having more turns to improve wind speed to connect DFIG [20]. RSC and GSC are used to regulate reactive power and slip power recovery.

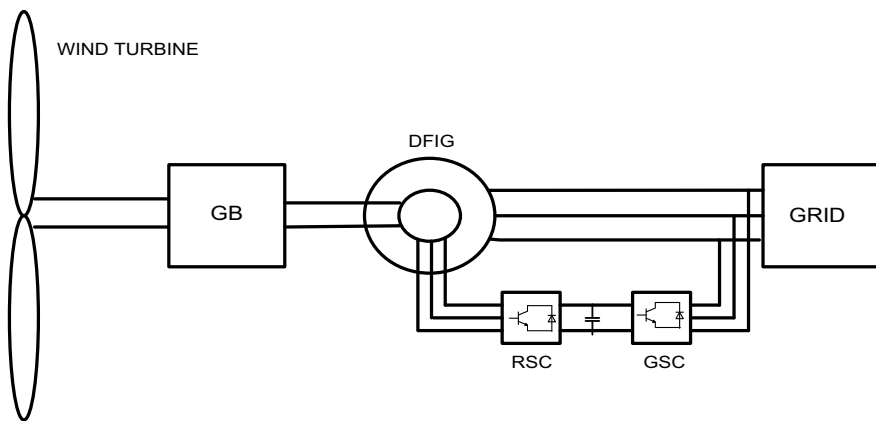


Fig. 1 The basic configuration of DFIG

2.1 Mathematical Modeling of DFIG

Wind turbines with DFIG are used more often due to lower capital investment. DFIG is dominating the wind turbine market with a total share of 84.5% to 86%. Based on the operational characteristics, grid integration of wind turbines will lead to small signal or transient stability issues. For the same wind turbine rating, DFIG wind turbines have better reactive power regulation capability and transient voltage stability characteristics when compared to traditional induction generators. This section presents the mathematical modeling of DFIG. The steady-state expressions of DFIG are assumed and they are represented by,

$$v_{ds} = -r_s i_{ds} + [(x_s + x_m)i_{qs} + x_m i_{qr}] \quad (1)$$

$$v_{qs} = -r_s i_{qs} - [(x_s + x_m)i_{ds} + x_m i_{dr}] \quad (2)$$

$$v_{dr} = -r_R i_{dr} + (1 - \omega_m)[(x_R + x_m)i_{qr} + x_m i_{qs}] \quad (3)$$

$$v_{qr} = -r_R i_{qr} - (1 - \omega_m)[(x_R + x_m)i_{dr} + x_m i_{ds}] \quad (4)$$

In the above equations, x_m and x_s are magnetizing reactance and stator reactance respectively. Similarly x_R and r_R are rotor reactance and resistance respectively [21, 22]. v_{ds} , v_{qs} are the stator voltages of d and q axes. Similarly v_{dr} , v_{qr} are the rotor voltages of d and q axes [23]. It may be noted that stator voltage mostly depends on the magnitude and phase angle, and they are expressed as,

$$v_{ds} = V \sin(-\theta) \quad (5)$$

$$v_{qs} = V \cos(\theta) \quad (6)$$

Here θ is the angle between V and v_{qs} . The active power (P) and the reactive power (Q) that are injected into the utility grid depends on the stator and grid-side currents of the converter. These are expressed as [24],

$$P = v_{ds}i_{ds} + v_{qs}i_{qs} + v_{dc}i_{dc} + v_{qc}i_{qc} \quad (7)$$

$$Q = v_{qs}i_{ds} - v_{ds}i_{qs} + v_{qc}i_{qc} - v_{dc}i_{dc} \quad (8)$$

These can be rewritten by considering the grid-side converter and converter power equations and they are expressed as,

$$P_c = v_{dc}i_{dc} + v_{qc}i_{qc} \quad (9)$$

$$Q_c = v_{qc}i_{dc} - v_{dc}i_{qc} \quad (10)$$

Rotor side active power (P_r) and reactive power (Q_r) are

$$P_r = v_{dr}i_{dr} + v_{qr}i_{qr} \quad (11)$$

$$Q_r = v_{qr}i_{dr} - v_{dr}i_{qr} \quad (12)$$

Further, if the converter is assumed to be lossless then the active power (P_c) and reactive power (Q_c) on the converter side are $P_c = P_r$ and $Q_c = 0$. Finally, the injected power into the grid is given by [25],

$$P = v_{ds}i_{ds} + v_{qs}i_{qs} + v_{dr}i_{dr} + v_{qr}i_{qr} \quad (13)$$

$$Q = v_{qs}i_{ds} - v_{ds}i_{qs} \quad (14)$$

where i_{ds} , i_{qs} are the stator currents of the d and q axes, respectively. i_{dr} and i_{qr} are the rotor currents of the d and q axes, respectively. In the generator, the motion equation of a single shaft model is utilized. In this work, it can be considered that converter controls can filter the dynamics of the shaft. Therefore,

$$\dot{\omega}_m = (T_m - T_e)/2H_m \quad (15)$$

$$T_e = \psi_{ds}i_{qs} - \psi_{qs}i_{ds} \quad (16)$$

The stator flux and generator currents relationship can be expressed as,

$$\psi_{ds} = -[(x_s + x_m)i_{ds} + x_m i_{dr}] \quad (17)$$

$$\psi_{qs} = -[(x_s + x_m)i_{qs} + x_m i_{qr}] \quad (18)$$

ψ_{ds} and ψ_{qs} are stator fluxes on the d-axis and q-axis respectively. Then, electrical torque (T_e) is expressed as,

$$T_e = x_m(i_{qr}i_{ds} - i_{dr}i_{qs}) \quad (19)$$

The mechanical torque (T_m) is given by [26],

$$T_m = \frac{P_w}{\omega_m} \quad (20)$$

2.2 *Implementation of Wind Turbine Integrated Models for TS Analysis Using PSAT Software*

Wind power grid integration creates stability problems. The world is facing a severe energy security problem with demand for energy going to be triple by 2050. Also, increasing restrictions on conventional energy sources to resist environmental change is giving rise to increased use of renewable resources for electricity production. Wind energy being uncertain and dynamically generates the issue of the storage facility when integrated into the grid. TS studies are addressed using PSAT which is MATLAB-compatible software. TS studies have been done by applying a 3 phase fault at time $t = 3$ s and the duration of fault is 150 ms. The step-by-step procedure to implement the wind turbine integrated models for the TS analysis using PSAT [27, 28] is presented next:

- **Step 1:** Install PSAT software in MATLAB R2009a version.
- **Step 2:** Create the new data file (SIMULINK model) in PSAT (MATLAB compatible toolbox) by clicking File/Open/New data file.
- **Step 3:** Construct SCIG wind turbine integrated to IEEE 14 bus system model with 3 phase fault (at time $t = 3$ s and fault clearing time is 50 ms) in MATLAB SIMULINK using PSAT library and save this file with a suitable name.
- **Step 4:** Give practical wind speed data as an input file to the wind turbine model by editing the PSAT data file (.m model).
- **Step 5:** Load the data file by clicking “File/Open/ datafile/select data file (from saved file)/load”.
- **Step 6:** After loading the data file, run power flow by clicking on the option “Power Flow” (for this select Newton–Raphson method which is available in settings).
- **Step 7:** After executing power flow, carry out time-domain simulation (for this select Trapezoidal method which is available in settings) by selecting the option as “Time Domain” and simulate for 20 s of time (for this keep ending time = 20 s). The system may reach a steady-state within 3–4 s. But to have further insight into system behavior the study period is extended to 20 s.
- **Step 8:** After time-domain simulation, plot the curves such as rotor angles, bus angles, and voltages, etc. for the time by clicking on the option “Plot” which is on the right side of the PSAT tool-bar.

3 Reliability Test System (RTS) 24 Bus Test System

In this chapter, an RTS-24 bus test system has been used for the TS analysis and the enhancement of grid-connected DFIG based wind turbine. This test system includes 10 generating units, one synchronous condenser, 4 transformers, and 38 transmission lines. These transmission lines have two different voltage levels, i.e., 230 and 138 kV. The 138 kV is in the lower portion whereas 230 kV is in the upper portion connected by 230/138 kV transformers at buses 11, 12, and 24. The wind turbine is connected

to RTS 24 bus system at bus number 14 as shown in Fig. 2. The total generation of all conventional generators is 2340 MW in the case of the RTS-24 bus system. As mentioned earlier, at bus number 14 wind turbine generator (i.e., DFIG) with the capacity of 240 MW (all wind turbines together) is integrated, which is more than 10% of total conventional generation. A three-phase fault was applied at the 11th bus at time $t = 3$ s, and fault clearing time is set to 50 ms. In RTS 24 bus system, the wind turbines are connected at bus number 14 which has been chosen randomly. A 3-phase fault is applied at the 11th bus as shown in Fig. 2. The fault is applied at $t = 3$ s and the fault clearing time is 50 ms.

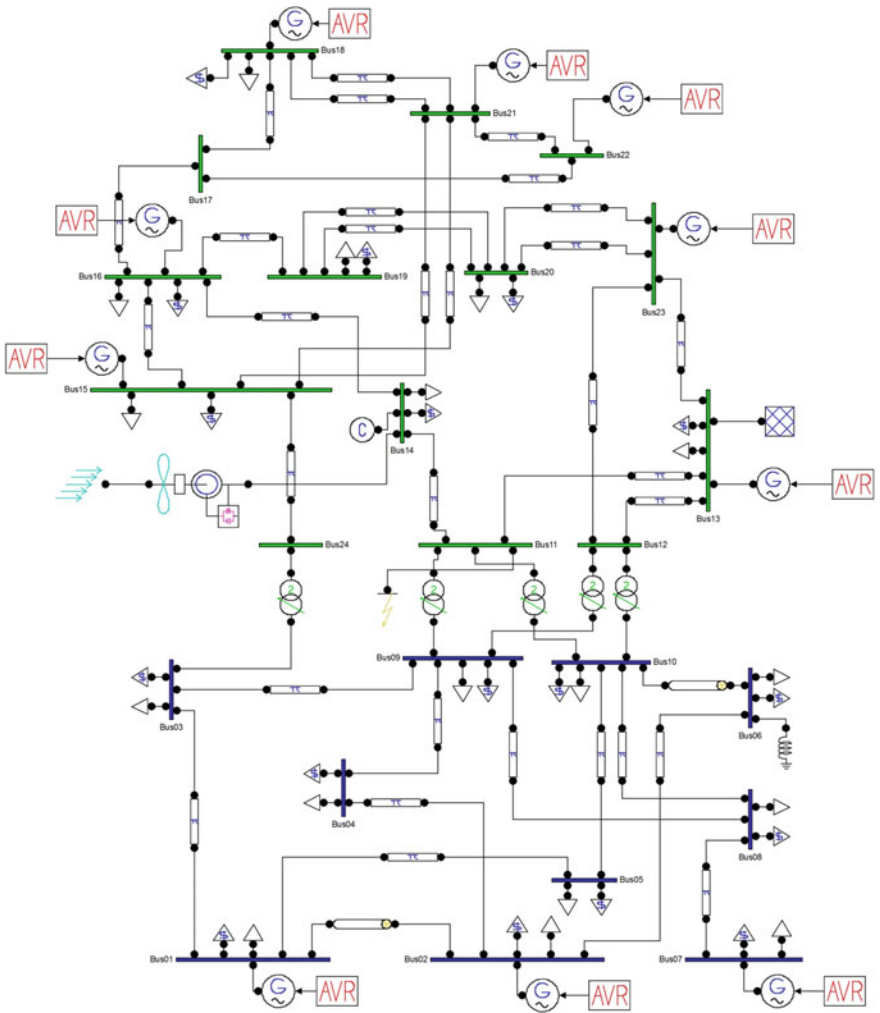


Fig. 2 PSAT Simulated RTS 24 bus system with DFIG wind turbine at bus 14 and fault at bus number 11

4 Results and Discussion

The analysis of bus angles, rotational speeds of generators, generator rotor angles, and voltages at all buses have been discussed in this section. The test system used for the analysis is RTS 24 bus system with the integration DFIG wind turbine. Comparisons of all the results of transient stability study under severe fault conditions are also presented. DFIG wind turbines can supply the active power at constant frequency and voltage despite rotor speed variation.

After execution of power flow, time-domain simulation has been carried out for 20 s. The fault is applied at t equal to 3 s to evaluate system transient stability and fault is cleared at 50 ms. Figures 3, 4, 5 and 6 show the variation of rotor angles, angular speed, bus angles, and voltage magnitudes of DFIG wind turbine integrated RTS 24 bus system which is subjected to three-phase fault at bus number 11.

Figures 3, 4, 5 and 6 show that due to the application of the 3-phase fault at bus 11, the rotor angles have varied from 1 to 1.4 radians, and finally reached to steady-state as shown in Fig. 3. Figure 4 describes the variation of angular speeds in the range of 0.97–1.1 p.u and reached steady on the removal of a fault. Figures 5 and 6 indicate that bus angles reached 0.15 radians, the voltage dropped to 0.3 p.u during the fault and all these values have reached a steady-state after removing fault within simulated time. From the above analysis, it can be concluded that the system is stable.

In the DFIG wind generator, the maximum peak overshoot is less, and hence the steady-state is achieved in less time after clearing the fault. Further, with DFIG transient stability can be improved using the rotor resistance control method and is discussed in Sect. 4.1.

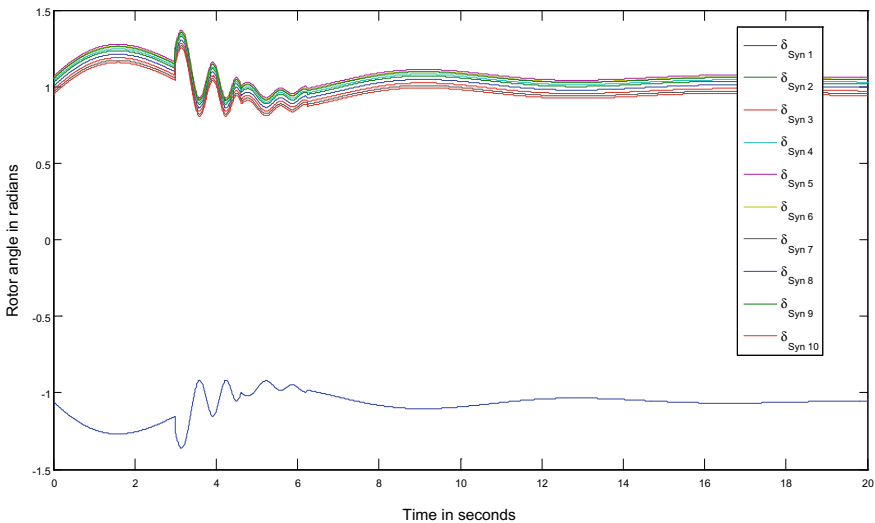


Fig. 3 Rotor angles of different generators for 24 bus system with DFIG wind turbine, fault at bus 11

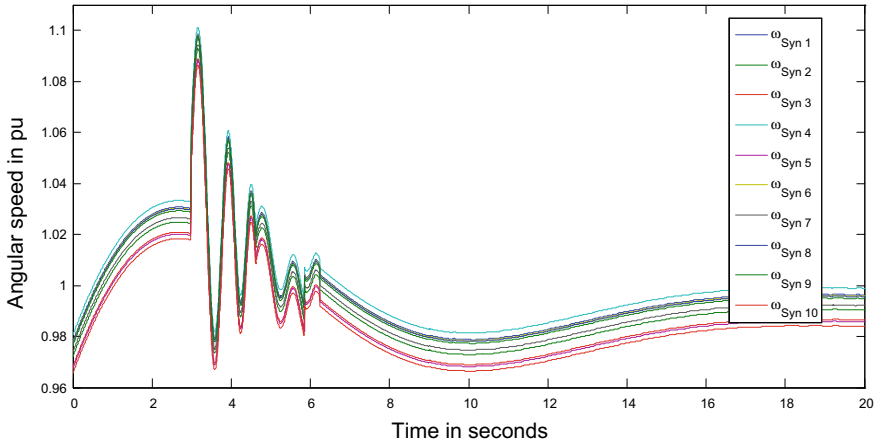


Fig. 4 Angular speeds at different synchronous generators for 24 bus systems with DFIG wind turbine, fault at bus 11

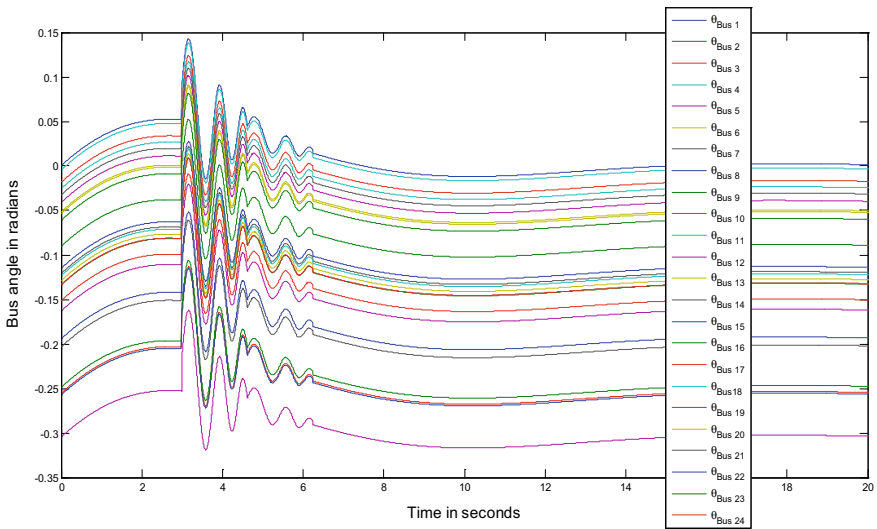


Fig. 5 Bus angles at various busses for 24 bus system with DFIG, fault at bus 11

4.1 Transient Stability Enhancement of DFIG Integrated RTS 24 Bus System

TS enhancement is the process of improving the system damping and reducing the maximum peak overshoot and thereby helping the system to reach a steady-state quickly. For stability improvement, external rotor resistance (variable resistance) is

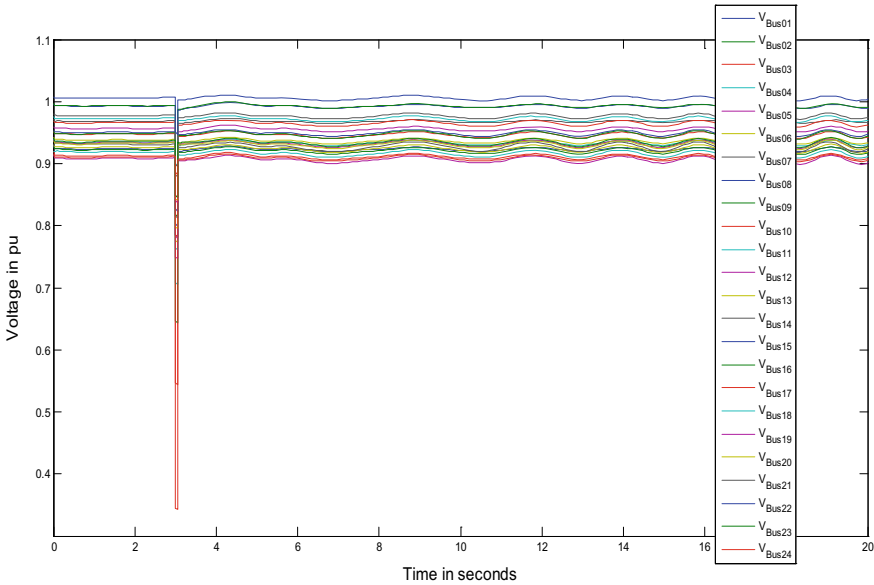
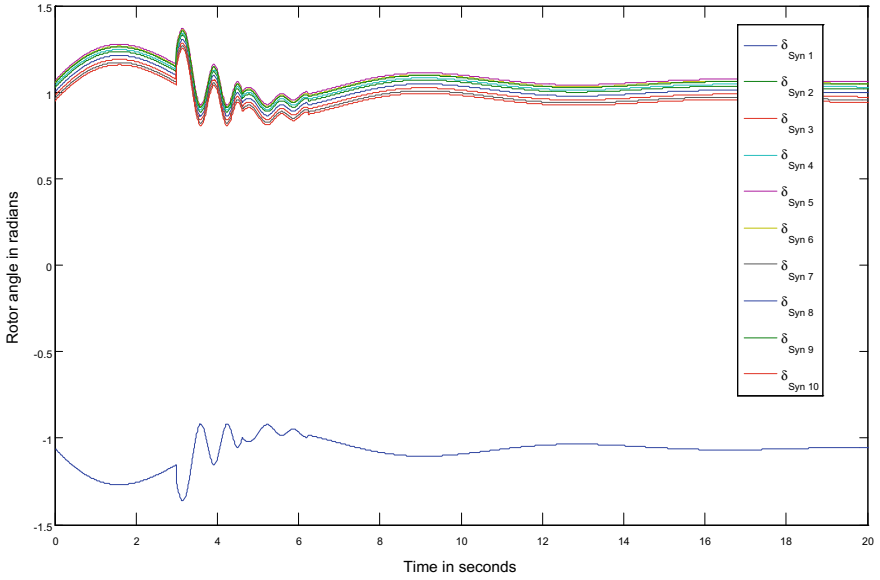


Fig. 6 The voltage at various busses for 24 bus systems with DFIG, fault at bus 11

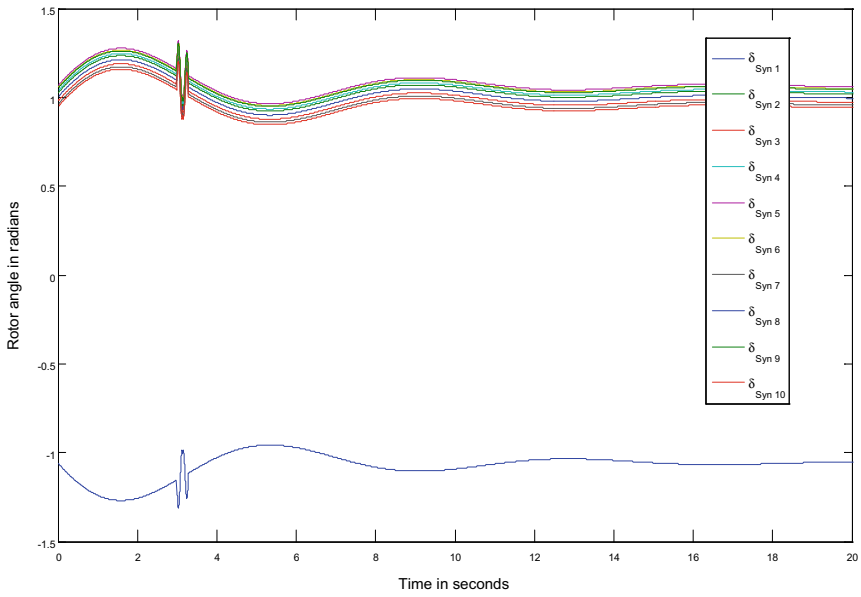
added on the rotor side which is possible in DFIG (slip ring) based wind turbines and this method is known as rotor resistance control. In this section rotor, the resistance control method is used to enhance the TS of the RTS 24 bus system. This is the usual practice in the case of a wound rotor (slip ring) induction generator to improve torque-slip controllability. In this method, an external resistor is added to the rotor windings through a power electronic converter. Adding external resistance on the rotor side causes more losses. So, resistance should be selected optimally to improve TS as well as considering losses. In the present work, external resistance is changed with different values and finally fixed at 50% of the original value. Studies are conducted on DFIG integrated RTS 24 bus system and results are discussed below. The rotor resistance has been modified from 0.01 to 0.015 p.u, and all other parameters remain unchanged in the waveforms shown below.

Figure 7 depicts the rotor angle enhancements with rotor resistance control of RTS 24 bus system, fault at bus 11. Figure 7a presents the rotor angle enhancements with R_s is 0.01 p.u, X_s is 0.10 p.u, R_r is 0.01 p.u and X_r is 0.08 p.u. Figure 7b presents the rotor angle enhancements with R_s is 0.01 p.u, X_s is 0.10 p.u, R_r is 0.015 p.u and X_r is 0.08 p.u. In Fig. 7, the maximum rotor angle is 1.4 radians (approximately) before adjustment of rotor resistance (from Fig. 7a) and after rotor resistance modification maximum rotor angle is limited to 1.3 radians (from Fig. 7b).

Figure 8 depicts the angular speed enhancements with rotor resistance control of RTS 24 bus system, fault at bus 11. Figure 8a presents the angular speed enhancements with R_s is 0.01 p.u, X_s is 0.10 p.u, R_r is 0.01 p.u and X_r is 0.08 p.u. Figure 8b presents the angular speed enhancements with R_s is 0.01 p.u, X_s is 0.10 p.u, R_r is

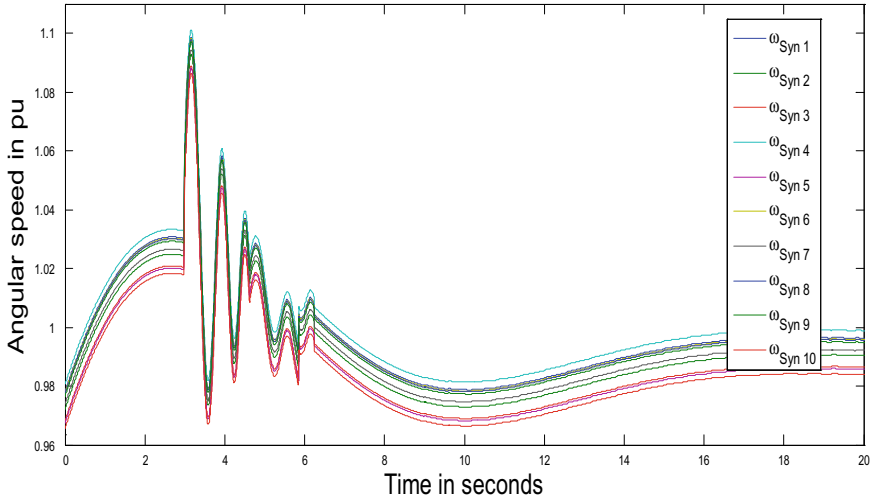


(a)

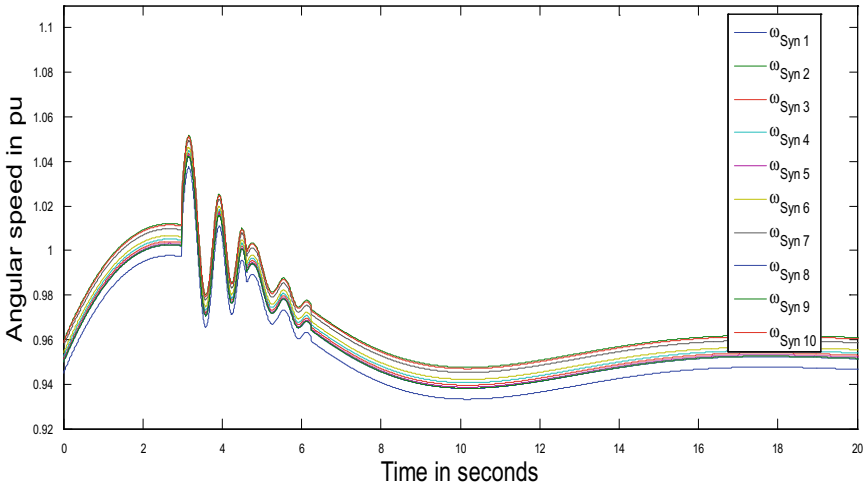


(b)

Fig. 7 Rotor angle enhancements with rotor resistance control of RTS 24 bus system, fault at bus 11



(a)



(b)

Fig. 8 Angular speed enhancements with rotor resistance control of RTS 24 bus system, fault at bus11

0.015 p.u and X_r is 0.08 p.u. In Fig. 8, the synchronous machine angular speed is 1.1 p.u before adjustment of rotor resistance (from Fig. 8a) and after modification of rotor resistance, it is less than 1.06 p.u (from Fig. 8b).

Figure 9 depicts the bus angle enhancements with rotor resistance control of RTS 24 bus system, fault at bus 11. Figure 9a presents the bus angle enhancements with R_s is 0.01 p.u, X_s is 0.10 p.u, R_r is 0.01 p.u and X_r is 0.08 p.u. Figure 9b presents the bus angle enhancements with R_s is 0.01 p.u, X_s is 0.10 p.u, R_r is 0.015 p.u and X_r

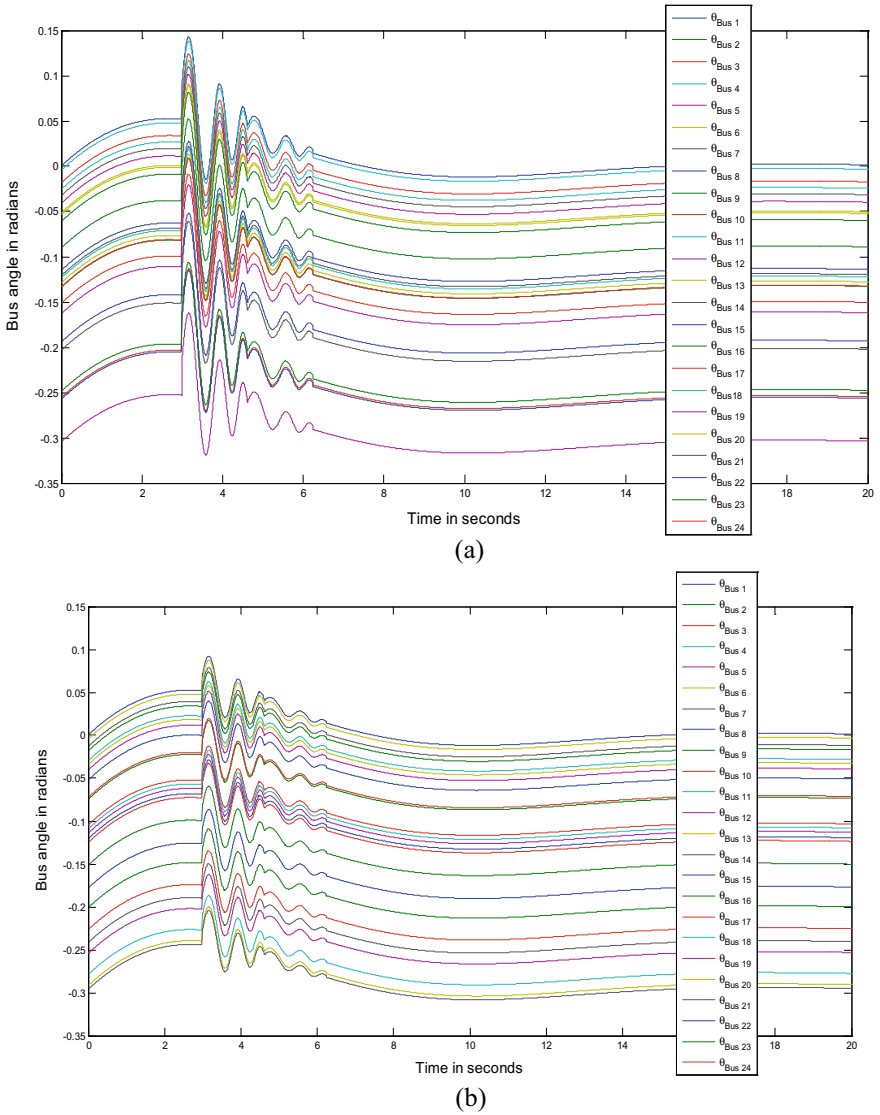


Fig. 9 Bus angle enhancements with rotor resistance control of RTS 24 bus system, fault at bus 11

is 0.08 p.u. In Fig. 9, bus angles peak values are near to 0.15 radians with R_r is 0.01 p.u (from Fig. 9a) and 0.1 radians after adding external rotor resistance to 0.015 p.u (from Fig. 9b).

The above case studies on test systems conclude that an increase in rotor resistance improves the TS of the system. This is because of the proportionality of the damping ratio with the resistance. As the damping ratio of the system increases the maximum

peak overshoot and the oscillations of the system reduce thereby improving the TS of the system. After execution of power flow, time-domain simulation has been carried out for the 20 s. A fault is applied at $t = 3$ s to evaluate system transient stability and fault is cleared at 50 ms. In DFIG wind turbine addition of external resistance has improved system transient stability and the system could reach steady-state quickly as damping ratio is enhanced due to proportional relationship with the external resistance being added.

5 Conclusions

This chapter presents the transient stability (TS) analysis of power systems by incorporating the wind energy generators by Power System Analysis Toolbox (PSAT) software. The detailed mathematical modeling of DFIG is also presented in this work. In DFIG, the control action is performed by using a power electronic-based converter that can be controlled by using rotor frequency, and hence the rotor speed. With the help of this converter, the DFIG can import or export the reactive power support from the main grid, and it has rotor-side control as well as power electronics-based control. These controlling methods make DFIG wind turbines efficient. Further, in DFIG wind turbine addition of external resistance has improved system transient stability and the system could reach steady-state quickly as damping ratio is enhanced due to proportional relationship with the external resistance being added. In the proposed TS analysis, rotor angle variation, rotational speeds of individual generators, bus voltages, and angles at all buses are analyzed. Simulation results are performed on the RTS-24 bus system. All the obtained results are visualized with graphical representation. It can be observed from the results that the deviations in the rotor angle are low in magnitude and can show better damping by using the DFIG. As time progresses, for the generator rotational speeds and voltage at individual busses, the oscillations, and maximum peak values have reduced in the case of DFIG. Wind power integration studies including the energy storage systems are the scope for future research work.

Acknowledgements This research work was funded by “Woosong University’s Academic Research Funding—2021”.

References

1. Karami ESZ (2013) Transient stability assessment of power systems described with detailed models using neural networks. *Int J Electr Power Energy Syst* 45(1):279–292. <https://doi.org/10.1016/j.ijepes.2012.08.071>
2. Lei Y, Mullane A, Lightbody G, Yacamini R (2006) Modeling of the wind turbine with a doubly fed induction generator for grid integration studies. *IEEE Trans Energy Convers* 21(1):257–264. <https://doi.org/10.1109/TEC.2005.847958>

3. Ullah NR, Thiringer T (2007) Variable speed wind turbines for power system stability enhancement. *IEEE Trans Energy Convers* 22(1):52–60. <https://doi.org/10.1109/TEC.2006.889625>
4. Goudarzi N, Zhu WD (2013) A review on the development of wind turbine generators across the world. *Int J Dyn Control* 1:192–202. <https://doi.org/10.1007/s40435-013-0016-y>
5. Li H, Chen Z (2008) Overview of different wind generator systems and their comparisons. *IET Renew Power Gener* 2(2):123–138. <https://doi.org/10.1049/iet-rpg:20070044>
6. Thomas PC, Sreerenjini K, Pillai AG, Cherian VI, Joseph T, Sreedharan S (2013) Placement of STATCOM in a wind integrated power system for improving the load ability. In: *IEEE international conference on power, energy and control, Dindigul, India*, pp 110–114. <https://doi.org/10.1109/ICPEC.2013.6527633>
7. Buch H, Bhagiya RD, Shah BA, Suthar B (2011) Voltage profile management in restructured power system using STATCOM. In: *Nirma University international conference on engineering, Ahmedabad, India*, pp 1–7. <https://doi.org/10.1109/NUIConE.2011.6153279>
8. Muljadi E, Nguyen TB, Pai MA (2008) Impact of wind power plants on voltage and transient stability of power systems. In: *IEEE energy 2030 conference, Atlanta, GA, USA*, pp 1–7. <https://doi.org/10.1109/ENERGY.2008.4781039>
9. Devaraj D, Jeevajyothi R (2011) Impact of wind turbine systems on power system voltage stability. In: *IEEE international conference on computer, communication and electrical technology, Tirunelveli, India*, pp 411–416. <https://doi.org/10.1109/ICCET.2011.5762510>
10. Azizi AH, Rahimi M (2018) Dynamic performance analysis, stability margin improvement and transfer power capability enhancement in DFIG based wind turbines at weak ac grid conditions. *Int J Electr Power Energy Syst* 99:434–446. <https://doi.org/10.1016/j.ijepes.2018.01.040>
11. Akhbari A, Rahimi M (2020) Control and stability analysis of DFIG wind system at the load following mode in a DC microgrid comprising wind and microturbine sources and constant power loads. *Int J Electr Power Energy Syst* 117. <https://doi.org/10.1016/j.ijepes.2019.105622>
12. Prajapat GP, Senroy N, Kar IN (2018) Modeling and impact of gear train backlash on performance of DFIG wind turbine system. *Electr Power Syst Res* 163(A):356–364. <https://doi.org/10.1016/j.epsr.2018.07.006>
13. Morshed MJ, Sardoueinassab Z, Fekih A (2019) A coordinated control for voltage and transient stability of multi-machine power grids relying on wind energy. *Int J Electr Power Energy Syst* 109:95–109. <https://doi.org/10.1016/j.ijepes.2019.02.009>
14. Bhukya J, Mahajan V (2019) Optimization of damping controller for PSS and SSSC to improve stability of interconnected system with DFIG based wind farm. *Int J Electr Power Energy Syst* 108:314–335. <https://doi.org/10.1016/j.ijepes.2019.01.017>
15. Pillai AG, Thomas PC, Sreerenjini K, Baby S, Joseph T, Sreedharan S (2013) Transient stability analysis of wind integrated power systems with storage using central area controller. In: *IEEE international conference on microelectronics, communications and renewable energy*, pp 1–5. <https://doi.org/10.1109/AICERA-ICMiCR.2013.6575991>
16. Ouyang H, Li P, Zhu L, Hao Y, Xu C, He C (2012) Impact of large-scale wind power integration on power system transient stability. In: *IEEE international conference on innovative smart grid technologies*, pp 1–6. <https://doi.org/10.1109/ISGT-Asia.2012.6303130>
17. Lopez YU, Navarro JAD (2008) Small signal stability analysis of wind turbines with squirrel cage induction generators. In: *IEEE international conference on transmission and distribution conference and exposition, Bogota, Colombia*, pp 1–10. <https://doi.org/10.1109/TDC-LA.2008.4641779>
18. Petersson TT, Harnefors L, Petru T (2005) Modeling and experimental verification of grid interaction of a DFIG wind turbine. *IEEE Trans Energy Convers* 20(4):878–886. <https://doi.org/10.1109/TEC.2005.853750>
19. Kadri A, Marzougui H, Aouiti A, Bacha F (2020) Energy management and control strategy for a DFIG wind turbine/fuel cell hybrid system with super capacitor storage system. *Energy* 192. <https://doi.org/10.1016/j.energy.2019.116518>
20. Xiong L, Li P, Wu F, Ma M, Khan MW, Wang J (2019) A coordinated high-order sliding mode control of DFIG wind turbine for power optimization and grid synchronization. *Int J Electr Power Energy Syst* 105:679–689. <https://doi.org/10.1016/j.ijepes.2018.09.008>

21. Zhang T, Yao J, Pei J, Luo Y, Zhang H, Liu K, Wang J (2020) Coordinated control of HVDC sending system with large-scale DFIG-based wind farm under mono-polar blocking fault. *Int J Electr Power Energy Syst* 119. <https://doi.org/10.1016/j.ijepes.2020.105943>
22. Jerin ARA, Prabaharan N, Palanisamy K, Umashankar S (2017) FRT capability in DFIG based wind turbines using DVR with combined feed-forward and feed-back control. *Energy Proc* 138:1184–1189. <https://doi.org/10.1016/j.egypro.2017.10.233>
23. Gebru FM, Khan B, Alhelou HH (2020) Analyzing low voltage ride through capability of doubly fed induction generator based wind turbine. *Comput Electr Eng* 86. <https://doi.org/10.1016/j.compeleceng.2020.106727>
24. Yao J, Pei J, Xu D, Liu R, Wang X, Wang C, Li Y (2018) Coordinated control of a hybrid wind farm with DFIG-based and PMSG-based wind power generation systems under asymmetrical grid faults. *Renew Energy* 127:613–629. <https://doi.org/10.1016/j.renene.2018.04.080>
25. Adetokun BB, Muriithi CM, Ojo JO (2020) Voltage stability assessment and enhancement of power grid with increasing wind energy penetration. *Int J Electr Power Energy Syst* 120. <https://doi.org/10.1016/j.ijepes.2020.105988>
26. Hossain MdE (2017) Performance analysis of diode-bridge-type non-superconducting fault current limiter in improving transient stability of DFIG based variable speed wind generator. *Electr Power Syst Res* 143:782–793. <https://doi.org/10.1016/j.epsr.2016.09.020>
27. Okedu KE (2017) Augmenting DFIG wind turbine transient performance using alternative voltage source T-type grid side converter. *Renew Energy Focus* 18:1–10. <https://doi.org/10.1016/j.ref.2017.02.004>
28. Milano F (2005) Power system analysis toolbox. Version 1.3.4, software and documentation, July 14, 2005

Design and Analysis of BLDC Motor Driver for Hybrid Electric Vehicles



Seong-Cheol Kim, Narasimha Sangam, Sravanthi Pagidipala,
and Surender Reddy Salkuti

Abstract This chapter presents the design and analysis of brushless DC (BLDC) motor driver for hybrid electric vehicles. Due to the combustion of petroleum, it is going to create a pollution problem. Therefore, it is needed that alternating energy resources for petroleum reserves which are exhaustible in potential are required to be determined. The majority of the automobiles right now are reliant on internal combustion engines (ICEs) for the operation and it the root cause of worry since they are accountable for smog. Therefore, the automobile companies are searching for alternate energy sources which could decrease pollution. As a result of arising pollution issue, the hybrid electric-powered vehicles are important for long term planning. The brushed DC machine works on a setup of wound wire coils and armature which acts as a two-pole electromagnet. The brushless DC machine, by comparison, uses a lasting magnet as it has an outside rotor. Additionally, it runs on 3 phases of coils along with a special sensor that monitors the rotor position. This chapter presents the relative evaluation of the electric vehicle (EV) that is powered by brushless DC (BLDC) motor and the corresponding impact on the state of ripples and charge in the DC voltage at the battery power. This comparison has been carried in the MATLAB application and the outcomes are explained clearly in the results section.

Keywords Brushless DC motor · Hybrid electric vehicles · DC-DC converters · Pulse width modulation · Regenerative energy · Voltage source converter

S.-C. Kim · S. R. Salkuti (✉)

Department of Railroad Electrical Systems, Woosong University, Daejeon 34606, Republic of Korea

e-mail: surender@wsu.ac.kr

N. Sangam

Department of Electrical and Electronics Engineering, TKR College of Engineering and Technology, Hyderabad, India

e-mail: sangamnarsimha@tkrcet.com

S. Pagidipala

Department of Electrical Engineering, National Institute of Technology Andhra Pradesh (NIT-AP), Andhra Pradesh, India

Nomenclature

BEV	Battery electric vehicle
BLDC	Brushless direct current
CO	Carbon monoxide
CO ₂	Carbon dioxide
EVs	Electric vehicles
ICE	Internal combustion engine
HEV	Hybrid electric vehicles
RBS	Regenerative braking system
PID	Proportional integral derivative
FLC	Fuzzy logic control
Li-ion	Lithium-ion
SOC	State of charge
PHEVs	Plug-in hybrid electric vehicles
NiMH	Nickel–Metal Hydride
VSI	Voltage Source Inverter
PWM	Pulse Width Modulation
SPWM	Sinusoidal pulse width modulation
VSC	Voltage Source Converters
IGBTs	Insulated gate bipolar transistors

1 Introduction

The transportation sector is growing rapidly throughout the world and it mostly depends on oils. The fossil fuels utilized in mainstream automobile will release various greenhouse gases such as carbon monoxide (CO), carbon dioxide (CO₂), and methane. The exorbitant of gases causes pollution associated with the environmental surroundings, climate modification, and warming. To reduce these affects, automobile industry is now certainly moving towards the electric vehicle (EV) technology [1, 2]. The electric vehicles (EVs) have reduced fuel price in conformity with fossil-fueled automobiles since they are primarily built with battery pack systems. The battery power coordination in an EV is the large amount of element this is certainly important in determining the distance. The electrical automobiles are trusted for pollution free transportation environment as they operate with an electrical battery [3]. In order to increase the distance travelled by the EVs and to increase the recapturing of the regenerative energy, one must enhance the performance of all components utilized in the EVs such as electric engine, energy converter, and power storage system, i.e., battery power or ultracapacitor.

In recent years, EVs have drawn much attention as compared to conventional internal combustion engine (ICE) vehicles. This contemplation is due to the economic and environmental troubles concerns linked with the utilization of natural gas and

petroleum fuels, and these are used as fuel in ICE vehicles. More advancement and researches on vehicles like fuel cell and hybrid cars, pure battery powered EVs, etc. are pursued actively [4]. Owing to the facts that these vehicles are reasoned to serve as an efficient means to deal with global warming caused by the tail pipe-auto emissions. In the case of eco vehicles, the compatibility between safety and running performance has to be ensured especially in the case of EVs where electric devices like batteries, converters and inverters are part of their propulsion force producing system. If such an electric device fails during the motion of the EV, the EVs shall fail to run safely and comfortably. This kind of failure in motion may constitute series traffic accidents like rear end collisions. As an advancement for developing the next generation of EVs, fail safe functions must be interlinked within the propulsion force generating system, there by the EV can persist to run safely even if malfunctions occurs during EV motion [5]. The hybrid electric vehicles (HEV), which mainly contains at a minimum of two sources of power, first one is a primary power source and the other one is named as secondary power source, which have the favors of both the EV and conventional ICE vehicles also had the ability to vanquish their disadvantages.

1.1 Related Work

Unlike the conventional vehicles, the running capability of battery electric vehicle (BEV) depends completely on the electric motor and battery unit; as there is no involvement of traditional ICEs. In order to recharge the battery to a sufficient amount, it should be plugged with an external electricity source [6, 7]. It can also be recharged by regenerative braking process like all EVs. These vehicles have the merits like no emissions, gases, free from compulsory oil changes, comparatively low cost of running, fast and real smooth acceleration, and also have the capacity to conveniently charge at home. But it also have the demerits like shorter range than gasoline vehicles and moderately expensive than its gasoline equivalent despite the fact that within the span of 2–3 years the gasoline savings will pay off.

Reference [8] reviews the technology and applications of electrical vehicles. It critically appraises the level of state-of-the-art research improvements in this industry developed in the last decade. It also highlights the technical issues of automobile technology. Reference [9] presents which converter or drive is suitable for the electric car. Regenerative stopping can improve power usage efficiency which in turn improves the driving distance of electric automobiles. The importance and characteristics of regenerative braking system (RBS) has been presented in the reference [10]. The RBS is adjusted to DC that is brushless BLDC engine, and it emphasizes in the circulation with this particular force that is powerful in stopping alongside BLDC motor control. In this work, BLDC motor control uses proportional integral derivative (PID) control; consequently, the flow of stopping force uses the fuzzy logic control (FLC). The braking torque could be managed in real-time by PID control because it is certainly slower than PID control.

Reference [11] has designed the effectiveness of DC engine which is highly inexpensive. The controller takes input that is individual manage the rate and drives the engine at that rate regardless of load. This permits fast, smooth motor response. A converter drives the motor by utilizing the power through the battery pack. Reference [12] is targeted at the optimization of core size power inductors in bidirectional DC-DC converters. It describes a characterization that is certainly experimental are large-signal for energy inductors in EV applications and an answer getting an inductance guide value when it comes to ability inductor in DC-DC converters simulation studies. A prototype of one kilowatt inductive wireless power transfer power converters with high frequency supply is modeled in reference [13]. Reference [14] proposes the modeling and evaluation of sizing of battery pack required by using the Simpson in R Studio.

1.2 Motivation and Contributions

This chapter provides the comparative analysis of DC machine powered electric vehicle and BLDC powered electric vehicle, and the corresponding effect on state of charge and ripples in the dc voltage at the battery. This comparison is carried out in the MATLAB software and the comparative results are given individually. The objective of this work is to provide a better percentage of the state of charge (SOC) to make the design much better and efficient. This work discusses the concerns related to the battery storage systems, their types along with their benefits and drawbacks. Also describes the types of converters and primarily DC-DC converters, their advantages, and just how they are found in this task is certainly proposed. Simulation results and analysis linked to the proposed work are also discussed. In short, the main objectives are to provide better SOC, much better design, improved efficiency, and less maintenance.

Organization of this chapter: In Sect. 2, the description and classification of battery storage system is presented. Section 3 describes the modeling of DC-DC converter. In Sect. 4, simulation results are described. In the last section, the whole chapter is concluded.

2 Battery Storage System

Generally, there are two types of batteries, primary and secondary. Normally, the standards for the secondary/rechargeable batteries rate the capacity over a 4, 8 h, or even longer discharge times. The lithium-ion (Li-ion) battery is used in the design of this hybrid EV due to its low cost and good performance and light weight [15]. It has a nominal voltage of 350 V and an initial state of charge (SOC) of 88%. A power kit is some sort of computer product comprising a genuine degree of electrochemical cells with outside junctions for powering devices which might be electric as flashlights,

cellular phones, and automobiles that happen to be electric. These cells are wet electrolytes fluids that are vulnerable to leakage and spillage [16]. Batteries convert chemical power directly to provide power that is electric.

The various energy sources like batteries, ultracapacitors and flywheels of EVs can retrieve and store regenerative energy effectively. Energy management subsystem unit along with vehicle controller unit processes the energy recovery and there by the regeneration process is controlled. In order to monitor the energy source usability and regulate the refueling, the energy refueling unit is utilized. For every EV auxiliaries including climate control and power steering unit, and the sufficient power with various voltage levels are delivered by the auxiliary power supply subsystem.

In plug-in hybrid electric vehicles (PHEVs), batteries reflect as the greatest means of source of energy. To accomplish the “all electric driving range” insistence the powertrains of PHEV's should carry large number of high rated battery packs with abundant energy and superior power density. Energy supplied from the high rated battery pack should be adequate enough for the impulses to sustain the continuous speed range [17]. Through within the all electric driving range the batteries also need to deliver power to the auxiliaries like air conditioning unit or power steering unit etc. But the use of large quantities of onboard high rated batteries bring up the questions about safety regarding with chances of fire threat, accidents or even the possibilities of short circuit during either operation cannot be avoided. It creates another critical situation; there by the selection of battery technology is highly crucial in consideration with their efficiency, price, and authenticity. The mostly acknowledged batteries in PHEVs are currently Lithium-ion (Li-ion) batteries. They can dispense sufficient-energy density and highly demanded-power density for the batteries of equal weight, and ensures wider all electric drive range with best ever performance of vehicle. One of the other kinds of commercialized battery for PHEVs is Nickel–Metal Hydride (NiMH) batteries.

The EVs are designed to steer with high voltage electrical energy stored batteries. By this way the exhaust emissions can be excluded which further reduces the air pollution since gasoline or other fossil fuels are not required for the propulsion. During the entire driving range, the noises and vibrations from engine is negligibly small in comparison with traditional ICEs. The electric motor employed in EVs is generally higher performance motors [18]. During the downhill or decelerating motion of the said vehicle the restoring of brake energy by regeneration can be employed and will be stored to the high voltage batteries. There by the driving range from single charging will be extended and also reduce the loss during the braking. In case existing charge of battery is not adequate to drive the vehicle, various charging methods like AC or DC charge is applied. The trickle charge can also be applied.

The incorporation of an ICE with electric motor is the most widely used combo for the generation of propulsion force in hybrid EVs. With this integration, energy efficiency will be improved and vehicle emissions will be fall off due to the electric motor and driving range will extended because of the ICE. The stereotypical ICE vehicles show good performances along with large operating range clearly because of the high energy-density yielded by the petroleum products. But these common ICE vehicles have the disadvantage of indigent fuel economy and greater risks of

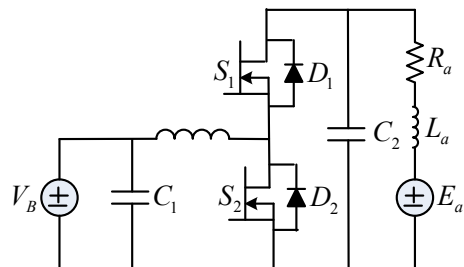
environmental contamination [19]. By far the reasons behind their indigent fuel economy are the contrast between real operation requirements and the vehicles fuel expertise, operating in urban areas, the wastage of kinetic energy during braking, and due to the stop and go driving pattern the productivity of hydraulic transmission in current day automobiles.

The existent EVs powered by battery packs have dominance over typical ICE vehicles by high energy productivity and almost zero environmental contamination. The comparison of these vehicles based on the performance of their driving range per battery charge ICEs hold the upper hand. However, due to the use of two power sources, hybrid electric vehicles can outsmart both traditional ICEs and EVs.

3 DC-DC Converter

The power electronic devices in PHEVs comprises of inverters, converters can be bidirectional or unidirectional, chargers etc. The inverter serves to transfer the battery DC power in to the required AC power for propulsion of electric motor(s). Another important fact is that, with the motor drive power electronic components, the retrieval of regenerative energy and their storage in batteries are possible. Diverse numbers of DC-DC converters are beneficial for applications that require multiple voltage levels [20]. In contemplation of regenerative energy storage in to battery bidirectional power flow has to be ensured regarding with the converter. Apart from these AC to DC converters are essential for battery chargers, as they transfigure the AC power flow of grid to suitable DC power to charge the battery unit. To achieve high efficiency batteries programmable digital controllers having proper voltage and current profiles are needed along with proper power factor correction. Figure 1 depicts the buck-boost converter connected with DC machine. The fuzzy logic control (FLC) finds the duty cycle of S_1 and S_2 to ensure the charge and discharge of battery. Buck-boost converter is a kind of DC-to-DC converter which contains a manufacturing voltage magnitude that is often more than or perhaps much less in comparison with the voltage magnitude of input, and this is equivalent to a flyback converter working with an inductor [21, 22].

Fig. 1 Buck-boost converter connected with DC machine



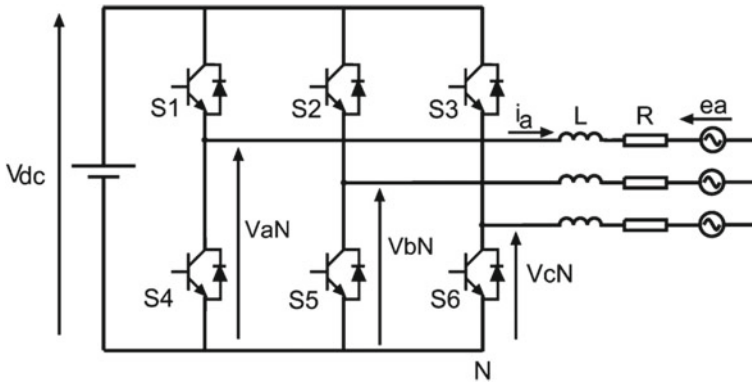


Fig. 2 The schematic diagram of VSI

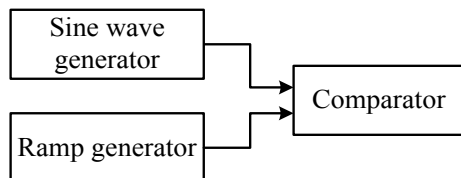
3.1 Voltage Source Inverter (VSI)

The main purpose of VSI is to convert a constant DC voltage into an AC voltage with variable magnitude and frequency. The VSI maintains a fixed polarity of DC voltage, and the reversal of power can be obtained without reversing the direction of the current. The schematic view of VSI is depicted in Fig. 2.

3.2 Pulse Width Modulation (PWM)

It is a modulation technique which is used to encode a pulsating signal. The switching frequency of PWM is much higher than what would affect the load. By doing that the resultant waveform is as smooth as possible [23, 24]. The main advantages of using PWM are cheap to create, consumes less energy, use of high frequencies (around 40 to 100 kHz), extremely efficient in energy-smart while dimming the radiant light or perhaps in voltage conversions, high control ability of power and high efficiency, i.e., around 90%. A modulation strategy is helpful to encode a communication as an illustration that is pulsing. This modulation strategy assists to encode information for transmission, and it allows the control related to the power supplied which could be electrical products and services. Figures 3 and 4 depict the block diagram and

Fig. 3 SPWM block diagram



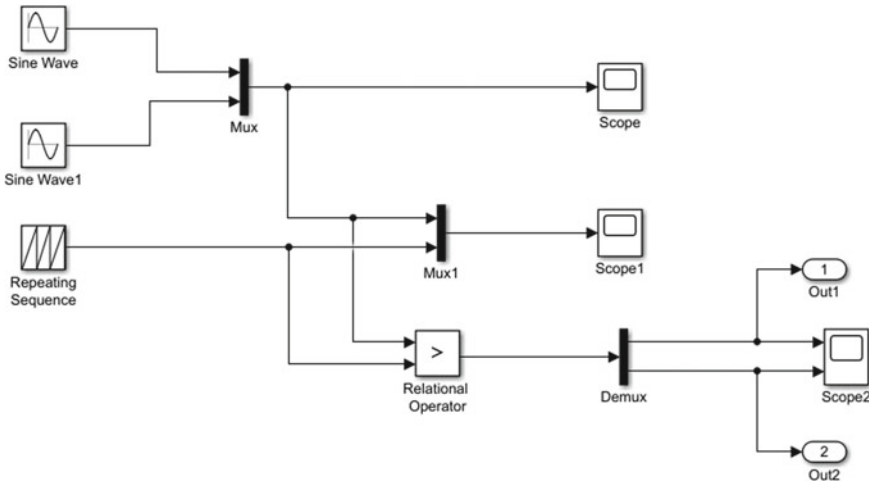


Fig. 4 SPWM simulation diagram

simulation diagram of sinusoidal pulse width modulation (SPWM). The (ON and OFF time frames) period of pulse is continuous. The (ON time and OFF period) about the pulse is called period with this pulse, and the ratio attached with the time that is full punctually that is from the period is named as duty cycle.

3.3 Voltage Source Converters (VSC)

The polarity of a DC voltage is typically fixed and it is smoothed by using a capacitance [14, 25]. Because of this, an HVDC converter utilizing insulated gate bipolar transistors (IGBTs) is often known as a voltage source converter (VSC). The controllability introduces several benefits; particularly the ability to change the ON/OFF status of IGBT's a couple of times per duration to have the ability to enhance harmonic performance. A two-level converter can function as the type that is most basic of three-phase VSC and will undoubtedly be seen as a six pulse bridge [26, 27]. Figure 5 depicts the two-level VSC for HVDC.

Some HVDC methods were constructed with three-level converters to improve the negative performance are harmonic the converter is unquestionably two-level. The three-level converters can synthesize 3 (instead of just two) discrete voltage quantities while in the AC terminal of the phase [28]: $+\frac{1}{2}U_d$, zero, $-\frac{1}{2}U_d$. Here, a common type of the converter is used [29], i.e., diode clamped converter with 4 IGBT valves in each phase.

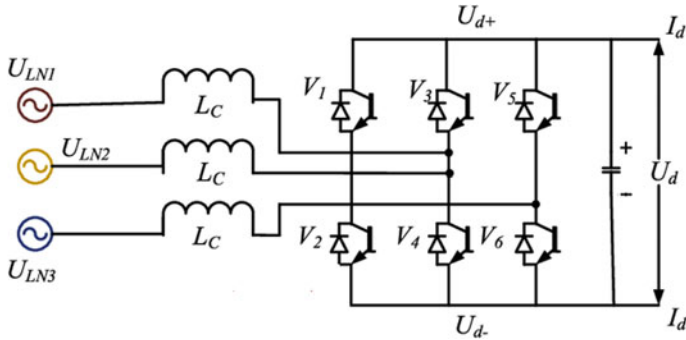


Fig. 5 Two-level VSC for HVDC

4 Results and Discussion

Batteries of PHEVs are charged with the assistance of EV supply equipment (EVSE), i.e., charging stations. The charging stations communicate along with vehicles to guarantee that electricity flows in to the system will be shielded and pertinent. The classifications of EVSE in plug-in vehicles are elicited from the rate at which batteries will charge. The two major kinds of EVSE are ‘AC level 1’ and ‘AC level 2’, which will be able to supply the vehicle with alternating current. The vehicle is equipped with an on board electrical equipment/charger which transfer AC to DC for charging the vehicle battery [30, 31]. DC fast charging might also appropriate for direct DC supply to automobile, simply named as DC level 2.

Converter circuit configuration of hybrid electric vehicle (HEV) using DC machine has been depicted in Fig. 6. The duty ratio is produced by fuzzy logic control (FLC) with ramp revolution of changing and hence the pulse created for

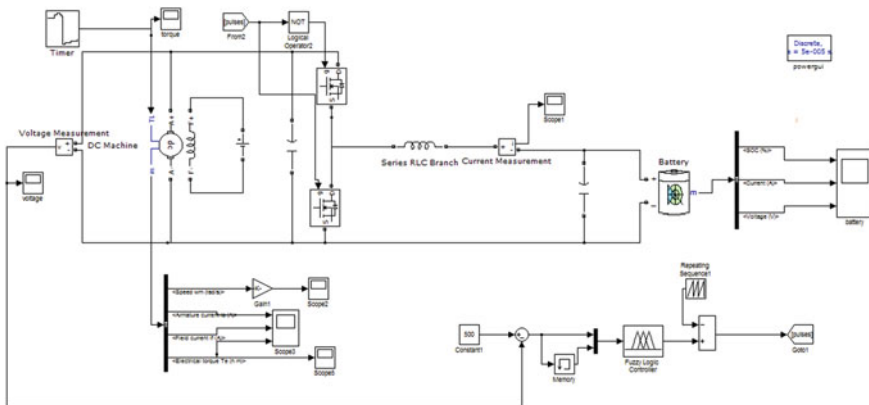


Fig. 6 Converter circuit configuration of hybrid electric vehicle using DC machine

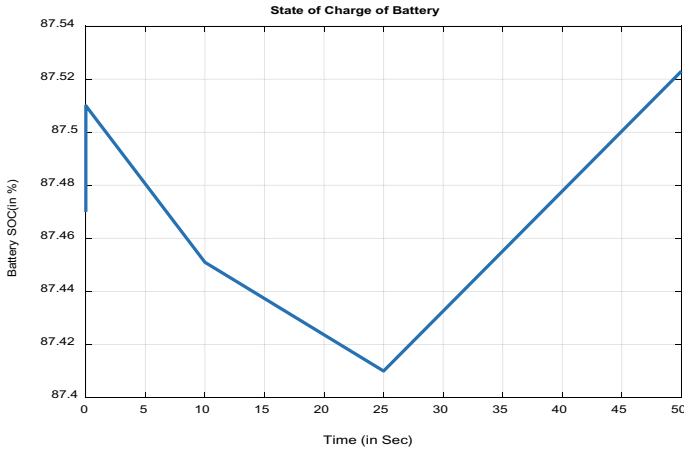


Fig. 7 Battery SOC (in %)

semiconductor switch to the group of zero and 25 moments. DC unit voltage is elevated on the worthiness that is needed.

The battery energy state of charge (SOC) is improved based on the simulation outcome. In the EV, the regenerative braking has happened in this state. The charge and also the discharge states of this particular battery energy are required for determining the distance of travel. Figure 7 depicts the plot of battery SOC (in percentage) versus time for the converter system with DC machine. The output waveforms of battery voltage and current are depicted in Fig. 8.

The proposed converter system with BLDC motor is simulated and it is shown in Fig. 9. Figure 10 depicts the plot of battery SOC (in percentage) versus time for the converter system with BLDC motor. The output waveforms of battery voltage and current are depicted in Fig. 11. The voltage waveform of BLDC motor has been depicted in Fig. 12.

The DC machines operate in generating mode in the case of battery is charged and also the bi-directional DC-DC converter operates in the buck mode. In the EV, regenerative braking has occurred in this state. In the BLDC machine, when the battery is charged, the machine is operated in generator mode. The battery SOC has been increased from 87.6 to 87.8%. Results being exemplary analysis are acquired straight into the MATLAB and all the simulation results are analyzed for different conditions alongside the SOC, the voltage quantities are also improved.

5 Conclusions

The charging and discharging states of battery plays an important role in determining the distance to travel the electric vehicle. This chapter has presented the design and

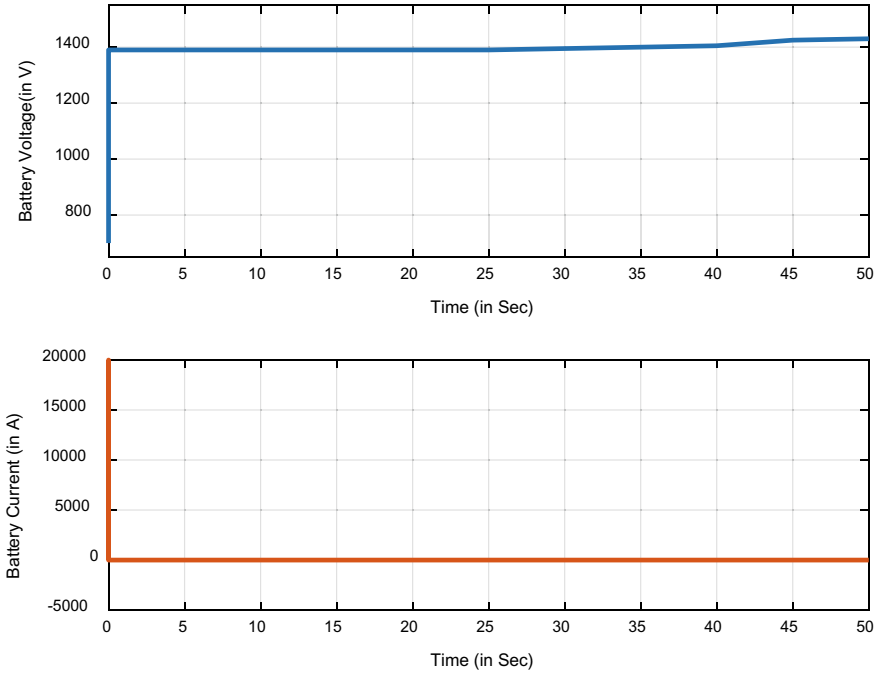


Fig. 8 Battery voltage and current versus time

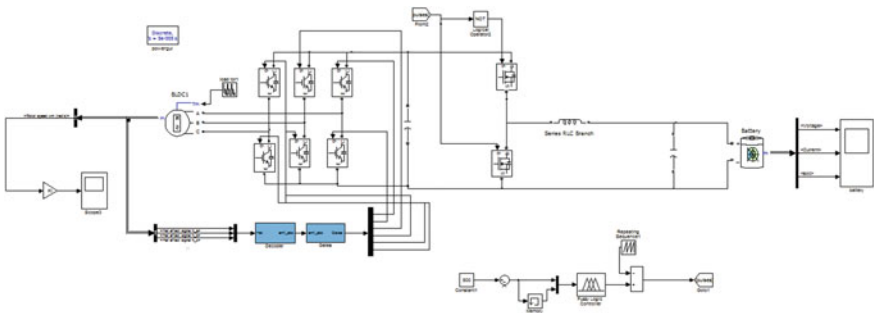


Fig. 9 Proposed converter system with BLDC motor

analysis of brushless DC (BLDC) motor driver for the hybrid electric vehicles. The relative evaluation of the electric vehicle (EV) that is powered by BLDC motor and the corresponding impact on the state of ripples and charge in the DC voltage at the battery power are also presented. This comparison has been carried in the MATLAB application and the outcomes are explained clearly in the results section. Battery pack energy has been enhanced from 87.47 to 87.55% according to the simulation effect. In the all-electric automobile, regenerative braking has occurred. The charge

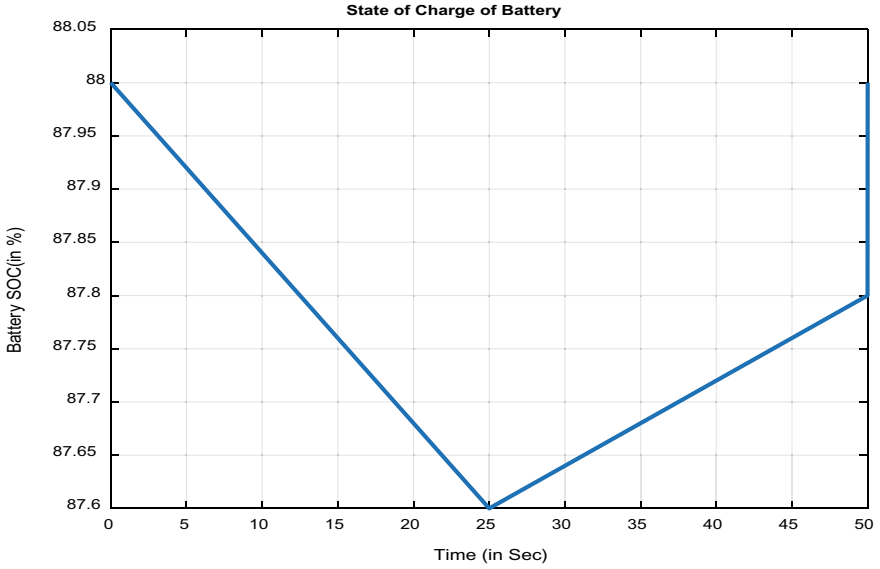


Fig. 10 SOC of battery (in %)

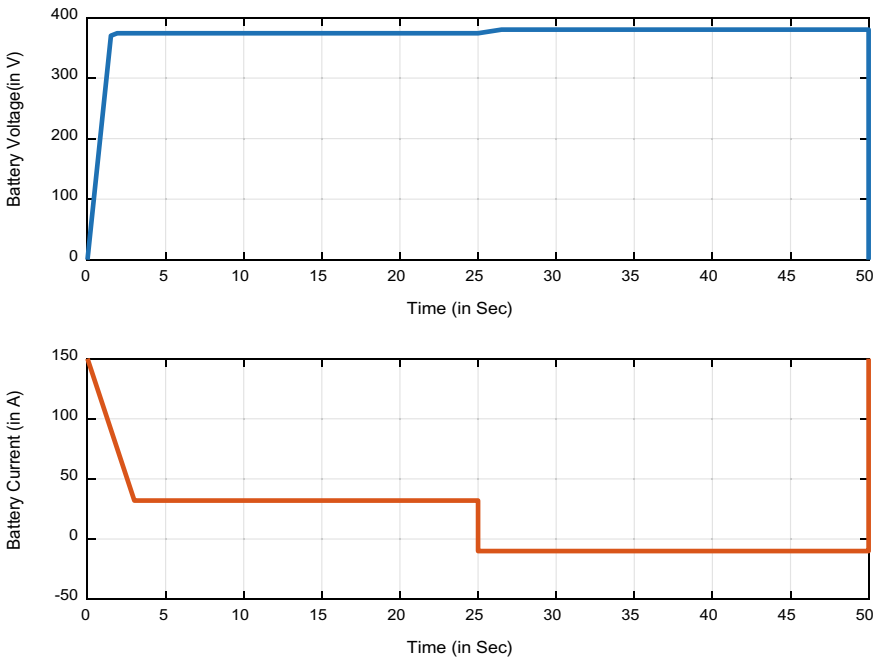


Fig. 11 Battery voltage and current of converter system with BLDC motor

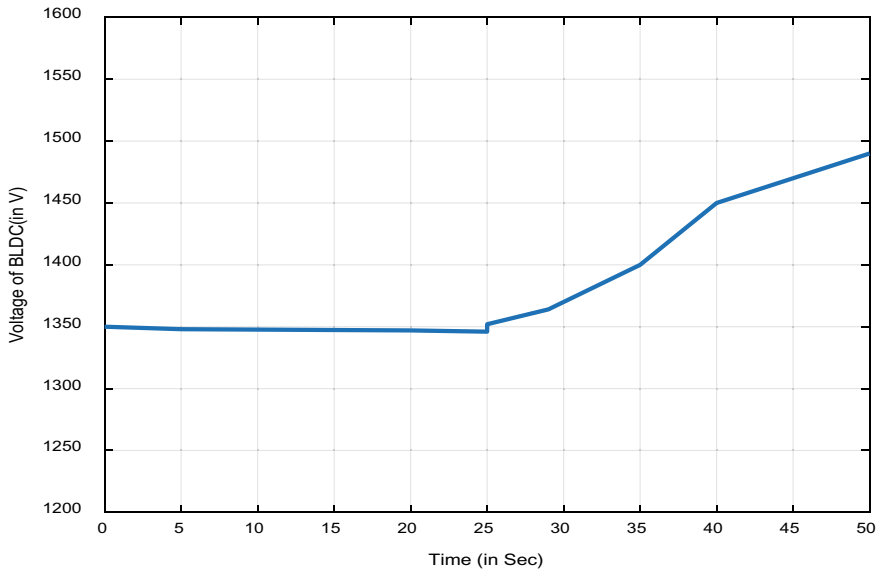


Fig. 12 Voltage of converter system with BLDC machine

and also discharge states of the electric battery may be many needed for distance to determining. If the battery pack is charged, the unit which is dc operated turbine setting and the bi-directional DC-DC converter will be operated in the buck mode. Adjustable torque which is unfavorable is placed about the BLDC device as well as influence the battery pack. Based upon the simulation results, the battery state of charge (SOC) has been improved from 87.6 to 87.8%.

Acknowledgements This research work was funded by “Woosong University’s Academic Research Funding-2021”.

References

1. Metin NA, Boyar A, Kabalci E (2019) Design and analysis of bi-directional DC-DC driver for electric vehicles. In: 1st global power, energy and communication conference (GPECOM), pp 227–232. <https://doi.org/10.1109/GPECOM.2019.8778532>
2. Yong JY, Ramachandaramurthy VK, Tan KM, Mithulananthan N (2015) A review on the state-of-the-art technologies of electric vehicle, its impacts and prospects. *Renew Sustain Energy Rev* 49:365–385. <https://doi.org/10.1016/j.rser.2015.04.130>
3. Zhang J, Shen T (2018) Receding horizon optimal control of PHEV with demanded torque estimation model. *IFAC-PapersOnLine* 51(31):183–187. <https://doi.org/10.1016/j.ifacol.2018.10.034>

4. İnci M, Büyük M, Demir MH, İlbey G (2021) A review and research on fuel cell electric vehicles: topologies, power electronic converters, energy management methods, technical challenges, marketing and future aspects. *Renew Sustain Energy Rev* 137. <https://doi.org/10.1016/j.rser.2020.110648>
5. Kahveci O, Kaya MF (2021) Hydrogen production from Al–Cu alloy using electric vehicle’s waste DC motor coils. *Int J Hydrogen Energy*. <https://doi.org/10.1016/j.ijhydene.2021.06.201>
6. Bayardo RG, Loukianov AG, Fuentes-Aguilar RQ, Utkin VI (2020) Adaptive speed tracking controller for a brush-less DC motor using singular perturbation. *IFAC-PapersOnLine* 53(2):3880–3885. <https://doi.org/10.1016/j.ifacol.2020.12.2100>
7. Aliasand AE, Josh FT (2020) Selection of motor foran electric vehicle: a review. *Mater Today: Proc* 24(3):1804–1815. <https://doi.org/10.1016/j.matpr.2020.03.605>
8. Zhang F, Zhang X, Zhang M, Edmonds ASE (2016) Literature review of electric vehicle technology and its applications. In: 5th international conference on computer science and network technology, pp 832–837. <https://doi.org/10.1109/ICCSNT.2016.8070276>
9. Tiwari A, Jaga OP (2017) Component selection for an electric vehicle: a review. In: International conference on computation of power, energy information and communication (ICCPEIC), pp 492–499. <https://doi.org/10.1109/ICCPEIC.2017.8290416>
10. Nian X, Peng F, Zhang H (2014) Regenerative braking system of electric vehicle driven by brushless DC motor. *IEEE Trans Ind Electron* 61(10):5798–5808. <https://doi.org/10.1109/TIE.2014.2300059>
11. Haishui Z, Dahu W, Tong Z, Keming H (2010) Design on a DC motor speed control. In: International conference on intelligent computation technology and automation, pp 59–63. <https://doi.org/10.1109/ICICTA.2010.795>
12. Perdigoão MS, Trovão JPF, Alonso JM, Saraiva ES (2015) Large-signal characterization of power inductors in EV bidirectional DC–DC converters focused on core size optimization. *IEEE Trans Ind Electron* 62(5):3042–3051. <https://doi.org/10.1109/TIE.2015.2402632>
13. Sandeep V, Shivanand MN, Reddy SS (2021) Design of a one kilowatt wireless charging system for electric vehicle in line with Bharath EV standards. *Int J Emerg Electr Power Syst* 22(3):255–267. <https://doi.org/10.1515/ijeeps-2020-0178>
14. Sandeep V, Shastri S, Sardar A, Salkuti SR (2020) Modeling of battery pack sizing for electric vehicles. *Int J Power Electron Drive Syst* 11(4):1987–1994. <https://doi.org/10.11591/ijpeds.v11i4.pp1987-1994>
15. Cipin R, Mach M, Toman M, Knobloch J (2017) Measurement and evaluation of DC motor starting torque. In: IEEE international conference on environment and electrical engineering and IEEE industrial and commercial power systems Europe, Milan, pp 1–5. <https://doi.org/10.1109/EEEIC.2017.7977475>
16. Suresh K, Arulmozhiyal R (2016) Design and implementation of bi-directional DC-DC converter for wind energy system. *Circuits Syst* 17:3705–3722. <https://doi.org/10.4236/cs.2016.711311>
17. Sandeep V, Shivanand MN, Reddy SS (2021) Design of a one kilowatt wireless charging system for electric vehicle in line with Bharath EV standards. *Int J Emerg Electr Power Syst* 22(3):255–267. <https://doi.org/10.1515/ijeeps-2020-0178>
18. Hur J, Sung HG, Lee BK, Won CY, Lee BH (2006) Development of high-efficiency 42V cooling fan motor for hybrid electric vehicle applications. In: IEEE vehicle power and propulsion conference, pp 1–6. <https://doi.org/10.1109/VPPC.2006.364307>
19. Pothirasan N, Rajasekaran MP, Muneeswaran V (2018) Real time reactive power compensation for battery/photovoltaic hybrid power source for internet of hybrid electric vehicle system. *Cogn Syst Res* 52:473–488. <https://doi.org/10.1016/j.cogsys.2018.07.030>
20. Gupte S (2014) Experimental analysis and feasibility study of 1400 CC diesel engine car converted into hybrid electric vehicle by using BLDC hub motors. *Energy Procedia* 54:177–184. <https://doi.org/10.1016/j.egypro.2014.07.261>
21. Salkuti SR (2021) Energy storage and electric vehicles: technology, operation, challenges, and cost-benefit analysis. *Int J Adv Comput Sci Appl* 12(4):40–45. <https://doi.org/10.14569/IJA.CSA.2021.0120406>

22. Salehifar M, Moreno-Eguilaz M, Putrus G, Barras P (2016) Simplified fault tolerant finite control set model predictive control of a five-phase inverter supplying BLDC motor in electric vehicle drive. *Electr Power Syst Res* 132:56–66. <https://doi.org/10.1016/j.epsr.2015.10.030>
23. Lee BC, Song CH, Kim DH, Kim KC (2020) Study on process derivation and characteristic analysis for BLDC motor design using dual rotor structure with high torque density. *Energies* 13(24):6745. <https://doi.org/10.3390/en13246745>
24. Kim H-J, Park H-S, Kim J-M (2020) Expansion of operating speed range of high-speed BLDC motor using hybrid PWM switching method considering dead time. *Energies* 13(19):5212. <https://doi.org/10.3390/en13195212>
25. Karki A, Phuyal S, Tuladhar D, Basnet S, Shrestha BP (2020) Status of pure electric vehicle power train technology and future prospects. *Appl Syst Innov* 3(35):1–28. <https://doi.org/10.3390/asi3030035>
26. Hassanin MA, Abdel-Kader FE, Amer SI, Abu-Moubarka AE (2018) Operation of brushless DC motor to drive the electric vehicle. In: Twentieth international Middle East power systems conference (MEPCON), pp 500–503. <https://doi.org/10.1109/MEPCON.2018.8635158>
27. Prasetyo HF, Rohman AS, Hariadi FI, Hindersah H (2016) Controls of BLDC motors in electric vehicle testing simulator. In: 6th international conference on system engineering and technology (ICSET), pp 173–178. <https://doi.org/10.1109/ICSEngT.2016.7849645>
28. Salkuti SR (2019) Optimal operation of microgrid considering renewable energy sources, electric vehicles and demand response. *E3S Web Conf* 87:1–6. <https://doi.org/10.1051/e3s/conf/20198701007>
29. Purwadi A, Dozeno J, Heryana N (2013) Testing performance of 10 kW BLDC motor and LiFePO₄ battery on ITB-1 electric car prototype. *Procedia Technol* 11:1074–1082. <https://doi.org/10.1016/j.protcy.2013.12.296>
30. Hwang MH, Lee HS, Yang SH, Cha HR, Park SJ (2019) Electromagnetic field analysis and design of an efficient outer rotor inductor in the low-speed section for driving electric vehicles. *Energies* 12(24):4615. <https://doi.org/10.3390/en12244615>
31. Carev V, Roháč J, Šipoš M, Schmirler M (2021) A multilayer brushless DC motor for heavy lift drones. *Energies* 14(9):2504. <https://doi.org/10.3390/en14092504>

A Novel Approach for Power Quality Improvement in Microgrid



Arvind R. Singh, Papia Ray, and Surender Reddy Salkuti

Abstract This chapter proposes an approach to improve the power quality (PQ) of the three-phase system by manipulating the grid-connected smart Photovoltaic Distribution Static Compensator (PV D-STATCOM) system with the help of a proposed dynamic voltage restorer (DVR) and a reweighted zero attracting (RZA) control technique containing adaptive features with P and O (perturb and observe) approach based maximum power point tracking (MPPT) method. The PV D-STATCOM is having a PV array alongside the quality of active filtering converter is essential to transform DC voltage into its equivalent AC voltage quantity with necessary PQ improvement measures such as harmonic distortion elimination, reactive power compensation in all 3 unbalanced phases of the concerned distribution system and with some other remedial measures. The implementation of the RZA strategy, which is discussed in this chapter, is showing reasonable steady-state behavior and transient responses. The proposed work on grid-connected PV systems can efficiently perform around the clock for constant and variable solar irradiation connected to a comparatively linear load. This approach is smart enough to operate in both modes, such as identifying solar PV power and the capability of bidirectional or multidirectional power flow without manual interventions. The proposed approach is designated as smart as it can automatically accomplish both modes, sensing the PV power and gifted of multidirectional power flow. The proposed system accomplishes the twin role of a PQ refining device by operating as D-STATCOM and by transferring solar power to the consumer and grid acquired from the PV array.

A. R. Singh
School of Electrical Engineering, Shandong University, Jinan, China

P. Ray
Department of Electrical Engineering, Veer Surendra Sai University of Technology (VSSUT),
Burla, Odisha, India
e-mail: papiaray_ee@vssut.ac.in

S. R. Salkuti (✉)
Department of Railroad and Electrical Engineering, Woosong University, Daejeon 34606,
Republic of Korea
e-mail: surender@wsu.ac.kr

Keywords Power quality · PV D-STATCOM · Dynamic voltage restorer · Voltage source inverter · Reactive power · Harmonics

Nomenclature

DG	Distributed Generation
MG	Microgrid
ESS	Energy Storage Systems
PCC	Point of Common Coupling
PV	Photovoltaic
PQ	Power Quality
RESs	Renewable Energy Resources
VSI	Voltage Source Inverter
DERs	Distributed Energy Resources
DVR	Dynamic Voltage Restorer
PV-DSTATCOM	Photovoltaic Distribution Static Compensator
SSC	Static Series Compensator
SVB	Series Voltage Booster
RZA	Reweighted Zero Attracting
AVR	Automatic Voltage Regulator
MPPT	Maximum Power Point Tracking
FFT	Fast Fourier Transform
THD	Total Harmonic Distortion
UPQC	Unified Power Quality Conditioner

1 Introduction

The issues related to power quality are a significant challenge in today's electricity distribution and transmission scenario. The objective of power quality improvement has enforced the introduction of susceptible and complex devices in the vicinity of electrical infrastructure. Nonstandard voltage, disturbing power, and frequency are a few of the power quality-related problems. This power quality problem results in damage or failure of end-user equipment. A microgrid (MG) is a coordinated combination of a group of unpredicted loads, energy storage systems (ESS), and distributed generation (DG) units that operate at the same level of distribution voltage to obtain a harmonious operation [1]. The point of common coupling (PCC) is a concept which indicates the node at which the MG is synchronized with the primary grid. Conventionally the MGs prefer to operate in grid-connected mode to acquire the benefits of a high inertial grid. Despite the choice of having grid connectivity, these MGs hold the potential to feed a sufficient amount of emergency power to the trailing loads even

when the grid is getting disconnected. The progress of traditional microgrids (MGs) has been followed with versatile objectives such as resolving the problem of growing power system efficiency, beneficial exploitation of the unconventional renewable energy resources (RESs) with minimum environmental impact, optimal management of power fluctuation along with other power quality improvement measures, and electrical network extension facilities deprived of violating the classical operating philosophies of conventional distribution systems [2]. For a reliable MG smooth operation, it is necessary to handle some of the most critical problems, such as power quality issues, energy balance, and safety. A unique and operative power quality improvement technique for the MG operation has been proposed in this chapter with necessary explanations.

Voltage Source Inverter (VSI) based MGs are being developed and designed with various control strategies concentrating on supplying sinusoidal current and voltage free of harmonics to the concerned system even when the non-linear or disturbed loads are connected to the grid [2]. The improvement of power quality uncertainties in the MGs is in demand to eradicate harmonics-related noises and deliver unpolluted sinusoidal waveform at rated frequency and voltage. Typically, MGs are more vulnerable to the power quality troubles due to comparatively lesser inertia level (because of the presence of intensive non-linear electronic devices in the concerned distributed energy resources (DERs) [3]), perturbation of the electricity consumptions and power generation, lower short circuit level, the existence of numerous vendors and decision-makers, the requirement of action mode changeover from a grid-allied to sophisticated island mode and vice-versa.

Power quality is expressed as maintaining the magnitude of concerned voltage waveform in its pure sinusoidal nature with prescribed magnitude, frequency within a recommended limit without any abnormality in shape. Power quality-related issues to the end-user equipment and consumers occur in the electrical system when there is any abnormality in the waveform's frequency and magnitude related to power beyond a specified range [4]. The diverse kinds of power quality disturbances comprise the unbalanced voltage, sags and swells in voltage waveform, harmonic distortion, transients, short term disturbances like the under-voltages and over-voltages, power outage, perceptible flicker, electrical noise, and voltage notching. Due to the high intermittent characteristics of the existing distributed energy generators like wind power, solar power, and fuel cells, the voltage generated from these resources cannot be connected directly to the primary grids. However, this can be achieved with the help of an interfacing converter between the outputs of these renewable energy resources and the ac power distribution systems. Harmonics are generally referred to as the distortion of the sinusoidal waveform by waveforms of different frequencies [5].

A developed MG model integrating solar generation, wind power systems, aqua electrolyzers, fuel cells, battery energy storage systems, and diesel generators are proposed in the reference [6]. A comprehensive survey on MG to improve the power quality parameters is taken as the main objective is presented in reference [7]. A decision-making approach based on the MATLAB-Simulink model has been suggested in [8] to evaluate the power quality features of the single-phase AC MG with necessary explanations. Reference [9] addresses the power quality improvement

of multi-area MGs. A new mathematical morphology-based shunt active filter for improving MG's power quality is described [10].

Similarly, the fuzzy logic control approach for the UPQC is discussed in reference [11] for unbalanced power networks like the low voltage distribution systems. This fuzzy logic control scheme proposed here is used for the current control in-place of proportional-integral controllers, which have a tolerable performance over a wide variety of operating nodes. A vigorous voltage control technique with an angle droop method to improve power quality is proposed in reference [12]. A robust control approach for multifunctional grid-connected inverters under an unbalanced loading condition and primary voltage environments is proposed [13]. Reference [14] suggested an integrated approach to alleviating power quality difficulties in an MG by optimally controlling the operational schedule of generation sources and load demands.

It has been observed from the literature survey that proper research is still needed for the development of an accurate scheme that can limit the harmonic disturbances without compromising the reactive power compensation and power balance in all three phases of the distribution system. This research gap is fulfilled in this chapter by developing two methods that compensate for various power quality disturbances like harmonic distortion. In the first method, a smart PV-DSTATCOM is suggested in this chapter to mitigate power quality problems. It acts as an active filter that nullifies the effect of non-linear load currents and improves the grid's power factor, regulating the DC-link voltage. The multidirectional flow of power has also been achieved in this model [15]. The proposed system works in both the modes of constant irradiation and variable irradiation with a constant load. The second method can safeguard the sensitive consumer loads from numerous perturbations in the power supply infrastructure by mitigating short-term power quality issues such as voltage sags and swells with a dynamic voltage restorer (DVR). PV-DSTATCOM and DVR's main objective is to reduce the harmonics, voltage sags, and swells and improve power quality. This chapter focuses on mitigating the short-term voltage disturbances like the voltage sag and swell in the low voltage unbalanced distribution networks by effectively implementing a DVR. The primary objectives of this chapter are as follows:

- The total harmonic distortion (THD) initiated by non-linear consumer loads should be reduced below 4% by implementing PV-DSTATCOM with maximum power point tracking (MPPT) controller. The reweighted zero attracting (RZA) control scheme with adaptive features should be installed at the point of the common coupling (PCC) node where the MG is connected with the primary grid to accomplish developed PQ performance in the MG. The PV-DSTATCOM also transforms the DC voltage into AC.
- The enhancement of the PQ by suppressing the harmonic distortions is made using a hysteresis controller.
- To increase the efficiency of PV cells, MPPT is implemented.
- Dynamic voltage restorer is used to mitigating voltage swells and voltage sags required by the customer and the reduced harmonics.

The rest part of this chapter is arranged as follows. Section 2 presents power quality improvement using a PV-DSTATCOM into the MG to eliminate the system's harmonics. Section 3 proposes an approach to eliminate any nonlinearities and mitigate voltage sag and swell with DVR for obtaining good performance of the system. Section 4 presents simulation results and discussion. Conclusions are drawn in Sect. 5 by comparing proposed approaches and drawing the contributions.

2 Power Quality Improvement by Developing PV-DSTATCOM

The RERs, such as solar PV, are manifested from free energy resources freely obtainable from solar radiation and have gained widespread acceptance amongst electricity consumers. The single-stage algorithm or topology is preferred as a DC-DC boost converter requirement is eradicated, reducing budget and improving the efficiency of the concerned system. The concept of PV-distribution static compensator (PV-DSTATCOM), which is used to transform the DC output voltage from the solar cell to equivalent AC, is regarded as a converter with a solar photovoltaic array with an operational amplifier based active filtering feature to improve the system performance by improving power quality and suppressing harmonic distortions with reactive power compensation in the unbalanced distribution system network [16].

The rising demand for energy, an increase of unwanted power outages, and high penetration of electronic circuit-based non-linear loads with the depreciating power infrastructure create a formidable challenge in front of researchers. A smart PV-DSTATCOM system acting as an active filter to counterbalance the aforementioned problems has been proposed in this work. It can nullify the effect of the harmful effects of non-linear load currents, standardize the voltage of DC-link, and develop the grid's power factor. It can also achieve power flow in multidirectional nodes. The discussed system can perform into two modes DSTATCOM and PV-DSTATCOM, and achieve two ways of sensing the PV power automatically. In this chapter, an adaptive reweighted zero attracting (RZA) control approach extracts the reference from measured grid currents [17]. The traditional control strategy with the LMS algorithm can provide an appropriate steady-state behaviour and transient response, but it has a wide range of mean square errors. The RZA control scheme proposed in this chapter uses a zero attractor generator in the adaptive iteration by incorporating parallel relaxation and comprehensive sensing to achieve improved performance of the control scheme. The RZA control provides accurate reference signals and improves the filtering process.

2.1 Power System Model

Let's assume a grid equivalent model comprising of 3 phase generating source model associated with loading in series and corresponding self-impedances [18, 19]. The current and voltage are measured at the node defined by the PCC. THD of the complete grid system is measured over FFT analysis. Figure 1. Depicts the simple arrangement of a grid with non-linear loads leading to the production of harmonics.

Total distribution in both 3-phase current and voltage waveforms and the total THD of the circuit with the help of the FFT study are shown in Figs. 2 and 3. Harmonics are introduced due to nonlinear consumer loads and generating units, which try to distort the current and voltage waveforms, as shown in Figs. 2 and 3. These unwanted harmonics can be reduced by installing a smart and flexible branch at PCC [20]. The harmonic load is only connected to the B phase; hence R and Y phases are pure sinusoidal, but the B phase is distorted. In Fig. 4, introduced THD due to non-linear load and generating units that distort current and voltage waveforms is portrayed. Hence, THD found here by utilizing the FFT analysis was 58.10%.

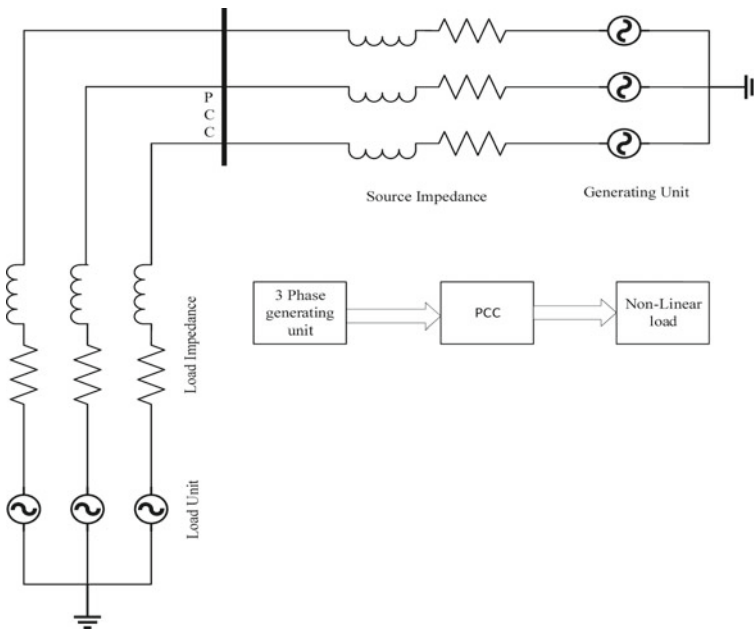


Fig. 1 The simple arrangement of a grid with non-linear loads leading to the production of harmonics

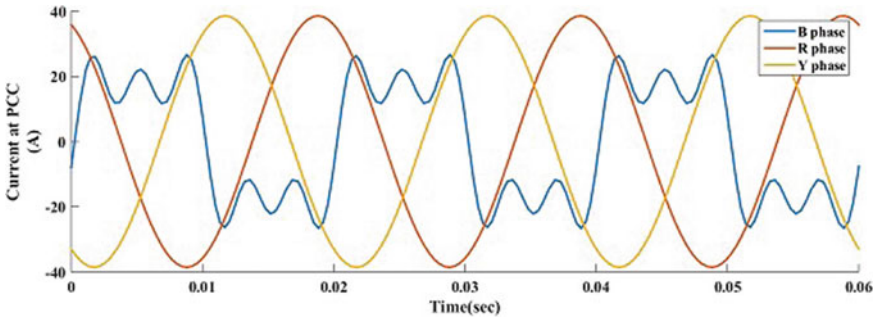


Fig. 2 Distortion in a current waveform due to 5th and 11th order harmonics existing in the R phase

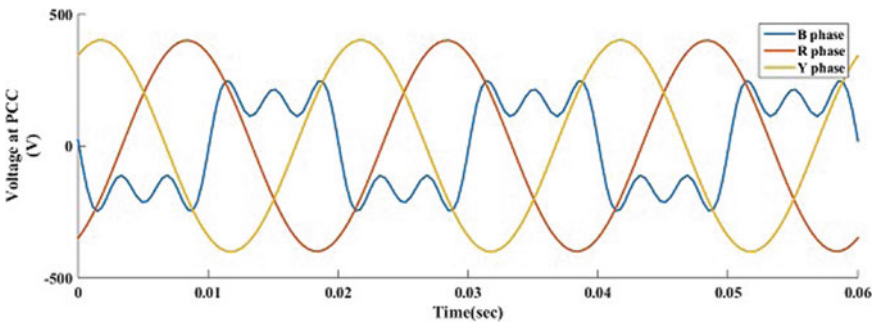


Fig. 3 Distortion in voltage waveform due to 5th and 11th order harmonics existing in the R phase

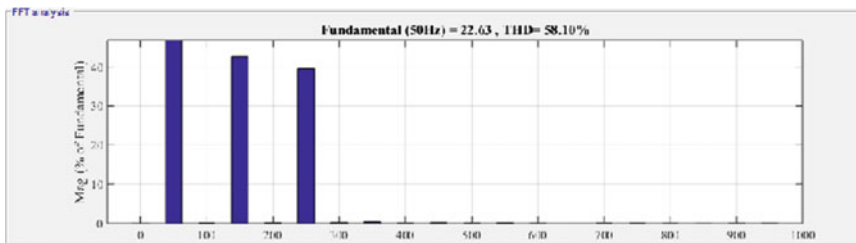


Fig. 4 THD without smart branch and controller

2.2 Grid Design and Its THD with PV-DSTATCOM

A smart PV-DSTATCOM system with an active filtering scheme that can nullify the unwanted non-linear load currents with power factor compensation at PCC and DC voltage connection regulation has been explained and proposed in this chapter with necessary illustrations [21]. The proposed system can automatically perform

two types of PV power sensing modes: the DSTATCOM mode and PV-DSTATCOM mode. An adaptive RZA scheme of control has been used in this work to identify the required grid reference current. A precise value of current and voltage can extract maximum power from a PV array with constant insolation; hence, the MPPT approaches have been presented, such as adaptive perturb and observe technique [22, 23]. Let's consider a conventional grid containing 3 phase generating sources coupled to a linear or nonlinear load connected in series with their corresponding self-impedances. Currents and voltages are measured at the traditional PCC. The harmonic distortion term defined by THD of the whole grid is measured during FFT analysis. Schematic diagram of proposed PV-DSTATCOM scheme topology has been depicted in Fig. 5.

Parameters utilized for the simulation of PV-DSTATCOM installed in the grid are presented in Table 1. It has been estimated that by inserting a suitable voltage at the sampling time period of (T_s), the current at PCC can be made harmonic-free. An adaptive RZA control technique was implemented to extract grid currents in the form of reference [24]. There present one particular significance of current and voltage at which extreme power can be found from PV array; hence the MPPT practices have been testified, such as adaptive P&O (perturb and observe) procedure.

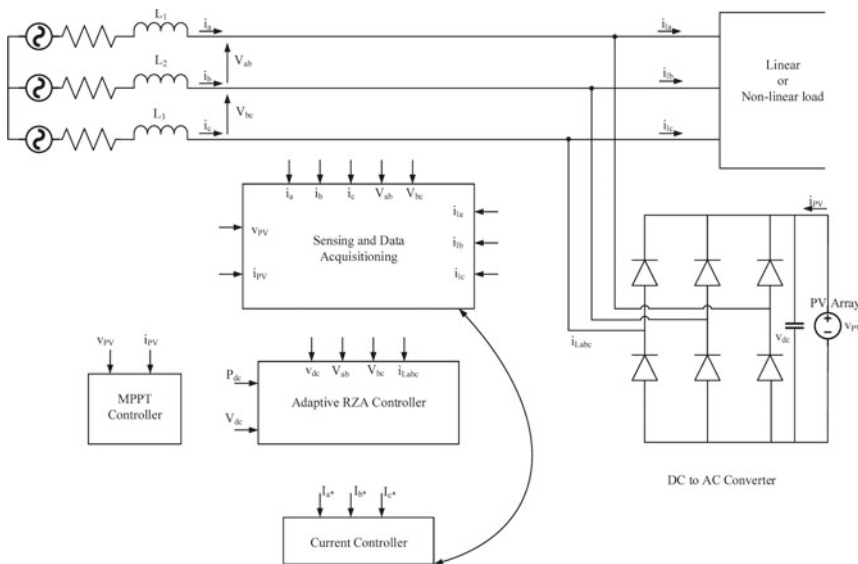


Fig. 5 Schematic diagram of proposed PV-DSTATCOM scheme topology

Table 1 Parameters used for the simulation of PV DSTATCOM installed in the grid

Parameters	Value
OC voltage of PV simulator array (V_{OCN})	394.80 V
SC current array (I_{SCN})	16.62A
Array power (P_{MPP})	5.35 kW
DC bus voltage (V_{Ref})	380 V
Interfacing inductor (L_f)	2.9mH
DC bus capacitor (C_{dc})	2350uF
Sampling time (T_s)	30us
Grid voltage (V_{LL})	220Vrms
Ripple filter (R_f and C_f)	5Ω,10uF
DC PI controller (K_{pd} and K_{id})	0.1,0.01
Non-linear load	1.1 kW load with a 3-phase diode bridge with
μ	0.054
ε	10.2
ρ	0.004

2.3 System Topology and Control Architecture

The suggested scheme comprises 5350 W solar PV array connected to the grid's 3-phase AC system to feed linear and non-linear load up through ripple filters [25]. The constraints of the default solar PV array at nominal working environments have been utilized in this work. The flowchart which depicts the operation of PV-DSTATCOM is presented in Fig. 6.

The voltage of 2-lines (v_{ab} and v_{bc}) that are sensed at PCC are applied to determine phase to ground voltages on PCC [26],

$$v_a = (2v_{ab} + v_{bc})/3 \quad (1)$$

$$v_b = (-v_{ab} + v_{bc})/3 \quad (2)$$

The unit of in-phase and templates of quadrature is calculated as [27],

$$u_{pa} = v_a/v_t \quad (3)$$

$$u_{pb} = v_b/v_t \quad (4)$$

$$u_{pc} = v_c/v_t \quad (5)$$

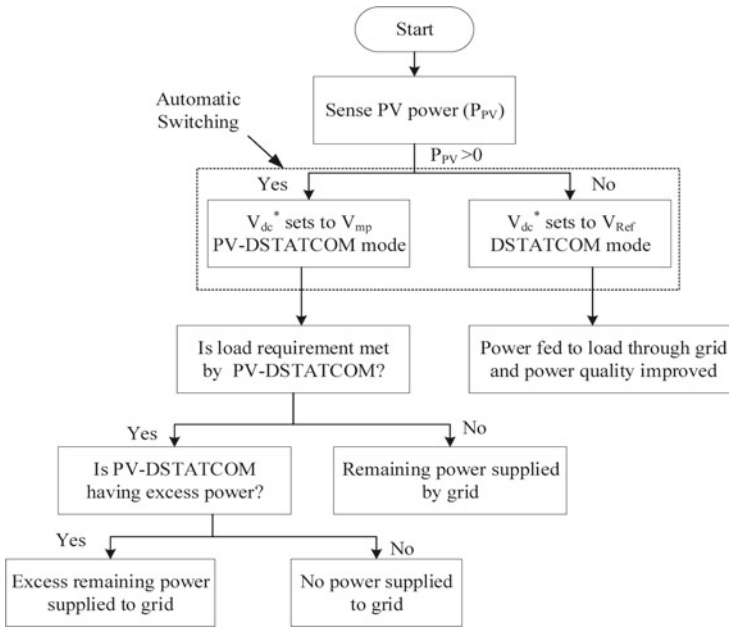


Fig. 6 Flowchart depicting the process of PV-DSTATCOM scheme

$$u_{qa} = (-u_{pb}/\sqrt{3}) + (-u_{pc}/\sqrt{3}) \quad (6)$$

$$u_{qb} = (\sqrt{3}u_{pa}/2) + ((u_{pb} - u_{pc})/2\sqrt{3}) \quad (7)$$

$$u_{qc} = (\sqrt{3}u_{pa}/2) + ((u_{pb} - u_{pc})/2\sqrt{3}) \quad (8)$$

The error of DC voltage (V_{de}) is determined as the variance among the reference voltage of DC bus (V_{dc}^*) achieved from the perturb and observe (P&O) MPPT and DC voltage that is sensed (V_{dc}). P&O's hill-climbing method works on the perturbation of solar output voltage and observing power sign, and consequently chooses the condition for the later perturbation to reach analogical hill-top or the extreme practical PowerPoint [28]. DC voltage fault at r th sampling instantaneous is expressed as,

$$V_{de}(r) = V_{dc}^* - V_{dc} \quad (9)$$

The component of active power loss (w_{cp}) which is adaptable DC bus voltage is approximate by using V_{de} and a Proportional Integral (PI) controller gains as,

$$w_{cp}(r+1) = w_{cp}(r) + K_{pd}[V_{de}(r+1) - V_{de}(r)] + K_{id}V_{de}(r+1) \quad (10)$$

where K_{pd} and K_{id} are proportional and integral gains, $G_p(s)$ is a transfer function of the concerned plant and $G_c(s)$ is a transfer function for the concerned PI voltage controller. Similarly, to regulate the PCC voltages observed voltage error ($V_{te}(n)$) is fed to another controller of PI nature [29]. Calculated fault and failure component of reactive power (w_{cq}) at r th the sampling period is evaluated as,

$$V_{te}(r) = V_t^* - V_t \tag{11}$$

$$w_{cq}(r + 1) = w_{cq}(r) + K_{pt}[V_{te}(r + 1) - V_{te}(r)] + K_{it}V_{te}(r + 1) \tag{12}$$

where K_{pt} and K_{it} Are proportional and integral gains used in this controller, which is having PI characteristics. For an upgraded error performance as the solar irradiance stage varies, the feed-forwards term of PV from the solar photovoltaic array is calculated by using,

$$w_{pv}(r) = 2P_{pv}(r)/3v_t \tag{13}$$

where P_{pv} is obtained PV power. Weight of the fundamental active element of the load current of phase ‘a’ under steady-state and dynamic conditions is calculated by using [30]

$$w_{pa}(r + 1) = w_{pa}(r) - \frac{\rho \text{sgn}(w_{pa}(r))}{1 + \varepsilon|w_{pa}(r)|} + \mu e_{pa}(r)u_{pa} \tag{14}$$

where,

$$e_{pa}(r) = i_{La}(r)u_{pa}(r)w_{pa}(r) \tag{15}$$

e_{pa} is a load component of the concerned active error, ρ is an invariable constant to switch the strength of zero attractors, K_a is the reweighted term for the zero attractors, u is the factor of convergence, sgn is a signum function, s is an independent constant, $w_{pa}(r)$, $i_{La}(r)$ and $u_{pa}(r)$ are the active reference component of the weight, load current, and in-phase unit template of phase ‘a’ at r th instant [31].

Similarly, weights of primary effective terms ($w_{pb}(r)$, $w_{pc}(r)$) of non-linear load currents and adaptive instrument faults of supplementary 2 phases ‘b’ and ‘c’ with steady-state and dynamic situations (when load unbalancing is undertaken) are conveyed as,

$$w_{pb}(r + 1) = w_{pb}(r) - \frac{\rho \text{sgn}(w_{pb}(r))}{1 + \varepsilon|w_{pb}(r)|} + \mu e_{pb}(r)u_{pb} \tag{16}$$

where,

$$e_{pb}(r) = i_{Lb}(r)u_{pb}(r)w_{pb}(r) \quad (17)$$

$$w_{pc}(r+1) = w_{pc}(r) - \frac{\rho \text{sgn}(w_{pc}(r))}{1 + \varepsilon|w_{pc}(r)|} + \mu e_{pc}(r)u_{pc} \quad (18)$$

where,

$$e_{pc}(r) = i_{Lc}(r)u_{pc}(r)w_{pc}(r) \quad (19)$$

Similarly, the weight of primary reactive share of the nonlinear current drawn by phase 'a' under steady-state and dynamic situations is represented by [32],

$$w_{qa}(r+1) = w_{qa}(r) - \frac{\rho \text{sgn}(w_{qa}(r))}{1 + \varepsilon|w_{qa}(r)|} + \mu e_{qa}(r)u_{qa} \quad (20)$$

where the reactive error $e_{qa}(r)$ is expressed as,

$$e_{qa}(r) = i_{La}(r) - u_{qa}(r)w_{qa}(r) \quad (21)$$

$$w_{qb}(r+1) = w_{qb}(r) - \frac{\rho \text{sgn}(w_{qb}(r))}{1 + \varepsilon|w_{qb}(r)|} + \mu e_{qb}(r)u_{qb} \quad (22)$$

where

$$e_{qb}(r) = i_{Lb}(r) - u_{qb}(r)w_{qb}(r) \quad (23)$$

$$w_{qc}(r+1) = w_{qc}(r) - \frac{\rho \text{sgn}(w_{qc}(r))}{1 + \varepsilon|w_{qc}(r)|} + \mu e_{qc}(r)u_{qc} \quad (24)$$

$$e_{qc}(r) = i_{Lc}(r) - u_{qc}(r)w_{qc}(r) \quad (25)$$

The active weight component (w_{sp}) of reference grid currents under dynamic and steady-state situations is represented by,

$$w_{sp} = w_{Lpa} + w_{cp} - w_{pv} \quad (26)$$

The reference active grid currents under dynamic and steady-state conditions are calculated by using,

$$i_{pa}^* = w_{sp}u_{pa}, \quad i_{pb}^* = w_{sp}u_{pb}, \quad i_{pc}^* = w_{sp}u_{pc} \quad (27)$$

Similarly, the total reactive weight component (w_{sq}) of reference grid currents under steady-state and dynamic conditions is represented by,

$$w_{sq} = -w_{Lqa} + w_{cq} \quad (28)$$

where,

$$w_{Lqa} = (w_{qa} + w_{qb} + w_{qc})/3 \quad (29)$$

The reference reactive grid currents under dynamic and steady-state situations are calculated by using,

$$i_{qa}^* = w_{sq}u_{qa}, i_{qb}^* = w_{sq}u_{qb}, i_{qc}^* = w_{sq}u_{pc} \quad (30)$$

Therefore, the total reference 3-phase grid currents under dynamic and steady-state situations are calculated by using,

$$i_{qa}^* = i_{pa}^* + i_{qa}^*, i_{sa}^* = i_{pa}^* + i_{qb}^*, i_{sc}^* = i_{pc}^* + i_{qc}^* \quad (31)$$

The difference between the reference grid and sensed current output is delivered through the hysteresis regulator to produce a pulse signal for the regulated switching by gate pulses of concerned VSC [13].

3 Power Quality Improvement by Developing Dynamic Voltage Restorer (DVR)

The nonstandard behaviour of concerned power system parameters like the current, voltage, and frequency that may damage the end-use equipment is regarded as the power quality disturbance [15]. Short-term power fluctuations like the power system swell or sag are some of the substantial concerns that occur frequently. A power quality enhancement device for the unbalanced distribution system known as the DVR is implemented effectively in this chapter to mitigate these short-term voltage fluctuations like voltage swell and voltage sags. DVR can deliver the optimum cost-effective solution to minimize the short-term voltage fluctuations such as voltage swells and sags required by end-use customers [16]. A DVR can be a resourceful solution to the required power quality problems with enormous rapid and flexible features.

3.1 Circuit Model of DVR

In an unbalanced distribution network, the solid-state (or static) power electronic component-based DVR can also be referred to as a static series compensator (SSC) or series voltage booster (SVB), which is preferably coupled in series with the concerned

primary distribution system with necessary arrangement [17]. The DVR refurbishes the load side voltage to a preferred pre-sag voltage amount by providing a series voltage of the preferred amplitude and frequency even when the source voltage is not balanced [18].

The DVR is usually connected with the primary unbalanced distribution system with the help of a series A voltage injection with the incoming 3 phase network. This helps to enhance the power quality of the disturbed system by necessary adjustment of the PCC voltage magnitude, phase shift, or wave shape. The short-term voltage sag's compensation can be achieved, and reactive and active power addition into an unbalanced power distribution network. Although the reactive component of power cannot be generated from any source, it is compensated by the help of a VSI inside DVR. This can protect the sensitive loads or end-user equipment in the parallel feeder with the necessary breaker action by disconnecting faulted feeder and limiting the fault current with necessary parameter modification [33]. DVR also improves harmonics present in the line voltage along with the mitigation of voltage swell and sag. Figure 7 depicts the primary DVR circuit and its components. A DVR coupled to the grid with a non-linear load is shown in this figure.

DVR comprises the energy storage unit, VSI, series injection transformer, filter, control unit, and bypass switch/circuit breaker. The energy storage section's function is to cater to VSI, which feeds to a series injection transformer. The VSI is a combination of power electronic devices that can switch the battery source's power with the necessary frequency. This works as a source of generating 3-phase voltage with the required magnitude phase and frequency to compensate for the unbalanced value of the concerned load voltage [19]. The transformer presented in Fig. 7 injects the generated voltage from VSI in sequence with the unstable distribution line. The HV part is coupled to a network, while the LV side is connected to VSI. The filter and control unit is used to sense the fluctuations related to power quality and filter the harmonics in the output of VSI [20]. Bypass switch/circuit breaker is used for isolation of DVR from the grid.

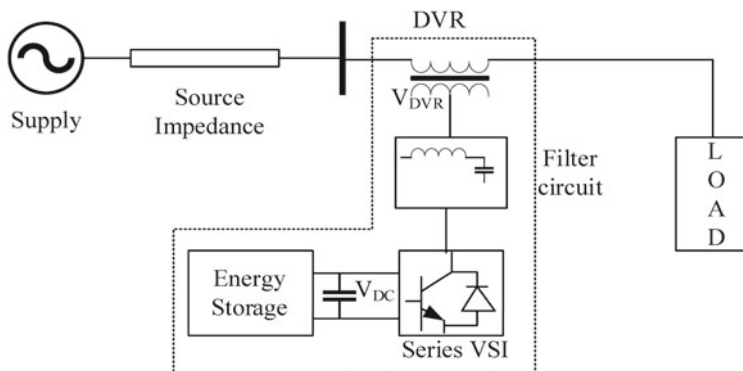


Fig. 7 Basic circuit model of DVR

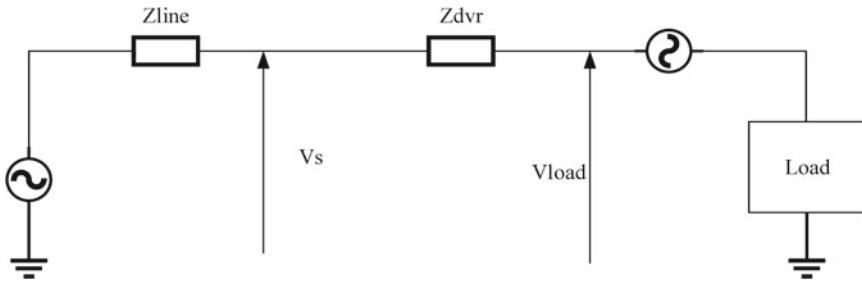


Fig. 8 Equivalent single line diagram of DVR

3.2 Proposed Technique

The DVR re-establishes the load side voltage to a preferred pre-sag voltage amount by delivering a voltage of the preferred frequency and magnitude even if it has an unbalanced source voltage [34, 35]. Following proposed objectives achieve this:

- A dc source is converted to a harmonic free ac source with AVR help connected with filter.
- A Series injection transformer is implemented to alleviate the voltage sag by inserting voltage at PCC.

Bypass switch further enhances the convenience of implementing the circuit. The basic diagram of a grid-connected DVR is depicted in Fig. 8, making it very convenient to understand its operation principle by considering a 3-phase fault. Hence, a DVR coupled to the grid with a non-linear load is depicted in Fig. 7.

4 Results and Discussion

In this portion, the proposed PV-DSTATCOM and DVR are implemented to improve the system’s power quality. The simulation results of these two approaches are presented next:

4.1 Improvement of Power Quality by Developing PV-DSTATCOM

Figure 9 shows the three-phase waveform obtained as the output of the simulating PV-DSTATCOM model. Also, the final THD found by applying the FFT analysis on illustrated in Fig. 10.

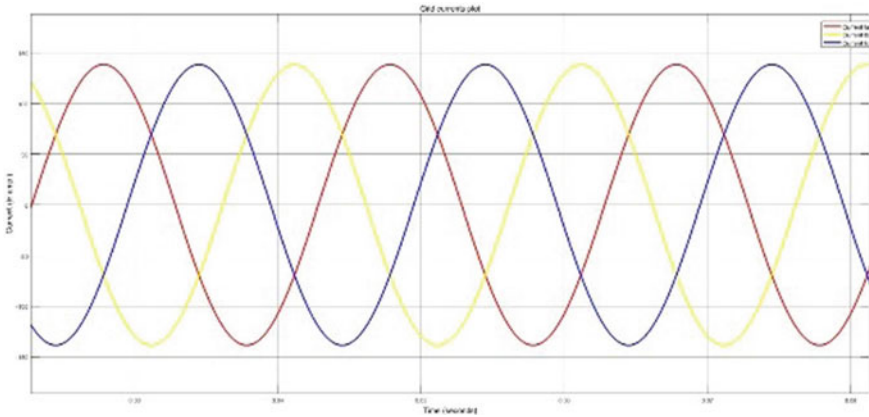


Fig. 9 The 3 phase waveform was obtained by simulating the PV DSTATCOM model

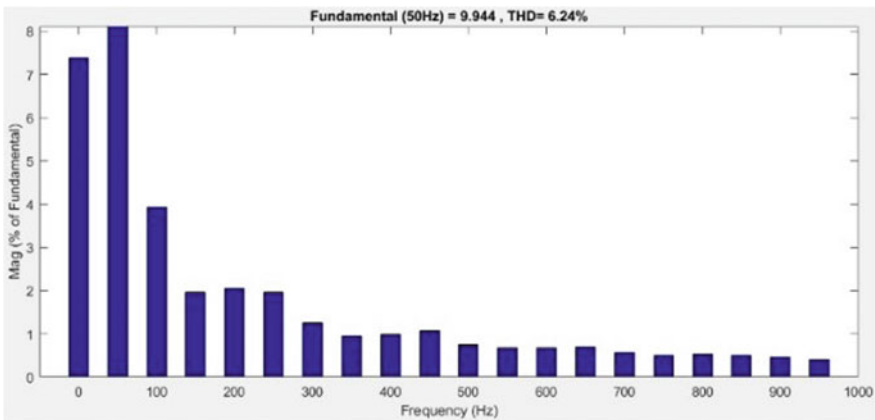


Fig. 10 The final THD was obtained by using the FFT analysis

From Figs. 9 and 10, it has been observed that the waveform is almost sinusoidal after incorporating the PV-DSTATCOM in the model, and the THD has also reduced to 6.64%, which was previously 48%. Further, the use of automated solar PV helps in uninterrupted supply. As a result of the simulation, the harmonics caused due to consumer loads which are non-linear and devices remain practically mitigated. THD was condensed from 58.7% instead of PV-DSTATCOM to 5% with PV-DSTATCOM. By increasing the generation voltage, the waveform gets smoother further.

4.2 Improvement of Power Quality by Developing DVR

The voltage at PCC due to 3 phase fault and the injected voltage and finally the recovered sag are depicted in Fig. 11. Figure 12 illustrates the THD during the 3-phase sudden short-circuit.

Now the proposed DVR is implemented to improve the PQ of the concerned system. Figure 13 depicts the THD during the 3-phase sudden short-circuit after using the proposed DVR. From this figure, it can be observed that the THD has also decreased by 8%, along with the waveform’s improvement. The voltage sag is mitigated and restored to the normal value. Hence in this way, it can be seen that the 3-phase short-circuit fault can be overcome without causing equipment failure or interrupting power supply and is one of the most convenient methods for low voltage applications.

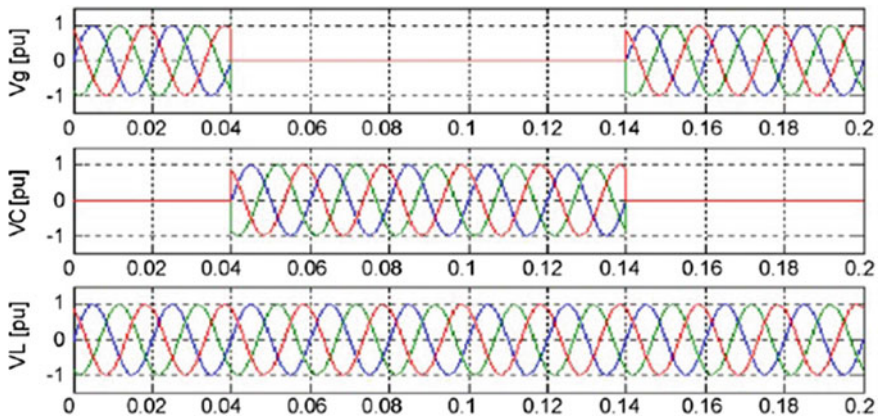


Fig. 11 Voltage sag injected voltage and recovered voltage waveforms

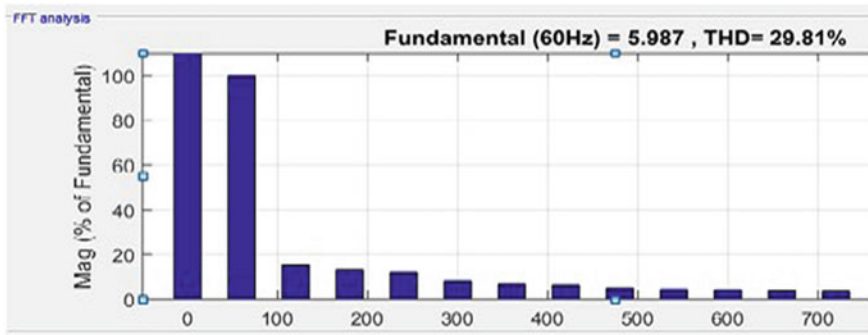


Fig. 12 THD during 3-phase sudden short circuit

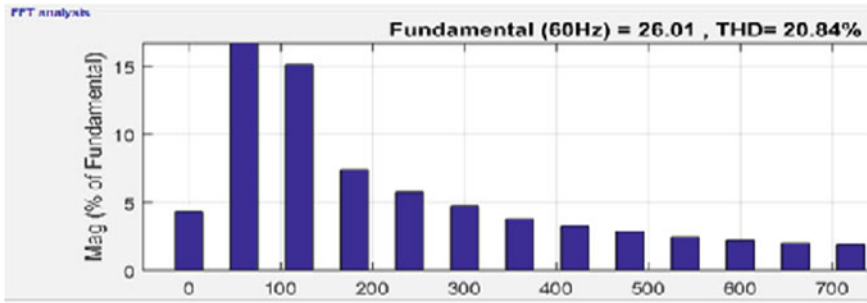


Fig. 13 THD during 3-phase sudden short-circuits after using DVR

DVR is used in various applications as it is less expensive. Compared to DSTATCOM and UPS, DVR is a lot cheaper, and the UPS requires a lot of maintenance due to battery leakage and replacement problems. DVR is tiny and is a better power-effective device than UPS, Superconducting Magnetic Energy Storage (SMES), and DSTATCOM. DVR also compensates for line voltage harmonics along with mitigation of voltage sag and swell.

5 Conclusions

This chapter presented a new power quality improvement approaches in microgrids (MGs) using a grid-connected smart photovoltaic distribution static compensator (PV-DSTATCOM) system implementing an adaptive RZA control technique through perturbing and observe (P&O) MPPT approach and the use of DVR for a three-phase system. These two techniques are verified by performing various recreations. The advantages of PV-DSTATCOM with MPPT and RZA controller were analyzed with sensitivity, and the DVR can be practicality taken into consideration. The proposed technique removes the necessity for non-linear current contribution amongst inverters by not negotiating voltage quality. The THD diminishes expressively by using these efficient techniques. Without using any of these methods, the THD was perceived to be roughly 58% in the output voltage, but after implementing the proposed strategies, the THD has reduced to about 21%. Thus, minimizing the disturbances in practice. Secondly, the IGBT-based controllers were introduced by PV-DSTATCOM, which includes an MPPT controller and an RZA controller. This resulted in a reduced THD of about (4 – 6) %. Later, DVR use in the smart grid was analyzed to mitigate voltage sag due to power quality disturbances and improved harmonics. The approaches proposed in this chapter provides the system with enough prediction ability and smartness for holding the required current and voltage quality at the PCC, and high power quality is achieved with significantly fewer expenses.

Acknowledgements This research work was supported by “Woosong University’s Academic Research Funding-2021”.

References

1. Yazdi F, Hosseinian SH (2019) A novel “Smart Branch” for power quality improvement in microgrids. *Int J Electr Power Energy Syst* 110:161–170. <https://doi.org/10.1016/j.ijepes.2019.02.026>
2. Lavanya V, Kumar NS (2018) Control strategies for power quality improvement in microgrid. *Int J Renew Energy Res* 8(1):151–154
3. Zhong QC (2013) Harmonic droop controller to reduce the voltage harmonics of inverters. *IEEE Trans Ind Electron* 60(3):936–945. <https://doi.org/10.1109/TIE.2012.2189542>
4. Wang R, Hsu SC, Zheng S, Chen JH, Li XI (2020) Renewable energy microgrids: Economic evaluation and decision making for government policies to contribute to affordable and clean energy. *Appl Energy* 274. <https://doi.org/10.1016/j.apenergy.2020.115287>
5. Singh B, Kandpal M, Hussain I (2018) Control of grid-tied smart PV-DSTATCOM system using an adaptive technique. *IEEE Trans Smart Grid* 9(5):3986–3993. <https://doi.org/10.1109/TSG.2016.2645600>
6. Veronica AJ, Kumar NS (2017) Development of hybrid microgrid model for frequency stabilization. *Wind Eng* 41(5):343–352. <https://doi.org/10.1177/0309524X17723203>
7. Bacha S, Picault D, Burger B, Otadui IE, Martins J (2015) Photovoltaics in microgrids: an overview of grid integration and energy management aspects. *IEEE Ind Electron Mag* 9(1):33–46. <https://doi.org/10.1109/MIE.2014.2366499>
8. Chitra N, Kumar AS, Priyadharshini P, Prabaakaran K (2014) Survey on microgrid: power quality improvement techniques. *ISRN Renew Energy* 2014:1–7. <https://doi.org/10.1155/2014/342019>
9. Kaushal J, Basak P (2018) A novel approach for determination of power quality monitoring index of an AC microgrid using fuzzy inference system. *Iran J Sci Technol Trans Electr Eng* 42:429–450. <https://doi.org/10.1007/S40998-018-0087-Z>
10. Hashempour MM, Lee T, Savaghebi M, Guerrero JM (2019) Real-time supervisory control for power quality improvement of multi-area microgrids. *IEEE Syst J* 13(1):864–874. <https://doi.org/10.1109/JSYST.2018.2823899>
11. Sahoo B, Routray SK, Rout PK (2020) Application of mathematical morphology for power quality improvement in microgrid. *Int Trans Electr Energy Syst* 30(5). <https://doi.org/10.1002/2050-7038.12329>
12. Eldin AAH, Mansour AA, Gamal ME, Youssef KH (2019) Power quality improvement of smart microgrids using EMS-based fuzzy controlled UPQC. *Turk J Electr Eng Comput Sci* 27:1181–1197. <https://doi.org/10.3906/elk-1807-166>
13. Qian H, Xu Q, Zhao J, Yuan X (2020) A robust GPS-based control scheme for power-sharing and quality improvement in microgrid. *Int J Electr Power Energy Syst* 123. <https://doi.org/10.1016/j.ijepes.2020.106324>
14. Safa A, Berkouk ELM, Messlem Y, Gouichiche A (2018) A robust control algorithm for a multifunctional grid tied inverter to enhance the power quality of a microgrid under unbalanced conditions. *Int J Electr Power Energy Syst* 100:253–264. <https://doi.org/10.1016/j.ijepes.2018.02.042>
15. Thomas D, Hoop GD, Deblecker O, Genikomsakis KN, Ioakimidis CS (2020) An integrated tool for optimal energy scheduling and power quality improvement of a microgrid under multiple demand response schemes. *Appl Energy* 260. <https://doi.org/10.1016/j.apenergy.2019.114314>

16. Kumar YVP, Bhimasingu R (2017) Electrical machines based DC/AC energy conversion schemes for the improvement of power quality and resiliency in renewable energy microgrids. *Int J Electr Power Energy Syst* 90:10–26. <https://doi.org/10.1016/j.ijepes.2017.01.015>
17. Kumar YVP, Ravikumar B (2016) A simple modular multilevel inverter topology for the power quality improvement in renewable energy based green building microgrids. *Electr Power Syst Res* 140:147–161. <https://doi.org/10.1016/j.epsr.2016.06.027>
18. Srivatchan NS, Rangarajan P, Rajalakshmi S (2015) Control scheme for power quality improvement in islanded microgrid operation. *Procedia Technol* 21:212–215. <https://doi.org/10.1016/j.protcy.2015.10.090>
19. Igual R, Medrano C (2020) Research challenges in real-time classification of power quality disturbances applicable to microgrids: a systematic review. *Renew Sustain Energy Rev* 132. <https://doi.org/10.1016/j.rser.2020.110050>
20. Shafiullah GM, Amanullah MT, Ali ABMS, Wolfs P, Arif MT (2013) Smart grids: opportunities, developments and trends. Springer, London. <https://doi.org/10.1007/978-1-4471-5210-1>
21. Steffel SJ, Caroselli PR, Dinkel AM, Liu JQ, Sackey RN, Vadhar NR (2012) Integrating solar generation on the electric distribution grid. *IEEE Trans Smart Grid* 3(2):878–886. <https://doi.org/10.1109/TSG.2012.2191985>
22. Wang T, O'Neill D, Kamath H (2015) Dynamic control and optimization of distributed energy resources in a microgrid. *IEEE Trans Smart Grid* 6(6):2884–2894. <https://doi.org/10.1109/TSG.2015.2430286>
23. Jager K, Isabella O, Smets AHM, Van Swaaij RACMM, Zeman M (2014) Solar energy fundamentals, technology and systems. UIT Cambridge, Cambridge
24. Wu TF, Chang CH, Lin LC, Kuo CL (2011) Power loss comparison of single- and two-stage grid-connected photovoltaic systems. *IEEE Trans Energy Convers* 26(2):707–715. <https://doi.org/10.1109/TEC.2011.2123897>
25. Das SR, Mishra DP, Ray PK, Salkuti SR, Sahoo AK (2021) Power quality improvement using fuzzy logic-based compensation in a hybrid power system. *Int J Power Electron Drive Syst* 12(1):576–584. <https://doi.org/10.11591/ijpeds.v12.i1.pp576-584>
26. Agarwal RK, Hussain I, Singh B (2016) LMF based control algorithm for single-stage three-phase grid integrated solar PV system. *IEEE Trans Sustain Energy* 7(4):1379–1387. <https://doi.org/10.1109/TSTE.2016.2553181>
27. Subudhi B, Pradhan R (2013) A comparative study on maximum power point tracking techniques for photovoltaic power systems. *IEEE Trans Sustain Energy* 4(1):89–98. <https://doi.org/10.1109/TSTE.2012.2202294>
28. Martinez JA, Arnedo JM (2006) Voltage sag studies in distribution networks—part I: system modelling. *IEEE Trans Power Delivery* 21(3):1670–1678. <https://doi.org/10.1109/TPWRD.2006.874113>
29. Das B, Panigrahi PK, Das SR, Mishra DP, Salkuti SR (2021) Power quality improvement in a photovoltaic based microgrid integrated network using multilevel inverter. *Int J Emerg Electr Power Syst*. <https://doi.org/10.1515/ijepes-2021-0040>
30. Choi SS, Li BH, Vilathgamuwa DM (2011) Dynamic voltage restoration with minimum energy injection. *IEEE Trans Power Syst* 15(1):51–57. <https://doi.org/10.1109/59.852100>
31. Vilathgamuwa D, Wijekoon HM, Choi SS (2012) A novel technique to compensate voltage sags in multilines distribution system the interline dynamic voltage restorer. *IEEE Trans Ind Electron* 53(5):1603–1611. <https://doi.org/10.1109/TIE.2006.882017>
32. Ray P, Salkuti SR (2020) Smart branch and droop controller based power quality improvement in microgrids. *Int J Emerg Electr Power Syst* 21(6). <https://doi.org/10.1515/ijepes-2020-0094>
33. Marei MI, EI-Saadany EF, Salama MMA (2012) A new approach to control DVR based on symmetrical components estimation. *IEEE Trans Power Deliv* 22(4):2017–2024. <https://doi.org/10.1109/TPWRD.2007.905537>
34. Mathur RM, Varma RK (2013) Thyristor-based FACTS controllers for electrical transmission systems. Wiley, New York
35. Kaushal J, Basak P (2020) Power quality control based on voltage sag/swell, unbalancing, frequency, THD and power factor using artificial neural network in PV integrated AC microgrid. *Sustain Energy Grids Netw* 23. <https://doi.org/10.1016/j.segan.2020.100365>

Characterization of Bifacial Passivated Emitter and Rear Contact Solar Cell



Suresh Kumar Tummala, Phaneendra Babu Bobba,
and Satyanarayana Kosaraju

Abstract A Passivated Emitter and Rear Contact Cell (PERC) defines a new architecture of solar cell which differs from standard cell architecture. PERC enhances light capture at the rear surface and to optimize electron capture. This leads to an increase (or) achieve better efficiency than when compared with standard cell which are reaching their physical limits. In this paper, the characterization of bifacial p-type PERC solar cell with various proportions of tallness and width, back Silicon Nitrate layer with various thickness are streamlined. Most elevated back productivity of the bifacial solar cell (~22%) was obtained at AM 1.5 (air mass), 1000 W/m², 26 °C standard test condition.

Keywords PERC · Bifacial · Finger · Generation profile · Reflection · Absorbtion

Nomenclature

PERC	Passivated Emitter Rear Contact
LCOE	Levelized Cost of Energy
c-Si	Crystalline Silicon
PV	Photovoltaic
EQE	External Quantum Efficiency
P _{MP}	Maximum Power
J _{SC}	Short Circuit Current
V _{OC}	Open Circuit Voltage
R _S	Series Resistance
R _{SH}	Shunt Resistance

S. K. Tummala (✉) · P. B. Bobba
Electrical and Electronics Engineering Department, Gokaraju Rangaraju Institute of Engineering and Technology, Hyderabad, India

S. Kosaraju
Mechanical Engineering Department, Gokaraju Rangaraju Institute of Engineering and Technology, Hyderabad, India

J_L	Current density generated inside the solar cell
$J_{ph}(\lambda)$	Incident Photon Current
$A(\lambda)$	Fraction of the incident light
$\eta(\lambda)$	Collection Efficiency
T_{nom}	Nominal Temperature
T	Operating Temperature
E_g	Band gap of the semiconductor
q	Charge on electron
k	Boltzmann's constant
N_F	Number of Finger
W_F	Width of Finger
P_F	Finger Pitch
S_F	Finger Spacing

1 Introduction

The mission for grid equality is the steady mission of the photovoltaic business and lessening the expense of power with high effective advances is a basic methodology for the business to achieve this mission. As PV modules are the center part of a PV framework, the consistent improvement of module productivity is the most immediate and great innovation course to accomplish lattice equality. Among high-effectiveness cell innovations [1], PERC (passivated emitter and rear cells) is without a doubt the most cost-effective. Contrasted and regular cell, the creation of PERC cell needs just to add back passivation [2] and laser opening areas, combined with metallization methods. This will adequately improve the change effectiveness of the cells [3]. In the previous a half year, the world record for PERC cell change productivity has been continually re-energized, exhibiting the solid likely potential gain of PERC. The exhibition of mechanical kind screen-printed 6-inch PERC sun powered cells has been fundamentally expanded during recent years. Crystalline silicon (c-Si) is the crystalline form of silicon, either polycrystalline silicon (poly-Si, consisting of small crystals) or monocrystalline silicon (mono-Si, a continuous crystal). Crystalline silicon is the dominant semiconducting material used in photovoltaic technology to produce solar cells. These cells are assembled into solar panels as part of a photovoltaic system to generate solar power from sunlight. The main comparison of the p-type PERC and standard PV cell are:

Standard PV cells are typically Crystalline Silicon cells with a high energy transformation effectiveness rate. This implies that the cells, framed into boards, can produce more power even though the boards are sufficiently enormous to find a way into restricted spaces like roofs, making them space-proficient and over the long haul, cost-effective. Whereas, PERC cell innovation is more direct as they just contrast marginally from the standard PV cells. It is likewise savvier as it permits energy yield to be amplified because of more productive energy transformation.

Bifacial PERC is additionally turning into a significant course in the advancement of the innovation [4]. The usually utilized assembling innovation for bifacial PERC cell is to change the printing cycle of the PERC single-sided cell and changing the back surface from entire aluminum layer to a neighborhood aluminum layer. This permits accidental light on the back surface to enter the cell from the uncovered layer [5, 6] and make photoelectric change on both the front and back sides. with an irrelevant expansion in assembling cost, bifacial PERC can accomplish a force age gain of 10%-25% at the framework level, which will essentially diminish the Levelized Cost of Energy [7] of the PV framework while enormously improving the intensity and advancement capability of PERC innovation.

Bifacial silicon cell is an exceptional sort of gem silicon solar cell structure, which can get daylight and produce electrical force from both the front and posteriors. These cells are planned with uncommon structure and finger contact, so they can ingest more daylight and produce a lot of intensity from the two sides. The effectiveness gains [8] of bifacial cells comparative with single-sided cells are hard to gauge by a solitary cell. Along these lines, much of the time, they should be made into modules. Bifacial modules can be introduced deftly [9, 10] in a wide scope of uses. The type of customary single-sided cell modules establishment applications, for example, ground photovoltaic force stations and rooftop photovoltaic frameworks, is similarly reasonable for bifacial modules. The bifacial modules are particularly useful for ground establishment since they exploit the ground's mirrored light [11], produce greater power under similar conditions, and are additionally appropriate for establishment on the rooftop. Ground and rooftop-mounted bifacial modules should be mounted inclined on the scene. The bifacial cell and module can likewise be liberated [12, 13] from the course of the establishment. The back is as wonderful as the front, particularly appropriate for the vertical establishment of the scene, for example, vertical establishment as a fence, soundproof divider, thruway guardrail [14], and so on Thusly, the bifacial modules are reasonable for establishment in different situations, for example, ground power station, uniaxial global positioning framework, water surface force station, daylight room, photovoltaic shed, thruway soundproof divider, drape divider, vehicle shed, fabricating coordinated PV, etc. In the interim, in some ground power plant or housetop power plant [15], bifacial cells and modules additionally were introduced and have been run consistently for quite a while.

To additionally understand the benefits of high force transformation of high-effectiveness cells, joining PERC cells with a creative module [16, 17] development procedure is a significant overhaul course for makers of PERC cells and modules. From an innovation viewpoint to improve module yield power, the half-cut cell is without a doubt an elite and ease item that is anything but difficult to execute in enormous scope creation [18]. The half-cut cell is the procedure that slices a traditional cell down the middle and afterward interfacing the two parts together [19]. Contrasted the regular cells, the lone activity required is to cut the entire cell into two sections by a laser prior to string welding them. The PV cell parting and transmission are completely programmed [20] and the string welder needs just slight alteration to accomplish enormous scope creation.

1.1 Methodology

The principle preferred position of utilizing bifacial solar modules to construct photovoltaic plants is high force age. In the most part, the bifacial cells are made into bifacial modules. At the point when the direction, tendency, and stature of the bifacial modules are fixed, the force age gain of the bifacial modules predominantly returns from the side, which improves the current and greatest yield intensity of the get together by accepting the environmental dissipated light and the mirrored light of the ground. Moreover, the force age gain of the back can be improved by raising the stature of the part and expanding the tendency point of the segment. In this chapter, characterization of bifacial PERC solar cell is presented with a focus on Reflection, External Quantum Efficiency, C-V measurements, Generation profiles, and photon currents.

1.2 Bifacial PERC

Presently, the worldwide market is overwhelmed by mono-facial PV cells and modules. In any case, the International Technology Roadmap for Photovoltaics 2019 predicts that bifacial cells will pick up 60% of the worldwide market in 10 years, and they will be utilized in both bifacial and mono-facial modules. This is fundamentally because of the assumption that bifacial cells would create more force. Nonetheless, genuine bifacial modules with bifacial cells and straightforward back covers are required to make up about half of worldwide piece of the overall industry by 2029. Bifacial modules cannot be rated the same way as mono-facial modules; therefore, further discussion into standard testing conditions are required. Nevertheless, the possible gain from this technology attracts attention from the photovoltaic market.

The electrical outputs of the solar cell or module are calculated by solving an equivalent-circuit model. The solution to that model shown [21] in Fig. 1 is an IV curve (i.e., the relationship between current and voltage), from which standard electrical outputs [22] like maximum power P_{MP} , short-circuit current J_{SC} , and open-circuit voltage V_{OC} are determined. The inputs are defined there are two possible exceptions: the series resistance R_s (optional) and the light-generated current J_L .

J_L represents the current density generated inside the solar cell and collected by the p–n junction. It's called the light-generated current density.

J_L is determined from the equation:

$$J_L = \int_0^{\infty} J_{ph}(\lambda)A(\lambda)\eta(\lambda)d\lambda \quad (1)$$

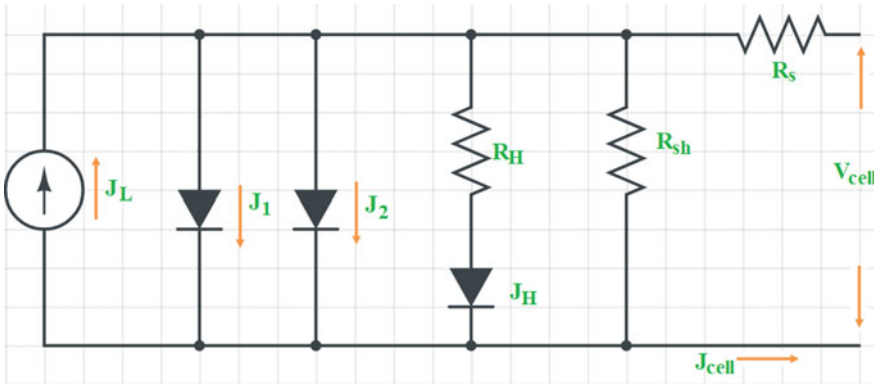


Fig. 1 Electrical equivalent circuit of bifacial cell

where $J_{ph}(\lambda)$ is the incident photon current, $A(\lambda)$ is the fraction of the incident light that becomes absorbed by the active region of the solar cell, and $\eta(\lambda)$ is the collection efficiency within that active region [23].

Inputs for equivalent-circuit models are commonly quoted at ‘nominal’ temperatures such as 25 °C or 300 K. When installed in the field, however, solar cells tend to operate at higher temperatures. The option of loading circuit inputs at a nominal temperature T_{nom} , setting the operating temperature T , and allowing SunSolve [24] to calculate the circuit inputs at T using the same approach as PV Syst, which applies these equations:

$$J_L = J_{Lnom}[1 + \mu_{IL}(T - T_{nom})] \tag{2}$$

$$m_1 = m_{1nom}[1 + \mu_{m1}(T - T_{nom})] \tag{3}$$

where μ_{IL} and μ_{m1} are coefficients for the light-generated current and ideality factor of the primary diode m_1 ; and

$$J_{01} = J_{01nom} \left(\frac{T}{T_{nom}} \right)^3 \exp \left[\frac{qE_g}{m_1 k} \left(\frac{1}{T} - \frac{1}{T_{nom}} \right) \right] \tag{4}$$

where E_g is the band gap of the semiconductor, q is the charge on an electron, and k is Boltzmann’s constant, giving the recombination current of the primary diode J_{01} at temperature T .

The Monte-Carlo algorithm (a Monte Carlo algorithm is a randomized algorithm whose output may be incorrect with a certain (typically small) probability) necessarily leads to uncertainty in the outputs. These uncertainties are calculated by dividing the number of rays traced into multiple sub-simulations, and then applying statistical analysis to determine a mean value and a 95% confidence interval for each

output. If, for example, the current absorbed within the solar cell is determined to be $J_{cell} = 36.23 \pm 0.45 \text{ mA/cm}^2$ after 100,000 rays are traced, this means that we can be 95% confident that J_{cell} would be between 35.78 and 36.68 mA/cm^2 after infinitely many rays are traced.

1.3 Algorithm

Step 1: Several rays are created. Each ray is assigned a wavelength, an intensity, a direction, and a location.

Step 2: Each light beam continues along a straight line until it converges with an aspect of the module's surface.

Step 3: At this interaction, and at all future interactions with an interface: reflectance, transmittance, and absorptance are calculated; the intensity of the ray is reduced by the value of the absorptance; the magnitudes of reflectance and transmittance are translated into probabilities.

Step 4: If the ray passes through an absorbing layer, its intensity is reduced by applying Beer's law.

Step 5: Steps 2–4 is repeated for each ray until the ray is lost from the module, the ray's intensity decreases below a threshold and the ray has intersected with the maximum allowable number of interfaces.

Step 6: The gains and losses are recorded for each ray and summed and averaged to give the results of the ray packet.

Step 7: Steps 1–6 is repeated for as many ray packets that are required for the total number of rays to equal the value entered.

2 Characterization of PERC

Passive layer of PERC will be acting as reflector for the unabsorbed light back to the cell for second absorption leading to increase the overall cell efficiency. Figure 2 shown is a typical PERC cell considered for the analysis which is having 4 rectangular interconnection, 5 busbars and 120 fingers on both the sides.

The geometry of the cell has the configuration of grid contact layout both in front and rear sides. Finger orientation is along X and bus bar orientation is along Y. Number of fingers (N_F) on both the sides is 120 with round rectangular cross section. The height (H) of the fingers is 15 μm and width of each finger (W_F) is 45 μm on both sides of the cell. Finger pitch (P_F) and finger spacing (S_F) are considered as 0.1306 cm and 0.1261 cm respectively. Similarly, bus bars are considered as 5 numbers (N_B with

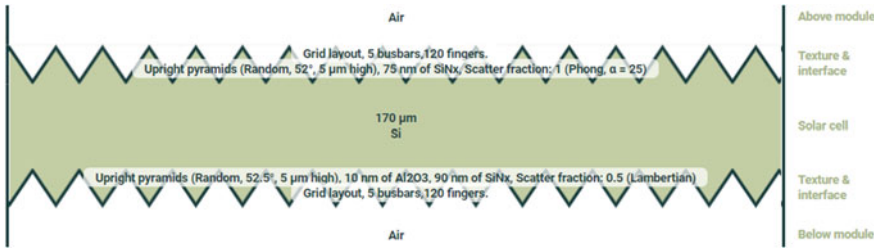


Fig. 2 c-Si bifacial PERC Cell

rectangular cross section having $15 \mu\text{m}$ height (H) and $1100 \mu\text{m}$ width (W_B). To calculate R_S , front and rear electrodes of the cell are designed with Ag, Dupont PV 19 conductor having resistivity $2.6 \times 10^{-6} \Omega\text{cm}$ (Fig. 3).

The shape of the cell is pseudosquare with length (X_C) 15.68 cm , diameter (D_C) 21 cm and cell area (A_C) 244.3 cm^2 . Entire analysis is carried out using sunlight spectrum with AM 1.5 g [Gue95] and scaling factor 1 covered for full area. Minimum wavelength of the spectrum is considered as 300 nm whereas the maximum wavelength is 1200 nm with wavelength interval of 20 nm . The Grid anode speaks to the standard H-bar plan for a cell cathode. It comprises of a bunch of fingers master-minded at the right points to a progression of bus bars. The two fingers and bus bars run the full degree of the substrate (for example to the edge of the wafer). This arrangement would regularly be utilized for the front cathode of a norm or PERC cell and for the back terminal of bi-facial cells. Simulation permits to set either the number of fingers as well as bus bars to zero.

The Coating terminal speaks to a surface covered totally by an anode. It is comprised of a progression of bus bars with a constant layer of metal between

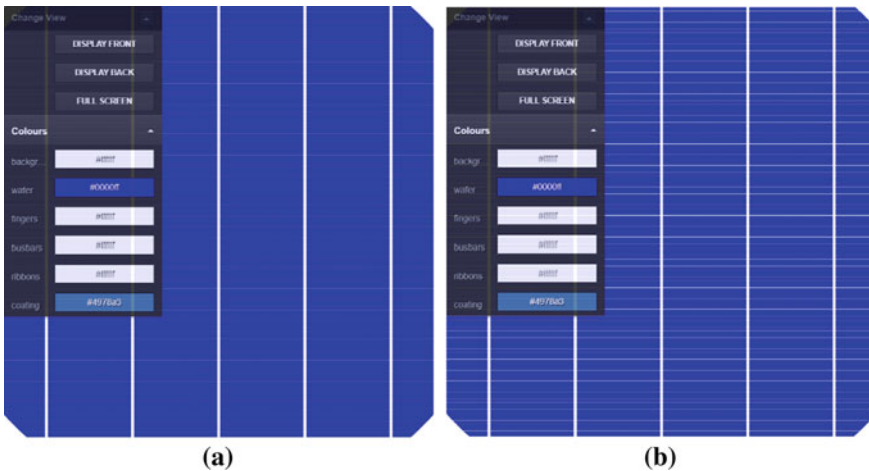


Fig. 3 **a** Cell image—front display, **b** cell image—back display

everyone. This setup is commonly be utilized to reproduce the backside of a standard screen print or PERC cell. Note that the coatings are applied right to the edge of the wafer and it is preposterous to expect to characterize a hole at the edge. All setups permit the meaning of cell interconnection strips. Strips are adjusted to a similar pivot as the bus bars. The length of the strip is equivalent to the degree of the unit cell for example the wafer size + any encompassing zone. Strips were applied to both the front and back of the cell.

Solar Cell Equivalent Circuit Parameters [21]:

The cell considered has the following equivalent circuit parameters

Light-collected current	(J_L)	39.36 mA/cm ²
Saturation current 1	(J_{01})	0.2 pA/cm ²
Ideality factor 1	(m_1)	1
Saturation current 2	(J_{02})	10 nA/cm ²
Ideality factor 2	(m_2)	2
Shunt resistance	(R_{sh})	20 k Ω cm ²
Non-grid resistance	(R_{ng})	0.5 Ω cm ²
Grid resistance	(R_{sg})	0.09807 Ω cm ²
Series resistance	(R_s)	0.5909 Ω cm ²
Nominal temperature	T_{nom}	26.85 °C
Operating temperature	T	26.85 °C

3 Results

Generation Profile

A generation profile describes the generation rate of electron–hole pairs G as a function of depth in the solar cell. Its units are cm⁻³ s⁻¹. G is calculated as a function of distance from both the uppermost point of the solar cell (z), and the nearest point on the front surface (ζ). Figure 4 explains the difference between z and ζ . The first figure in Fig. 4 shows how z and ζ are defined, giving the example of generation occurring at point 1 and point 2 (inside a pyramid); the second figure plots contours of ζ within a textured cell [24].

Additionally, is known that G is characterized regarding the cell territory. That is the reason $G(z)$ diminishes with diminishing z when z is not exactly the height of the pyramids. Although the age rate may be high inside the silicon part of a pyramids, $G(z)$ is here characterized over the whole cell territory instead of simply the zone contained inside the pyramids. The explanation we characterize $G(z)$ this way is so the necessary of $G(z)$ and $G(\zeta)$ are the equivalent and liken to the current thickness consumed in the cell $J_{A,cell}$:

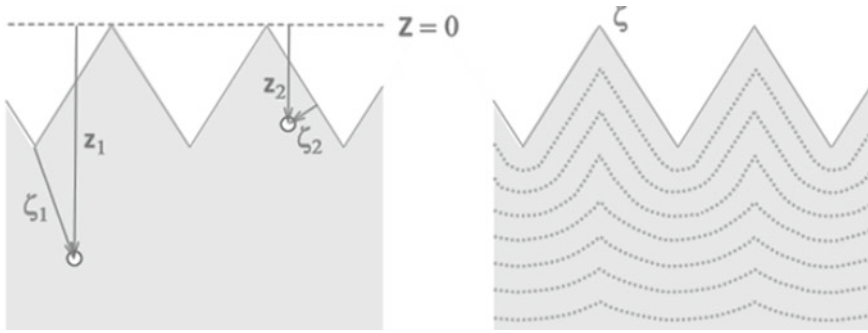


Fig. 4 Difference between z and ζ

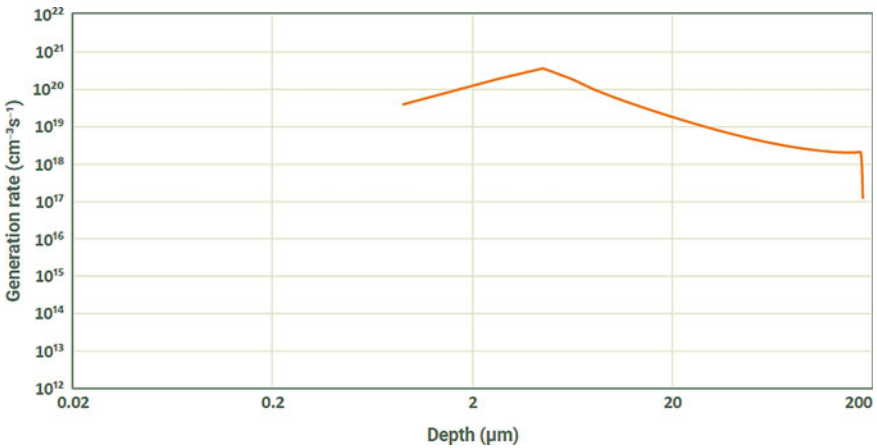


Fig. 5 Generation rate versus depth

$$\int_0^w G(z)dz = \int_0^{w'} G(\zeta)d\zeta = J_{A,\text{cell}} \tag{5}$$

- W Thickness of the cell including the height of the front and rear texture, and
- W' Thickness of the cell including the height of the rear texture but excluding the height of the front texture.

Figures 5 and 6 shows the plot of the generation rate with respect to depth and zeta of the cell respectively. The depth and zeta of the cell is represented in μm , and the generation rate is defined as $\text{cm}^{-3} \text{s}^{-1}$.

The intensity (W/m^2) of an illuminating source is determined by incorporating the spectral ($\text{W}/\text{m}^2/\text{nm}$) intensity of the chosen range over the chosen frequency scope and multiplying by the scaling factor. The spectrum of the chose range is thought

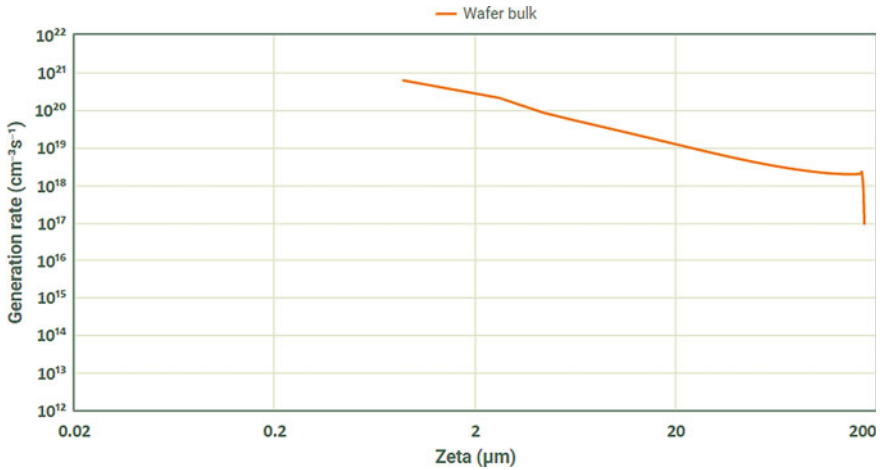


Fig. 6 Generation rate versus zeta

to be the incident power on an \perp ar plane. Thusly must scale any custom spectra that have estimated by instruments not perpendicular to the light source.

RAT (Reflection, Absorption and Transmission) analysis is performed using Sunsolve simulation tool. There are two ways to deal with figuring the division of incident rays that are scattered. The main methodology is to set a consistent dissipating portion Λ . This implies that for each beam that collaborates with the surface, Λ of these will be dissipated by the picked dispersing model, and the rest of not be dispersed. In this manner, setting $\Lambda = 0$ will imply that there is no dispersing, regardless of what the dissipating model is chosen. The subsequent methodology is to apply a scalar dispersing model. With this model, the dissipating part Λ isn't consistent yet diminishes with expanding frequency. This division additionally relies upon the episode point, the refractive list of the materials, and whether the beam is reflected or consumed.

For Reflection

$$\Lambda = 1 - e^{\left[-\left(\frac{2\pi}{\lambda} \sigma_{rms} * 2 * n_i * \cos \theta_i\right)^2\right]} \tag{6}$$

For Transmission

$$\Lambda = 1 - e^{\left[-\left(\frac{2\pi}{\lambda} \sigma_{rms} * |n_i * \cos \theta_i - n_t * \cos \theta_t|\right)^2\right]} \tag{7}$$

where σ_{rms} is the root mean square roughness of the surface.

Reflection of sunlight in the front panel, Esc in both front and rear side are computed and plotted on a graph as shown in the Fig. 7 without considering spectral intensity. Figure 8 shows the Reflection, Absorption when considering spectral intensity.

Quantum efficiency is given as a function of wavelength. No sunlight is absorbed below the bandgap, so the quantum efficiency is zero in larger wavelengths. From Fig. 9 after 1150 nm the QE is zero. QE is not measured below 300 nm as the power from AM1.5 g is low and the response is reduced due to front surface recombination. The quantum efficiency for the cell considered is maintained constantly 94% ($\pm 2\%$) between wavelengths of 460–970 nm, this efficiency is good for a better power

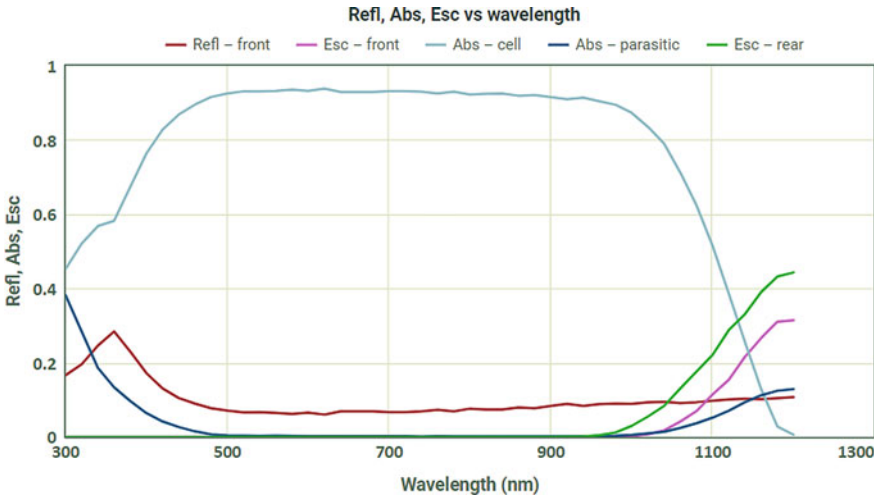


Fig. 7 Refl, Abs, Esc versus wavelength without considering spectral intensity

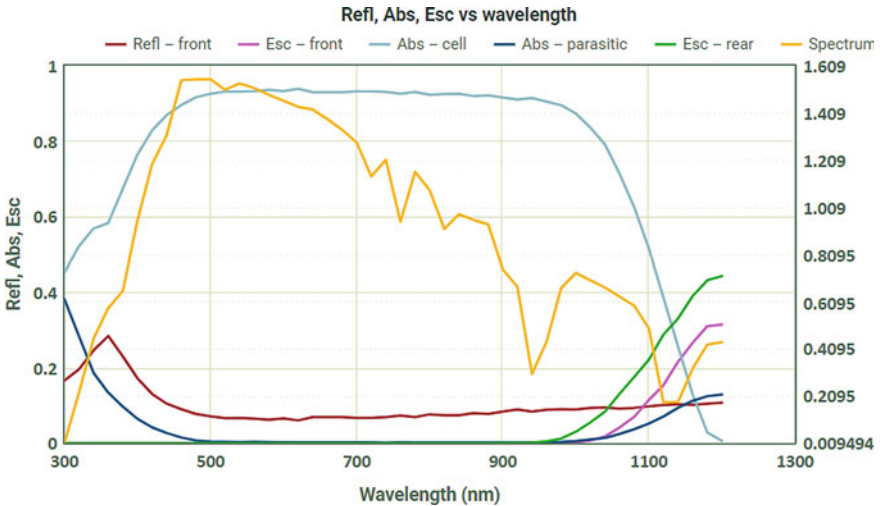


Fig. 8 Refl, Abs, Esc versus wavelength considering spectral intensity

generation in the solar cell as the number of carriers collected are more. Equivalent current densities in solar cell are plotted in Fig. 10.

Figure 11 shows main losses versus λ , where the stacked columns are the current densities measured in mA/cm² (Tables 1 and 2).

Table 3 represents equivalent parameters of the cell like temperature, maximum output power, maximum power point voltage, maximum power point current, fill factor of the solar cell, open circuit voltage and short circuit current.

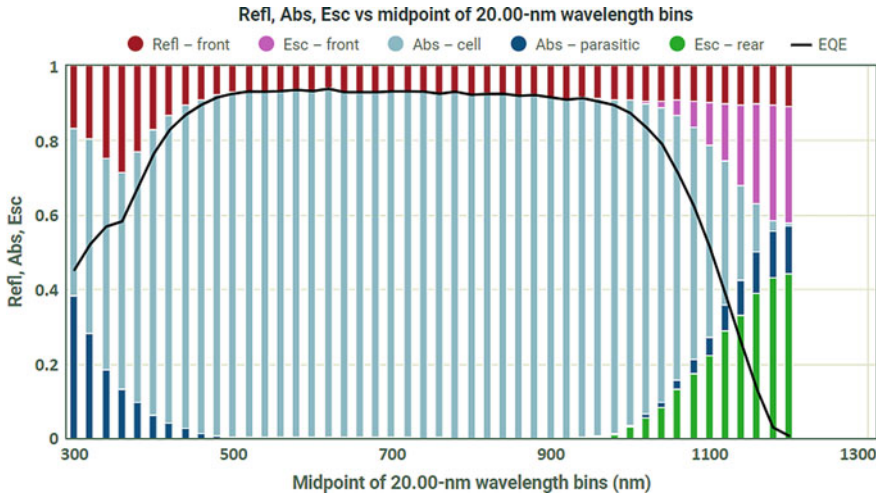


Fig. 9 External quantum efficiency in solar cell

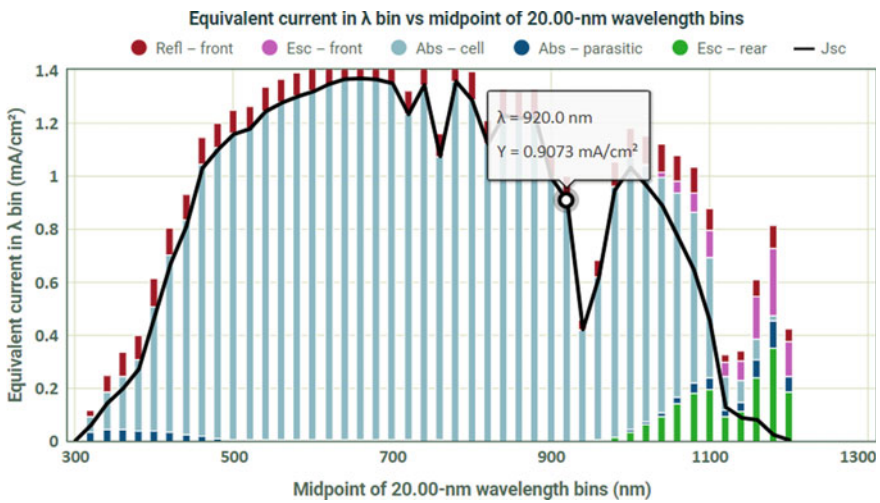


Fig. 10 Equivalent current densities in solar cell

Figure 12 shows the IV graph of the cell which is producing an output power of 5.068 W with a fill factor of 0.795. Maximum Point (MP) is shown in the graph at which the voltage generated is 563.2 mV and the current is 8.998 A. The equivalent data of the IV plot is recorded in Table 3 and grid resistance of the cell is recorded in Table 4.

Total amount of carriers that have been reflected from the cell with respect to spectrum or wavelength is plotted and represented in Fig. 13. As discussed in Fig. 9, reflection will be more below 460 nm and above 970 nm as the power is less. During 460-970 nm the reflection will be minimum. Similarly, the total reflection from the

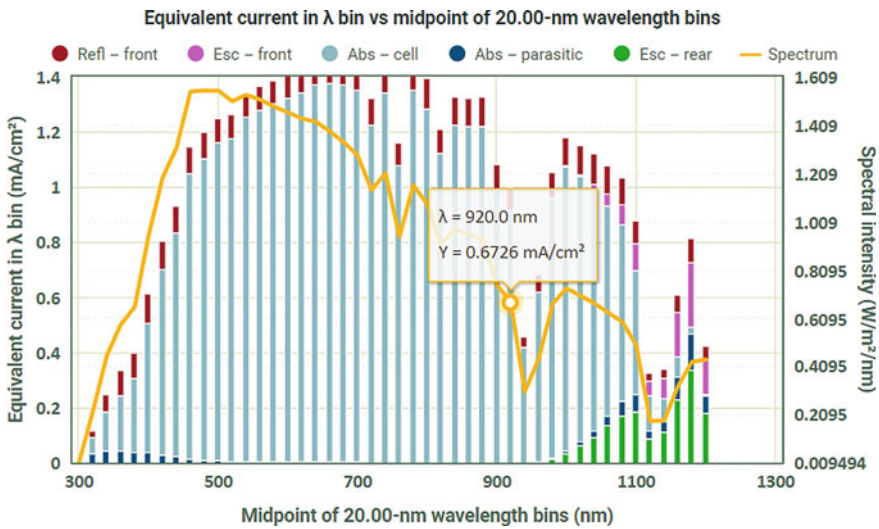


Fig. 11 Main losses with respect to spectral intensity

Table 1 Equivalent photon current densities (mA/cm²)

	Mean (mA/cm ²)	95% CI (mA/cm ²)	Fraction of J_{inc} (%)
Incident	46.32	–	100.0
<i>Lost to environment</i>			
Reflected front	3.901	0.03894	8.423
Escaped front	0.9209	0.01120	1.988
Escaped rear	1.712	0.01575	3.696
<i>Absorbed in components</i>			
Cell absorption	39.00	0.03879	84.20
Parasitic absorption	0.7792	–	1.682
Remainder	0.006600	0.001614	0.01425

Table 2 Equivalent photon current densities (A)

	Mean (mA/cm ²)	95% CI (mA/cm ²)	Fraction of J_{inc} (%)
Incident	11.32	–	100.0
<i>Lost to environment</i>			
Reflected front	0.9531	0.009515	8.423
Escaped front	0.2250	0.002737	1.988
Escaped rear	0.4183	0.003847	3.696
<i>Absorbed in components</i>			
Cell absorption	9.528	0.009476	84.20
Parasitic absorption	0.1904	–	1.682
Remainder	0.001612	3.944×10^{-4}	0.01425

Table 3 Current voltage (IV) data

Parameter	Abb	Units	Output
Temperature	T	K	300.0
Maximum power	P _{MP}	W	5.068
Maximum-power-point voltage	V _{MP}	mV	563.2
Maximum-power-point current	I _{MP}	A	8.998
Fill Factor	FF		0.795
Open-circuit voltage	V _{OC}	mV	669.1
Short-circuit current	I _{SC}	A	9.528

rear side of the cell is plotted in Fig. 14. Up to 950 nm the reflection from rear side is zero. As the spectrum increases beyond 950 nm capturing of carriers will decrease at the rear side which is shown in the plot of Fig. 14.

Total amount of carriers that have been absorbed from the cell with respect to spectrum or wavelength is plotted and represented in Fig. 15. As discussed in Fig. 9, reflection will be more below 460 nm and above 970 nm as the power is less. During 460–970 nm the absorption will be maximum. Similarly, the total absorption from the rear side of the cell is plotted in Fig. 16. Up to 500 nm the absorption from rear side is zero. As the spectrum increases beyond 950 nm capturing of carriers will decrease at the rear side which is shown in the plot of Figs. 16 and 17.

Figure 18 shows the plot of the total amount of sunlight escaped in the front side of the cell with respect to wavelength. Front surface escape can be read as the sunlight (photons) that has entered the cell but was unable to absorb by the cell and escaped in the front surface. Front surface escape is referred as advance loss in the cell, and this is due to surface texture and light trapping properties. Further to the analysis presented an attempt is made to show the effect of haze on the cell. Figures 19 and 20 show respectively the effect of total haze on reflection, absorption, Esc and EQE for different spectrums and the same are plotted.

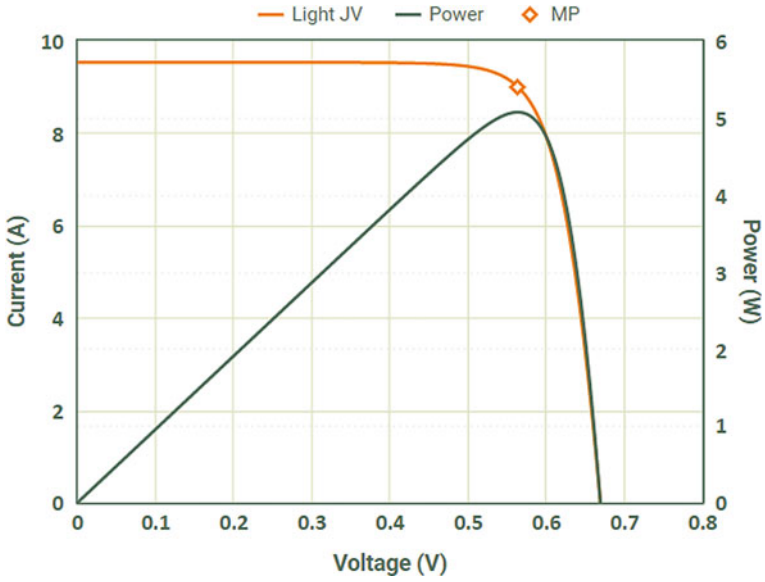


Fig. 12 I-V Plot showing maximum point

Table 4 Grid resistance of solar cell

	R_s grid ($\Omega \cdot \text{cm}^2$)	R_s contact ($\Omega \cdot \text{cm}^2$)	R_s total ($\Omega \cdot \text{cm}^2$)	Metal coverage (%)	A (cm^2)	V (cm^3)
<i>Front elements</i>						
Busbars	0.01248	0	0.01248		8.621	0.01293
Fingers	0.04611	0	0.04611		8.120	0.01044
Front metal total	0.05859	0	0.05859	6.852	16.74	0.02337
<i>Rear elements</i>						
Busbars	0.01245	0	0.01245		8.621	0.01293
Fingers	0.01523	0	0.01523		21.11	0.02940
Rear metal total	0.02769	0	0.02769	12.17	29.73	0.04233
Total for cell	0.08628	0	0.08628	19.02	46.47	0.06570

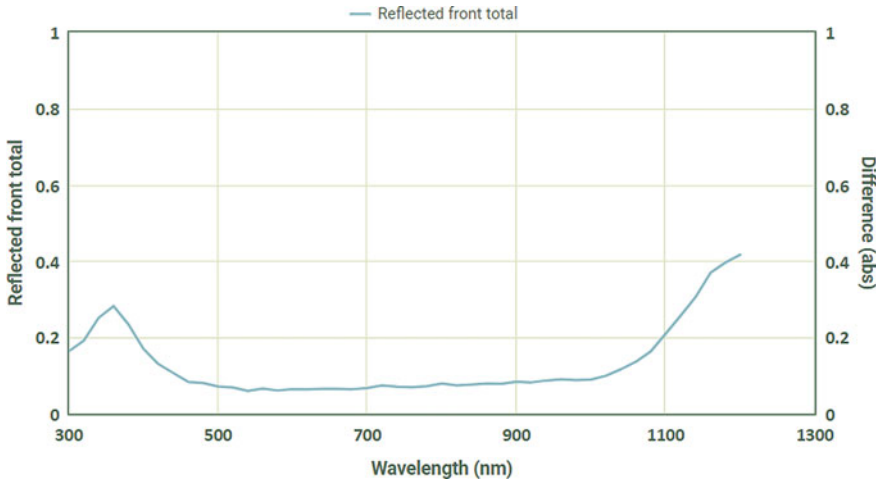


Fig. 13 Total reflection from front side of cell versus wavelength

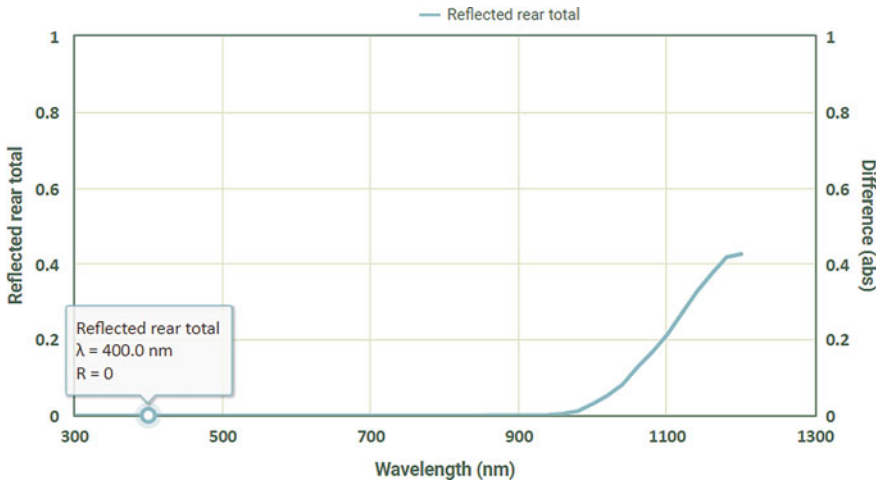


Fig. 14 Total reflection from rear side of cell versus wavelength

Color outputs are calculated from the upward hemispherical spectrum (front color), the downwards hemispherical spectrum (rear color), and, if a detector is included, the spectrum incident to the detector (detector color). The program effectively ‘averages’ the color of the module components that reflect light. If a module contains a dark blue cell surrounded by a white back sheet, its ‘averaged’ color might appear light blue; and if the cell also had fingers, then the ‘averaged’ color might be a bluey grey (Fig. 21).

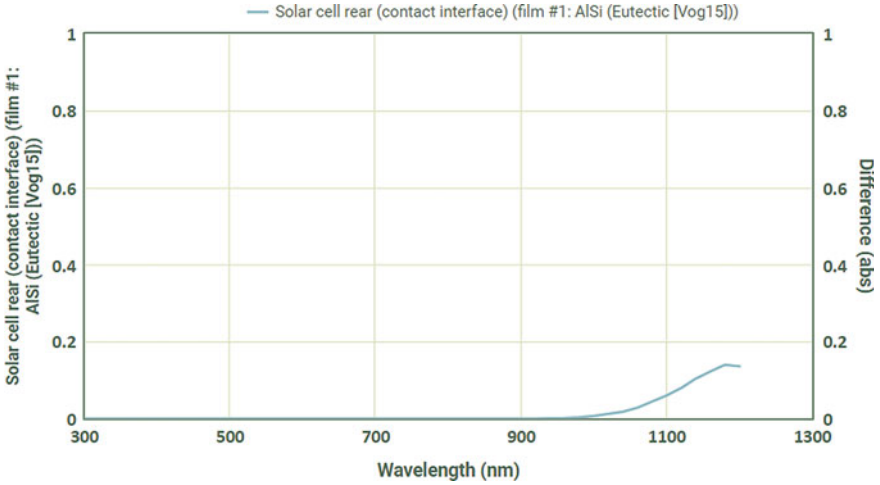


Fig. 15 Total absorption from front side of cell versus wavelength

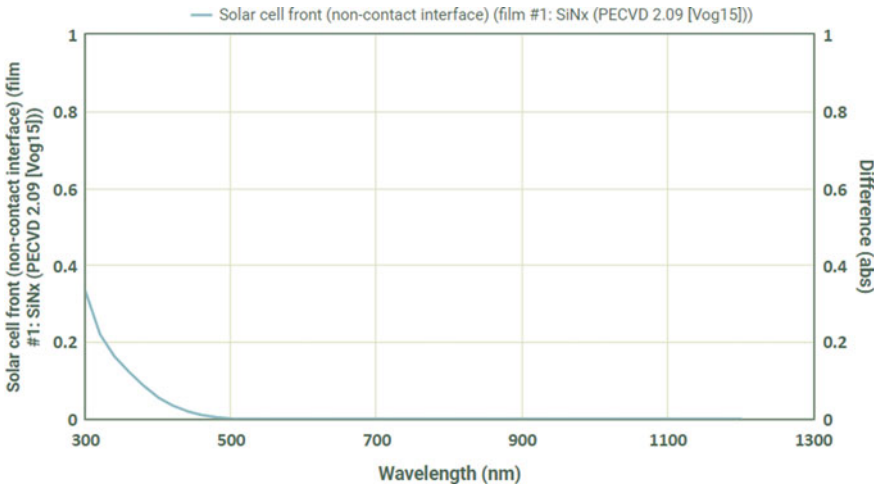


Fig. 16 Total absorption from rear side of cell versus wavelength

The color of the cell has been determined using CIE 1964, 10°, Wyman 2013_Eq 3 [24] color matching function and the chromatic display type is sRGB, 6504 K, standard. The shading coordinating capacities were dictated by estimating the mean shading view of an example of human eyewitnesses over the visual reach from 360 to 970 nm. XYZ is a device-independent representation of colour. It does not depend on the display monitor. The precision of XYZ increases as the number of rays increases and as the wavelength interval decreases (down to 1 nm). XYZ is scaled such that Y = luminosity. XYZ depends on the incident spectrum as well as the reflection,

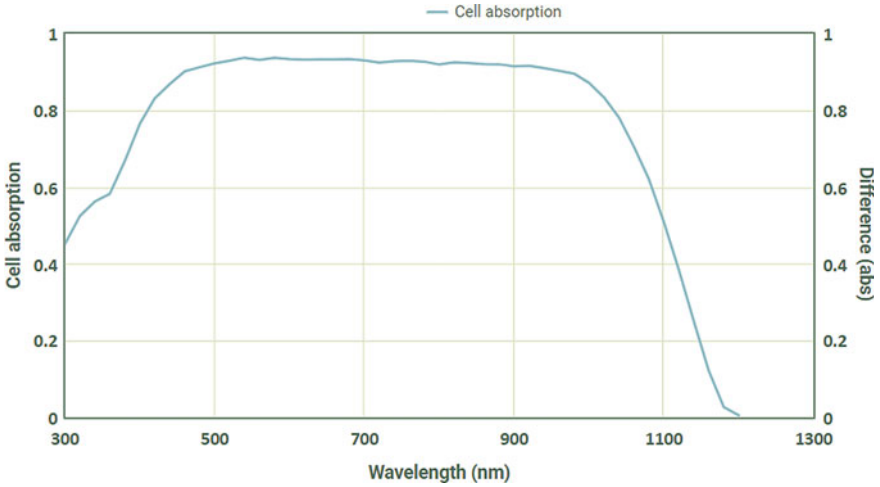


Fig. 17 Cell absorption versus wavelength

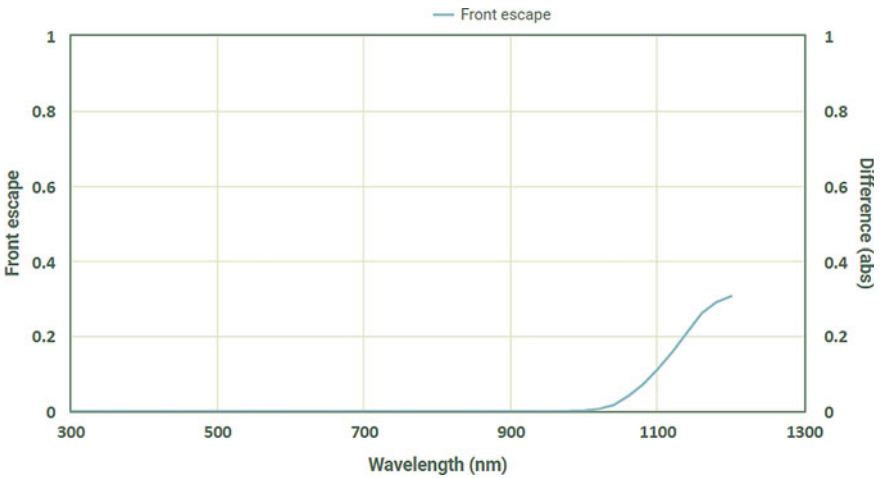


Fig. 18 Front surface escape of light versus wavelength

absorption, and transmission of the simulated structure. XYZ will only be calculated if the inputs for the minimum and maximum wavelengths are ≤ 360 nm and ≥ 970 nm, respectively.

$$X = \Delta\lambda \sum_{\lambda=360}^{970 \text{ nm}} \bar{x}_\lambda P(\lambda) \tag{8}$$

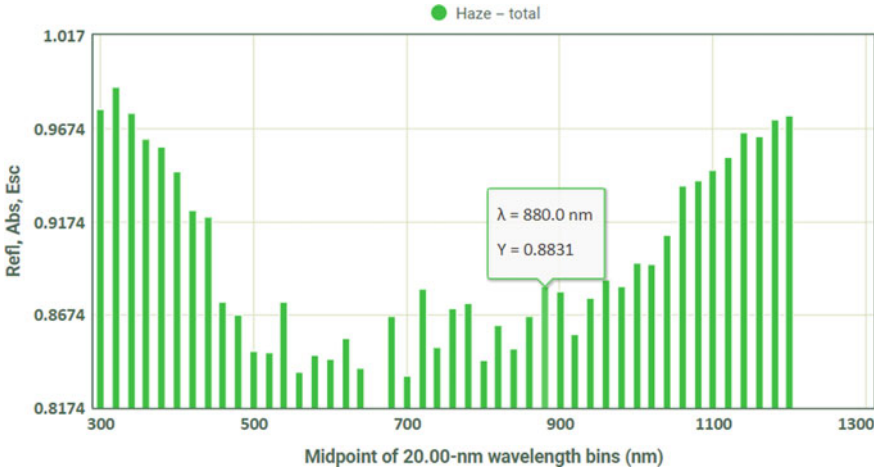


Fig. 19 Haze effect on Refl, Abs, Esc versus wavelength

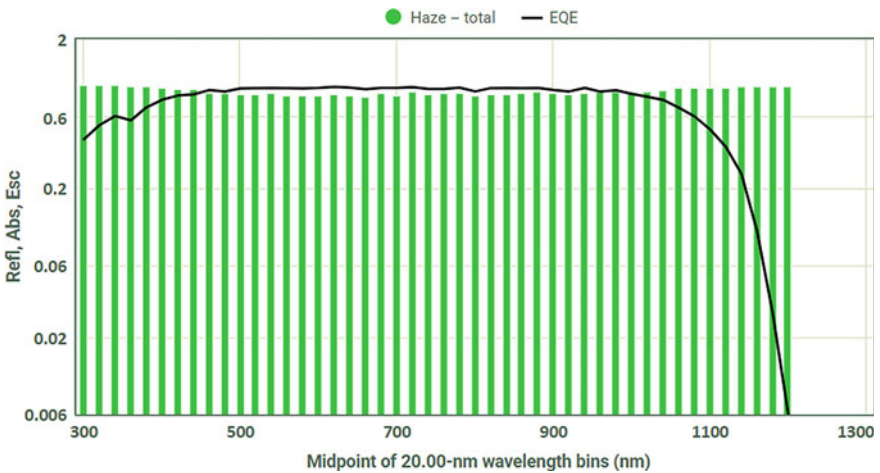


Fig. 20 Haze effect versus EQE on Refl, Abs, Esc and spectrum

$$Y = \Delta\lambda \sum_{\lambda=360}^{970 \text{ nm}} \bar{y}_{\lambda} P(\lambda) \tag{9}$$

$$Z = \Delta\lambda \sum_{\lambda=360}^{970 \text{ nm}} \bar{z}_{\lambda} P(\lambda) \tag{10}$$

The X and Z parts give the shading or chromaticity of the range. Because the apparent tone depends just upon the general extents of X, Y, and Z, we characterize

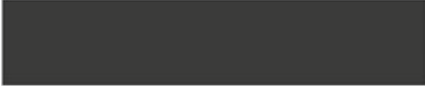
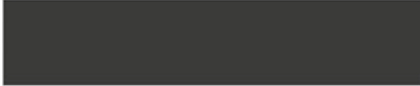
Front	Detector
	
XYZ: (0.05165, 0.05000, 0.06888)	XYZ: (0.04886, 0.05000, 0.04695)
RGB: (67, 61, 72)	RGB: (68, 62, 58)
LAB: (26.73, 5.192, -6.009)	LAB: (26.73, 1.710, 3.550)
LUV: (26.73, 2.463, -7.658)	LUV: (26.73, 3.524, 3.664)

Fig. 21 Cell Color using color matching function

its chromaticity coordinates as:

$$x = \frac{X}{X + Y + Z} \tag{11}$$

$$y = \frac{Y}{X + Y + Z} \tag{12}$$

$$z = \frac{Z}{X + Y + Z} \tag{13}$$

Now

$$x + y + z = \frac{X + Y + Z}{X + Y + Z} = 1 \tag{14}$$

z may be obtained from x and y

$$z = 1 - (x + y) \tag{15}$$

RGB, LAB and LUV are all calculated from XYZ. These outputs depend on the white point of the chromatic display type. Most computer monitors have a sRGB display type where the white point is based on the 6504 K spectrum. RGB also depends on the chromaticity coordinates and gamma curves of the chromatic display type.

4 Conclusion

Characterization of bifacial p-type PERC solar cell with various proportions of size and width are presented in this paper. Back Silicon Nitrate layer with various thickness are streamlined and most elevated back productivity of bifacial solar cell (~22%)

was obtained at AM1.5 g standard test condition. Absorption, Reflection and Escape factors are presented to verify the advance losses in the PERC cell. Total reflected sunlight on the front side of the cell is recorded as 8.4%, escaped front side and rear side are noted as 1.9% and 3.5% respectively. The Cell absorption is found to be 86.215% which included parasitic absorption of 1.925%. p-type PERC when compared to normal c-Si cell has 10.79% more absorption rate.

Acknowledgements Authors would like to thank FIST (Fund for Improvement of S&T Infrastructure), Department of Science & Technology, Ministry of Science & Technology, Govt. of INDIA and GRIET Management for their sanction of grants to the institution. Grant Number: SR/FST/College-29/2017 dt: 16 Jan 2018.

References

1. Sporleder K, Bauer J, Richter S, Hähnel A, Großer S, Turek M, Hagendorf C (2019) Local corrosion of silicon as root cause for potential-induced degradation at the rear side of bifacial PERC solar cells. *Phys Status Solidi RRL Rapid Lett.* <https://doi.org/10.1002/pssr.201900163>
2. Cai X, Ni Z, Chen C, Ke P, Chen H, Cao H, Zhang Q (2019) The study on anti-PID performance of high efficiency bifacial cell module. *IOP Conf Ser: Mater Sci Eng.* <https://doi.org/10.1088/1757-899X/556/1/012033>
3. Ye F, Deng W, Guo W, Liu R, Chen D, Chen Y, Yang Y, Yuan N, Ding J, Feng Z (2017) 22.13% efficient industrial p-type mono PERC solar cell. *IEEE PVSC, Washington.* <https://doi.org/10.1109/PVSC.2016.7750289>
4. Zhang S, Hu D, Qian H, Jie J, Ni Z, Zhang X, Xie L (2019) Application of silicon oxide on high efficiency mono-crystalline silicon PERC solar cells. *Energies.* <https://doi.org/10.3390/en12061168>
5. Renshaw JS, Upadhyaya A, Upadhyaya V, Rohatgi A (2012) Crystalline silicon solar cells with segmented selective emitter by ultraviolet laser doping. 38th IEEE PVSC, TX. <https://doi.org/10.1109/PVSC.2012.6317794>
6. Lee E, Lee H, Choi J, Oh D, Shim J, Cho K, Kim J, Lee S, Hallam B, Wenham SR, Lee H (2011) Improved LDSE processing for the avoidance of overplanting yielding 19.2% efficiency on commercial grade crystalline Si solar cell. *Sol Energy Mater Sol Cells.* <https://doi.org/10.3390/en13061388>
7. Dahlinger M, Eisele SJ, Lill PC, Kohler JR, Werner JH (2012) Full area laser doped boron emitter silicon solar cells. 38th IEEE PVSC, Austin. <https://doi.org/10.1109/PVSC.2012.6317778>
8. Kim C, Lee J, Lim S, Jeong C (2015) Enhanced absorption and short circuit current density of selective emitter solar cell using double textured structure. *Solar Energy.* <https://doi.org/10.1016/j.solener.2015.04.010>
9. Hirata K, Saitoh T, Ogane A, Sugimura E, Fuyuki T (2011) Selective emitter formation by laser doping for phosphorous-doped n-type silicon solar cells. *Appl Phys Exp.* <https://doi.org/10.1143/APEX.5.016501>
10. Wang KS, Lin D, An XR, Mai L, Mitchell E, Wenham SR (2012) 18.8% Efficient laser-doped semi-conductor fingers screen-printed silicon solar cell with light-induced plating. 38th IEEE PVSC, Austin. <https://doi.org/10.1109/PVSC.2012.6317805>
11. Zhang QZ, Shu BF, Chen MB, Zhong NB, Luo JJ, Wu XL (2017) Numerical investigation on selective emitter formation by laser doping for phosphorous-doped silicon solar cells. *J Laser Appl* 02-2003. <https://doi.org/10.2351/1.4979303>

12. Lopez G, Ortega P, Colina M, Voz C, Martin I, Morales-Vilches, Orpella A, Alcubilla R (2015) Emitter formation using laser doping technique on n- and p-type c-Si substrates. *Appl Surface Sci* 336:182–187. <https://doi.org/10.1016/j.apsusc.2014.10.140>
13. Takahashi K, Kurosawa M, Ikenoue H, Sakashita M, Takeuchi W, Nakatsuka O, Zaima S (2016) Low thermal budget n-type doping into Ge surface using ultraviolet laser irradiation in phosphoric acid solution. *Appl Phys Lett* 108:052104. <https://doi.org/10.1063/1.4941236>
14. Dullweber T, Wehmeier N, Nowack A, Brendemühl T, Kajari-Schröder S, Brendel R (2016) Industrial bifacial n-type silicon solar cells applying a boron co-diffused rear emitter and an aluminum rear finger grid. *Phys Status Solid* 213(11):3046–3052. <https://doi.org/10.1002/pssa.201600346>
15. Jager U, Wolf A, Steinhäuser B, Benick J, Nekarda J, Preu R (2012) Laser doping for high efficiency silicon solar cells. *Laser Mater Proc* 847309. <https://doi.org/10.1063/1.4915326>
16. Sun X, Khan MR, Deline C, Alam MA (2018) Optimization and performance of bifacial solar modules: a global perspective. *Appl Energy* 212:1601–1610. <https://doi.org/10.1016/j.apenergy.2017.12.041>
17. Castillo-Aguilella JE, Hauser PS, Castillo J (2016) Multi-variable bifacial photovoltaic module test results and best-fit annual bifacial energy yield model. *IEEE Access* 4:498–506. <https://doi.org/10.1109/ACCESS.2016.2518399>
18. Park H, Chang S, Park S, Kim WK (2019) Outdoor performance test of bifacial n-type silicon photovoltaic modules. *Sustainability* 11(22):6234. <https://doi.org/10.3390/su11226234>
19. Liu J, Janssen GJM, Koppes M, Kossen EJ, Tool K, Komatsu Y, Anker J, Gutjahr A, Vlooswijk A, Luchies JM (2015) Selective emitter in n-type c-Si solar cells. 31st European photovoltaic solar energy conference, Hamburg, pp 633–636. <https://doi.org/10.1016/j.egypro.2016.07.122>
20. Richter A, Benick J, Feldmann F, Fell A, Hermle M, Glunz SW (2017) n-Type Si solar cells with passivating electron contact: identifying sources for efficiency limitations by wafer thickness and resistivity variation. *Solar Energy Mater Cells* 173:96–105. <https://doi.org/10.1016/j.solmat.2017.05.042>
21. Bhang BG, Lee W, Kim GG, Choi JH, Park SY, Ahn H-K (2019) Power performance of bifacial c-Si PV modules with different shading ratios. *IEEE J Photovoltaics* 9(5):1413–1420. <https://doi.org/10.1109/JPHOTOV.2019.2928461>
22. Simayi S, Kida Y, Shirasawa K, Suzuki T, Takato H (2017) Method of removing single-side doped layer while maintaining pyramid textured surface of n-type bifacial solar cells. *IEEE J Photovoltaics* 7:458–462. <https://doi.org/10.1109/JPHOTOV.2016.2646060>
23. Lu G, Zheng F, Wang J, Shen W (2017) Thin Al₂O₃ passivated boron emitter of n-type bifacial c-Si solar cells with industrial process. *Prog Photovoltaics: Res Appl* 25(4):280–290. <https://doi.org/10.1002/pip.2859>
24. PV Lighthouse: SunSolve™, accessed 12 Dec 2020, <https://www.pvlighthouse.com.au>

Network Reconfiguration of Distribution System with Distributed Generation, Shunt Capacitors and Electric Vehicle Charging Stations



Surender Reddy Salkuti

Abstract This chapter presents a heuristic-based technique for solving the optimal network reconfiguration (ONR) in a radial distribution system (RDS) using the fuzzy-based multi-objective methodology. Minimization of real power losses and deviation of nodes voltage is considered as the multiple objectives in this work and they are modeled with fuzzy sets. The developed algorithm determines the optimal reconfiguration of feeders with the minimum number of tie-line switch operations. This work focuses on different combinations of ONR along with renewable-based distributed generation (DG) units, shunt capacitors, and electric vehicle charging stations (EVCSs). The load flow analysis implemented in this chapter is based on an iterative approach of the receiving end voltage of RDS. The effectiveness of the proposed heuristic-based methodology has been implemented on the IEEE 69 bus RDS.

Keywords Network reconfiguration · Distributed generation · Power loss · Voltage stability · Distribution system load flow · Radial distribution system · Shunt capacitors · Electric vehicles

Nomenclature

NR	Network reconfiguration
DG	Distributed generation
DSLFL	Distribution system load flow
RDS	Radial distribution system
EVs	Electric vehicles
DERs	Distributed energy resources
PEVs	Plugin electric vehicles

S. R. Salkuti (✉)

Department of Railroad and Electrical Engineering, Woosong University, 171 Dongdaejon-ro (155-3 Jayang-dong), Dong-gu, Daejeon 34606, Republic of Korea
e-mail: surender@wsu.ac.kr

BFS	Backward forward sweep
LIM	Load impedance matrix
OFR	Optimal feeder reconfiguration
ONR	Optimal network reconfiguration
N_{EV}^c, N_{EV}^d	Number of EVs charging and discharging
P_{G2V}, P_{V2G}	Active powers from vehicle-to-grid and grid-to-vehicle
η_c, η_d	Charging and discharging efficiencies
R_c, R_d	Charging and discharging rates
N_{tie}	Number of tie-line switches

1 Introduction

The distribution system plays a crucial role among the other components of the electrical power system that is generation and transmission. The power system is becoming more and more complex with the increasing demand. In developing countries, power generation is usually insufficient to meet the increasing load demand. Therefore, it is necessary to reduce the total losses in the network of which the major part is contributed by the distribution system. The power industry is adopting deregulation to obtain the economic efficiency of power system operation. In the deregulated scenario, both generation and distribution companies are dedicated to their function [1], which avoids the monopoly and creates a competitive market environment between them. This forces the power utilities to fulfill the energy demand of the consumers at a reasonable cost.

Recently the electric vehicles (EVs) have gained importance due to the increasing air pollution, climate change, and increased oil prices. Distributed energy resources (DERs) such as EVs and distributed generation (DG) are growing as an opportunity to decarbonize the energy system. The necessity of EVs is very clear with their great potential to electrify the transportation sector [2]. The renewable-based DG sources create uncertainty in the power distribution system. At the same time, they also pose new technical challenges to the power system, which can be addressed with increased flexibility. For better utilization of electrical energy, the optimization of both distribution system operation and control becomes necessary. This can be achieved through the automation of the distribution system. One of the methods adopted is the remote control of the configuration by which losses in the branches of the entire system can be minimized. The distribution system reconfiguration is carried out by modifying the topological structure of the network by changing the status of the sectionalizing and tie-line switches [3, 4]. And also, the optimal switch operations may reduce losses in the system. Both of these are met by reconfiguration. Hence, both the ONR and less number of switching operations will reduce the power losses and they are met by the proposed ONR approach.

Most of the distribution systems generally operated in radial topology which enables suitable voltage and power flow control, reduced fault current, and easier

protection coordination schemes over the meshed system. Typically, the radial distribution systems (RDSs) have two types of switches, namely, sectionalizing switches which are usually open, and tie-line switches which are usually closed [5]. When the fault occurs either on distributors or feeders, the tie-line switch allows some portion of the faulted part to be restored promptly, thereby enhancing the reliability of the system. According to Ref. [2], the power loss in the distribution network constitutes 70% of the total power loss. Therefore, the major cause of power interruption is due to problems in the distribution system.

1.1 Related Work

There has been considerable interest in the recent past to develop algorithms for feeder reconfiguration (FR) of the distribution system under various operating contingencies. Usually, distribution companies try to keep active power losses below the standard ones to gain profit rather than paying penalties. Thus the active power loss minimization is a major concern of the distribution system researchers, which has a significant impact on the maximum loadability of the network and hence, on the power system stability particularly in overburdened networks. Some of the established techniques to handle distribution systems under such a competitive scenario include network reconfiguration (NR), DG allocation, shunt capacitor placement, and simultaneous NR and DG allocation [6]. Hence, the existing distribution system requires to be optimized to satisfy the demand in the most reliable, economical, and environmentally friendlier way, while meeting the associated geographical or operational constraints.

A high-performance nonlinear sliding mode controller has been proposed in Ref. [7] for an EV charging system to improve the power factor (pf) to handle the unbalanced EV chargers and to compensate for voltage distortions. The super sense genetic algorithm (SSGA) is applied in Ref. [8] to solve the problem of complex combinatorial NR problem of RDSs. An approach for the optimal network rearrangement by incorporating the plugin electric vehicles (PEVs) proposed in Ref. [9] is based on the random programming model of the Monte Carlo simulation method. An approach for optimal placement and sizing of electric vehicle charging stations (EVCSs) on a distribution network is proposed in [10]. A fuzzy approach-based multi-objective heuristic technique for ONR in distribution systems considering the DGs is proposed in [11]. A single-phase ($1-\varphi$) EV charging coordination approach with the three-phase ($3-\varphi$) supply and chargers connected to the EVs with the less loaded phase of the feeder at the starting of charging has been proposed in [12]. The optimal planning approach of EVCSs and shunt capacitors is proposed in [13] and it is solved by using the dragonfly algorithm (DA).

An equilibrium optimizer algorithm has been applied to the ONR problem in Ref. [14] with loss reduction, voltage magnitude enhancement, and reliability indices improvement objectives. An efficient technique for balanced and unbalanced RDSs optimization by ONR and optimal capacitor placement has been proposed in [15].

The ONR allows better penetration of renewable energy sources (RESs) in the RDS and it is solved in Ref. [16] using the mixed particle swarm optimization (PSO) for loss minimization and voltage profile enhancement improvement. Reference [17] proposes optimal battery energy storage systems and allocation of PV-based DG have been solved by the PSO algorithm.

1.2 Scope and Contributions

From the literature on ONR with loss minimization objective in the distribution system, the research gap has been identified and explored the work area with current research performance and its limitations. From the literature, it has been identified that there is a requirement for solving the ONR problem by simultaneously installing the renewable-based DG units, shunt capacitors, and EVCSs. Renewable-based DG units, i.e., wind plants and solar PV farms have wind speed and solar insolation as input parameters and they are highly intermittent. The distribution load flow (DLF) used in this chapter is based on the iterative approach. The potential of this approach has made the ONR approach is very powerful and can be applied to any size of the distribution network. The ONR and DG allocation to strengthen the efficiency of distribution systems based on power loss minimization and voltage deviation minimization, as these are two major issues in the recent competitive power scenario, and they are considered as the objective functions with the presence of shunt capacitors and EVCSs. The simulation has occurred to both balanced as well as unbalanced radial distribution systems (RDSs).

This chapter is organized as follows: The description of RDS, ONR, and the summary of the literature work has been presented in Sect. 1. A brief description of distribution load flow (DLF) analysis has been presented in Sect. 2. Section 3 describes the modeling of shunt capacitors and EVCSs in the distribution system. Problem formulation is presented in Sect. 4. Section 5 describes the solution methodology. Section 6 describes the results and discussion on the 69 bus test system. The conclusions of this chapter have been summarized in Sect. 7.

2 Distribution Load Flow (DLF) Analysis

The analysis of DLF is basic but it is an essential mathematical tool for the analysis of distribution systems in both the planning and operational stages. The primary aim of the power flow analysis is to determine the magnitude and phase of steady-state voltage at all buses, active and reactive power flows in each line, for a specified loading. There are numerous power flow methods like Newton Raphson, Gauss-Seidel, fast decoupled methods, and many more methods with a modification in conventional ones. Due to the different properties of the distribution systems, these methods are not suitable for load flow analysis [18]. Certain applications including

distribution automation and power system optimization require efficient and robust load flow solutions. Over the last few decades, these load flow methods have been evolved in several different dimensions to handle both static and dynamic power distribution system problems. Traditionally, the Backward Forward Sweep (BFS) load flow techniques are applied to distribution systems and it has two-step analyses. Other load flow methods include little modification into existing techniques for their advantage over the older ones. In literature, several conventional methods have been utilized to solve distribution system problems [19]. The open branches are electrically represented with very high impedance. Whenever a branch is connected, then its parameters are replaced with actual values (i.e., resistance and reactance values) and vice versa when a branch is removed or disconnected. In other words, when a branch exchange takes place, only those parameters will be modified accordingly for further processing. This saves a lot of computation burden.

The proposed load flow solution presented in this chapter depends on an iterative approach of the receiving end voltage of the RDS. It is successfully applied on ill-conditioned RDS with consideration of realistic load [20]. In the first step, the effective power at each bus is determined after forming adjacent branches and adjacent node matrices. A sparse technique is used to determine the branches and nodes beyond a particular node. The detailed mathematical formulation is given below considering the electrical equivalent of a branch connected between the nodes a and b of RDS, and it is shown in Fig. 1.

The amount of current flowing from node a to node b can be expressed as [20],

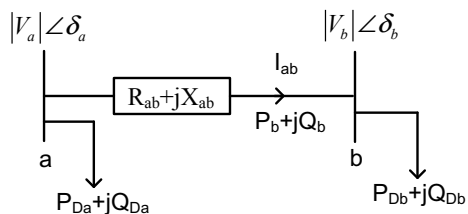
$$I_{ab} = \frac{|V_a|\angle\delta_a - |V_b|\angle\delta_b}{R_{ab} + jX_{ab}} = \frac{P_b - jQ_b}{(|V_b|\angle\delta_b)^*} \tag{1}$$

where active power (P_b) can be expressed in terms of active power load at a bus/node i (P_{Di}) and active power loss of line k ($P_{loss,k}$). Mathematically, it can be expressed as,

$$P_b = \sum_{i=1}^{N_b} P_{Di} + \sum_{k=1}^{N_{br}} P_{loss,k} \tag{2}$$

where N_b shows all the buses beyond the bus b. N_{br} shows all the branches beyond the bus b. From Eq. (1), P_b can be expressed as [21],

Fig. 1 Electrical equivalent of a typical distribution system branch



$$P_b = \frac{|V_a||V_b| \sin(\delta_a - \delta_b) + R_{ab}Q_b}{X_{ab}} \quad (3)$$

From the above equation, the voltage magnitude ($|V_b|$) and angle (δ_b) at the end of receiving node can be calculated by using,

$$\begin{aligned} |V_b| = & - \left[|V_a| \left(\frac{R_{ab}}{X_{ab}} \sin \delta - \cos \delta \right) \right] \\ & + \left[\left(|V_a| \frac{R_{ab}}{X_{ab}} \sin \delta - \cos \delta \right)^2 - 4Q_b \left(\frac{R_{ab}^2}{X_{ab}} + X_{ab} \right) \right]^{1/2} \end{aligned} \quad (4)$$

where $\delta = \delta_a - \delta_b$.

$$\delta_b = \delta_a - \tan^{-1} \left[\frac{P_b X_{ab} - Q_b R_{ab}}{|V_b|^2 + P_b R_{ab} + Q_b X_{ab}} \right] \quad (5)$$

The active and reactive power losses are calculated by using Eq. (3), and they are expressed as,

$$P_{loss,ab} = \frac{(P_b^2 + Q_b^2) R_{ab}}{|V_b|^2} \quad (6)$$

$$Q_{loss,ab} = \frac{(P_b^2 + Q_b^2) X_{ab}}{|V_b|^2} \quad (7)$$

All such techniques work well with static systems where there is no change in the topology of the network [22]. Again under critical loading conditions, there is no guarantee of their convergence. Even in converged cases, these methods are very inefficient in respect of storage requirements and solution speed. Moreover, for dynamic systems, it is a challenge to arrange the line data as per the load flow requirement and to maintain the radiality, and ensure connectivity. This necessitates the utilization of improved data structure-based techniques.

3 Modeling of Shunt Capacitor and EVCS in the Distribution System

The ever-growing population leads to a significant increment in customer load demand. It leads to the placement of DGs in RDS being nearer to the load demand. Among the various renewable-based DGs, solar PV and wind energy are widely used as they are abundantly available. As there is a rapid growth in load demand, the line losses in the distribution network are quite high and need to be taken care of [23].

Various techniques have been implemented to RDSs apart from the DG penetration to optimize the power losses in the RDS. This section presents the modeling of shunt capacitors and EVCSs in the RDS.

3.1 Modeling of Shunt Capacitor

Shunt capacitors supply the amount of reactive power to the RDS at the bus where they are connected. This in turn causes a reduction in reactive power flowing in the line. If the reactive power and the system voltage are assumed to be constant, then the losses are inversely proportional to the power factor, and hence improvement in the power factor causes a reduction in system losses. The other benefits of installing the shunt capacitors are voltage profile improvement, decrease in kVA loading, and reduces system improvement cost/kVA of load supplied [24]. And also, to overcome the compensation during the light load conditions, the automatic switching units can be provided but this switching equipment is costly and this, in turn, will limit the number of capacitors and thus the minimum capacity of the capacitor bank that has to be provided on the feeder.

The placement of shunt capacitors in the DS reduces the system losses, enhances the voltage profile, and also corrects the power factor. Figure 2 depicts the representation of the shunt capacitor in the DS. This capacitor injects reactive power (Q_c) into the system.

Amount of reactive power injected at bus b ($Q_{inj,b}$) can be expressed by [25],

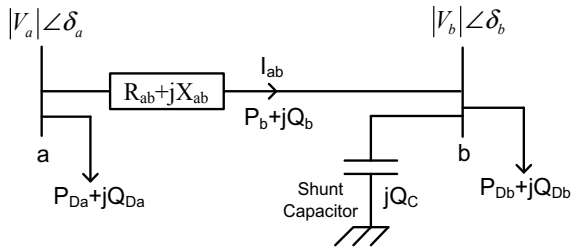
$$Q_{inj,b} = Q_{Db} - Q_c \tag{8}$$

Now the active power loss with shunt capacitor ($P_{loss,ab}^c$) can be expressed as [25],

$$P_{loss,ab}^c = \frac{(P_b^2 + Q_{inj,b}^2)R_{ab}}{|V_b|^2} = \frac{[P_b^2 + (Q_{Db} - Q_c)^2]R_{ab}}{|V_b|^2} \tag{9}$$

$$P_{loss,ab}^c = \frac{(P_b^2 + Q_b^2)R_{ab}}{|V_b|^2} + \frac{(Q_c^2 - 2Q_{Db}Q_c)R_{ab}}{|V_b|^2} = P_{loss,ab} + \Delta P_{loss,ab}^c \tag{10}$$

Fig. 2 Representation of shunt capacitor in the distribution system



where $\Delta P_{loss,ab}^c$ is the reduction in power loss, i.e., active power loss before and after placing the shunt capacitor [26], and it can be expressed from Eq. (10) as,

$$\Delta P_{loss,ab}^c = \frac{(Q_c^2 - 2Q_{Db}Q_c)R_{ab}}{|V_b|^2} \tag{11}$$

3.2 Modeling of EVCS in the Distribution System

Figure 3 depicts the representation of EVCS in the distribution system.

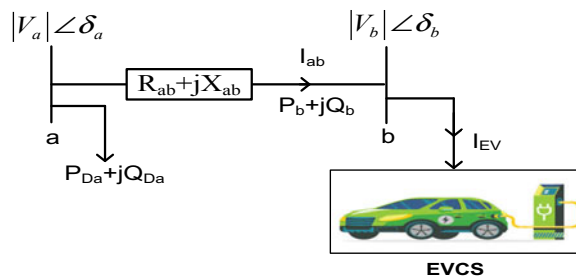
The power demand of EVCS at bus b (P_{Db}^{EVCS}) can be calculated by using [27, 28],

$$P_{Db}^{EVCS} = N_{EV}^c P_{G2V} \eta_c R_c - N_{EV}^d P_{V2G} \eta_d R_d \tag{12}$$

4 Problem Formulation

This section presents the general description of distribution systems and the mathematical modeling of optimal feeder reconfiguration (OFR) or optimal network reconfiguration (ONR). Factors that are affecting the increase in the power losses in the distribution network are feeder length, low voltage, low power factor, poor workmanship in fittings, and reduction of line losses. Various methods used for the reduction of distribution system losses are the construction of a new substation, reinforcement of feeder, reactive power compensation, HV distribution system, grading of conductors, and feeder reconfiguration [29]. In this work, two objectives, i.e., real power loss and voltage deviations are modeled with fuzzy sets [29, 30]. Some heuristics are developed to reduce the number of tie-line switching operations.

Fig. 3 Representation of EVCS in the RDS



4.1 Fuzzy Membership Function for Active Power Loss Reduction (μL_i)

The basic purpose for membership function, i.e., objective in the fuzzy domain is to minimize the active power loss of the system. The variable α_i can be defined as

$$\alpha_i = \frac{P_{loss}(i)}{P_{loss}^0} \quad \text{for } i = 1, 2, \dots, N_k \quad (13)$$

where N_k is total number of lines in loop including the tie-line, when the k th tie-switch is closed, $P_{loss}(i)$ is total active power loss when i th line in the loop is opened, and P_{loss}^0 is total real power loss before the NR. Membership/objective function for active power loss reduction (μL_i) can be written as [30],

$$\mu L_i = \begin{cases} \frac{\alpha_{\max} - \alpha_i}{\alpha_{\max} - \alpha_{\min}} & \text{for } \alpha_{\min} < \alpha_i < \alpha_{\max} \\ 1 & \text{for } \alpha_i \leq \alpha_{\min} \\ 0 & \text{for } \alpha_i \geq \alpha_{\max} \end{cases} \quad (14)$$

4.2 Fuzzy Membership Function for Maximum Node Voltage Deviation (μV_i)

The main aim of this function is to minimize the deviation of nodes' voltage. The variable β_i can be expressed as

$$\beta_i = \max(|V_{i,j} - V_s|) \quad \text{for } i = 1, 2, \dots, N_k; \quad j = 1, 2, \dots, N_B \quad (15)$$

where N_B is total number of buses in RDS, V_s is substation voltage, and $V_{i,j}$ is j th bus voltage corresponding to the opening of the i th line [29, 30]. The fuzzy membership function for maximum bus voltage deviation (μV_i) can be expressed as,

$$\mu V_i = \begin{cases} \frac{\beta_{\max} - \beta_i}{\beta_{\max} - \beta_{\min}} & \text{for } \beta_{\min} < \beta_i < \beta_{\max} \\ 1 & \text{for } \beta_i \leq \beta_{\min} \\ 0 & \text{for } \beta_i \geq \beta_{\max} \end{cases} \quad (16)$$

4.3 Constraints

The active and reactive power balances of the RDS system including the DG units, shunt capacitors, and EVCSs are expressed as [31, 32],

$$P_D = P_G^{Grid} + P_{Db}^{EVCS} + \sum_{i=1}^{N_{DG}} P_{DG,i} \quad (17)$$

$$Q_D = Q_G^{Grid} + \sum_{i=1}^{N_{DG}} Q_{DG,i} + \sum_{j=1}^{N_c} Q_{c,j} \quad (18)$$

Voltages at each bus can be expressed as,

$$0.95 \leq V_i \leq 1.05 \quad (19)$$

Active and reactive powers of DG units can be expressed as [33, 34],

$$P_{DG,i}^{\min} \leq P_{DG,i} \leq P_{DG,i}^{\max} \quad (20)$$

$$Q_{DG,i}^{\min} \leq Q_{DG,i} \leq Q_{DG,i}^{\max} \quad (21)$$

4.4 Selection of Best-Compromised Solution

When optimizing two or more objectives simultaneously, a best-compromised solution needs to be determined [35]. The procedure for determining the best-compromised solution using the min-max principle is determined next:

The membership function values of the two objectives are determined. When the k th tie-line switch of RDS is closed, a loop is formed with number of lines in the loop N_k . After opening the i th line in the loop, run the DLF to determine μL_i and μV_i for $i = 1, 2, \dots, N_k$. Determine the fuzzy decision for overall satisfaction [36, 37] by using,

$$D_{k,i} = \min(\mu L_i, \mu V_i) \quad \text{for } 1, 2, \dots, N_k \quad (22)$$

The optimal solution is the maximum of overall degrees of satisfaction, and it is expressed as [38],

$$OS_k = \max(D_{k,i}) \quad \text{for } 1, 2, \dots, N_k \quad (23)$$

5 Solution Methodology

This section presents heuristics for minimizing the number of operations of tie-line switches. Here, heuristic rules are developed to minimize the number of tie-line switch operations [39, 40]. The flow chart of the proposed solution methodology has been depicted in Fig. 4, and the step-by-step approach is presented next:

- **Step 1:** Read the RDS test system data.

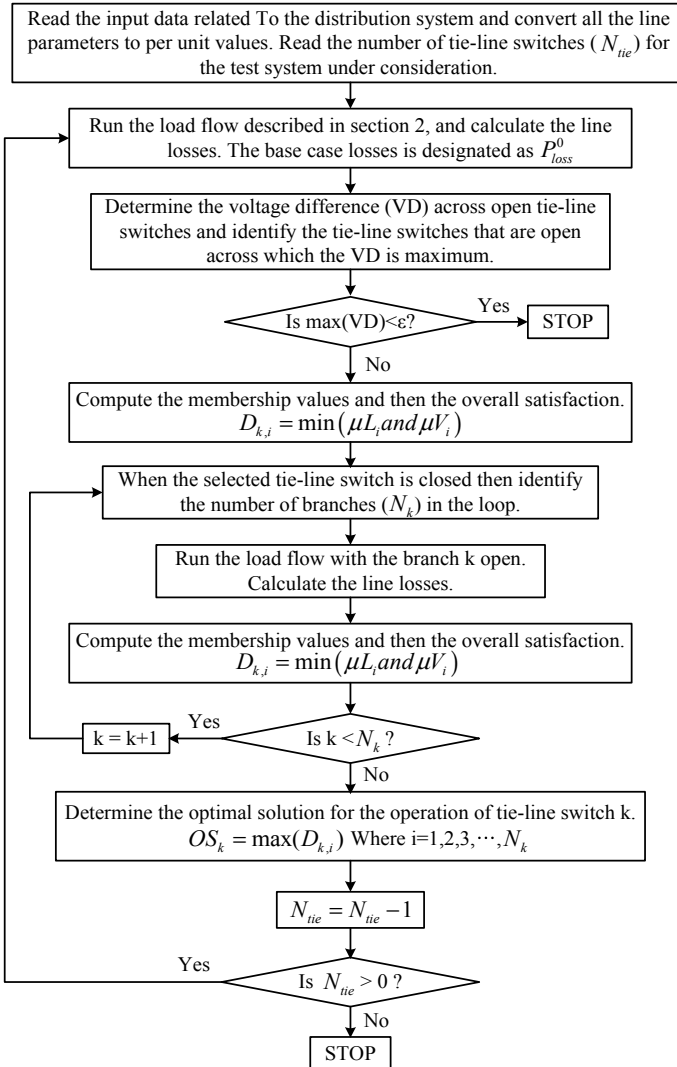


Fig. 4 Flow chart of the proposed ONR/OFR algorithm

- **Step 2:** Execute the load flow solution as described in Sect. 2.
- **Step 3:** Determine voltage difference (ΔV_{tie}) across the open tie-line switches.
- **Step 4:** Identify the open tie-line switch across which ΔV_{tie} is maximum, and it can be represented as (ΔV_{tie}^{\max}).
- **Step 5:** If $\Delta V_{tie}^{\max} >$ specified value (ϵ), then go to Step 6 else go to Step 11.
- **Step 6:** When the selected tie-line switch is closed then identify the number of branches (N_k) in the loop.
- **Step 7:** Open one line at a time in the loop, and determine the membership value for each objective function. Compute μL_i and μV_i using the Eqs. (14) and (16), respectively.
- **Step 8:** Compute the overall degree of satisfaction using Eq. (22).
- **Step 9:** Determine the optimal solution for the operation of the k th tie-line switch using Eq. (23).
- **Step 10:** Make the number of tie-line switches (N_{tie}) equal to $N_{tie} - 1$, and rearrange the coding of the rest of the tie-line switches, and go to Step 2.
- **Step 11:** Display the output results.

6 Results and Discussion

The proposed ONR methodology has been implemented on IEEE 69 bus test system which has a single feeder with a single substation [41]. Figure 5 depicts the single-line diagram of 69 bus RDS. System load demand, line, and tie-line data have been taken from Ref. [42]. This system has 68 lines, i.e., sectionalizing switches, they are 1–68 and they are normally closed. Five tie-line switches (which form 5 loops) considered in this work are 69, 70, 71, 72, and 73, they open tie switches. The base voltage and kVA are 12.66 kV and 1000 kVA, respectively. The real and reactive power load of 3,802 kW and 2,694 kVA, respectively. In this test system, the DG units are placed at buses 5, 28, 45, and 60; shunt capacitors are placed at buses 22, 36, and 64; EVCSs are placed at buses 18 and 59.

In the present work, the convergence criterion (ϵ) is considered as 0.01, and it has been assumed that α_{\min} is 0.5, α_{\max} is 1, β_{\min} is 0.05 and β_{\max} is 0.10. The active power loss obtained in the base case condition is 224.96 kW, and all the tie-line switches, i.e., 69, 70, 71, 72, and 73. The minimum voltage obtained in this base case is 0.9066 p.u. at bus 54.

6.1 Case 1: Tie-Line Switch Operation 1

In this case, the voltage difference across each tie-line switch is determined. The voltage differences across tie-line switches 69, 70, 71, 72 and 73 are 0.0031 p.u., 0.0008 p.u., 0.0416 p.u., 0.0742 p.u. and 0.0471 p.u., respectively. From these voltages, it can be observed that voltage difference across line number 72 is maximum,

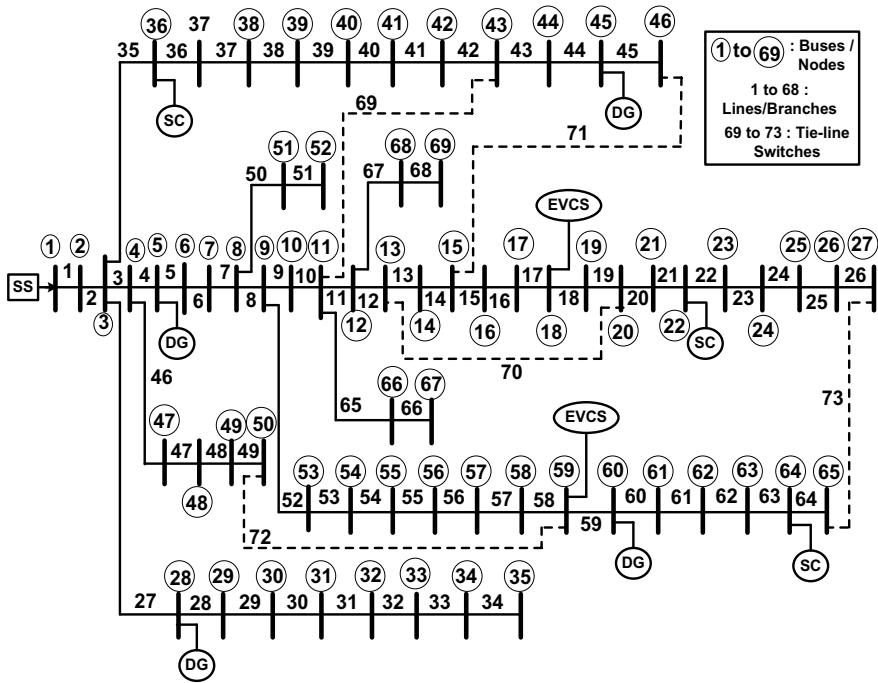


Fig. 5 SLD of IEEE 69 bus RDS before ONR

i.e., 0.0742 p.u. Table 1 presents the membership values of power loss and voltage deviation, and the overall satisfaction for tie-line switch operation 1. In this case, line number 72 is closed and the membership values for opened lines are presented in Table 1. The overall satisfaction has been determined by using Eq. (23), and they are presented in the table. From the results obtained, it is observed that by using the fuzzy set intersection, the fuzzy decision for overall satisfaction is obtained when line 46 is open and line 72 is closed. The obtained value of overall satisfaction is 0.7362, which is the maximum of $D_{k,i}$.

6.2 Case 2: Tie-Line Switch Operation 2

The voltage differences across tie-line switches 69, 70, 71, 72 and 73 are 0.00312 p.u., 0.0008 p.u., 0.0416 p.u., 0.0742 p.u. and 0.0471 p.u., respectively. From these voltages, after the tie-line switch operation 1, it can be observed that voltage difference across line number 73 is maximum, i.e., 0.0471 p.u. Table 2 presents the membership values of power loss and voltage deviation, and the overall satisfaction for tie-line switch operation 2. In this case, line number 73 is closed and the membership values for opened lines are presented in Table 2. The overall satisfaction has been determined

Table 1 Membership values for tie-line switch operation 1

Closed line	Opened line	Membership values of power loss and voltage deviation		$D_{k,i} = \min(\mu L_i, \mu V_i)$
		μL_i	μV_i	
Base case		1	0.5654	0.5654
72	38	0	0.4378	0
72	37	0	0.3937	0
72	36	0	0.3515	0
72	35	0	0.3518	0
72	47	0.7353	0.8742	0.7353
72	46	0.7362	0.8745	0.7362
72	45	0.7352	0.8734	0.7352
72	44	0.7350	0.8734	0.7350
72	43	0.7224	0.8642	0.7224
72	42	0.7082	0.8540	0.7082
72	41	0.7052	0.8540	0.7052
72	8	0	0.1457	0
72	7	0	0	0
72	6	0	0	0
72	5	0	0	0
72	4	0	0	0

by using Eq. (23), and they are presented in the table. From the results obtained, it is observed that by using the fuzzy set intersection, the fuzzy decision for overall satisfaction is obtained when line 53 is open and line 73 is closed. The obtained value of overall satisfaction is 0.7575 which is the maximum of $D_{k,i}$.

6.3 Case 3: Tie-Line Switch Operation 3

The voltage differences across tie-line switches 69, 70, 71, 72 and 73 are 0.00312 p.u., 0.0008 p.u., 0.0416 p.u., 0.0742 p.u. and 0.0471 p.u., respectively. From these voltages, after the tie-line switch operations 1 and 2, it can be observed that voltage difference across line number 71 is maximum, i.e., 0.0416 p.u. Table 3 presents the membership values of power loss and voltage deviation, and the overall satisfaction for tie-line switch operation 3. In this case, line number 71 is closed and the membership values for opened lines are presented in Table 3. The overall satisfaction has been determined by using Eq. (23), and they are presented in the table. From the results obtained, it is observed that by using the fuzzy set intersection, the fuzzy decision

Table 2 Membership values for tie-line switch operation 2

Closed line	Opened line	Membership values of power loss and voltage deviation		$D_{k,i} = \min(\mu L_i, \mu V_i)$
		μL_i	μV_i	
After tie-line switch operation 1		0.7386	0.8632	0.7386
73	26	0.7203	0.8621	0.7203
73	25	0.7225	0.8520	0.7225
73	24	0.7265	0.8505	0.7265
73	23	0.7071	0.8248	0.7071
73	22	0.7078	0.8246	0.7078
73	21	0.7046	0.7051	0.7046
73	20	0.6199	0.7056	0.6199
73	19	0.6175	0.7062	0.6175
73	18	0.6163	0.7120	0.6163
73	17	0.5656	0.6485	0.5656
73	16	0.5152	0.5836	0.5152
73	15	0.4420	0.5352	0.4420
73	14	0.4447	0.5360	0.4447
73	13	0.4338	0.5225	0.4338
73	12	0.4232	0.5122	0.4232
73	11	0.0774	0.1995	0.0774
73	10	0	0	0
73	9	0	0	0
73	8	0	0	0
73	7	0	0	0
73	6	0	0	0
73	5	0	0	0
73	4	0	0	0
73	53	0.7575	0.9129	0.7575
73	52	0.7548	1	0.7548
73	51	0.7542	1	0.7542
73	50	0.7435	0.9792	0.7435
73	49	0	0	0
73	48	0	0	0
73	72	0	0	0
73	38	0	0	0
73	37	0	0	0
73	36	0	0	0

(continued)

Table 2 (continued)

Closed line	Opened line	Membership values of power loss and voltage deviation		$D_{k,i} = \min(\mu L_i, \mu V_i)$
		μL_i	μV_i	
73	35	0	0	0

The bold values in the table represent the fuzzy decision for overall satisfaction by using the fuzzy set intersection

Table 3 Membership values for tie-line switch operation 3

Closed line	Opened line	Membership values of power loss and voltage deviation		$D_{k,i} = \min(\mu L_i, \mu V_i)$
		μL_i	μV_i	
After tie-line switch operation 2		0.7252	0.8625	0.7252
71	14	0.8618	0.9321	0.8618
71	13	0.8712	0.9652	0.8712
71	12	0.8706	0.9025	0.8706
71	11	0.8568	0.9158	0.8568
71	10	0.7990	0.9198	0.7990
71	9	0.7887	0.9138	0.7887
71	8	0.7458	0.9166	0.7458
71	7	0.3452	0.8252	0.3452
71	6	0.2898	0.7879	0.2898
71	5	0.2898	0.7842	0.2898
71	4	0.2858	0.7840	0.2858
71	68	0.7365	0.9198	0.7365
71	67	0.7165	0.9174	0.7165
71	66	0.7138	0.9133	0.7138
71	65	0.7086	0.9165	0.7086
71	64	0.7152	0.9114	0.7152
71	63	0.7098	0.9144	0.7098
71	62	0.6954	0.9100	0.6954
71	61	0.6788	0.9152	0.6788
71	60	0.6763	0.9126	0.6763
71	59	0.6552	0.9126	0.6552
71	58	0.6466	0.9126	0.6466

The bold values in the table represent the fuzzy decision for overall satisfaction by using the fuzzy set intersection

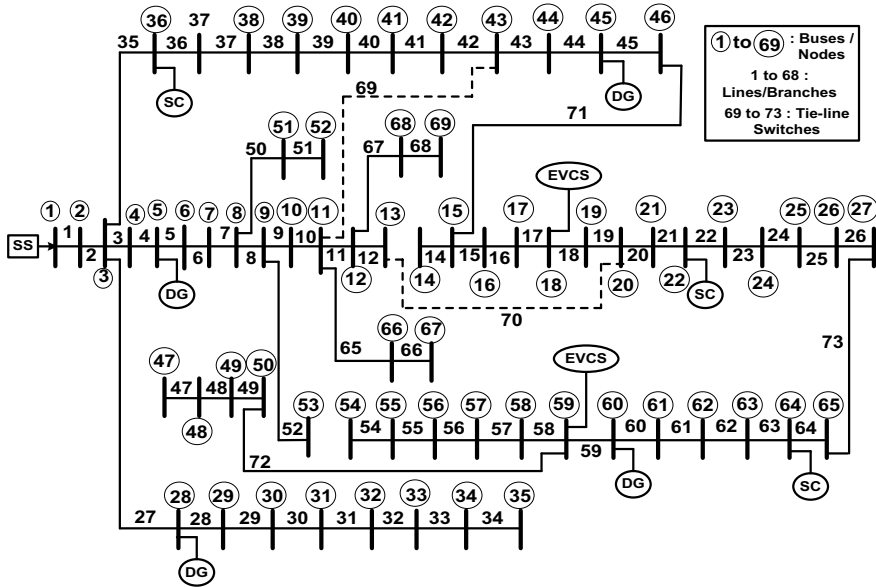


Fig. 6 SLD of IEEE 69 bus RDS after ONR

for overall satisfaction is obtained when line 13 is open and line 71 is closed. The obtained value of overall satisfaction is 0.8712 which is the maximum of $D_{k,i}$.

6.4 Case 4: Tie-Line Switch Operation 4

The voltage differences across tie-line switches 69, 70, 71, 72 and 73 are 0.0031 p.u., 0.0008 p.u., 0.0416 p.u., 0.0742 p.u. and 0.0471 p.u., respectively. From these voltages, after the tie-line switch operations 1, 2, and 3, it can be observed that voltage difference across line number 69 is maximum, i.e., 0.0031 p.u. However, this voltage difference is less than ϵ (0.01). Therefore, there is no further network reconfiguration is required. Figure 6 depicts the final topology of IEEE 69 bus RDS after ONR. Bus voltages before and after the ONR are presented in Table 4. From this table, it can be observed the voltage profile has been improved after the proposed ONR approach.

7 Conclusions

This paper proposes an optimal network/feeder reconfiguration (ONR/OFR) problem of the radial distribution system (RDS), and it is solved by simultaneously allocating the distributed generation (DG), shunt capacitors, and electric vehicle charging

Table 4 Bus voltages before and after the ONR

Bus number	Before ONR	After ONR	Bus Number	Before ONR	After ONR
1	1.0000	1.0000	36	0.9998	0.9997
2	1.0000	1.0000	37	0.9990	0.9965
3	0.9999	0.9999	38	0.9967	0.9855
4	0.9998	0.9998	39	0.9962	0.9828
5	0.9989	0.9996	40	0.9756	0.9921
6	0.9889	0.9968	41	0.9756	0.9932
7	0.9784	0.9941	42	0.9720	0.9921
8	0.9759	0.9934	43	0.9687	0.9920
9	0.9748	0.9932	44	0.9643	0.9919
10	0.9698	0.9896	45	0.9599	0.9920
11	0.9687	0.9890	46	0.9374	0.9922
12	0.9655	0.9879	47	0.9264	0.9919
13	0.9626	0.9874	48	0.9221	0.9458
14	0.9597	0.9875	49	0.9171	0.9411
15	0.9568	0.9872	50	0.9097	0.9342
16	0.9563	0.9871	51	0.9094	0.9339
17	0.9554	0.9856	52	0.9090	0.9336
18	0.9554	0.9856	53	0.9071	0.9327
19	0.9549	0.9850	54	0.9066	0.9820
20	0.9546	0.9846	55	0.9686	0.9889
21	0.9542	0.9840	56	0.9686	0.9889
22	0.9541	0.9844	57	0.9652	0.9876
23	0.9541	0.9838	58	0.9652	0.9876
24	0.9539	0.9835	59	0.9999	0.9999
25	0.9538	0.9837	60	0.9997	0.9993
26	0.9537	0.9828	61	0.9996	0.9986
27	0.9537	0.9827	62	0.9995	0.9984
28	0.9999	0.9999	63	0.9995	0.9984
29	0.9999	0.9999	64	0.9988	0.9947
30	0.9997	0.9997	65	0.9986	0.9925
31	0.9997	0.9997	66	0.9985	0.9924
32	0.9996	0.9996	67	0.9985	0.9923
33	0.9993	0.9993	68	0.9984	0.9916
34	0.9990	0.9990	69	0.9984	0.9919
35	0.9989	0.9989			

stations (EVCSs). In the proposed ONR problem, the objectives, i.e., active power loss and voltage deviation minimizations are solved by using the fuzzy-based multi-objective methodology. An iterative approach-based distribution load flow (DLF) has been used in this work. The proposed algorithm identifies the ONR of feeders with the minimum number of tie-line switch operations. Simulation studies have been performed on 69 bus RDS.

Acknowledgements This research work was funded by “Woosong University’s Academic Research Funding-2021”.

References

1. Uniyal A, Sarangi S (2021) Optimal network reconfiguration and DG allocation using adaptive modified whale optimization algorithm considering probabilistic load flow. *Electr Power Syst Res* 192. <https://doi.org/10.1016/j.epsr.2020.106909>
2. Aman MM, Jasmon GB, Bakar AHA, Mokhlis H, Karimi M (2014) Optimum shunt capacitor placement in distribution system—a review and comparative study. *Renew Sustain Energy Rev* 30:429–439. <https://doi.org/10.1016/j.rser.2013.10.002>
3. Das S, Das D, Patra A (2017) Reconfiguration of distribution networks with optimal placement of distributed generations in the presence of remote voltage controlled bus. *Renew Sustain Energy Rev* 73:772–781. <https://doi.org/10.1016/j.rser.2017.01.055>
4. Srinivasan G, Visalakshi S (2017) Application of AGPSO for power loss minimization in radial distribution network via DG units, capacitors and NR. *Energy Procedia* 117:190–200. <https://doi.org/10.1016/j.egypro.2017.05.122>
5. Biswas PP, Mallipeddi R, Suganthan PN, Amaratunga GAJ (2017) A multiobjective approach for optimal placement and sizing of distributed generators and capacitors in distribution network. *Appl Soft Comput* 60:268–280. <https://doi.org/10.1016/j.asoc.2017.07.004>
6. Manbachi M, Sadu A, Farhangi H, Monti A, Palizban A, Ponci F, Arzanpour S (2016) Impact of EV penetration on volt–VAR optimization of distribution networks using real-time co-simulation monitoring platform. *Appl Energy* 169:28–39. <https://doi.org/10.1016/j.apenergy.2016.01.084>
7. Farkoush SG, Kim CH, Jung HC, Lee S, Umpon NT, Rhee SB (2017) Power factor improvement of distribution system with EV chargers based on SMC Method for SVC. *J Electr Eng Technol* 12(4):1340–1347. <https://doi.org/10.5370/JEET.2017.12.4.1340>
8. Agrawal P, Kanwar N, Gupta N, Niazi KR, Swarnkar A (2020) Network reconfiguration of radial active distribution systems in uncertain environment using super sense genetic algorithm. *Int J Emerg Electr Power Syst* 21(2). <https://doi.org/10.1515/ijeeps-2019-0051>
9. Tabatabaei J, Moghaddam MS, Baigi JM (2020) Rearrangement of electrical distribution networks with optimal coordination of grid-connected hybrid electric vehicles and wind power generation sources. *IEEE Access* 8:219513–219524. <https://doi.org/10.1109/ACCESS.2020.3042763>
10. Chen L, Xu C, Song H, Jermisittiparsert K (2021) Optimal sizing and sitting of EVCS in the distribution system using metaheuristics: a case study. *Energy Rep* 7:208–217. <https://doi.org/10.1016/j.egy.2020.12.032>
11. Gampa SR, Das D (2017) Multi-objective approach for reconfiguration of distribution systems with distributed generations. *Electr Power Comp Syst* 45(15):1678–1690. <https://doi.org/10.1080/15325008.2017.1378944>
12. Vega-Fuentes E, Denai M (2019) Enhanced electric vehicle integration in the UK low-voltage networks with distributed phase shifting control. *IEEE Access* 7:46796–46807. <https://doi.org/10.1109/ACCESS.2019.2909990>

13. Rajesh P, Shajin FH (2021) Optimal allocation of EV charging spots and capacitors in distribution network improving voltage and power loss by quantum-behaved and Gaussian mutational dragonfly algorithm (QGDA). *Electr Power Syst Res* 194. <https://doi.org/10.1016/j.epsr.2021.107049>
14. Cikan M, Kekezoglu B (2021) Comparison of metaheuristic optimization techniques including equilibrium optimizer algorithm in power distribution network reconfiguration. *Alex Eng J*. <https://doi.org/10.1016/j.aej.2021.06.079>
15. Sedighzadeh M, Bakhtiary R (2016) Optimal multi-objective reconfiguration and capacitor placement of distribution systems with the Hybrid Big Bang-Big Crunch algorithm in the fuzzy framework. *Ain Shams Eng J* 7(1):113–129. <https://doi.org/10.1016/j.asej.2015.11.018>
16. Essallah S, Khedher A (2020) Optimization of distribution system operation by network reconfiguration and DG integration using MPSO algorithm. *Renew Energy Focus* 34:37–46. <https://doi.org/10.1016/j.ref.2020.04.002>
17. Mukhopadhyay B, Das D (2020) Multi-objective dynamic and static reconfiguration with optimized allocation of PV-DG and battery energy storage system. *Renew Sustain Energy Rev* 124. <https://doi.org/10.1016/j.rser.2020.109777>
18. Wang Y, Zhang N, Chen Q, Yang J, Kang C, Huang J (2017) Dependent discrete convolution based probabilistic load flow for the active distribution system. *IEEE Trans Sustain Energy* 8(3):1000–1009. <https://doi.org/10.1109/TSTE.2016.2640340>
19. Murari K, Padhy NP (2019) A network-topology-based approach for the load-flow solution of AC–DC distribution system with distributed generations. *IEEE Trans Industr Inf* 15(3):1508–1520. <https://doi.org/10.1109/TII.2018.2852714>
20. Nagaraju K, Sivanagaraju S, Ramana T, Prasad PV (2011) A novel load flow method for radial distribution systems for realistic loads. *Electr Power Comp Syst* 39(2):128–141. <https://doi.org/10.1080/15325008.2010.526984>
21. Liu J, Wang X, Fang W, Cheng L, Niu S, Huo C, Wang J (2016) A novel load flow model for distribution systems based on current injections. In: *China international conference on electricity distribution (CICED)*, pp 1–6. <https://doi.org/10.1109/CICED.2016.7576094>
22. Sereeter B, Markensteijn AS, Kootte ME, Vuik C (2021) A novel linearized power flow approach for transmission and distribution networks. *J Comput Appl Math* 394. <https://doi.org/10.1016/j.cam.2021.113572>
23. Muthukumar K, Jayalalitha S (2017) Integrated approach of network reconfiguration with distributed generation and shunt capacitors placement for power loss minimization in radial distribution networks. *Appl Soft Comput* 52:1262–1284. <https://doi.org/10.1016/j.asoc.2016.07.031>
24. Tolabi HB, Lashkar Ara A, Hosseini R (2020) A new thief and police algorithm and its application in simultaneous reconfiguration with optimal allocation of capacitor and distributed generation units. *Energy* 203. <https://doi.org/10.1016/j.energy.2020.117911>
25. Available. [Online]: https://assets.researchsquare.com/files/rs-281250/v1_stamped.pdf?c=1620244094
26. Esmaeilian HR, Fadaeinedjad R (2015) Distribution system efficiency improvement using network reconfiguration and capacitor allocation. *Int J Electr Power Energy Syst* 64:457–468. <https://doi.org/10.1016/j.ijepes.2014.06.051>
27. Salkuti SR (2020) Optimal network reconfiguration with distributed generation and electric vehicle charging stations. *Int J Math Eng Manage Sci* 6(4):1174–1185. <https://doi.org/10.33889/IJMEMS.2021.6.4.070>
28. Manan WIABWA, Bin Saedi A, Peeie MHB, Abu Hanifah MSB (2021) Modeling of the network reconfiguration considering electric vehicle charging load. In: *8th international conference on computer and communication engineering (ICCCE)*, pp 82–86. <https://doi.org/10.1109/ICCCE50029.2021.9467143>
29. Das D (2006) A fuzzy multiobjective approach for network reconfiguration of distribution systems. *IEEE Trans Power Deliv* 21(1):202–209. <https://doi.org/10.1109/TPWRD.2005.852335>

30. Das D (2006) Reconfiguration of distribution system using fuzzy multi-objective approach. *Int J Electr Power Energy Syst* 28(5):331–338. <https://doi.org/10.1016/j.ijepes.2005.08.018>
31. Syahputra R, Robandi I, Ashari M (2012) Reconfiguration of distribution network with DG using fuzzy multi-objective method. In: International conference on innovation management and technology research, pp 316–321. <https://doi.org/10.1109/ICIMTR.2012.6236410>
32. Stojanović B, Rajić T (2017) Novel approach to reconfiguration power loss reduction problem by simulated annealing technique. *Int Trans Electr Energy Syst* 27(12). <https://doi.org/10.1002/etep.2464>
33. Sun Q, Yu Y, Li D, Hu X (2021) A distribution network reconstruction method with DG and EV based on improved gravitation algorithm. *Syst Sci Control Eng* 9(2):6–13. <https://doi.org/10.1080/21642583.2020.1833781>
34. Amin A, Tareen WUK, Usman M, Memon KA, Horan B, Mahmood A, Mekhilef S (2020) An integrated approach to optimal charging scheduling of electric vehicles integrated with improved medium-voltage network reconfiguration for power loss minimization. *Sustainability* 12(21). <https://doi.org/10.3390/su12219211>
35. Hota AP, Mishra S, Mishra DP, Salkuti SR (2021) Allocating active power loss with network reconfiguration in electrical power distribution systems. *Int J Power Electron Drive Syst* 12(1):130–138. <https://doi.org/10.11591/ijpeds.v12.i1.pp130-138>
36. Salkuti SR (2021) Feeder reconfiguration in unbalanced distribution system with wind and solar generation using ant lion optimization. *Int J Adv Comput Sci Appl* 12(3):31–39. <https://doi.org/10.14569/IJACSA.2021.0120304>
37. Shi Q, Li F, Olama M, Dong J, Xue Y, Starke M, Winstead C, Kuruganti T (2021) Network reconfiguration and distributed energy resource scheduling for improved distribution system resilience. *Int J Electr Power Energy Syst* 124. <https://doi.org/10.1016/j.ijepes.2020.106355>
38. Agrawal P, Kanwar N, Gupta N, Niazi KR, Swarnkar A (2021) Resiliency in active distribution systems via network reconfiguration. *Sustain Energy Grids Netw* 26. <https://doi.org/10.1016/j.segan.2021.100434>
39. Kanwar N, Gupta N, Niazi KR, Swarnkar A (2015) Improved meta-heuristic techniques for simultaneous capacitor and DG allocation in radial distribution networks. *Int J Electr Power Energy Syst* 73:653–664. <https://doi.org/10.1016/j.ijepes.2015.05.049>
40. Salkuti SR (2021) Feeder reconfiguration in unbalanced distribution system with wind and solar generation using ant lion optimization. *Int J Adv Comput Sci Appl* 12(3):86–95. <https://doi.org/10.14569/IJACSA.2021.0120304>
41. Banarjee S, Chanda CK, Das D (2013) Reconfiguration of distribution networks based on fuzzy multiobjective approach by considering loads of different types. *J Inst Eng (India): Ser B* 94:29–42. <https://doi.org/10.1007/s40031-013-0043-2>
42. Savier JS, Das D (2007) Impact of network reconfiguration on loss allocation of radial distribution systems. *IEEE Trans Power Deliv* 22(4):2473–2480. <https://doi.org/10.1109/TPWRD.2007.905370>

Role of Advanced Control Technologies in the Evolution of Smart



Raseswari Pradhan

Abstract In power system, only electric grid means to a vast and variable setup of electrical components that distribute electrical energy from the generating locations to the user end. The components are transmission buses, substations, feeder buses etc. The electric grid is deliberated to be a technological prodigy in handling so many generating units, high megawatts of generating capacity and several miles of transmission lines. However, in recent scenario the electricity disruption like a blackout is very common not in India but in advanced countries like United State of America. A grid would be more efficient when more resiliency is added into the existing electric network and made ready for diffident unavoidable tragedies and natural calamities. Therefore, if some extra powerful features are supplemented to the existing grid, then it becomes a smart grid. The extra powerful features can be advanced control techniques application in grid operation. This will make the existing grid network more efficient, faster in power transmission and self-repair after power disturbances, inexpensive, improved security etc. This chapter presents a discussion on the various challenges in execution of smart grid. After that, some of recent proposed control techniques designed and applied to handle those issues. Various control applications in smart grid are supplemented with appropriate test bench problem and experimental or simulation results.

Keywords Smart grid · Definition · Evolution · Challenges · Control technologies · Communication technologies · Commercial applications

Nomenclature

IC	Integrated-Circuit
IoT	Internet of Things
PHEV	Plug-in Hybrid Electric Vehicles

R. Pradhan (✉)

Department of Electrical Engineering, VSSUT, Burla, Odisha 768018, India

e-mail: rpradhan_ee@vssut.ac.in

CPS	Cyber Physical Systems
RFID	Radio Frequency Identification
AMI	Advanced Metering Infrastructure
MPPT	Maximum Power Point Tracking
V2G	Vehicle-to-Grid
PMU	Phasor Measurement Units
GPS	Global Positioning System Satellite
IT	Information Technology
GIS	Geographic Information System
ERP	Enterprise Resource Planning
EAM	Enterprise Asset Management
CRM	Customer Relationship Management
SCADA	Supervisory Control and Data Acquisition
DMS	Distribution Management System
OMS	Outage Management Systems
DSM	Demand Side Management
S/S	Sub-Station
WAMS	Wide Area Measurement System
GPP	Generator Protection Panels
DGT	Directorate General of Training
UPS	Uninterruptible Power Supply
ATS	Automatic Transfer Switch
TVSS	Transient Voltage Surge Suppression
PSG	Peer-to-Peer Semantic Grid
GE	General Electricals
NIST	National Institute of Standard and Technology

1 Introduction

Electricity is one of the greatest findings of the nineteenth century as all other scientifically, socially and economically based revolutionary advancement depends on electricity only. Therefore, in recent scenario, electricity became a fundamental requirement for human being. This is the energy that can be generated and transmitted easily and economically over long distance. It is also easier to transform from this form to other form of energy. However, the entire process of utilization of electricity from generation to used end need a very complex structure of network which is known as electric grid [1].

An electric grid is well-known as an electrical-network of multiple number of well-synchronized generating stations and feeder stations. In between them, a large number of transmission and distribution buses are constructed for efficient transmission from generation to consumers. Again, the whole complicated structure is

controlled by one or more control centres. These are definitely some massive interconnected physical networks. Also, electrical grid is the backbone infrastructure for electricity industry [2]. According to various report, the existing grid is not up-to-date to meet demand of current twenty-first century [3]. Still, the structure of the existing grid is so large that it is a very matter of concern to manage, to maintain and to look after too so that it efficiently works [4]. Also, it is difficult and expensive to coordinate between generation and user ends so as less energy wastage will be there. When intelligence is incorporated into the existing massive network of electrical grid, it becomes smart grid [5].

Smart grid provides the opportunity for small scale distributed generation fulling the local electricity demands. This helps in establishing partial or full independence from centralized grid network. So, these types of grids are easy to control and maintain. Further, in case of occurrence of any kind fault in the system, it can be isolated from the main grid by intentional islanding process. Since the size is small, its components can be placed in proper locations to have efficient working environment.

2 Generalized Definition of Smart Grids

It is a highly adopted research topic in current days. Hence, numerous types of definition are available in literature. In some papers, smart grids are defined as the electrical systems with state-of-the-art observers, controllers and communiqué machineries to convey trustworthy and secure form of electricity. This technology has enhanced the efficacies of both generators and feeders. They too provide flexible choices for consumers. In other words, smart grid is an amalgamation of the existing complex physical network system and new advanced cyber network systems [6]. Here, physical network system serves as the skeleton whereas cyber network system is its brain and nervous system to deal the technological challenges of the grid.

In different parts of world, smart grid has different meanings. In USA, smart grid is usually means to the renovation of the electric sectors from a centralized and service-provider-controlling system to that of largely consumer collaborative system [7]. In Europe, it means the public participation in broad ways and also amalgamation of all its belonging nations [8]. Smart grid in China refers a safer, reliable, fast responding, sustainable and inexpensive physical network [9]. Recently, the Chinese Government is paying more attention to building new structures and improving the existing infrastructure in order make the system more consumer-centric and market-oriented [10].

Power network is very vast and hence its grid structure is also very large having many sections like generation, transmission, distribution etc. Smart grids are usually enabled with recent advanced technologies like Integrated-Circuit (IC) techniques in all of these sectors. Therefore, smart grid is continuously becoming more inexpensive, competent and sustainable. For further improvement in it, there is requirement of following a universal standard. For grid, that bench-mark level is delivered by U.S. National Institute of Standards and Technology. According to it, there are seven

number of vital sections such as customers, functioning, amenity supplier, generation, conduction and feeder.

Figure 1 presents a generalized layout of a smart grid. In this figure, it is shown as the amalgamation of a large number of conventional power plants, nonconventional plants, micro-grids, large demand sectors, small residential consumers, energy storage technologies and smart grid managing them [1]. According to IEEE Grid Vision 2050 [11], massive emphasis is required from smart grids on bidirectional flow of management in operations and control.

A Smart grid is becoming stronger and powerful by employing different kind of advanced inventive technologies and facilities. Some of them are listed as follows.

- Advanced generation technologies for all sizes of generators
- More involvement of consumers in optimized operation of the system
- Making the system more consumer-centric
- Enhancing self-recovery capability of the whole electricity supply system
- Increase in reliability and security of electricity supply
- Taking care of the standard, government regulation and market as well commercial requirement.

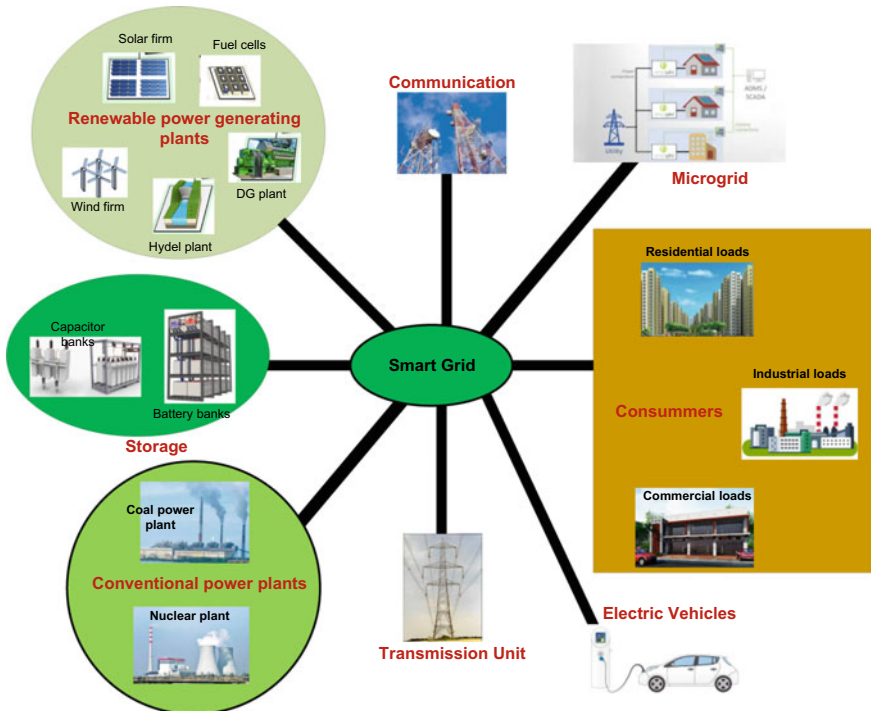


Fig. 1 Layout of a smart grid [1]

Table 1 Comparison of conventional grid with smart grid [8]

Parameters	Conventional grid	Smart grid
Generation	Centralized	Distributed
Operation	Electromechanical	Digital
Grid fault conditions	Failures and blackouts	Adaptive and islanding
Real-time observing	Nil	Extensive
Response	Slow	Very fast
Data lost	Manual restoration	Self-healing
Communication	One way	Two ways
Back ups	No storage of energy	Present
Control	Utility based	A large part is consumer based

Table 2 Per hour revenue generated in various industries of USA

Industry	Amount (in thousands of dollars)
Cellular communications	41
Telephone ticket sales	72
Airline’s reservation system	90
Semiconductor manufacturer	2000
Credit card operation	2580
Brokage operation	6480

Source US Department of Energy

Table 1 expresses a comparative study of the conventional electric grid and that of the smart grid. According to department of Energy of USA, the average revenue wasted if there is power interrupt in the country for one hour as shown in Table 2. This justifies smart grid introduction in power sectors.

3 Evolution of Smart Grids

Conventional grids are basically designed with exhaustible sources like coal, gas, petroleum product etc. Due to massive use of these commodities, their quantities are decaying and for next stock, thousands of years will be required. Again, they environmental impact too. Therefore, trends have been inclined towards use of cleaner and inexhaustible energy sources like wind, solar etc. However, there is need of making changes to the existing grid for this purpose and hence evolution of smart grid happened.

Rendering to a report of World-Energy-Outlook [12] in the year 2014, the energy requirement globally will be increased up to nearly 40% by 2040. In that situation, it is difficult to maintain the standard of energy without any harm to environments if conventional grids are continued to be used. Even though renewable energy sources are abundantly available but their harvesting technologies is complicated. Hence, there is requirement of advanced technologies as well as government support for efficient, reliable and secured harvesting of these sources. Also, there is need of proper methods, support and policies for their integration with grid. In this regard, globally many countries including India have their non-renewable ministries to make new energy policies and incentives for adapting those policies.

In the USA, these kinds of initiation have been started in the tenure of President Obama and became doubled by 2008. Report is there that enhancement in implementation of sustainable energy sources will be around 20% by 2020 in both USA and Europe [13, 14]. In this regards China is also not far behind. It has set target of around 15% by 2020 and 86% by 2050 [15, 16]. However, for these types of implementation smart grids are required.

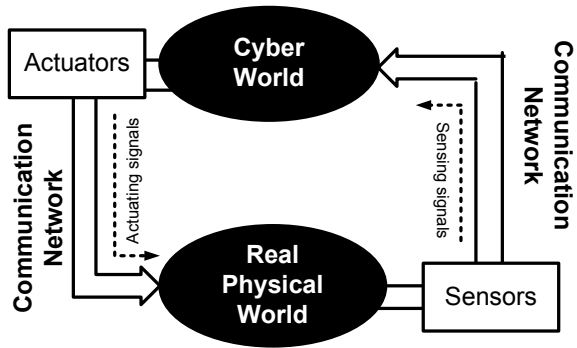
Smart grids are designed and commissioned in such a way that both supply as well as usage would be more reliable, proficient, secured, cost-effective and viable to environment. Their primary target is to integrate intelligence to the working of all of its components from supply side to consumer side including the transmission and distribution lines. The better they integrate intelligence to physical world, the more will be their success. For intelligence integration, usually cyber systems are used. They primary jobs are sensing, processing and collecting information for intelligent management and control of the grid. Therefore, a new technology has been immersed that is the cyber–physical system (CPS). This system is capable of better handle of integration and interaction issues of physical systems and cyber systems in smart grids [17].

4 Challenges in Implementation of Smart Grids

Implementation of CPS technologies in smart grids will no doubt strengthen them. However, new challenges arise due to the use of CPSs handling the systems unusual characteristics.

The acceptance of a smart grid in future will be decided by certain special features like compact, flexible, portable, safe and secure etc. For this there is always a requirement of good interaction between its various stakeholders in physical worlds (power network and consumers) and cyber worlds as shown in Fig. 2. However, it has many technical, social and environmental challenging factors while its implementation [9].

Fig. 2 Interaction between physical world and cyber system



4.1 Technical Challenges

In this kind of grid, so many types of technical challenges are there to be attended. One of such condition is irregularity in some generating sources like the renewable energy generations such as solar plant, wind farm, etc. In this case, it supplies substandard quality of electricity. Further, in some of the huge power networks including smaller dispersed energy sources, such as, solar plant, battery banks, wind-firms, plug-in hybrid electric vehicles (PHEVs) suffer unpredictable operation because of various conflicting energy market policies. Another important technical factor is the variance of peak and average electricity demands of an area. It may be some cases present where only slight reduction in peak demand may accommodate the present power generation capacity. Therefore, there is no need of building new power plants. But, for some cases, the difference between peak and average electricity demand is so high that introduction of some new power plants is unnecessary for feeding these peak loads. A smart grid needs to handle these kinds of situations in multi area power networks. In these kind of grids, wastage of electricity in transmission can be reduced by implementing distributed generation concept. In consumer sides also efficiency can be enhanced by introducing various advanced technologies such as usage of smart measurement, sensors, transmitters and processors. There is requirement of several vital techniques for the above matters. Some are listed as follows.

- Necessity in scattered control machineries with high grade of communication network. Here, sources, loads, and storage units can enjoy self-control or local-control not always the centralized control.
- Need of approximately correct prediction of load side demand well before in advance.
- Requirement of accurate estimation of renewable energy sources generation taking account the weather forecasting. So that the grid operation would be smooth even if the intermittent natures of these energy sources.
- Enhancement of grid efficiency by reducing the peak demand by implementing smart load management, active tariff and power-cut if required.

- Prerequisite of efficient and smart energy storage equipment that helps in cutting down the peak demand to some extent, shave peaks in energy demands [18].

To deal with all the above discussed factors, it needs completely systematic and dedicated steps of involvement while doing modification to the existing grid to make it smarter. CPS are capable of such kind of paradigm. Figure 2 is showing such type network that relate physical world with cyber world.

4.2 *Environmental Challenges*

Although CPS has great help in maintaining smartness of a smart grid is, there are some environmental issues exist in implementation of smart grids due to this CPS. However, even if these issues can't be isolated from each other. They are interrelated to one and another. These issues are now tried to be discussed precisely as follows.

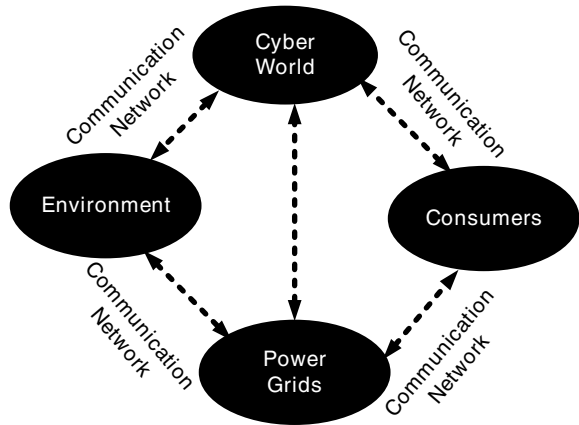
4.2.1 **Eco System**

Eco system is means to be a natural community [19]. Development of a smart grid should not hamper the eco system of its surrounding areas. Decisions in these developments need to be taken considering the area's ecological, social and financial prospects. These decisions must be very future-perspectives without neglecting the present scenario. The approach needs to be always a cross-functional type approach. Taking an example; as in a grid with thermal power plant, the details of systematic functioning need to be considered like expenditures, profits, influence coal mining, transportation, burning, waste dumping, pollution control and other side-effects to surrounding environment. Eco system of a smart grid has many numbers of connected and interconnected networks starting from raw resources to demand side consumers involving many physical, cyber and social-economic systems.

Individual life cycles of each element of such a large-scale system are to be considered during the designing stage itself. The ecosystem of a smart grid always requires an internal feedback mechanism that would monitor its self-regulation, regaining after disturbances and controlling power. Smart grid ecosystems must be structured as interaction between ecological, societal and commercial systems as shown in Fig. 3.

In this figure, power system is the physical world that is required to be is the components whose physical behaviours need to be supervised and controlled. Here, the cyber system denotes to intelligence involvement by implementing the innovative software and hardware for better data-exchange between various physical components of the systems. The society and economy systems mean the involvement of consumers in grid operation, tariff and service provide. Eventually, the term nature and environments mean to surrounding nature of a grid. Grids as well as nature

Fig. 3 Layout showing energy ecosystem



have great impact on each other. The arrows demarcate the communication networks enabling data flows between each unit of this grid eco system.

4.2.2 Big Data

This term is usually applied in the data assembly and its analysis. It has five significant features like bulk size, speed, authenticity, alteration, and cost [20]. Data can be captured by using smart meters as smart meters have these features. In smart system, it needs to efficient manage a huge bulk of data related to consumers. Data analysis needs to handle real time scrutiny of such massive data collected by smart meters from both utilities and users. It must be fast but authenticate. It also capable of handle variation in data but must not be very costly. This is more appropriate in case of sensors and any such kind of devices generated information. For analysis of these data some advanced analytical algorithms are required. However, these analytical algorithms need large sets of available information. In smart grids, data can be collected either conventionally from industries or with new technologies like web-cams, climate predicting systems, atlases, charts and images [21]. The issues in big data are related with smart architecture and design of a smart grid having faster information technologies and specialized computation [20].

4.2.3 Cloud Computing

Real-time, fast and smooth management of big data is necessary in smart grids. For this work, there is a need of efficient tool for storage, computation and complex webbing of computing resources. Cloud computing is such a very latest paradigm service provider these packages [21]. Some of its remarkable benefits are self-service, flexibility in usage, resource sharing etc. Some other advantages are easy supervision,

enhance in revenue by lessening cost, continuous services, tragedy controlling and intelligence in analysis of data [22].

The first cloud-based measurement device was introduced in Denmark in small-scale. Next, some other countries have also implemented it. In England, a Smart Energy Cloud system is used that is supporting the countries' cloud-based measurement device program. Report is there that the number of units will cross beyond 100 million by 2020. Again, this technology is showing tremendous results like more correct billing, smarter functioning and visibility. Therefore, cloud computing platforms has a great future in power sector. There are a number of cloud computing platforms established and in service in power systems. IBM Core metrics and Google Big Query are two big players in this field.

However, there are some risks in involving cloud computing in service like issues of security and privacy. This is because the cloud computing service providers are exposed to much confidential information of the consumers and may misuse them. Therefore, there is requirement of bound the service provider with some regulatory constraints [23]. But these issues should not affect the operation of the grid.

4.2.4 Internet of Things (IoT)

In IoT, the term “things” involves some entities like physical uniqueness, physical characteristics, virtual behaviours and intelligence of users. IoT is the extension of the Internet amenities to physical world like smart grid. In this recent service, the conventional Internet service is made enriched by applying some new expertise like RFID, sensors, smart devices [24]. IoT is growing very fast. Smart grid consists of a large communication network that link all power apparatus from the transmission and distribution sectors. This includes meters handling electricity, water, gas, heating systems and building automation systems. Efficient operations of the smart grid can be accomplished by using the global standards for IoT. Using IoT, smart grid becomes more linked, profitable and intelligent. Recently, there is beginning of a new era of power grid that is Internet of Energy. It consists of intelligent transmission and distribution of electricity smarter substation and well-organized feeder. The future of IoT lies in designing a secure and closer to real-time responses. Because, current existing structure of IoT is prone to cyber-attacks and poor qualities of responses. For effective architecture and design of smart grid, there is need of effective and optimal interaction and communication between all stakeholders of a smart grid [25].

4.2.5 Networking

Networking is becoming very important in recent era in every sectors so in smart grid too. In smart grid many complex networks are involved like communication networks, living systems, societal networks, cyber networks and physical electrical networks [26]. This gives diversity to the grid. But, due to this many problems too arises as follows.

- The dynamics of these networks are simplified to make them linearized for better analysis. However, they are physically far away from the real network.
- The links are assumed to be static where as in actual case they may be dynamic too.
- Smart grids have heterogeneous combinations of many dynamic, static, nonlinear models interconnected to each other whereas the networking systems represented as having homogeneous components.
- Power networks may have different functional layers involving telecommunication, smart measuring units and feeder management systems etc. There are always issues involved in prioritizing the components of each functional layers and dealing with their problems while functioning.

4.2.6 Legislation and Regulation

As discussed before, to secure the personal data of consumers' and prevention from misuse of them, there is a high demand of development some standard legislations and regulations across the globe. Currently, the practice is that different countries have set their own rules and regulation that different from others. So, there is no uniformity in implementation of constraints and barriers on numerous analyses [27]. The vital issues in application of smart grid are mostly cyber related. Extend of involvement of the stakeholders is one of the major issues. Similarly, incentive related problem is another issue. Legitimate barriers in developing and regulating smoothly are some other important issues too.

Since, the power sectors and organizations are different country to country. Therefore, legal and regulatory systems too are different. Therefore, cyber issues are required to be addressed accordingly following the respective system of each country.

Smart grid standardization is necessary in order to make it uniform worldwide. IEEE has a significant part in this field. IEEE has over 100 Smart Grid-related approved standards. It also has several Smart Grid-related pending standards [3]. Some of the standards in Communication Protocols are as follows [28].

- From one Regulatory body to other, i.e., IEC 60870-6/TASE.2
- From one Regulatory body to site apparatus, i.e., IEEE 1815 (DNP3) for USA and IEC 60870-5 for UK
- Site apparatus, i.e., IEC 61850 and IEEE 1815 (DNP3).

5 Control Issues in Implementation of Smart Grids

The vital control issues in the operation of a smart grids are involved in strengthening the grid-structure, improvement in its intelligence, communications, integration of various intermittent generating units, moving offshore, harvesting the goodness of

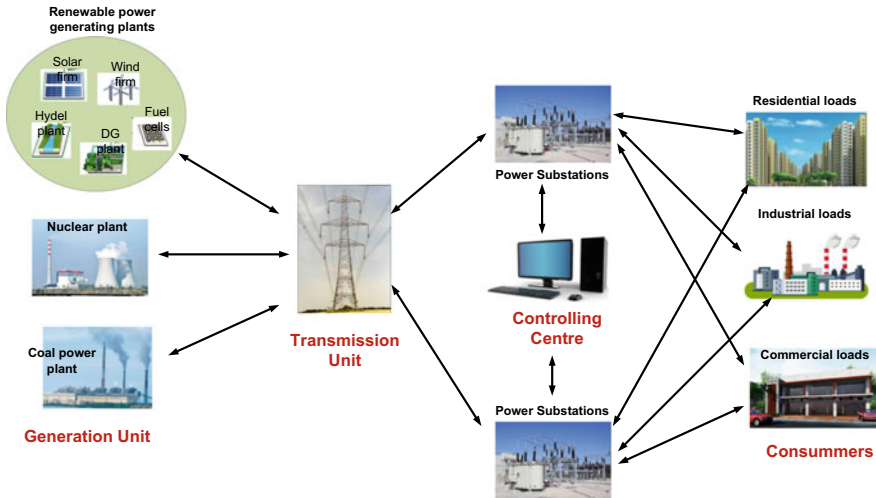


Fig. 4 Control structure in smart electrical grid and its interfaces

distributed generation and storage units. The control structure of a smart grid is shown in Fig. 4.

5.1 Reinforcement of the Grid

The existing conventional grid is very old. Further, they are very huge and complicated. Again, the grid intimately related to social and economic growth of an area. Therefore, it is required to ensure enhancement in grid power by integration of renewable resources, power handling capabilities and control.

5.2 Improvement in Intelligence

FREEDM substations are established to improve the stake of sustainable energy. They involve large number of advanced and prototype components. The prospective grids are going to be different from that of the existing grids in terms of organization and application. Figure 4 shows such a futuristic set-up of grid. It comprises mostly distributed types of generation and storage systems. This trademarks the grid more flexible and consistent in operation. This system uses a large scale of power electronics devices in order to make them automatic, adaptive and superiority in energy management and power quality improvement [29].

However, in these kinds of set-up, the current flow during fault condition is very small. Hence, fault can't be detected using that of conventional fault detection

methods. Further, source and load sides are not symmetrical in nature. Therefore, normal symmetrical based analysis is not applicable to these systems. The traditional protection systems are also not appropriate for these systems [30].

5.3 Betterment in Communications

In a smart grid, usually almost all of its components are linked by communication network for the effective exchange of information. Correct and fast exchange of information is necessary for quick response of the devices in certain situations. Feeder systems are basically constructed taking care of a fixed toleration level in voltage and current in normal operating conditions. Beyond that the protection systems become active. In a smart grid, the exchange of information about any contingency situation and required command after decision making to the respective protection devices must be faster and smoother. This can be possible by using two-way digital communication like wired phones and mobile phones, radios, Fiber-optical-devices, Power line transporter transmission, Satellite and web [31].

5.4 Participation of Intermittent Sources

Cost is one of the main factors in all commercial sectors including the power sectors. Therefore, optimal economic power dispatch of various available generating units is necessary [32]. To solve this problem, calculation of optimal load sharing of the generating station is required. Previously, only conventional sources were present. Therefore, this problem was simpler dealing with only stock of fossil fuels and their cost. Recently, more and more intermittent and distributed sources are getting added to the system. So, the problem becomes more complicated. The challenges lie in location of power plants away from load centers. So, it will be not economical to install communication networks too [31].

Different distributed generation technologies are available such as wind-plant, solar arrays etc. It is always necessary to select right one among these technologies for a particular location for better performance. In addition to that some supplementary technologies need to be implemented to the existing systems like use of Maximum Power Point Tracking (MPPT) in wind and solar plants to minimize energy losses [33].

5.5 Offshore Movement

This term is mostly applied in case of wind farms. Now-a-days, it is applied in smart grids as wind farms are part of them. Therefore, smart grid technology is

now capable of controlling and operating remote plants efficiently and optimally. Such an innovative technology is proposed in paper [34]. It can enable a grid to tackle uncertainties in monitoring and maintenance equipment of a power plant. An adaptive condition-based maintenance scheme is discussed here.

5.6 Capturing the Benefits of Back-Up Devices

As discussed in the previous sections, some of the generating systems of a smart grids are intermittent in nature basically the renewable energy-based systems. This may inject unwanted disturbances to the stable grid and through it to other components of the grid. Therefore, a disturbance created in a small part of grid may imbalance the whole grid causing black-out like situations. Therefore, there is need of some back-up devices to be installed with the other generating systems such as battery banks. These devices are usually installed at the distribution level. Now-a-days, back-up devices are very essential elements in off-grid application. In grid integrated application also, back-up devices are installed in order to enhance the system robustness against intermittent supply of energy. Apart from batter banks, diesel generators, flywheels, fuel cells, ultra-capacitors etc. are also very popular back-up systems in power sectors [32]. The combination of generating systems with back-up systems are known as hybrid systems.

However, the back-up systems must be selected, designed and commissioned in such a way that the quality of power and voltage level will not be hampered both in short and long terms. In addition to it, stability of the whole system will be retained even with bulk injection of back-up powers. A vast research is going in this area. However, those are not sufficient and competent enough to use commercially [33, 34]. Different hybrid systems have different issues and hence they are required to be addressed differently. For an example, in wind farm-based hybrid systems, back-up devices are designed to handle intermittence generation as well as ramp rates that limits its generation level. Similarly, in solar based hybrid systems, both intermittence and power angle correction factors are vital issues [35].

5.7 Plug-In Hybrid Vehicles Usage

Smart grids are characterized with distributed generations and dispersed consumers. A smarter grid needs to address them all proficiently. Electric vehicles have a great future and their injection volumes are increasing. However, they are highly movable and discrete in nature. The new technology to it is the plug-in hybrid vehicles and known as vehicle-to-grid (V2G). V2G does not means only its utilization as means of transportation but also its usage of electric-rechargeable batteries. For batteries recharging, grid support is necessary. Therefore, in near future, they will emerge as a major challenge for grid network, the future electricity networks. V2G is still not

commercially famous. To make it more reliable, more research is required. In some of the researches [36], V2G systems are developed with in a confined area of grids called micro grids.

5.8 Advanced Technologies Implementation

Recently, a number of advanced technologies are designed and formulated to be applied in different section of a power network like monitoring, sensing, measurement, data acquisition, control etc. Phasor measurement units (PMUs) are such an advanced technology. These are well-synchronized with the real-time power grid network and widely used as measuring devices. Their advanced characters are very beneficial in system observation, protection and controlling. Here, synchronization is accomplished by maintaining equal sampling frequency of voltage and current waveforms using Global Positioning System Satellite (GPS) [37].

6 Digital Control of Smart Grids

Digital control is usually a combination of energy and information technology (IT). Introduction of digital control in power sector has enabled it with two-way-communication between consumer and energy provider. This technology is expected to come to picture in 1980s. However, 2015 onwards its utilization paradigm has covered smart grid, smart homes, digital billing, distributed generation, maintenance services, smart interconnection etc. The utilization of digital control in power sector is very vast. Some of its distinct components are shown in Fig. 5. It consists of smart grid, smart homes, renewable energy sources, consumer engagement, distribution intelligence and plugin-vehicle.

Recently, digital control technology offers smart grid solutions from generation sites to the utility sides of electrical energy. Its services include protection and control of all kind of generator sets of the grid. It also ensures safety and smooth operation of a hybrid generation system with renewable energy sources. It facilitates continuous transfer to power backup units in order to provide uninterrupted power supply. Therefore, using digital control technologies, power grid reliability is enhanced. In future, digital control technologies will play big roles in smooth functioning of a smart city. Figure 6 shows how it can help in the operation of smart city.

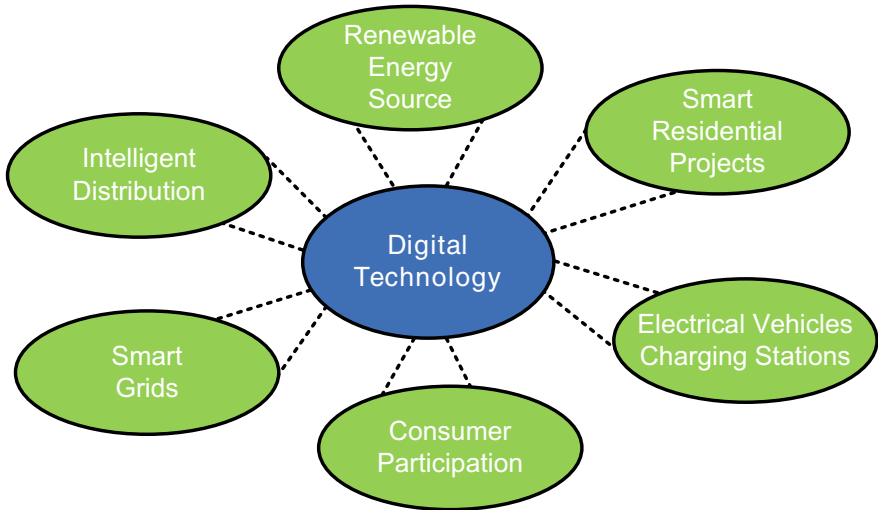


Fig. 5 Components of digital control in power sectors

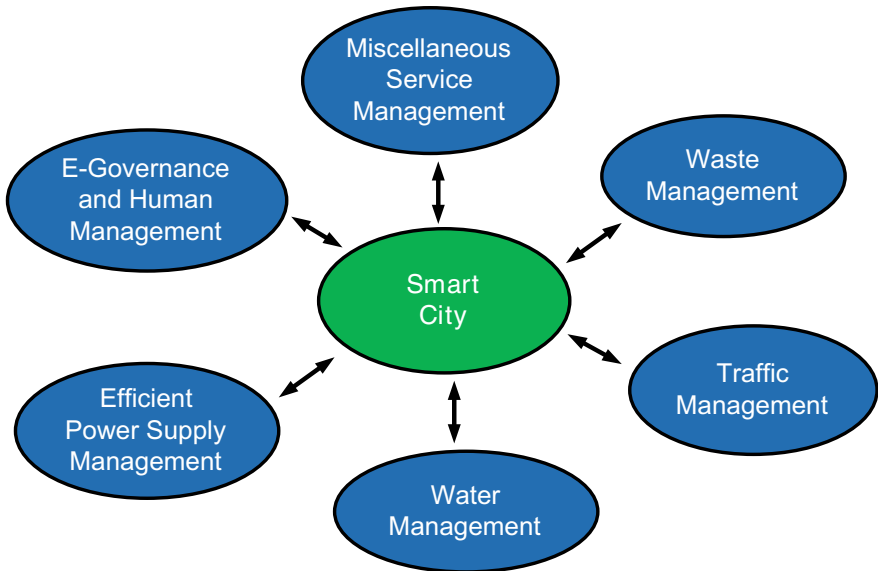


Fig. 6 Future of digital control in smart city

7 Adaptive Control Technologies for Smart Grid

With adaptive control technology, an advanced distribution system can be managed. Advanced distribution system can manage both demand and efficiency more proficiently. This can be possible due to use of adaptive optimization techniques and grid improvement tasks. The usage of adaptive enable the grid to analyze and manage distributed energy resources. It also makes them automatic, self-healing and self-sustaining. Advanced distribution system further supports closed-loop type control structure. Here, the operator sects the adaptive schemes studying the forecasted grid conditions data collected using advanced data acquisition devices.

A layout of an advanced distribution system based adaptive control system is shown in Fig. 7. Its advanced management system takes care of real-time services like sub-station (S/S) automation, feeder automation and functioning of intelligent devices. It also looks after enterprise services like GIS, ERP, CRM and EAM. In this

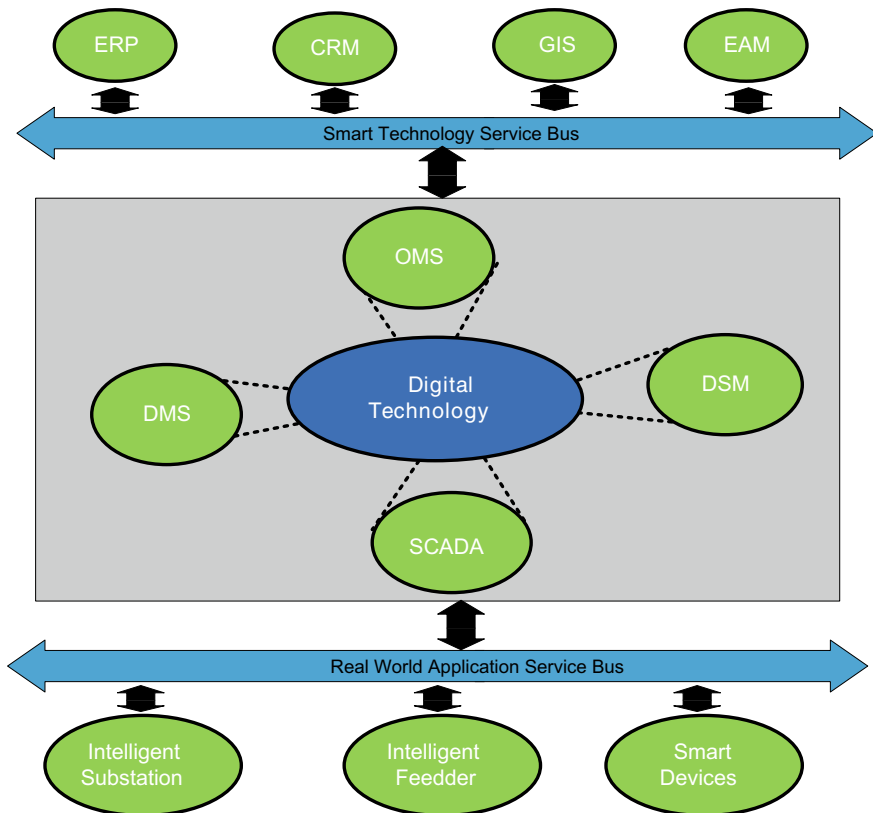


Fig. 7 Paradigm of adaptive control technologies in smart grid

management system, various advanced technologies have been used like SCADA, DMS, OMS and DSM [38].

Adaptive control technology has future in smart grid in the following fields.

7.1 Advanced Metering Infrastructure (AMI)

It serves as an interface between the grid and consumers. The information exchange is bidirectional in nature. It is enabled with accurate load data acquiring, advanced control, real-time tariff and outage detection. In AMIs, data acquisition interval is programmed to be at 5, 15, 30 or 60 min of time intervals depending upon the types of loads. It has a Home Automation Network (HAN) gateway. It also includes remote connect/disconnect switch.

7.2 Phasor Measurement Unit (PMUs)

PMUs are controlled by GPS. They are specifically synchronized with the real-time system voltage and current waveforms. By this they can remotely measure data of a grid by catching its electrical waves. It is very effective in fault detection without even physically attached to the network.

7.3 Distributed Weather Sensing

It helps in gathering weather data like cell temperature, solar irradiance, wind speed, etc. in case of renewable energy-based hybrid systems. Thereby the power outage can be forecasted in advanced and required modification in grid are carried out. It is an effective tool for efficient power management [39].

7.4 Wide Area Measurement System (WAMS)

In this system, a chain of PMUs is made in service. This network provides continuous real-time monitoring and data acquisition for a wide range of areas.

8 Adaptive Control Technologies for Smart Grid

As discussed earlier, communication between different sections of a smart grid very vital. Therefore, there is requirement of innovative communication skills. Classification of these communication technologies has been done depending upon their utilization. They are as follows.

8.1 Integrated Communications

Any interference in this network may severely affect its quality of wireless sensing capabilities. Various features of integrated communications are fast, fully unified and bidirectional data exchange. So that the smart grid becomes vibrant and collaborative [40].

8.2 Secure Web Mechanism

The advanced technologies must be protected, secured and reliable [41].

8.3 Wireless Sensor System

These systems must handle severe environments, packet faults, changing link capability, constrained in resources and maintain required standard.

8.4 Communication Infrastructure

In this system, a chain of PMUS is made in service. This network provides continuous real-time monitoring and data acquisition for a wide range of areas.

These are used as the back-bone of a communication network. Some of the components are given as follows.

- System Integrators
- WAN Network
- LAN Network
- Data Storage Management and Analytics
- CRM.

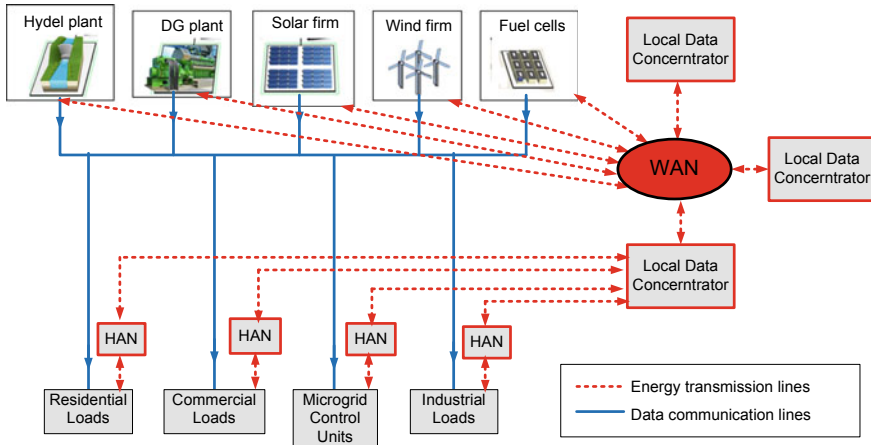


Fig. 8 Advanced communication technologies in smart grid

The future advanced communication technologies in smart grid are shown in Fig. 8 [42].

9 Some Commercially Available Smart Grid Technologies

Some leading companies like GE are involved in this field. Some of its products are shown in Table 3.

Table 3 Various commercial smart grid based products by GE

Protection and control	Distributed grid management	Micro grid control
Generator protection: G60 G30 489	Wireless trip control: DGT wireless transfer trip	Optimized generation and grid interconnect relays: F60 C30
Generator protection panels: GPP	Advanced load shedding and restoration: C90Plus	Load management/load shedding relays: C90Plus F35
Plant system optimization: PMCS C90Plus	Quick standby devices: UPS ATS TVSS PSG	Wireless LAN extension: Mercury iNET-II entra NET

Source GE Technologies

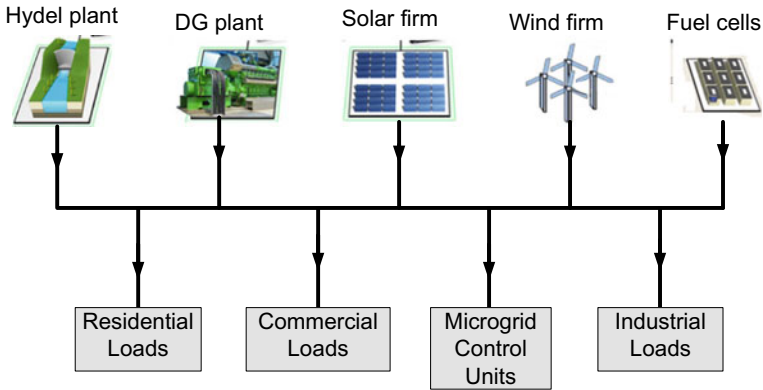


Fig. 9 Layout of GE Microgrid Control System. *Source* GE Technologies

The GE Microgrid Control System offers an advanced technique in which different power generation and feeder data are accumulated efficiently. Then that data is utilized to formulate the optimal cost-effective scheme so as to provide uninterrupted supply. It also rich with the presence of controllable and optimized generating units, storage units and delivery of clean power. A layout of GE Microgrid Control System is shown in Fig. 9.

GE is also providing solution for advanced digital communication from generation to utility sectors to the user ends. This is possible by a fast and secured two-way wireless network. It can send quick trip signals to dispersed generation units. Then, acknowledge report after work done is also sent back for confirmation. This kind of wireless arrangement cuts costs and ensured safety (Fig. 10).

Many other smart grids related commercial products are available across the world. In USA, Plug-in Electric Vehicles are in high demand and are being sold very fast. It is expected that by 2020, the sold unit will cross beyond one Million. Two big companies have been ventured in this field such as Nissan Leaf and Chevrolet Volt.

Since, smart grid is growing day by day in USA, Major government and local agencies are involved in its smooth operation and control like National Institute of Standard and Technology (NIST), LOS Alamos, Edison, Oak Ridge, NSF, Ercot etc.

Back up technologies also very vital in case of smart grid operation to support during peak load period. For back up batter bank is an important component. Therefore, many companies are serving in sectors like Ktech Corp, California’s Central Valley etc.

For transmission systems, Midwest Energy Inc. Project, Hays, KS are providing solution. They are supplying nine relay-based PMUs and synchro phasor communications network for watching power-angle and signal-frequency. It also analyses disturbances and resulting faults, monitors signals, their stability status etc. Similarly, SGIG Distribution Automation Project, Atlantic City, NJ; Golden Spread Electric Cooperative Project in Amarilo, TX; Whirlpool Corporation Smart Grid Project,

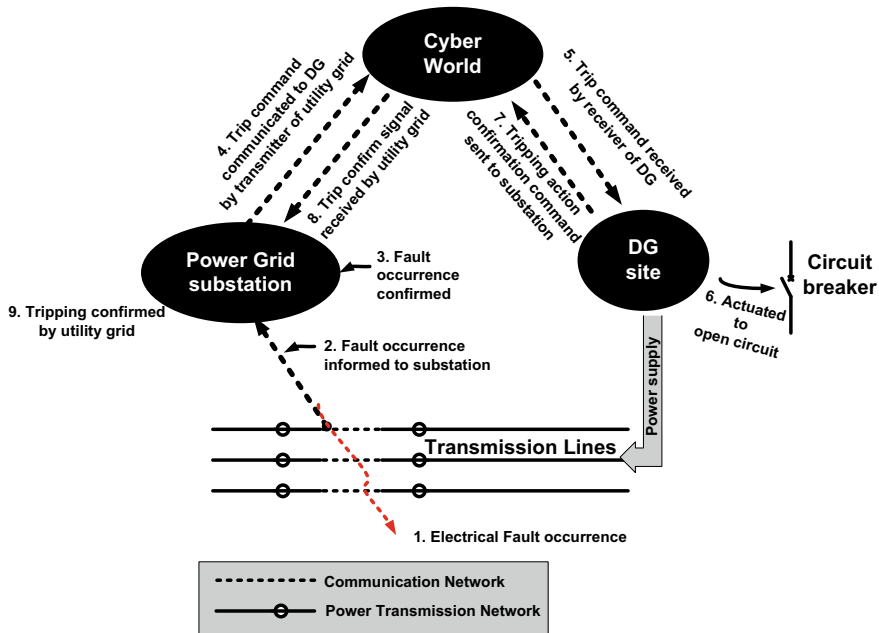


Fig. 10 Wireless infrastructure solution by GE. *Source* GE smart grid https://www.gegridsolutions.com/multilin/smartgrid_innovations.htm

Benton Harbor, MI; Peak Energy Agriculture Rewards (PEAR) in Fresno, CA and AMI Project in Lubbock, TX are some other famous companies that have ventured to provide smart grid solution commercially.

10 Conclusion

This chapter gives an overview about different aspects of a smart grid. It has presented that smart grid technology has eradicated various age-old problems like incorporated controlling, vast capacity sources, dependency on unsustainable sources etc. It also problems in automation increasing responsiveness from consumers. With the help of better communication systems, now smart grid is being powered with two-ways smooth and authenticate data flows. A comparison has made with that of the conventional to justify its superiority. This chapter also has a brief discussion on different challenges and issues faced by smart grid like technical, ecological, social, control, protocols etc. It has also discussion on on-going expansion and future technologies of smart grid like smart city applications. Further this chapter has elaborated usage of adaptive control techniques and advanced communication technologies to make smart grid more intelligent and user-end friendly. It is also discussed with some IEEE and other universal standards, how this technology is made universally

uniform, secured and protected. It is seen that smart grid offers a very vast area of research. This chapter can be a very good reference for the aspirant researchers and engineers working in various field of smart grid.

References

1. Meng W, Ma R, Chen HH (2014) Smart grid neighborhood area networks: a survey. *IEEE Netw* 28:24–32. <https://doi.org/10.1109/MNET.2014.6724103>
2. Gungor VC, Sahin D, Kokac T, Ergut S, Buccella C, Cecati C, Hancke GP (2011) Smart grid technologies: communication technologies and standards. *IEEE Trans Ind Inf* 7:529–539. <https://doi.org/10.1109/TII.2011.2166794>
3. Wang W, Xu Y, Khanna M (2011) A survey on the communication architectures in smart grid. *Comput Netw* 55:3604–3629. <https://doi.org/10.1016/j.comnet.2011.07.010>
4. Wu FF, Moslehi K, Bose A (2005) Power system control centers: past, present, and future. *Proc IEEE* 93:1890–1908. <https://doi.org/10.1109/JPROC.2005.857499>
5. Tushar W, Yuen C, Saha TK, Morstyn T, Chapman AC, Alam MJE, Poor HV (2021) Peer-to-peer energy systems for connected communities: a review of recent advances and emerging challenges. *Appl Energy* 282:116131. <https://doi.org/10.1016/j.apenergy.2020.116131>
6. Cecati C, Mokryani G, Piccolo A, Siano P (2010) An overview on the smart grid concept. In: *IECON 2010—36th annual conference on IEEE industrial electronics society*, Nov 2010. IEEE, pp 3322–3327. <https://doi.org/10.1016/j.asej.2020.05.004>
7. Gunduz MZ, Das R (2020) Cyber-security on smart grid: threats and potential solutions. *Comput Netw* 169:107094. <https://doi.org/10.1016/j.comnet.2019.107094>
8. Narayanan SN, Khanna K, Panigrahi BK, Joshi A (2019) Security in smart cyber-physical systems: a case study on smart grids and smart cars. In: *Smart cities cybersecurity and privacy*. Elsevier, pp 147–163. <https://doi.org/10.1016/B978-0-12-815032-0.00011-1>
9. Jha AV, Appasani B, Ghazali AN, Pattanayak P, Gurjar DS, Kabalci E, Mohanta DK (2021) Smart grid cyber-physical systems: communication technologies, standards and challenges. *Wireless Netw* 27:2595–2613. <https://doi.org/10.1007/s11276-021-02579-1>
10. Xin C, Chen X, Chen H, Chen S, Zhang M (2020) Green product supply chain coordination under demand uncertainty. *IEEE Access* 8:25877–25891. <https://doi.org/10.1109/ACCESS.2020.2963944>
11. Stoustrup J, Annaswamy A, Chakraborty A, Qu Z (2019) *Smart grid control*, vol 10. Springer International Publishing, pp 978–983. <https://doi.org/10.1007/978-3-319-98310-3>
12. US Energy Information Administration (ed) (2011) *Annual energy outlook 2011: with projections to 2035*. DOI-DOE/EIA-0383. Government Printing Office
13. Lins C (2010) Renewable energy technology roadmap: 20% RES by 2020. In: *Local governments and climate change: sustainable energy planning and implementation in small and medium sized communities*, vol 39, p 131. <https://doi.org/10.1007/978-1-4020-9531-3>
14. Koronen C, Åhman M, Nilsson LJ (2020) Data centres in future European energy systems—energy efficiency, integration and policy. *Energy Effic* 13:129–144. <https://doi.org/10.1007/s12053-019-09833-8>
15. Tan Q, Yu S (2021) Dynamics of renewable energy in China: drivers and challenges. In: *Renewable energy transition in Asia: policies, markets and emerging issues*, vol 1, pp 113–135. https://doi.org/10.1007/978-981-15-8905-8_6
16. Hai T, Sharafati A, Mohammed A, Salih SQ, Deo RC, Al-Ansari N, Yaseen ZM (2020) Global solar radiation estimation and climatic variability analysis using extreme learning machine based predictive model. *IEEE Access* 8:12026–12042. <https://doi.org/10.1109/ACCESS.2020.2965303>

17. Sun D, Li W, Yao X, Liu H, Chai J, Xie K, Feng L (2021) Research on IoT architecture and application scheme for smart grid. In: Proceedings of the 9th international conference on computer engineering and networks, vol 1. Springer, Singapore, pp 921–928. https://doi.org/10.1007/978-981-15-3753-0_90
18. Bullich-Massagué E, Cifuentes-García FJ, Glenny-Crende I, Cheah-Mañé M, Aragüés-Peñalba M, Díaz-González F, Gomis-Bellmunt O (2020) A review of energy storage technologies for large scale photovoltaic power plants. *Appl Energy* 274:115213. <https://doi.org/10.1016/j.apenergy.2020.115213>
19. Marrone M, Linnenluecke MK, Richardson G, Smith T (2020) Trends in environmental accounting research within and outside of the accounting discipline. *Account Audit Account J* 33:2167–2193. <https://doi.org/10.1108/AAAJ-03-2020-4457>
20. Lytras M, Visvizi A, Zhang X, Aljohani NR (2020) Cognitive computing, big data analytics and data driven industrial marketing. *Ind Mark Manag* 90:663–666. <https://doi.org/10.1016/j.indmarman.2020.03.024>
21. Talaat M, Alsayyari AS, Alblawi A, Hatata AY (2020) Hybrid-cloud-based data processing for power system monitoring in smart grids. *Sustain Cities Soc* 55:102049. <https://doi.org/10.1016/j.scs.2020.102049>
22. Priyanka EB, Thangavel S, Gao XZ (2021) Review analysis on cloud computing based smart grid technology in the oil pipeline sensor network system. *Pet Res* 6:77–90. <https://doi.org/10.1016/j.ptlrs.2020.10.001>
23. Hashmi SA, Ali CF, Zafar S (2021) Internet of things and cloud computing-based energy management system for demand side management in smart grid. *Int J Energy Res* 45:1007–1022. <https://doi.org/10.1002/er.6141>
24. Rath M, Tomar A (2021) Smart grid modernization using Internet of Things technology. In: *Advances in smart grid power system*, vol 1. Academic Press, pp 191–212. <https://doi.org/10.1016/B978-0-12-824337-4.00007-2>
25. Babu RG, Glorindal G (2021) Big data security using IoT-based smart grid communications. In: *Cognitive informatics and soft computing*. Springer, Singapore, pp 391–401. https://doi.org/10.1007/978-981-16-1056-1_32
26. Ahmadzadeh S, Parr G, Zhao W (2021) A review on communication aspects of demand response management for future 5G IoT-based smart grids. *IEEE Access*. <https://doi.org/10.1109/ACCESS.2021.3082430>
27. Lopes JAP, Madureira AG, Matos M, Bessa RJ, Monteiro V, Afonso JL, Magalhães P (2020) The future of power systems: challenges, trends, and upcoming paradigms. *Wiley Interdiscip Rev Energy Environ* 9:e368. <https://doi.org/10.1002/wene.368>
28. Gunduz MZ, Das R (2020) Cyber-security on smart grid: threats and potential solutions. *Computer Netw* 169:107094. <https://doi.org/10.1016/j.comnet.2019.107094>
29. Nazir M, Enslin JH, Burkes K (2021) Hybrid bypass protection of hybrid smart transformers for advanced grid support. In: *2021 IEEE 12th international symposium on power electronics for distributed generation systems (PEDG)*. IEEE, pp 1–5. <https://doi.org/10.1109/PEDG51384.2021.9494212>
30. Wu Y, Wu Y, Guerrero JM, Vasquez JC (2021) Digitalization and decentralization driving transactive energy Internet: key technologies and infrastructures. *Int J Electr Power Energy Syst* 126:106593. <https://doi.org/10.1016/j.ijepes.2020.106593>
31. Li Y, Wang T, Wang S (2020) Cost-efficient approximation algorithm for aggregation points planning in smart grid communications. *Wireless Netw* 26:521–530. <https://doi.org/10.1007/s11276-019-02152-x>
32. Arya A, Sisodia S, Mehroliya S, Rajeshwari CS (2020) A novel approach to optimize bidding strategy for restructured power market using game theory. In: *2020 IEEE international symposium on sustainable energy, signal processing and cyber security (iSSSC)*. IEEE, pp 1–6. <https://doi.org/10.1109/iSSSC50941.2020.9358902>
33. Das L, Munikoti S, Natarajan B, Srinivasan B (2020) Measuring smart grid resilience: methods, challenges and opportunities. *Renew Sustain Energy Rev* 130:109918. <https://doi.org/10.1016/j.rser.2020.109918>

34. Rathor SK, Saxena D (2020) Energy management system for smart grid: an overview and key issues. *Int J Energy Res* 44:4067–4109. <https://doi.org/10.1002/er.4883>
35. Wang Y, Das R, Putrus G, Kotter R (2020) Economic evaluation of photovoltaic and energy storage technologies for future domestic energy systems—a case study of the UK. *Energy* 203:117826. <https://doi.org/10.1016/j.energy.2020.117826>
36. Das S, Acharjee P, Bhattacharya A (2020) Charging scheduling of electric vehicle incorporating grid-to-vehicle and vehicle-to-grid technology considering in smart grid. *IEEE Trans Ind Appl* 57:1688–1702. <https://doi.org/10.1109/TIA.2020.3041808>
37. Siamak S, Dehghani M, Mohammadi M (2020) Dynamic GPS spoofing attack detection, localization, and measurement correction exploiting PMU and SCADA. *IEEE Syst J* 15:2531–2540. <https://doi.org/10.1109/JSYST.2020.3001016>
38. Duan P, Soleimani H, Ghazanfari A, Dehghani M (2020) Distributed energy management in smart grids based on cloud-fog layer architecture considering PHEVs. *IEEE Trans Ind Appl*. <https://doi.org/10.1109/TIA.2020.3010899>
39. Al Kadhimi BM, Mohammed AB (2020) The aspect of power quality in a wind generation: overview. *J Phys Conf Ser* 1530:12104. IOP Publishing
40. Shi L, Crow ML (2008) Power and energy society general meeting-conversion and delivery of electrical energy in the 21st century. IEEE, Pittsburgh
41. Ari AAA, Ngangmo OK, Titouna C, Thiare O, Mohamadou A, Gueroui AM (2020) Enabling privacy and security in Cloud of Things: Architecture, applications, security & privacy challenges. *Appl Comput Inform*. <https://doi.org/10.1016/j.aci.2019.11.005>
42. Li C, Wang Q, Jing Z, Zhu H, Wang P, Yu C (2021) A method of data transmission technology for line condition monitoring in smart transmission grid. *E3S Web Conf* 252:01002. EDP Sciences. <https://doi.org/10.1051/e3sconf/202125201002>

Application of Solar Energy as Distributed Generation for Real Power Loss Reduction in Radial Distribution Network



Aliva Routray, Khyati D. Mistry, and Sabha Raj Arya

Abstract This work discusses the integration of solar energy as Distribution Generation in radial distribution systems. It improves the system reliability and integrity by minimizing the losses. To generate solar power, daily solar radiation data are generated using obstructed astronomical model to get accurate radiations as solar panel input. The global radiation is modelled with obstructed astronomical technique, self-shadowing effect, and photovoltaic temperature. The hourly data distribution pattern of solar radiation is non-parametric. This issue proceeds to the implementation of Kernel Density Estimation techniques in this work. The solar energy as DG is implemented to IEEE-15 and IEEE-28 bus distribution networks separately. The optimum location and capacity of DG in the distribution system are determined by employing Grey Wolf Optimization (GWO) technique.

Keywords Distributed Generation · Grey Wolf Optimization · Radial distribution system · Self-shadowing effect · Temperature model

Nomenclature

RDS	Radial Distribution System
DG	Distribution Generation
GMA	Greenwich Meridian Angle
AST	Apparent Solar Time
STC	Standard Test Condition
NOCT	Nominal Operating Cell Temperature
KDE	Kernel Density Estimation
MCS	Monte Carlo Simulation
PDF	Probability Density Function
RTS	Reliability Test System

A. Routray · K. D. Mistry · S. R. Arya (✉)

Department of Electrical Engineering, Sardar Vallabhbhai National Institute of Technology Surat, Gujarat 395007, India

GWO	Grey Wolf Optimization
PV	Photovoltaic
P_o	Power Generated from PV Module
Y_o	Solar module's rated capacity (kW) at STC
I_{Geff}	Solar Irradiance (kWh/m ²)
$I_{Geff,STC}$	Solar Irradiance at STC (kWh/m ²)
K	Temperature coefficient
T_o	PV Cell Temperature (°C)
$T_{o,STC}$	PV Cell temperature at STC (°C)
T_{amb}	Ambient temperature (°C)
$T_{o,NOCT}$	PV Cell temperature at NOCT (°C)
$T_{amb,NOCT}$	Nominal atmospheric temperature (°C) at NOCT (°C)
$\eta_{o,STC}$	Panel Efficiency at STC
τ_o	Solar transmittance
A_o	Solar absorptance
$I_{Geff,NOCT}$	Solar radiation at NOCT (kWh/m ²)
dS	Distance between consecutive panels
a	Azimuth angle of the shadow
L_{Sh}	Length of the shadow
Ang	Solar altitude angle

1 Introduction

The transmission and distribution systems are operated with heavy loading conditions. The distribution system is the bigger point of concern as it stays close to the consumer side. Enhanced Efficiency and power quality are the parameters those need to provide a favorable economic environment for the minimization of power losses in the system [1]. Several approaches for the loss minimization problem have been identified in many existing works of literatures. These methodologies are different from each other in terms of employed method, problem formulation, loss minimizing tool and the obtained solution. Capacitor placements, network reconfiguration, Distributed Generation (DG) allocation, feeder grading, high voltage distribution, usage of power electronics devices etc. are some of the methods for power loss minimization. However, few techniques like capacitor placement, network reconfiguration and DG allocation are more often used for reducing the line losses by improving the efficiency of distribution system [2]. There are many benefits of DG integration such as exploitation of renewable energies, decreased environmental impacts, improved energy efficiency, good congestion management, bus voltage increment and power loss reduction in the distribution system [3]. The DGs are also economical because of less maintenance cost. Moreover, this methodology of DG penetration is comparatively more effective and very much beneficial than the other methods of loss minimization. The main reason for the extensive popularity of DGs is, their

green technology and environmental concern for the world. Apart from it, the penetration of DGs into the distribution system is widely increased as it can be used as a small-scale power generation source and can be easily placed to the consumer side [4]. DGs can use renewable as well as non-renewable power sources for power generation.

Solar energy as DG has the potential to meet the energy needs and to achieve the environmental goal. Much research has been carried out on the penetration of solar energy as DG into the distribution system because of clean energy [5]. Photovoltaic incorporation is the medium for solar energy to serve commercial and residential customers. The construction of solar panels is taken place from the fundamental unit of PV cell which is doped with silicon semiconductor. The PV cell forms the module and further the modules form the PV array. The PV cell absorbs the solar radiation and the electricity is produced in DC form [6]. The solar energy can be stored for future use as solar cell only operates during the day time. Apart from the solar power generation, PV-based energy also takes part in space programs as it sends power to the satellite equipment, direct application for home lighting, water pumping, road lighting etc. in remote areas and supplies excessive load demands during the peak hour of the summer days. However, the penetration level potentially creates challenges in fields of reliability, power quality, over-voltage issues and protection due to the intermittent energy produced during the daytime.

The PV application area is the vast area of study which can be the current research areas of many researchers. Solar energy can be integrated into the grid with an acceptable level of penetration else it can cause an adverse effect on the entire system. The adverse impact can be a reverse power flow that damages the transformer operation. When properly sized and placed, the PV system can help the distribution system in minimizing the feeder loss. In literature [7], solar panels are utilized on the rooftops to provide additional energy for domestic application. Optimal allocation of solar energy as DG using any optimization technique is widely implemented in the distribution system. In [8], solar-based DGs are used in the distribution system and the optimal allocation is found by bat algorithm. In [9], the PV-DG placement is accomplished for assessment of PV potential in a distribution system using optimization technique. At different load levels, the performance of the distribution system is studied using PV-based DG [10]. A novel optimization technique is implemented in [11], to a distribution system for optimal solar energy as DG allocation. The results with DG connection in the distribution system are obtained to have low power losses in the lines and bus voltage improvement. Resiliency analysis of a distribution system with solar energy as DG has been carried out in literature [12]. Demand-side management using solar energy as DG for a micro-grid is studied in [13]. Active power, reactive power and the bus voltages values are considered after solar integration onto the distribution system and the stability of the system is studied [14].

Solar energy is used as DG for active power loss reduction which is the primary objective of this work. In this work, hourly solar radiation is formed from the Kernel Density Estimation followed by Monte Carlo Simulation. The obtained radiation is implemented through several astronomical models using obstruction and scaling factors. The self-shadowing effect and ambient temperature effect are added to the

solar farm to get the accurate solar radiations. The hourly load demand is considered during the Distribution System Load Flow analysis. The position and capacity of solar farm as DG are decided by applying Grey Wolf Optimization technique. The IEEE-15 and IEEE-28 bus standard distribution systems are studied for the loss minimization analysis using solar energy. The power losses as well as the bus voltages are determined with DG and the results are analyzed.

2 Effect of External Parameters on Solar Radiation

A few challenges take place in the process of solar power generation such as solar radiation data generation using measuring tools or data prediction with algorithms, the effect of temperature and other climatic factors on the PV panel efficiency, grid integration and its impact on power electronics components etc. Extensive active researches are carried out on these challenging areas.

2.1 Irradiance Astronomical Model

The available global radiation is termed instantaneous solar radiation (I_{Gsol}). An irradiance astronomical model is used for converting the instantaneous radiation into effective radiation (I_{Geff}) falling on PV panels [15]. The effective solar radiation depends on many parameters such as solar declination angle (Δ), latitude of installed PV panel's location, tilt angle of the panel, day of the year, hour of the day etc. [6, 16, 17]. The sinusoidal relationship of solar declination angle for spring equinox day ($D = 81$) can be expressed as given in Eq. (1).

$$\Delta(D) = 23.45 \sin(F(D)) \quad (1)$$

where $\Delta(D)$ is the solar declination angle, $\Delta(D) \in [-23.45^\circ, 23.45^\circ]$ and $F(D) = 360(D - 81)/365$. The equation of time ($T(D)$) is expressed in Eq. (2) which gives the time difference between clock time and solar time.

$$T(D) = (9.87 \sin 2F(D) - 7.53 \cos F(D) - 1.5 \sin F(D)) * (1/60) \quad (2)$$

Again the time difference (T_M) between the installed solar panel time zone and the reference Greenwich Meridian Angle (GMA) can be given as in Eq. (3).

$$T_M = (L_o - GMA)/15^\circ \quad (3)$$

where L_o is the longitude of the location, $GMA = UTC_{off} - 15^\circ$ and UTC_{off} is the time offset between Greenwich and time zone of installed solar panel location. Now

the Apparent Solar Time (AST) is calculated as given in Eq. (4) and its time in hour range belongs to [0, 24].

$$AST(t, D) = t + T(D) \tag{4}$$

The hour angle is the Hr(t, D) is determined as,

$$Hr(t, D) = 15(AST(t, D) - 12) \tag{5}$$

Here, t is the clock time of the day in hour. Now the angle of incidence (A_i) between the solar panel and the solar radiation can be generalized as given in Eq. (6).

$$\begin{aligned} \cos A_i(t, D) = & \sin \Delta(t, D) \times \sin L_A \times \cos \phi - \sin \Delta(t, D) \times \cos L_A \\ & \times \sin \varphi \times \cos \eta + \cos \Delta(t, D) \times \cos L_A \times \cos \varphi \\ & \times \cos Hr(t, D) + \cos \Delta(t, D) \times \sin L_A \times \sin \phi \times \cos \eta \\ & \times \cos Hr(t, D) + \cos \Delta(t, D) \times \sin \phi \times \sin \eta \times \sin Hr(t, D) \end{aligned} \tag{6}$$

where L_A is the latitude of the location, ϕ is the inclination angle of the solar panel towards the sun, and η is the solar azimuthal displacement. The incidence angle $A_i(t, D)$ determines the effective solar irradiance as given by Eq. (7).

$$I_{Geff}(t, D) = I_{Gsol}(t, D) \times \cos A_i(t, D) \tag{7}$$

The solar declination angle and incidence angle for the month of June is determined using the above equations and can be observed from Fig. 1. However, the cosine of incidence angle is considered for 1st June and implemented in this chapter. The astronomical model helps in tracking the incidence angle being a function of time. Similarly, the incidence angle can be calculated for any day with all the solar hours in a year. The solar declination angle is required to determine the effective solar

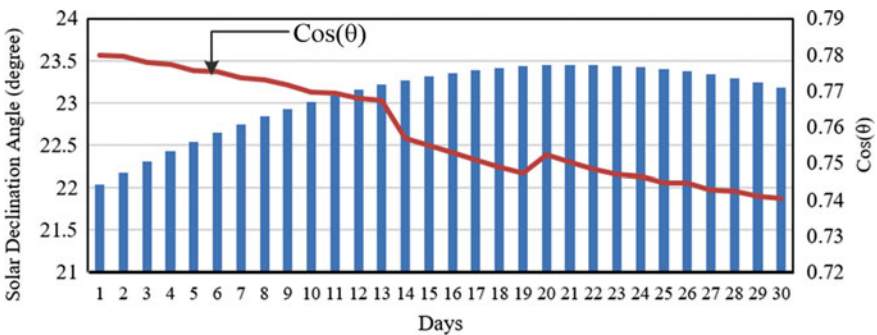


Fig. 1 Solar declination angle and cosine of incidence angle for the month of June

radiation from the global radiation fall on the earth's surface. This accurate radiation on the PV panel gives the real power output obtained from it helps to realize the system practically.

2.2 Obstructed Solar Astronomical Model

The solar panel efficiency is practically hindered with objects like buildings, trees, birds, weather etc. These are known as the obstructions on the way of solar power production. In the solar astronomical model these factors are not taken into consideration. Hence, the calculations lack precision in solar radiation with large deviation. This astronomical model is always an advantage for actual radiation fetching. It uses multiplying factors to determine the closest solar radiation that falls on the PV panels [18]. In this work, the radiation values are fetched from the installed solar farm in Bagalkot, Karnataka, India during the month of June, 2017. The global solar radiation can be obtained for any location from the NASA web application [19]. These radiation values are modelled using obstruction factor and the effective radiation is used in further work.

Here, $G1(t, D)$ is the radiation obtained from the basic irradiance model, $G2(t, D)$ is the radiation obtained after using the scaling factor in astronomical model, $G3(t, D)$ is an effective radiation obtained after using obstruction factor, $M(t, D)$ is the measured value of radiation from the farm and $O(t, D)$ be the obstruction factor. Scaling factor is the ratio of measured solar radiation data to the radiation formed from the solar astronomical model. Mathematically, the scaling factor (SF) is expressed as,

$$SF = \frac{M(t, D)}{G1(t, D)} \quad (8)$$

Now, the obstruction factor can be defined as the ratio of the difference between radiations obtained by using scaling factor and the global solar radiation with respect to radiation value obtained after using scaling factor. Mathematically, the expression is given in Eq. (9).

$$O(t, D) = \frac{G2(t, D) - M(t, D)}{G2(t, D)} \quad (9)$$

The relation between scaled radiation and obstructed radiation is given in Eqs. (10) and (11).

$$G2(t, D) = SF \times G1(t, D) \quad (10)$$

$$G3(t, D) = G2(t, D) \times (1 - O(t, D)) \quad (11)$$

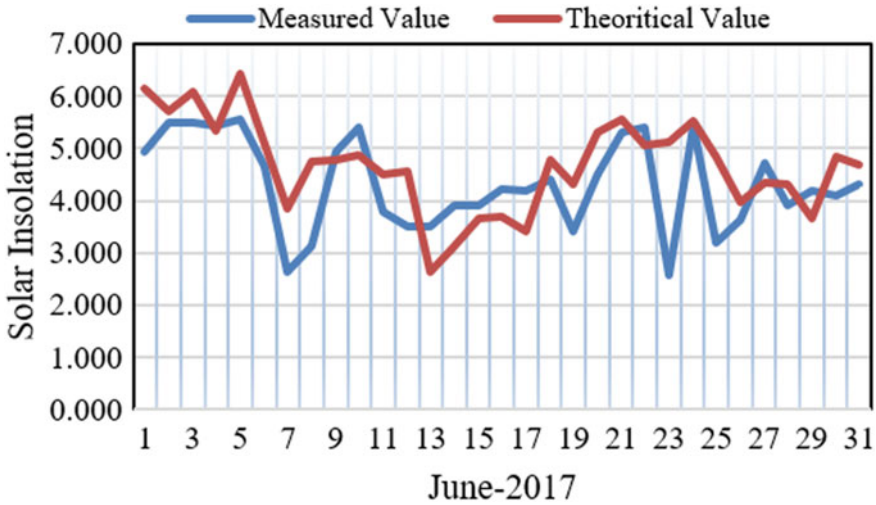


Fig. 2 Irradiance data at Bagalkot, Karnataka

The solar insolation is calculated from the astronomical model and is compared with the measured radiation values from the respective solar farm. From Fig. 2, it can be observed that, there is a significant difference between both the radiation values. The solar insolation is obtained for all 30 days of June 2017. However, 1st June is further considered for the purpose of analysis.

The obstruction factor is useful for obtaining the closest solar radiation value on PV panels for any random day. The scaling and obstruction values are 0.9227 and 0.0773 respectively. Using these factors, the analysis is extended for effective radiation calculation in June 2019.

The final solar irradiance value is obtained after executing the radiation from NASA with the several astronomical models. The radiations that are determined using these models are given in Table 1. The relative difference between the radiations in each astronomical modelling can be observed in Fig. 3.

The obstructed model helps in finding the practical insolation data for the respective solar farm location. After using the scaling and the obstruction factors with the astronomical model, from Table 1, the radiations for 1st June with basic, scaled, and obstructed models are found to be 4.858 kW/m², 4.483 kW/m² and 4.136 kW/m² respectively. The daily average solar insolation is calculated from the above values and it is found to be decreased by 14.863% after implementing the obstructed astronomical model. The solar power is obtained from the radiation obtained using the obstructed astronomical model and employed for further study.

Table 1 Effective solar radiation from different models in June 2019

Days in June	From NASA(kW/m ²)	Cosine of incidence angle	Using astronomical model (kW/m ²)	Using scaled astronomical model (kW/m ²)	Using obstructed astronomical model (kW/m ²)
1	6.23	0.7799	4.858777	4.483194	4.1366
2	6.33	0.7795	4.934235	4.552819	4.2009
3	6.05	0.7777	4.705085	4.341382	4.0058
4	5.56	0.7773	4.321788	3.987714	3.6795
5	6.38	0.7756	4.948328	4.565822	4.2129
6	6.13	0.7752	4.751976	4.384648	4.0457
7	4.77	0.7736	3.690072	3.404829	3.1416
8	5.02	0.7731	3.880962	3.580964	3.3042
9	6.31	0.7716	4.868796	4.492438	4.1452
10	6.32	0.7696	4.863872	4.487895	4.141
11	6.38	0.7692	4.907496	4.528147	4.1781
12	4.46	0.7678	3.424388	3.159683	2.9154
13	4.06	0.7673	3.115238	2.87443	2.6522
14	5.93	0.7569	4.488417	4.141462	3.8213
15	6.09	0.7548	4.596732	4.241405	3.9135
16	5.87	0.7528	4.418936	4.077352	3.7622
17	5.53	0.7509	4.152477	3.831491	3.5353
18	6.16	0.749	4.61384	4.25719	3.9281
19	5.7	0.7472	4.25904	3.929816	3.626
20	5.18	0.7523	3.896914	3.595683	3.3177
21	5.49	0.7502	4.118598	3.80023	3.5065
22	2.48	0.7483	1.855784	1.712332	1.58
23	4.66	0.7469	3.480554	3.211507	2.9633
24	4.96	0.7463	3.701648	3.415511	3.1515
25	5.21	0.7447	3.879887	3.579972	3.3032
26	5.16	0.7445	3.84162	3.544663	3.2707
27	4.88	0.7427	3.624376	3.344212	3.0857
28	3.12	0.7425	2.3166	2.137527	1.9723
29	3.46	0.741	2.56386	2.365674	2.1828
30	2.96	0.7404	2.191584	2.022175	1.8659

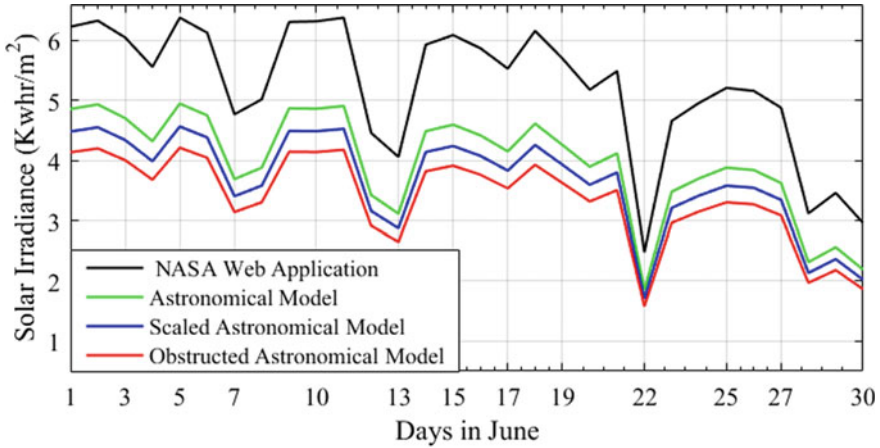


Fig. 3 Solar irradiance values with different models in June-2019

2.3 PV Cell Temperature Model

Ambient temperature significantly affects the solar power generation from PV modules [6, 20]. The increase in the ambient temperature, decreases the efficiency of solar panel output. The analysis is carried out in this subsection for the same location and month. A solar panel is designed to give maximum efficiency when it is operated in Standard Test Condition (STC). The PV generated solar panel output can be expressed as,

$$P_o = Y_o \times \frac{I_{Geff}}{I_{Geff,STC}} \times [1 + \kappa \times (T_o - T_{o,STC})] \tag{12}$$

Mathematically, the solar cell temperature is calculated as given in Eq. (13),

$$T_o = T_{amb} + \frac{\left(\frac{I_{Geff}}{I_{Geff,STC}}\right)(T_{o,NOCT} - T_{amb,NOCT})\left[1 - \frac{\eta_{o,STC}(1 - \kappa \times T_{o,STC})}{\tau_o \times A_o}\right]}{1 + (T_{o,NOCT} - T_{amb,NOCT})\left(\frac{I_{Geff}}{I_{Geff,NOCT}}\right)\left(\frac{\kappa \times \eta_{o,STC}}{\tau_o \times A_o}\right)} \tag{13}$$

The solar panel which is considered in this work, has a peak power of 335 W. The electrical datasheet for the solar panel is collected from Ref. [21]. The electrical data for PV solar cell at Standard Test Condition (STC) and Nominal Operating Cell Temperature (NOCT) is mentioned.

The temperature of the atmosphere for June 2019, is extracted from the recorded past weather data [22]. The PV cell temperature is determined using the above equations with available solar irradiance data. Here the solar absorptance and solar trans-

mittance values are taken as 0.6 and 0.9 as per the best classification [20]. The ambient temperature is less than the solar module temperature and can be observed from Fig. 4.

The temperature model is implemented to the astronomically generated solar radiations. The effective radiations is reduced after considering PV temperature and astronomical model as shown in Fig. 5. To meet the customer demand requirement in any distribution system, a number of solar panels can be installed in a solar farm. As per the daily average solar radiation value and PV cell temperature value, the effective solar power is generated and fed to the distribution system as DG.

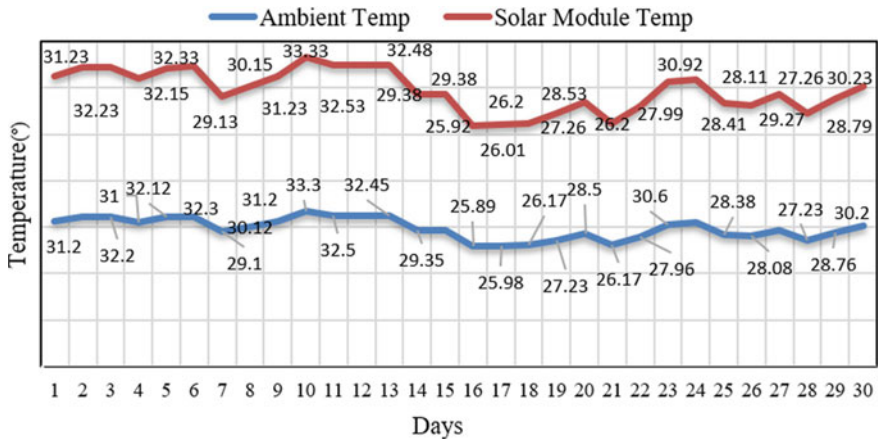


Fig. 4 Daily average ambient temperature and solar module temperature

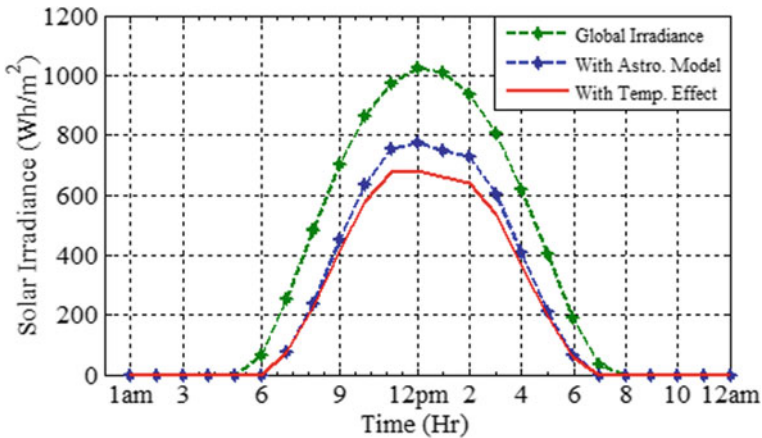


Fig. 5 Hourly solar irradiance with astronomical model and temperature effect

2.4 Panel Size and Location

PV panels always work in stand-alone mode for any grid operation. The number of solar panels or the size of the farm depends on the degree of maximum electrical load connected to the system. A radial distribution system consists of load buses except for one source node as generating node. The solar farm power is injected into any of these load buses depending on the total consumer demand and DG constraint. In this work, the solar farm location is considered to be Bagalkot, Karnataka, India. The solar power penetration is assumed to be 30% of the total load demand of the distribution system [23]. Hence, the number of solar panels are calculated as per the load demand requirement.

2.5 Shadowing Effect in Solar Panels

Solar panels are installed in a certain location forming a solar farm. The inter-row distance between two consecutive solar panel rows is maintained to avoid the shading of solar panels. This shading of solar panels is known as the self-shadowing effect. This effect prevents unshaded solar cells from operating at maximum power. In this section, a preventive measure has been taken to eliminate the power loss caused by the shadowing effect. An illustration of the self-shadowing effect is given in Fig. 6. The installation of solar panels has specific mounting guidelines as the length of the uppermost tip and the lower most tip of the solar panel which are 3 m and 2.168 m respectively [24]. The distance between the consecutive solar panel rows is calculated using Eqs. (14)–(17) [25].

$$dS = L_{Sh} \times \cos(a) \tag{14}$$

$$L_{Sh} = \frac{3}{\tan(ang)} \tag{15}$$

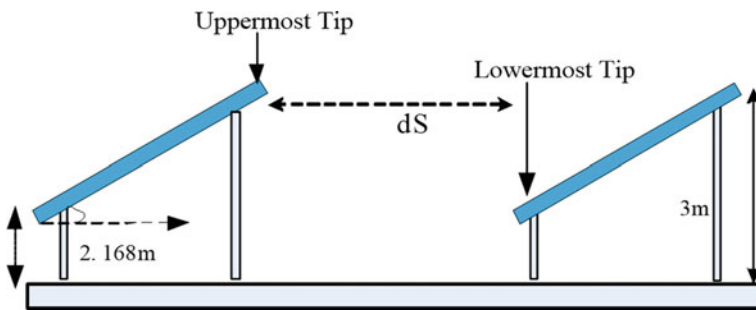


Fig. 6 Solar panel dimension and self shadowing of consecutive panels

Table 2 Number of solar panels for different test systems

Test system	Total load demand (kW)	30% of load demand (kW)	Solar farm area (m ²)		No. of required solar panels
			Without self-shadowing	With self-shadowing	
IEEE-15	1266.4	380	242	941	350
IEEE-28	761.05	230	403	1568	210

$$\sin(ang) = \cos(L_A) \times \cos(\Delta) \times \cos(t) + \sin(L_A) \times \sin(\Delta) \quad (16)$$

$$a = \frac{\cos(\Delta) \times \sin(t)}{\cos(ang)} \quad (17)$$

The panel elevation angle is assumed to be 30° with respect to the horizontal surface [25]. Hence the horizontal component of the panel becomes 0.866 times the original panel length. Now the effective length becomes 1.44 m. The effective spacing is calculated using the above equations and found to be 4.14 m [25]. The test systems with total load demand and number of solar panels needed after considering the self-shadowing effect are given in Table 2.

2.6 Stochastic Modelling of Solar Irradiance

The solar radiation data are needed to find the solar power output. With the high uncertainty and non-parametric behaviour of hourly solar radiation pattern, the stochastic method is implemented to generate the hourly radiation dataset. The process needs very large amount of data to come out with better results. The solar database resources are found in NREL website which provides vast information regarding solar radiation for several locations in the United States [26]. In this work, hourly solar radiation data is considered for over 10 years that is from 1991 to 2010. Kernel Density Estimation is implemented to the uncertain radiation data as the Probability Density Function of the data cannot be identified using available standard distribution functions [15]. After finding the Probability Distribution Function for solar radiation data, Cumulative Probability Distribution is determined and therefore generating the random radiation samples for application in Monte Carlo Simulation. The hourly histogram plots for all the solar hours are obtained and given in Figs. 7, 8, 9, 10, 11, 12, 13, 14, 15, 16, 17 and 18.

The Kernel Density Function uses the following equations. Here, PDF_{Hr} is the hourly probability function, RR_n is the random variable, $KDE(.)$ is the Kernel Function Estimator, ss is the sample size and sp is the smoothing parameter.

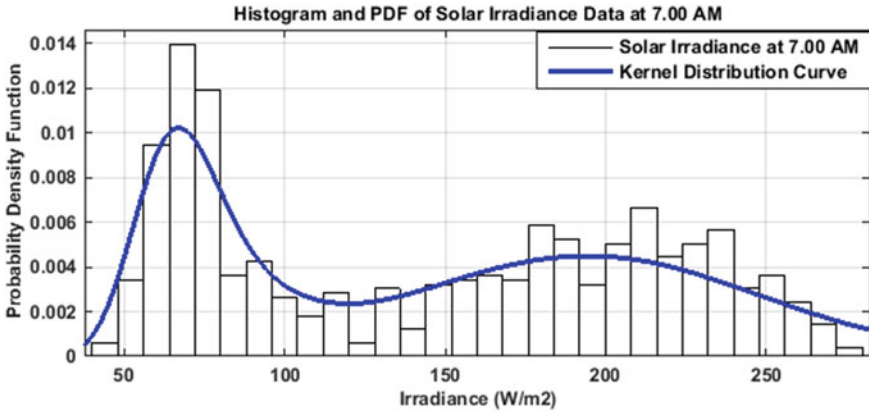


Fig. 7 Histogram and probability density function of solar irradiance data at 7.00 a.m.

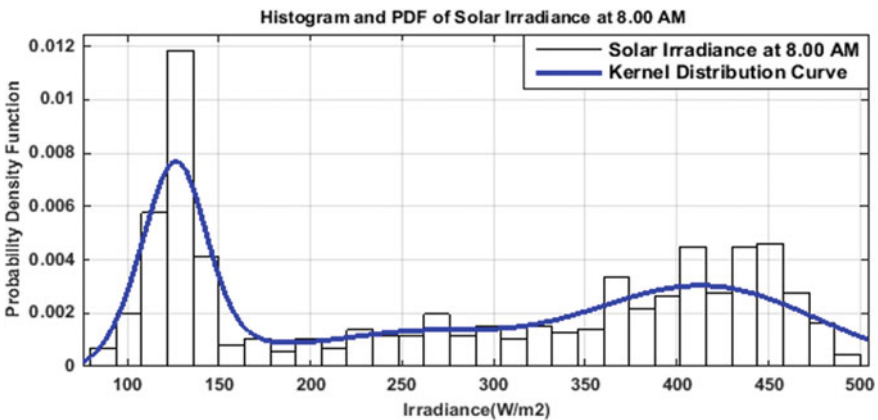


Fig. 8 Histogram and probability density function of solar irradiance data at 8.00 a.m.

$$PDF_{Hr}(RR_n) = \frac{1}{ss \times sp} \sum_{i=1}^{ss} KDE\left(\frac{RR_n - RR_{ni}}{sp}\right) \tag{18}$$

Solar radiation is generated using the above method for location Surat, Gujarat, India on an hourly basis and given in Table 3. In this chapter, the solar radiation is considered as a daily average radiation and is fetched from NASA for the specified location as mentioned before.

The radiation data of those having more than the threshold radiation value ($I_{TH} = 50 \text{ Wh/m}^2$) are considered for power calculation. The radiations below the threshold value are assumed to be zero.

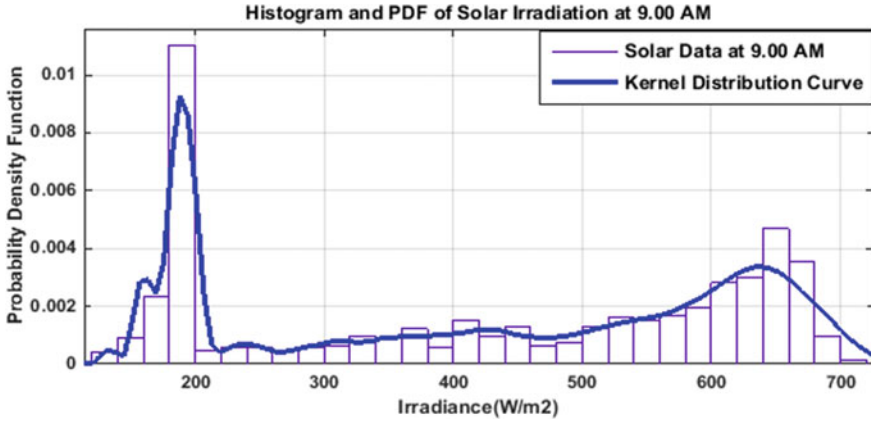


Fig. 9 Histogram and probability density function of solar irradiance data at 9.00 a.m.

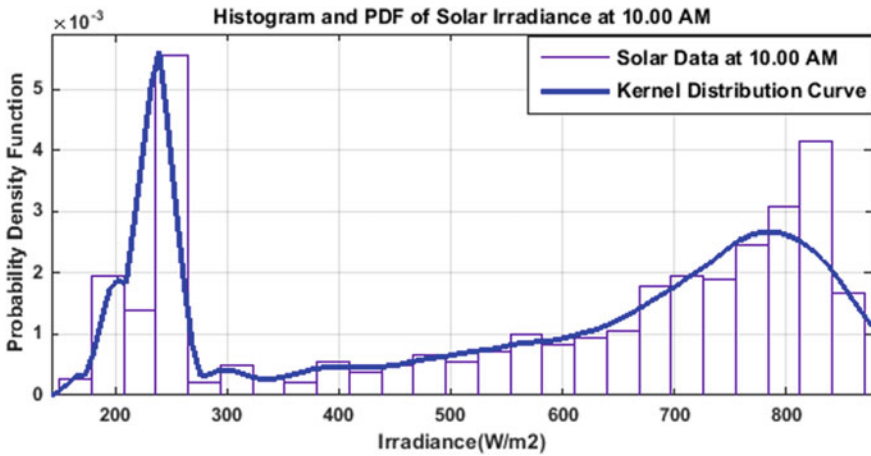


Fig. 10 Histogram and probability density function of solar irradiance data at 10.00 a.m.

3 Load Modelling Profile

The hourly analysis of active power loss in distribution lines is carried out in this chapter. In this work, a constant load model is taken into consideration for hourly power flow calculation in the distribution lines. The percentage of loads for every weekday or weekend and every hour is different. This percentage load profile data is considered from IEEE-Reliability Test System (RTS) [27]. The hourly average load percentage values for a summer season are proposed with the time-varying solar power. The load values are mentioned in percent for weekday hourly load and

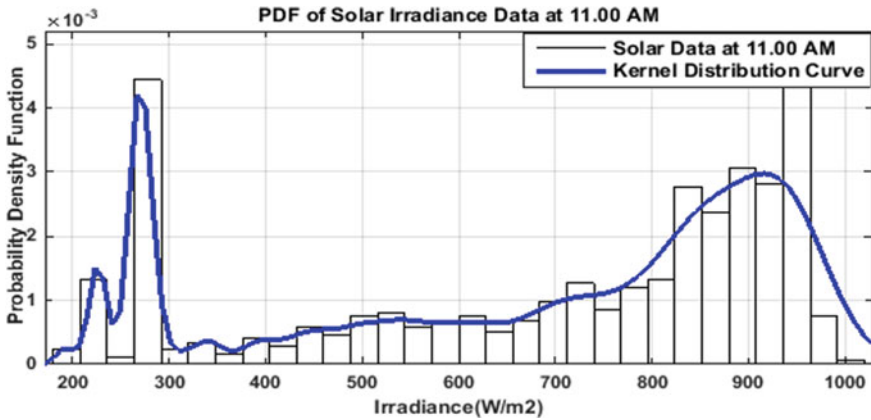


Fig. 11 Histogram and probability density function of solar irradiance data at 11.00 a.m.

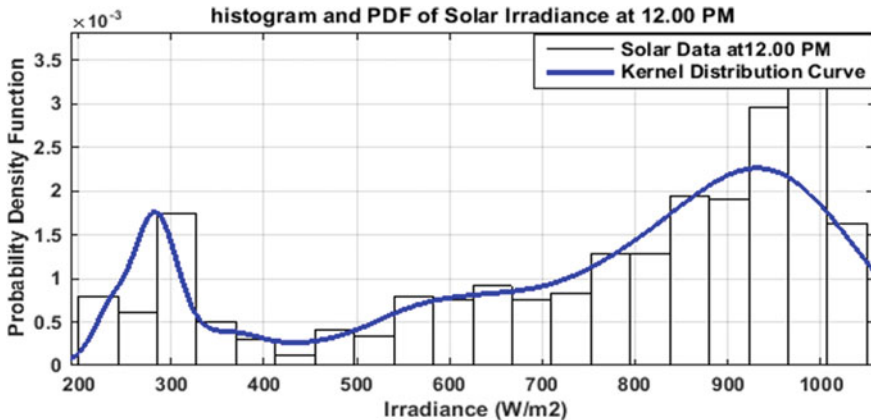


Fig. 12 Histogram and probability density function of solar irradiance data at 12.00 p.m.

weekend hourly load as given in Table 4. In this chapter, peak of load demand is considered for the study that is at 12.00 p.m. of the day.

The tabulation gives the information about the hourly peak load in the percentage of daily peak load. Since for weekdays all the peak percentage of loads are equal, the power or energy consumption graph for all the five days is similar. Saturday and Sunday are the weekend days. The hourly peak values are different from the weekdays load values. The PV generation is independent and the power generation values are obtained from the solar irradiance values which is distinct at the different times of the day and position of the sun as well as the rotation of the earth.

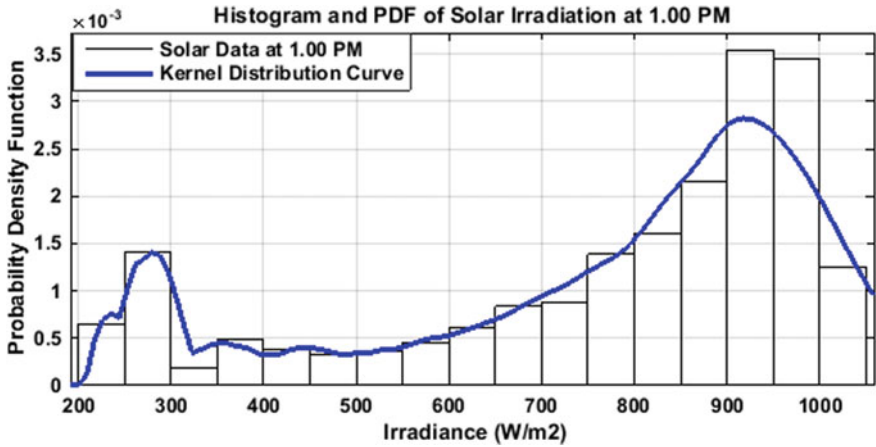


Fig. 13 Histogram and probability density function of solar irradiance data at 1.00 p.m.

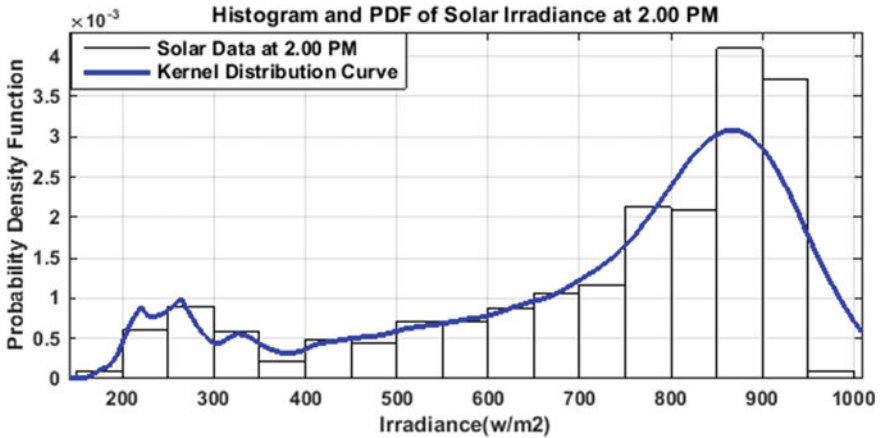


Fig. 14 Histogram and probability density function of solar irradiance data at 2.00 p.m.

4 Problem Formulation

The objective function of the work is to determine the active power losses in the distribution system using DG. Here bus number varies from *i* to *nn*. Few operational constraints are to be satisfied to ensure system integrity. The power balance equation at bus ‘*i*’ after DG is connected to the grid is given in Eq. (19).

$$P_{xDGi} = P_{xi} - P_{xDi} \tag{19}$$

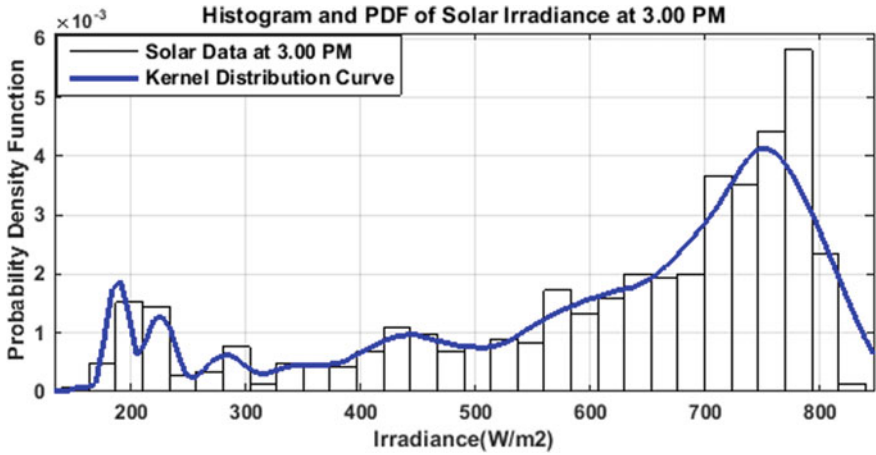


Fig. 15 Histogram and probability density function of solar irradiance data at 3.00 p.m.

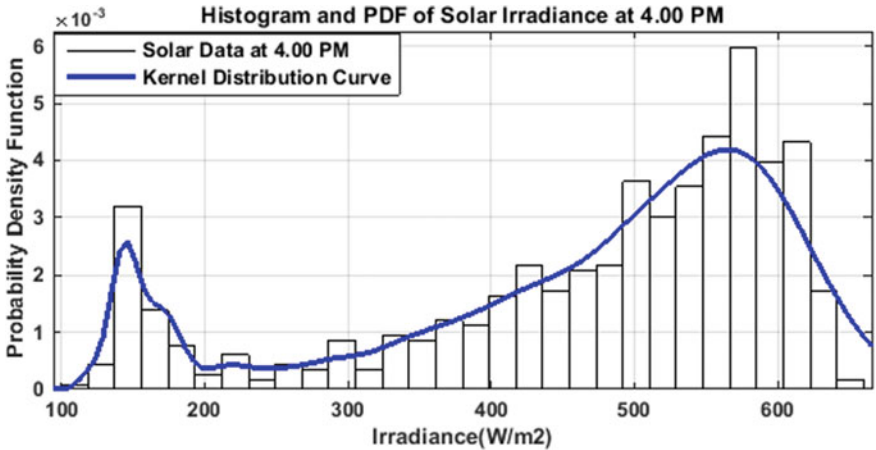


Fig. 16 Histogram and probability density function of solar irradiance data at 4.00 p.m.

Here, P_{xDGi} is the power generation from DG, P_{xi} is the bus power generation and P_{Di} is the power supplied to the loads connected at the nodes at bus ‘i’ respectively. Mathematically, the objective function in this work can be expressed as,

$$\text{Total Power Loss} = \sum_{i=1}^{nm} P_{xiLoss} \tag{20}$$

The constraints to the objective function are described below.

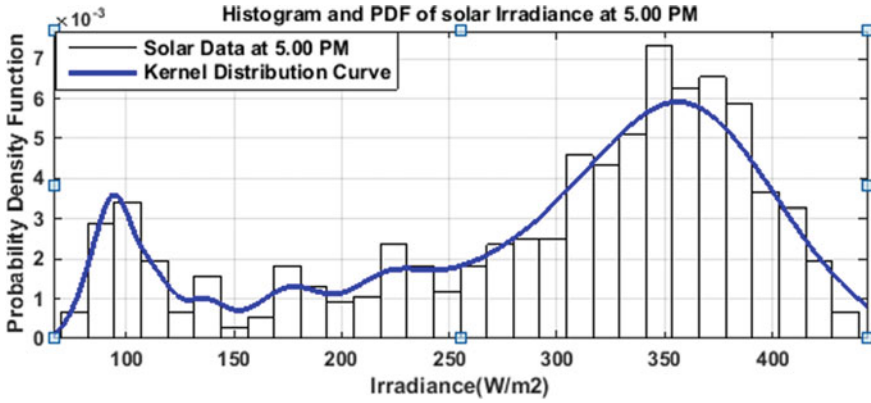


Fig. 17 Histogram and probability density function of solar irradiance data at 5.00 p.m.

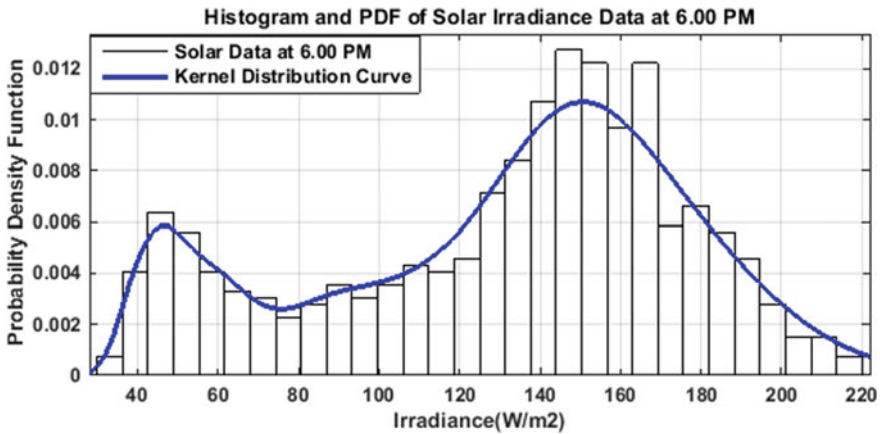


Fig. 18 Histogram and probability density function of solar irradiance data at 6.00 p.m.

Constraints of Equality

The power losses in the lines and the power consumed by the consumers as loads must be equal to the sum of power generation from the grid as well as from the DG. The power balance equation is given by,

$$P_{xG} + P_{xDG} = P_{xD} + P_{xLOSS} \tag{21}$$

Here, P_{xG} is the power generated from the grid, P_{xD} is the consumed power by the consumers, P_{xDG} is the power generation from the DG source and P_{xLOSS} is the losses in the distribution lines.

Table 3 Hourly generated solar irradiance

Sl. No.	Time	Solar radiation (Wh/m ²)	
		Using Monte Carlo simulation	Using astronomical modeling
1	1.00 a.m.	0	0
2	2.00 a.m.	0	0
3	3.00 a.m.	0	0
4	4.00 a.m.	0	0
5	5.00 a.m.	0	0
6	6.00 a.m.	64	5.6576
7	7.00 a.m.	251	76.6554
8	8.00 a.m.	483	238.5537
9	9.00 a.m.	700	448.77
10	10.00 a.m.	861	634.6431
11	11.00 a.m.	974	755.0448
12	12.00 p.m.	1026	772.3728
13	1.00 p.m.	1010	749.925
14	2.00 p.m.	939	728.2884
15	3.00 p.m.	805	602.3815
16	4.00 p.m.	619	409.9637
17	5.00 p.m.	405	212.058
18	6.00 p.m.	188	64.2208
19	7.00 p.m.	33	4.2471
20	8.00 p.m.	0	0
21	9.00 p.m.	0	0
22	10.00 p.m.	0	0
23	11.00 p.m.	0	0
24	12.00 a.m.	0	0

Constraints of Inequality

In every distribution line, there is some limit to the current flow in the line due to the current-carrying capacity. If $I_{x\max}$ is the maximum current limit for the respective line and I_x is the flowing current, then the equation is given as in Eq. (22).

$$I_x \leq I_{x\max} \tag{22}$$

Similarly, the nodal voltage of the system must be in its limitation or tolerance range. If V_x is the actual voltage at any node and $V_{x\min}$ is the minimum and $V_{x\max}$ is the maximum voltage limits, then the equation can be given as in (23).

$$|V_{x\min}| \leq |V_x| \leq |V_{x\max}| \tag{23}$$

Table 4 Hourly peak load in percentage of daily peak load [27]

Day/time (h)	01:00	02:00	03:00	04:00	05:00	06:00
Weekday	64	60	58	56	56	58
	07:00	08:00	09:00	10:00	11:00	12:00
	64	76	87	95	99	100
	13:00	14:00	15:00	16:00	17:00	18:00
	99	100	100	97	96	96
	19:00	20:00	21:00	22:00	23:00	00:00
	93	92	92	93	87	72
Day/time	01:00	02:00	03:00	04:00	05:00	06:00
Weekend	74	70	66	65	64	62
	07:00	08:00	09:00	10:00	11:00	12:00
	62	66	81	86	91	91
	13:00	14:00	15:00	16:00	17:00	18:00
	93	92	91	91	92	94
	19:00	20:00	21:00	22:00	23:00	00:00
	95	95	100	93	88	80

Constarints of DG

DG is connected as an additional part of the existing system. Hence it also follows some limitations as, the maximum capacity of DG should be less than its maximum limits. If P_{xDG} is the DG power generation at any time and P_{xDGmax} is the maximum power that can be generated using the DG, then the constraint is given in Eq. (24).

$$|P_{xDG}| \leq P_{xDGmax} \tag{24}$$

This helps the system to stay stable and maximum benefits can be obtained to the system with consideration of DG constraints.

5 Optimization Technique

Optimum placement and capacity of solar energy as DG is a very important segment of the work. To minimize the active power losses in the distribution lines of the test systems, Grey Wolf Optimization (GWO) technique is implemented in this work. GWO is a metaphor-based algorithm that imitates the hunting process of grey wolves to determine the global optimum of complex optimization problems. Its multiguide and multi-stage mechanism enables it to explore the search space

thoroughly. However, complex computation mechanism and presence of multiple algorithm-specific parameter (which needs to be tuned) makes its implementation difficult [28].

The size of a grey wolf pack generally varies from 5 to 12 and every grey wolf pack follows a very strict social hierarchy. The leader of the pack is termed as L1-wolf and it takes a decision regarding hunting, which is followed by other wolves in the pack. In this social hierarchy of grey wolves, the position of L2-wolf lies just below L1-wolf. L2-wolf plays the role of an advisor for L1-wolf for decision making. Responsibilities of L2-wolf also include carrying out the command of L1-wolf throughout the pack and providing feedback to L1-wolf. The lowest rank wolf in the hierarchy is known as L3-wolf. L3-wolf follows the order of other dominant wolves. Apart from L1-wolf, L2-wolf and L3-wolf, other wolves in the pack are called L4-wolf. They obey the orders of L1-wolf and L2-wolf but dominate L3-wolf. L4-wolves generally carry out the task of watching the boundaries of the pack and warning the pack of impending danger. It should be observed that every wolf in the pack contributes to the hunting process, even though the hunting is mainly guided by L1 and L2-wolves.

5.1 Mathematical Model of GWO

Stage-1: Initialization and Hierarchy Assignment

In this stage, a set of feasible random feasible solutions are generated and their fitness is evaluated. The solution having the best fitness value is designated as L1-wolf while solutions having second and third best fitness values are termed as L2 and L3 wolf respectively. Other solutions in the solution pool are called L4-wolves. In the GWO technique, generally, search process is guided by L1, L2 and L3-wolves.

Stage-2: Encirclement of Prey

In this stage, grey wolves encircle prey before their hunting. This phenomenon mathematically is modeled by positioning solutions (grey wolves) around prey which is the optimum solution. Mathematical operations are carried in this stage and they are given in the below equations.

$$\vec{C}1 = \left| \vec{C}2 \cdot \vec{P}_p(t) - \vec{P}(t) \right| \tag{25}$$

$$\vec{P}(t + 1) = \vec{P}_p(t + 1) - \vec{C}3 \cdot \vec{C}1 \tag{26}$$

In these equations, ‘t’ denotes current iteration, $P_p(t)$ and $P(t)$ represent the position vector of the prey and grey wolf respectively. $C2$ and $C3$ are coefficient vectors whose values are determined as given below.

$$\vec{C} 3 = 2\vec{c}_3 \cdot \vec{r}r_1 - \vec{c}_3 \tag{27}$$

$$\vec{C} 2 = 2 \cdot \vec{r}r_2 \tag{28}$$

In the above equations, rr_1 and rr_2 are random vectors in the range $[0, 1]$, while components of vector c_3 linearly decrease from 2 to 0 with an increase in iteration. Random vector rr_1 and rr_2 play a crucial role in positioning the wolves around the prey.

Stage-3: Hunting

Generally, the hunting process is guided by L1, L2 and L3 wolves. Mathematically, the hunting process is modeled by adjusting the position of L4 wolves according to the positions of L1, L2 and L3 wolves. Following mathematical operations are carried out in this stage.

$$\vec{C} 1_{L1} = \left| \vec{C} 2_1 \cdot \vec{P}_{P_{L1}} - \vec{P} \right| \tag{29}$$

$$\vec{C} 1_{L2} = \left| \vec{C} 2_2 \cdot \vec{P}_{P_{L2}} - \vec{P} \right| \tag{30}$$

$$\vec{C} 1_{L3} = \left| \vec{C} 2_3 \cdot \vec{P}_{P_{L3}} - \vec{P} \right| \tag{31}$$

$$\vec{P}_1 = \vec{P}_{P_{L1}} - \vec{C} 3_1 \cdot \vec{C} 1_{L1} \tag{32}$$

$$\vec{P}_2 = \vec{P}_{P_{L2}} - \vec{C} 3_2 \cdot \vec{C} 1_{L2} \tag{33}$$

$$\vec{P}_3 = \vec{P}_{P_{L3}} - \vec{C} 3_3 \cdot \vec{C} 1_{L3} \tag{34}$$

$$\vec{P}(t + 1) = \frac{\vec{P}_1 + \vec{P}_2 + \vec{P}_3}{3} \tag{35}$$

In the above equations, P_1 , P_2 and P_3 are the updated positions of L4 wolf P according to the L1, L2 and L3 wolves. The final position of 4 wolf P is represented by $P(t + 1)$.

Stage-3(a): Attacking Prey (Exploitation)

When the prey stops moving, the grey wolf attacks the prey and finishes the hunting process. This is mathematically modeled by linearly decreasing ‘ c ’ from 2 to 0 with increasing iteration which in turn decreases the range of $C3$. From the above equations, it is clear that, $C3$ lies in the range $[-2c, 2c]$ and ‘ c ’ generally decreases from 2 to 0. When the values of $C3$ lies in the range of $[-1, 1]$, then the updated

position of the search agent will be in between the current position of prey and the search agent. Hence the value of $|C3| < 1$ makes the wolves move towards the prey.

Stage-3(b): Searching for Prey (Exploration)

This operator brings diversity to the search process. When $C3$ lies in the range $[1, 2]$ and $[-2, -1]$, $L1, L2$ and $L3$ wolves diverge in the search space in search of prey. Hence, $|C3| > 1$ causes through exploration of search space.

6 Test System Under Study

IEEE-15 [29] and IEEE-28 [30] standard radial distribution systems are examined in this work. These test systems with single line diagram are mentioned below. These standard systems are balanced distribution systems.

6.1 IEEE-15 Bus System

IEEE-15 [29] standard radial distribution systems are examined in this work. The base voltage and base power values for IEEE-15 bus system are 10 kV and 11 MVA. The single line diagram for these test bus systems is given in Fig. 19.

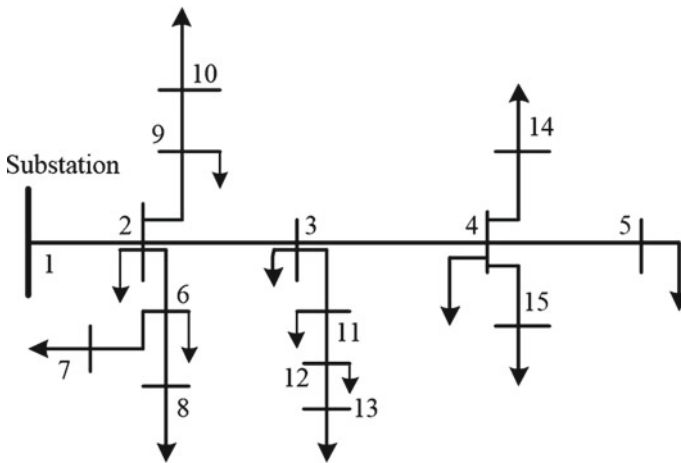


Fig. 19 IEEE-15 node radial distribution system

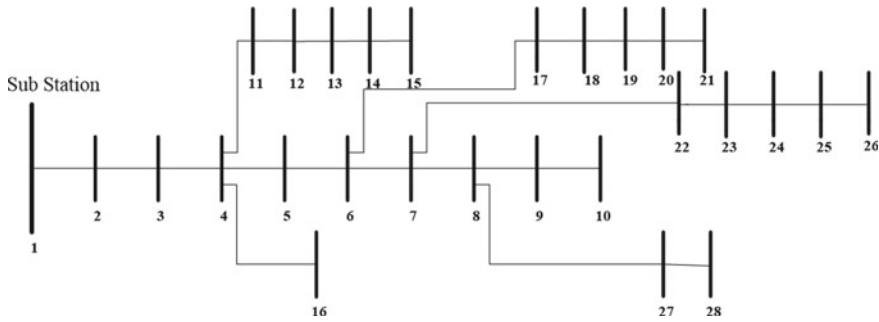


Fig. 20 IEEE-28 node radial distribution system

6.2 IEEE-28 Bus System

IEEE standard 28 bus [30] radial distribution system is studied and is shown in Fig. 20. The system base voltage and base MVA of the system are 11 kV and 100 MVA respectively.

7 Result and Discussion

The test systems are studied with the obstructed astronomical model, temperature model, self-shadowing effect, load model and optimization algorithm. The solar radiation obtained from the meteorological website is implemented with the obstructed astronomical model. The power generated from the solar farm is fed to the test systems as DG. The generated power output is fed to the test distribution system after considering all the factors. Then the system is run with a power flow algorithm to find the current flow in the branch, power losses and bus voltage at the nodes. The proposed power flow technique is executed in MATLAB 2016b. The system parameter is examined without DG and with DG. The system performance in terms of power losses, bus voltages and optimization characteristics are given under this result section.

7.1 Real Power Loss Minimization

The power flow method is implemented and the line losses are found as active and reactive power losses. With DG penetration, the system losses are remarkably minimized. After considering the daily peak load on 1st June (Saturday) to be 96%, the active and reactive power losses are minimized from 56.71 to 34.24 kW and 52.58 to 30.71 kVAR with DG in case of IEEE-15 bus system. Similarly, the active

Table 5 Reduction in power loss minimization with DG in percentage

Date	IEEE-15 bus RDS		IEEE-28 bus RDS	
	%age reduction in Ploss	%age reduction in Qloss	%age reduction in Ploss	%age reduction in Qloss
01-Jun-19	65.45	71.21	143.23	150.34
02-Jun-19	65.37	71.12	142.86	149.96
03-Jun-19	64.67	70.39	139.85	146.86
04-Jun-19	64.59	70.30	139.51	146.51
05-Jun-19	65.3	71.08	142.67	149.77
06-Jun-19	65.62	71.39	144	151.12
07-Jun-19	65.54	71.30	143.6	150.73

and reactive power losses are minimized from 62.98 to 25.89 kW and 42.13 to 16.83 kVAR with DG in case of IEEE-28 bus system. The power losses in the distribution lines can be calculated for other days with DG penetration. A noticeable decrement in power losses with DG connection has been observed from the results. The solar power is extracted from the solar farm and is injected into the test system from 1st June to 7th June 2019. The percentage reduction in power losses for both the test systems is given in Table 5.

7.2 Bus Voltage Improvement

The DG injection into the distribution system increases the nodal voltage, being an additional advantage of DG penetration. The daily bus voltages are found for the complete week in June for distribution test systems. The bus voltages after DG penetration have a remarkable effect on bus voltage improvement at the system nodes. The bus voltage before DG penetration and after DG penetration for 1st June (Saturday) is given in Tables 6 and 7 for IEEE-15 and IEEE-28 bus respectively. Likewise, the bus voltages for other days of the week can also be found with DG and the results are given in Tables 6 and 7 for IEEE-15 and IEEE-28 bus respectively. The bus voltages are observed to be significantly improved for both the system with DG allocation.

The systems are realized with peak load and available solar power at the peak hour of the day. From the availability of hourly DG power, the bus voltages are found at 12.00 p.m. The bus voltages for both the test systems are given in Figs. 21 and 22, respectively. The voltage profiles are improved with DG connection.

Table 6 Nodal voltage with DG connection in IEEE-15 bus system

Bus\days	Saturday		With DG (p.u)					
	No DG (p.u)	With DG (p.u)	2nd Jun	3rd Jun	4th Jun	5th Jun	6th Jun	7th Jun
Bus-1	1	1	1	1	1	1	1	1
Bus-2	0.9725	0.9787	0.9791	0.983	0.9835	0.9794	0.9778	0.9782
Bus-3	0.9585	0.97	0.9706	0.9761	0.9767	0.971	0.9687	0.9693
Bus-4	0.953	0.9682	0.9689	0.9747	0.9754	0.9692	0.9668	0.9675
Bus-5	0.952	0.9673	0.968	0.9739	0.9746	0.9683	0.9659	0.9666
Bus-6	0.96	0.9663	0.967	0.9731	0.9738	0.9674	0.9648	0.9655
Bus-7	0.9579	0.9641	0.9649	0.9714	0.9722	0.9653	0.9626	0.9634
Bus-8	0.9588	0.965	0.9658	0.9722	0.9729	0.9662	0.9635	0.9643
Bus-9	0.9693	0.9755	0.9761	0.9805	0.981	0.9763	0.9745	0.975
Bus-10	0.9683	0.9745	0.9751	0.9797	0.9802	0.9753	0.9734	0.974
Bus-11	0.9521	0.9636	0.9644	0.971	0.9718	0.9648	0.962	0.9628
Bus-12	0.9481	0.9597	0.9606	0.9679	0.9688	0.961	0.958	0.9589
Bus-13	0.9469	0.9585	0.9594	0.967	0.9678	0.9598	0.9567	0.9576
Bus-14	0.9508	0.966	0.9668	0.973	0.9737	0.9671	0.9646	0.9653
Bus-15	0.9506	0.9703	0.9709	0.9763	0.977	0.9713	0.969	0.9696

7.3 Optimum DG Location and Capacity

The optimization technique is used to find the optimum DG capacity and its location at the test system node. Grey Wolf Optimization algorithm is used for minimizing the line losses in the distribution system. The DG capacity is considered as 30% of entire load demand of both the distribution systems. The DG location is found to be at bus number-15 bus number-24 in the case of IEEE-15 and IEEE-28 radial test distribution systems. The system after combined optimization technique and load flow technique, the active power losses are minimized and bus voltage is improved with DG injection.

8 Conclusion

In this work, solar energy is used as a DG to minimize the line losses in the distribution system. The solar radiation from the meteorological website is modelled with an astronomical model and obstructed astronomical model. The scaling factor and the obstruction factor from the obstructed astronomical model are calculated to find the effective solar radiation fall on the solar panels. This causes the decrease in daily average solar radiation value to 14.867%. The radiation is further modelled with the

Table 7 Nodal voltage with DG connection in IEEE-28 bus RDS (p.u)

Bus/days	Saturday		With DG					
	No DG (p.u)	With DG (p.u)	2nd Jun	3rd Jun	4th Jun	5th Jun	6th Jun	7th Jun
Bus-1	1	1	1	1	1	1	1	1
Bus-2	0.9868	0.9911	0.9913	0.9929	0.9931	0.9914	0.9907	0.9909
Bus-3	0.9679	0.9785	0.979	0.9829	0.9834	0.9792	0.9776	0.9781
Bus-4	0.9544	0.9697	0.9703	0.9759	0.9765	0.9706	0.9683	0.969
Bus-5	0.9409	0.9626	0.9634	0.9703	0.9711	0.9638	0.9609	0.9617
Bus-6	0.9308	0.9578	0.9587	0.9665	0.9674	0.9592	0.9559	0.9569
Bus-7	0.922	0.9555	0.9565	0.9647	0.9656	0.957	0.9536	0.9545
Bus-8	0.9197	0.9532	0.9543	0.9629	0.9639	0.9548	0.9512	0.9522
Bus-9	0.9194	0.953	0.954	0.9626	0.9637	0.9545	0.9509	0.952
Bus-10	0.9192	0.9528	0.9538	0.9625	0.9635	0.9543	0.9507	0.9517
Bus-11	0.9485	0.9638	0.9646	0.9712	0.972	0.965	0.9622	0.963
Bus-12	0.9468	0.9622	0.963	0.9699	0.9707	0.9634	0.9605	0.9613
Bus-13	0.9458	0.9612	0.962	0.9691	0.97	0.9624	0.9595	0.9603
Bus-14	0.9455	0.9609	0.9617	0.9689	0.9697	0.9622	0.9592	0.96
Bus-15	0.9453	0.9607	0.9615	0.9687	0.9696	0.962	0.959	0.9598
Bus-16	0.9398	0.9615	0.9623	0.9694	0.9702	0.9628	0.9598	0.9607
Bus-17	0.9291	0.9561	0.9571	0.9651	0.9661	0.9576	0.9542	0.9552
Bus-18	0.9282	0.9552	0.9562	0.9644	0.9654	0.9567	0.9533	0.9542
Bus-19	0.9266	0.9537	0.9547	0.9632	0.9642	0.9552	0.9516	0.9526
Bus-20	0.9257	0.9529	0.9539	0.9626	0.9636	0.9544	0.9508	0.9518
Bus-21	0.9251	0.9523	0.9533	0.9621	0.9631	0.9538	0.9502	0.9512
Bus-22	0.9193	0.9571	0.958	0.9659	0.9668	0.9585	0.9552	0.9561
Bus-23	0.9178	0.9586	0.9595	0.9671	0.968	0.96	0.9568	0.9577
Bus-24	0.9167	0.96	0.9609	0.9682	0.9691	0.9613	0.9582	0.9591
Bus-25	0.9164	0.9598	0.9606	0.968	0.9689	0.9611	0.958	0.9589
Bus-26	0.9163	0.9596	0.9605	0.9679	0.9688	0.9609	0.9578	0.9587
Bus-27	0.9192	0.9528	0.9538	0.9625	0.9635	0.9543	0.9507	0.9518
Bus-28	0.9191	0.9527	0.9537	0.9624	0.9634	0.9542	0.9506	0.9516

temperature effect to get the actual radiation on PV panels. A Solar farm is formed after considering the self-shadowing effect and the solar power generated from it is penetrated to the distribution system as DG. The solar insolation values are considered for June 2019 in Bagalkot, Karnataka, India. The best location and capacity of DG are found using the GWO optimization technique to get the most minimum power losses in the distribution lines. The optimum size of DG is assumed to be 30% of the total load demand of the test system that is produced by the solar farm. The number

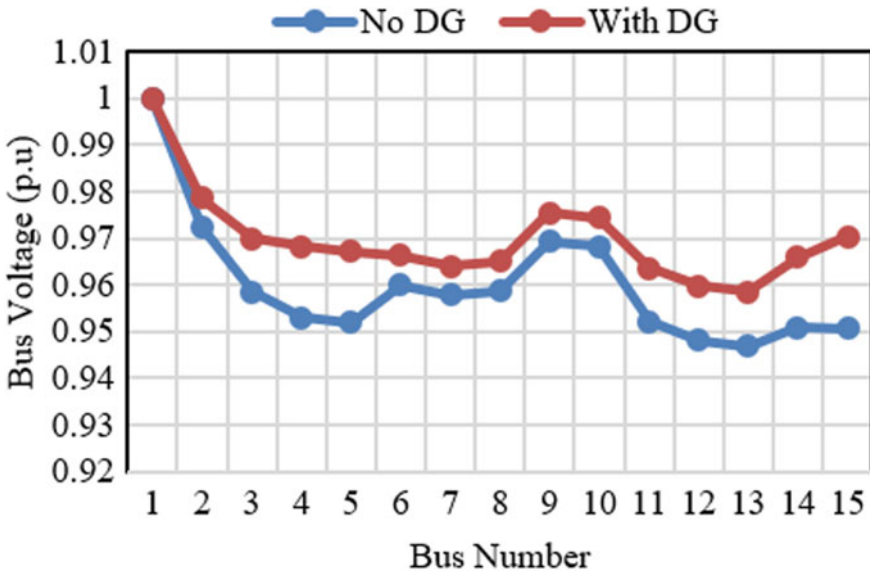


Fig. 21 Bus voltage improvement in IEEE-15 RDS

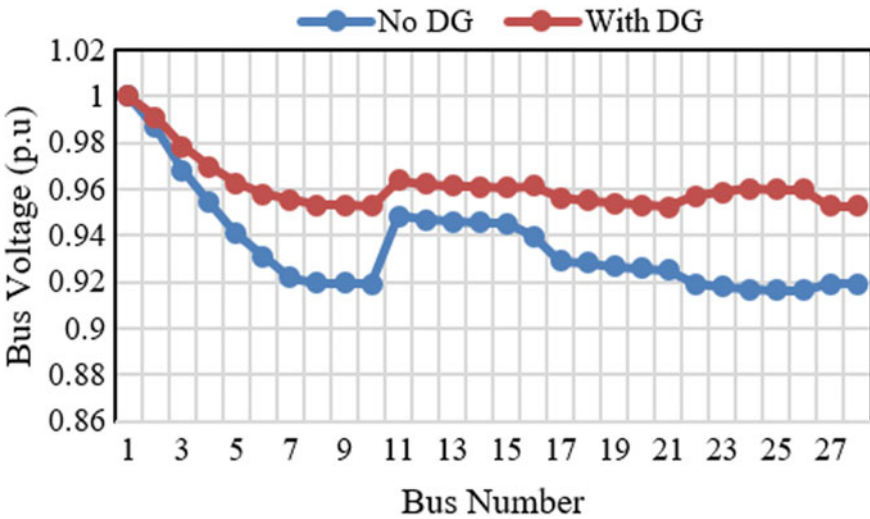


Fig. 22 Bus voltage improvement in IEEE-28 RDS

of solar panels is determined for each test systems under study to match the necessary load demand. For system analysis, the LIM load flow technique is implemented to the distribution systems. IEEE-15 and IEEE-28 bus RDS are used as system under study for the loss minimization using DG. The system parameters like active power

loss and bus voltages with DG are compared with system performance without DG. From the result, the power losses in both the test systems are significantly decreased and the bus voltages are improved remarkably with DG placements.

References

1. Nguyen TT (2021) Enhanced sunflower optimization for placement distributed generation in distribution system. *Int J Electr Comput Eng* 11(1):10. <https://doi.org/10.11591/ijece.v11i1.pp107-113>
2. Kalambe S, Agnihotri G (2014) Loss minimization techniques used in distribution network: bibliographical survey. *Renew Sustain Energy Rev* 29:184–200. <https://doi.org/10.1016/j.rser.2013.08.075>
3. Rathore A, Patidar NP (2021) Optimal sizing and allocation of renewable based distribution generation with gravity energy storage considering stochastic nature using particle swarm optimization in radial distribution network. *J Energy Storage* 35:102–282. <https://doi.org/10.1016/j.est.2021.102282>
4. Oda ES, Abd El Hamed AM, Ali A, Elbaset AA, Abd El Sattar M, Ebeed M (2021) Stochastic optimal planning of distribution system considering integrated photovoltaic-based DG and DSTATCOM under uncertainties of loads and solar irradiance. *IEEE Access* 9:26541–26555. <https://doi.org/10.1109/access.2021.3058589>
5. Goswami DY, Kreith F (2007) Handbook of energy efficiency and renewable energy. CRC Press. <https://doi.org/10.1201/9781420003482>
6. Solanki CS (2015) Solar photovoltaics: fundamentals, technologies and applications. PHI Learning Pvt. Ltd., India. ISBN 987-81-203-5111-0
7. Uzum B, Onen A, Hasanien HM, Muyeen SM (2021) Rooftop solar PV penetration impacts on distribution network and further growth factors—a comprehensive. *Rev Electron* 10(1):55. <https://doi.org/10.3390/electronics10010055>
8. Sudabattula SK, Kowsalya M (2016) Optimal allocation of solar based distributed generators in distribution system using Bat algorithm. *Perspect Sci* 8:270–272. <https://doi.org/10.1016/j.pisc.2016.04.048>
9. Bawazir RO, Cetin NS (2020) Comprehensive overview of optimizing PV-DG allocation in power system and solar energy resource potential assessments. *Energy Rep* 6:173–208. <https://doi.org/10.1016/j.egy.2019.12.010>
10. Ahmed IM, Kamel S, Abdel-Mawgoud H, Yu J (2018) Optimal allocation of PV based DG in distribution networks at different load levels. In: Twentieth international Middle East power systems conference, pp 649–654. <https://doi.org/10.1109/mepcon.2018.8635122>
11. Saha S, Mukherjee V (2021) A novel multi-objective modified symbiotic organisms search algorithm for optimal allocation of distributed generation in radial distribution system. *Neural Comput Appl* 33(6):1751–1771. <https://doi.org/10.1007/s00521-020-05080-6>
12. Janamala V (2021) A new meta-heuristic pathfinder algorithm for solving optimal allocation of solar photovoltaic system in multi-lateral distribution system for improving resilience. *Appl Sci* 3(1):1–17. <https://doi.org/10.1007/s42452-020-04044-8>
13. Panda S, Rout PK, Sahu BK (2021) Demand side management by PV integration to micro-grid power distribution system: a review and case study analysis. In: Green technology for smart city and society, pp 417–432. https://doi.org/10.1007/978-981-15-8218-9_35
14. Salih ZH, Hasan GT, Mohammed MA, Klib MAS, Ali AH, Ibrahim RA (2019) Study the effect of integrating the solar energy source on stability of electrical distribution system. In: 22nd international conference on control systems and computer science (CSCS), pp 443–447. <https://doi.org/10.1109/CSCS.2019.00081>

15. Marco M, Zordan D, Dini P, Rossi M (2014) Solar stat: modeling photovoltaic sources through stochastic Markov processes. In: IEEE international energy conference (ENERGYCON), pp 688–695. <https://doi.org/10.1109/ENERGYCON.2014.6850501>
16. Zobia AF, Ramesh CB (2011) Handbook of renewable energy technology. World Scientific
17. Dave JV, Halpern P, Myers HJ (1975) Computation of incident solar energy. IBM J Res Dev 19(6):539–549. <https://doi.org/10.1147/rd.196.0539>
18. Jeong J, Culler D (2012) A practical theory of micro-solar power sensor networks. ACM Trans Sens Netw 9(1):1–36. <https://doi.org/10.1145/2379799.2379808>
19. <https://power.larc.nasa.gov/data-access-viewer/>
20. HOMER (2019) The hybrid optimization model for electric renewable. [Online]. Available: <http://www.homerenergy.com>
21. “TRINASOLAR: homepage”. [Online]. Available: <http://www.trinasolar.com/us/product/duo-max72/duomax-peg14>
22. “TIMENDATE: homepage”. [Online]. Available: <https://www.timeanddate.com/weather/india/bagalkot/historic?month=6&year=2019>
23. Duong MQ, Nam Tran NT, Sava GN, Scripcariu M (2017) The impacts of distributed generation penetration into the power system. In: International conference on electromechanical and power systems (SIELMEN), pp 295–301. <https://doi.org/10.1109/SIELMEN.2017.8123336>
24. Weinstock D, Appelbaum J (2009) Optimization of solar photovoltaic fields. J Sol Energy Eng 131(3):031003-1–9. <https://doi.org/10.1115/1.3142705>
25. Gurupira T, Rix AJ (2017) Constrained optimization of photovoltaic (PV) module layouts. In: IEEE AFRICON, Cape Town, pp 1179–1184. <https://doi.org/10.1109/AFRCON.2017.8095649>
26. “NREL: renewable resource data center home page”. [Online]. Available: <http://www.nrel.gov/rredc/>
27. Probability Subcommittee (1979) IEEE reliability test system. IEEE Trans Power Appar Syst 98(6):2047–2054. <https://doi.org/10.1109/TPAS.1979.319398>
28. Mirjalili SM, Lewis A (2014) Grey wolf optimizer. J Adv Eng Softw 69:46–61. <https://doi.org/10.1016/j.advengsoft.2013.12.007>
29. Das D, Kothari DP, Kalam A (1995) Simple and efficient method for load flow solution of radial distribution networks. Int J Electr Power Energy Syst 17(5):335–346. [https://doi.org/10.1016/0142-0615\(95\)00050-0](https://doi.org/10.1016/0142-0615(95)00050-0)
30. Das D, Negi HS, Kothari DP (1994) Novel method for solving radial distribution networks. Proc IEE Gener Transm Distrib 141(4):291–298. <https://doi.org/10.1049/ip-gtd:19949966>

Author Index

A

Abdelaziz, Almoataz Y., 125
Annamraju, Anil, 221
Ansari, Salauddin, 77
Arunkumar, C. R., 181
Arya, Sabha Raj, 403

B

Battapothula, Gurappa, 221
Battu, Neelakanteshwar Rao, 257
Bhat, Sunil, 49
Bobba, Phaneendra Babu, 333

G

Gupta, Om Hari, 77

K

Kim, Seong-Cheol, 297
Kosaraju, Satyanarayana, 333
Krishna, Perka, 257

M

Manthati, Udaya Bhasker, 181
Mistry, Khyati D, 403

N

Namrata, Kumari, 153

P

Pagidipala, Sravanthi, 1, 297

Pradhan, Raseswari, 377
Punna, Srinivas, 181

R

Rakesh Chandra, D., 103, 279
Ray, Papia, 1, 153, 313
Routray, Aliva, 403

S

Salkuti, Surender Reddy, 1, 29, 103, 279,
297, 313, 355
Samadhiya, Akshit, 153
Sangam, Narasimha, 297
Satish, Raavi, 125
Singh, Arvind R., 49, 313
Srinivasarathnam, C., 221
Srivastava, Ishan, 49

T

Tummala, Suresh Kumar, 333

V

Vaisakh, K., 125
Veeramsetty, Venkataramana, 103, 279

Y

Yammani, Chandrasekhar, 221
Yarlagadda, Venu, 257

Subject Index

A

Absolute error, 226
Acceleration coefficients, 232, 234
Access, 3, 7, 8, 16, 43, 69, 70, 224, 225
Accuracy, 11, 29, 103, 112, 113, 125, 139, 140, 153, 174, 225–227
Active filters, 259, 268, 269, 316, 317
Active frequency drift, 160, 162
Active islanding, 153, 160, 169, 174
Active power load, 103–105, 109, 110, 359
Active power loss, 126, 322, 357, 359, 361–363, 366, 373, 405, 416, 418, 422, 428, 431
Adaptive control technologies, 393–395
Adjustable speed drives, 149
Advanced communication technologies, 396, 398
Advanced metering infrastructure, 5, 6, 8, 10, 51, 394
Algorithm-specific parameters, 221, 232, 234, 423
Alternate energy sources, 225, 297
Analytical method, 226–228, 240
Angular speed, 287–289, 291
Anti-islanding (AI), 157, 158
Apparent solar time, 407
Artificial immune system, 226
Artificial neural network, 14, 103, 104
Astronomical model, 405–410, 412, 428
Automatic meter reading, 51, 60
Automatic phase drift, 163
Automatic Transfer Switch (ATS), 396
Azimuthal displacement, 407

B

Back propagation algorithm, 107, 108, 113, 114
Backward/forward sweep method, 126
Backward pass, 114, 118
Bacterial foraging algorithm, 226
Band stop filter, 269
Bandwidth, 57, 58, 62, 64, 68, 72, 196–199, 202
Battery, 1, 5, 12, 19–24, 29, 31, 35, 37–40, 53, 181, 183–186, 188, 191–194, 196, 197, 199, 202–209, 211–213, 217, 218, 259, 268, 297–302, 305–309, 326, 330, 390
Battery bank, 39, 383, 390
Battery electric vehicles, 20, 24, 299
Battery energy storage, 29, 30, 35, 315, 358
Best solution, 226, 231, 233, 235
Beta distribution, 38
Bias parameters, 104, 108, 113–117, 119, 121, 122
Bidirectional DC–DC converters, 181, 185, 186, 188, 195, 300
Bifacial PERC, 335, 336, 339
Biomass energy, 3, 29, 31, 44
Blockchain technology, 1, 13, 15–18
Bode plot, 198, 199, 202, 205
Boltzmann constant, 228
Boost, 81, 104, 194, 204, 206, 213, 262
Boost converter, 81, 88, 89, 167, 195, 205, 212, 217, 257, 258, 262, 270, 273, 276, 302, 317
Box plot, 109
Brushless DC (BLDC) motor, 297, 299, 306–308

- Buck, 81, 193, 204, 262, 302, 306, 309
- Buck boost converter, 262
- Buck converter, 262
- Building area network, 63
- Bulk generation, 52, 53
- Bus, 57, 60, 68, 125, 127–150, 167, 203, 279, 281, 282, 285–293, 321, 322, 338–340, 355, 358, 359, 361–364, 366, 367, 371–373, 377, 378, 403, 406, 413, 418, 419, 425–430
- Bus voltage, 128, 132, 133, 136, 138, 182, 203, 204, 293, 321, 322, 363, 371, 372, 405, 406, 426–428, 430, 431

- C**
- Capacitor banks, 127, 132, 139, 149, 268, 361
- Capital investment, 35, 225, 283
- Carbon-dioxide, 43, 44, 224, 298
- Cascaded H-type inverter, 268
- Current stress, 181, 185
- Centralized places, 223
- Characteristics, 3, 4, 19, 21, 23, 24, 30, 54, 65, 68, 73, 77, 91, 93, 94, 111, 112, 128, 157, 181, 183, 184, 187, 188, 225, 227, 228, 230, 240–242, 244–249, 263, 265, 283, 299, 315, 323, 382, 386, 426
- Characterization, 300, 333, 336, 338, 352
- Charge of electron, 228
- Charging, 17, 19–24, 31, 39, 40, 181, 185, 186, 191, 193–196, 204, 205, 213, 217, 218, 301, 305, 306, 355, 357, 371
- Chemical energy, 222
- Chopping fraction, 160, 162, 166
- Circuit breaker switching strategy, 168
- Coal, 52, 224, 381, 384
- Cognitive component, 233
- Collection efficiency, 337
- Communication systems, 5, 8, 49, 57, 62, 64, 65, 73, 153, 398
- Comparison phase, 235, 236
- Compensation-based method, 127
- Complex power generation, 135
- Composite residential loads, 149
- Computer, 223, 300, 352
- Conclusions, 79, 105, 127, 317, 358
- Congestion, 7, 9, 72, 280, 404
- Consistency, 39, 226
- Constant load model, 416
- Constant speed wind turbine, 281
- Constant voltage method, 263
- Contact resistance, 227
- Control strategy, 55
- Control issues, 387
- Controller design, 185, 196
- Control parameter, 234
- Control strategy, 155–157, 181, 185, 213, 258, 315, 317
- Control target, 203
- Conventional energy, 30, 224, 259, 260, 263, 280, 285
- Convergence criterion, 136, 236, 237, 366
- Converter control circuit, 129
- Converters, 19, 35, 81, 129, 155, 156, 181, 183–186, 188, 189, 191, 195, 196, 201, 202, 204, 205, 210, 212, 218, 258, 259, 262, 276, 280, 282–284, 293, 298–300, 302, 304–309, 313, 315, 317
- Correlation, 5, 103–107, 113
- Crossover probability, 234
- Crystalline silicon, 261, 334
- Current sensor, 212
- Current source, 127, 227, 263
- Current source inverter, 266
- Current sweep method, 263
- Current temperature coefficient, 229, 236, 237, 240
- Customer Relationship Management (CRM), 393, 395
- Cyber physical systems, 382, 384

- D**
- DC-DC converters, 181, 184–186, 188, 195, 259, 262, 300, 302, 306, 309
- DC grid voltage, 181, 186, 188, 203, 206, 207, 209, 210, 212–214, 217, 218
- DC microgrid, 181–185, 187–189, 191, 193–197, 204, 208, 212, 213, 217, 218, 281
- Dead time, 161, 162, 190, 192
- Degradation cost, 39, 40
- Demand, 3, 5, 6, 11, 12, 14, 15, 18, 19, 22, 25, 29, 30, 40, 49–56, 104, 155, 167, 169, 170, 183, 191, 203, 207, 209, 213, 223, 224, 258, 280, 281, 285, 315, 317, 356, 357, 362, 379, 380, 383, 384, 387, 393, 397, 405, 412–414
- Demand side management, 225
- Depth of discharge, 39
- Detection time, 153, 156–159, 164, 165, 167, 169, 172, 174, 176

- Deterministic algorithms, 225
 - DG capacity, 3, 428
 - DG constraints, 413, 422
 - DG location, 428
 - Digital control of smart grid, 391
 - Diode clamped inverters, 268
 - Diode ideality factor, 90, 226, 228, 236, 237, 240, 245
 - Diode reverse saturation current, 227, 228, 236, 237, 240, 245
 - Direct-drive synchronous generator, 281
 - Directorate General of Training (DGT), 396
 - Discharging, 22, 39, 40, 181, 185, 186, 188–190, 193, 194, 196, 204, 205, 217, 218, 306
 - Distributed energy resources, 10, 25, 315, 356, 393
 - Distributed generation, 3, 5, 23, 53, 125, 155, 156, 167, 176, 257, 280, 314, 355, 356, 371, 379, 383, 388–391, 403, 404
 - Distributed generator, 153, 158, 271
 - Distribution management system, 6, 55
 - Distribution networks, 3, 49, 53, 55, 58, 62, 64, 65, 125–127, 130, 157, 316, 325, 326, 357, 358, 360, 362, 403
 - Distribution system, 4, 6, 13, 24, 54, 55, 104, 153, 271, 313, 315–317, 325, 326, 355–362, 393, 403–406, 412, 413, 418, 425–430
 - Doubly fed induction generator, 279, 282
 - dSPACE DS1104, 212
 - Duty cycle, 88, 190, 192, 193, 201, 302, 304
 - Dynamic programming, 225
 - Dynamic voltage restorer, 313, 316, 325
- E**
- Economical, 31, 49, 50, 53, 56, 64, 73, 153, 282, 357, 389, 404
 - Effective solar radiation, 406, 408, 410, 428
 - Effective spacing, 414
 - Efficiency, 2, 5–7, 9–11, 20, 21, 24, 25, 31, 32, 35, 36, 39–42, 44, 45, 78, 79, 81, 89, 97–99, 104, 162, 184, 185, 225, 226, 261–263, 265, 266, 270, 299–303, 315–317, 333, 338, 343, 356, 358, 383, 393, 404, 406, 411
 - Electrical energy, 9, 15, 19–21, 42, 56, 81, 88, 187, 222–224, 259, 261, 301, 356, 377, 391
 - Electric grid, 18, 24, 54, 181, 377, 378, 381
 - Electric vehicles, 1, 7, 17–20, 22, 24, 125, 297, 298, 300, 306, 307, 355–357, 371, 390, 397
 - Elitism probability, 234
 - Encirclement of prey, 423
 - Energy density, 20, 21, 39, 183, 185, 193, 301
 - Energy management systems, 6, 185
 - Energy service interface, 55
 - Energy storage, 1, 3, 10, 12, 19, 22, 40, 53, 181, 185, 326, 380, 384
 - Energy storage systems, 1, 30, 181, 183, 293, 314
 - Enterprise Asset Management (EAM), 393
 - Enterprise resource planning, 393
 - Environmental challenges, 280, 384
 - Environmental impact, 11, 12, 29, 51, 315, 381, 404
 - Equation of time, 406
 - Equivalent Series Resistance (ESR), 204
 - Error detection ratio, 158–160
 - Evolutionary algorithm, 234
 - Evolution of smart grid, 381
 - EV supply equipment, 305
 - Exploitation, 70, 315, 404, 424
 - Exploration, 10, 43, 425
 - External quantum efficiency, 336, 344
- F**
- Fast Fourier Transform (FFT), 318
 - Fault detection, 5, 13, 52, 55, 388, 394
 - Feature selection, 103, 113
 - FFT analysis, 318, 320, 327, 328
 - Filter inductor, 195, 196
 - Filters, 88, 89, 195, 196, 258, 259, 266, 268–274, 276, 284, 321, 326, 327
 - Finger contact, 335
 - Finger pitch, 338
 - Finger spacing, 338
 - Fitness, 235–237, 423
 - Fitness function, 230, 231, 240
 - Fixed excitation voltage type, 128
 - Fixed Speed Induction Generator (FSIG), 127
 - Fixed-speed wind generator, 279
 - Flow chart, 88, 160, 161, 165, 166, 194, 227, 263, 264, 365
 - Fluorescent light banks, 149
 - Flying capacitor inverters, 268
 - Flywheels, 12, 21, 301, 390
 - Forecasting, 14, 53, 55, 103, 104, 112, 113, 383

Forward pass, 113, 116, 122
 Fossil fuels, 3, 19, 22, 24, 29, 40, 42, 43, 45,
 221, 224, 258, 268, 298, 301, 389
 Frequency drift, 160, 162
 Fuel cell hybrid electric vehicle, 24
 Fuel cells, 5, 19, 21, 24, 126, 127, 156, 259,
 299, 315, 390
 Full bridge inverter, 266, 267
 Fundamental power flow algorithm, 131
 Fundamental voltage, 142, 144, 146, 148,
 149, 269
 Fuzzy logic control, 299, 302, 305, 316

G

Gauss-Seidel, 358
 Gearbox, 31, 282
 Gem silicon solar cell structure, 335
 General Electricals (GE), 396–398
 Generation, 1–7, 9–15, 17–19, 21, 29–32,
 35, 39, 45, 51–53, 55, 56, 60, 62–64,
 73, 77–79, 104, 136, 154, 155, 169,
 182, 207, 209, 221, 223–225,
 234–236, 257, 258, 261, 268,
 280–282, 286, 299, 301, 315, 316,
 328, 340–342, 344, 356, 378–381,
 383, 388, 390, 391, 396, 397, 403,
 405, 406, 411, 417, 419, 420, 422
 Generation profile, 336, 340
 Generator protection panels, 396
 Genetic algorithm, 226, 234, 357
 Geographic information system, 6
 Geometric programming, 225
 Geothermal energy, 31, 42, 43, 45
 Global best solution, 231, 232
 Global positioning system satellite, 391
 Global radiation, 403, 406, 408
 Global warming, 3, 19, 43, 44, 224, 299
 Greenhouse gas emission, 7, 126
 Greenwich meridian angle, 406
 Grey wolf optimization, 403, 406, 422, 428
 Grid, 1–18, 23, 25, 31, 35, 41, 42, 44,
 49–58, 61, 64–73, 126, 127,
 155–159, 162–165, 167, 168, 170,
 172, 174, 183, 185, 191, 199,
 211–213, 217, 224, 227, 257, 259,
 268–274, 276, 279–285, 293, 302,
 313–321, 324–327, 330, 334, 338,
 339, 347, 377, 379–391, 393–399,
 405, 406, 412, 418, 420
 Grid connected, 126, 153, 155, 156, 160,
 163, 167, 169, 176, 259, 273, 276,
 279

Grid resistance, 340, 345, 347
 Grid volatility, 8
 Gross Domestic Product (GDP), 223

H

Half bridge inverter, 266
 Harmful gases, 224
 Harmonic current injections, 129, 136, 138
 Harmonic detection, 165
 Harmonic distortion elimination, 313
 Harmonic load composition, 139
 Harmonic pollution, 146
 Harmonic Power Flow Algorithm (HPFA),
 126, 127, 129, 136, 137, 139, 140,
 146
 Harmonics, 60, 89, 125–127, 129, 136,
 138–141, 144–147, 165, 257–259,
 262, 267–271, 273, 276, 281, 304,
 315–320, 326–328, 330
 Harmonic source current spectrum, 127
 Harmonic spectrum, 127
 Harmony memory, 234
 Head branch, 130–132
 Head bus, 130–132
 High pass filter, 269
 Home area network, 55, 63
 Hour angle, 407
 Hybrid electric vehicle, 19, 20, 22, 24, 183,
 185, 218, 297, 299, 301, 302, 305,
 307, 383
 Hybrid energy storage systems, 181, 183
 Hybrid inverters, 268
 Hybrid islanding detection, 157, 160, 165
 Hydro Power, 41, 260, 261

I

Impedance measurement, 164
 Incidence angle, 407
 Incident photon current, 337
 Incremental conductance method, 263
 Independent system operators, 53, 56
 Indian Government, 224
 Induction generator, 126, 128, 129, 280,
 282, 283, 289
 Inequality constraints, 421
 Inertia weight, 232–234, 237, 240
 Information technology, 385, 391
 Insulated gate bipolar transistors, 304
 Integrated-circuit, 379
 Intelligent electronic devices, 9, 49, 51
 Internal combustion engines, 18–20, 297,
 298

- Internet of things, 18, 386
- Inverter, 19, 20, 24, 35, 88, 157, 160, 162–165, 167, 176, 257–259, 265–268, 270, 271, 273, 275, 276, 280, 299, 302, 316, 330
- Irradiance, 30, 35, 37, 38, 45, 77, 81, 90–96, 98, 228–230, 236, 237, 240–242, 244–249, 251–253, 259, 263, 323, 394, 406–409, 412, 414–421
- Islanding detection, 153, 154, 156–158, 160, 167, 169, 172, 174–176
- Isolated converters, 184, 262
- Iterative procedure, 131, 132, 136

- J**
- Jaya algorithm, 221, 227, 234, 236–238, 240, 242–247, 249–253

- K**
- Kelvin, 228
- Kernel density estimation, 403, 405, 414

- L**
- Lambert W function, 226
- Laterals, 129, 130
- Lead-acid battery, 212
- Leakage current, 227
- Levelized cost of energy, 335
- Levenberg parameters, 226
- Life expectancy, 6, 223
- Light-generated current, 336, 337
- Linear loads, 127, 136, 138, 149, 313
- Literacy rate, 223
- Lithium-ion (Li-ion) battery, 20, 38, 300, 301
- Load demand, 1, 29, 30, 38, 53, 54, 104, 181, 186, 205, 207, 209, 210, 212, 216–218, 221, 316, 356, 360, 366, 405, 406, 413, 414, 417, 428–430
- Load flow, 355, 358–360, 366, 373, 406, 428, 430
- Load modelling, 55, 416
- Local generation, 167, 170, 171
- Local islanding detection, 160
- Local load, 89, 155, 167, 169–175
- Low pass filter, 269

- M**
- Machine learning, 1, 13–15, 103, 104
- Mathematical modelling, 240
- Matlab, 77, 89, 99, 130, 139, 167, 205, 221, 237, 257, 279, 285, 297, 300, 306, 307, 315, 426
- Maximum power point, 81, 187, 229, 230, 236, 237, 240, 344
- Maximum power point tracking, 77, 187, 257, 259, 263, 273, 313, 316, 389
- Mean square error, 79, 317
- Meta-heuristic techniques, 227, 240, 245
- Metaphor based algorithm, 422
- Meter data management system, 55
- Metropolitan area network, 67
- Microgrid, 10, 17, 18, 30, 53, 125, 153, 155, 169, 183–185, 189, 218, 313–315, 330, 397
- Model predictive control, 181, 185
- Modified ROCOF, 167, 169, 170, 172–176
- Modified sine wave inverter, 265
- Module, 37, 86, 87, 89, 90, 183, 188, 221, 222, 226–228, 236, 237, 240, 242, 243, 245, 246, 249, 334–336, 338, 348, 405, 411, 412
- Mono-crystalline, 221, 226, 227, 240, 242, 245
- Monocrystalline cells, 261
- Monte carlo simulation, 357, 405, 414
- MOSFET switch IRFP460, 212
- Motion energy, 222
- Multi-directional power flow, 313, 316
- Multi input bidirectional DC-DC converter, 181, 185
- Multiple PWM inverter, 267
- Mutation probability, 234

- N**
- NASA, 408–410, 415
- National institute of standard and technology, 397
- Negative component of current injection, 164
- Neighborhood area network, 62
- Neural network, 14, 259, 280
- Newton method, 226
- Nickel–metal hydride batteries, 301
- Nitrogen-oxide, 224
- Nominal operating cell temperature, 411
- Nominal temperature, 337, 340
- Non-conventional energy sources, 259, 260
- Non detection zone, 153, 156, 158
- Non-isolated converters, 184, 262
- Non-linear, 77, 125–127, 136, 144, 146, 149, 187, 221, 225, 226, 315–319, 321, 323, 326–328, 330

- Non-linear loads, 125–127, 136, 138, 144, 146, 149, 316–319, 321, 323, 326, 327
- Nuclear energy, 222
- Numbering scheme, 129
- O**
- Objective function, 226, 231–235, 358, 363, 366, 418, 419
- Obstructed astronomical model, 403, 409, 426, 428
- Obstruction factor, 408, 409, 428
- Open circuit voltage, 229, 236, 237, 344
- Operating temperature, 35, 240, 337, 340
- Operating voltage, 83, 85, 188, 229, 236, 237, 240
- Operational constraints, 357, 418
- Optimization, 5, 8, 13, 19, 30, 51, 72, 221, 226, 231, 234, 237, 240, 300, 356–359, 396, 422, 426
- Optimization algorithm, 146, 225, 234, 236, 426
- Optimization technique, 30, 221, 222, 226, 228, 231–233, 240, 259, 393, 405, 422, 428, 429
- Outage management systems, 6
- Output of solar, 37
- Over/under current, 167, 169, 172, 174, 175
- Over/under frequency, 167, 169
- Over/under voltage, 167, 169
- P**
- Pass band filters, 269
- Passivated emitter, 333, 334
- Passive filters, 269
- Passive islanding detection, 160
- Peak loads, 3, 126, 383, 397, 417, 422, 426, 427
- Peak overshoot, 186, 209–211, 218, 287, 288, 293
- Peak-peak inductor current, 196
- Peer-to-peer semantic grid, 396
- Perturb and observe, 77, 79, 82, 188, 259, 263, 264, 313, 320, 322
- Perturb and observe algorithm, 259, 263
- Phase Jump Detection (PJD), 168
- Phase Locked Loop (PLL), 281
- Phasor measurement units, 6, 9, 24, 51, 391, 394
- Photoelectric, 35, 36, 335
- Photon current densities, 345, 346
- Photon currents, 336
- Photovoltaic, 10, 35, 77–79, 81, 126, 127, 257, 259, 273, 334–336, 403, 405
- Photovoltaic array, 317, 323
- Photovoltaic cell, 35, 259
- Photovoltaic distribution static compensator, 313, 330
- Photovoltaic power, 261
- Plug-in hybrid electric vehicles, 20, 22, 24, 301, 383
- Point of common coupling, 65, 158, 258, 314
- Polycrystalline cells, 261
- Positive feedback, 162, 163, 165
- Positive sequence impedance, 134
- Positive sequence voltage, 164
- Power flow, 49, 51, 52, 55, 57, 68
- Power line communication, 57, 58
- Power converter, 167, 183, 280, 300
- Power density, 24, 39, 181, 183, 185, 193, 280, 301
- Power electronic converter, 19, 129, 280, 289
- Power factor, 128, 160, 163, 270, 302, 316, 317, 319, 357, 361, 362
- Power factor control mode, 128
- Power flow, 127, 132, 136, 139, 141, 145, 147, 184, 185, 189, 191, 193, 194, 196, 217, 218, 285, 287, 293, 302, 313, 317, 356, 358, 405, 416, 426
- Power flow algorithms, 125, 426
- Power flow program, 131
- Power loss minimization, 357, 358, 404, 426
- Power quality, 54, 126, 146, 153, 155–160, 162–165, 167, 169, 174, 176, 259, 268, 270, 281, 313–317, 325–327, 329, 330, 388, 404, 405
- Power system analysis toolbox, 279, 293
- Probability density function, 414–420
- Problem formulation, 227, 228, 358, 362, 404, 418
- Proportional integral, 181, 322
- Proportional integral derivative, 299
- Pulse width modulation, 267, 270, 303
- Pumped hydro energy systems, 30, 40
- PV array, 167, 187, 205, 259, 313, 320, 321, 405
- PV bus sensitivity matrix, 134
- PV cell, 35–37, 79, 187, 225, 261, 263, 265, 316, 334–336, 405
- PV cell modelling, 263
- PV cell temperature, 37, 411, 412

PV generation, 170–175, 181, 186, 188,
191, 205–210, 212, 213, 215, 217,
218, 417
PV node, 126, 134, 135
PV panel, 35, 37, 81, 83, 86–89, 186–188,
195, 206, 208, 209, 227, 229, 406,
408, 409, 413, 429

Q

Quality factor, 158, 264

R

Radial distribution network, 126, 403
Radial distribution system, 355, 357, 358,
371, 403, 413, 425, 426
Radiant energy, 222
Radio frequency identification, 386
Random number, 234, 235
Rate of change of frequency, 67, 157
Reactive power, 55
Reactive power compensation, 55, 313,
316, 317, 362
Reactive power generation, 134–136, 141
Reactive power loss, 360, 426, 427
Real power generation, 134, 135, 141
Real power loss, 138, 355, 362, 363, 403,
426
Real-time distribution networks, 126
Rechargeable batteries, 20, 300, 390
Reflection, 223, 336, 342, 345, 346, 348,
349, 353
Regenerative energy, 298, 301, 302
Regional transmission operators, 53
Regulated power supply, 212
Regulating excitation voltage type, 128
Reliability test system, 279, 282, 285, 416
Reliable, 1, 3, 5, 6, 8, 25, 31, 43, 69, 73,
103, 104, 157, 169, 174, 223–225,
279, 315, 357, 379, 382, 391
Remote islanding detection, 160
Renewable energy resources, 1, 3, 11, 29,
30, 45, 280, 315
Renewable energy sources, 10, 16, 18, 51,
125, 153, 155, 181–183, 221, 225,
257, 263, 358, 382, 383, 391
Reverse saturation current, 187
Reweighted zero attracting, 313, 316, 317
R.M.S value of voltage, 138
Root mean square error, 226, 231
Rotor resistance, 288, 289, 291, 292
Rotor resistance control, 279, 281, 287,
289–292

S

Sandia frequency shift, 162, 166
Sandia voltage shift, 162
SCADA system, 53, 71
Scaled astronomical Model, 410
Scaling factor, 339, 341, 405, 408, 428
Search space, 226, 231, 233, 234, 236, 237,
240, 422, 425
Self shadowing effect, 413
Semi-conductor device, 262
Sequential programming, 226
Series filter, 269
Series resistance, 37, 227, 228, 236, 237,
240, 245, 336, 340
Settling time, 186, 207, 209–211, 218
Shading of solar panels, 413
Shape parameter, 38
Short circuit current, 36, 90, 229, 236, 237,
240, 344
Short-circuit fault, 329
Shuffle frog leap algorithm, 226
Shunt active filter, 257–259, 269, 270, 272,
276, 316
Shunt filter, 269
Shunt resistance, 36, 37, 227, 228, 236,
237, 240, 244, 340
Silicon nitrate, 333, 352
Simulation annealing, 226
Sine wave inverter, 265
Single diode modelling, 225
Single phase inverter, 266
Single PWM inverter, 267
Sinusoidal pulse width modulation, 304
Sinusoidal PWM inverter, 267
Sinusoidal voltage waveform, 136
Slip, 128, 282, 289
Slip mode frequency shift, 163
Slope, 3, 30, 81, 83, 163, 189–192, 230
Small hydro energy, 30, 40
Small signal linear averaged model, 186,
196, 197, 199
Smart appliances, 9
Smart grid technologies, 49, 389, 396, 398
Smart meter, 7–10, 24, 49, 51, 52, 55, 56,
63, 67, 69, 70, 385
Smart power distribution network, 125
Social, 13, 224, 237, 280, 382, 384, 388,
398, 423
Social component, 233, 234
Social learning rate, 233
Society, 10, 12, 223, 384
Solar absorptance, 411
Solar based DGs, 167

Solar declination angle, 406, 407
 Solar energy, 3, 17, 34, 35, 37, 77–79, 81, 88, 225, 257, 259, 261, 263, 403, 405, 406, 422, 428
 Solar farm, 406, 408, 409, 412–414, 426, 427, 429
 Solar insolation, 30, 358, 409, 429
 Solar irradiation, 29, 35–37, 81, 189, 313
 Solar panel efficiency, 408
 Solar photovoltaic, 3, 29, 30, 167, 169, 317, 323
 Solar power, 6, 35, 37, 79, 89, 90, 225, 258, 259, 313, 315, 334, 403, 405, 406, 408, 409, 411–414, 416, 427, 429
 Solar transmittance, 412
 Spot loads, 144, 149
 Square wave inverter, 265
 Squirrel cage induction generator, 127, 281, 282
 Stability, 23–25, 53, 155, 159, 162, 169, 183, 185, 213, 280–283, 285, 288, 357, 390, 397, 405
 Standard Test Condition (STC), 37, 229, 250, 333, 353, 411
 State of charge, 39, 186, 300, 306, 309
 Static compensator, 281, 317
 Static Voltage Characteristic Model (SVCM), 128
 Steady-state behaviour, 317
 Stochastic algorithm, 225, 226, 231
 Stochastic gradient descent optimizer, 104, 107, 108, 113, 114
 Stochastic modelling, 414
 Strengthened, 223
 Sub-station, 23, 24, 393
 Substation bus voltage, 131
 Sulphur dioxide, 224
 Supercapacitor, 12, 183–186, 188, 191–197, 202, 204, 205, 212, 218
 Superconducting magnetic energy storage, 330
 Supervisory Control And Data Acquisition (SCADA), 8, 10, 71, 168, 393, 394
 Sustainability, 5, 10, 11, 31, 78
 Sustainable energy, 6, 42, 382, 388
 Swarm intelligence algorithm, 234
 Swarm size, 232, 233
 Switching frequency, 197, 268, 303
 Synchronous based-renewable DG, 125, 129, 144, 146
 Synchronous generators, 128, 281, 288
 Synchronous machine, 291

T

Technical challenges, 15, 153, 356, 383
 Tail branch, 130, 131
 Tail bus, 130–132, 138
 Teaching learning based optimization, 226
 Temperature, 30, 35–37, 39, 42, 43, 77, 79, 81, 86, 87, 89–96, 98, 99, 104, 187, 228–230, 236, 237, 240–242, 244–249, 251–253, 263, 265, 337, 344, 346, 394, 403, 405, 406, 411, 412, 429
 Temperature coefficient, 87, 90
 Temperature method, 263
 Temperature model, 412, 426
 Test system, 68, 285, 287, 292, 358, 365, 366, 414, 422, 425–431
 Thermal energy, 29, 222, 260
 Thermal voltage, 228
 Thin-film, 226, 227, 240, 242, 245
 Thin film cells, 261
 Three phase inverter, 266, 267, 271
 Three-phase PFA, 126
 Three-phase system, 313, 330
 Threshold radiation, 415
 Tidal energy source, 260
 Tolerance limit, 132, 138
 Total harmonic distortion, 139, 257, 258, 270, 272, 276, 316
 Transfer function, 196, 198, 199, 202, 204, 323
 Transformers, 31, 35, 41, 42, 89, 127, 167, 184, 262, 285, 326, 327, 405
 Transient response, 313, 317
 Transient stability, 279–281, 283, 287, 288, 293
 Transient Voltage Surge Suppression (TVSS), 396
 Transmitted, 20, 58, 223, 378
 Transportation sector, 298, 356
 Two-diode model, 226
 Two-way communication, 6, 8, 9, 49, 51, 54, 55, 57, 64, 73

U
 Ultracapacitors, 298, 301
 Unbalanced load, 126
 Uncertainty, 3, 11, 29, 30, 39, 221, 281, 315, 337, 356, 390, 414
 Uncertainty modeling, 30, 37
 Unified controller, 181, 185, 186, 196, 218
 Unintentional islanding, 153–157, 167
 Uninterruptible Power Supply (UPS), 396

Update phase, 235, 236
 Urbanization rate, 223
 Utility grid, 29, 88, 89, 126, 159, 162, 167, 269, 271, 280, 282, 283
 Utilization, 3, 5, 11, 12, 19, 22, 49, 153, 158, 223, 225, 298, 356, 360, 378, 390, 391, 395

V

Vector Shift IDM, 167
 Vehicle-to-grid, 390
 Velocity, 231–234, 237
 Voltage control mode, 128, 262
 Voltage fluctuation injection, 166
 Voltage mismatches, 133, 134
 Voltage mismatch matrix, 134
 Voltage regulator, 127, 149, 269
 Voltage sag, 60, 269, 281, 316, 317, 325–327, 329, 330
 Voltage sensor, 212
 Voltage source converter, 258, 280, 304
 Voltage source inverter, 164, 257, 266, 303, 315
 Voltage stabilization, 185

W

Wafer, 261, 339, 340

WAMS, 6, 53, 394
 Wave energy source, 260
 Weekend hourly load, 417
 Weibull PDF, 32, 34, 37
 Weights, 38, 104–108, 110–114, 116–122, 269, 300, 301, 323, 324
 Wide area measurement system, 6, 394
 Width of finger, 338
 Wind energy, 5, 29–31, 45, 260, 280–282, 285, 360
 Wind energy generators, 33, 279, 293
 Wind energy source, 260
 Wind power, 11, 31–34, 225, 260, 279, 281, 282, 285, 293, 315
 Wind power generation, 280
 Wind speed prediction, 13
 Wind turbines, 5, 10, 31, 32, 127, 155, 260, 279–283, 285–289, 293
 Wireless mesh network, 62
 World, 3, 6, 8, 10, 11, 29, 30, 44, 160, 223–225, 260, 261, 280, 285, 298, 334, 379, 382–384, 386, 397, 405
 Worst solution, 235

Z

Zero time, 160
 Zero voltage switching, 185